Advances in Polymer Science 258

Walter Kaminsky *Editor*

Polyolefins: 50 years after Ziegler and Natta II

Polyolefins by Metallocenes and Other Single-Site Catalysts

Springer

258
Advances in Polymer Science

For further volumes:
http://www.springer.com/series/12

Aims and Scope

The series Advances in Polymer Science presents critical reviews of the present and future trends in polymer and biopolymer science. It covers all areas of research in polymer and biopolymer science including chemistry, physical chemistry, physics, material science.

The thematic volumes are addressed to scientists, whether at universities or in industry, who wish to keep abreast of the important advances in the covered topics.

Advances in Polymer Science enjoys a longstanding tradition and good reputation in its community. Each volume is dedicated to a current topic, and each review critically surveys one aspect of that topic, to place it within the context of the volume. The volumes typically summarize the significant developments of the last 5 to 10 years and discuss them critically, presenting selected examples, explaining and illustrating the important principles, and bringing together many important references of primary literature. On that basis, future research directions in the area can be discussed. Advances in Polymer Science volumes thus are important references for every polymer scientist, as well as for other scientists interested in polymer science - as an introduction to a neighboring field, or as a compilation of detailed information for the specialist.

Review articles for the individual volumes are invited by the volume editors. Single contributions can be specially commissioned.

Readership: Polymer scientists, or scientists in related fields interested in polymer and biopolymer science, at universities or in industry, graduate students.

Special offer:
For all clients with a standing order we offer the electronic form of Advances in Polymer Science free of charge.

Walter Kaminsky
Editor

Polyolefins: 50 years after Ziegler and Natta II

Polyolefins by Metallocenes and Other Single-Site Catalysts

With contributions by

M. Anselm · L. Boggioni · H.H. Brintzinger · L. Cui · D. Fischer · K. Hakala · T. Halbach · W. Kaminsky · E. Kokko · A. Kurek · P. Lehmus · S. Lipponen · B. Löfgren · G.A. Luinstra · R.S.A. Meyer · T.C. Mike Chung · R. Mülhaupt · A. Pakkanen née Malmberg · A. Razavi · J. Seppälä · T. Shiono · H. Sinn · W.-H. Sun · M. Stürzel · N.H. Tarte · I. Tritto · S. Woo

Springer

Editor
Walter Kaminsky
Dept. of Chemistry
Inst. for Techn. and Macromol. Chemistry
University of Hamburg
Hamburg
Germany

ISSN 0065-3195 ISSN 1436-5030 (electronic)
ISBN 978-3-642-40804-5 ISBN 978-3-642-40805-2 (eBook)
DOI 10.1007/978-3-642-40805-2
Springer Heidelberg New York Dordrecht London

Library of Congress Control Number: 2013955573

Printed on acid-free paper

Springer is part of Springer Science+Business Media (www.springer.com)

Preface

Fifty years after the Nobel Prize was awarded to Karl Ziegler and Giulio Natta in 1963, the polymerization of olefins by metallorganic catalysts has grown to one of the most fascinating areas in academic and industrial polymer science and now has the largest use in polymer production. Ziegler had discovered 10 years earlier that a mixture of transition metal compounds, especially titanium chlorides and aluminum alkyls, was able to polymerize ethene by an insertion reaction. This spectacular milestone was expanded a year later when Natta prepared and characterized isotactic polypropylene and introduced stereospecific polymerization. In contrast to the high-pressure ethene polymerization invented in 1935 by ICI (Imperial Chemical Industries, Great Britain), the catalyzed olefin polymerization requires only low pressure and low temperature.

Today, more than 130 million tons of polyolefins are produced worldwide per year, the major part with the help of Ziegler–Natta catalysts. Polyolefins have changed the world! They are not only the polymers with the highest production volume, but they also show an unbroken production increase. Containing only carbon and hydrogen atoms, polyolefins are sustainable materials, light in weight, and offer a wide variety of properties. The production requires only easily available and nontoxic monomers and proceeds with almost no losses or side reactions. After their end of use, polyolefins can easily be recycled through mechanical procedures to simple articles, by pyrolysis to gas and oil, or by incineration to energy.

In recent decades, new generations of catalysts with higher activities and stereospecificities and modern production processes have been invented to produce a great variety of polyolefins ranging from high density polyethylene (HDPE) to linear low density polyethylene (LLDPE), high melting polypropylene, high modulus polyolefin fibers, ethene–propene rubber (EPR), ethene–propene–diene monomer rubber (EPDM). The chromium-based Phillips catalysts opened the field of gas phase polymerization for HDPE. New supported Ziegler–Natta catalysts make it possible to increase the activity, to control the morphology, and for polypropylene to increase the isotacticity by adding different kinds of donors.

A great development in this research field was the discovery of metallocene and other transition metal complexes activated by methylaluminoxane. These catalysts

are up to 10 times more active than Ziegler–Natta catalysts, are soluble in hydrocarbons, show only one type of active site (single site catalysts), and can easily be modified in their chemical structure. These properties make it possible to predict the properties of the resulting polyolefins very accurately from the knowledge of the structure of the catalyst, and thus to control molecular weight and distribution, comonomer content, and tacticity by careful selection of the appropriate reactor conditions. The single site character of metallocene-based catalysts leads to a better understanding of the mechanism of olefin polymerization and to the introduction of other bulky cocatalysts.

The different chapters in this book deal with the development of olefin polymerization 50 years after the pioneering work of Ziegler and Natta. Academic and industrial developments of ethene and propene polymerizations are presented, including short biographies of Ziegler and Natta, research on Phillips catalysts, kinetic and active site measurements, and polyolefin characterization. Review chapters also describe the latest results of olefin homo-, living-, and copolymerizations by metallocene and other single site catalysts, such as the synthesis of ansa metallocenes, supported iron catalysts, syndiotactic polypropylene, long chain branched polyolefins, and cyclic and functional copolymers. Remarkable progress has been achieved in the synthesis of polyolefin nanocomposites by an in-situ polymerization process using clay, layered silicates, carbon fibers, and carbon nanotubes as fillers.

I thank all the authors very much for giving their time to write these exciting chapters.

Hamburg, Germany Walter Kaminsky

Contents

Adv Polym Sci (2013) 258: 1–28
DOI: 10.1007/12_2013_226

Published online: 12 June 2013

Methylaluminoxane: Key Component for New Polymerization Catalysts

Walter Kaminsky and Hansjörg Sinn

Abstract The use of methylaluminoxane (MAO) as cocatalyst for the polymerization of olefins and some other vinyl compounds has widely increased the possibilities for more precisely controlling the polymer composition, polymer structure, tacticity, and special properties. Highly active catalysts are obtained by different transition metal complexes such as metallocenes, half-sandwich complexes, and bisimino complexes combined with MAO. These catalysts allow the synthesis of polyolefins with different tacticities and stereoregularities, new cycloolefins and other copolymers, and polyolefin composite materials of a purity that cannot be obtained by Ziegler–Natta catalysts. The single-site character of metallocene/MAO or other transition metal/MAO catalysts leads to a better understanding of the mechanism of olefin polymerization.

Keywords Metallocene catalysts · Methylaluminoxane · Olefin polymerization · Single-site catalysts

Contents

W. Kaminsky (✉)
Institute for Technical and Macromolecular Chemistry, University of Hamburg,
Bundesstraase 45, 20146 Hamburg, Germany
e-mail: kaminsky@chemie.uni-hamburg.de

H. Sinn
Guest at the Technical University Clausthal,
Institute for Technical and Macromolecular Chemistry, University of Hamburg,
Bundesstraase 45, 20146 Hamburg, Germany
e-mail: sinnalox@t-online.de

Abbreviations

Ac	Acetyl
Bu	Butyl
CNF	Carbon nanofiber
Cp	Cyclopentadienyl
Cp*	Pentamethyl cyclopentadienyl
En	Ethylidene
Et	Ethyl
Flu	Fluorenyl
Ind	Indenyl
$IndH_4$	Tetrahydro indenyl
MAO	Methylaluminoxan
Me	Methyl
M_w/M_n	Molecular weight distribution
MWCNT	Multiwalled carbon nanotube
Naph	Naphthyl
NmCp	Neomenthyl cyclopentadienyl
NMR	Nuclear magnetic resonance
PE	Polyethylene
Ph	Phenyl
PP	Polypropylene
*t*Bu	*Tertiary*-butyl
TEM	Transmission electron microscopy
TIBA	Triisobuthyl aluminum
TMA	Trimethylaluminum

1 Introduction

Shortly after the discovery of the polymerization catalyst by Ziegler [1], in 1957 Breslow [2] and Natta [3] used the newly synthesized titanocene as a transition metal component in combination with aluminum alkyls for the polymerization of ethene. Compared with the heterogeneous Ziegler catalyst based on titanium tetrachloride or titanium trichloride and triethylaluminum, the titanocene/$Al(C_2H_5)_2Cl$ catalyst is homogeneous and soluble in hydrocarbons. It therefore was preferentially studied in order to understand the elementary steps of the polymerization, which is simpler in homogeneous than in heterogeneous systems. On the other hand, there was

less industrial interest in this homogeneous Ziegler catalyst because of the low polymerization activity.

The most investigated homogeneous catalyst systems are based on bis(cyclopentadienyl)titanium(IV), bis(cyclopentadienyl)zirconium(IV), tetrabenzyltitanium, vanadium chloride, and trialkylaluminum or alkylaluminum halides as cocatalysts. Subsequent research on these and other systems with various alkyl groups has been conducted by Patat and Sinn [4], Shilov [5], Henrici-Olivé and Olivé [6], Reichert and Schoetter [7], and Fink et al. [8].

The polymerization of olefins, promoted by homogeneous Ziegler catalysts based on biscyclopentadienyltitanium(IV) or analogous compounds and aluminum alkyls, is accompanied by a series of other reactions such as alkylation, hydrogen transfer, and reduction that greatly complicate the kinetic interpretation of the polymerization. It was found that the polymerization takes place primarily into a Ti–C bond where the titanium exists as the titanium(IV) alkyl cation formed by alkylation and dissociation (1) and (2) [8–11]:

$$(C_5H_5)_2TiCl_2 + AlR_2Cl \rightarrow (C_5H_5)_2TiRCl + AlRCl_2 \quad (1)$$

$$(C_5H_5)_2TiRCl + AlRCl_2 \rightarrow \left[(C_5H_5)_2TiR\right]^+ + \left[AlRCl_3\right]^- \quad (2)$$

In the case of β-hydrogen transfer by ethyl alkylated titanium complexes, Ti–CH_2–CH_2–Ti units are formed (3), which are unstable and decompose within some seconds into titanium(III) species and ethene (4) [12, 13]:

$$2\,Cp_2Ti(Cl)CH_2 - CH_3 \rightarrow Cp_2(Cl)Ti - CH_2 - CH_2 - Ti(Cl)Cp_2 + CH_3 - CH_3 \quad (3)$$

$$Cp_2(Cl)Ti - CH_2 - CH_2 - Ti(Cl)Cp_2 \rightarrow 2\ Cp_2TiCl + CH_2 = CH_2 \quad (4)$$

The bridged titanium complexes as well as the reduced titanium(III) species are polymerization inactive. Analogous zirconium complexes have been used to isolate intermediates and to study alkyl exchange and β-hydrogen transfer because zirconium is less easily reduced than titanium [14, 15]. Sinn and Kolk isolated a stable $Cp_2(Cl)Zr$–CH_2–CH_2–$Zr(Cl)Cp_2$ complex [16]. Zirconium–aluminum alkyl complexes with unusual bonding angles (75.9°) between the bridging angles were obtained (Fig. 1), showing the force in these complexes [17]. It looks like an ethene is complex bonded between two zirconium complexes, but NMR measurements show that the chemical C–C bond of the bridge (bond length 0.151 nm) is normal.

In the Institute of Technical and Macromolecular Chemistry at the University of Hamburg we investigate these side reactions, especially the hydrogen transfer reactions. The main goal of the research is to be able to engineering the polymer reaction. The kinetics of polymer reactions are studied as well as the analysis of polymers and different side pathways. In the Hamburg Institute, research groups for polymer synthesis and characterization, polymer physics, and polymer recycling work together [18, 19].

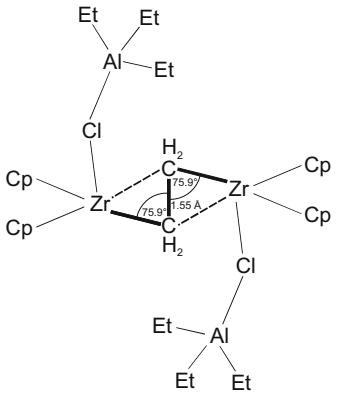

Fig. 1 X-ray structure of a CH_2–CH_2 bridged dizirconocene–triethylaluminum complex

To decrease the reduction rate of the titanium system, we investigated (instead of the ethyl-containing system) the reaction of biscyclopentadienyl–titanium dimethyl and trimethylaluminum (TMA), mainly by NMR analysis at low temperatures. The formation of new CH_2-bridged titanium aluminum complexes were observed by a slow α-hydrogen transfer (5) [20]:

$$Cp_2Ti(CH_3)_2 + Al(CH_3)_3 \rightarrow Cp_2(CH_3)Ti - CH_2 - Al(CH_3)_2 + CH_4 \qquad (5)$$

This slow reaction and the complexation by ethene was analyzed by NMR measurements, because no reduction of titanium(IV) and no polymerization take place. The unintentional condensation of water into the NMR tube led in 1975 to the astonishing formation of polyethylene [21]. This unexpected observation was confirmed in a larger scale experiment in a 1 L autoclave [22]. More details of this discovery can be found in [23–26]. Some years before, Reichert [26] had found an approximately twofold increase in the activity through the addition of small amounts of water to the halogen-rich homogeneous system $Cp_2TiEtCl/EtAlCl_2$, and Breslow [27] obtained similar results with the Cp_2TiCl_2/Me_2AlCl system. Obviously, there are great differences between the halogen-free and the halogen-containing catalysts. The polymerization rate in the halogen-free $Cp_2Ti(CH_3)_2/Al(CH_3)_3/H_2O$ catalyst reaches a maximum when high amounts of water, up to a molar ratio water/TMA of 1:1, are added.

2 Formation and Structure of MAO

Karl Ziegler describes the formation of alkyl aluminum oxides and the subsequent reaction of the primary produced dialkyl aluminum hydroxide [28]. It was also recognized that bis(diethylaluminum)oxide decomposes by disproportionation into triethyl-aluminum and a solid, non-volatile compound [29]. Bis(dimethylaluminum) oxide is mentioned in the literature but not exactly described [30].

It was clear that TMA reacts rapidly with water in a toluene solution. The next step was therefore to isolate the product formed in a 1:1 mixture of water and TMA. The general reaction is shown by (6):

$$n\,H_2O + (n+1)\ Al(CH_3)_3 \rightarrow\ (H_3C)_2Al - [O - AlCH_3]_n - CH_3 + 2n\,CH_4 \quad (6)$$

At these water levels, explosions could happen, therefore in first experiments inorganic salts were used containing bonded water, such as $CuSO_4 \bullet 5H_2O$ or $Al_2(SO_4)_3 \bullet 14H_2O$ in toluene suspension [31]. After 20 h, the reaction mixture was filtered and the solvent evaporated. The white powder obtained was dried and analyzed. The compound was named methylaluminoxane (MAO).

MAO prepared by the use of $CuSO_4 \bullet 5H_2O$ contains small amounts of copper compounds. To produce a pure MAO and to prevent any side reactions it is necessary to use TMA and water or ice only. This allows the calculation of mass-balances and a better characterization. The research group of Sinn used an ice-plate that was washed with a stream of a TMA solution [32]. The reaction takes place at the surface only, forming a white film. This film is dissolved if the stream of the solution on the top of the plate exceeds turbulence. A rotating scraper was used in such a way that it did not erode the ice. A detailed description of the equipment can be found in [33].

Although the experiments using this procedure are reproducible, the conditions of the reaction are inconsistent. The linear flow-viscosity of the solution decreases with the distance from the center if the solution is added in the center of the plate, and the linear velocity of the scraper increases with the radius. This produces different Reynolds numbers along the surface and different heat transfer conditions and, as a result, different temperatures are obtained by the strongly exothermic reaction of TMA and frozen water at the surface. To have more constant reaction conditions, a thin-film reactor was constructed [34]. A cooled and rotating steel band picks up ice by sublimation in a sublimation chamber and introduces the ice into the reaction chamber. Here, the ice reacts with a solution of TMA, producing MAO and methane. The better heat transfer on the steel band makes it possible to have more constant reaction temperatures.

The obtained MAO was investigated by element analysis, cryoscopic and NMR measurements, and decomposition with HCl. It was found that MAO is a mixture of different oligomers, including some ring structures (Fig. 2).

Even today, the exact structure is not known because there are equilibria between the oligomers and complexation of the oligomers with each other and with unreacted TMA. MAO is a compound in which aluminum and oxygen atoms are arranged alternately and free valences are saturated by methyl substituents. There is evidence that, in a first step, TMA reacts with water to form a hydroxyl compound (7):

$$H_2O + Al(CH_3)_3 \rightarrow (H_3C)_2Al - OH + CH_4 \quad (7)$$

$(H_3C)_2Al$–OH is unstable and reacts even at −40°C with a second TMA to form a dimer MAO (8):

$$(H_3C)_2Al - OH + Al(CH_3)_3 \rightarrow (H_3C)_2Al - O - Al(CH_3)_2 + CH_4 \quad (8)$$

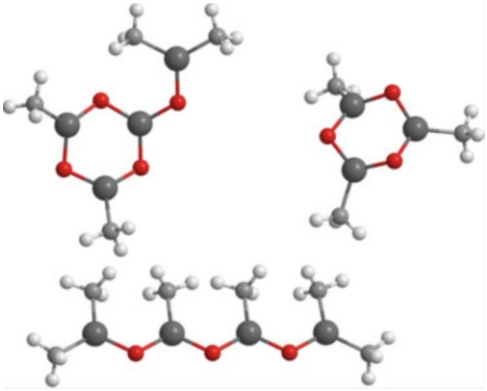

Fig. 2 Unit structures of cyclic and linear MAO: *big balls* aluminium, *small balls* oxygen and methyl groups

In the case of MAO there is no evidence that the dimer $(H_3C)_2Al–O–Al(CH_3)_2$ will be stable unless the reaction is done in homogeneous solution (for instance, hexadeutero benzene) with concentrations of TMA <100 mmol/L and the products are stabilized by donors (for instance, diethyl ether).

If highly dispersed water is added to a 20 mM solution of TMA in hexadeutero benzene (which is able to solve the introduced amount of water) a reaction evolving methane takes place within <100 s. The H-NMR integral of TMA, which was found at −0.351 ppm with a value of 778.4, was reduced equivalently to the amount of water added and showed an integral value of 532.1; only a very small broadening of the signal could be seen. However, if diethyl ether was added, the signal at −0.351 ppm disappeared and two new signals were found, one at −0.472 ppm with an integral value of 324.8 and another at −0.607 ppm with an integral value of 157.3. The signal at −0.607 ppm was identified as TMA-diethyetherate.

The solution with added diethyl ether was stable for some days. A very small reduction in size of the integral values can be seen within some hours, but the postulated condensation (9) with evolving TMA has not yet been proved to be simple:

$$2\,(H_3C)_2Al-O-Al(CH_3)_2 \rightarrow (H_3C)_2Al-O-Al(CH_3)-O-Al(CH_3)_2 + Al(CH_3)_3 \quad (9)$$

However, there is no doubt that MAO structures have the ability to condense with splitting off of TMA. A MAO sample with a vapor tension of <0.001 mbar was sealed in 1997 under argon and contained, when opened in 2007, serious amounts of TMA, which were condensed off and characterized [35]. The splitting off of TMA seems to be a general property of methylaluminum compounds and able to cause the formation of long-chained, advanced MAO products by curious reactions [36, 37].

According to investigations by Sinn [38], there is evidence that a compound with a ratio $CH_3/Al = 1.5$ plays an important role in the formation of MAO. If diethyl ether is added to a solution of MAO and TMA in toluene, a phase separation takes place. After the separation is finished, all TMA will be found in the upper phase.

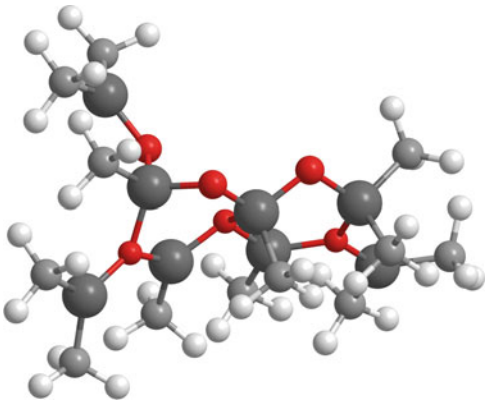

Fig. 3 MAO association of two linear unit structures: *big balls* aluminium; *small balls* oxygen and methyl groups

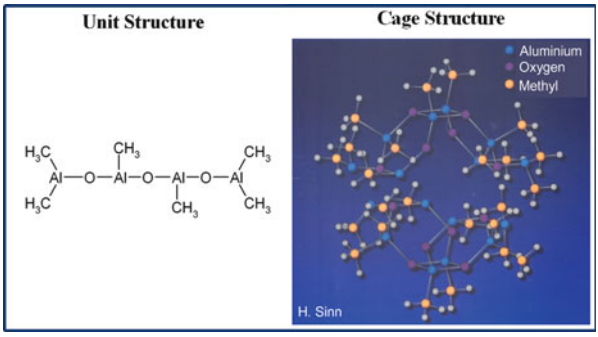

Fig. 4 MAO cage formed by four linear unit structures

The lower phase has, after washing with toluene, a composition of 1 diethyl ether molecule for 8 aluminum atoms, 12 methyl groups, and 6 oxygen atoms. If the lower phase is washed by diethyl ether the composition changes to 1 toluene molecule, 3–4 diethyl ether molecules for 16 aluminum atoms, 24 methyl groups, and 12 oxygen atoms. Cryoscopic measurements in tetrahydrofuran results in a molecular mass of 250–300. Therefore, MAO consists mainly of units of the basic structure $[Al_4O_3Me_6]$, a hexa-methyl-tetra-aluminoxane, which contains four aluminum, three oxygen atoms and six methyl groups. The ratio $CH_3/Al = 1.5$ for MAO was confirmed by the studies of Eilertsen, Rytter, and Ystenes [39].

As the aluminum atoms in the unit structures of MAO are coordinatively unsaturated, the units join together to form clusters and cages. These have molecular weights from 1,200 to 1,600 (as measured by cryoscopy in benzene) and are soluble in hydrocarbons, especially in aromatic solvents. A probably association of two and a cage structure of four $[Al_4O_3Me_6]$ units are shown in Figs. 3 and 4.

The association is destroyed when the complexes are treated with diethyl ether. In the case of MAO, an ideal cluster structure of $[Al_4O_3Me_6]_4$ could not be isolated although such a cluster with *tertiary*-butyl groups instead of methyl groups was isolated and characterized by Barron [40, 41]. It was also possible to synthesize similar aluminoxane with ethyl groups. This ethylaluminoxane has a molecular

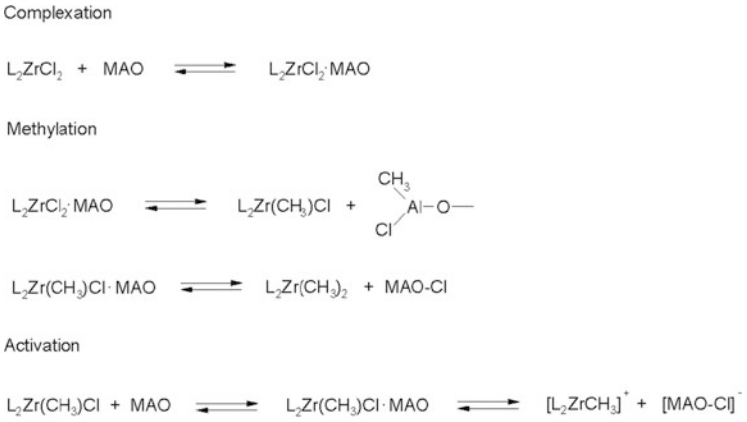

Fig. 5 Reaction scheme of the alkylation, complexation and ion pair formation of zirconocene dichloride and MAO. *L* cyclopentadienyl, indenyl, or fluorenyl

weight of 1,000 but has only a very poor polymerization activity compared with MAO [42].

The use of separately produced MAO together with $Cp_2Ti(CH_3)_2$ further increased the activity by a factor of 100 compared to the system of $Cp_2Ti(CH_3)_2$/$Al(CH_3)_3$/H_2O [31]. For the first time it was possible to polymerize propene with a soluble biscyclopentadienyl-titanium/MAO catalyst to obtain atactic polypropylene and to generate ethene/propene copolymers. We used bis(cyclopentadienyl)zirconium dimethyl and MAO for polymerization of ethene and propene and obtained extremely high activities, higher than for the titanium system. To date, biscyclopentadienyl–zirconium complexes, activated by aluminum alkyls have been described as totally inactive for olefin polymerization. A patent application was written covering these exciting results [43], but the interest in industry was not very enthusiastic for this new catalyst system. It was also discovered that Cp_2ZrCl_2, which can be synthesized more easily and is more stable than $Cp_2Zr(CH_3)_2$, is also an active catalyst precursor in combination with MAO. The nature of the active site and the role of MAO are not totally clear. One function of MAO is the alkylation of the metallocene complex if a dichloride is used. The other function is the formation of an ion pair. Shilov and Dyachkovsky [44], Eisch [45], Jordan [46], and Bochmann [47] all showed that the activity of metallocene catalysts depends on the formation of cationic species. Today, most research groups agree with this statement. The bulky MAO cluster takes a chlorine atom or a methyl group from the metallocene together with an electron to form a cationic metallocene and an anionic MAO complex (Fig. 5). Important for the polymerization activity is the formation of bulky anions, which have a weak bonding to the metallocene cation. It is difficult to explain the function of MAO during the polymerization and why it is necessary to have such a high excess, i.e., Al(MAO)/Zr = 1,000 and more. One explanation for the high excess is the fact that MAO is also needed to destroy impurities.

Other explanations are side reactions such as deactivation of MAO with the -metallocene-like α-hydrogen transfer reactions or that only a part of MAO with a special structure is suitable for the activation. Knowing that the bulky structure of MAO could be necessary for the activation of metallocene catalysts, other bulky and weakly coordinating cocatalysts such as tris(pentafluorophenyl)borane or organic salts of the non-coordinating tetrakis(pentafluorophenyl)borate $[(C_6F_5)_4B]^-$, and aluminum fluorides were introduced by Marks [48, 49] and others [50–53]. With these cocatalysts, a metallocene/cocatalyst ratio of 1:1 is used, but only if a high excess of an aluminum alkyl as scavenger is present. Details of the polymerization using other cocatalysts are described by Shiono [54].

Meanwhile, the polyolefin industries used MAO-containing catalysts on a large scale. Companies such as Albermale, Akzo, Chemtura, and Mitsui produce hundreds of tonnes of MAO by reaction of water or ice with TMA and in some cases add other aluminum alkyls to increase the solubility.

3 New Polyolefins

3.1 Homopolymers

Metallocenes, especially zirconocenes but also titanocenes, hafnocenes, and other transition metal complexes treated with MAO are highly active for the polymerization of olefins, diolefins, and styrene. The polymerization activity, which is up to 100 times higher than for classical Ziegler catalysts, as well as the possibility to easily tailor the microstructure of the polymer chain and to obtain polymers with special properties have motivated research groups worldwide to produce thousands of patents and publications in the last 20 years. An overview can be found in selected review articles and books [55–68]. A metallocene/MAO catalyst containing 1 g zirconium produced 40×10^6 g polyethylene in 1 h at 95°C and 8 bar ethene pressure (Table 1).

Nearly every zirconium atom forms an active center as shown by Tait [69] and Chien [70] and produces about 46,000 polymer chains per hour. The insertion time of one ethene unit is only 3×10^{-5} s. For the first time, it could be shown that a soluble catalyst such as Cp_2ZrCl_2/MAO is able to produce polyethylene with high molecular weights and a narrow molecular weight distribution of approximately two. All active sites are similar and form polymers with the same average chain length (single-site catalysts). Only traces of low molecular weight oligomers are formed.

Zirconocenes with different symmetries and substitutions are shown in Fig. 6. There are a great variety of structures of metallocenes that can be used for the polymerization. The cyclopentadienyl, indenyl, and fluorenyl ligands can be hydrated or substituted by alkyl, aryl, methoxy, siloxy, or other groups. Ethanediyl (C_2H_4), dimethylsilandiyl [$(CH_3)_2Si$], or isopropandiyl [$(CH_3)_2C$] are mainly used as interannular bridges between the rings. Central metals could be Ti, Zr, or

Table 1 Polymerization activity of Cp_2ZrCl_2/MAO at 95°C and 8 bar ethene pressure [134]

Activity	39.8×10^6 $g_{PE}/(g_{Zr}\ h)$
Zirconocene concentration	6.2×10^{-8} mol/L
MAO concentration (molecular weight 1,200 g/mol)	7.1×10^{-4} mol/L
Molecular weight polyethylene	78,000 g/mol
Polymerization degree	28,000
Time for formation of one polyethylene chain	0.087 s
Turnover time (insertion) of ethylene	3.1×10^{-5} s

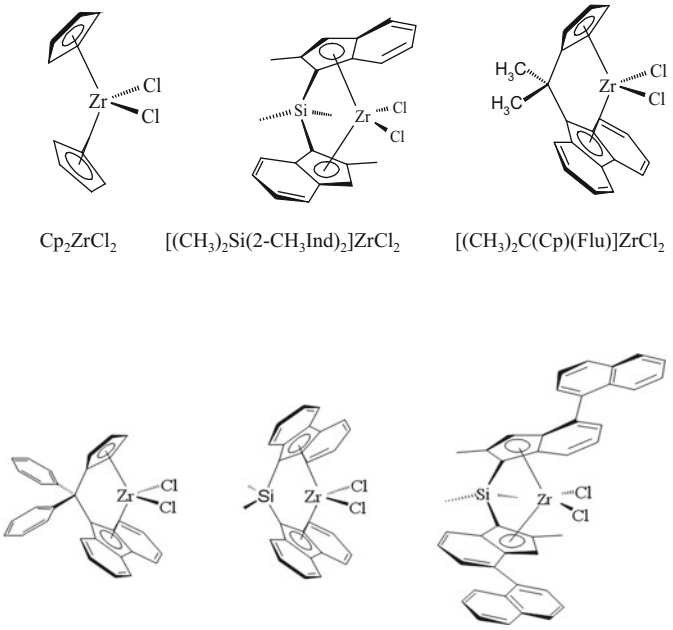

Fig. 6 Zirconocenes with different symmetries suitable for the polymerization of olefins

Hf. Such and similar metallocenes are used for the polymerization of ethene, propene, and other olefins. Table 2 compares the polymerization of ethene by selected metallocene/MAO catalysts [71, 72].

Generally, zirconium catalysts are more active than hafnium or titanium systems. Trimethyl-substituted bisindenyl systems show very high activities, exceeding those of sterically less-hindered Cp_2ZrCl_2. The activities are much lower for bridged cyclopentadienyl–indenyl or fluorenyl zirconocenes. If pentamethylcyclo pentadienyl–zirconium dichloride ($Cp^*_2ZrCl_2$/MAO) is used instead of Cp_2ZrCl_2/MAO, polyethylene with much higher molecular weight is formed, but at lower activity. This means that chain transfer reactions are much slower in this substituted zirconocene complex. The metallocene/MAO catalysts have a long-lasting activity; even after

Table 2 Comparison of ethene polymerization[a] with different metallocene/MAO catalysts at the same polymerization conditions

Metallocene[b]	Activity[c]	Molecular weight (g/mol)
Cp_2TiCl_2	34,200	400,000
Cp_2ZrCl_2	60,900	620,000
Cp_2HfCl_2	4,200	700,000
Cp_2TiMe_2	1,200	500,000
Cp_2ZrMe_2	14,000	730,000
$Cp^*_2ZrCl_2$	1,300	1,500,000
$(NmCp)_2ZrCl_2$	12,200	1,000,000
$[O(SiMeCp)_2]ZrCl_2$	57,800	930,000
$[En(IndH_4)_2]ZrCl_2$	22,200	1,000,000
$[En(Ind)_2]ZrCl_2$	12,000	350,000
$[En(Ind)_2]HfCl_2$	2,900	480,000
$[En(2,4,7\text{-}Me_3Ind)_2]ZrCl_2$	78,000	190,000
$[Me_2Si(Ind)_2]ZrCl_2$	36,900	260,000
$[Ph_2Si(Ind)_2]ZrCl_2$	20,200	320,000
$[Bz_2Si(Ind)_2]ZrCl_2$	12,000	350,000
$[Me_2Si(IndH_4)_2]ZrCl_2$	30,200	900,000
$[Me_2Si(2,4,7\text{-}Me_3Ind)_2]ZrCl_2$	111,900	250,000
$[Me_2Si(2Me\text{-}4Ph\text{-}Ind)_2]ZrCl_2$	16,600	730,000
$[Me_2C(Ind)(Cp)]ZrCl_2$	15,500	25,000
$[Ph_2C(Ind)(Cp)]ZrCl_2$	3,300	18,000
$[Me_2C(Ind)(3MeCp)]ZrCl_2$	2,700	30,000
$[Me_2C(Flu)(Cp)]ZrCl_2$	2,000	500,000
$[Ph_2C(Flu)(Cp)]ZrCl_2$	2,800	630,000
$[Me_2C(Flu)(Cp)]HfCl_2$	890	560,000

[a]Polymerization conditions: ethene pressure 2.5 bar, temperature 30°C, [metallocene] 6.25×10^{-6} mol, metallocene/MAO ratio 250, solvent toluene

[b]*Cp* cyclopentadienyl, *Me* methyl, *Ind* indenyl, $IndH_4$ tetrahydroindenyl, *En* C_2H_4, *Flu* fluorenyl, *NmCp* neomenthyl cyclopentadienyl, *Bz* benzyl

[c]Activity is expressed as $kg_{PE}/(mol_{metallocene}$ h [ethene])

more than 100 h of polymerization time they are still active. Bridged bis(fluorenyl) zirconocenes are also reported to be very active [73]. Polyethylenes synthesized by metallocene/MAO catalysts have a molecular weight distribution (M_w/M_n) of 2 and show 0.9–1.2 methyl side groups, 1.1–1.8 vinyl and 0.2 *trans*-vinyl groups per 1,000 C atoms in the backbone polymer chain. The molecular weight of metallocene polyethylenes varies in a wide range between 18,000 and 1.5 million and can be easily lowered by increasing the temperature, raising the metallocene/ethene ratio, or by adding small amounts of hydrogen (0.1–2 mol%) [74]. The molecular weight distribution can be decreased down to 1.1 by living polymerization using bis(phenoxy-imine)titanium complexes (FI-catalysts) or other half-sandwich complexes [75–78].

For an industrial use, it can be necessary to support the MAO cocatalyst on silica or alumina. Silica with up to 30 wt% of MAO is obtained. In such a case, a

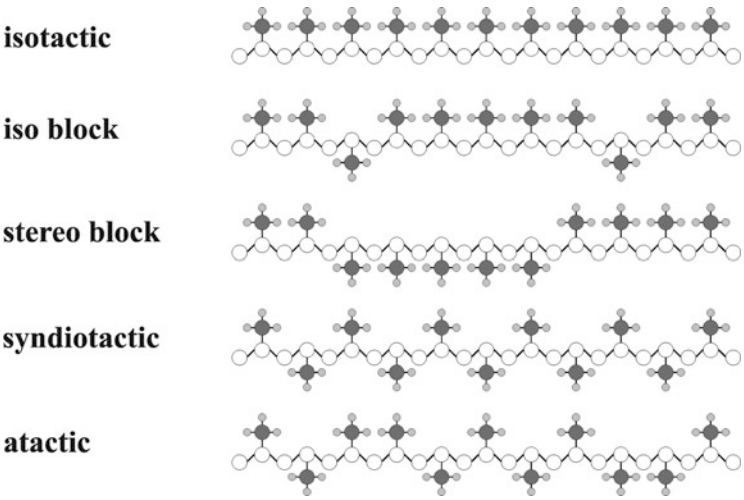

Fig. 7 Microstructures of polypropylenes obtained by various metallocene catalysts (hydrogen atoms of the backbone chain are not shown)

heterogeneous catalyst is formed by adding the metallocene and then the same technical process as for heterogeneous Ziegler–Natta catalysts can be used (drop-in technology) [79]. By this procedure, a better particle morphology control is possible and there is less reactor walling. Another advantage is that the ratio MAO/metallocene can be decreased to a ratio Al(MAO)/Zr = 100. On the other hand, the activity decreases to about half that of the homogeneous system.

By using metallocene/MAO catalysts it is possible to produce polypropylenes with different kinds of microstructures and of a purity that cannot be obtained by Ziegler–Natta catalysts (Fig. 7). Pino and Mülhaupt [80] analyzed a sample and found that the polypropylene synthesized by a symmetric Cp_2ZrCl_2/MAO catalyst was the purest atactic polypropylene they had ever seen. The metal atom in titanocene and zirconocene complexes is linked to two rings of five carbon atoms and to two other groups (methyl, chlorine). The angles between the rings and their substitution pattern play a key role in the activity and stereospecificity. Using different ligand substituents, it was now possible to obtain isotactic, isoblock, stereoblock, syndiotactic, and atactic polypropylenes in high purity.

Brintzinger [81] was the first to isolate chiral *ansa* titanocenes. *Ansa* metallocenes such as $[En(Ind)_2]ZrCl_2$ or $[Me_2Si(Ind)_2]ZrCl_2$ form three different molecular structures (Fig. 8). It was shown in 1984 for the first time that the racemic mixture of the *R* and *S* forms of $[En(IndH_4)_2]ZrCl_2$ produces highly isotactic polypropylene (iPP) in combination with MAO in toluene solution [82]. By synthesis of the *ansa* bisindenyl-zirconocene, mainly the racemic mixture is obtained.

Ewen [83] reported some months before the use of a mixture of the racemic and *meso* forms (56:44%) of the analog $[En(Ind)_2]TiCl_2$ and obtained a mixture of isotactic and atactic polypropylene. The non-chiral *meso* form of $[En(Ind)_2]TiCl_2$

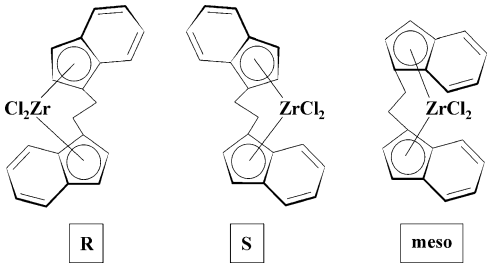

Fig. 8 *R*, *S*, and *meso* forms of ethanediyl-bridged bis (indenyl)zirconium dichloride

gives atactic polypropylene by a much slower polymerization rate. Stereo-errors in the polypropylene chain produced especially by $[En(Ind)_2]HfCl_2$/MAO are randomly distributed along the polymer chain, whereas in polypropylene made with Ziegler–Natta catalysts the errors are concentrated at chain ends and in oligomers.

Researchers of the Hoechst company later optimized the structure of *ansa* zirconocene complexes by using different bridges and substituents at the indenyl rings, such as $[Me_2Si(2Me\text{-}4PhInd)_2]ZrCl_2$ or $[(CH_3)_2Si(2\text{-}CH_3\text{-}4\text{-}Naph\text{-}Ind)_2]$ $ZrCl_2$ (structure shown in Fig. 6) [84]. They were able to obtain iPP with an activity of 15,000 kg_{PP}/mol_{Zr} h, a molecular weight of 650,000 g/mol, an isotacticity of 99%, and a melting point of 160°C. At a polymerization temperature of 70°C in liquid propene, the activity can reach 875,000 kg_{PP}/mol_{Zr} h.

In 1987, Ewen, Jones, and Razavi [85] obtained pure syndiotactic polypropylene using a C_s-symmetric $[Me_2C(Flu)(Cp)]ZrCl_2$ complex with a bridged cyclopentadienyl and a fluorenyl ring. This metallocene offers two different bonding positions for the inserted propylene and forms an alternating polypropylene structure. Higher activities are obtained if a $[Ph_2C(Cp)(Flu)]ZrCl_2$/MAO catalyst is used with phenyl groups in the bridge (see Fig. 6 and Table 3).

Table 3 compares the activities of the propene polymerization by different metallocene/MAO catalysts, the molecular weights, the isotacticities calculated from the ^{13}C NMR-measured mesopentades (mmmm), the microstructures, and the melting points of the obtained polypropylenes. The activities vary between 130 and 15,000 kg_{PP}/mol_{Zr} h at 30°C and the molecular weights between 2,000 and 750,000 g/mol. Bridged bisindenyl zirconocenes are more active than hafnocenes. The highest isotacticity of 99% was obtained using $[En(2,4,7\text{-}Me_3Ind)_2]ZrCl_2$ as catalyst component. Unsubstituted bisindenyl-zirconocenes such as $[En(Ind)_2]ZrCl_2$ or $[Me_2Si(Ind)_2]ZrCl_2$ produce polypropylenes with melting points below 160°C because there are stereo-errors along the polymer chain. One propene unit is inserted in a wrong position and the others have the same stereo-position. This metallocene iso-block polypropylene (see Fig. 6) is characterized by a higher film transparency because the crystal size is in the nanoscale.

We discovered that unbridged biscyclopentadienyl zirconocenes with bulky substitutions such as neomentyl produce syndioblock polypropylenes with elastic properties [86]. Such a bulky ligand could stabilize an asymmetric (chiral) active site for a short time. During this time, some propene units could be inserted with the same stereospecificity, forming an isotactic block, followed by a change in

Table 3 Comparison of propene polymerization[a] with different metallocene/MAO catalysts at the same polymerization conditions

Metallocene[b]	Activity[c]	Molecular weight (g/mol)	Isotactacticity mmmm (%)	Microstructure[d]	Melting point (°C)
Cp_2ZrCl_2	140	2,000	7	a	–
$(NmCp)_2ZrCl_2$	170	3,000	23	sb	118
$[En(Ind)_2]ZrCl_2$	1,690	32,000	91	i	136
$[En(Ind)_2]HfCl_2$	610	446,000	85	ib	126
$[En(2,4,7Me_3Ind)_2]ZrCl_2$	750	418,000	>99	i	162
$[Me_2Si(Ind)_2]ZrCl_2$	1,940	79,000	96	i	148
$[Ph_2Si(Ind)_2]ZrCl_2$	2,160	90,000	96	i	136
$[Me_2Si(2,4,7Me_3Ind)_2]ZrCl_2$	3,800	192,000	95	i	155
$[Me_2Si(2Me\text{-}4PhInd)_2]ZrCl_2$	15,000	650,000	99	i	160
$[Me_2Si(2Me\text{-}4,5BenzInd)_2]ZrCl_2$	6,100	380,000	98	i	157
$[Me_2C(Ind)(Cp)]ZrCl_2$	180	3,000	19	sb	–
$[Ph_2C(Fluo)(Cp)]ZrCl_2$	1,980	729,000	0.4	s	141
$[Me_2C(Fluo)(Cp)]ZrCl_2$	1,550	159,000	0.6	s	138
$[Me_2C(Fluo)(Cp)]HfCl_2$	130	750,000	0.7	s	138
$[Me_2C(Fluo)(3\text{-}t\text{BuCp})]ZrCl_2$	1,045	52,000	89	ib	130

[a]Polymerization conditions: propene pressure 2 bar, temperature 30°C, [metallocene] 6.25×10^{-6} mol, metallocene/MAO ratio 250, solvent 200 mL toluene
[b]*Cp* cyclopentadienyl, *Nm* neomenthyl, *Ind* indenyl, *En* C_2H_4, *BenzInd* benzoindenyl, *Flu*fluorenyl
[c]Activity is expressed as $kg_{PP}/(mol_{Zr/Hf}$ h [propene])
[d]*a* atactic, *i* isotactic, *s* syndiotactic, *sb* stereoblock, *ib* isoblock

conformation. Non-chiral *ansa* metallocenes such as $[(CH_3)_2Si(Flu)_2]ZrCl_2$ (see Fig. 6) produce again atactic polypropylene. Detailed information on propene polymerization by *ansa* metallocene catalysts can be found in the chapters by Brintzinger and Fischer [87] and Razavi [88].

Surprisingly, it was also possible to homopolymerize cyclic olefins such as cyclobutene, cyclopentene, and norbornene by metallocene/MAO catalysts to partially crystalline materials and to copolymerize them with ethene [89]. We observed only double bond opening by the homo- and copolymerization of cyclic olefins, in contrast to Ziegler–Natta catalysts where ring and double bond opening occur simultaneously. Poly(cyclopentene), synthesized by isotactically working metallocene catalysts are crystalline, have a low solubility, and a melting temperature of about 395°C. The unusual formation of 100% of 1,3-enchainments for poly(cyclopentene) was shown by Collins [90]. The melting point of crystalline polynorbornene obtained by metallocene/MAO catalysts is higher than the decomposition temperature of about 400°C. It is therefore difficult to process such a polymer [91].

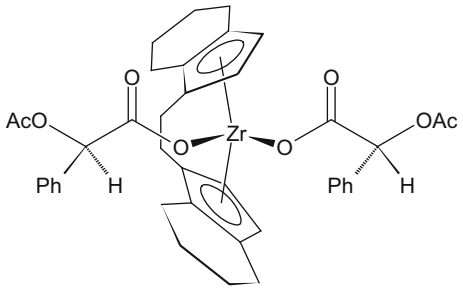

Fig. 9 *R*-Ethanediyl-bridged bis(indenyl)zirconium bis-mandelate

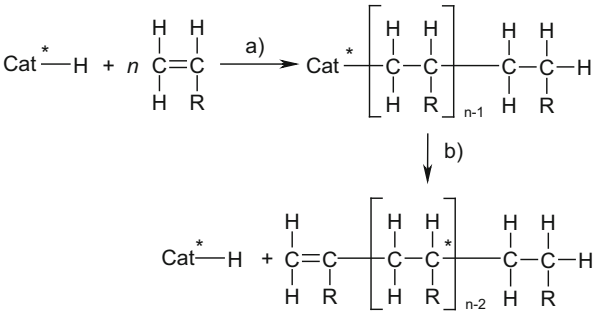

Fig. 10 Mechanism of the isotactic polymerization of propene using an alkylzirconocenium ion generated from a C_2-symmetric bis(indenyl) zirconocene: (**a**) polymerization reaction, (**b**) termination reaction. *Asterisks* indicate chiral catalyst or chiral carbon atom

A separation of the racemic mixture of chiral zirconocene compounds into the optically active pure enantiomers is performed using *O*-acetyl-(*R*)-mandelic acid as chiral auxillary [92] (Fig. 9). Only the *S-ansa* zirconocene forms a complex, while the *R*-form does not react with the *R*-mandelate. The complex can be separated by crystallization from the unreacted form and is obtained in a purity of 99%. The mandelate complex shows a similar catalytic activity to that of the corresponding dichloride [93].

The polymerization starts when an olefin undergoes insertion into the Zr–C bond formed by methylation with MAO (Fig. 10).

Chain growth termination takes place by β-hydrogen transfer to the transition metal center or a metal-bound olefin, resulting in formation of a zirconocene hybrid or alkyl and an olefin-terminated polymer or oligomer chain. The trimeric propene is the first to have one chiral carbon. Although the polymer shows no optical activity, trimers and higher oligomers prepared by optically active metallocene catalysts are optically active.

The conditions used to obtain oligomers were extreme since the catalyst normally produces high molecular weight polymer chains. High *S*-zirconocene and very low propene concentration, fed continually, were chosen for this oligomerization at different reaction temperatures. The yield of trimers was up to 14%. They were separated by distillation from the other oligomers. But, the trimers were also a mixture of different isomers. The composition varied with the oligomerization temperature and the propene feed. At a propene feed of 10 mL/min, more than 80% of the trimeric fraction consists of 2,4-dimethyl-1-heptene with one chiral

carbon in the molecule (see Fig. 10). Other trimeric isomers were formed by double bond migration, 2,1-, and 1,3-insertion and were evidence for the mechanism of chain termination in the olefin polymerization by metallocene catalysts. It was possible to obtain the propene trimer 2,4-dimethyl-1-heptene with 95.3 enantiomeric excess at 20°C oligomerization temperature [94]. The tetrameric oligopropylene, under the same preparation conditions, shows a higher optical rotation than the trimer because the molecule consists of two chiral carbon atoms.

These measurements were direct proof that a chiral (pure enantiomer) soluble zirconocene/MAO catalyst inserts the propene units in the same stereospecific manner and produces optically active oligomers and, by a continued insertion, isotactic polymers. Such polymer chains contain a vinyl group at the end formed by the main termination reaction, and all methyl groups are found at the top or the bottom. Using a racemic mixture of the zirconocene, 50% of the polymer chains show the methyl groups at the top and the other 50% at the bottom.

3.2 Copolymers

Because metallocene/MAO catalysts were found to be highly active polymerization catalysts not only for ethene and propene but also for longer chained 1-olefins, they are suitable for different copolymerizations. Copolymers with new microstructures can be obtained, such as:

Ethene–propene (EP) [25]
Ethene–propene, diene (EPDM) [95]
Ethene–1-butene, hexene (LLDPE) [96]
Ethene–1-octene (LLDPE) [97]
Ethene–1,5-hexadiene elastomer [95]
Ethene–cyclopentene (COC) [98]
Ethene–norbornene (COC) [91, 98]
Ethene–1,3-butadiene (elastomer) [95]
Ethene–styrene (elastomer) [99, 100]

EP, EPDM (ethene propene diene monomers), and LLDPE (linear low-density polyethylene) are of high interest for the polymer industry. All copolymers produced by metallocene catalysts are characterized by a narrow molecular weight distribution of 2 and a uniform microstructure. Although the comonomers are distributed randomly in the polymer chain, only low amounts are needed to decrease the density and the melting point of ethene copolymers. The low amount of oligomers compared to copolymers produced by Ziegler–Natta catalysts is responsible for a high tensile strength and other mechanical properties of the obtained LLDPE. Mechanical properties can be increased if there are some long chain branches in the polymer chain. In particular, half-sandwich complexes (constrained geometry catalysts) are able to incorporate higher 1-olefins into the growing chain (Fig. 11) [78]. These complexes are activated by MAO or fluorinated phenylborates.

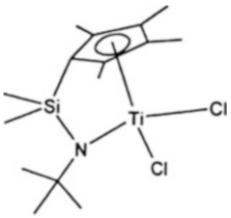

Fig. 11 Pentamethyl cyclopentadienyl titanium amido complex

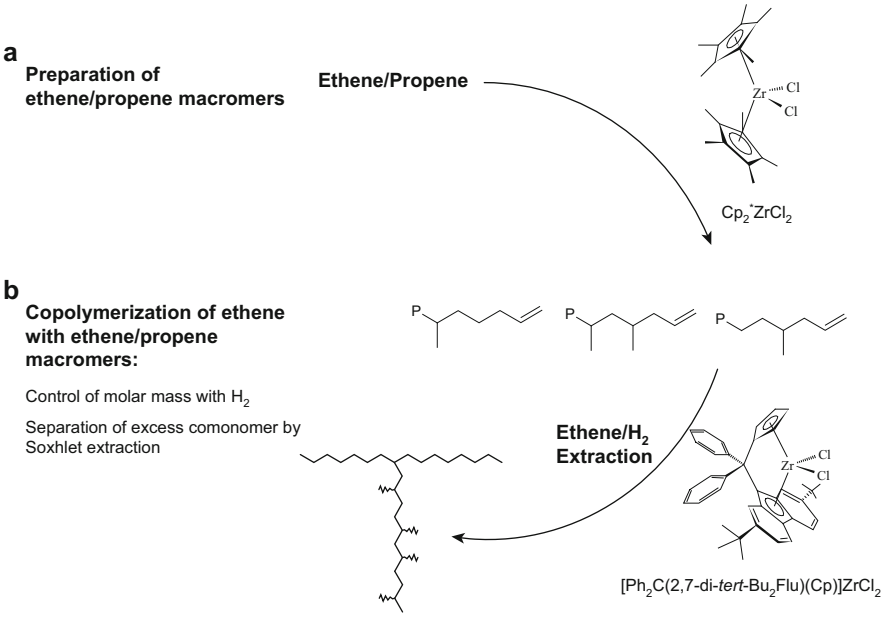

Fig. 12 Reaction scheme for ethene-graft ethene/propene copolymers by two different zirconocene/MAO catalysts in two steps

Long-chain branched polyethylenes can be also obtained by copolymerization of ethene with ethene oligomers by tandem polymerization in one step [100] or with ethene/propene oligomers in two steps [101]. In the latter case, polymers are obtained with crystalline polyethylene backbone chains and amorphic ethene/propene copolymer side chains [102].

Figure 12 shows a scheme for the preparation of long-chain branched polyethylene by using two different metallocene catalysts in two steps [101]. In a first step, ethene/propene macromers with molecular weights of 8,000–25,000 g/mol were produced by a $[C_5(CH_3)_5]_2ZrCl_2$/MAO catalyst (Step A). The propene content varied from 13 to 23 wt%. The macromers are amorphic, soluble in toluene, and show a high content of vinyl end groups. In the subsequent copolymerization of the ethene/propene macromers with ethene, a different metallocene $[Ph_2C(2,7\text{-di-}t\text{Bu}_2\text{Flu})(Cp)]ZrCl_2$

Table 4 Copolymerization[a] of norbornene and ethene by different metallocene/MAO-catalysts

Metallocene[b]	Time (min)	Activity (kg/mol h)	Norbornene incorporation (wt%)
Cp_2ZrCl_2	30	1,200	21.4
$[En(Ind)_2]ZrCl_2$	10	9,120	26.1
$[Me_2Si(Ind)_2]ZrCl_2$	15	2,320	28.4
$[En(IndH_4)_2]ZrCl_2$	40	480	28.1
$[Me_2C(Flu)(Cp)]ZrCl_2$	10	7,200	28.9
$[Ph_2C(Flu)(Cp)]ZrCl_2$	10	6,000	27.3
$[Ph_2C(Ind)(Cp)]ZrCl_2$	15	2,950	33.3

[a]Polymerization conditions: ethene pressure 2 bar, [norbornene] 0.05 mol/L, temperature 30°C, [metallocene] 5×10^{-6} mol/L, metallocene/MAO ratio 200, solvent toluene
[b]*Cp* cyclopentadienyl, Me methyl, *Ind* indenyl, *En* C_2H_4, *Flu* fluorenyl, *Ph* phenyl

was used to catalyze the copolymerization (Step B). Small amounts of hydrogen were added to reduce the molecular weight for easier rheological measurements.

The incorporation of the macromer was investigated and calculated by ^{13}C NMR measurements. The maximum incorporation rate was 0.52 mol%. This means that about 59.7 wt% of the polymer is composed of macromer units and, on average, every 400th carbon atom of the backbone chain is branched. The melting point of the long-chain branched polyethylene decreases from 136 to 121°C, and the zero shear-rate viscosity increases from 142 to 280 Pa s. Such long-chain branched copolymer can be produced much more easily by metallocene/MAO catalysts than by Ziegler–Natta catalysts.

By the copolymerization of cyclic olefins such as cyclopentene or norbornene with ethene and other α-olefins, it is possible to obtain cycloolefin copolymers (COC) representing a new class of thermoplastic, amorphous materials [89, 103].

Cyclopentene, norbornene, or other cyclic olefins are incorporated exclusively by 1,2-insertion into the growing copolymer chain; no ring opening occurs. The insertion of the huge norbornene monomer is very fast by metallocene/MAO catalysts.

Table 4 compares the activities and incorporation of norbornene by different catalysts. Under special conditions, the polymerization rate of a 1:1 molar mixture of ethene and norbornene is higher than the homopolymerization of ethene (comonomer effect) [24].

The $[Ph_2C(Ind)(Cp)]ZrCl_2$/MAO catalyst shows not only high activities for the copolymerization of ethene with norbornene, but also gives an alternating structure.

Most metallocenes produce copolymers with a statistical structure, and a few produce polymers with an alternating structure. Statistical copolymers are amorphous if more than 10–15 mol% of cycloolefins are incorporated into the polymer chain. The glass transition temperature can be varied over a wide range by selection of norbornene as cycloolefin and variation of the amount of norbornene incorporated into the polymer chain [104].

Cycloolefin copolymers are characterized by excellent transparency, high glass transition temperatures of up to 200°C, and excellent long-life service temperatures.

They are resistant to polar solvents and chemicals and can be melt-processed. Due to their high carbon/hydrogen ratio, these polymers have a high refractive index (1.53 for an ethene/norbornene copolymer at 50 mol% incorporation). Their stability against hydrolysis and chemical degradation, in combination with their stiffness, makes them interesting materials for optical applications, for example in compact discs, lenses, optical fibers, or films [105]. Meanwhile, ethene/norbornene COC material is commercially available under the name of TOPAS (Ticona, Celanese). Details of the polymerization of cyclic olefins with single-site catalysts can be found in the contribution by Boggioni and Tritto [106].

3.3 Polyolefin Nanocomposites

In the last few years, a lot of research in academic and industrial laboratories has focused on polyolefin nanocomposites because of their high potential as materials with novel properties [96]. The properties of the nanocomposites are not only influenced by the kind of filler but also by the microstructure of the polyolefins and the preparation process. Nanofillers commonly used are metal oxides, sulfides, silica and layered silica as well as fibers such as carbon nanotubes (CNT), carbon nanofibers (CNF), and polymer fibers [107–111].

In the past, most composites have been prepared by mechanical blending of the particles or fibers above the melting temperature of the desired matrix. Melt compounding of polyolefins with nanoparticles often leads to an insufficient filler dispersion, especially at a high filler content, which leads to aggregation and intercalation, which in turn causes a deterioration of the mechanical properties. Such disadvantages can be solved by in-situ polymerization, whereby the cocatalyst (e.g. MAO) can be adsorbed or anchored on the surface of nanofillers such as particles, fibers, CNF, or multi-walled carbon nanotubes (MWCNT), thus changing the surface to a hydrophobic one [112, 113]. The MAO reacts, for example, with the OH groups of silica or with the carboxy groups of oxidized CNTs or is physically absorbed at the surface (Fig. 13). The chemical reaction of MAO with polar groups results in the formation of methane. Excess MAO is washed out.

In a second step, the metallocene is added and forms catalytically active polymerization sites on the nanosurface. The thickness of the polymer films, formed by addition of ethene or propene, depends on the polymerization conditions, especially the polymerization time, the kind of metallocene catalyst, and the pressure of the monomer. The in-situ polymerization leads to composite materials in which the particles or fibers are intensively covered with the polymer.

Metallocene/ MAO and other single-site catalysts are soluble in hydrocarbons and therefore can be perfectly absorbed on the surface of particles and fibers or they can penetrate the layers of layered silicates and oxides. For a detailed description of polyolefin nanoparticles and layered silicate nanocomposites see [114–116].

The composite materials show, for example, an improved stiffness with a negligible loss of impact strength, high gas barrier properties, significant flame retardant properties, better clarity and gloss, as well as high crystallization rates.

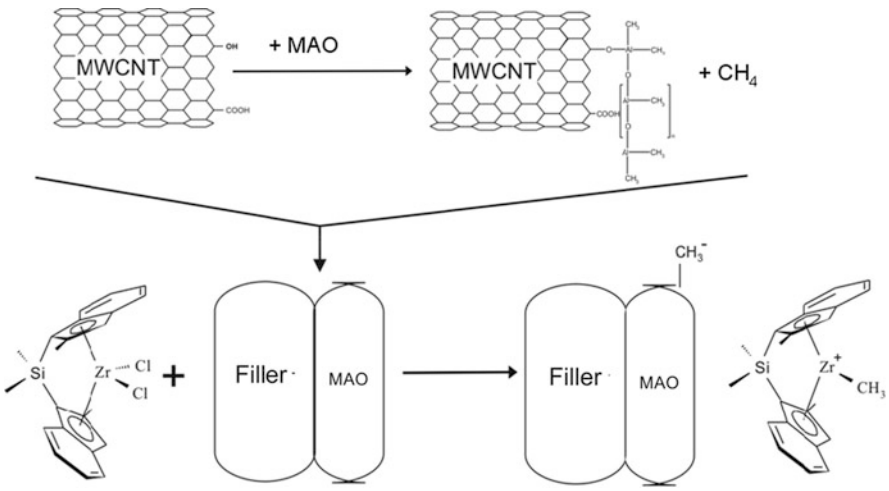

Fig. 13 Formation of polymerization active sites by absorption of MAO on oxidized multiwall carbon nanotubes (MWCNT) followed by addition of a zirconocene

Even low nanoparticle contents are sufficient to obtain new or modified material characteristics, especially a faster crystallization rate and a higher crystallization temperature.

To increase the stiffness of polypropylene, we investigated the in-situ polymerization of propene and silica balls (monopheres) with a diameter of 250 nm. The zirconocene [(pMePh)$_2$C(Cp)(2,7-bis-*t*BuFlu)]ZrCl$_2$ was used. The polymerizations were carried out in toluene as solvent and TIBA as scavenger. To determine whether MAO-impregnated silica balls are suitable for storage, 2.55 g silica balls were impregnated with 11 mL of MAO solution (10% MAO). Polymerizations of propene were carried out at 30°C directly after preparation, 2 weeks later, and 11 weeks later. As can be seen from Table 5, the activities decreased only slightly, even after 11 weeks, to 81% of the original activity. This shows that nanofiller/MAO precursors can be stored for a long period.

CNFs or MWCNTs are an especially attractive class of fillers for polymers because of their intriguing mechanical and thermal properties [117]. CNFs were dispersed in toluene solution, then MAO, an isotactic working zirconocene, and propene were added and the suspension stirred for approximately 30 min. As expected for in-situ polymerization, the polymer grew directly on the fiber surface and covered it with a thin polypropylene layer. The dried polypropylene nanocomposites were obtained in powder form. The morphology of the iPP/CNF nanocomposites was investigated using transmission electron microscopy (TEM). Figure 14 shows a TEM micrograph of iPP/CNT nanocomposite material synthesized by in-situ polymerization. It can be seen that there is no agglomeration of the nanofibers. The CNFs with a diameter of 100 nm are covered by a coat of about 50 nm iPP. Separated polymerization active sites at the surface of fibers form

Table 5 Stability of MAO-impregnated nanosilica balls in syndiotactic propene polymerization[a]

Weeks after preparation	Activity[b]	Filler content (%)
0	3,700	11
2	3,300	9
11	3,000	10

[a]Polymerization conditions: temperature 30°C, time 30 min, propene pressure 2 bar, solvent 200 mL toluene, silica/MAO 0.55 g, [zirconocene] 1.3×10^{-6} mol/L, TIBA 2 mmol
[b]Activity is expressed as $kg_{PP}/(mol_{Zr}$ h [propene])

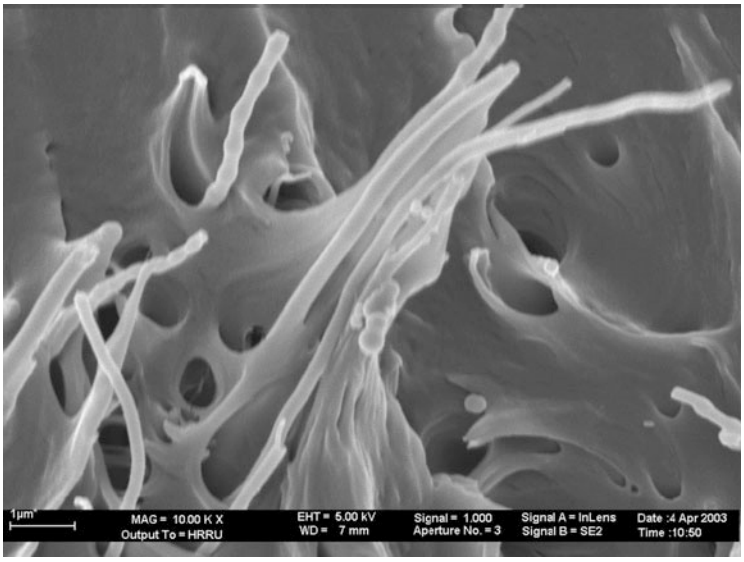

Fig. 14 TEM micrograph of an iPP/CNT composite material containing 14 wt% of carbon nanotubes. The nanotubes are covered by a coating of about 50 nm iPP

string-of-pearl-like structures. The polypropylene material is fitted on the fiber, showing the excellent adhesion between polymer and fibers.

With longer polymerization times, the thickness of the polyolefin covering the fiber increased. The fiber/MAO/zirconocene system works like a supported catalyst. Filler contents between 0.5 and 50 wt% were possible.

In the case of MWCNTs, these were sonicated in a toluene suspension, treated with MAO, stirred for 24 h, filtered, and washed with hot toluene. After adding the chiral *ansa* zirconocene $[(CH_3)_2Si(2\text{-}CH_3\text{-}4\text{-Nap-Ind})_2]ZrCl_2$ and propene, isotactic high molecular weight polypropylene iPP/MWCNT composites with 0.9–50 wt% filler content were obtained. The molecular weights of the polypropylene matrix in the nanocomposites were in the range $M_w = 1{,}200{,}000$–$1{,}700{,}000$. The polymerization activity reached 5,000 kg_{PP}/mol_{Zr} h [propene]. It was independent of the filler content.

It can be seen from Fig. 15 that the nanotubes are coated by a thin film of iPP. The diameter of the MWCNT used (about 20 layers) is 20 nm and the thickness of

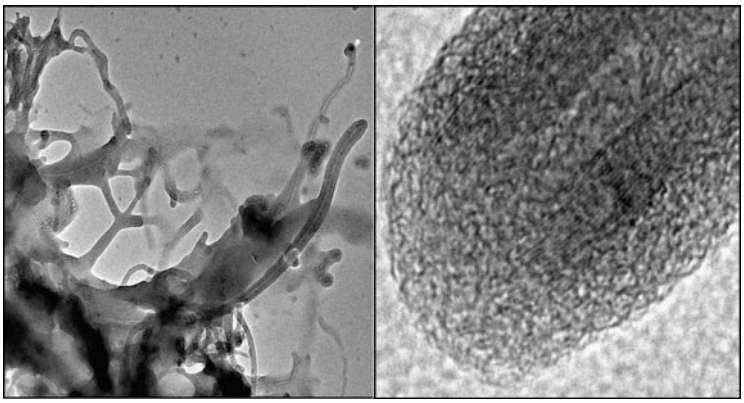

Fig. 15 TEM micrographs of a MWCNT composite prepared by in-situ polymerization: *left* nanotubes covered by iPP; *right* higher resolution image of the top of a nanotube/iPP composite

the iPP coat about 8 nm. Even the loose network of polymer-layered nanotubes on the lower left side, which are partially conglomerated by polypropylene but still mostly separated from each other, is permeated with polymer and seems to be widening by the growth of the polymer chains.

The morphology of nanocomposites prepared by in-situ polymerization is, in comparison to melt compounded composites, generally characterized by a good MWCNT separation, homogeneous distribution in the matrix, and a good adhesion of the polymer on the MWCNT surface [118].

The main advantage of polypropylene filled with CNF or MWCNT is the change in mechanical properties. High molecular weight iPP filled with MWCNT is an exceptionally strong composite material. The tensile strength of a composite film increases by 20% if only 1 wt% of MWCNT is incorporated, but also the form stability and the crystallization rate from a melt increase strongly and make this composite material suitable for new applications, such as in the automotive plastic industries. Figure 16 shows the dynamic mechanical analysis of iPP/MWCNT for measuring the form stability. The temperature is measured at which a deflection of an iPP/MWCNT sample caused by a force is not reversible.

The high molecular weight unfilled polypropylene prepared by the same catalyst has a form stability of 48.7°C (Table 6). A composite polypropylene with 0.9 wt% of MWCNT shows form stability up to 60.4°C, and a composite polypropylene with 2.3 wt% of MWCNT a form stability of up to 71.5°C. Other important parameters are the crystallization temperature and the half time of crystallization. The addition of only 0.9 wt% of MWCNT led to an increase in crystallization temperature from 118 to 123°C. The half time of crystallization was significantly reduced (faster crystallization rate) by low amounts of nanotubes. At 135°C it was 4.5 min for a composite with 0.9 wt% MWCNT and 2.4 min for a composite with 2.2 wt% MWCNT. The higher crystallization rate increases the economy of an industrial forming process.

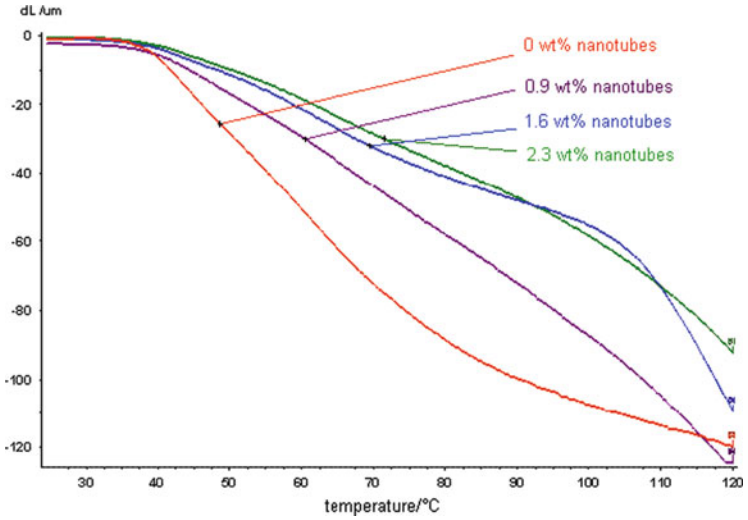

Fig. 16 Dynamic mechanical measurements of iPP/MWCNT composites measuring the form stability in dependence of the filler content and temperature

Table 6 Form stability of iPP/MWCNT samples with different amounts of MWCNT filler at a force of 1.8 MPa

MWCNT in iPP (wt%)	Temperature (°C)
0	48.7
0.9	60.4
1.6	69.5
2.3	71.5

4 Outlook

Mechanistic studies of metallocene/MAO catalysts have strongly increased the knowledge of olefin polymerization catalysis. This knowledge has made it possible to find new bulky and weakly coordinating cocatalysts such as perfluorophenylborate anions and boranes. The discovery of new transition metal complexes activated by MAO or other cocatalysts that show special polymerization properties is still ongoing. It is another task to decrease the amount of MAO needed for the activation. Supporting the MAO on silica, alumina, or on new organic polymers [119] is one step towards this.

Metallocene/MAO and other single-site catalysts allow the synthesis of tailored polyolefin structures in a way that was impossible in previous years. The known dependence of the kind of metallocene-based polymer on the catalyst structure allows the modeling of the reaction kinetics and the polymerization process [120]. Reactor models could be developed using mass and energy balances and they describe the polymer composition as well as the reactor operating conditions required for a given polymer architecture. It should be possible to design polyolefins with tailored molecular weight, comonomer content, long and short

chain branching [121, 122], and comonomer distribution. Control of morphology is possible by suspension, cascade, or multizone reactors that improve melt viscosity and processing.

Late transition metal complexes, which are more stable in water, can be used for emulsion polymerization [123–125]. Very small and stable polyethylene particles with diameters of 100 nm are obtained by microemulsion polymerization using nickel(II) complexes and diphenylphosphine benzene sulfonate as cocatalyst [126].

A lot can be done to tailor the microstructure of copolymers. Today it is only possible to create statistically ordered or alternating copolymers of polyolefins [127]. It is not possible to design polyolefins with a required sequence order of two or more monomers, which will be essential to establish self-organization of the polymer chain. To design three dimensional crystallizing polyolefins for materials with special properties, such as cages for catalysts or membranes, the controlled self-organization will be necessary. Easier synthesis of polyolefins with polar comonomers is important for this and for polymer blends of polyolefins with other polymers, such as polyamides or polyesters [128]. Polar monomers incorporated consist of hydroxyl, carboxyl, ether, ester, siloxy, or amino groups. Blends containing small amounts of such functional metallocene-based copolymers are tougher and stiffer than non-compatibilized polymers [120, 129–131].

There has been some initial success in forming block copolymers using single-site catalysts. These catalysts have to show no or only a slow chain transfer reaction, like living systems [132]. In a first step, only propylene is polymerized, forming a hard polypropylene block, then by addition of ethene a soft ethene/propene copolymer or a polyethylene block follows because ethene is inserted much faster.

Another method is described using a chain-shuttling agent to form block copolymers [133]. Two different single-site catalysts and monomers are used in one reactor. The cocatalyst is a fluorinated phenylborate. One catalyst is able to homopolymerize from a mixture of ethene and 1-octene only or mainly ethene, forming a hard polyethylene segment; the other catalyst copolymerizes ethene and 1-octene to a soft copolymer segment. By the addition of zinc diethyl as a chain transfer agent, the growing polymer chain shuttles between the two catalysts. A block copolymer results with soft and hard segments with elastomeric properties. In the future, it could also be possible to use MAO-activated catalysts for chain-shuttling.

Polyolefin nanocomposites open up the approach to new classes of materials with great property combinations. A soft polyolefin matrix can be combined with hard inorganic particles, or strong layers of silicates or graphene, or with fibers of extreme high tensile strength, such as carbon fibers, carbon nanotubes or polymer fibers. An easy way for the preparation of such polyolefin nanocomposites is in-situ polymerization using nanoparticles or fibers activated by metallocene/MAO or other single-site catalysts. Materials with high gas barrier resistance, high thermal and electric conductivity, and high form stability can be obtained as well as a good dispersion of the nanofiller in the polymer matrix.

The development and commercialization of metallocene/MAO and other single-site catalysts have just started and have already expanded the product range of

polyolefins. New, designed catalysts will enlarge the polyolefin industry and the applications of polymers.

References

1. Ziegler K, Holzkamp E, Breil H, Martin H (1955) Angew Chem 67:541
2. Breslow DS, Newburg NR (1957) J Am Chem Soc 79:5072
3. Natta G, Pino P, Mazzanti G, Longi P (1957) Gazz Chim Ital 87:549
4. Patat F, Sinn H (1958) Angew Chem 70:496
5. Shilov AE (1960) Dok Akad Nauk SSS 132:599
6. Henrici-Olivé G, Olivé S (1969) J Organomet Chem 16:339
7. Reichert KH, Schoetter E (1968) Z Phys Chem 57:74
8. Fink G, Rottler R (1981) Angew Makromol Chem 94:2
9. Waters JA, Mortimer GA (1972) J Polym Sci A1 10:895–907
10. Chien JCW (1959) J Am Chem Soc 81:86
11. Fink G, Schnell D (1982) Angew Makromol Chem 105:39
12. Sinn H, Patat F (1963) Angew Chem 75:805
13. Sinn H, Hinck H, Bandermann F, Grützmacher HF (1968) Angew Chem 80:190
14. Kaminsky W, Sinn H (1975) Justus Liebigs Ann Chem 1975:424
15. Kaminsky W, Vollmer HJ, Heins E, Sinn H (1974) Makromol Chem 175:443
16. Sinn H, Kolk E (1966) J Organomet Chem 6:373
17. Kaminsky W, Kopf J, Sinn H, Vollmer HJ (1976) Angew Chem Int Ed Engl 15:629
18. Sinn H (1974) Chem Ing Technol 46:579
19. Sinn H, Kaminsky W, Janning J (1976) Angew Chem 88:737
20. Heins E, Hinck H, Kaminsky W, Oppermann G, Raulinat P, Sinn H (1970) Makromol Chem 134:125
21. Mottweiler R (1975) Thesis. University of Hamburg, Hamburg
22. Andresen A, Cordes HG, Herwig J, Kaminsky W, Merck A, Mottweiler R, Pein J, Sinn H, Vollmer HJ (1976) Angew Chem Int Ed Engl 15:630
23. Sinn H, Kaminsky W (1980) Ziegler–Natta catalysis. Adv Organomet Chem 18:99
24. Kaminsky W (2004) J Polym Sci A Polym Chem 42:3911
25. Kaminsky W (2012) Macromolecules 45:3289
26. Reichert KH, Meyer KR (1973) Makromol Chem 169:163
27. Long WP, Breslow DS (1975) Justus Liebigs Ann Chem 1975:463
28. Lehmkuhl H, Ziegler K (1970) In: Houben J, Weyl T (eds) Methoden der organische Chemie (Houben-Weyl) vol XIII, part 4. Thieme, Stuttgart, p 76
29. Storr A, Jones K, Laubengayer AW (1968) J Am Chem Soc 90:3173
30. Bähr G (1946) Fiat review of German Science. Inorganic chemistry, Part II, p 161
31. Herwig J, Kaminsky W (1983) Polym Bull 9:464
32. Sinn H, Bliemeister J, Clausnitzer D, Tikwe L, Winter H, Zarncke O (1988) In: Kaminsky W, Sinn H (eds) Transition metals and organometallics as catalysts for olefin polymerization. Springer, Berlin, p 257
33. Bliemeister J, Hagendorf W, Harder A, Heitmann B, Schimmel I, Schmedt E, Schnuchel W, Sinn H, Tikwe L, vThienen N, Urlass K, Winter H, Zarncke O (1995) In: Fink G, Mülhaupt P, Brintzinger HH (eds) Ziegler catalysts. Springer, Berlin, p 57
34. Sinn H, Schimmel I, Ott M, vThienen N, Harder A, Hagendorf W, Heitmann B, Haupt E (1999) In: Kaminsky W (ed) Metalorganic catalysts for synthesis and polymerization. Springer, Berlin, p 105
35. Sinn H, Namyslo J (2012) Colloquium at Chemistry Department, University Hamburg, 30 May 2012
36. Smith GM, Palmaka SW, Rogers JS, Malpass DB, Monfiston DJ (1998) US Patent 5,831,109 to Akzo Nobel

37. Malpass DB, Palmaka SW, Smith GM, Rogers JS (1997) Int Patent Appl WO 9,723,288, A1 19,970,703 to Akzo Nobel
38. Sinn H (1995) Macromol Symp 97:27
39. Eilertsen JL, Rytter E, Ystenes (1999) In: Kaminsky W (ed) Metalorganic catalysts for synthesis and polymerization. Springer, Berlin, p 136
40. Mason MR, Smith JM, Bott SG, Barron R (1993) J Am Chem Soc 115:4971
41. Koide Y, Bott SG, Barron AR (1996) Organometallics 15:2213
42. Kaminsky W, Miri M, Sinn H, Woldt R (1983) Makromol Chem Rapid Commun 4:417
43. Sinn H, Kaminsky W, Vollmer HJ, Woldt R (1980) DE Patent 3,007,725
44. Dyachkovskii FS, Shilova AK, Shilov AE (1967) Polym Sci C 16:2333
45. Eisch JJ, Pombrick SI, Zheng GX (1993) Organometallics 12:3856
46. Jordon RF, Dasher WE, Echols SF (1968) J Am Chem Soc 108:1718
47. Bochmann M, Wilson LM (1986) J Chem Soc Chem Commun 1610
48. Yang X, Stern CL, Marks TJ (1991) Organometallics 10:840
49. Sishta C, Hathorn RM, Marks TJ (1992) J Am Chem Soc 114:1112
50. Hlatky GG, Turner HW, Eckmann RR (1989) J Am Chem Soc 111:2728
51. Chien JCW, Tsai WM, Rausch MD (1991) J Am Chem Soc 113:8570
52. Bochmann M, Lancaster SJ (1993) Organometallics 12:633
53. Zambelli A, Longo P, Grassi A (1989) Macromolecules 22:2186
54. Shiono T (2013) Trialkylaluminum-free modified methylaluminoxane as a cocatalyst for living polymerization of olefins. Adv Polym Sci. doi:10.1007/12_2013_211
55. Brintzinger HH, Fischer D, Mülhaupt R, Rieger B, Waymouth R (1995) Angew Chem 107:1255, Angew Chem Int Ed Engl 34:1143
56. Scheirs J, Kaminsky W (eds) (2000) Metallocene-based polyolefins: preparation, properties, and technology, vols 1 and 2. Wiley, Chichester
57. Coates GW (2000) Chem Rev 100:1223
58. Rieger B, Baugh LS, Kacker S, Striegler S (eds) (2003) Late transition metal polymerization catalysis. Wiley-VCH, Weinheim
59. Keii T (2004) Heterogeneous kinetics: theory of Ziegler–Natta–Kaminsky polymerization, vol 77, Springer series in chemical physics. Springer, Berlin
60. Razavi A, Thewalt U (2006) Coord Chem Rev 250:155
61. Kaminsky W (ed) (2005) Olefin polymerization. Macromol Symp 236
62. Chum PS, Swogger KW (2008) Prog Polym Sci 33:797
63. Baugh LS, Canich JAM (eds) (2008) Stereoselective polymerization with single-site catalysts. CRC, Boca Raton
64. Busico V (2009) Dalton Trans 41:8794
65. Severn J, Robert L (2010) In: Hoff R, Mathers RT (eds) Handbook of transition metal polymerization catalysts. Wiley, New York, p 157
66. Nomura K, Liu KJ (2011) Dalton Trans 40:7666
67. Heurtefen B, Bouilhac C, Cloutet E, Taton D, Deffieux A, Cramail H (2011) Prog Polym Sci 36:89
68. Delferro M, Marks TJ (2011) Chem Rev 111:2450
69. Tait P (1988) In: Kaminsky W, Sinn H (eds) Transition metals and organometallics as catalysts for olefin polymerization. Springer, Berlin, p 309
70. Chien JCW, Wang BP (1989) J Polym Sci A 27:139
71. Kaminsky W, Engehausen R, Zoumis K, Spaleck W, Rohrmann J (1992) Makromol Chem 193:1643
72. Kaminsky W (1996) Macromol Chem Phys 197:3907
73. Alt GH, Milius W, Palackal SJ (1994) J Organomet Chem 472:113
74. Kaminsky W, Lüker H (1989) Makromol Chem Rapid Commun 5:225
75. Erker JKG, Fröhlich R (1997) J Am Chem Soc 119:11165
76. Kawai K, Fujita T (2009) Top Organomet Chem 26:3–41
77. Shiono T (2011) Polym J 43:331

78. Stevens (1993) Proceedings worldwide metallocene conference, MetCon 93, Houston, 26–28 May 1993. Catalyst Consultants, Houston, p 157
79. Hlatky GG (2000) Chem Rev 100:1347
80. Pino P, Mühlhaupt R (1980) Angew Chem 92:869
81. Wild FR, Zsolnai L, Huttner G, Brintzinger HH (1982) J Organomet Chem 232:233
82. Kaminsky W, Külper K, Brintzinger HH, Wild FR (1985) Angew Chem Int Ed Engl 24:507
83. Ewen JA (1984) J Am Chem Soc 106:6355
84. Spaleck W, Aulbach M, Bachmann B, Kueber F, Winter A (1995) Macromol Symp 89:237
85. Ewen JA, Jones RL, Razavi A, Ferrara JP (1988) J Am Chem Soc 110:6255
86. Kaminsky W, Buschermöhle M (1987) In: Fontanille M, Guyot A (eds) Recent advances in mechanistic and synthetic aspects of polymerization. Reidel, Dordrecht, p 503
87. Brintzinger HH, Fischer D (2013) Development of ansa-metallocenes for isotactic olefin polymerization. Adv Polym Sci. doi:10.1007/12_2013_215
88. Razavi A (2013) Syndiotactic polypropene: discovery, development, and industrialization via bridged metallocene catalysts. Adv Polym Sci. doi:10.1007/12_2013_220
89. Kaminsky W, Spiehl R (1989) Makromol Chem 190:515
90. Collins S, Kelly WM (1992) Macromolecules 25:233
91. Tritto I, Boggioni L, Ferro DR (2006) Coord Chem Rev 250:212
92. Schäfer A, Karl E, Zsolnai L, Huttner G, Brintzinger HH (1987) J Organomet Chem 328:87
93. Kaminsky W, Ahlers A, Möller-Lindenhof N (1989) Angew Chem Int Ed Engl 28:1216
94. Kaminsky W, Ahlers A, Rabe O, König W (1992) In: Enders D, Gais H-J, Keim W (eds) Organic synthesis via organometallics. Vieweg, Braunschweig, p 151
95. Kaminsky W, Miri M (1985) J Polym Sci A Polym Chem 23:2151
96. Kaminsky W, Schlobohm M (1986) Makromol Chem Rapid Symp 4:103
97. Kaminsky W (1994) Catal Today 20:257
98. Jüngling S, Mülhaupt R, Fischer D, Langhauser F (1995) Angew Makromol Chem 229:93
99. Kaminsky W (2000) Catal Today 62:23
100. Frediani M, Bianchini C, Kaminsky W (2006) Kinet Catal 47:207
101. Arikan B, Stadler FJ, Kaschta J, Münstedt H, Kaminsky W (2007) Macromol Rapid Commun 28:1472
102. Stadler FJ, Arikan-Conley B, Kaschta J, Kaminsky W, Münstedt H (2011) Macromolecules 44:5053
103. Kaminsky W, Boggioni L, Tritto I (2012) In: Matyjaszewski K, Möller M (eds) Polymer science: a comprehensive reference, vol 3. Elsevier, Amsterdam, p 843
104. Kaminsky W, Bark A, Arndt M (1991) Makromol Chem Macromol Symp 47:83
105. Cherdron H, Brekner MJ, Osan F (1994) Angew Makromol Chem 223:121
106. Boggioni L, Tritto I (2013) Polyolefins with cyclic comonomers. Adv Polym Sci. doi:10.1007/12_2013_217
107. Dong M, Wang L, Jiang G, Sun T, Zhao Y, Yu H, Chen T (2006) J Appl Polym Sci 101:1291
108. Alexandre M, Martin E, Dubois P, Garcia-Marti M, Jerome R (2000) Macromol Rapid Commun 21:931
109. Xalter R, Halbach TS, Muelhaupt R (2006) Macromol Symp 236:145
110. Funck A, Kaminsky W (2007) Compos A Technol 67:906
111. Guo N, Benedetto SA, Tewari P, Lanagan MT, Ratner MA, Marks TJ (2010) Chem Mater 22:1567
112. Xalter R, Mülhaupt R (2010) Macromol Reaction Eng 4:25
113. Etcheverry M, Ferreira ML, Capiati NJ, Pegoretti A, Barbosa SE (2008) Compos A Appl Sci 39:1915
114. Stürzel M, Kurek A, Anselm M, Halbach T, Mülhaupt R (2013) Polyolefin nanocomposites and hybrid catalysts. Adv Polym Sci. doi:10.1007/12_2013_219
115. Tarte NH, Cui L, Woo S (2013) Polyolefin/layered silicate nanocomposites prepared by in-situ polymerization. Adv Polym Sci. doi:10.1007/12_2013_228

116. Meyer RSA, Luinstra GA (2013) Iron catalyst in the preparation of polyolefin composites. Adv Polym Sci. doi:10.1007/12_2013_223
117. Kaminsky W (2008) Macromol Chem Phys 209:459
118. Kaminsky W, Funck A, Klinke C (2008) Top Catal 48:84
119. Klapper M, Jang YJ, Bieber K, Nemnich T, Nenov N, Müllen K (2004) Macromol Symp 213:131
120. Busico V, Cipullo R, Corradini P (1993) Macromol Chem Rapid Commun 117:195
121. Stadler FJ, Arikan B, Kaschta J, Kaminsky W (2010) Macromol Chem Phys 211:1472
122. Malmberg A, Kokko E, Lehmus P, Löfgren B, Seppälä JV (1998) Macromolecules 31:8448
123. Ittel SD, Johnson LK, Brookhart M (2000) Chem Rev 100:1169
124. Mecking S (2007) Colloid Polym Sci 285:605
125. Möller HM, Baier MC, Mecking S, Talsi EP, Bryliakov KP (2012) Chem A Eur J 18:848
126. Zhang D, Guironnet D, Goettker-Schnetmann I, Mecking S (2009) Organometallics 28:4072
127. Kaminsky W (2009) J Chem Soc Dalton Trans 2009:8003
128. Heinemann J, Muelhaupt R, Brinkmann P, Luinstra GA (1999) Macromol Chem Phys 200:384
129. Lipponen S, Seppälä J (2011) Organometallics 30:528
130. Seppälä J, Kokko E, Lehmus P, Pakkanen A, Hakala K, Lipponen S, Löfgren B (2013) Functional polyolefins through polymerizations by using bis(indenyl)zirconium catalysts. Adv Polym Sci. doi:10.1007/12_2013_210
131. Chung TCM (2013) Functional polyolefins: synthesis and energy storage applications. Adv Polym Sci. doi:10.1007/12_2013_209
132. Saito J, Mitani M, Matsui S, Kashiwa T, Fujita T (2000) Macromol Rapid Commun 21:1333
133. Arriola DJ, Carnahan EM, Hustad PD, Kuhlman RL, Wenzel TT (2006) Science 312:714
134. Kaminsky W (1986) In: Seymour RB, Cheng T (eds) History of polyolefins. Reidel, New York, p 257

Adv Polym Sci (2013) 258: 29–42
DOI: 10.1007/12_2013_215

Published online: 16 May 2013

Development of *ansa*-Metallocene Catalysts for Isotactic Olefin Polymerization

Hans H. Brintzinger and David Fischer

Abstract The development of *ansa*-metallocene catalysts is considered along several lines of interest – *ansa*-metallocene complexes with different ligand frameworks, insights gained with regard to relevant reaction intermediates and contributions of *ansa*-metallocene catalysts to industrial polymer production – with a view toward the present state of the art in these fields of catalysis research.

Keywords Activation · *ansa*-Zirconocene catalysts · Constrained-geometry catalysts · ethene/propene rubbers · Isotactic polypropylene · Linear low-density polyethylene · Molar-mass distribution · Olefin polymerization · Reaction mechanisms · Single-site catalysts · Stereosectivity

Contents

H.H. Brintzinger (✉)
University of Konstanz, Konstanz D-78457, Germany
e-mail: hans.brintzinger@uni-konstanz.de

D. Fischer
Albemarle Corporation, Baton Rouge, LA 70801, USA
e-mail: david.fischer@albemarle.com

1 Introduction

In this article, we try to give a brief account of the development of *ansa*-metallocene catalysts for isotactic olefin polymerizations, especially with regard to some points of particular interest to the authors of this article. For this, we will refer to appropriate previous reviews and then try to assess the state of the art.

2 Structural Variants of *ansa*-Metallocene Catalysts

In the three decades that have passed since the first syntheses of chiral ethanediyl-bridged bis(indenyl)titanium and bis(indenyl)zirconium complexes [1, 2] and the first reports on their use – together with methylalumoxane as activator [3] – as catalysts for isotactic olefin polymerization [4, 5], this field of catalysis research has seen many structural variations on the *ansa*-metallocene theme.

Among *ansa*-metallocene catalysts with different group IV transition metals, *ansa*-titanocene-based catalysts (with rare exceptions [6]) lose most of their activity above 0°C, whereas *ansa*-hafnocene catalysts usually give lower activities than the analogous *ansa*-zirconocene catalysts [7, 8], which have thus received most research interest.

Variations in catalyst structures mostly involved changes in the substitution patterns of the *ansa*-metallocene ring ligands, since catalyst properties are clearly influenced most directly by the steric environment of the metallocene coordination sites [7–9]. Much interest has been directed at the possibility of obtaining polyolefins with tacticities different from those of the isotactic polymers obtained with C_2-symmetric *ansa*-metallocene catalysts. The observation that zirconocene catalysts with C_S-symmetric geometry, i.e. with enantiotopic metallocene coordination sites, generate syndiotactic polypropylene [10] thus helped to establish explanations for the enantioselectivity of the chain-growth process; these explanations are universally accepted today [11, 12].

Especially interesting in this regard are *ansa*-metallocene catalysts with a C_1-symmetric structure, in which the steric environments of the metallocene coordination sites are unrelated to each other. Depending on the steric environment of each coordination site, polypropylene tacticities can range here from almost atactic to highly isotactic [7, 13]. Due to the possibility of finely adjusting stereoerror frequencies, and thereby tuning the flexibility of polymer chains and the ensuing properties of polymer materials, this type of catalysts continues to be of practical interest [14].

With regard to variations in bridging units, interanular bridging via a $(CH_3)_2Si$ unit proved to endow *ansa*-metallocene catalysts with higher degrees of stereoselectivity and with higher activities than bridges with two-atom or longer chains [15], probably due to a greater stereorigidity of the ligand framework and a wider opening of the interanular wedge angle [7, 8, 16]. Bridging units with spatially more demanding, asymmetric or chiral substituents have likewise been shown to influence the catalytic properties of *ansa*-metallocene catalysts [17], especially those with C_1 symmetry [7], presumably via their effects on ring-ligand conformation.

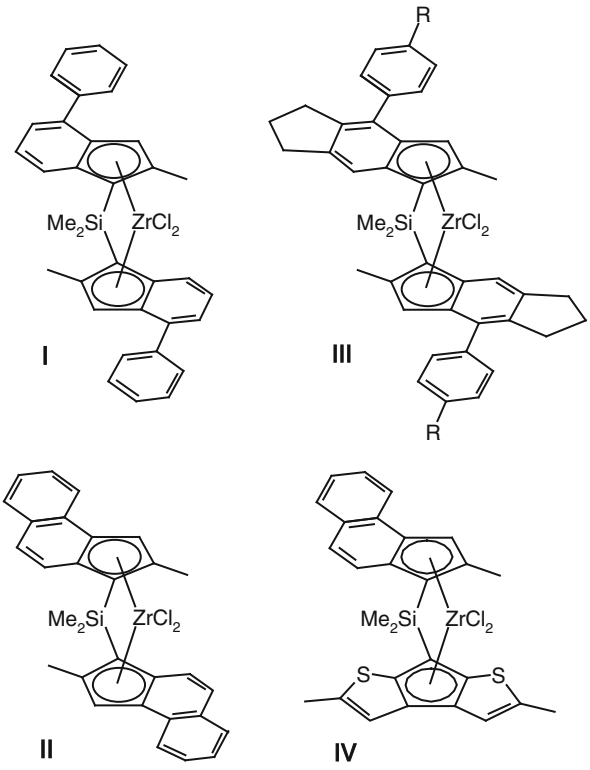

Fig. 1 Representative *ansa*-zirconocene precatalysts: After activation with MAO, **I** and **II** give highly active catalysts for isotactic propene polymerization [20, 21], **III** gives further activity increase [22] and C_1-symmetric **IV** gives partly isotactic polypropylene [14]

Ansa-metallocene catalysts with ring ligands connected by a semi-labile electron donor–acceptor bond have been shown to produce polypropylene with interesting elasticity properties [18]. Similar observations had also previously been made with unbridged zirconocene catalysts, the indenyl ligands of which are hindered in their mutual rotation by phenyl substituents in their 2-position [19]. In both cases, an interchange between alternative ring ligand rotamers appears to occur on a time scale that is comparable to that required to complete a polyolefin chain. Whether this gives rise to polymer chains containing alternating blocks of preponderantly isotactic and atactic sequences as a cause of elastomeric properties, or to reactor blends of mainly isotactic and mainly atactic chains (or both), is still under debate [8].

Major research interests have been aimed at the adjustment of *ansa*-metallocene catalysts to the requirements of industrial polymer production, i.e. high activities, high molar masses and high degrees of isotacticity. Remarkable achievements in this regard by use of *ansa*-zirconocene complexes with methyl-substituted 2-positions and extended anulation and/or "frontal" substitution of their C_5-ring ligands (Fig. 1) were reported rather early on [20, 21] and were further optimized more recently [22, 23].

A "frontal" extension of the ring ligands appears to be responsible for increased activities, most likely by way of destabilizing some (still unidentified) resting state of the chain-growth process. On the other hand, methyl substituents in the

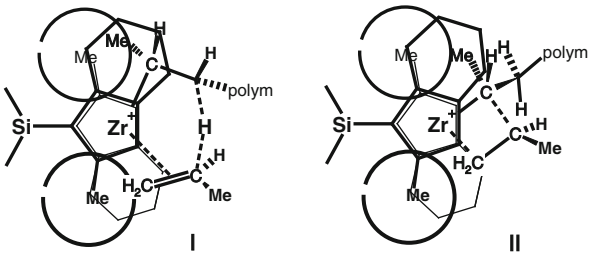

Fig. 2 The transition state for β-H transfer to monomer (**I**) after a 2,1-insertion requires more space in the mid-plane of the metallocene wedge than the insertion transition state (**II**); it is thus disfavored by methyl substituents next to the bridgehead positions [21, 24]

2-position, next to the interanular bridge, were shown to suppress chain release via β-H transfer to an olefin monomer, particularly after a 2,1-misinsertion, due to their interference with a space-demanding β-H transfer transition state (Fig. 2) [21, 24].

A more recent variation of this theme concerns the utilization of *ansa*-zirconocene catalysts of the bis-indenyl type for the industrial production of elastomeric propene/ethene copolymers (EP rubbers, see Sect. 4) [8]. Here, a drastic reduction in molar mass occurs in the presence of ethene. This problem was overcome by further decreasing the space in the *ansa*-metallocene coordination plane through replacement of one of the 2-positioned methyl substituents by an isopropyl group [25]. This feat represents a rare case where a prediction based on computational studies actually preceded the experimental outcome and shows the usefulness of clear conceptions concerning relevant reaction paths.

3 Mechanisms of Catalyst Activation and Polymerization Catalysis

The first reports of isotactic α-olefin polymerization by homogeneously dissolved *ansa*-metallocene catalysts were greeted by the expectation that the mechanisms responsible for this stereoselective catalysis might now be more thoroughly clarified than had been possible for solid-state Ziegler–Natta catalysis. Although progress has been made toward that goal during recent decades, our basic understanding of homogeneous polymerization catalysis is still not quite satisfactory in some respects.

Activation of *ansa*-metallocene dichloride precursors by methylalumoxane (MAO) – a partial-hydrolysis product of trimethylaluminum [3] – was the initial door-opener for the polymerization of propene and higher olefins by *ansa*-metallocene catalysts [4, 5]. It is still being quoted as the most frequently used route to activate these catalyst systems [26]. Evidence has recently been presented that activation by MAO might involve highly reactive $AlMe_2^+$ cations [27]. Yet it remains unknown which structural features of MAO might be responsible for its unique reactivity.

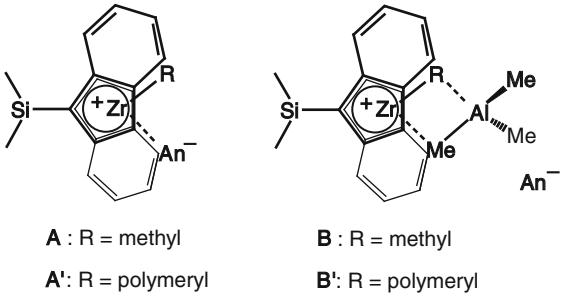

Fig. 3 Inner-sphere ion pairs **A**, containing a methyl zirconocenium cation, and outer-sphere ion pairs **B**, containing a heterobinuclear $AlMe_3$ adduct of the latter, together with a weakly coordinating anion An^-, such as $MeB(C_6F_5)_3^-$, $B(C_6F_5)_4^-$ or $MeMAO^-$, observed in *ansa*-zirconocene systems activated with $B(C_6F_5)_3$, $Ph_3CB(C_6F_5)_4$ or MAO, respectively [26, 28, 29]. The corresponding species **A′** and **B′** with R = polymeryl, observed in active catalyst systems in the presence of olefin [30, 31]

Highly active and more well-defined catalyst systems have become accessible by reaction of a zirconocene alkyl precursor with one of several "cationization" reagents that contain a trityl or dimethylanilinum cation capable of abstracting an alkyl anion from this precursor. An inert tetra(perfluorophenyl) borate or related anion coordinates only weakly to the resulting alkyl zirconocenium cation in an inner-sphere ion pair of type **A** (Fig. 3) [26, 28, 29].

In MAO-activated catalyst systems, alkyl zirconocenium cations are likewise thought to be present, presumably in weakly bound inner-sphere ion pairs with anions of the type $MeMAO^-$ [26, 29]. These anions – still only vaguely characterized as large agglomerates [32] – are assumed to be formed from MAO by uptake of a methyl anion from the alkyl zirconocene precursor. In equilibrium with these inner-sphere ion pairs **A**, outer-sphere ion pairs **B** (Fig. 3) are observed in MAO-activated pre-catalyst systems [29, 32–34] that contain a heterobinuclear cationic $AlMe_3$ adduct [35], presumably together with $MeMAO^-$ as counter-anion.

With regard to the growth of metal-bound polymer chains from a metallocene pre-catalyst activated in this manner, it is undisputed that successive monomer molecules are incorporated by *cis*-insertions into the metal–alkyl bond, first of an ion pair **A**, and then of the ensuing metal-polymeryl species A′ [7]. The latter reaction, i.e. growth of a Zr-bound polymer chain, has been found to be much faster than the initial insertion into a Zr–Me bond in most cases studied [30, 36, 37].

For the growth of isotactic polypropylene chains and higher polyolefin chains at the chiral coordination sites of *ansa*-metallocene catalysts, the following explanation is now firmly established [11, 12]: Formation of the new C–C bond requires that the α-olefin substituent and the C(α)–C(β) bond of the metal-bound polymeryl chain are oriented *anti* to each other along the incipient C–C bond, while the C(α)–C(β) chain segment must reside in an open quadrant of the chiral metallocene coordination site. The latter is thus considered to control the enantiofacial orientation of the α-olefin in the insertion transition state **TS** (Fig. 4) by way of the C(α)–C(β) chain-segment "lever".

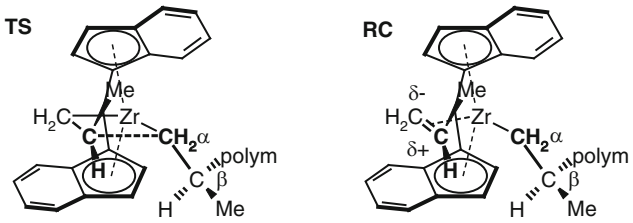

Fig. 4 Transition state **TS** for favored si-facial olefin insertion into a Zr–polymeryl bond according to the model of chain-segment-mediated catalytic site control [11, 12] (*left*) and reaction complex **RC**, which is thought to precede transition state formation [7] (*right*)

This model of chain-segment mediated enantiomorphic site control for isotactic polyolefin formation by C_2-symmetric *ansa*-metallocene catalysts has received experimental support from several lines of stereochemical evidence [38, 39]. It has also provided convincing explanations for the generation of syndiotactic polypropylene at the enantiotopic coordination sites of C_S-symmetric *ansa*-metallocene catalysts [10] and for the variable stereoregularities of polymers obtained with C_1-symmetric catalysts cf. Sect. 2) [7, 13].

Useful insights regarding the transition states of side reactions, which occur in competition to olefin insertion, such as chain release by β-H transfer and chain-end isomerizations, have also been derived from experimental data on kinetics [21, 40, 41], kinetic isotope effects and isotope label redistributions [39, 42].

Little experimental evidence is available, on the other hand, with regard to a metal-olefin reaction complex **RC** (Fig. 4), which is considered to precede formation of the insertion transition state **TS**. Steady-state concentrations of such a species are obviously insufficient for spectroscopic detection. Experimental studies on cationic metallocene–olefin complexes, where olefin insertion is slow or impossible for one reason or another, as well as a number of computational studies, portray such reaction complexes as having some finite stability, a rather polarized C=C double bond and a low barrier of rotation around the olefin–metal bond [7, 28].

Insufficiently explored is also the ubiquitous reaction by which a metallocene-bound polymer chain is transferred to an Al center of the co-catalyst/activator in exchange for a methyl group. While there is little doubt that intermediates of type **B′** (Fig. 3) are involved in such an alkyl exchange [28], only scant experimental data concern the effects of different chain-ends and *ansa*-metallocene structures on the rate, extent and direction of these exchange reactions. As these can be used to transfer polymer chains between catalysts with different stereoselectivities [43], further exploration might be useful for a production of polypropylene that contains chain segments with different tacticities.

Rather glaring deficits in our understanding of metallocene-catalyzed olefin polymerization concern the catalyst resting state(s), i.e. the identity of those species that make up the majority of the total metallocene concentration of a catalyst system "at work." At first glance, it would appear quite feasible to identify at

least the major species of such a working catalyst, e.g. by NMR spectroscopy. In this manner, inner-sphere ion pairs of type **A′** (Fig. 3), with a polymeryl chain and a $MeB(C_6F_5)_3^-$ anion attached to the cationic metal center, have indeed been identified in toluene solution at –40°C as the catalyst resting state in an *ansa*-zirconocene catalyst system activated with the Lewis-acidic borane $B(C_6F_5)_3$ [30].

Under conditions more closely approaching practically useful polymerization catalysis, i.e. in working catalyst systems that contain less "sticky" counter-anions and a substantial olefin excess and that operate at ambient or higher temperatures, it is not yet clear which fractions of the total catalyst content in a given catalyst system correspond to ion pairs of type **A′** or to several other resting-state candidates with regio-irregular [44], allylic [45] or agostically bound [46] chain ends.

During polymerization of 1-hexene by an MAO-activated ansa-zirconocene catalyst system, species of types A, B and B' were detected by NMR spetroscopy but found to account for less than half of the initial metallocene concentration [31]. Major parts of the metallocene content of this catalyst system thus remain unaccounted for.

Further efforts to identify the resting state(s) and the major modes of deactivation [47] of typical *ansa*-metallocene catalysts would appear worthwhile, since – to quote a recent review [26] – "in the absence of this information, a rational analysis of the effects of structural variations on catalyst activities … must remain fragmentary."

4 Industrial Use of *ansa*-Metallocene Catalysts

The first isospecific propene polymerization with an ethanediyl-bridged bis (indenyl)-titanium complex demonstrated in 1983 the capability of *ansa*-metallocenes to control the tacticity of a growing polypropylene chain [4, 48], thus creating a strong interest in exploring the potential use of *ansa*-metallocenes for industrial polypropylene production. A first step towards industrially suitable systems was the use of much more stable zirconium complexes, which when activated by the methylaluminoxane co-catalyst [3] allowed higher polymerization temperatures and thus higher activities [5].

However, these first *ansa*-zirconocenes delivered at temperatures of 70°C and above, as typical for industrial PP processes, only oligomeric or low molecular weight polypropylene and moderate isotacticities, both still insufficient for industrial usage. Further increases in activity and better stereospecifities were obtained using the more rigid dimethylsilylene bridge, which was patented by Fina Technology in 1987 [15, 49] and has since become the most widely used bridging unit.

However, only the introduction of methyl substituents in the 2-position, by the former Hoechst AG in 1990 [20, 50], led to polypropylenes with sufficiently high molar mass under industrially relevant polymerization conditions. In 1990, *rac*-dimethylsilylene-bis(2-methylindenyl)zirconium dichloride thus became the first *ansa*-metallocene to combine all these improvements and be suitable for industrial use [50, 51]. Since then, the basic concept of dimethylsilylene-bridged,

2-methyl-substituted bisindenyl zirconocenes has been further optimized, e.g. by substitution at the 4-position [52–54] and by pseudo C_2-symmetric bisindenyl *ansa*-zirconocenes with one 2-isopropyl and one 2-methyl substituent [25, 55].

Probably to circumvent the former Hoechst AG's strong patent position on bisindenyl-type *ansa*-metallocenes, alternative structures were developed by Mitsubishi Chemical Corporation [23, 52] and by former Montell [14, 56], based on azulenyl and heterocenyl ligands, respectively.

Although *ansa*-metallocene catalysts are intrinsically homogeneous catalysts, all industrial polypropylene processes had been developed for heterogeneous Ziegler–Natta catalysts. Therefore, an absolute requirement for the industrial use of *ansa*-metallocenes was their heterogenization on a solid carrier material to avoid polymer growth on reactor walls and to achieve control over polymer particle morphology [57, 58]. Fixation of an *ansa*-metallocene catalyst on a solid support allows its use as a "drop-in" replacement for traditional Ziegler–Natta solid-state catalysts in preexisting polyolefin production plants, where it then produces polyolefin materials with properties closely similar to those produced by it in homogeneous solution. The necessity to heterogenize metallocene catalysts was first recognized by ExxonMobil and patented in 1985 [59]. Since then, suitable recipes for heterogenized metallocene catalysts, which yield polymer products with controlled spherical morphology, and the elementary processes responsible for this outcome have been thoroughly researched and described in detailed reviews [57, 58, 60, 61].

Industrial use of *ansa*-metallocenes for the production of isotactic polypropylene had to overcome not only technical hurdles, but has also been restricted by a complicated and scattered patent landscape. Basic patent rights like the activation of metallocene complexes by MAO, supported metallocenes [59, 62], silanediyl-bridges [49] and 2-methyl substitution [50], all of which were required for the use of *ansa*-metallocenes in industrial polypropylene production, were owned by different companies such that no player had the freedom to move. Only in 1995, 5 years after *rac*-dimethylsilylenbis(2-methylindenyl)zirconium dichloride had been described for the first time in a patent [50], did ExxonMobil and the former Hoechst AG announce independently their first commercial production of metallocene-catalyzed, isotactic polypropylene. Most likely, these 5 years were needed not only to solve technical problems, but also to gain access to all the necessary patent rights.

Today, at least five companies are known to use *ansa*-metallocenes for industrial production of isotactic polypropylene: TOTAL Petrochemicals & Refining (Lumicene®) [63], LyondellBasell (Metocene) [64], Japan Polypropylene (WINTEC™), ExxonMobil (Achieve™ PP) and LyondellBasell's licensee PolyMirae (Metocene). In addition, technology for the industrial production of polypropylene by use of *ansa*-metallocenes is offered for licensing by LyondellBasell (Metocene) [64] and Lummus Novolen Technology GmbH (Novocene™) [65]. Although Japan Polypropylene's WINTEC™ is produced by a bis-azulenyl-type ansa-metallocene [23, 52] and also uses a MAO-free activator support, all others are believed to use bis-indenyl-type metallocenes.

In industrial use, *ansa*-metallocene catalyst systems compete with the well-established traditional Ziegler–Natta catalysts. Because their precursors, in particular the racemic *ansa*-metallocenes and suitable activators like MAO, are more costly than the relatively simple raw materials for Ziegler–Natta catalysts, the industrial success of *ansa*-metallocene catalysts is contingent on their ability to produce polymer materials with superior properties, which can be priced so as to compensate for the higher costs of synthesizing, activating and handling these advanced organometallic catalysts.

For isotactic polypropylene (i-PP), currently produced at a world-wide scale of about 50 million tons per year with classical Ziegler–Natta catalysts, the situation can be viewed as follows [66]: For many applications, the rather wide molar-mass distribution of i-PP generated by solid-state Ziegler–Natta catalysts is an advantage compared to the narrow molar-mass distribution of i-PP produced with supported *ansa*-metallocene catalysts, since a wide molar-mass distribution leads to a more pronounced shear-induced viscosity decrease of the polymer melt and, hence, to higher through-put rates in typical extrusion processes. It also provides higher polymer-melt strengths, which is desirable in thermoforming and biaxally oriented polypropylene (BOPP) film production, both very large application segments for i-PP. Other i-PP applications (e.g. melt-blown or spun-bonded non-woven fabrics), however, benefit from metallocene-produced i-PP because they run more stably at higher speeds in these spinning processes, thus providing processing advantages. The uniform polymer chain lengths also cause a higher orientation in the spinning process, thus providing higher tenacities of the final non-woven fabric [67].

Besides its narrow molar-mass distribution, metallocene-produced i-PP benefits from a much more efficient control of its molar mass by hydrogen, eliminating the need for post-reactor chain degradation using peroxides. Metallocene-produced i-PP is thus normally free of oligomeric chain fragments and low molecular weight residues from peroxides, which both cause spinning fumes and deposits on the spinning dies. This reduces emissions during the spinning process and the frequency of shutdowns necessary to clean the spinning dies.

Although the wider molar-mass distribution of conventional i-PP is generally preferred in thick-wall injection molding, where the shear-induced drop of the melt viscosity helps to fill the mold faster, *ansa*-metallocene-catalyzed i-PP offers advantages in thin-wall injection molding, where i-PP with higher melt flow rate (lower viscosity) is generally used: The uniform polymer chain length distribution brings a higher number of tie-molecules capable of connecting different crystallites. This translates into higher toughness, whereas the absence of excessively long polymer chains (with very long relaxation times) reduces warpage and gives injection-molded articles higher dimensional stability and superior mechanical strength; consequently, thinner walls allow material savings.

Other advantages of these materials result from their crystallization characteristics: Due to its compositional homogeneity, polypropylene obtained with *ansa*-metallocene catalysts gives rise to a more controlled initial crystallite formation in a narrow temperature window. The ensuing crystallization process can thus be guided so as to yield smaller crystallites than in polymers obtained with

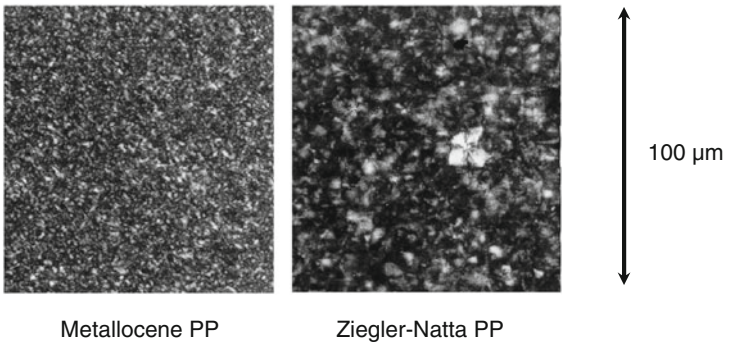

Fig. 5 Crystallite sizes in polypropylenes produced with an *ansa*-zirconocene catalyst (*left*) and with a solid-state Ziegler–Natta catalyst (*right*), both clarified with a nucleating agent (Courtesy of Basell Polyolefins GmbH and of Rendiconti Lincei: Scienze Fisiche e Naturali for permission to reproduce this figure from [66])

classical solid-state catalysts (Fig. 5). Therefore, films and thin-walled articles made from these materials have substantially reduced haze and close-to-perfect transparency, together with a decreased permeability for oxygen and water.

Ansa-metallocene catalysts, and metallocene catalysts in general, deliver particularly clear-cut improvements in product properties of ethene/α-olefin copolymers [68], such as linear low-density polyethylene (LLDPE) or ethene/propene (EP) rubbers, which command large polymer market segments. Solid-state Ziegler–Natta catalysts, which strongly prefer ethene, need a large excess of α-olefin in the monomer feed to incorporate sufficient co-monomer fractions. Higher α-olefin contents are mostly built into short polymer chains, which grow at less-selective centers of these non-uniform catalysts. The resulting copolymers thus usually contain significant fractions of soft, short-chain materials, which are extracted from the surface of packaging films upon contact with lipids or cause other undesirable effects.

Metallocene-based single-site catalysts, on the other hand, incorporate propene and higher α-olefins more readily, easily generating copolymer chains with much higher co-monomer contents, controlled co-monomer distribution along the chains and uniform chain lengths [7, 8]. Their selectivities with regard to co-monomer uptake and co-monomer distribution within chains – from alternating to random or even blocky microstructures – can be tuned almost without limitations so as to allow access to copolymer materials with high suitability for various form-giving processes and with mechanical and optical properties widely adaptable to various end-user demands [8, 69]. In particular, films produced from metallocene-catalyzed LLDPE (m-LLDPE) show drastically improved mechanical strength, gloss and transparency compared with films of LLDPE obtained from conventional Ziegler–Natta catalysts. Therefore, Single-site catalysts, including metallocene and *ansa*-metallocene catalysts, are widely used for the production of ethene/α-olefin copolymers and, in particular, m-LLDPE.

A majority of all polyethylene grades are ethene/α-olefin copolymers (LLDPE, MDPE), which benefit directly from the use of single-site catalysts like *ansa*-metallocenes. Most polypropylenes, on the other hand, are homo-polymers, with one exception: biphasic i-PP reactor blends contain elastomeric ethene/propene copolymers (EP rubbers) dispersed in a matrix of crystalline i-PP homo-polymer. Such reactor blends, used e.g. in the manufacture of automobile parts, retain the high mechanical strength of isotactic polypropylene while being endowed with increased toughness, also at lower temperatures, from the dispersed EP rubber particles. However, these ethene/propene copolymers, for which similar considerations should hold as for m-LLDPE, were not accessible by first-generation 2-methyl-substitued bisindenyl *ansa*-metallocenes because of a drastic reduction in polymer chain length in the presence of ethene. Therefore, the development of catalysts bearing a ligand framework with suitably substituted α-positions [25, 55, 70], as discussed in Sect. 2, was a prerequisite for the production of i-PP reactor blends with metallocene catalysts. Such a specially adapted *ansa*-zirconocene catalyst is used by LyondellBasell to produce EP/i-PP "impact" polymer blends, which belong to their family of "Clyrell" grades [71].

The unique properties of i-PP produced with *ansa*-metallocene catalysts, including their low content of easily migrating short-chain polymer, desirable in particular for food and medical packaging and related purposes [72], has driven the industrial use of i-PP produced with *ansa*-metallocene catalysts in some demanding market sectors. However, higher costs, the dominance of homo-polypropylene, improved Ziegler–Natta catalysts and, last but not least, a complicated patent situation have as of today restricted their use in the i-PP field to specialized niche applications.

The possibility of controlling the interanular wedge angle of *ansa*-metallocene catalysts and their resulting capability to also enchain olefins, which are otherwise not readily amenable to insertion polymerization, allows the production of copolymers of ethene with cyclic olefins, in particular with norbornene or its substituted derivatives. Based on first observations in this regard [73, 74], ethene/norbornene copolymers, e.g. with alternating microstructures [75–77] and with excellent optical and barrier properties, are now commercially produced with *ansa*-metallocene catalysts by Topas Advanced Polymers (TOPAS®) [78] and by Mitsui Chemical (Apel) [79].

5 Concluding Remarks

Since the first reports on their usage for isospecific propene polymerization [4, 5, 48], *ansa*-metallocenes have inspired industrial and academic research for almost 30 years. Initially introduced for isospecific olefin polymerization, the concept of bridging their two ring ligands has substantially enhanced the variability and design options of metallocene catalysts in general. In addition to paving the way for industrial i-PP

production with single-site catalysts, this concept has also led to the first industrial production and market introduction of syndiotactic polypropylene by former Fina Inc. (today TOTAL Petrochemicals & Refining USA, Inc.) and of ethene/norbornene copolymers by former Hoechst AG (today TOPAS Advanced Polymers).

The possibility of preventing the mutual rotation of the ring ligands [4, 5] and to vary the interanular wedge angle [16] has secured for *ansa*-metallocenes an important role in metallocene-produced polyethylene, together with simple unbridged metallocenes and non-metallocene single-site catalysts. Even Dow's "constrained-geometry catalysts", where a bridge links cyclopentadienyl-type with non-cyclopentadienyl-type (e.g. alkylamido) ligands to form a half-sandwich complex with a titanium center [80, 81], to become the basis for DOW's INSITE™ technology and ENGAGE™ polyolefin elastomer product line, might thus be regarded as evolutions of the *ansa*-metallocene concept.

The role of *ansa*-metallocenes for the industrial production of i-PP (initially the primary aim of their development) is still limited to specialized niche applications with relatively small market shares and thus – ironically – is less important than for other polymers such as m-LLDPE. Besides the specifics of isotactic propene homopolymers and their applications in injection molding and BOPP, higher costs for the use of *ansa*-metallocene catalysts and rather severe patent hurdles have limited their full success in industrial i-PP production so far. However, LyondellBasell and Lummus Novolen Technology GmbH, the two active licensors of metallocene technology for the isospecific polymerization of propene, have both reported the development of highly active *ansa*-metallocene catalysts for i-PP, which reduces the cost gap between such catalysts and modern Ziegler–Natta catalysts [82, 83]. At the same time, many of the basic patents, by which access to *ansa*-metallocene technology for i-PP had been limited to only a handful of players, have now expired or will expire in the near future. It will be interesting to see whether this will finally open the path for a wider use of *ansa*-metallocene catalysts in the industrial production of i-PP.

Acknowledgments We thank Rendiconti Lincei: Scienze Fisiche e Naturali for permission to use for this review materials published in [66] and Deutsche Forschungsgemeinschaft for support of research in this field at the University of Konstanz (grant Me 1388/9-1).

References

1. Wild F, Zsolnai L, Huttner G, Brintzinger HH (1982) J Organomet Chem 232:233
2. Wild F, Wasiucionek M, Huttner G, Brintzinger HH (1985) J Organomet Chem 288:63
3. Sinn H, Kaminsky W (1980) Adv Organomet Chem 18:99
4. Ewen JA (1984) J Am Chem Soc 106:6355
5. Kaminsky W, Külper K, Brintzinger HH, Wild F (1985) Angew Chem Int Ed Engl 24:507
6. Llinas GH, Day RO, Rausch MD, Chien JCW (1993) Organometallics 12:1283
7. Resconi L, Cavallo L, Fait A, Piemontesi F (2000) Chem Rev 100:1253
8. Resconi L, Chadwick JC, Cavallo L (2007) In: Crabtree RH, Mingos DMP (eds) Comprehensive organometallic chemistry III, vol 4. Elsevier, Amsterdam, p 1005

9. Möhring PC, Coville MJ (2006) Coord Chem Rev 250:18
10. Ewen JA, Jones RL, Razavi A, Ferrara J (1988) J Am Chem Soc 110:6255
11. Cavallo L, Guerra G, Vacatello M, Corradini P (1991) Macromolecules 24:1784
12. Guerra G, Longo P, Cavallo L, Corradini P (1997) J Am Chem Soc 119:4394
13. Rieger B, Jany G, Fawzi R, Steimann M (1994) Organometallics 13:647
14. Resconi L, Guidotta S, Camurati I, Frabetti R, Focante F, Nifant'ev IE, Laishevtsev IP (2005) Macromol Chem Phys 206:1405
15. Ewen JA, Haspeslagh L, Atwood JL, Zhang H (1987) J Am Chem Soc 109:6544
16. Köpf H, Pickardt J (1981) Zeitschr f Naturforsch 36B:1208
17. Kirillov E, Marquet N, Bader M, Razavi A, Belia V, Hampel F, Roisnel T, Gladysz JA, Carpentier JF (2011) Organometallics 30:263
18. Ostoja Starzewski KA, Kelly WM, Stumpf A, Freitag D (1999) Angew Chem Int Ed Engl 38:2439
19. Coates GW, Waymouth RM (1995) Science 267:217
20. Spaleck W, Küber F, Winter A, Rohrmann J, Bachmann B, Antberg M, Dolle V, Paulus E (1994) Organometallics 13:954
21. Stehling U, Diebold J, Kirsten R, Röll W, Brintzinger HH, Jüngling S, Mühlhaupt R, Langhauser F (1994) Organometallics 13:964
22. Nifant'ev IE, Ivchenko PV, Bagrov VV, Churakov AV, Chevalier R (2012) Organometallics 31:4340
23. Sugano T (1999) Novel metallocene catalysts for propylene polymerization. In: Proceedings Schotland conference on specialty polyolefins (SPO'99), October 12–13, 1999, Houston, Texas. Schotland Business Research, p 33
24. Jüngling S, Mülhaupt R, Stehling U, Brintzinger HH, Fischer D, Langhauser F (1995) J Polym Sci A 33:1305
25. Elder M, Okumura Y, Jones RL, Seidel N, Richter B (2004) MOSPOL conference. Book of abstracts. MOSPOL, Moscow, 59
26. Bryliakov KP, Talsi EP (2012) Coord Chem Rev 256:2994
27. Tanskanen J, Linnolahti M, Severn J, Bochmann M (2012) In: Abstracts of papers, 243rd ACS National Meeting & Exposition, San Diego, PHYS-291
28. Bochmann M (2010) Organometallics 29:4711
29. Chen EYX, Marks TJ (2000) Chem Rev 100:1391
30. Landis CR, Rosaaen KA, Sillars DRJ (2003) J Am Chem Soc 125:1710
31. Babushkin DE, Brintzinger HH (2010) J Am Chem Soc 132:452
32. Babushkin DE, Brintzinger HH (2002) J Am Chem Soc 124:12869
33. Tritto I, Donetti R, Sacchi MC, Locatelli P, Zannoni G (1997) Macromolecules 30:1247
34. Babushkin DE, Semikolenova NV, Zakharov VA, Talsi EP (2000) Macromol Chem Phys 201:558
35. Bochmann M, Lancaster SJ (1994) Angew Chem Int Ed Engl 33:1634
36. Busico V, Cipullo R, Esposito V (1999) Macromol Rapid Commun 20:116
37. Al-Humydi A, Garrison JC, Youngs WJ, Collins S (2005) Organometallics 24:193
38. Pino P, Cioni P, Wei J (1987) J Am Chem Soc 109:6189
39. Leclerc MK, Brintzinger HH (1996) J Am Chem Soc 118:9024
40. Tsutsui T, Mizuno A, Kashiwa N (1989) Polymer 30:428
41. Resconi L, Camurati I, Sudmeijer O (1999) Top Catal 7:145
42. Abrams MB, Yoder JC, Loeber C, Day MW, Bercaw JE (1999) Organometallics 18:1389
43. Lieber S, Brintzinger HH (2000) Macromolecules 33:9192
44. Busico V, Cipullo R, Romanelli V, Ronca S, Togrou M (2005) J Am Chem Soc 127:1608
45. Landis CR, Christianson MD (2006) Proc Natl Acad Sci USA 103:15349
46. Alonso-Moreno C, Lancaster DJ, Wright JA, Hughes DL, Zuccaccia C, Correra A, Macchioni A, Cavallo L, Bochmann M (2008) Organometallics 27:5474
47. Fischer D, Mülhaupt R (1991) J Organomet Chem 417:C7
48. Ewen JA (1983) US 4,522,982

49. Ewen JA (1987) Patent EP 284,708 B1
50. Winter A, Antberg M, Spaleck W, Rohrmann J, Dolle V (1990) Patent EP 485,821 B1
51. Spaleck W, Antberg M, Rohrmann J, Winter A, Bachmann B, Kiprof P, Behm J, Herrmann WA (1992) Angew Chemie Int Ed Engl 31:1347
52. Sugano T, Uchino H, Imaeda K, Taniyama E, Iwama N (1994) Patent EP 697,418 B1
53. Karl E, Roell W, Brintzinger HH, Rieger B, Stehling U (1991) Patent EP 519,237 B1
54. Küber F, Bachmann B, Spaleck W, Winter A, Rohrmann J (1992) Patent EP 576,970 B1
55. Schottek J, Oberhoff M, Bingel C, Fischer D, Weiss H, Winter A, Fraaije V (2001) Patent WO 01/48034 A2
56. Ewen JA, Elder M, Jones RL, Dubitsky YA (1996) Patent WO 98/22486
57. Hlatky GG (2000) Chem Rev 100:1347
58. Severn JR, Chadwick JC, Duchateau R, Friederichs N (2005) Chem Rev 105:4073
59. Welborn HC (1985) Patent EP 206794 B2
60. Fink G, Steinmetz B, Zechlin J, Przybyla C, Tesche B (2000) Chem Rev 100:1377
61. Alexiadis A, Andres C, Ferrari D, Korber F, Hauschild K, Bochmann M, Fink G (2004) Macromol Mater Eng 289:457
62. Ewen JA, Welborn HC (1983) Patent EP 129,368 B2
63. Total Petrochemicals (2010) Lumicene. http://www.totalrefiningchemicals.com/EN/aboutus/products_markets/Pages/Lumicene.aspx. Accessed 27 March 2013
64. Lyondellbasell (2008) Metocene PP technology. http://www.lyondellbasell.com/Technology/LicensedTechnologies/Metocene/. Accessed 27 March 2013
65. Novolen Technology (2009) Metallocenes. http://www.novolentechnology.com/catalyst/metallocenes.html. Accessed 27 March 2013
66. Brintzinger HH (2007) Rend Fis Acc Lincei 18:257
67. Pasquini N (2005) In: Pasquini N (ed) Polypropylene handbook. Hanser, Munich, p 506
68. Resconi L, Camurati I, Malizia F (2006) Macromol Chem Phys 207:2257
69. Resconi L, Fritze C (2005) In: Pasquini N (ed) Polypropylene handbook. Hanser, Munich, p 107
70. Schottek J, Oberhoff M, Bingel C, Fischer D, Weiss H, Winter A, Fraaije V (2002) World Pat Appl WO 02/02575
71. Basell Service Company B.V. (2008) Products. https://polymers.lyondellbasell.com/portal/binary/com.vignette.vps.basell.BasellFileServlet?parentId=bf24bb0ed4995110VgnVCM100000646f3c14RCRD&childId=en&rel=vignette-mgmt-user-BASTBROCHURE&keyAttr=BAS-TTEXT-LANGUAGEID&docAttr=BASTBROCHURE-DOCUMENT. Accessed 21 April 2013
72. Schütz B, Konrad R (2005) In: Cooper E (ed) Business briefings 2005: medical device manufacture and technology. Business Briefings, London, pp. 1–4, 39–41
73. Kaminsky W, Bark A, Brekner HJ (1988) Patent DE 3,835,044 A1
74. Kaminsky W, Bark A, Arndt M (1991) Makromol Chem Macromol Symp 47:83
75. Arndt M, Beulich I (1998) Macromol Chem Phys 199:1221
76. Ruchatz D, Fink G (1998) Macromolecules 31:4684
77. Shin JY, Park JY, Liu C, He J, Kim SC (2005) Pure Appl Chem 77:801
78. TOPAS Advanced Polymers (2012) TOPAS COC Polymers. http://www.topas.com/products/topas-coc-polymers. Accessed 22 April 2013
79. Mitsui Chemicals America (2013) APEL Cyclo olefin copolymer (COC). http://www.mitsuichemicals.com/apel_prop.htm. Accessed 27 March 2013
80. Stevens JC, Neithamer DR (1989) Patent EP 418,044 B2
81. Braunschweig H, Breitling FM (2006) Coord Chem Rev 250:2691
82. LyondellBasell (2009) New single-site catalyst boosts process performance of LyondellBasell's Metocene PP technology. http://lyondellbasell.mediaroom.com/index.php?s=43&item=678. Accessed 27 March 2013
83. Winter A (2004) The new MCC catalyst generations. In: Proceedings Maack PP 2004 congress, Zürich. Maack Business Services, Zurich

Adv Polym Sci (2013) 258: 43–116
DOI: 10.1007/12_2013_220

Published online: 26 September 2013

Syndiotactic Polypropylene: Discovery, Development, and Industrialization via Bridged Metallocene Catalysts

Abbas Razavi

Abstract This chapter covers the discovery that enabled, for the first time, the manufacturing of high molecular weight, highly stereoregular syndiotactic polypropylene polymers with narrow molecular weight distribution via the new class of metallocene molecules with bridged cyclopentadienyl-fluorenyl ligands. First, the salient crystal structural features of the neutral metallocene molecules and the crystal structure of the corresponding mono-alkyl-zirconocenium cation is introduced. Then, by employing the structural and geometrical data, a realistic working model for the active site precursor is developed and presented. The stereochemistry of the catalytic propylene poly-insertion reaction and the formation of syndiotactic polypropylene according to the enantiomorphic site control mechanism at the enantiotopic cationic active sites, formed after the activation of the prochiral metallocene dichloride with methylaluminoxane, MAO, is reviewed and further delineated. In the following sections, the impact of the introduction of substituents with proper size and composition at some selected positions of the ligand is discussed and the methods for increasing the molecular weight and stereoregularity of syndiotactic polypropylene polymers are elaborated. With the aid of computational calculations on real and hypothetical catalyst systems with substitutionally altered ligand structures, it is shown that the degree of enantioselectivity of syndiospecific catalyst systems can be determined and/or predicted for these systems quantitatively and with high precision. The calculations confirm that the introduction of substituent(s) reinforcing the preferential conformational orientation of the polymer chain enhances the overall enantioselectivity of the active site, and to certain extends stereoselectivity in general, by affecting the site epimerization processes. The computational calculations reveal that to account correctly for the frequency of the site epimerization-dependent m-type stereo-errors it is essential to include the counter-ion, as an integrated part of the

A. Razavi (✉)
35 Domaine de la Brisee, 7034 Obourg, Belgium
e-mail: abbasrazavi@skynet.be

catalyst system, into the calculations. The relevance of the symmetry and stereorigidity of the metallocene structure for the syndiospecificity of the final catalyst is debated by presenting a few "non-conforming" catalyst examples.

Finally, the challenges involved in the manufacture of syndiotactic polypropylene in commercial scale continuous production processes are highlighted as well as the polymer's unique structural, physical, mechanical and rheological properties.

Keywords Counter-anion effects · C_s symmetric zirconocene catalyst · Enantioselectivity · Enantiomeric mis-insertion · Heterogenization · Site epimerization · Syndiotactic polypropylene

Contents

1 Introduction

Syndiotactic polypropylene was first isolated by Natta and coworkers as a minor by-product of an isotactic polypropylene (i-PP) produced with a $TiCl_3$-based Ziegler–Natta (ZN) catalyst, $TiCl_3/Et_2AlCl$ [1–9]. The nature of the active sites and the mechanism of formation of this polymer (discovered more than half a century ago) are not very well known and still a matter of much debate. It is, however, believed that they are formed on catalytic sites with C_2 symmetry and of low chlorine coordination (Fig. 1) via a chain-end controlled mechanism. Later, Zambelli and coworkers produced syndiotactic polypropylene (s-PP) directly, at subzero polymerization temperatures, using a vanadium-based catalyst. In this case, more is known about the nature of the active site (Fig. 1) and the mechanism of the polymerization has been elucidated satisfactorily [10–17]. It is assumed that the polymer chains are formed at low temperatures at the homogeneous active sites according to a mechanism that is controlled by the chirality of the last inserted monomer unit located at the metal-end of the growing polymer chain. No single-crystal X-ray structure of the catalyst precursor is available due to the very temperature-sensitive nature of the catalytic species and its precursor.

After discovery of the bridged cyclopentadienyl-fluorenyl metallocene-based syndiotactic-specific catalyst systems and the resulting s-PP polymers [18–27] it was possible for the first time to make ever more accurate statements about the nature of the syndiospecific active site and the mechanism of the polymerization of these fascinating yet very complex systems. By studying the available X-ray structural data of the metallocene molecules and their stabilized alkylmetallocenium cation [19–21] (as the immediate active site precursor), it has become possible to make reasonable deductions on the nature of the active sites and their mode of functioning during the different stages of the polymerization, i.e., monomer coordination, activation, insertion, and propagation. On the other hand, the facile availability of large syndiotactic polymer samples, prepared at different and precise polymerization temperatures/conditions, and statistical analysis of the data extracted from their high-resolution ^{13}C NMR spectra, provided the means for accurate statements on the mechanism of the polymerization and the relationship between catalyst structure and polymer microstructure. The bridged cyclopentadienyl-fluorenyl ligand-based metallocene structure proved to be a very versatile precatalyst system. Depending on the substitutional modifications performed on different parts of the organic ligand, the bridge,

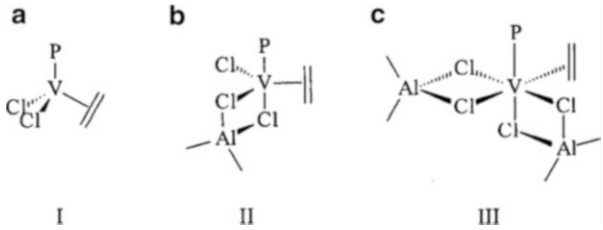

Fig. 1 (**a**–**c**) Zambelli's models (*I*–*III*) for hypothetical active sites in VCl_4-based catalysts

fluorenyl, and/or cylopentadienyl moieties it is possible to create new catalysts systems that can produce s-PP polymers with increased molecular weights, stereoregularities, and melting points. The ligand modifications can bring about, in certain cases, even a change in the tactic behavior of the resulting catalysts, leading to the development of a whole range of new polypropylene macromolecules whose chain tacticities include hemi-isotactic and stereoblock in addition to syndiotactic and isotactic [28–34].

2 Bridged Cyclopentadienyl-Fluorenyl Metallocene Molecules

In late 1987, a simple coupling reaction between the reagent 6,6-dimethylfuvene and the fluorenyl anion in tetrahydrofuran (THF) led to the formation of 2-cyclopentadienyl-2-fluorenyl-propane, a new bi-functional ligand whose double deprotonation with an alkyl lithium, and subsequent reaction with MCl_4 (M = Zr, Hf) resulted in the successful synthesis of two bridged metallocene molecules, (η^5-C_5H_4-μ-CMe_2-η^5-$C_{13}H_8$) MCl_2, where M = Zr (**1**) or M = Hf (**2**). Complexes **1** and **2**, after their activation with methylaluminoxane (MAO), become very active catalysts for olefin polymerization. More importantly, they promote the catalytic polymerization of propylene to highly syndiotactic polypropylene. Complexes **1** and **2** have been characterized by single-crystal X-ray diffraction methods and NMR spectroscopy [19, 20]. Figure 2 presents two different perspective views of the molecular structures of **1** and **2** as determined by single-crystal X-ray diffraction. The structural characteristics of these two complexes were discussed at length soon after their discovery in a series of publications [18–27, 28–34]. However, some of the prominent structural features that are relevant to their catalytic performance with respect to stereoselective propylene polymerization are reiterated here with an emphasis on the zirconium-based complex **1** as an example.

The fact that the metallocene complexes **1** and **2** are active for olefin polymerization was, of course, of no surprise; Kaminsky and Sinn had discovered in the mid-1970s that MAO obtained from partial hydrolysis of tri-methylaluminum (TMA) could activate metallocene dichloride complexes to very efficient olefin

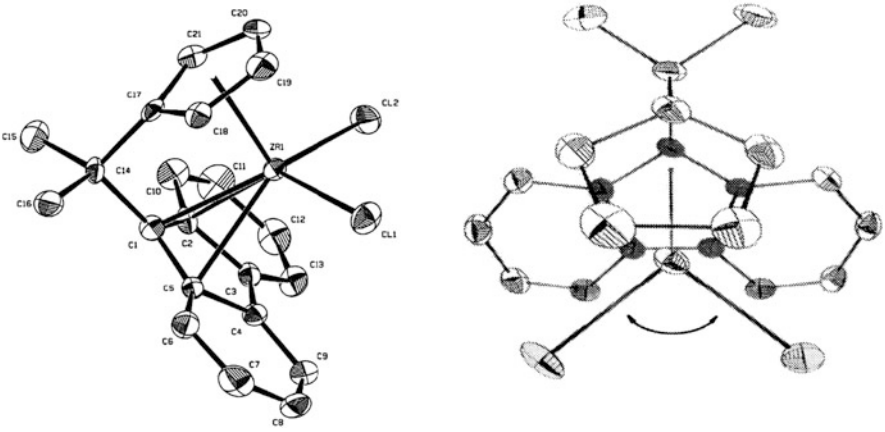

Fig. 2 Side (*left*) and top (*right*) views of the molecular structure of **(η^5-C_5H_4-μ-CMe_2-η^5-$C_{13}H_8$)MCl_2**; M = Zr (**1**), M = Hf (**2**)

polymerization catalysts [35–42]. The rationalization of the activation processes of the metallocene complexes with MAO and the mechanistic aspects of the their olefin polymerization (such as monomer coordination, activation, insertion, propagation, and possible pathways for chain termination) were in many ways identical or very similar, except for minor details, to catalyst systems that were discovered by Ziegler and Natta in 1953. Also, the fact that homotopic metallocene/MAO catalysts polymerize propylene to stereoregular crystalline polypropylene was already known. In the mid-1980s, after the discovery of the bridged chiral *ansa*-bis-indenyl metallocene complexes [43–45], it was shown, in a series of polymerization tests, that MAO activation of C_2 symmetric chirotopic bis-indenyl-based metallocene complexes very efficiently promotes the isospecific polymerization of propylene to highly stereoregular i-PP [46–55]. In this case, the rationalization for the nature and behavior of catalytically active species and the formation of i-PP was again very similar to the activation processes and mechanistic routes that had been proposed, and generally accepted, for stereospecific polymerization of propylene with heterogeneous ZN catalyst systems [56–63]. The polymerization mechanism involving the face-selective coordination of propylene, its activation, insertion, and stereoselective propagation at a C_2 symmetric active metal center could satisfactorily explain the formation of i-PP with these metallocene-based catalysts according to the same mechanism, and in a similar way, as proposed much earlier for the heterogeneous titanium trichloride-based ZN catalyst systems. With the exception of some minor differences, the enantio- and stereoselectivity as well as regioselectivity of the poly-insertion reaction and chain termination path ways were very similar to those processes that had been proposed for heterogeneous ZN catalysts [64–76].

What was unprecedented in the polymerization behavior of the newly discovered catalyst systems, however, was the fact that an initially nonchiral metallocene

(prochiral!) molecule, after activation with MAO, could provide an enantiotopically chiral catalyst that could produce a crystalline polypropylene with syndiotactic chain architecture according to a new mechanism that follows, in a rhythmic alternation, the *si*/*re* prochiral face-selective coordination and insertion of propylene molecules at its two available enantiotopic coordination positions.

To understand the functioning mode of this catalyst system and the mechanistic aspects of the stereochemical events involved in the formation of s-PP chains, it is very important to first examine more closely the molecular structure and structural characteristics of the complex **1** (and/or **2**). The structural data can be then correlated to the information gleaned from different polymer analyses in order to determine the polymerization mechanism and the elementary steps involved in the formation of s-PP chains on the basis of the well-established principle of catalyst structure–polypropylene chain microstructure interrelationship.

2.1 *Molecular Structure of Isopropylidene(cyclopentadienyl-fluorenyl)MCl_2 (M = Zr, Hf): Bonding and Symmetry*

Two different views of the molecular structures of the metallocene complexes isopropylidene(cyclopentadienyl-fluorenyl)MCl_2, where M = Zr (**1**) or Hf (**2**), are depicted in Fig. 2. As evident from the molecular views presented in Fig. 2, the stereorigid metallocene molecule **1** (and **2**) possess, in the solid state, a bilateral symmetry (or a plane of symmetry, σ_v). Consequently, the left and right halves of the molecule, if bisected by the imaginary symmetry plane, would be mirror image related. Apart from this global observation, detailed examination of the structural data, particularly those concerning the Zr–C and C–C bond distances, reveals the following facts. Despite the presence of a relatively short bridge (basically a carbon atom) as the inter-annular tie between the two aromatic ring systems (the cyclopentadienyl and fluorenyl centroids), the bonding relationship of these rings to the zirconium metal is very strong and of a η^5 nature. The thermal stability of **1** (and **2**) also favors the notion of a doubly η^5-bonded centroid–M–centroid molecular structure. The observed variation in the bond distances with a progressive increase in the $Zr–C_{flu}$ bond distances from the bridge-head carbon to the proximal carbons, extending to the distal carbons, is believed to be caused by the nonbonding repulsive steric interaction between the two σ-bonded chloride ligands and the distal C–H groups of the two six-membered rings of the fluorenyl section [19]. Similar reasoning applies to the $Zr–C_{cp}$ bond distance variation due to different carbon atoms in the cyclopentadienyl moiety. The Zr–C bond distance lengthening, on average about 0.2 Å, due to nonbonded contact and repulsive interaction between the σ-ligands and the distal C–H groups of both aromatic systems is of prime importance for the stereoselectivity and the degree of enantioselectivity of the resulting catalysts (Sect. 2.4). The distal parts of cyclopentadienyl and fluorenyl moieties of the ligand are positioned exactly above and below the two

chloride groups, occupying the prospective coordination sites designated for future monomer coordination and polymer chain growth. By interacting with their substituents, they regulate and direct the orientation of the growing polymer chain, determine the *re* or *si* selective coordination of propylene, and govern the whole scenery of the stereospecific polymerization process.

For future discussions, it is also important to know that the fluorenyl–Zr–cyclopentadienyl bond angle in the zirconium complex **1** is 118.6° (119.4° for hafnium complex **2**) and deviates by about 10° from the ideal tetrahedral angle of 109.5° (tetrahedral formed around the bridging carbon and the bonds with its four substituents, two methyl groups plus fluorenyl and cyclopentadienyl groups) and a Cl–Zr–Cl bond angle of 98.2° (Cl–Hf–Cl = 97.5°).

2.2 *Crystal Structure of the Metallocenium–Monoalkyl Cation and the Structure of the Putative Active Site*

Before the discovery of the metallocene-based syndiospecific catalyst system there existed, thanks to intensive investigations by several research groups worldwide, sufficient evidence to assume that the active species involved in metallocene-based olefin polymerization catalysis are cationic in nature [77–96]. It is now widely accepted that the active site species are cationic metallocenium–monoalkyl complexes. They are formed generally during the activation step(s) when the catalyst precursor, the metallocene dichloride, is treated with the alkyl-aluminum co-catalysts/activators in a "two-step" alkylation and alkyl abstraction reaction (in reality the alkylation process comprises a rather complex multi-step halide/alkyl exchange with reversible and nonreversible reactions and side reactions leading to the final cationic species and some unspecified nonreactive or dormant species. See also [97] and the quoted references). Therefore it is reasonable to assume that similar cationic species are being formed during the activation stages of **1** (and **2**)/MAO catalyst systems with MAO or other alkylating, ionizing agents.

It was recognized that for mechanistic elucidation of the elementary steps involved in stereospecific propylene polymerization catalysis with **1** (and **2**)/MAO, access to the molecular structure of the corresponding zirconocenium–methyl cation of complex **1** would be very useful. Its molecular structure and X-ray determined interatomic parameters could help to design a practical and realistic model for the hypothetical active site at which the actual syndiospecific polymerization of propylene is actually taking place. The geometrical data for the cationic complex allow better visualization and insight into the immediate stereo-electronic environment of the hypothetical active site, and elaboration of its functioning.

The metallocenium complex **3**, $[(\eta^5\text{-}C_5H_4\text{-}\mu\text{-}CMe_2\text{-}\eta^5\text{-}C_{13}H_8)Zr^+Me][B(C_6F_5)_4]^-$, is prepared via the double methylation of complex **1** and the subsequent reaction of the di-methylated reaction product with an equivalent of the reagent trityl-tetrakis-pentaflurophenylborate, $(C_6H_5)_3C\text{-}B(C_6F_5)_4$, in toluene at room temperature.

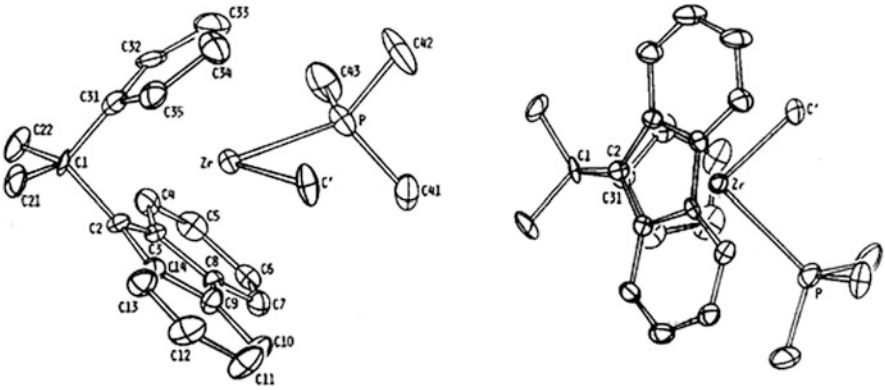

Fig. 3 Two different views of the molecular structure of $[(\eta^5\text{-}C_5H_4\text{-}\mu\text{-}CMe_2\text{-}\eta^5\text{-}C_{13}H_8)Zr^+Me(PMe)_3][^-B(C_6F_5)_4]$ as determined by X-ray single-crystal analysis. The anion is omitted for the sake of clarity

As expected, complex **3** is very active for catalytic polymerization of propylene to s-PP, and the microstructures and molecular weights of the s-PP polymers it produces are very close to the properties of syndiotactic polymers obtained with the complex **1**/MAO catalyst system, prepared under the same polymerization condition. All attempts to isolate the polymerization active cationic reaction intermediate, $[(\eta^5\text{-}C_5H_4\text{-}\mu\text{-}CMe_2\text{-}\eta^5\text{-}C_{13}H_8)Zr^+Me][B(C_6F_5)_4]$, in crystalline form for X-ray structure determination failed. However, it could be isolated, in its stabilized form, after the addition of one equivalent of the reagent tri-methyl-phosphine, PMe_3, to a solution of the catalytically active complex **3** in toluene. The resulting dark purple reaction product, complex **4**, $[(\eta^5\text{-}C_5H_4\text{-}\mu\text{-}CMe_2\text{-}\eta^5\text{-}C_{13}H_8)Zr^+Me(PMe_3)][^-B(C_6F_5)_4]$ could be crystallized out of the solution and was isolated in pure form and identified by its ^1H NMR spectrum and single-crystal X-ray structure determination [21] (see Fig. 3).

The general feature of the crystal structure of complex **4** is very similar to that of the X-ray structure of complex **1** (or **2**). The centroid–Zr–centroid bonds are η^5 in nature and, as for similar metallocene having a $C_5H_4CR_2C_{13}H_8$ ligand, the least squares planes defined by the two C_5 fragments in **4** are inclined towards the zirconium atom with respect to the C1–C2 and C1–C31 vectors (see Fig. 3 left). The effect is more pronounced for the cyclopentadienyl ring than for the fluorenyl group, with inclination angles of 15.5° and 11.8°, respectively. A noteworthy feature of this structure is the unusually small Me–Zr–PMe_3 angle of 88.4°. An α-agostic Zr–H–C interaction (vide infra) could be responsible for this phenomenon by forcing the Zr–C bond to move closer to the Zr–P bond. However, we have no experimental evidence for this, except the fact that the H–Zr distance for one of the three methyl hydrides seems to be spatially shorter than the other two H–Zr distances [21].

Table 1 Polymerization conditions and results with (**1** and **2**)/MAO

Metal	Temperature (°C)	Activity (kg/g)	M_w (×1,000)	rrrr (%)
Zr	60	180	90	82
Zr	40	120	138	86
Hf	60	2.7	778	73
Hf	40	0.2	1,322	64

Polymerization conditions: 1 L liquid propylene; 5 mL MAO (11 wt% in toluene); 60 min

Table 2 Presentation of the relevant ^{13}C NMR normalized spectroscopic stereo-sequence distributions (%) for syndiotactic polypropylene samples produced with (**1** and **2**)/MAO at different temperatures

Metal	Temperature (°C)	rrrr (%)	rrmr (%)	rmmr (%)	mmmm (%)
Zr	60	82	2.70	1.65	0
Zr	40	86	1.15	1.55	0
Hf	60	73	7.20	3.80	0.5
Hf	40	64	10.50	3.50	1.8

2.3 *Polymerization Behavior of 1/MAO and 2/MAO Catalyst Systems*

As mentioned above, the activation of the metallocene dichlorides **1** and **2** with MAO provides very efficient catalysts for polymerization of propylene to high molecular weight, highly crystalline s-PP polymers. Detailed propylene polymerization conditions, results, and polymer analysis with **1** and **2**/MAO catalyst systems are presented in Tables 1 and 2. Inspection of the data presented in Table 1 reveals, aside from the fact that all the produced polypropylene polymer samples are syndiotactic in nature (apparent from the large rrrr pentads), other important information.

The molecular weights (M_w) of s-PP polymers produced with **2**/MAO are much higher than those of the corresponding polymers produced with **1**/MAO, and the molecular weights of all the s-PP polymers produced with either one of the two catalysts systems decrease with increasing polymerization temperature. On the other hand, the polymers produced with **1**/MAO are much more stereoregular than the corresponding polymers produced with **2**/MAO. And, finally, for both (**1** and **2**)/MAO catalyst systems, the catalysts' stereoselectivity decreases with increasing polymerization temperature. The methyl region of the ^{13}C NMR spectra of the s-PP polymers produced with (**1** and **2**)/MAO at 60°C are depicted in Fig. 4. On the left hand side of the figure is shown the ^{13}C NMR spectrum of the s-PP produced with the Zr-based catalyst and on the right hand side of Fig. 4 is the ^{13}C NMR spectrum corresponding to the s-PP produced with Hf-based catalyst. The ^{13}C NMR spectra reveal that the basic architectures of the two sets of polymers are basically the same (steric pentads, chemical shifts) [19]. It can be seen pictorially from these spectra that the polymer produced with (**1** and **2**)/MAO catalysts systems are highly syndiotactic, as evident from the predominant rrrr pentads signals with the chemical shift at 20.15 ppm. They represent long uninterrupted syndiotactic sequences of *racemic*

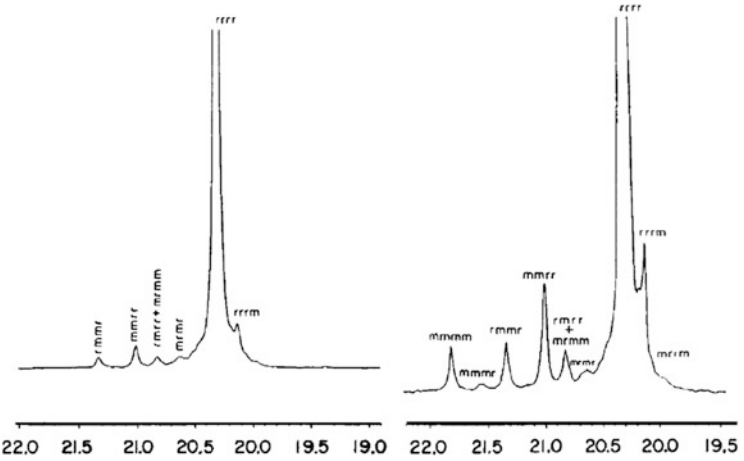

Fig. 4 The methyl region of ^{13}C NMR spectra of syndiotactic polypropylene produced with Zr- (*left*) and Hf-based (*right*) metallocene catalysts. The chemical shift scale is recorded in ppm downfield from tetramethylsilane signal with a 300 MHz spectrometer

dyads, r, in the backbone of the individual polymer chains. The ^{13}C NMR spectra also reveal the appearance of other small signals characteristic for stereodefects in the backbone syndiotactic polymer chains due to occasional errors made by the catalyst during the propylene enchainment process. The s-PP polymers produced with Zr-based catalyst have all the basic finger print microstructure . . .rrrrrrrrmmrrrrrrrmrrrrrrr. . .. The mm and m units seen in the backbone of the chain are the so-called isotactic *meso* triad and isotactic *meso* dyad characteristic stereo-defects ubiquitous in all s-PP chains produced with enantiotopic metallocene catalysts. The corresponding, less stereoregular, Hf-based s-PP polymer's microstructure . . .rrrrrrmmrrrrrrmrrrrmmmmrrr. . . exhibits, in addition to the two mentioned mm and m stereodefects, about 1.8% of short sequences of isotactic pentads, mmmm, centered at 21.65 ppm of the ^{13}C NMR spectrum (see Fig. 4, right spectrum, and Table 2). Table 2 presents the microtacticity variations in the s-PP chains occurring with the changes in polymerization temperature. As the stereoselectivity decreases with increasing polymerization temperature, so does the rrrr pentad concentration, due to the simultaneous increase in stereodefects in the related pentads, rmmr and rrmr. However, whereas the increase in rmmr stereodefect related pentads is very moderate to negligible, the rrmr stereo-defect related pentads increase much faster with increasing polymerization temperature for s-PPs produced with both catalyst systems. For polymers produced with the Zr-based **1**/MAO catalyst system they more than double for every 20°C increase in the polymerization temperature.

In spite of their almost identical structures [19], catalyst systems prepared with complexes **1**/MAO and **2**/MAO, show substantial differences in their catalytic behavior and polymerization performance. The mechanism of propylene polymerization with (**1** and **2**)/MAO catalyst systems will be discussed further in some length. For now, it should be just mentioned that since the polymerization proceeds

in both cases according to the same basic mechanism and they both produce similar s-PP chains, it could be reasonably assumed that the even the isotactic stereodefects (mmmm) in the backbone of polymer chains formed with (**1** and **2**)/MAO catalyst systems are also generated following the same basic mechanism, operating only with slightly less efficiency in the case of **2**/MAO. As for the substantial differences related to the activities of the two catalysts and molecular weights of their polymers, different kinetic behavior for **1**/MAO and **2**/MAO catalyst systems is suspected.

2.4 Mechanism of Syndiospecific Polymerization

In order to describe correctly the mechanism of the syndiospecific polymerization with (**1** and **2**)/MAO catalyst systems, as mentioned before, access to a realistic model representing the active site is of utmost importance. The information extracted from the molecular structures of complexes **1** and **4** provides all necessary elements required to construct such a "realistic" active site model. From the discussion in Sects. 2.1 and 2.2, it can be reasonably assumed that the structure of the actual active centers, at least during the π-complex formation, are very similar and close to the structures of complex **4** depicted in Fig. 3. All is needed is to imagine the PMe_3 molecule as removed and replaced by a propylene molecule. In this form, it can be used to describe the different stereochemical events, step by step, during different stages of polymerization, activation, monomer selection/coordination, monomer insertion, chain propagation and chain termination responsible for the formation of s-PP with the microstructure ...rrrrrrmmrrrrmrrr... with complex **1**/MAO:

1. The stereorigid bridged metallocene dichloride **1**, as depicted in Fig. 2, is a prochiral molecule and possesses bilateral symmetry. The activation of metallocene dichloride **1** leads to the formation of enantiomeric metallocenium–monoalkyl cationic species that are both electron-deficient and coordinatively unsaturated and structurally very similar to the enantiomeric molecule depicted in Fig. 3. These enantiomeric metallocenium–monoalkyl species have the necessary vacant coordination position and energetically low lying, accessible empty fragment orbitals to be used for coordination and activation of incoming propylene molecules via interaction with their available π orbitals.
2. The cationic metallocenium–monoalkyl species [21] are composed of equal numbers of *R* and *S* mirror-image related enantiomers and have monomer *re*/*si* π-face selective properties (Fig. 5).
3. The *re* or *si* face-selectivity is induced by the unique steric arrangement of the chelating ancillary ligand engulfing the resident chiral transition metal center via a delicately balanced, cooperative and nonbonded steric interactions between different parts of the "active" catalytic species, ligand, polymer chain, and coordinating monomer. The nonbonded steric interactions govern the whole scenery of the syndiospecific polymerization process during all its individual steps.

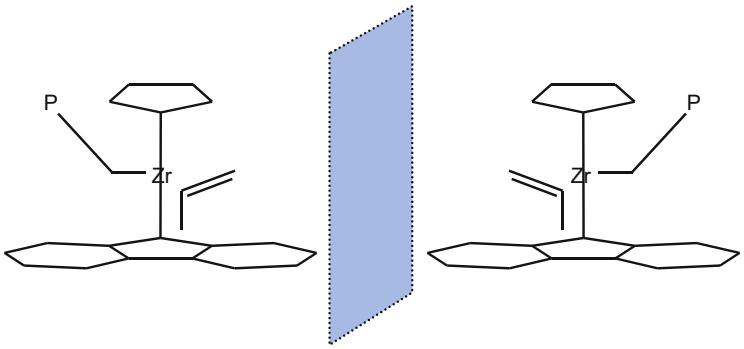

Fig. 5 The hypothetical *re*/*si* propylene face-selective *R* and *S* enantiomeric active species formed after activation of the metallocene molecule

4. Since according to this mechanism each enantiomer *R* or *S*, independently, would produce isotactic chains, and yet exclusively syndiotactic polymer chains are formed, it has to be concluded that the active enantiomeric species "enantiomerize" via an intramolecular mechanism and interconvert individually after each monomer insertion.
5. The systematic transformation of the *R* and *S* antipodes into one another implies that the relative positions of at least two of the four ligands or ligand moieties surrounding the transition metal center must be changed systematically.
6. Since the η^5-bonded aromatic ligands are tied together by a structural bridge and their rearrangement is impossible and excluded, such a reversible interconversion can take place only when the alkyl group (polymer chain) and the coordinating monomer exchange their positions uninterruptedly and systematically after each insertion; i.e., chain migratory insertion! [64–76].
7. The *meso* triad-based, enantiomorphic site control type of stereochemical errors, mm, are formed whenever the said balanced nonbonded steric interaction is perturbed, and the correct alignment of the substituents of the three main participants (ligand, polymer chain and monomer) is not materialized perfectly. In such a case, a monomer with "wrong face" is inserted and a unit with inverted configuration is enchained. The ability of occasional reverse face selectivity emanates from the inherent structural factors of the metallocene-based catalyst. It is independent of monomer concentration and counter-ion pairing nature; however, it is dependent on polymerization temperature.
8. The *meso* dyad-based stereo-errors, m, arise from occasional back migration of the polymer chain before the insertion of the next monomer unit. As a consequence of this active site epimerization (see Fig. 6), a double monomer insertion at the same enantiotopic coordination site will takes place and units of two monomers with identical stereogenic centers (m) are enchained (vide infra).

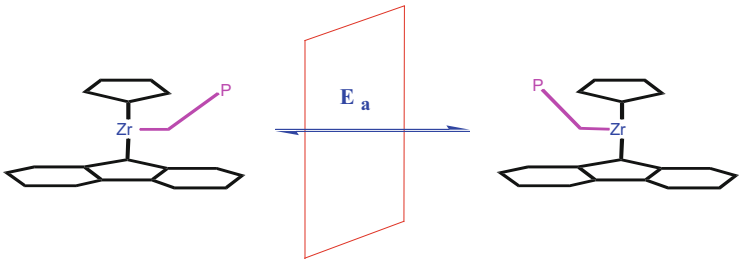

Fig. 6 Representation of the endothermic active site epimerization (chain migration without insertion) process. E_a activation energy

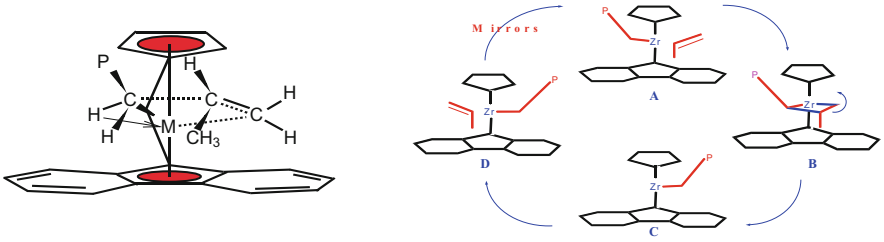

Fig. 7 The syndiospecific transition state structure (*left*). Representation of the syndio-insertion catalytic cycle (*right*); the bridge is omitted for the sake of clarity. (*A*) Large substituted cyclopentadienyl group, the fluorenyl group, and a smaller unsubstituted cyclopentadienyl group are tied together by an isopropylidene bridge. (*B*) Steric interaction with the fluorenyl ligand forces the growing polymer chain to orientate towards the free space left or right of the unsubstituted cyclopentadienyl moiety. (*C*) Trioordinated polymeryl-Zironocenium cation. (*D*) Incoming monomer orients itself with its methyl group *trans* to the growing polymer chain

2.5 *Syndiospecific Transition State Structure and Syndio-Insertion Catalytic Cycle*

To delineate how these many factors operate in a concerted manner to provide the necessary and sufficient conditions for the syndiospecificity of the catalytic site created with complex **1**, we can now employ the constructed molecular model to devise a transition state structure that explains in a plausible manner the behavior of this very complex system and the important steps involved in the catalytic cycles.

Figure 7 (left) represents the hypothetical active site transition state structure for syndiospecific polymerization of propylene to polypropylene. The model is constructed on the basis of data obtained from the X-ray structure of complex **1** and **4**; it is further refined to include an α-agostic bond between the transition metal and the alky group, representing the growing polymer chain, and a coordinated propylene monomer. On the right-hand side of Fig. 7 a syndioselective insertion cycle is shown involving the cationic active site and a migratory inserting polymer chain. The hypothetical transition state geometry reveals the relative importance of

the nonbonded steric interactions operating on different parts of the catalytic species and on the polymerization active participants, the aromatic ligand, the polymer chain, and the coordinating monomer in the following order. The organic ligand consists of a large substituted cyclopentadienyl group, the fluorenyl group, and a smaller, sterically less challenging, unsubstituted cyclopentadienyl group tied together with an isopropylidene bridge. The steric interaction between the flat and spatially extended fluorenyl ligand forces the growing polymer chain, during the polymerization, to adopt the conformation that permits its orientation towards the free space left (or right) of the unsubstituted cyclopentadienyl moiety of the ligand. The incoming monomer in turn (to avoid an excessive repulsive steric exposure) orients itself in a manner such that its methyl group is "trans" positioned with respect to the growing polymer chain (alkyl group).

The system thus reaches its minimum energy during the formation of the metalacyclobutane transition state. In this coordination mode, the coordinated monomer points with its methyl group head-down into the empty space in the central region of the fluorenyl ligand with little or no direct interaction with the ligand. The importance of the "head-down" orientation of the monomer with respect to the "upward" orientation of the chain during the π-complex formation and transition state was recognized and proposed early on after extensive molecular mechanics and force field calculations performed by Corradini and coworkers [64, 69, 71, 73–75]. The model underwent later additional refinement and took its current form after experiments conducted by several research groups supported the idea of the formation of an α-hydride agostic Zr bond assisting and stabilizing the chain conformation orientation in the metalacyclobutane transition state geometry, before the actual propylene insertion [98–106]. It implies that the insertion transition state relies on the formation of an α-agostic bond between either one of the two available hydrides on the last carbon (α-C) of the growing polymer chain and the transition metal center. This agnostic interaction provokes the rotation of the highly directional sp^3 orbital of the α carbon towards the π orbital of the 1,2-coordinated propylene monomer, allowing for larger orbital overlapping and contributing to the stabilization of the insertion transition state and thus affecting profoundly the stereochemistry of insertion; selection of one or the other α-hydride for agostic interaction could bring the growing polymer chain either into the congested quadrant of the ancillary ligand or its free quadrant left or right of the cyclopentadienyl group [99].

After insertion of the first monomer, the alkyl group (polymer chain), now enlarged by one monomer, is moved to the coordination side that has become vacant after the monomer insertion and is replaced itself by a new incoming propylene monomer presenting a different face. Thus, another cycle begins with another monomer face at the other enantiotopic coordination site (see Fig. 7, right). The systematic and repetitious cycles would then lead to the formation of polypropylene chains with alternatively inverted stereogenic centers. The systematic transformation of the two *S* and *R* enantiomorphic antipodes into one another, after each olefin insertion, ensures that the relative positions of the σ-and π-bonded ligands in the equatorial plane of the transition metal are exchanged and that monomers with

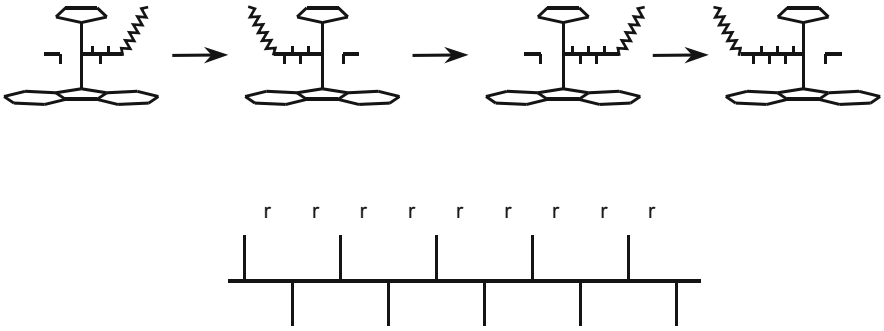

Fig. 8 Representation of mechanism of syndiospecific polymerization and formation of syndiotactic polypropylene (*top*). Fischer projection of a perfect syndiotactic chain sequence (*bottom*)

alternative faces are coordinated and inserted, resulting in the formation of sequences of monomer units with alternating relative configuration, i.e., formation of syndiotactic chains (Fig. 8).

The description involving an enantiotopic, cationic active species combined with the chain migratory insertion mechanism is perfectly fit to explain the formation of s-PP polymers. According to the scheme shown in Fig. 8, reproducing several catalytic cycles, the regularly alternating enantio-facial preference for the *re* and *si* prochiral faces of the monomer arises from the propylene insertion taking place at regularly alternating sides (enantiotopic coordination site) of the pseudo-tetrahedral geometry of the active site.

The working hypothesis, active site model, and the transition state structure discussed in the preceding paragraphs not only account for the syndiospecificity of the catalysts and formation of the s-PP chain but they also warrant the formation of microstructural chain defects or stereo-errors due to monomer misplacements in the backbone of the syndiotactic polymer chains, as shown pictorially in Fig. 9.

From the two types of stereo-errors, the *meso* triads (mm) and *meso* dyads (m), encountered in the backbone microstructure of the syndiotactic polymer chains, the formation mechanism of the so-called enantiomorphic site control type errors (mm) is straightforward and well understood. They could be produced at the step A (or D) in the cycle shown in Fig. 7 whenever the chain/monomer arrangement is not in *trans* mode configuration, and either the growing polymer chain or the propylene is mis-oriented with respect to the ligand and to each other (Fig. 9, top). These types of stereo-errors have been detected and were explained in connection with isotactic polymers prepared with the classical $TiCl_3$-based ZN catalyst systems [56–63, 64–76]. They are also ubiquitous in the backbone of the i-PP formed with isotactic-specific metallocene catalysts. Formation of the *meso* dyad (m) stereo-errors, unique to s-PP chains, are related to the epimerization of the active center and can take place in step C of the catalytic cycle (see Figs. 7 and 9) whenever the polymer chain migrates, without inserting a propylene monomer, to the other coordination position of the active site before arrival of the next propylene

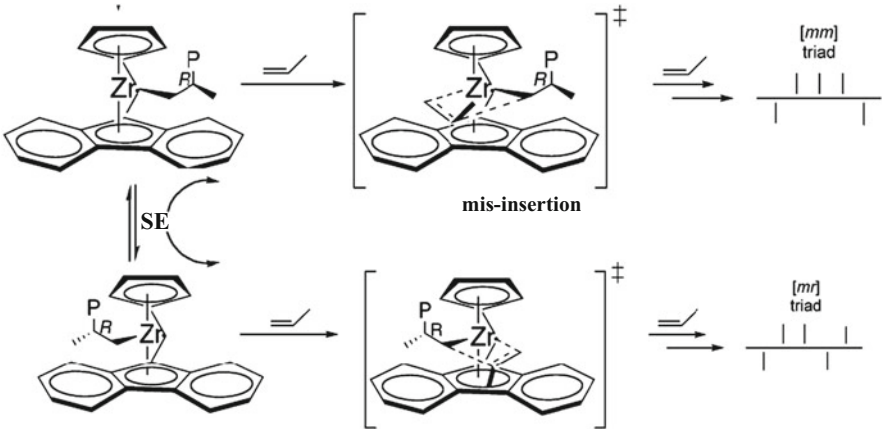

Fig. 9 Mechanisms of the enantiofacial mis-insertion and of the site epimerization (SE), and their corresponding signature pentad distributions

monomer. Their formation will be discussed in some detail later. The mechanism of the enantio-facial mis-insertion and site epimerization are presented more explicitly in Fig. 9 (bottom).

To summarize the above points, it can be generally stated that in order to form highly syndiotactic polypropylene chains with **1**/MAO or any other enantiotopic metallocene-based catalyst system, it is required that the chain assumes a dual responsibility. Whereas its "static" or steric interactions with the ligand and the monomer substituents are crucial for the degree of enantioselectivity, its dynamic behavior of regular and systematic, back and forth, migrations determine the frequency of site epimerization and the overall stereoselectivity. A "malfunctioning" of the latter leads to an increasing amount of m-type stereodefects and, in extreme cases, could even lead to a reversal of stereospecificity, from syndio- to isospecificity [28–34]. Whenever the chain plays both roles efficiently, the inherently enantiotopic catalyst produces s-PP with high stereoregularity. Its dysfunctioning in fulfilling one of these two roles can cause a lowering in the degree of enantio- or stereospecificity, leading to lower stereoregularity of the resulting s-PP.

3 Structural Modifications to Enhance the Syndiospecific Catalytic Performance

The s-PP samples produced with **1**/MAO catalyst system all have long enough chain lengths and high enough stereoregularities and melting points to provide polymeric materials with crystallinities and mechanical properties sufficient for general purpose applications. However, to enlarge the field of s-PP polymer resin applications for broader usage, it is necessary to further widen the range of melting points and molecular weights of the industrially produced s-PP polymers.

In order to increase the melting point of the semicrystalline s-PP polymers, it is necessary to increase the stereoregularity of the individual polymer chains. This in turn requires the suppression of the concentration of both types of stereodefects (m and mm) in the backbone of the polymer chains, whose combined numbers determine the crystallinity, melting point, and most of the physical properties, such as crystallization rate, optics, etc.

In the following sections, a few examples are presented as case studies to show how these substitutional modifications are realized and in what way they bring about the desired improvements. The discussion starts with the topic of modification of the bridge and bridge substituents to increase the syndiotactic polymer's molecular weight. We continues with the subject of structural modifications for improving the stereoselectivity of the catalyst and the stereoregularity of the resulting s-PP.

Before entering the discussions, it should be noted from the onset that there exist only limited options for substitutional modifications with the aim of increasing molecular weight and/or improving the enantioselectivity of the **1**/MAO catalyst system without tampering with its salient syndiospecific characteristics. Therefore, for these investigations, only limited substitution modification patterns have been selected that can bring about the desired improvement but otherwise leave the syndiotactic selective behavior of the system intact.

3.1 Modification of the Bridge and Syndiotactic Polymer Molecular Weight

The importance of the bridge in *ansa*-metallocene catalysts was recognized early on during the development of chiral metallocene catalysts for olefin polymerization [43–45]. Its existence is the prerequisite for stereorigidity of the metallocene structure, designed to prevent the free rotation of the aromatic ring(s) and to maintain the appropriate chirality of the corresponding cationic active species during the initial stages and the entire process of the polymerization. Later, it was recognized that the size of the bridge connecting the two aromatic rings could be additionally used as a regulating tool for modifying the active site's bite angle. For example, by replacing a one-carbon bridge such as $=CR_2$ with a two-carbon bridge like –RC–CR– or a silicon bridge like $=SiR_2$ it is possible to decrease the opening around, and control the monomer accessibility to, the transition metal center and thus influence the activity of the catalyst [107, 108, 109–112].

Based on a series of molecular mechanic calculations and polymerization experiments performed with a number of *ansa*-bis-(fluorenyl)zirconium dichloride complexes, Alt et al. [109–112] demonstrated that the size of the bridging unit plays an important role in the final catalytic activity of these complexes towards ethylene polymerization. A bigger bite angle, i.e., bigger opening around the active site, is supposed to increase the catalytic activity because of a less-hindered monomer

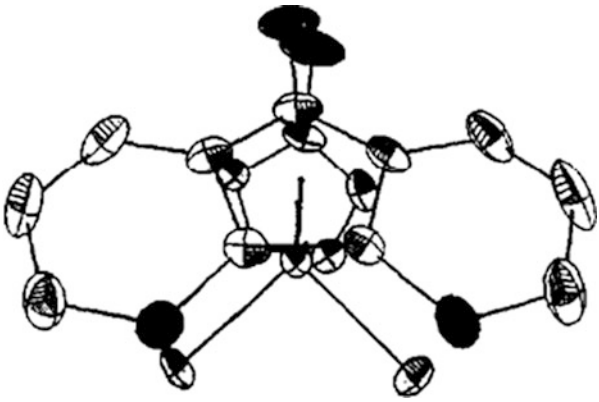

Fig. 10 Top view of the molecular structure of complex (η^5-C_5H_4-μ-Et-η^5-$C_{13}H_8$)$ZrCl_2$, **5**

approach as it passes through a wider entrance. However, the authors note that in addition to the "purely" steric effect, some degree of electronic influence has also to be taken into consideration to account for the overall change in catalyst behavior. Naturally, a large opening also translates into better incorporation of higher α-olefins and better comonomer incorporation in copolymerization reactions involving larger comonomers.

Little was known about the influence of the bridge and bridge substituent(s) on the catalytic performance with respect to the molecular weight of the resulting polymer until the advent of the syndiotactic-selective metallocene catalyst systems. The following two sections describe the modifications of the size and substituents of the inter-annular bridge in complex **1** and their impact on the catalytic performance and resulting s-PP.

3.2 Bridge Size Modification: 1,2-Ethano-Bridge Versus 2,2-Propano-Bridge

Syndiotactic-selective precatalyst complexes **1** and **2** have a ligand system in which the inter-annular bridge, connecting the two aromatic rings together, is the single carbon atom of the isopropylidene, or 2,2-dimethyl-propano group. It appeared intriguing to know what would be the effect on the polymerization behavior of the resulting catalyst of an increase in the number of carbon atoms of the bridge (i.e., an increase in the size) by one additional carbon atom. To answer this question, a review of the polymerization behavior of the complex [1,2-(cyclopentadienyl-fluorenyl)ethane]$ZrCl_2$, **5**, whose single-crystal X-ray structure is depicted in Fig. 10, is very helpful [34, 113]. As revealed by the molecular structure shown in Fig. 10, and similar to complex **1**, the molecule in complex **5** is prochiral and can be divided into two almost equivalent halves by a symmetry plane, σ_v, bisecting the Cl–Zr–Cl angle (only the two carbon atoms in the bridge lie on a skew line with respect to the mirror plane and are not symmetry related (cf. Fig. 10). Consequently,

Table 3 Polymerization conditions, results, and polymer analyses with 5

Temperature (°C)	Activity (kg/g)	M_w (×1,000)	MWD	rrrr (%)	Melting point (°C)
20	25	491	4.7	84.30	133
40	35	248	3.4	82.90	125
60	50	171	3.7	74.31	111
80	35	71	2.7	56.71	–

Polymerization conditions: 1 L liquid propylene, 10 mL MAO 10% in toluene

Table 4 Presentation of the relevant ^{13}C NMR normalized spectroscopic stereosequence distributions (%) for syndiotactic polypropylene samples produced with **5**/MAO at different polymerization temperatures

Temperature (°C)	rrrr (%)	rrrm (%)	rrmr (%)	rmmr (%)
20	84.30	4.15	4.62	1.63
40	82.90	5.95	4.29	1.98
60	74.31	8.94	6.91	2.48
80	56.71	13.54	13.49	2.91

the catalyst prepared from **5** and MAO bears close resemblance to **1**/MAO catalyst system and behaves accordingly by efficiently polymerizing propylene to s-PP after its activation.

The polymerization conditions, results, and polymer analyses for the **5**/MAO catalyst system and the corresponding s-PP polymers are presented in Tables 3 and 4. A comparison of the data listed in Tables 3 and 4 with the data listed in Tables 1 and 2 reveals that the catalyst derived from **5**/MAO produces, as expected, s-PP chains but with higher molecular weight (almost double in size). The data also show that the ethano-bridged catalyst system is less active and less stereoselective (cf. the percentage of rrrr, rmmr, and rrmr pentads!) than the corresponding propano-bridged catalyst system made with **1**/MAO, at all polymerization temperatures tested. Interestingly and surprisingly, all the polymers produced with **5**/MAO, particularly those produced at lower polymerization temperatures, exhibit broad molecular weight distribution (MWD, 4–5), which is very unusual for polymers produced with single-site catalysts. However, analysis of the methyl signal pattern and pentad intensity distributions obtained from the ^{13}C NMR spectra of syndiotactic polymers produced with **5**/MAO at different polymerization temperatures (see Table 4) show that they are, in general, architecturally and microstructurally very similar to the polymers produced with the **1**/MAO catalyst system [34, 113]. These macromolecules also exhibit all the chain microtacticity fine structures ...rrrrrrrrrmmrrrrmrrr... with two types of configurational defects; *meso* triad (mm) and *meso* dyad (m).

Table 4 presents the variation in steric pentad distributions with the polymerization temperature. The precipitous decrease in rrrr steric pentads concomitant with a rapid increase in rrmr pentad sequences and a moderate but noticeable increase in rmmr pentads with increasing polymerization temperature (particularly for the temperature range between 40°C and 60°C and higher) is also reminiscent of the microstructure–temperature interdependence of s-PP polymers formed with

1/MAO. It is an indication of a rampant site epimerization setting in faster and faster with increasing polymerization temperature. The concentrations of the site epimerization related rrmr pentads in the syndiotactic polymers produced with the **5**/MAO catalyst system have, however, almost triple the size of corresponding rrmr pentads found in polymers produced with **1**/MAO. The enantioselectivity related (rmmr) pentad concentrations in s-PP chains produced at the same polymerization temperature with both catalyst systems are less different in size and do not change as dramatically with the change in polymerization temperature, within the range tested (see data on related pentads in Table 4).

The observed general similarities in catalytic behavior between **5**/MAO and **1**/MAO catalyst systems corroborate the molecular structural resemblance of **1** and **5** but are in contradiction with the displayed discrepancies regarding larger polydispersity, higher molecular weight, and lower stereoregularity. The complete interpretation of the polymerization data can, however, be given in an elegant and convincing way, as least with respect to larger polydispersity, by close inspection of the single-crystal X-ray structure and associated data [34, 113] (similar results have been reported by Kim et al. [114]) and by inspecting more closely the impact of the bridge as the potential source of behavioral dissimilarity.

Let us first start the discussion with the polydispersity and focus on the reasons for a relatively large molecular weight distribution (up to 4.7) observed for s-PP polymers produced with **5**/MAO catalyst systems. It follows from the theory [115] that for polymers produced with single-site type catalysts the expected molecular weight distributions should have a value of 2. Accordingly, values of 2 (or close to 2) have been measured generally for all polymers produced in homogeneous olefin polymerization catalysis with activated metallocenes under controlled polymerization conditions. Large deviations from this value are generally indicative of the presence of diffusion phenomena or temperature variations during the polymerization process. In the absence of the said factors, broader molecular weight distribution reflect, unambiguously, the presence of more than one population of active species in the polymerization medium. Closer inspection of the crystal structure data for **5** confirms this fact and provides the clue for this apparently rather unusual phenomenon.

The in-depth examinations of the X-ray data for **5** by Atwood and colleagues [113] revealed that the unit cell of the crystalline lattice of **5** accommodates two types of molecules, i.e., two different conformers. The formation of two conformers arises from the fact that the ligand structure of complex **5** contains a two-carbon atom unit in its ethano-based bridge that has a fluxional character. The ethano ($–CH_2–CH_2–$) group can assume two different spatial arrangements with respect to the aromatic rings, being able to oscillate about the center of inertia lying mid-way between the two CH_2 groups. These arrangements give rise to two energetically identical, stable, but different conformers, δ and λ, whose structures are presented in Fig. 11. The two independent molecules populate equally the unit cells of the crystalline lattice in the solid state.

These conformers, as neutral molecules, interconvert very quickly in solution at room temperature and are indistinguishable (in a temperature range measured from −80°C to 90°C) in the ^{1}H NMR timescale [34]. The ^{1}H NMR spectrum of **5**

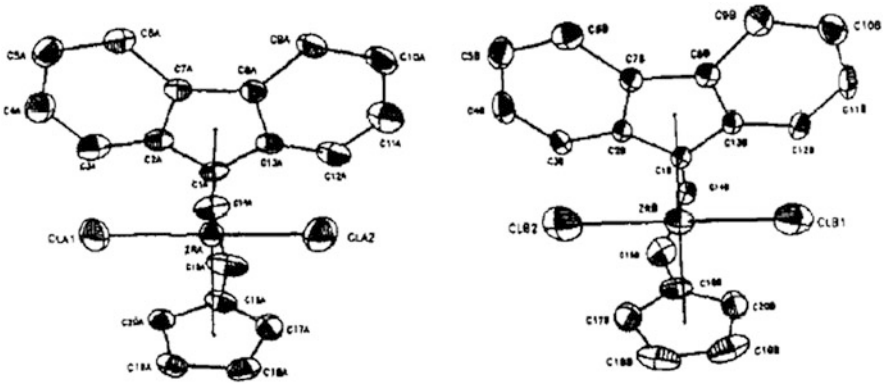

Fig. 11 The two δ/λ-(η^5-C_5H_4-μ-Et-η^5-$C_{13}H_8$)$ZrCl_2$ conformers of **5**

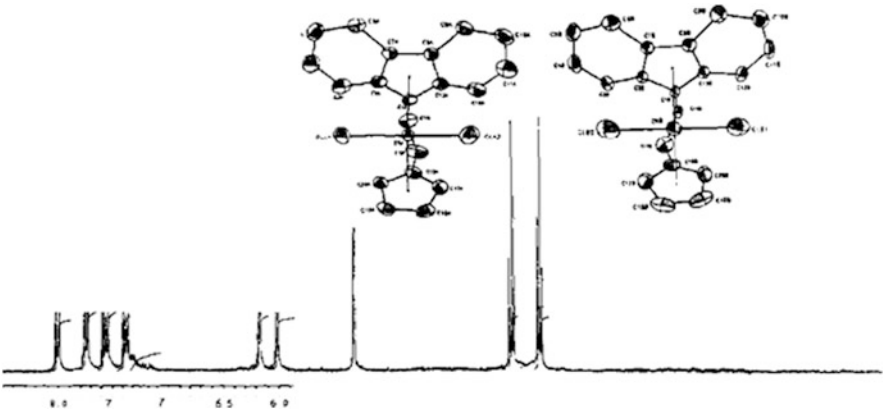

Fig. 12 ^{1}H NMR spectrum of δ/λ-**5** conformers in toluene at room temperature. Only aromatic proton chemical shifts are shown

(displayed in Fig. 12) reflects this fact by exhibiting for each proton pair of the two conformers only one time-averaged signal.

After the activation with MAO, the interconversion mobility of their cationic species seems to become severely restricted, probably due to the electronic differences between the cationic molecule and the neutral molecule and/or because of ion pairing dynamics between the cationic zirconium alkyl conformers and the MAO anion [34, 113]. Since the two conformers have different enough structural characteristics (two sets of bond angles and bond distances) they consequently behave differently as catalytic species after their activation and transformation to cationic species. The two cationic conformational species thus have slightly different catalytic properties and produce two different populations of active species, giving rise to two populations of polymer chains distinguishable by the difference in their polymer chain lengths. In this respect, the catalytic system generated with **5**/MAO resembles very much a dual-site catalyst system [116–121].

At higher polymerization temperatures, however, the energy for overcoming the interconversion barrier is apparently provided even for cationic systems and the polydispersity of the polymers begins to decrease with the gradually increasing polymerization temperature, as the difference between the two populations of active species vanishes due to very fast δ–λ interconversion. The two polymer chain populations coalesce around 80°C into one single population. At 90°C, the catalyst produces an amorphous polypropylene polymer that contains a large portion of atactic pentads but a narrow molecular weight distribution.

At higher temperatures, at the same time as the polydispersity decreases because of the rapid reversible δ–λ interconversion, the rigid structural integrity is also more and more compromised. The concentration of enantiomorphic site control related stereo-errors (rmmr) increases, but the rate of site epimerization and concentration of rrmr pentads increase much more dramatically, parallel to the increase in the conformational interconversion rate and the resulting molecular flexibility.

The explanation for the formation of the longer polymer chains with the **5**/MAO catalyst system requires a different approach and necessitates a comparative evaluation of the interatomic parameters for structures **5** and **1**, including some important bond angles and bond distances. It is apparent from structural data [113] that the substitution of one carbon atom (in the bridge of **1**) with two carbon atoms (in the bridge of **5**) provokes the increase in centroid–Zr–centroid angle (a smaller bite angle!) by several degrees (127.28°/127.08° versus 118.6° for **1**). The cyclopentadienyl and fluorenyl ring systems are forced to move closer and adopt a more parallel position. This new ring arrangement causes the increase in the average cyclopentadienyl Zr–centroid bond distance ($Zr–C_{cp}$ = 2.268 Å/2.285 Å for **5**, **5′** versus 2.170 Å for **1**) and the decrease in the average fluorenyl Zr–centroid bond distance ($Zr–C_{flu}$ = 2.196 Å/2.196 Å for **5**, **5′** versus 2.240 Å for **1**). The net effect is that under these conditions slightly more ligand coverage is provided for the transition metal's coordination sites. The increase in the centroid–Zr–centroid angle at the same time is accompanied by an increase in the frontier orbital energies and a change in the degree of their hybridization [107, 108, 122]. Furthermore, the increased steric congestion around the coordination sites increases the nonbonded steric contacts between the ligand and the growing chain substituents, preventing it from getting close enough to the Zr center for an adequate orbital overlapping between the metal fragment orbitals and hydrides for a meaningful α- or β-agostic exchange. The lower probability of the β-agostic approach favors the formation of a longer chain and, on the other hand, the lower probability of α-agostic interaction is favorable for enhanced conformational orientation of the chain and faster insertion/propagation steps, resulting in a lower degree of enantioselectivity and lower activity due to lower insertion rate (and also smaller bite angle!). Thus both from a steric and a valence orbital energetic point of view, the approach and subsequent orbital overlapping between chain-end hydride orbitals and transition metal fragment orbitals for a proper agostic interaction (of any kind) will be less favored for the new catalyst formed with **5** (similar results have been reported by Kim et al. [114]).

3.3 Bridge Substituents and Syndiotactic Polypropylene Molecular Weight

An increase in the size of the bridge, exemplified by replacement of the single-carbon isopropylidene inter-annular bridge with a two-carbon ethano-bridge, in syndiospecific catalyst system **5**/MAO provides the desired increase in the molecular weight of the s-PP polymer, but is unfortunately accompanied by some undesired side effects such as a decrease in the catalytic activity and stereospecificity and a lowering of the stereoregularity of the s-PP polymer. Other investigations related to the increase in the size of the bridge have also shown, for example, that the replacement of the carbon bridge with a silicon bridge has a similar deleterious effect on the enantioselectivity of the final catalysts [123, 124]. These findings are suggestive of the fact that any bridge modification with the purpose of improving the overall final catalyst properties must maintain the single-carbon arrangement of the bridge in the basic skeleton of complex **1**. This leaves only one remaining option for further consideration: modification of the bridge substituents.

The effect of the bridge substituents on the molecular weight of s-PP polymer was accidentally discovered during a systematic study of structural modifications for syndiospecific catalyst systems. The aim of the study was initially to perform substitutional modifications on the ligand without destroying the bilateral symmetry in the original metallocene molecule **1**. In the course of the study, by us and other research groups, the two methyl substituents of the bridge were exchanged individually or simultaneously for one or two phenyl groups, one or two hydride groups, and a series of other potential aliphatic or aromatic groups [125–127]. Of the many bridge substituent modifications, the effect of replacing the two methyl substituents of the bridge in **1** with two phenyl groups causes the most spectacular results with respect to increasing the molecular weight of s-PP and is discussed below in some detail.

3.4 Polymerization Behavior of Diphenylmethylidene (cyclopentadienyl-fluorenyl)MCl_2/MAO: Methyl Versus Phenyl Substituent in the Bridge

The replacement of the two methyl groups in the isopropylidene bridge of the complex **1** (and **2**) by two phenyl groups leads to the formation of two new complexes, diphenylmethylidene(cyclopentadienyl-fluorenyl)MCl_2 or (η^5-C_5H_4-CPh_2-η^5-$C_{13}H_8$)MCl_2; M = Zr, (**6**) or Hf (**7**). Complexes **6** and **7** can be prepared according to a method very similar to that used for the preparation of **1** and **2** (see Sect. 8).

Two different views of the molecular structure of **6** (and **7**) are portrayed in Fig. 13. From both a molecular symmetry point of view and from solid structural characteristics (bond distances and bond angles) point of view, complexes **6** and **7** appear almost indistinguishable from **1** and **2** [20]. It was, therefore, expected that

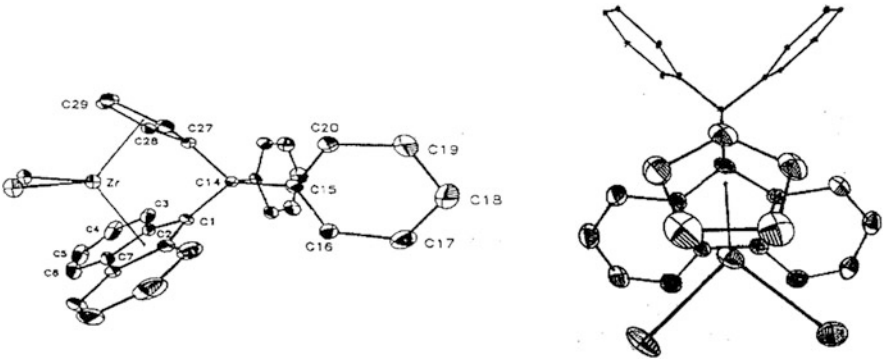

Fig. 13 Two different views of single-crystal X-ray molecular structure of complexes (η^5-C_5H_4-CPh_2-η^5-$C_{13}H_8$)MCl_2; M = Zr (**6**), Hf (**7**)

Table 5 Polymerization results and conditions for (**6** and **7**)/MAO

Complex	Temperature (°C)	Activity (g/g)	M_w (×1,000)	rrrr (%)	Melting point (°C)
Zr	20	11,800	1,243	145.60	91.04
Zr	40	26,000	785	89.74	144.45
Zr	60	138,000	478	86.78	133.40
Hf	40	17,500	2,863	76.60	103.81
Hf	60	27,500	1,950	7.03	102.17

Polymerization conditions: 1 L liquid propylene; 10 mL MAO (11 wt% in toluene); 60 min

Table 6 Presentation of ^{13}C NMR normalized spectroscopic stereosequence distributions (%) for syndiotactic polypropylene samples produced with (**6** and **7**)/MAO at different polymerization temperatures

Complex	Temperature (°C)	rrrr (%)	rrmr (%)	rmmr (%)	mmmm (%)
Zr	20	91.04	1.07	0.92	0.00
Zr	40	89.74	1.21	2.08	0.00
Zr	60	86.78	1.95	2.40	0.11
Hf	40	76.60	2.71	4.55	0.58
Hf	60	74.03	1.37	3.46	0.86

their activated forms as catalysts would produce very similar, if not identical, s-PP chains when polymerizing propylene. Correspondingly, after activation with MAO or other ethylating/ionizing agents, complexes **6** and **7** are transformed into excellent catalysts for promoting the polymerization of propylene to highly syndiotactic polypropylene. Table 5 presents the polymerization conditions, results, and polymer analysis for (**6** and **7**)/MAO catalyst systems. Table 6 compares the microtacticities of s-PP produced with catalyst systems (**6** and **7**)/MAO and (**1** and **2**)/MAO at different polymerization temperatures.

A cursory comparison of the data given in Table 5 for s-PP samples produced with complexes (**6** and **7**)/MAO and the data in Table 1 for complexes (**1** and **2**)/MAO

reveals that, under similar polymerization conditions, the catalyst systems **6**/MAO (and **7**/MAO) produce s-PP polymers with much higher molecular weights compared to polymers produced with **1**/MAO (and **2**/MAO) catalyst systems. On the other hand, for both systems the polymers' stereoregularities and microtacticities, as measured by the size of the related pentad (rmmr and rrmr) intensities, within the expected experimental errors, were very close.

The general model and mechanism that was discussed in Sect. 2.4 and proposed for the mechanism of the syndiospecific polymerization of propylene with the C_S symmetric metallocene catalyst system **1**/MAO vindicate the similar microtacticity and stereoregularity of the syndiotactic polymers perfectly, but does not in any way account for or rationalize, the polymerization behavior of catalyst system diphenylmethylidene-μ-(cyclopentadienyl-fluorenyl)zirconium dichloride **6**/MAO (**7**/MAO) with respect to the dramatic increases in the molecular weights of the resulting s-PP polymers.

The molecular structures of **1** and **6**, depicted in Figs. 2 and 13, expose their extraordinary overall resemblance and the reason for the production of s-PP chains with very similar microstructures. They do not, however, provide any clue as to why the molecular weights of their corresponding s-PP polymers are so different. A review of the solid state interatomic bond distances obtained from crystal structure data for complexes **1** and **6** [19, 20] also does not give, at the first sight, any indications that might justify the different catalytic performance in this respect. It seems that upon introduction of the phenyl groups in the bridge, the important Zr–C bond distances in the modified complex **6** have not undergone palpable changes. Both aromatic ring systems in complex **6** are η^5-bonded to the zirconium center and the observed slight variations in Zr–C and C–C bond distance are, in general, well within the expected experimental uncertainties.

However, closer inspection of the bond angles reveals some minor changes. The centroid–Zr–centroid (and Cl–Zr–Cl) bond angle in complex **6** is smaller than the corresponding bond angles for complex **1**.The angle has decreased from a value of 118.60° (and 98.20°) to a value of 117.60° (and 96.60°), i.e., by 1.00° (and 1.60°). These angular changes imply that in complex **6**, as a result of the repulsive interaction between the two aromatic phenyl substituents in the bridge, the external tetrahedral angle, i.e. the angle including the bridging carbon and the bonds connected to the two phenyl groups, is increased and as a direct consequence the internal tetrahedral angle, including the bridging carbon and its bonds to cyclopentadienyl and fluorenyl bridge-head carbon atoms, is decreased.[1] The smaller internal angle forces the transition metal Zr (Hf) to move slightly outward in order to fit better inside the ligand and to have a more efficient *d* orbitals overlapping with their aromatic ring π-systems.[2]

[1] (a) Tetrahedral formed by the bridging carbon and the four bonds connecting it to two phenyl groups, a cyclopentadienyl, and a fluorenyl group. (b) Interpretation of the X-ray data in [20] was given by Professor Jerry Atwood (private communication) with respect to Zr displacement.

[2] See footnote 1, part b.

A comparison of the ^{1}H NMR spectra [19, 20, 128] of complexes **1** and **6** reveals further that the structural differences may be more substantial in solution phase. Comparison of ^{1}H NMR spectra of the complexes **1** and **6** shows that for both molecules the proton signals related to the cyclopentadienyl groups of both catalyst systems have very similar chemical shift values and present the same coupling pattern (two virtual triplets) [20]. Examination of the fluorenyl's proton signals indicates that some of the protons belonging to the fluorenyl part of complex **6** have been subjected to major different shielding and deshielding forces, giving rise to completely different chemical shifts and signal patterns. Fluorenyl protons attached to carbons 3,3′ and 4,4′ (see Fig. 13 for numbering) closest to the bridge substituents, the phenyl groups, in complex **6** experience the most dramatic up-field shift. Their signals appear more than 1.5 and 0.5 ppm shifted to higher field, respectively, whereas the chemical shift variations for protons 5,5′ and 6,6′ (attached to carbon 5,5′ and 6,6′ in Fig. 13), more distant from the bridge, are negligible (see Sect. 8) [20, 129, 130]. Apparently, the introduction of the phenyl groups in the C1 bridge (vide supra) causes important changes in the electron density distribution of the aromatic π-system of the fluorenyl's six-membered rings. This in turn provokes a redistribution of the electron densities concentrated on the different C–H atom groups and their chemical shift repositioning [20, 129, 130]. It is also possible that the magnetic field anisotropy caused by the ring currents of the two phenyl substituents in the bridge is responsible for the observed differences in the chemical shifts and signal patterns for the said protons.

The slight outward repositioning of the metal center and dramatic differences in chemical shifts and signal pattern of the fluorenyl protons for compounds **1** and **6**, on the other hand, could be indicative of fact that the fluorenyl moieties of the ligands of these complexes are engaged in different bonding relationship or hapticities with the transition metal in the solution phase. In other words, the redistribution of the electron densities and changes in the Zr–C bonds in fluorenyl carbon atoms may be associated with, or a result of, an eventual hapticity change from η^5-bonding to η^3-bonding. It is in essence speculated that different Zr–C_{flu} bond hapticities, η^5 or η^3, (or even a η^1-type bonding) are at the origin of the different catalytic performances of (**1** and **2**)/MAO, and (**6** and **7**)/MAO catalyst systems [129, 130]. To prove the veracity of the hypothesis concerning different η-bonding in complexes **1** and **6** in solution phase, a hydrogenation experiment was undertaken that proved to be very revealing.

The aim of the hydrogenation experiment was, first, to verify the assumption that whether in either one of the complexes a η^3 Zr–C_{flu} is operative and, if so, to assign the correct Zr–C_{flu} centroid hapticities to each of the two metallocene complexes **1** and **6**. Theoretically, the η^3 nature of the five-membered ring of Zr–fluorenyl bond in one of the metallocenes would basically imply that the corresponding two six-membered rings are fully aromatic and not easily subject to hydrogenation. On the contrary, if in one of the metallocenes the Zr–C_{flu} centroid bond is η^5 in nature, then the fused six-membered rings are not "quite" aromatic and more hexadiene like in nature and therefore subject to facile hydrogenation. Figure 14 shows the hydrogenation scheme for the two metallocene complexes **1** and **6** and the formation

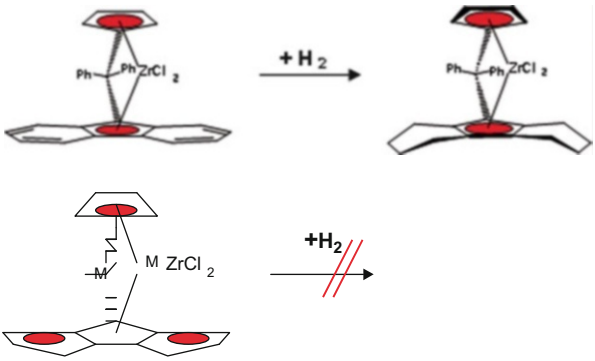

Fig. 14 Representation of **1** (*bottom left*) and **6** (*top left*) and the hydrogenation scheme. The structure of complex **8** is shown (*right*). The *solid areas* in the rings represent their aromatic nature

of the complex, diphenylmethylidene-μ-(cyclopentadienyl-octahydrofluorenyl)$ZrCl_2$, **8**, as the only hydrogenation product. Metallocene **8** was obtained from **6** under mild hydrogenation conditions [28, 30].

All attempts to hydrogenate metallocene **1** under similar and even more vigorous conditions failed. It can be therefore concluded that an η^3 bonding scenario represent the correct Zr–fluorenyl bond hapticity for complex **1** in solution phase and an η^5 bonding correctly describes the bonding of the Zr–fluorenyl centroid for complex **6** both in solution phase and solid state. The structures of complexes **1** and **6** with correct Zr–Centroid bonding for **1** and **6** are presented in Fig. 14. The solid areas in the rings reflect their aromatic nature in each case.

The hydrogenation experiment clearly shows that the complexes **1** and **6** are chemically different from each other in solution, at least with respect to the fluorenyl–Zr bond hapticities, despite their solid state apparent close resemblance.

The displacement of the transition metal towards the more open section of the ligand leads, at the same time, to a greater exposure of the transition metal and its protruding frontier orbitals in **6**. Even though it is difficult to establish a direct link between the hapticity of the $Zr–C_{flu}$ centroid bonds of the two catalyst systems and the molecular weights of their s-PPs, it is conceivable that the more exposed orbitals and the different electronic characteristics of the ligand changes the electrophilicity of the transition metal active site and its bond strength to carbon (of the polymer chain). The alteration of the shape, direction, and spatial extension of the frontier orbitals and the Lewis acidity of the transition metal of the metallocenium–monoalkyl cation can potentially influence the kinetics of the polymerization reaction by requiring new reaction pathways and different insertion transition state energies and chain transfer transition state energies. For the catalyst systems **1**/MAO and **6**/MAO it seems that the stereo-electronics in the former are conducive to a higher probability of β-hydride agostic interaction/transfer and formation of shorter chains, whereas the geometry in the latter is more prone to a rather frequent α-hydride agostic interaction and formation of longer chains.

4 Fluorenyl Substituents and Catalyst Enantioselectivity

As in the case of the bridge substituent modifications, this section describes the results of a systematic investigation involving fluorenyl substitution patterns. The investigations have shown that any modification of cyclopentadienyl substitution in complex **1** is at best ineffective [proximal position(s)] or completely disruptive [distal position(s)] to syndiospecificity of the final catalyst. As far as the fluorenyl substitution pattern is concerned, the combined substitutions at position 4 and 5 proved to be generally disruptive to enantioselectivity and had some adverse effects on polymer stereoregularity due to blockage of the central space in the frontal positions of the fluorenyl that accommodate the propylene methyl group [131–136]. By contrast, substitution at the 2 and 7 positions of the fluorenyl does not bring about any improvement in enantioselectivity of the parent complex **1**. On the other hand, double substitution involving positions 3 and 6 of the fluorenyl moiety of the ligand proved to bring about the desired improvements in catalyst stereoselectivity and in the resulting polymer's stereoregularity, melting point, and crystallinity. This will be discussed below as a successful case study. The study also shows that, as well as the position of the substituents, the size of the substituent is an important factor such that the larger the substituents, the more dramatic the effect they exert.

4.1 Stereoregularity Improvement and Frontal Substituents

The zirconocene complex (η^5-C_5H_4-μ-CPh_2-η^5-3,6-di-^{t}Bu-$C_{13}H_6$)$ZrCl_2$, **9**, can be synthesized according to a similar synthetic procedure that describes the synthesis of **6** (see Sect. 8 and [20]) with only difference being that, instead of the unsubstituted fluorene used for preparation of **6**, the 3,6-di-*tert*-butyl-substituted fluorene is employed for the synthesis of the ligand of complex **9**. The procedures for the aromatization of the ligand, its reaction with $ZrCl_4$, and isolation and identification of complex **9** all follow similar reaction procedures and work-up steps as for the preparation of **1** and **6** (see Sect. 8). Complex **9** is identified by its ^{1}H NMR spectrum and its single-crystal X-ray structure. The molecular structure of complex **9** is depicted in Fig. 15. As can be seen from molecular views, the metallocene molecule **9** projects the overall symmetry and bonding characteristics that were described for **6** except for the presence of two protruding *tert*-butyl substituents at positions 3 and 6 in its frontal section. When activated with MAO, complex **9** polymerizes propylene to highly syndiotactic polypropylene very efficiently. Catalyst prepared with the complex **9**/MAO is more active than the corresponding catalysts prepared with complexes **1** and **6** under the same polymerization conditions. Tables 7 and 8 present the polymerization conditions, results, and polymer analyses of the syndiotactic polymers produced with the **9**/MAO catalyst system at different polymerization temperatures [28–30]. A quick comparative

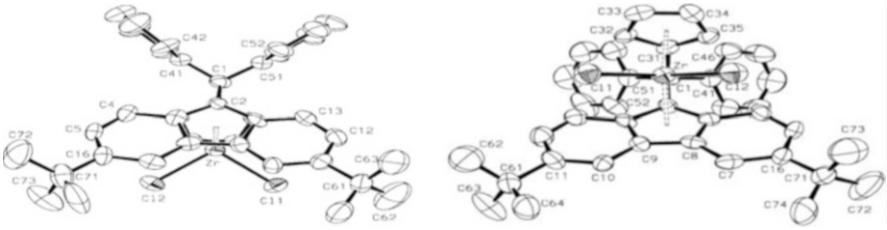

Fig. 15 Two perspective views of the single-crystal X-ray determined molecular structure of (η^5-C_5H_4-μ-CPh_2-η^5-3,6-di-^{t}Bu-$C_{13}H_6$)$ZrCl_2$, **9** [28–30]

Table 7 Polymerization results, polymer analysis, and stereodefects generated in the polymers produced with **9**/MAO at different polymerization temperatures

Temperature (°C)	M_W (kDa)	rrrr (%)	rmmr (%)	rrmr (%)	Melting point (°C)
40	766	91.0	0.73	0.93	150
60	590	88.5	0.85	1.65	143
80	443	79.0	1.06	3.79	128

Table 8 Comparison of ^{13}C NMR normalized spectroscopic stereosequence distributions (%) of syndiotactic polypropylene samples produced with **1**/MAO and **9**/MAO at different polymerization temperatures

	9/MAO catalyst system		**1**/MAO catalyst system	
Temperature (°C)	rmmr (%)	rrmr (%)	rmmr (%)	rrmr (%)
40	0.73	0.93	1.55	1.15
60	0.85	1.99	1.65	2.70
80	1.06	3.79	2.20	4.82

glance at the data given in Tables 1, 2, 7, and 8 reveals that the introduction of *tert*-butyl groups in positions 3 and 6 of the fluorenyl moiety of the ligand causes substantial improvements with respect to enantio- and stereoselectivity of the resulting catalysts **9**/MAO and the stereoregularity of the s-PP polymers it produces. The data presented in Table 8, compares the microtacticity variations of **1** and **9** under changing polymerization temperatures.

The data clearly shows, as anticipated, a substantial decrease in rmmr pentad concentrations related to *meso* triad (mm) stereoerrors in the backbone of syndiotactic polymer chains produced with **9**/MAO compared to the corresponding polymers produced with **1**/MAO at comparable polymerization temperatures. Interestingly, even the rrmr pentad concentrations in polymers produced with **9**/MAO, directly proportional to the catalyst's site epimerization frequency, are lower than the observed rrmr pentad concentration for polymers produced with **1** (and **6**). For syndiotactic polymers produced with both catalyst systems, the rrmr pentad concentrations almost double with every 20°C increase in polymerization temperature with the same rate. On the other hand, the enantiomorphic site control related rmmr pentad concentrations in syndiotactic polymers produced at different temperatures

with catalyst **9**/MAO are about half those of the corresponding rmmr pentad concentrations determined for polymers produced with catalysts of complexes (**1** and **6**)/MAO. Additionally, rmmr pentads in syndiotactic polymers produced with **9**/MAO show an even more moderate temperature dependency than the rmmr temperature dependency observed for polymers of (**1** and **6**)/MAO.

The improved enantioselectivity, reflected in lower percentage of rmmr pentads, for catalyst system **9**/MAO could be explained by the beneficial presence/action of the bulky *tert*-butyl substituents placed at positions 3 and 6 of the fluorenyl section of the ligand. These direct the polymer chain to the most preferred "upward" conformation away from fluorenyl part of the ligand and toward available quadrants left or right of the cyclopentadienyl group (see Sect. 3.2) and, at the same time, provide a more effective guidance for the preferred head-down propylene coordination mode (*anti* position with respect to the polymer chain via creation of a tighter "chiral pocket"). The explanation for the lower site epimerization related rrmr pentad concentration in polymers produced with **9**/MAO versus **1**/MAO, at the same polymerization temperature and monomer concentration is, however, less straightforward. It is most likely related to the steric bulk of the *tert*-butyl group's action in pushing the counter-ion (the anion) further away from the active cationic site, preventing a tight ion-pair formation and affecting the dynamic cation/anion association/dissociation processes [137, 138]. A cursory glance at the top and front views of the molecular structure of (η^5-C_5H_4-μ-CPh_2-η^5-3,6-di-^{t}Bu-$C_{13}H_6$)$ZrCl_2$, **9**, presented in Fig. 15, reveal the fact that due to substantial steric bulk of the *tert*-butyl substituents, the tight contact ion-pairing with MAO anion would be more difficult or harder for **9**/MAO systems than with the corresponding cations formed with (**1** and **6**)/MAO, rendering the site epimerization more difficult by forcing the anion to rearrange to the other coordination position after each insertion rather than associate back immediately. Thus, the immediate contact ion-pairing preventive effect of the *tert*-butyl substituents in **9** is an additional factor for the improved stereoselectivity of **9**/MAO as a result of slower active site epimerization. Most importantly, less tight ion-pairing is concomitant with higher activities due to easier availability of the coordination site to monomer coordination/insertion and chain propagation.

The two bulky *tert*-butyl groups in the fluorenyl moiety of the ligand affect the catalytic performance of **9**/MAO probably due to steric factors (interactions with polymer chain, monomer, and counter-ion as suggested above) rather than electronic factors. Use of a similar catalyst system in which the two *tert*-butyl substituents are placed at the 2 and 7 positions of the fluorenyl moiety of the ligand (η^5-C_5H_4-μ-CPh_2-η^5-2,7-di-^{t}Bu-$C_{13}H_6$)$ZrCl_2$/MAO [131–136] does not show any marked improvement in the enantioselectivity or stereoselectivity of the resulting syndiospecific catalyst or in the stereoregularity of its s-PP.

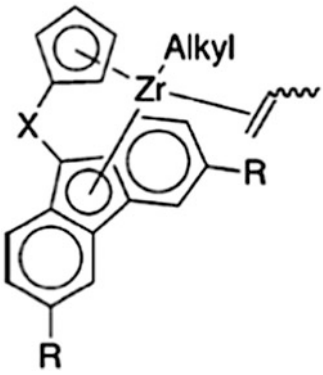

Scheme 1 C_s symmetric catalyst systems studied in computational investigation. R = H (system 1); R = methyl (system 2); R = *tert*-butyl (system 3); X = CMe_2; *Alkyl* = isobutyl

4.2 *Computational Calculations: Determination and/or Prediction of Enantioselectivity of Syndiospecific Catalyst Systems*

The experimental results concerning the effect of frontal substituent on the enantioselectivity of syndiotactic-specific metallocene catalysts can be further consolidated by computational calculations in a general and universal way. The computational calculations deliver the means for not only calculating the enantioselectivity of real and experimentally tested catalyst systems but also the ability to predict the enantioselectivity of hypothetical systems. In this section, the results of such computational calculations for three catalyst systems with a basic isopropylidene-bridged cyclopentadienyl-fluorenyl ligand skeleton are presented. The three chosen structures, for the reasons mentioned above, differ only by the gradually increasing size of the substituents located at positions 3 and 6 of their fluorenyl moieties. For the real catalyst systems, the catalysts **1**/MAO (system 1) and **9**/MAO (system 3) were selected. Additionally, a catalyst with a hypothetical structure, the isopropylidene(cyclopentadienyl-bis-3,6-dimethyl-fluorenyl)$ZrCl_2$, 3,6-dimethyfluorenyl-substituted version of complex **1** (system 2), is included for the calculation. The geometry of the model active sites for the three systems are depicted in Scheme 1 in which the bridge is represented by CMe_2, an isopropylidene group; R represents the substituents placed at positions 3 and 6 of the fluorenyl group, i.e., H, Me, and a *tert*-butyl group. The polymer chain is represented by an isobutyl group.

The basic system 1, with R = H, (fluorenyl without substituents), represent the catalysts system of complex **1** activated with MAO. It has been studied by many research groups including Angermund and colleagues [139–144] using a combination of density functional theory (DFT) functionals and a basis set very similar to the one chosen for this calculation by us [145–147]. The hypothetical system 2, is a modified version of complex **1** in which the ligand bears two methyl substituents in the 3 and 6 positions of its fluorenyl moiety. Furthermore, the insertion transition states are optimized for system 3 with two *tert*-butyl groups in the 3,6 positions of the fluorenyl ligand, representing catalysts system prepared with **9**/MAO [146].

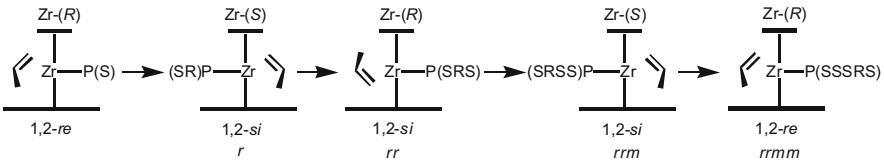

Scheme 2 Representation of the stereo-error sequence following an enantiomeric mis-insertion

It is commonly accepted that the syndiotactic-specific catalyst systems are highly regioselective (the regio-errors are either not present or very low in concentration and not easily detectable), and the single main source of the stereo-errors in the syndiospecific polymerization of propylene is enantiomeric mis-insertion, i.e., the insertion of a monomer unit with the "wrong" enantio-face. The "right" enantio-face would be the one that allows minimization of repulsive steric interactions between the olefin's side group and the growing polymer chain, as well as between the ligands and the growing polymer chain. This arrangement is best attained when the olefin's substituent and the alkyl (polymer) chain are in an "anti" relationship (versus a "syn" relationship), while at the same time the polymer (alkyl) chain is as far away as possible from the bulkier sections of the ligand. An enantiomeric mis-insertion event in the syndiospecific polymerization of propylene leads to the occurrence of a *meso* triad (mm) type stereo-error, as depicted in Scheme 2, whereas a perfect syndiotactic polymer is composed exclusively of *racemic* r dyads (Fig. 8). The preferred, dominant enantioselective enchainment sequence versus an enantiomeric mis-insertion event could be therefore presented schematically as in Scheme 2 (see also Fig. 9).

Each step in Scheme 2 represents a full catalytic cycle from the depicted π-complex to the one obtained after insertion, followed by uptake or coordination of the next monomer unit. At each step, the polymer chain is expected to be oriented away from the bulky fluorenyl ligand ("chain-away"). The four possible diastereomeric conformations are depicted in Fig. 16. In the most preferred stereochemical sequence, the methyl groups of propylene and the polymer chain are in an "anti" stereochemical relationship (the "chain-away/*anti*" diastereomeric conformation, (Fig. 16a) and one of the two faces of propylene, termed *re* or *si*, is inserted preferentially.[3] The 1,2-*si* enantiomeric mis-insertions take place either when the polymer chain points away from the fluorenyl group and the propylene's methyl group is "syn" oriented to it (diastereomeric conformation "chain-away/*syn*," Fig. 16c), or when the polymer chain points toward the fluorenyl group, while maintaining an "anti" relationship with the olefin substituent (diastereomeric

[3] For parent syndiospecific catalyst systems, the propylene π-complexes in which the Zr center has an *S* configuration insert the monomer in a 1,2-*si* fashion, and the configuration of the chiral center on the alkyl chain closest to the metal center is *R*. Alternatively, when the configuration of the Zr center is *R*, the closest chiral center on the chain is of *S* configuration and a 1,2-*re* insertion occurs. After each insertion, the alkyl chain "migrates" from one coordination site to the other. Due to the enantiotopic nature of the metallic active center, to have a complete picture it is sufficient to study only one of the two possibilities.

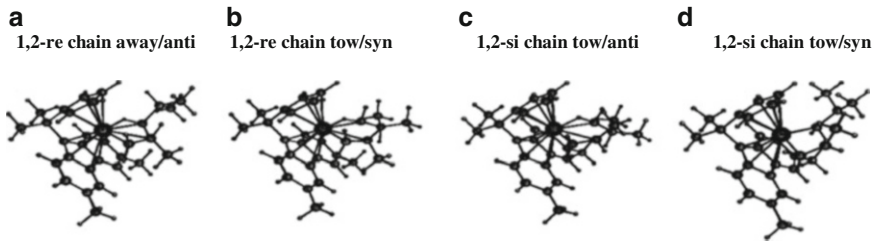

Fig. 16 Gas-phase optimized transition states for the insertion of propylene into the Zr–C bond of system 2: (**a**) 1,2-*re* chain away/*anti*; (**b**) 1,2-re chain toward/*syn*; (**c**) 1,2-si chain toward/*anti*; (**d**) 1,2-*si* chain toward/*syn*

conformation "chain-toward/*anti*," Fig. 16d). The situation in which the polymer chain points toward the fluorenyl ligand and is in a "syn" relationship with the methyl group of propylene (conformation "chain-toward/*syn*," Fig. 16b) would lead to 1,2-*re* insertion with the "correct" enantio-face, but it is expected to be the highest in energy; it is the least preferred stereochemical event due to two unfavorable steric interactions.

The gas-phase energies for propylene π-complexes and of the resulting insertion transition states (TSs) have been computed for all four possible diastereomeric conformations mentioned (chain-away/*anti*, chain-toward/*anti*, chain-toward/*syn*, chain-away/*syn*) for systems 1–3; the structures are shown in Scheme 1 and can be found in reference [146]. As expected, for all three ligand systems the lowest energy conformation is the one in which the alkyl chain points away from the fluorenyl moiety (chain-away/*anti* conformation) and the spatial relationship between the chain and the methyl group of propylene is *anti*. This corresponds to a 1,2-*re* approach (since the *R* chirality has been arbitrary chosen for the Zr metal center). The 1,2-*si* insertions are energetically slightly less favorable because one of the two interactions (either alkyl chain–monomer or alkyl chain–catalyst) is not energy-minimized. When both interactions are unfavorable, there is a dramatic increase in the relative energy for the remaining channel, ch-tow/syn, following a 1,2-*re* approach considerably higher in energy than all the others.

The substitution pattern on the fluorenyl moiety of the ligand plays an important role in the enantioselectivity. Adding bulky groups to the 3,6-positions strengthens repulsive interactions and increases the energy gap between the four conformations, as can be seen in the series 1–3. The calculated selectivity for system 1 is 2.0 kcal/mol [145, 147], for system 2 it increases and reaches the value of 2.4 kcal/mol, and for system 3 it is 2.6 kcal/mol. Because of its bulk, the *tert*-butyl substituent exerts the greatest conformational constraints on the growing polymer chain and consequently exhibits the highest enantio-facial selectivity. The increased selectivity comes only at a marginal expense of reactivity. In fact, in the gas phase the energy of the most favorable transition state for the hypothetical system 2, the dimethyl-substituted ligand system, (TS2 away/*anti*) is 7.4 kcal/mol below the reference energy point (zirconocenium isobutyl complex + propylene), whereas that of the

most favorable transition state for system 3 (TS3 away/*anti*) is 5.0 kcal/mol below the reference energy point. It should be noted that when the counter-ion is taken into account, both transition states would be destabilized because in the reference state the anion and cation interact closely.

Due to the different bulks of the substituents, it is likely that the ion-pair energy is, however, weaker in system 3. On the other hand, the anion does not play any important role in stabilizing one particular conformation of the diastereomeric cations versus the other. Therefore, enantio-face selectivity is hardly affected by including the anion in the picture and the anion can be disregarded in the calculations. The influence of toluene solvation, mimicking the polymerization medium, has been estimated by calculating the solvation energies of the gas-phase optimized geometries. The relative energies of the species involved in the insertion process are reported in [146]. Unsurprisingly, for all the different ligand systems, solvation effects are comparable for the four competing conformational channels. $\Delta\Delta E$ ranges between 0.1 and 0.2 kcal/mol. Thus, differential solvation plays a minimal role.

From the above calculation and discussion, two conclusions can be drawn regarding the origin and factors impacting the enantioselectivity of the syndiospecific catalyst systems:

1. The enantioselectivity does not emanate from a particular molecular symmetry of the catalyst structure but is tightly related to the steric arrangement of the organic ligand that engulfs the transition metal and its direct interaction with the growing polymer chain, which dictates its conformation and final spatial orientation (further ensured through a-H–Zr agnostic interaction). The combination of the steric arrangement of the ligand and the particular spatial orientation of the polymer chain (directing the coordination mode of the propylene) creates an overall repulsive steric force that "blocks" a large space in and around the coordination sphere of the transition metal center. The remaining "free" and accessible space forms a shape-selective "chiral pocket" that can only accept monomers of a certain shape, i.e., unique π-face that fits in that pocket easily without much repulsive interaction.
2. Any new substituent(s) at proper position(s) that could enhance the shape-selectivity of the chiral pocket via enforcing and stabilizing the spatial orientation of the growing polymer chain, regardless of its impact on the symmetry, would enhance the enantioselectivity of the final catalyst, be it of C_s or C_1 symmetry (see below). The substitution(s) at position 3(6) or 3,6 of the fluorenyl group, just beneath the growing polymer chain, provide exactly that enhancing effect.

4.3 Importance of the Frontal Substituents

To emphasize the importance of fluorenyl's frontal substituents at positions 3 and 6 and to confirm the findings of the computational calculations presented in Sect. 3.2, two new syndioselective catalysts systems are introduced whose ligands

Table 9 Polymerization conditions and results for μ-(Me_2Si)(3,6-di-^{t}BuFlu)(^{t}BuN)$TiCl_2$/MAO system

Temperature (°C)	Activity (kg/g)	M_W (×1,000)	rrrr (%)	Melting point (°C)
40	222	703	81.6	123.0
60	371	351	75.8	105.1
80	226	226	60.1	–

Table 10 Presentation of ^{13}C NMR spectroscopic stereosequence distributions (%) for syndiotactic polypropylene samples produced with **10**/MAO at different polymerization temperatures

Temperature (°C)	rrrr (%)	rmmr (%)	rrmr (%)
40	81.6	1.6	3.6
60	75.8	1.7	6.5
80	60.1	2.2	10.60

differ completely from the ligands of complexes **1**, **5**, **6**, and **9** by lacking a cyclopentadienyl ring. Let us start first with the complex η^1,η^5-*tert*-butyl (3,6-bis-*tert*-butylfluorenyl-dimethylsilyl)amido$TiCl_2$, the half-sandwich complex **10**. After activation with MAO, complex **10** very efficiently polymerizes propylene to high molecular weight s-PP chains [32].

Tables 9 and 10 presents the polymerization conditions, results, and polymer analyses of syndiotactic polymers produced with the **10**/MAO catalyst system. The degree of the syndiotacticity of the polypropylene polymer that it produces at 40°C (measured as the concentration of *racemic* pentads rrrr) is higher than 81%. The s-PP polymers that are produced at higher polymerization temperatures have lower stereoregularity but still high enough (74.00% at 60°C and 69.40% at 70°C) to impart to the resulting polymers measurable crystallinity and melting points (see Table 9). Only for polymers produced at 80°C is the crystallinity lost and no melting point observed.

The microstructure . . .rrrrmmrrrrmrrrr. . . of the s-PP polymers that are produced with **10** MAO includes the two characteristic types of stereodefects and is similar in nature to the microstructure of the s-PP polymers produced with other syndiotactic-specific metallocene catalysts (**1**, **5**, **6** and **9**)/MAO. From these results it can be concluded that the η^1,η^5-bonded dimethylsilyl-bridged amido-fluorenyl-based ligand is perfectly capable of imparting the needed stereorigidity and steric environment prerequisite for syndioselectivity of the transition metal active site. Additionally, the microstructural similarity between the s-PP polymers produced with **1**, **5**, **6**, **9**, and **10** indicate clearly that the formation of the s-PP polymers with **10** also proceeds according to the chain migratory insertion mechanism operating on enantiomorphic coordination sites.[4] Table 10 lists the variation in the relevant

[4] Due to the presence of a high number of site epimerization errors, the microstructure of the syndiotactic polypropylene polymers prepared with the catalyst system **10**/MAO looks deceptively similar to the microstructure of the syndiotactic polypropylene polymers prepared via chain-end control mechanisms; cf. [29] on syndiotactic polypropylene from [Me_2Si(3,6-^{t}Bu$_2$-9-fluorenyl)(N-^{t}Bu]$TiCl_2$-based catalysts.

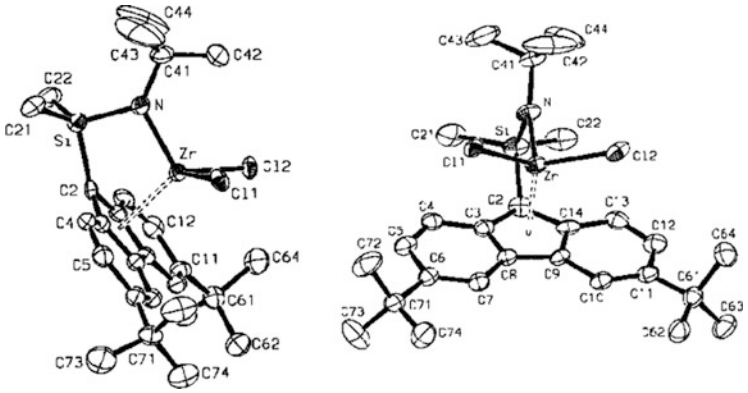

Fig. 17 Side and front view of the molecular structure of the complex η^1,η^5-*tert*-butyl(3,6-bis-*tert*-butylfluorenyl-dimethylsilyl)amidodichlorozirconium, **10**

stereopentad intensities with polymerization temperature. The data indicate that the syndiotacticity of the polymers produced with the **10**/MAO catalyst system at different polymerization temperatures, measured as the concentration of *racemic* pentads rrrr, are relatively high. The catalysts' enantioselectivity, judged by the concentration of the rmmr pentad sequences, are also very high and close to the enantioselectivities measured as rmmr pentads for the catalyst systems consisting of (**1**, **5**, **6** and **9**)/MAO.

The overall stereoregularity and melting points of the polymer are, however, lower for the syndiotactic polymers produced with the **10**/MAO catalyst system due to the presence of high concentration of site epimerization related stereo-errors (rrmr pentads). A rather frequent or fast site epimerization rate at higher polymerization temperatures is probably facilitated by the flexibility of the molecular structure of **10** (dynamic umbrella-type reversible inversion at the amido-nitrogen center see: [148]) and the rapid "same site" contact ion-pairing.

The single-crystal X-ray molecular structure of the complex μ-(Me_2Si)(3,6di-^{t}BuFlu)(^{t}BuN)$TiCl_2$ **10**, is depicted in Fig. 17. It shows a striking similarity to crystal structure of complex **9** with respect to its overall symmetry, despite the exchange of one of the aromatic rings, the cyclopentadienyl, in the molecule and its replacement with an amido group. Complex **10** exemplifies one of the rare examples of a titanium-based syndiotactic-specific metallocene catalyst systems.

It is in many other aspects different from all the catalyst systems t discussed in previous sections. It is based on a half-sandwich metallocene molecule that contains an amido-type N–Ti bond and is a 12-electron system (14-electron system at the most if one considers the contribution of the nitrogen's lone pair of electrons to the overall N–Ti bonding) leaving a cationic 10-electron (maximum 12 including the lone pair electrons of N) electron configuration active site.[5]

[5] As a comparison group, 4B neutral metallocenes have a 16-electron configuration and 14-electron configuration in their monoalkyl-cationic forms.

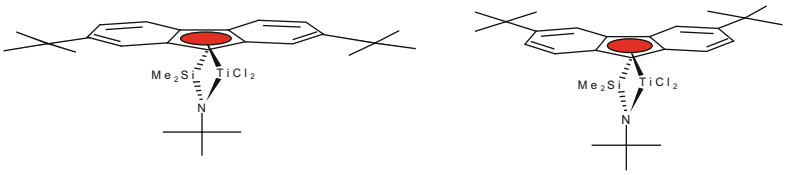

Fig. 18 Computer drawn structure of the complex η^1,η^5-*tert*-butyl(2,7-bis-*tert*-butylfluorenyl-dimethylsilyl)amidodichlorotitanium, **11** (*left*). On the *right*, the structure of **10** is shown for comparison

Table 11 Polymerization conditions and results for μ-(Me_2Si)(2,7-di-^{t}BuFlu)(^{t}BuN)$TiCl_2$/MAO system

Temperature (°C)	Activity (kg/g)	M_W (×1,000)	MWD	rrrr (%)	Melting point (°C)
40	27	605	2.6	75.74	111
60	160	506	3.2	63.92	–
80	75	367	3.1	55.89	–

Table 12 Presentation of ^{13}C NMR spectroscopic stereosequence distributions (%) for syndiotactic polypropylene samples produced with **5**/MAO at different polymerization temperatures

Temperature (°C)	rrrr (%)	rmmr (%)	rrmr (%)
40	75.74	3.15	4.72
60	69.05	3.03	8.55
80	55.89	3.46	11.23

The fact that the catalyst system **10**/MAO owes its high enantioselectivity mainly to the presence and the steric bulk of the *tert*-butyl substituents implanted at positions 3 and 6 of the fluorenyl moiety of its ligand can be demonstrated by reviewing the polymerization behavior of a similar complex, namely η^1,η^5-*tert*-butyl(2,7-bis-*tert*-butyl-fluorenyl-dimethylsilyl)amido-$TiCl_2$, **11** [29]. The only difference between the structures of complexes **11** and **10** lies in the different positions of the fluorenyl moiety where the *tert*-butyl substituents have been introduced. Complex **11** is prepared according to known synthetic procedures developed for constrained geometry, half-sandwich-type metallocene complexes. Its computer-drawn structure is shown in Fig. 18.

A glance at the molecular structure of **11** shown in Fig. 18 reveals again that from a molecular symmetry point of view complex **11** (like complex **10**) has all the structural and symmetry characteristics required to be classified as a syndiotactic-specific catalyst system after its activation. In practice, after activation with MAO, complex **11** does polymerize propylene to a high molecular weight s-PP very efficiently [29]. Tables 11 and 12 present the polymerization conditions, results and polymer analyses for **11**/MAO and the syndiotactic polymers it produces. According to these data, only the syndiotacticity of the polymers produced at and below 40°C (measured as the concentration of *racemic* pentads rrrr; about 75%) are

high enough to generate measurable crystallinity and melting points. The syndiotactic polymers that were produced at higher polymerization temperatures have much lower stereoregularity and exhibit no crystallinity and/or melting points.

Here again, like in the case of s-PP polymers produced with the **10**/MAO catalyst system, the main reason for lower stereoregularity is the rapidly increasing concentration of the site epimerization related (rrmr pentad) stereodefects. They double in size by increasing the polymerization temperature from 40°C to 60°C and reach values of over 10% at a polymerization temperature of 80°C and above for the very same reasons explained for syndiotactic polymers produced with the **10**/MAO catalyst system. The enantiomorphic site control related stereo-errors (rmmr pentads) are high but remain almost unchanged (as for **10**/MAO-produced polymers) over the entire measured temperature range.

The large enantioselectivity difference between the two catalyst systems involving complexes **10** and **11** (with rmmr pentad concentration of over 3% for **11**/MAO and about 1.7% for **10**/MAO) demonstrate the crucial role of the positions 3,6 for introducing the substitutions in the fluorenyl moiety of the ligand.

The syndiospecific catalysts systems (**10** and **11**)/MAO in which one of the ligand's main ingredients, an η^5-bonded cyclopentadienyl moiety, is exchanged for an η^1-bonded amido group with respect to the parent syndiospecific system made with complex **1**, are convincing examples for the validity of the fact that the proper steric balance between the three participants (ligand, polymer chain, and propylene) in the active transition state structure and the preference for one of the two monomer enantio-faces at each of the two enantiotopic coordination positions rather than for any particular geometry or symmetry, are the origin of syndiospecificity.

The polymerization behavior of (**10** and **11**)/MAO catalyst systems also demonstrates nicely that no matter what the chemical makeup of the metallocene precursor, composition of the ligand, or nature of the transition metal, the resulting catalysts (once their structure fulfills the prerequisites discussed based on the model given in Sect. 3.2) will act in a syndiotactic-specific manner and produce crystalline s-PP. The overall stereoselectivity is, however, determined by the frequency and rate of the site epimerization process. The lower stereoregularity of the new syndiotactic chains is probably the related to higher flexibility of the structures of complexes **10**/**11** in solution due to the absence of one of the η^5-bonded aromatic ring systems and the dynamic environment of a reversibly inverting amido group (dynamic umbrella-type reversible inversion at the amido-nitrogen center see: [148]) imparting a high degree of flexibility to the structure and/or facilitating fluorenyl ring slippage (see Sect. 4), leading occasionally to the dissymmetry of the site and the formation of lop-sided tight contact ion-pairing and short *meso* dyad units/sequences.

It is worth mentioning that the zirconium analogue of **10** produces only oligomeric materials.

5 Stereorigidity of Bridged Metallocenes and Stereoselectivity of the Catalysts

The lower stereorigidity and structural flexibility in complexes **5**, **10**, and **11** were associated with the more frequent occurrence of site epimerization and the lower stereospecificity of the resulting catalyst systems. In complex **5**, the conformational interconversion due to the fluxional behavior of the ethano-bridge, and in complexes **10** and **11**, the highly flexible structure as a result of the replacement of a strongly η^5-bonded ligand moiety (an aromatic ring) by a single atom η^1-bonded –N–R amido group (and the resulting amine-type umbrella interconversion[6] were considered to be the underlying reasons for lower skeletal rigidity and a probable source for higher site epimerization rate. However, one should be aware that even for bridged metallocene structures that have doubly η^5-bonded ligand systems such as in complexes **1** (**2**), **6** (**7**), and **9** the idea of high rigidity conveyed from solid state, X-ray images are somehow deceptive and should be taken as relative. The images extracted from X-ray crystal structural analysis project molecules contained in the unit cells in the solid state under the crystal packing effects. These rigid and static images reflect only a snapshot of the constantly vibrating, bending, and "breathing" molecules (the inward/outward movement of the two centroids towards and from the transition metal). In solution, the individual molecules freely float in the solvent and interact with the solvent molecules (the medium); they are much more mobile and dynamic than one would imagine.

Thus the question arises as to how rigid the stereorigid metallocene structures are in solution. In this context, it is important to be aware of at least two dynamic phenomena regarding the fluxional behavior of metallocene molecules in solution, namely, the phenomena of haptotropy [149–156] and ring slippage. The haptotropy and ring slippage [157–160, 161, and references therein] [162, 163], depicted schematically in Fig. 19, could influence the electronic properties of the active site and the steric environment surrounding it, particularly in the cationic state and in the presence of a counter-ion.

In Sect. 2.3 it was shown by the example of complexes **1** (**2**) and **6** (7), that the phenomenon of hapticity change or bond order variation between the transition metal and the aromatic ligands can change the kinetic pathways of the polymerization process and its outcome dramatically. The haptotropic behavior of metallocenes is a known phenomenon in transition organometallic chemistry and homogeneous catalysis [149–156].

The hapto-flexible aromatic ligands bonded to the transition metal can facilitate the ligand exchange reaction by "temporarily" lowering the hapticity in the transition state and permitting the increase in the formal coordination number without breaking the canonic electronic rules [157–160, 161, and references therein; 162, 163]. As a general rule, the hapticity change should be considered to be involved in almost all

[6] See footnote 5.

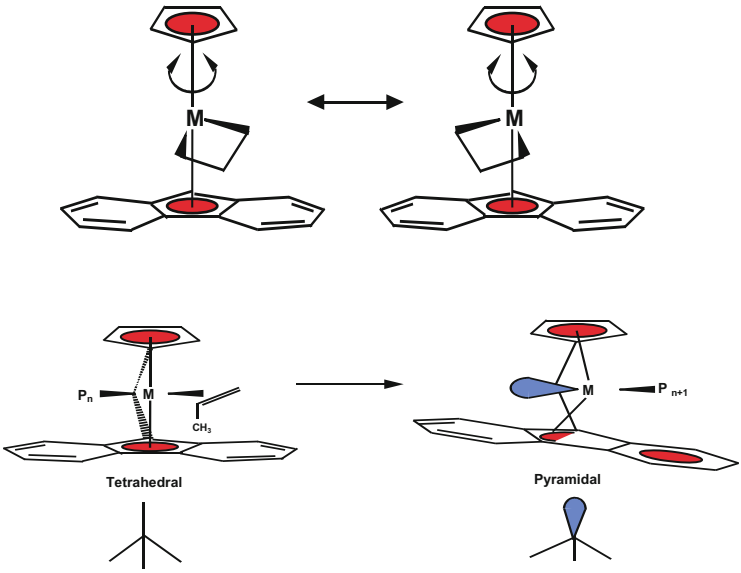

Fig. 19 *Top*: Lateral displacement of ligand system around the centroid–Zr bond axis (the bridge is omitted for the sake of clarity). *Bottom*: Geometry change

metallocenes catalyses particularly those comprising at least a fluorenyl and an indenyl, and possibly those with substituted cyclopentadienyl ring system(s). Whether or not any change in hapticity influences the polymerization behavior of the catalysts depends on the individual case and particularities of the catalysts/polymerization processes under discussion.

In this context, it is also noteworthy to mention another ligand/transition metal related, dynamic behavior, namely, the lateral displacement of the whole ligand system around the imaginary axis connecting the transition metal bonds to the centroids, which was first described by Petersen [164]. This movement can be described as a kind of windshield wiper-type oscillation of the MCl_2 moiety within the fixed ligand framework and could facilitate or influence the steps involved in the counter-ion-assisted site epimerization and chain migratory insertion processes (Fig. 19, top).

Finally, it is important to be aware of another, but slightly different, phenomenon that is related to the geometry change in the catalyst structure during the coordination and insertion steps. The pseudo-tetrahedral geometry, which is assumed for the tetra-coordinated transition metal site in the transition state, cannot be further extended to the step just after insertion. At this stage, the tetra-coordinated structure collapses due to the disappearance of one of the ligands, the monomer/counter-ion, leaving a tri-coordinated species behind in which the repulsive forces acting upon the bonding electron pairs are different and require a new geometry. The most logical structure that can be suggested for this step is a pyramidal structure and an empty fragment orbital. After the next monomer coordination (or the anion

association) the structure will again adopt the tetrahedral geometry (Fig. 19, bottom). This counter-ion-assisted change in geometry operates on all metallocenic catalyst systems, but is probably more crucial for the syndiotactic-specific catalyst systems and syndiospecific polymerization where dynamic processes such as chain migration and, particularly, site epimerization are vital or fatal for its existence. In this aspect, the syndiospecific polymerization process resembles a poly-insertion reaction following at each step the mechanism of a SN2-type reaction. For the isospecific system, the reagent propylene "always" attacks the tri-coordinated intermediate from the same side with the same face because of its homotopicity. For the syndiospecific case, the stereochemistry is determined by the reagent, propylene, attacking the tri-coordinated intermediate form on the opposite side with different faces because of the enantiotopic nature of the active site.

5.1 Catalysts Stereorigidity and Site Epimerization

In the preceding sections, the term "site epimerization" was frequently used as the phenomenon responsible for the formation of the *meso* dyad (m) stereodefects and the lower stereoregularity and crystallinity of the s-PP polymers. To increase the stereoregularity and melting point of these polymers, obviously, the concentration of the rrmr pentads must be suppressed in the polymer chain's backbone by devising means that enable circumventing their formation during syndiospecific polymerization of propylene.

The occurrence of site epimerization is generally explained [165–172] in the following manner: The *R* and *S* configured active sites that are formed during the initial stages of the activation are equi-energetic and can interconvert (epimerize) during the polymerization, particularly in the absence of a coordinating monomer or a stabilizing solvent molecule, particularly at higher polymerization temperatures. The interconversion occurs when occasionally the polymer chain swings back ("back-skip") to its initial coordination position after an insertion before the coordination of the next monomer (Fig. 6). Under these conditions, two (and more than two in the case of Hf-based catalyst **2**) consecutive insertions will take place at the same enantiomorphic coordination position, resulting in enchainment of two monomer units with the same prochiral face and insertion of two units with same stereogenic center. This leads to the formation of *meso* dyad, m-type, stereodefects in the s-PP polymer chains (and/or short isotactic blocks for the Hf analogue).

Little was known initially about the driving forces underlying the phenomenon of site epimerization. Empirically, it has been observed that (in addition to low monomer concentration and higher polymerization temperature dependency) the catalysts formed with metallocene structures with inherently lower stereorigidity or higher flexibility (such as structures **5**, **10**, and **11**) tend to undergo a more frequent site epimerization than those known to be less flexible, as can be seen from data presented in Table 13. Additionally, it was shown that the frontal substituents in more stereorigid catalysts systems impact the site epimerization rate (see **9**/MAO rrmr in

Table 13 Comparison of ^{13}C NMR stereo-error-related normalized spectroscopic stereosequence distributions (%) for syndiotactic polypropylene samples produced with **1**, **5**, **6**, **9**, **10** and **11**/MAO at polymerization temperatures of 40, 60, and 80°C

	Pentad rmmr (%)			Pentad rrmr (%)		
Catalyst	40°C	60°C	80°C	40°C	60°C	80°C
1	1.55	1.65	2.20	1.15	2.70	04.82
5	1.98	2.48	2.91	5.95	8.94	13.49
6	2.08	2.40	–	1.21	1.95	–
9	0.73	0.83	1.63	0.93	1.65	03.79
10	1.60	1.70	2.20	6.50	8.30	10.60
11	3.15	3.03	3.46	4.72	8.55	11.23

Table 13). Section 4.2 describes how computational calculations can be applied for different catalysts systems in the gas phase and solution phase in an attempt to pinpoint the origin(s) of site epimerization and possible ways to circumvent it.

5.2 *The Origin of Site Epimerization: Computational Investigation*

In order for site epimerization to occur during the syndiospecific polymerization of propylene with metallocene-based catalysts, two different mechanisms can be envisaged. Either the site epimerization occurs without inclusion of the counter-ion or it relies on its assistance.

5.3 *Site Epimerization in the "Absence" of the Counter-Ion*

The first and simplest mechanism starts with the naked anion and does not take into account the presence of a counter-ion, the anion (Fig. 6). It was originally presented as the mechanism responsible for the formation of the *meso* dyad (m) stereodefects based on the fact that the transition state geometries before and after a site epimerization are equi-energetic and therefore the assumption is that the activation energy barrier for the site epimerization is be very high.

However, the calculations performed by Angermund et al. [145] on a simple zirconocene complex catalyst model demonstrated that these assumptions do not corroborate with the energy barriers to be surmounted during the site epimerization process. According to the authors, the nonbonded repulsive interaction exerted between the polymer chain and different parts of the ligand, during its insertion-less migration from one coordination position to other, implicates several agostic bond making and breaking transition states, requiring large activation energies (in the order of more than 10 kcal/mol). According to our calculations for the

parent syndiospecific catalyst system **1**/MAO, the energy barrier for the site epimerization is even higher and reaches above 13 kcal/mol [146].

The polymer chain's passage between the two available coordination sites involves many nonbonded repulsive steric interactions with different parts of the ligand and the transformation of the β-agostic resting state into a symmetrical β′-agostic state, via a symmetric transition state in which the alkyl chain rests approximately in the plane formed by the metal and the ligands' centroids, half way between the two coordination positions. During the transformation, on either side of the reaction energy profile, other intermediates with α- and α′-agostic bonds are also formed [170]. Overall, the site epimerization mechanism that does not take into account the role of the counter-anion in the process has a very large activation energy compared to the propagation activation energy. Such a mechanism does not agree with the experimental results, which show that the pentad distributions are in reality influenced by a rather frequent site epimerization.

5.4 Counter-Ion-Assisted Site Epimerization

In the regular and real olefin polymerization processes with metallocene catalysts, the anion is an ever-present participant and an integral part of the functioning catalyst system. It is systematically displaced and moves (in and) out of the coordination sphere in a concerted action, while the monomer units approach for coordination to be paired again with the cation after the insertion process is complete. Assuming that the monomer approach proceeds along the most favorable path (i.e., via a *cis* approach with respect to the anion), immediately after the monomer insertion the anion is positioned at the outer coordination sphere, on the side of the polymer chain (Fig. 20a).

The resulting metalloocenium–polymeryl cation has an empty coordination site available for the re-formation of a close-contact ion pair with the anion. To avoid unnecessary steric interaction with the alky group (polymer chain), the anion can first undergo a spatial reorganization in the outer coordination sphere and then approach the free coordination site unhindered (Fig. 20b) [168, 169]. Alternatively, it can approach the cation directly, forcing in the process the polymer chain to move to the empty coordination site. The first process is what normally occurs during a syndiospecific propagation step (Fig. 20c), while the second process leads to the site epimerization since the immediate ion pairing and the simultaneous displacement of the polymer chain, results in a complex in which the polymer chain occupies the same coordination site as in the previous catalytic cycle (Fig. 20d).

Intuitively, it can be reasonably assumed that the anion reorganization in the outer coordination sphere is spontaneous and occurs freely; its rearrangement is governed purely by diffusion. Indeed, our gas-phase calculations [146] show that for the cation/anion model system, $Me_2C(CpFlu)ZrMe\text{-}Me\text{-}B(C_6F_5)_3$, the energy barrier is about 0.5 kcal/mol, and well within the error associated with the computational method. On the other hand, the formation of the close-contact ion pair is also an exothermic and

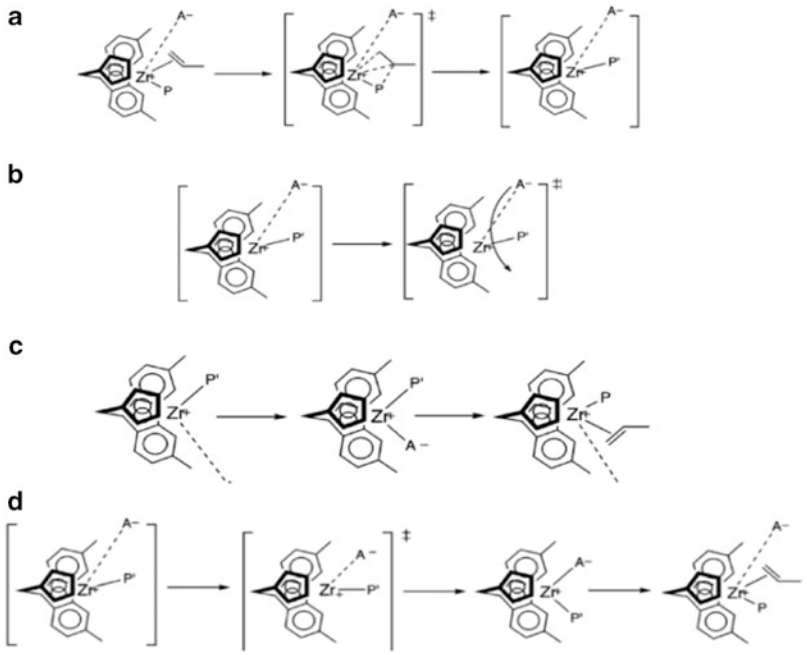

Fig. 20 Cation/anion (A^-) dynamics in the normal propagation process and in site epimerization. (**a**) The concerted process of monomer coordination and anion dissociation. (**b**) Diffusion-controlled process of anion rearrangement. (**c**) Normal chain migratory insertion/propagation. (**d**) Site epimerization

spontaneous process on the potential energy surface, as can be seen from the reaction coordinate shown in Fig. 21, which depicts the re-association of the $MeB(C_6F_5)_3^-$ anion to the metallocenium cation. The exothermicity of the ion pairing is so high (~20 kcal/mol) that the process is irreversible [146].

Ion pairing without previous anion reorganization has an activation barrier due to the fact that the agostic metal–alkyl interaction must be weakened, while repulsive interactions increase as the anion pushes the polymer chain to the other coordination site. During site epimerization, the β-agostic interaction is, however, maintained. The agostic interaction is only lost past the transition state, at a point where the energetic cost of its loss is overcompensated by the gain from the exothermic ion pairing reaction. The extent of the energy barrier depends on the overall charge distribution of the anion and on the substitution pattern of the ligand system.

The computed barriers to the site epimerization with the set of ligands selected for systems 1, 2, and 3 (shown in Scheme 1; see Sect. 3.2) in the gas phase and in toluene solution are given in Table 14. The counter-ion used for all these calculations is the $MeB(C_6F_5)_3^-$ anion. The calculated site epimerization energy barrier seems to decrease from system 1 (barrier of 3.3 kcal/mol) to system 2 (barrier of 2.6 kcal/mol). Only when the substituents are large enough, as is the case for system 3, are repulsive steric interactions increased and the barrier to site epimerization reaches its maximum (5.3 kcal/mol in the gas phase [146]).

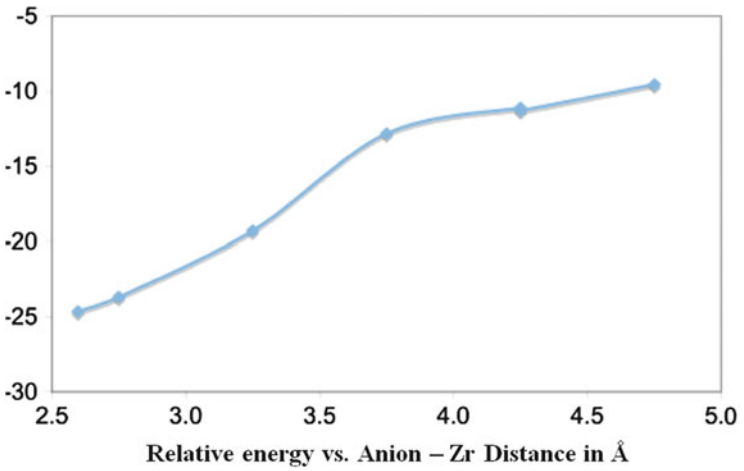

Fig. 21 Ion pairing in the regular polymerization mechanism in system 2, after the diffusion-controlled anion reorganization. Plot shows relative energy (in kcal/mol) versus anion–Zr distance (in Å)

Table 14 Dependence of the relative energies of the species involved in the site epimerization on the nature of the ligand system

	Gas phase			Solution (toluene)		
Catalyst	β-Agostic product	TS_{SE}	Ion pair	β-Agostic product	TS_{SE}	Ion pair
1	−5.3	−2.0	−23.9	−9.9	−5.9	−25.6
2	−4.3	−1.7	−23.0	−9.9	−6.5	−25.5
3	−5.9	−0.6	−22.9	−11.3	−4.8	−20.9

The counter-anion is $MeB(C_6F_5)_3^-$. All energies are relative to the respective parent close-contact ion-pair precursor and propylene. Relative energies in kcal/mol

As can be seen from Table 14, for all three systems, in general, the effect of solvation is to stabilize the transition state species involved, relative to the reactants, i.e., the $L_2Zr\text{-}iBu^+$ $MeB(C_6F_5)_3^-$ close-contact ion pair plus propylene.

To estimate the importance of the anion's charge distribution in the differential solvation of the species involved, the site epimerization of system 2 in the presence of three different anions was investigated. In addition to the already mentioned $MeB(C_6F_5)_3^-$, the site epimerization was studied with an anion developed by Marks, the fluoro-tris-perfluoro-biphenylaluminate, $FAl(Bif_f)_3^-$ anion [168, 169], and also with a model representing methylated MAO, MAO-Me^- [171, 172]. The reaction profiles in the gas phase and in toluene (marked COSMO) are shown in Fig. 22. The energies of the species are reported in Table 15. Marks' anion is much bulkier than $MeB(C_6F_5)_3^-$ and its negative charge is more concentrated on the fluorine, which bridges with the zirconocenium cation. The model for the methylated MAO also has the negative charge more concentrated in the part that interacts with the cation, compared to $MeB(C_6F_5)_3^-$, while its steric bulk is lower

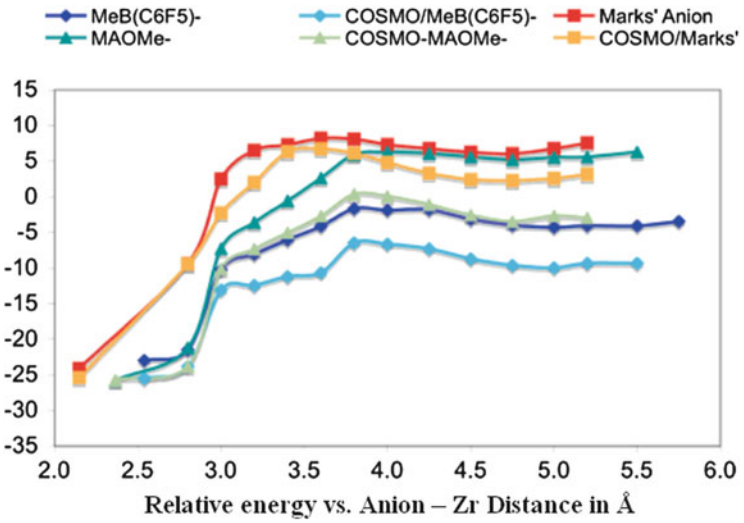

Fig. 22 Influence of the counter-ion on the site epimerization reaction profile in the gas phase and in toluene solution. The anions studied are $MeB(C_6F_5)_3^-$, $FAl(Bif_f)_3^-$ (Marks' anion), and a model for MAO-Me^-. Energies are relative to the respective parent ion pairs plus propylene of system 2. Plot shows relative energy (in kcal/mol) versus anion–Zr distance (in Å). *COSMO* (conductor-like screening model) relates to calculation in the solution phase, toluene [146]

Table 15 Dependence of the relative energies of the species involved in the site epimerization on the nature of the counter-anion

	Gas phase			Solution (toluene)		
Anion	β-Agostic product	TS_{SE}	Ion pair	β-Agostic product	TS_{SE}	Ion pair
$MeB(Ph_f)_3$	−4.3	−1.7	−23.0	−9.9	−6.5	−25.5
MAO	5.2	6.3	−25.8	−3.4	0.4	−25.7
$FAl(Bip_f)_3$	6.1	8.2	−24.1	2.3	6.7	−25.4

The ligand system is 2. All energies are relative to the respective parent close-contact ion-pair precursor and propylene. Relative energies in kcal/mol
TS_{SE} transition state for site epimerization

than that of $FAl(Bif_f)_3^-$ and comparable to $MeB(C_6F_5)_3^-$. The results obtained from gas-phase calculations suggest that site epimerization should occur most easily with a catalyst system that employs the MAO-Me^- anion ($\Delta E = 1.1$ kcal/mol) than with the catalysts formed with Marks' anion ($\Delta E = 2.1$ kcal/mol). The $MeB(C_6F_5)_3^-$ should be the best anion for suppressing the site epimerization to a minimum ($\Delta E = 2.6$ kcal/mol) [146].

However, when the solvation effects are considered, the correct qualitative trend is obtained: Marks' anion is the most effective in reducing the site epimerization ($\Delta E = 4.4$ kcal/mol), with the likelihood of site epimerization increasing when methylated MAO or $MeB(C_6F_5)_3$ are used to activate the Zr–Me bond of the precatalyst ($\Delta E = 3.8$ and 3.4 kcal/mol, respectively). The reason for this behavior

is twofold. First, Marks' anion interacts more strongly with the solvent than the other anions because its charge is the most localized. Therefore, solvent destabilization of the transition state with respect to the reactant is highest for Marks' anion. Second, the steric bulk makes it more difficult for the fluoroaluminate to get close to the zirconocenium cation. The MAO-Me^- model also has a more concentrated charge than $MeB(C_6F_5)_3^-$, which in solution has an effect similar to that found for Marks' anion but it is smaller and therefore the steric effects do not contribute as much to the barrier. The two effects combined are capable of explaining the experimental results.

It seems that the site epimerization mechanism, complex as it is, can be related to three main factors. Optimization of each would contribute to the lowering of its frequency of occurrence and to improvement in the stereoregularity and physical properties of the produced s-PP. Whereas a direct link could be establish between site epimerization and the ligand substituents' bulkiness and positions on one hand, and the anion's size and charge distribution on the other hand, the connection between structural flexibility and site epimerization, though proven empirically, is not very clear.

However, although optimization of the stereorigidity and substitutional factors are, more or less, controllable and within practical grasp, the anion–cation interaction, although very well understood, is in practice very difficult to implement in a large-scale catalyst manufacturing plant for commercial purposes. Understanding the effect of anion size, charge, and charge distribution on the site epimerization transition energy barrier in particular and controlling site epimerization in general, is of utmost importance not just for academic reasons but also for the commercialization of s-PP using large-scale supported catalysts.

6 Metallocene Molecular Symmetry and the Catalyst's Syndiotactic Specificity

In the previous sections, various factors affecting the stereospecificity of the syndiotactic-specific catalysts systems were discussed. A final topic that should be covered to complete these discussions is the relevance of the symmetry of the metallocene molecules and its role in the tactic behavior of the final catalyst. As shown in previous sections, for many different reasons the perfect bilateral symmetry of the original metallocene structure is most likely not maintained in the solution phase. The enantioselectivity calculations with model catalysts have also revealed that the catalyst system will behave in a syndioselective way as long as the conditions for the proper arrangement of ligand, polymer chain and minimum energy monomer coordination mode is provided at each coordination position. Thus, the legitimate question to be answered is whether the C_s or bilateral symmetry of a metallocene molecule is a good indicator for the syndiospecificity of the final catalyst.

All syndiotactic-specific catalysts that have been discussed so far had one principal element in common: their precatalyst's metallocene molecules in solid phase all presented bilateral molecular symmetry or a vertical plane of symmetry (σ_v) in the solid state. However, from the discussions in Sect. 4.3 it is clear that the whole notion of a "perfect" molecular symmetry, bilateral or otherwise, in the solution phase should be handled with caution and not t taken very literally. We saw that even with initially "perfect" bilateral symmetric metallocene molecules like **1** (**2**) and **6** (**7**), the perfect symmetry may be lost, at least in part, in solution and during different stages of the polymerization due to incessant η^5, η^3, and possibly η^1 reversible hapticity change or occasional ring slippage [149–160, 161, and references therein; 162, 163]. Thus, the question to be answered is whether or not the bilateral symmetry embodies the necessary and/or sufficient condition(s) for syndiotactic specificity of a catalyst system. It is apparent that a catalyst's syndiospecificity, as defined in preceding sections, is the result of the combined actions of several factors, the absence of any one of which could lead to the malfunctioning of the catalyst and destruction of the whole syndiospecificity process. The delicate steric balance between the three main participants (ligand, polymer chain, and monomer) as well as the interaction of cation with the counter-ion and proper functioning of the dynamic processes are all essential for its existence. Therefore, it should not be surprising if, occasionally, catalysts prepared with structurally "acceptable" metallocenes and with perfect bilateral symmetry do not function accordingly.

6.1 *Syndio- and Nonsyndiospecific Catalyst Systems with C_s Symmetric Metallocene Structures*

A disappointing example of this kind is the performance of the bilaterally symmetric complex dimethysilyl-(cyclopentadienyl-tetramethyl-cyclopentadienyl)$ZrCl_2$. After its activation with MAO and exposure to propylene, the resulting enantiotopic catalyst system does not function in a syndiotactic-specific manner and the polypropylene polymers that it produces are completely atactic. Here, obviously the presence of constantly rotating, relatively voluminous methyl groups, particularly those two placed in the distal positions (with respect to the bridge-head carbon of the substituted cyclopentadienyl group), blocks the central free space in front of the active site and interferes vigorously with the proper "head-down" coordination mode of propylene and disrupts completely the enantio-face selective process of the system.

Another example demonstrating the determining role of the molecular bilateral symmetry versus the (delicate and fragile) steric balance between the chain, monomer, and ligand substituents for the syndiospecificity process is the polymerization behavior of the metallocene complex diphenylmethylidene-(cyclopentadienyl-octahydrofluorenyl)$ZrCl_2$, with the chemical formula (η^5-C_5H_4-μ-CPh_2-η^5-$C_{13}H_{16}$)$ZrCl_2$, **8**.

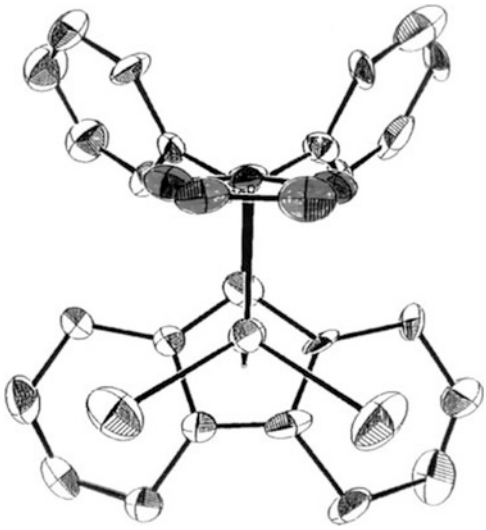

Fig. 23 Single-crystal X-ray-determined molecular structure of (η^5-C_5H_4-μ-CPh_2-η^5-$C_{13}H_{16}$)$ZrCl_2$, **8**

As mentioned in Sect. 2.4, complex **8** is prepared by selective hydrogenation of the fluorenyl moiety of the parent highly syndiotactic-specific metallocene molecule **6**. Its crystal structure is presented in Fig. 23. Complex **8** fulfills all symmetry requirements that one would expect a priori from a would-be syndiotactic-specific precatalyst molecule, nevertheless, after its activation with MAO and its exposure to propylene, complex **8** produces polypropylene chains with perfectly atactic microstructure [28, 30].

At a first glance, one could imagine that the minor changes in the size of the "substituents" resulting upon transformation of benzenic CH groups to slightly larger cyclohexylic CH_2 groups in the distal cyclic positions would be tolerated by the system and would not disturb the proper chain orientation and monomer coordination mode essential for the syndiospecific polymerization process. Closer look at the metallocene molecule **8** reveals that the change in substituent size from CH to CH_2, even though negligible, is concomitant with a dynamic phenomenon that might be the real disturbing factor. Hydrogenation of the six-membered rings transforms a flat "cyclohexatrien"-like cyclic system to a sterically more demanding, cyclohexene/cyclohexane-like aliphatic ring system involving dynamic boat/chair conformation interconversion. The flexible pseudo-cyclohexylic rings of the hydrogenated fluorenyl ligand moiety probably interfere more with proper chain orientation and the face-selective coordination mode of the monomer than the slight increase in the size of the substituents. This situation does not favor systematic and consecutive face-selective enchainment of the propylene monomers in an enantioselective manner conducive to formation of a stereoregular polymer chain.

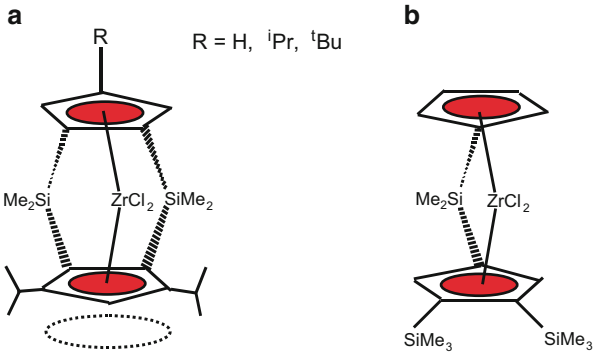

Fig. 24 Double-bridged syndiospecific (**a**) and nonsyndiospecific (**b**) structures [173–175]. *Dotted circle* indicates free space in the central position in front of the active site

6.2 *Other Types of C_s Symmetric Metallocene Catalysts with Syndio- and Nonsyndiospecific Behavior*

The double-bridged bis-cyclopentadienyl-based metallocene catalyst systems developed by Bercaw et al. [173–175] are excellent examples that can be employed to test further the universality of the syndiospecificity requirements for an independent check and verification by a new catalysts system with different ligand settings. The double-bridged zirconocene molecules shown in Fig. 24 do not contain any fluorenyl groups and yet they fulfill all structural and symmetry prerequisites for a potentially syndiotactic-selective metallocene catalyst. They resemble in their general molecular structure the molecules shown in Fig. 2 in that they have a bilateral symmetry and an unsubstituted cyclopentadienyl ring linked to a symmetrically substituted cyclopentadienyl ring (replacing fluorenyl) via a structural bridge.

Of these two structures, only the structure depicted in Fig. 24a acts in a syndiotactic-specific manner and, after activation with MAO, produces s-PP polymers. The structure depicted in Fig. 24b, despite its bilateral symmetry, behaves completely in a nonstereospecific way and, after activation with MAO and exposure to propylene monomer, produces atactic polypropylene. What makes the difference for these two systems is the fact that in the structure shown in Fig. 24a, the free space in the central position in front of the active site is maintained by the substituted cyclopentadienyl group and can accommodate the "head-down" oriented propylene's methyl group with respect to the growing polymer chain. This arrangement cannot be accommodated by the catalyst resulting from the metallocene structure presented in Fig. 24b. The two sterically encumbering germinal tri-methylsilyl groups entirely "fill" the central space and block the space needed for the methyl group "head-down" coordination mode of propylene (see Fig. 25). According to the authors, the double-bridge system exhibits very high stereospecificity (high stereorigidity!) and some of the doubly silylene-bridged zirconocene catalysts investigated by them have shown very high enantioselectivity (rrrr >99.5%) for insertion of α-olefins into zirconium–polymeryl bonds. Loss of stereospecificity in these catalysts occurs mainly by stereochemical inversion at the metal center, i.e., by site epimerization.

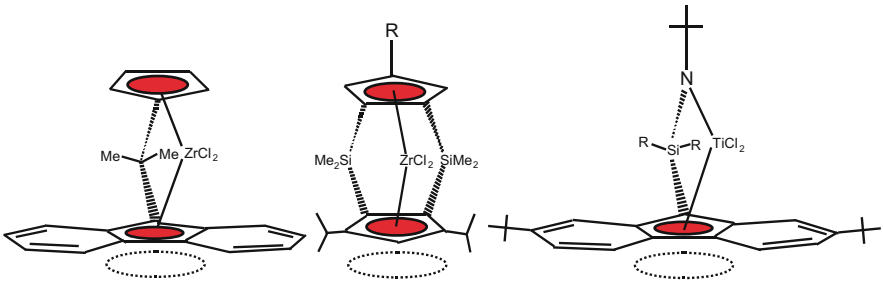

Fig. 25 Presentation of the central free space (*dotted circles*) and its importance for active site syndiospecificity

6.3 C_1 Symmetric Structures: Syndio- and Nonsyndiospecific Catalyst Systems

In the preceding section, the lack of syndiospecificity in certain catalyst systems prepared with bilaterally symmetric, prochiral metallocene molecules was discussed. On the other side of the spectrum, there are reports supporting the existence of many examples of syndiotactic-selective catalyst systems that are produced with metallocene molecules lacking any symmetry. These C_1 symmetric metallocene molecule precursors are capable of producing highly syndiotactic polypropylene [132, 133, 176, 177]. Several syndiotactic-specific catalysts produced with a C_1 symmetric metallocene precursor have been reported by several groups [132, 133, 176]. In these systems, the fluorenyl moiety of the ligand in complexes **1** and **6** is expanded via substitution, in a lop-sided manner, e.g., by fusing another aliphatic or aromatic six-membered ring to it. In these reported cases, the lack of C_s symmetry does not perturb the enantioselectivity of the resulting catalysts and even leads to a slight improvement in their enantioselectivity with respect to the parent catalysts made from complex **1**/MAO.

The most striking example for a C_1 symmetric syndiotactic-specific case is, however, the catalysts prepared with metallocene molecule, diphenylmethylidene-(cyclopentadienyl-3-*tert*-butyl-fluorenyl)zirconium dichloride **12**, with chemical formula (η^5-C_5H_4-μ-CPh_2-η^5-3-^{t}Bu-$C_{13}H_6$)$ZrCl_2$. Complex **12** is clearly a C_1 symmetric molecule, as can be seen from its single-crystal X-ray molecular structure depicted in Fig. 26 (right) [132, 133, 176, 177]. The symmetry-breaking substituent, a large *tert*-butyl group, is positioned at close proximity to the active transitional metal coordination sphere and one of its coordination positions; it interferes strongly with the growing polymer chain in a nonbonded steric manner. Nonetheless, after its activation with MAO, metallocene complex **12** polymerizes propylene to highly stereoregular s-PP chains. The syndiotacticities of the polymers produced with the **12**/MAO catalyst system are higher than of all the syndiotactic polymers produced with **1**/MAO, **5**/MAO, and **6**/MAO catalyst systems and ranks only below polymers produced with the **9**/MAO catalyst system. The s-PP produced

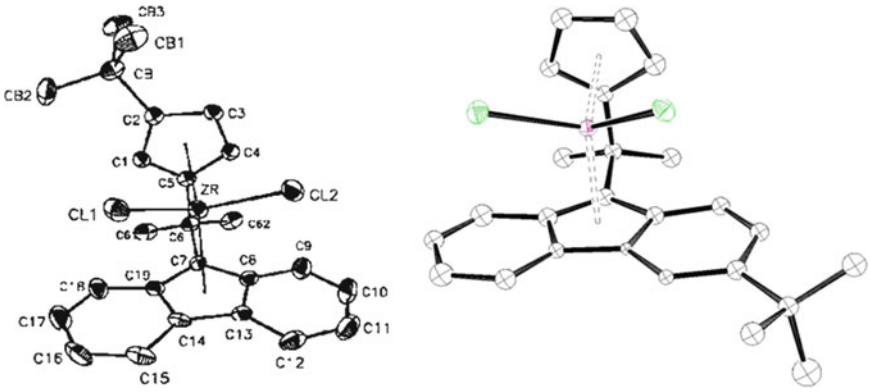

Fig. 26 Single-crystal X-ray molecular structures of (η^5-C_5H_4-μ-CPh_2-η^5-3-^{t}Bu-$C_{13}H_6$)$ZrCl_2$, **12** (*right*) and (η^5-3-^{t}Bu-C_5H_3-μ-CPh_2-η^5-$C_{13}H_7$)$ZrCl_2$, **13** (*left*)

with **11**/MAO at 60°C shows a stereoregularity-related rrrr pentad distribution of higher than 88% and a melting point of 143°C, with a molecular weight of 240 kDa [177].

The polymerization behavior of **12**/MAO might appear at first very surprising; however, a quick review of the principles discussed in previous sections discloses that the catalyst's performance is perfectly in line with all the principal elements, cited as prerequisites for having a high catalyst syndiotactic specificity. The *tert*-butyl group, located at position 3 of the fluorenyl moiety of the ligand, not only does not perturb the delicate balance described for catalyst systems **1** (and **6**)/MAO but also further enhances some of the steps involved in the enantioselective process. The bulky *tert*-butyl group is positioned just below one of the two coordination positions of the active site and interacts with the growing polymer chain strongly, in a "constructive" way, whenever it occupies this position. It reinforces the fluorenyl's role in pushing the polymer chain to move away from it and to adopt the mentioned "upward" chain conformation (this chiral chain conformation is conducive to a proper α-agostic interaction with the active site in the transition state). By doing so, it stabilizes further the enantioselective diastereomeric conformer's transition state and reduces the probability of occasional mis-insertion. The symmetry-breaking *tert*-butyl group makes this coordination position even more enantioselective and renders the catalyst **12**/MAO more enantioselective than the corresponding catalyst **1** (or **6**)/MAO. In this respect, catalyst **12**/MAO can be considered as having an intermediate enantioselectivity state between catalysts **6**/MAO and **9**/MAO.

The catalytic behavior of **12**/MAO is in direct contrast to another, structurally similar, C_1 symmetric catalyst system also prepared via modification of complex **1** with a *tert*-butyl group. However, in this case the *tert*-butyl group is placed at position 3 of the cyclopentadienyl moiety of its ligand. The metallocene molecule isopropylidene-(3-*tert*-butyl-cyclopentadienyl-fluorenyl)$ZrCl_2$, **13**, is prepared according to procedures described in Sect. 8. After its activation with MAO, the catalyst system becomes highly active for polymerization of propylene to

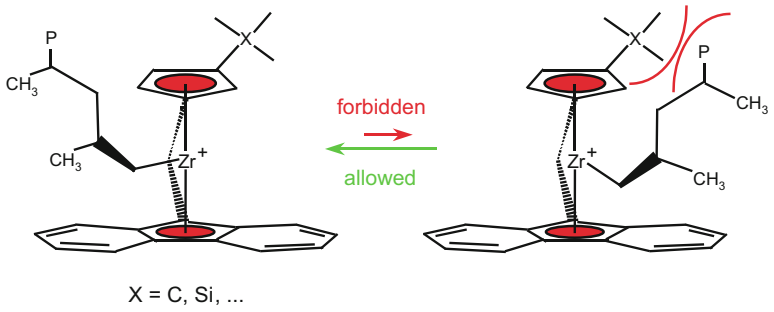

Fig. 27 Nonbonded steric repulsion between polymer chain and β-substituent provoking the systematic and predominant site epimerization

crystalline i-PP. In contrast to complex **12**, the bulky *tert*-butyl group in position 3 of the cyclopentadienyl in complex **13** poses a huge steric challenge to the polymer chain conformational orientation and blocks its systematic migration practically to a halt. Instead of the familiar chain migratory insertion, the polymerization process is dominated by systematic site epimerization, via forcing the growing polymer chain to return to its previous position after each insertion, effectively depriving the originally enantiotopic active site of one of its coordination positions. The overall effect of this *tert*-butyl substitution is the transformation of an originally syndiotactic-specific catalyst system to an isotactic-specific catalyst system. The molecular structure of complex **13** is depicted in Fig. 26 left. Figure 27 demonstrates schematically the ligand-induced site epimerization with the **13**/MAO catalyst system. Metallocene molecule **13** is the first example in a series of C_1 symmetric molecules that form the basis for a new important class of highly isospecific metallocene catalysts [32, 178–185].

6.4 *Other C_1 Symmetric but Syndiospecific Catalyst Systems*

Finally, to close this section, other examples of C_1 symmetric syndiospecific metallocene catalysts system that were reported by Waymouth et al. [186] are presented here briefly. Systematic investigations of the stereoselectivity of metallocene catalysts by these authors revealed that *ansa*-(3-*R*-indenyl)(Cp) zirconocene dichloride complexes whose representative example is depicted in Fig. 28 can generate, after their activation with MAO and exposure to propylene, s-PPs of low to intermediate stereoregularity. The authors report that the introduction of a substituent at position 3 of the indenyl moiety of the ligand will render the second coordination sites of these metallocene catalysts, initially nonstereoselective, stereoselective. Additionally, each of the coordination sites in these catalyst systems is selective and discriminatory with respect to the opposite "enantio"-faces of the propylene molecule. On the basis of the propylene concentration dependency of the

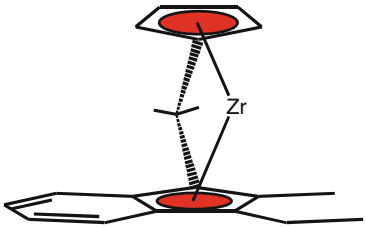

Fig. 28 Generic structure of syndiotactic-specific C_1 symmetric metallocene reported by Waymouth [186]

stereochemistry and an investigation of statistical modeling they implicate site epimerization or "back-skip" as the predominant contributor to the low stereospecificity of these metallocene catalysts. They claim that the indenyl's 2-substituent (the bridge-head position being position 1) in these catalyst systems helps to decrease their tendency to undergo site epimerization [186].

6.5 Industrial Production of Syndiotactic Polypropylene

In 1993, just about 5 years after the initial discovery of the metallocene-based syndiospecific catalyst systems and crystalline s-PP, the large scale commercial production of s-PP was announced by Fina Oil & Chemicals, at the time a subsidiary of Petrofina Belgium now itself an integrated part of the Total Petrochemical company. To reach this stage, 5 years of intensive preparatory work was needed by research groups and engineering teams from three companies: Fina Oil & Chemicals USA, Fina Research/Petrofina Belgium, and Mitsui Toatsu Japan (Mitsui Chemicals Inc). The preparations for the first industrial run with a supported metallocene catalysts focused mainly on challenges that were expected to be encountered during the following stages:

1. Pre-production phase: Large scale production, storage, and safe transportation of the supported metallocene catalyst to the production site.
2. Production phase: Employment of the Phillips loop reactor technology for the large-scale production of polypropylene with a supported metallocene catalyst for the first time ever.
3. Post-production phase: The processing conditions (addition, extrusion, pelletization, etc.) and product handling.

The general efforts to meet these challenges are described in the rest of this section, without the details and specifics that are given in the corresponding patents. These measures are common to all supported metallocene catalysts in commercial runs employing loop bulk or slurry processes.

6.6 Optimization of the Procedure for Synthesis of the Metallocene Molecule

The initial synthetic procedure developed for the synthesis and isolation of the pure metallocene dichloride samples included steps that required subambient reaction temperatures and chlorinated solvents such as methylene chloride [19, 20]. The recipe, though very convenient at smaller scales, was not very practical for the preparation of large quantities of, e.g., structures **1** or **6**. A new synthetic procedure that did not require the application of sub-zero temperatures and also eliminated the methylene chloride as solvent by replacing it with pentane resolved this issue [187, 188]. In the new procedure for the preparation of the metallocene molecule, the exact stoichiometric amount of the ligand's di-anion and $ZrCl_4$ are suspended in pentane and are reacted together. The procedure is effective in such a way that it does not necessitate any purification steps if the starting reagents are reacted together in stoichiometrically exact molar ratios. In this new "pentane procedure" the yield is practically quantitative.

6.7 Proper Choice of the Silica and MAO

For the industrial preparation of supported metallocene catalysts, selection of the inorganic support, generally a type of silica, is very important. There are many varieties of silica available in the market and each has different specifications with respect to the particle surface area, pore size (diameter, volume), bulk density, and mechanical properties [189–194]. The silica pore diameter and volume must be chosen bearing in mind that these pores will be partially filled with MAO.

Once the silica with desired properties is selected, the physically absorbed and chemically bonded (OH groups) excess water molecules have to be removed to reduce the number of OH groups and adjust their concentration to the selected MAO type and concentration in order to minimize excess usage the of MAO. The amount of fines formation during the polymerization, the bulk density of the polymer particles, and even the morphology of the final polymer particles depend, aside from the initial silica type, largely on the silica heat treatment regime and proper MAO treatment [189–194]. The heat treatment of the silica is also essential in ensuring optimum catalyst activity and, as mentioned, reducing the amount of MAO needed. It helps to reduce the amount of catalyst required and consequently the overall production cost. In contrast to silica, there are only a few known sources of MAO available commercially, with more or less similar compositions but different tri-methyl aluminum contents. No matter which of these MAO types is chosen, care must be taken to ensure the freshness and constancy of the product in each delivered batch to maintain the consistency of the resulting catalyst properties and of polymer production in the plant.

6.8 Large-Scale Preparation of the Supported Metallocene Catalysts

There are many different ways to combine the three main ingredients (metallocene molecule(s), MAO, and the silica) chemically to obtain the final supported metallocene catalysts. One of the most recommended procedures in the patent literature is to first treat the silica with MAO and then combine it with metallocene molecules. No matter which procedure is used, one must be aware that the resulting final heterogeneous metallocene catalyst is very reactive towards moisture, leading to its destruction, and to polar molecules that act as a very effective poison and deactivate the catalyst in an irreversible manner. The "long-term" storage of different batches of supported catalyst under inert atmosphere, in a temperate environment that excludes excessive heat, and with no exposure to light is essential for its constant activity and reliability.

6.9 Large-Scale Production of Syndiotactic Polypropylene

The Phillips process technology involving loop reactors, using liquid propylene both as the reaction medium and monomer, requires like any other continuous process meticulous control of polymerization conditions. Any deviations in temperature, pressure, liquid circulation velocity, etc. must be maintained within a very narrow range during the entire period of production. The process is very sensitive to formation of fines (very fine polymer particles), which are formed gradually during the polymerization and adhere to the reactor walls if the catalyst composition is not well defined or the set polymerization conditions not respected. With time, under the influence of the reactor wall temperature, these fines are transformed into a thin layer of polymer film that can act as an insulator and interfere with the reactor's temperature control system, leading to temperature and pressure fluctuations in the reactor. In severe cases, this phenomenon can lead to reactor fouling and shut down. The build-up of fines is generally avoided by the proper choice of silica particles, adjustment of the heat treatment regime, and the reaction conditions between silica support and MAO. The use of an antistatic agent is also not uncommon in moderate cases.

The polymer particle size, morphology, and bulk density are other important parameters for the maximum efficiency of the loop bulk process. Spherical or semi-spherical polymer particles of an average size of about 50–100 μm, with narrow particle size distribution and bulk densities close to or higher than 4 g/ml are generally desired. This is achieved primarily by the proper choice of silica particle morphology and the catalyst preparation conditions but also by adding a pre-polymerization step to the process during which the catalyst is first contacted with propylene, or other polymerizable monomers, at low concentration and moderate temperatures, before entering the main reactor.

6.10 Processing of Syndiotactic Polypropylene Polymers

Highly stereoselective metallocene catalysts, undergoing few site epimerization errors, that produce high crystallinity s-PP with melting points close to or higher than 160°C and fast crystallization rates are available for homogeneous polymerization [195–197]. The very same catalysts systems, however, when supported on a silica carrier, produce s-PP polymers with much lower melting points and crystallinities. Consequently, the crystallinities and crystallization rates decrease in heterogeneously produced s-PP polymer samples. For example, the same MAO-activated metallocene structure, in homogeneous and heterogeneous polymerization reactions, would produce two s-PP polymers whose melting points could differ by 5–20°C. Strangely, the higher the stereospecificity of the metallocene precatalyst and the higher the melting point of the homogeneous s-PP polymer, the lower is the melting point of the heterogeneously produced s-PP polymer counterpart, e.g., a metallocene structure providing s-PP polymers with a melting points around 132°C in homogeneous polymerization, produces s-PP polymers having melting points of about 127°C in heterogeneous polymerization under the same conditions. However, if the improved metallocene catalyst produces a s-PP polymer with a melting point of 160°C in a homogeneous polymerization [195–197, 198–202], the same structure under the same polymerization conditions produces a s-PP polymer with a melting point of only 140°C in heterogeneous polymerization. The analysis of the two polymers reveals that the heterogeneously produced polymer samples contain a much larger number of site epimerization-related errors, whereas the *meso* triad-related errors remain basically unchanged and almost equal for both polymer samples.

Therefore, and inadvertently, the s-PP resins that are produced industrially with supported metallocene catalysts have lower crystallinity and relatively low crystallization rates, which makes their processing challenging. The s-PP polymer melt that exits the extruder does not solidify quickly enough to proceed effectively with the pelletization process. In practice, one can mitigate the problem by addition of a nucleating agent or by cooling the extrudate. Another side-effect of the low crystallinity is that the commercially produced s-PP resins, with melting points below 130°C, contain a substantial amount of absorbed propylene monomer, which is released with time and necessitates vigorous aeration of the storage hanger. These handicaps hamper the fast and efficient extrusion and pelletization of very large quantities of commercially produced s-PP and have so far prevented its vast market penetration as a commodity product compared to other olefin-based thermoplastics.

7 Properties of Syndiotactic Polypropylene Polymers

7.1 Polymorphism of Syndiotactic Polypropylene

Syndiotactic polypropylene (s-PP) presents a very complex polymorphic behavior (the first part of this section on s-PP modifications is reported in the publication [203–212]). s-PP chains crystallize to various polymorphic crystalline phases and,

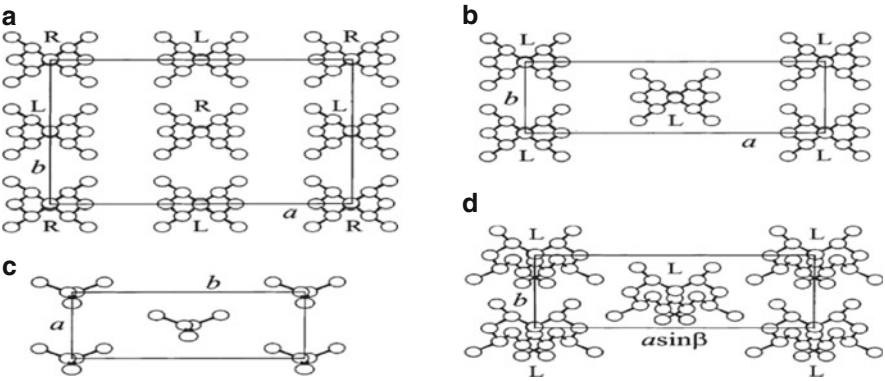

Fig. 29 Models of packing of the limit ordered (**a**) form I (axes $a = 14.5$ Å, $b = 11.2$ Å, $c = 7.4$ Å), (**b**) form II ($a = 14.5$ Å, $b = 5.6$ Å, $c = 7.4$ Å), (**c**) form III ($a = 5.22$ Å, $b = 11.7$ Å, $c = 5.06$ Å), and (**d**) form IV ($a = 14.17$ Å, $b = 5.72$ Å, $c = 11.6$ Å, $\beta = 108.8°$) of s-PP. *R* right-handed helix, *L* left-handed helix

depending on the degree of stereoregularity and the mechanical and thermal history, different degrees of statistical disorder are present in the crystal packing. Four crystalline forms (I–IV) have been described so far and are shown in Fig. 29. The most stable modification, which crystallizes under high crystallization temperature ($T_c > 130°C$) from melt or solution is defined as form I (Fig. 29a) and belongs to the space group Ibca. It is characterized by chains in the s(2/1)2 helical conformation packed in orthorhombic unit cells with axes $a = 14.5$ Å, $b = 11.2$ Å, and $c = 7.4$ Å. The axes of the helices are in the positions (0, 0, *z*) and (1/2, 0, *z*) of the unit cell, and the main X-ray peak in the powder spectrum appear at $d = 7.25$, 5.60, 4.70, and 4.31 Å ($2\theta = 12.2$, 15.8, 18.8, and 20.6°, Cu Kα). In an ideal lattice of form I, right handed (TTG^+G^+) and left handed (G^-G^-TT) helices alternate along the *a* and *b* axes, as imposed by the presence of the (211) reflection. Form II (Fig. 29b), was discovered during investigation of the X-ray diffraction spectra of drawn fibers of s-PP, and is characterized by chains in s(2/1)2 helical conformation packed in orthorhombic unit cells with axes $a = 14.5$ Å, $b = 5.60$ Å, and $c = 7.4$ Å. The axes of the helices are at $d = 7.25$, 5.22, and 4.31 Å ($2\theta = 12.2$, 17.0, and 20.6°, Cu Kα). The space group proposed for form II modification is $C222_1$, for which helices of the same chirality are included in the unit cell. The two metastable modifications, form III (Fig. 29c) and form IV (Fig. 29d), present chains in *trans*-planar and (T6G2T2G2) *n* helical conformations, respectively, and can be obtained only in oriented fibers. Form III is obtained by stretching at room temperature the compression-molded samples, as found by Natta et al. It is characterized by chains in zigzag *trans*-planar conformation. Its crystal structure has been reported recently [203–212] and belongs to the space group $P2_{1cn}$. In this form, the *trans*-planar chains are packed in orthorhombic unit cells with axes $a = 5.22$ Å, $b = 11.17$ Å, and $c = 5.06$ Å. The *trans*-planar form III has been, indeed, obtained by cold drawing procedures of low stereoregular s-PP samples or by stretching at room

temperature highly stereoregular samples prepared with metallocene catalysts. Finally, a form IV was obtained by exposing fiber specimens in the zigzag *trans*-planar form to various organic solvents (e.g., benzene, toluene) at room temperature. This form is characterized by helices with $(T_6G_2T_2G_2)_n$ conformation. A monoclinic unit cell has been proposed for this modification with $a = 5.72$ Å, $b = 7.64$ Å, and $c = 11.6$ Å (chain axis), $\alpha = 73.1°$, $\beta = 88.8°$, and $\Upsilon = 112.0°$. The hypothetical X-ray diffraction powder spectrum of this form would present main peaks at $d = 6.84$, 5.26, and 4.46 Å ($2\theta = 29°$, 16.8°, and 19.9°, Cu Kα).

The formation of the four crystalline modifications depends, as mentioned above, on the conditions of crystallization and the stereoregularity of the polymer sample. Form I, the thermodynamically stable form of s-PP is obtained under the most common conditions of crystallization, from the melt and/or precipitation from solution, in powder samples and single-crystals of s-PP. Form II is a metastable polymorph of s-PP and has been obtained only in oriented fibers of s-PP and, recently, by melt-crystallization at elevated pressure [203–212]. It can be also obtained by room temperature stretching of compression-molded specimens of low stereoregular s-PP samples prepared with vanadium-based Ziegler–Natta catalysts [10–17] or upon releasing the tension in stretched fibers of highly stereoregular s-PP samples initially in form III.

In fact, when highly stereoregular samples, prepared with homogeneous metallocene catalysts, are stretched at room temperature, the *trans*-planar form III is obtained, which transforms into the isochiral helical form II by releasing the tension. In powder of unoriented s-PP samples, only disordered modifications of form II, characterized by conformationally disordered chains containing *trans*-planar sequences (kink band defects) [213–215], can be obtained at atmospheric pressure, for instance, by precipitation from solutions of low stereoregular samples and in copolymers of s-PP with ethylene as the co-monomeric units. The metastable polymorphic forms II, III, and IV generally transform into the stable form I by annealing.

The complex polymorphic behavior of s-PP influences its macroscopic properties. For instance, oriented fibers of s-PP show an elastic behavior that is related to the structural organization. Unoriented compression-molded samples of s-PP behave like a typical highly crystalline material showing a plastic deformation upon stretching at room temperature. The crystalline domains, with chains in helical conformation, tend to assume a preferred orientation along the stretching direction to originate a plastic, irreversible, deformation. High orientation of the crystalline phase is generally achieved. Along with this plastic deformation, a phase transition from the most stable helical form into form III, with chains in the *trans*-planar conformation, gradually occurs. The phase transition is reversible: after release of the tension, the crystalline domains remain nearly oriented with the *c*-axis parallel to the preferred (stretching) direction, and the *trans*-planar form III transforms again into the more stable helical form. As a result, for previously unoriented material, a partial recovery of the macroscopic dimensions of the sample is attained. Therefore, unoriented samples show only fair or poor elastic properties. Stress-relaxed fibers show instead very good elastic behavior upon successive

stretching and relaxation; the helical form transforms by stretching into the *trans*-planar form, which transforms again into the helical form by releasing the tension, and a nearly total recovery of the initial dimensions of the fiber samples is observed. When the crystalline domains are already oriented along the stretching direction, i.e., when the sample has already undergone the plastic deformation, the fibers show good elastic properties. Of course, during the mechanical cycles the chains in the amorphous regions are also subjected to a reversible conformational transition from the "random coils" into extended conformations, and vice versa.

This reversibility of the transition is possibly assisted and is, somehow, favored by the polymorphic transition occurring in the crystalline regions. It has been suggested that although the driving force that induces the recovery of the initial dimensions in common elastomers upon release of the stress is mainly entropic, in the case of s-PP it is basically linked to the enthalpy gain achieved when the sample is relaxed due to the metastability of the *trans*-planar form III. On the other hand, it has been also hypothesized that the elastic behavior is mainly due to the conformational transition occurring in the amorphous phase for chains connecting the crystalline domains.

7.2 *Thermal Properties and the Origin of Multiple Melting Behavior of s-PP*

Differential scanning calorimetry (DSC) studies that were performed on the isothermal bulk crystallization and subsequent melting behavior of various s-PP resins from laboratory and commercially produced samples, indicate that most DSC endothermic traces exhibited two (or three) distinct melting endotherms, depending on the temperature at which the samples were crystallized. The DSC scans performed at different heating rates on as-polymerized or melt-crystallized forms of such samples generally present endotherms with a double peak shape. The increase in the enthalpy of the high-melting peak with decreasing heating rate is indicative of the occurrence of a recrystallization phenomenon during the heating process, whereby the less-ordered form II is partially transformed to the more ordered form I. This observation was made mainly for s-PP samples with stereoregularity lower than 90% (rrrr $< 90\%$); disordered modifications of form I are always obtained by melt crystallization. For highly stereoregular samples (rrrr $> 93\%$), only a single endothermic peak is observed, independent of the crystallization temperature of the isothermally melt-crystallized samples and the heating rate. The equilibrium melting temperature, T_m of the fully s-PP estimated to be 182°C, which is close to the value of 186°C found for i-PP [128]. Multiple melting behavior is not an exclusive phenomenon for s-PP. In fact, similar observations have been made on a number of other semicrystalline polymers, including some flexible polymers and some semi-stiff polymers.

Supaphol et al. [216–218] reviewed a number of hypotheses that have been proposed to explain the occurrence of multiple melting endotherm phenomena. In the studies on isothermal crystallization under quiescent conditions (i.e., crystallization is only a function of temperature), the multiple melting behavior of these semicrystalline polymers have been attributed to the following four phenomena: (1) the presence of two (or more) crystal modifications in the sample; (2) the presence of two (or more) crystalline morphologies; (3) the presence of two populations of crystal lamellae of different thicknesses; and (4) the simultaneous melting, recrystallization, and re-melting of the lamellae initially formed at the crystallization conditions.

7.3 *Syndiotactic Polypropylene: Physical and Mechanical Properties*

Compared to conventional i-PP produced with ZN catalysts, the s-PP produced commercially with supported metallocene catalyst has, due to its relatively low crystallinity, on the one hand, lower density, hardness, tensile strength, and flexural modulus and, on the other hand, higher clarity or transparency, impact strength, toughness (or elasticity), and stiffness. The melting point, density, hardness, crystallization temperature, heat of fusion, tensile strength at break, flexural modulus, and percent haze of s-PP all increase with increasing syndiotacticity of the polymer. The crystallization rate (defined customarily as the inverse of the time needed to attain one half of the final crystallinity multiplied by 100), crystallization temperature, and melting point are also all affected by the degree of stereoregularity of the polymer chains. The low temperature impact strength of s-PP decreases with decreasing temperature, but at 0°C it has still about two to three times higher impact strength than that of i-PP. Syndiotactic polypropylene also has different thermal properties to conventional i-PP and its glass transition temperature and heat of fusion are lower than those of i-PP. Unique properties of s-PP include good γ-ray internal stability and very low melting point for heat sealing. s-PP has also different thermal properties than the conventional i-PP. Its heat of fusion is lower than that of i-PP. Syndiotactic polypropylene also has different rheological behavior to i-PP; for example, regardless of the degree of its tacticity, s-PP has a much smaller melt flow than i-PP with comparable molecular weight. The rheological behavior of s-PP seems to indicate that, owing to its more flexible chain backbone structure, it contains a significantly higher number of molecular entanglements per unit volume than i-PP (see following section).

7.4 Syndiotactic Polypropylene: Processing and Rheology

Syndiotactic polypropylene has proven to process very differently from conventional i-PP, both in melt-phase processes and in solid-phase processes. At high shear rates, s-PP is more viscous and has higher elastic modulus than conventional i-PP, regardless of the degree of the tacticity. s-PP, has also a much smaller melt flow than that of the corresponding i-PP with the same molecular weight. s-PP has a lower crystallization rate than i-PP, and minor modifications are necessary when existing processing equipment designed for conventional i-PP is used for s-PP, e.g., s-PP needs a longer cycle time.

With a melting point of approximately 130°C (versus 160°C for i-PP) and crystallinity of approximately 30% (versus 55% for i-PP) for commercially produced s-PP, the discrepancies and the differences in solid-phase properties and processing seem obvious. As for the melt phase, the narrow molecular weight distribution of 2 for metallocene catalyst-based s-PP provides only part of the explanation for the observed differences in melt-phase properties. A cursory comparison with controlled-rheology i-PP (an ex-situ, extruder tailormade i-PP of very narrow MWD) makes one realize that must still be other reason(s), for the observed melt behavior. Polymer microtacticity could be one parameter to considered. When considering the molecular networks in high molecular weight polymer melts, the molecular weight and MWD are usually the only parameters compared at length for such linear polymers (long-chain branching does not usually exist in ZN polypropylenes). The effects of polymer chain tacticity are widely ignored in these rheological treatments. One reason is probably that it does not seem obvious why there should be a difference between amorphous polymer melts of i-PP and s-PP, each containing freely rotating molecules of similar chemistry (equal monomer units) in motion. However, polymer microtacticity appears to be the only other parameter that could provide the necessary explanations for the observed melt property differences for s-PP and i-PP.

Rheological studies have confirmed [219–221] that s-PP forms significantly more entanglements in the melt than its isotactic counterpart. Melt property effects are thus justified with this inherent difference in molecular chain flexibility and entanglement in mind. It is generally accepted that above a minimum (critical) molecular weight for each polymer type, there exists an equilibrium level (or distribution) of molecular entanglements in the molten phase. These chain entanglements contribute in expected ways to the observed rheological behaviors. In particular, they are imagined to act as minor "crosslinks," providing resistance to flow beyond the normal friction of molecule against molecule. In addition, each polymer backbone defines a characteristic flexibility (or rigidity) for interaction with its neighboring molecules. This also contributes to a polymer molecule's ability to move and fold around and amongst other like molecules in the melt. These two properties are obviously related.

The calculations performed by Wheat [220] for i-PP and s-PP also give surprising differences in these quantities. Essentially, based on this study, s-PP is

predicted to contain nearly three times the number of entanglements as i-PP, due primarily to tacticity differences alone! This would begin to explain many of the effects observed.

7.5 Market Applications

Although s-PP resins were originally designed for specialty markets, not yet served by conventional i-PP, it has the potential to compete against conventional i-PP, low density polyethylene (LDPE), linear low-density polyethylene (LLDPE), and polyvinyl chloride (PVC) in certain markets because of its toughness, impact strength, transparency, and low heat-seal temperature. As pure polymer, s-PP has found new applications and as a blend with i-PP it yields new properties that can be exploited in existing applications as a substitute for other polymers. Potential application areas include: (1) adhesives such as hot melt and functional grafting-type adhesives; (2) clear containers for sub-zero temperature usages; (3) preparation of color and/or additive concentrates; (4) elastomers; (5) extrusion products, especially those that must be sterilized by radiation, such as flexible bags and tubing; (6) fibers; (7) films, especially those requiring high clarity, toughness, and a low heat-sealing temperature, such as for snack food packaging; (8) injection molded products, especially those that must be sterilized by radiation, such as containers, rigid bottles, and syringes for medical use; (9) modifier and/or clarifier for resins such as i-PP; (10) modifier for polypropylene film; and (11) transparent sheets. A few important applications are reviewed below.

7.5.1 Injection Molding

The cycle time in injection molding with s-PP is significantly increased compared to that for i-PP. Because s-PP polymer thins less than i i-PP under shear, s-PP requires a longer boost time in injection molding and has a lower die swell than i-PP. Injection-molded s-PP samples and articles have lower haze, higher gloss, much higher notched Izod impact strength, lower flexural modulus (thus higher flexibility), lower Vicat softening temperature, and lower heat distortion temperature than similarly molded i-PP and copolymer containing 2% ethylbenzene. Their tensile properties are lower than that of i-PP and are comparable to that of the copolymer. s-PP homopolymer and clear impact resin also have higher Gardner impact at room temperature, higher light transmittance, and lower flexural modulus and haze than i-PP, i-PP copolymer, and s-PP-modified i-PP copolymer. After aging at room temperature, the tensile properties and flexural modulus of s-PP increases during the first 48 h, then the tensile properties begin to decrease and the flexural modulus begins to level off. s-PP also has a higher percentage decrease in elongation with time than i-PP homo- and copolymer at room temperature, probably due to the more pronounced secondary crystallization effect. The elongation at break of s-PP remains relatively stable at 130°C up to about 1,000 h. Injection-molded s-PP

samples were found to break up like a flexible polymer when exposed to 500 h of UV radiation, and the reduction in its intrinsic viscosity (or molecular weight) due to γ-ray irradiation is lower than that for i-PP.

7.5.2 Injection Blow Molding

Syndiotactic polypropylene resins allow the production of small flexible containers with very good γ-radiation resistance and a degree of transparency never achieved before with any polypropylene. Moreover, the final objects transmit a feeling by contact that has been qualified as "soft and warm." Only some highly expensive specialty and engineered polymers can achieve the same combination of properties, but require a significantly longer cycle time.

7.5.3 Films

Syndiotactic polypropylene can be heat-sealed at a lower temperature than conventional i-PP copolymers containing high levels of ethylene (sealing initiation temperature of around 100°C versus 110–120°C). s-PP films can be heat-sealed at a lower temperature than conventional ethylene/propylene copolymers containing 6% ethylene, e. g., $<$113°C versus $>\sim$119°C to develop a seal strength of 500 g/in., When compared with conventional i-PP, cast and blown films extruded from s-PP have much lower haze, much higher gloss, slightly higher elongation at yield, and comparable tensile strength at yield. Bi-axially oriented polypropylene (BOPP) films with improved shrink versus conventional BOPP films are obtained by blending a few wt% of s-PP into i-PP. The tensile, elongation, and optical properties and the impact strength of s-PP cast films are influenced by the melt temperature and chill roll temperature. Lowering the chill roll temperature leads to production of films with slightly higher tensile strength and elongation. Film extruded from an s-PP-modified random propylene copolymer has much lower haze, much higher gloss, slightly higher elongation at yield, comparable tensile strength at yield, slightly lower Elmendorf tear strength, and much lower Dart drop impact than that extruded from a ultra-low-density polyethylene (ULDPE)-modified random copolymer. It also has higher haze, gloss, Elmendorf tear strength, Dart drop impact, and elongation, and lower tensile strength at yield than films extruded from a propylene copolymer containing 2% ethylene and a conventional homopolypropylene.

7.5.4 Fibers

Addition of a few wt% of s-PP to i-PP before spinning dramatically improves the bulk and the softness of spun laid or staple nonwovens, two important techniques in fiber application. Moreover, the thermal bonding temperature is lowered by about 5–10°C, whereas the mechanical properties of the nonwovens are retained or slightly improved.

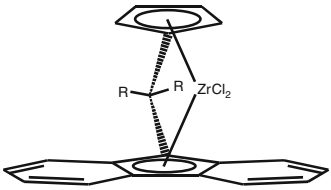

R = methyl (**1**), R = phenyl (**6**)

1

Fig. 30 Generic structure representing the simplest members of bridged cyclopentadienyl-fluorenyl zirconocenes (**1**)

7.5.5 Additive, s-PP/i-PP Blends

Syndiotactic polypropylene can be used as an impact modifier. Indeed, the addition of s-PP to i-PP can improve impact characteristics over pure i-PP [222–225]. When s-PP is blended with i-PP, the resulting resin has a processability better than that of i-PP and impact and transparency properties better than those of pure i-PP. As an impact modifier to a controlled rheology i-PP copolymer, s-PP does not crosslink or affect the peroxide efficiency of the copolymer while improving the Izod notched impact and maintaining the similar processability of the copolymer.

8 Experimental Details [187, 188]

8.1 Synthesis of Bridged, Cyclopentadienyl-Fluorenyl Zirconocenes.

The unsubstituted cyclopentadienyl-fluorenyl zirconocenes **1** and **6** (Fig. 30) are synthesized in two steps starting from the respective fulvenes and fluorene. All reactions are performed under inert gas atmosphere. All solvents are dry and free of oxygen.

For synthesis of the ligand, a solution of 150 mmol of fluorene dissolved in 200 mL of THF is cooled to 0°C. At this temperature, 93.75 mL (150 mmol) of a 1.6 M solution of methyllithium in diethylether is added dropwise. After the addition is completed, the resulting orange solution is stirred at room temperature for 4 h. Then, a solution of 150 mol of the respective fulvene in 100 mL of THF is added dropwise. After stirring at room temperature for 16 h, the mixture is hydrolyzed by careful addition of 200 mL of a saturated aqueous solution of ammonium chloride. The product **2** (Fig. 31) is extracted with diethyl ether as a white solid. Recrystallization from methanol:chloroform results in white needle-like crystals. Yield is 80% (R = Ph) to 100% (R = Me).

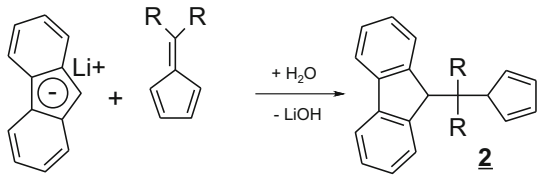

Fig. 31 General synthetic scheme for the preparation of bridged cyclopentadienyl-fluorenyl ligand (**2**)

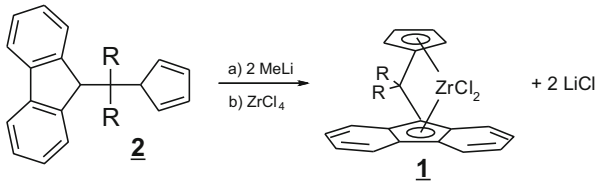

Fig. 32 General synthetic scheme for the preparation of bridged cyclopentadienyl-fluorenyl zirconocenes (**1**)

For synthesis of cyclopentadienyl-fluorenyl zirconocenes (Fig. 32), a solution of 42 mmol of **2** in 300 mL of THF is cooled to −78°C. At this temperature, 56.33 mL (84 mmol) of a 1.6 M solution of methyllithium in diethylether is added dropwise.

After 2 h, the cooling bath is removed and the red solution is stirred at room temperature for 8 h. Then, the solvent is removed in vacuo, resulting in an orange powder. This powder is suspended in 300 mL of pentane. Then 42 mmol of zirconium tetrachloride suspended in 100 mL of pentane is added. The mixture is stirred at room temperature for 6 h. Then, the insoluble red raw product is isolated by filtration. To separate from the lithium chloride, the raw product is taken up in 500 mL of methylene chloride and the turbid solution filtered over dried kieselgur. The resulting clear red solution is slowly evaporated and the product is isolated as a red crystalline precipitate [187, 188].

In Fig. 32, for R = Me the formula is $C_{21}H_{18}Cl_2Zr$. Percentage composition by analysis: C, 58.06; H, 4.14; Cl, 16.34; Zr, 20.99%. Percentage composition by calculation: C, 58.17; H, 4.19; Cl, 16.34; Zr, 20.07%.

For R =Me, results of ^{1}H NMR (CD_2Cl_2) ppm: δ = 8.1 (2H, m, 4,5-Flu), 7.8 (2H, m, 1,8-Flu), 7.5 (2H, m, 3,6-Flu), 7.2 (2H, m, 2,7-Flu), 6. 3 (2H, t, 3,4-Cp), 5.7 (1H, t, 2,5-Cp), 2.3 (6H, s, bridge-CH_3), where m, t and s signify multiplet, triplet and singlet, respectively.

For R = Ph, results of ^{1}H NMR (CD_2Cl_2) ppm: δ = 8.19 (2H, m, 4,5-Flu), 7.95 (2H, m, 2-Ph), 7.88 (2H, m, 5-Ph) 7.56 (2H, m, 3,6-Flu), 7.47 (2H, m, 4-Ph), 7.35 (2H, m, 3-Ph), 6.99 (2H, m, 2,7-Flu), 6.43 (2H, m, 1,8-Flu), 6.37 (2H, t, 3,4-Cp), 5.80 (2H, t, 2,5-Cp).

9 Outlook

The development of syndiospecific metallocene catalyst systems and s-PP from laboratory to commercial production has been one of the most successful projects both from scientific and technological points of view; it was driven mainly by the discovery of a new metallocene structure. During the 5 years of research and development there were many scientific, technical, and technological challenges, for example, regarding optimization of metallocene structure, its large scale production, supported catalyst development, process compatibility issues, polymer processing, and development of new product markets. Although the industrial production of s-PP has been a successful undertaking from both the technical and economic points of view, the production of s-PP has remained limited in volume and s-PP has been introduced to the market as rather a specialty product. There still exist afew handicaps that have hampered its large market penetration despite the attractiveness of its properties, particularly its excellent optical properties and its unusually high radiation resistance. The stumbling block on this road was and still is the slow crystallization rate of industrially manufactured s-PP. This originates from the low crystallinity, which in turn emanates from the presence of high numbers of the site epimerization-dependent *meso* dyad stereodefects in s-PP samples produced with supported catalyst systems.

Despite our good understanding of cation/anion dynamics in solution, our current understanding of the changes that the anionic MAO species undergo upon heterogenization on the silica is still limited and therefore our capability to control and or prevent the site epimerization processes is restricted.

We suspect either that the nature of the anionic species of MAO changes dramatically upon heterogenization to favor site epimerization-related pathway(s) or that, in heterogeneous polymerization, limitations in monomer-to-active site diffusion lower the effective monomer concentration at the active site and change the balance between the propagation rate and site epimerization rate in favor of the latter.[7]

[7] Incidentally, a very similar phenomenon is observed with C_2 symmetric bis-indenyl-based isospecific zirconocene dichloride catalysts. For example, the metallocene dimethylsilyl-bridged 2-methyl-4-phenyl-bisindenylzirconocenedichloride, once activated with MAO, produces an isotactic polypropylene with a melting point close to 160°C in liquid propylene at 60°C. However, the same catalyst, once supported on a silica carrier, produces i-PP polymers that have melting points ranging between 150 and 152°C, at the same polymerization conditions. In this case, the formation of larger amounts of region-irregular units in the heterogeneously produced i-PP is the melting point lowering factor. Interestingly, the bridged cyclopentadienyl-fluorenyl ligand-based C_1 symmetric isospecific catalyst systems are immune to this flaw. The homogeneously and heterogeneously produced isotactic polypropylenes with these catalysts show no or very few regio-irregular errors and their isotactic polypropylene polymer pairs have similar melting points that reach, for polymers produced with highly selective C_1 symmetric catalyst systems, values close to or even higher than 160°C.

No matter what the real causes behind the increased site epimerization rate in heterogeneous polymerization might be, the major challenge to s-PP resins becoming commodity products is the development of a heterogeneous catalyst system that does not trigger the mechanisms responsible for the acceleration of site epimerization processes. While waiting for this development, there exist two options for circumventing this dilemma in the short- or medium-term. Either operate the plant at lower temperatures and/or select the solution process as the technology of choice for the production of s-PP so that the heterogenization step becomes redundant. The first option will lead naturally to higher production costs and the second requires complete revision of the process conditions for the companies owning the technology.

References

1. Natta G, Pasquon I, Zambelli A (1962) J Am Chem Soc 84:1488
2. Natta G (1956) Chim Ind 38:751–765 (Chem. Abstr. 1957, 57, 11063)
3. Natta G (1960) Macromol Chem 35:94–131
4. Natta G, Pino P, Mazzanti G (1957) Gazz Chem Ital 87:528–548 (Chem. Abstr. 57, 88347)
5. Natta G, Corradini P, Ganis P (1960) Makromol Chem 39:238
6. Natta G, Pasquon I, Corradini P, Peraldo M, Pegoraro M, Zambelli (1960) A Atti Accad Nazl Lincei Rend Classe Sci Fis Mat Nat 28:539
7. Natta G, Pasquon I, Corradini P, Peraldo M, Pegoraro M, Zambelli A (1961) Rend Acc Naz Lincei 8(28): 539
8. Corradini P, Natta G, Ganis P, Temussi PA (1967) J Polym Sci C 16:2477
9. Natta G, Peraldo M, Allegra G (1964) Makromol Chem 75:215
10. Zambelli A, Gatti G, Sacchi C, Crain WO Jr, Roberts JD (1971) Macromolecules 4:45–477
11. Bovey FA, Sacchi MC, Zambelli A (1974) Macromolecules 7:752–754
12. Zambelli A, Tosi C, Sacchi C (1972) Macromolecules 5:649–654
13. Zambelli A, Wlofsgruber C, Zannoni G, Bovey FA (1974) Macromolecules 7:750–752
14. Zambelli A, Natta G, Pasquon I (1964) J Polym Sci 4:411
15. Zambelli A, Longo P, Terenghi S, Recupero D, Zannoni G (2000) J Mol Catal A 152:25–31
16. Lehr MH (1967) Macromolecules 1:178–184
17. Zambelli A, Sessa I, Grisi F, Fusco R, Accomazzi P (2001) Macromol Rapid Commun 22(5):297
18. Ewen JA, Jones LR, Razavi A, Ferrara JJ (1988) J Am Chem Soc 110:6255
19. Razavi A, Ferrara JJ (1992) J Organomet Chem 435:299
20. Razavi A, Atwood JA (1993) J Organomet Chem 459:117
21. Razavi A, Thewalt U (1993) J Organomet Chem 445:111
22. Razavi A, Ewen JA (2001) Syndiotactic polypropylene. Patent US 6,184,326, Fina Technology, Inc
23. Ewen JA, Razavi A (1995) Highly crystalline syndiotactic polypropylene. Patent US 5,476,914, Fina Technology, Inc
24. Razavi A, Ewen JA (1994) Patent US 5,334,677, Fina Technology, Inc
25. Ewen JA, Razavi A (1990) Process and catalyst for producing syndiotactic polyolefins. Patent US 4,892,851, Fina Technology, Inc
26. Elder MJ, Razavi A, Ewen JA (1993) Patent US 5,225,500, Fina Technology, Inc
27. Elder MJ, Razavi A, Ewen JA (1992) Patent US 5,155,080, Fina Technology, Inc

28. Razavi A, Bellia V, De Brauwer Y, Hortmann K, Peters L, Sirol S, Van Belle S, Thewalt U (2004) Macromol Chem Phys 205:347–356
29. Razavi A, Bellia V, De Brauwer Y, Hortmann K, Peters L, Sirol S, Van Belle S, Thewalt U (2004) Macromol Symp 213:157–171
30. Razavi A, Thewalt U (2006) Coord Chem Rev 250:155–169
31. Razavi A, Bellia V, Brauwer Y, Hortmann K, Peters L, Sirol S, Van Belle S, Marin V, Lopez M (2003) J Organomet Chem 684:206–215
32. Razavi A, Thewalt U (2001) J Organomet Chem 621:267–276
33. Razavi A, Vereecke D, Peters L, Den Dauw K, Nafpliotis L, Atwood JL (1995) Homogeneous Ziegler–Natta catalysts. In: Fink G, Muelhaupt R, Brintzinger HH (eds) Ziegler catalysts. Springer, Berlin, pp 112–147
34. Razavi A, Peters L, Nafpliotis L (1997) J Mol Catal A Chem 115:129
35. Sinn H, Kaminsky W, Vollmer HJ, Woldt R (1980) Angew Chem 92:396
36. Sinn H, Kaminsky W, Vollmer HJ, Woldt R (1980) Angew Chem Int Ed 19:390
37. Kaminsky W, Sinn H (1982) Homogeneous and high active Ziegler–Natta catalysts with alumoxane as component. In: Proceedings of the IUPAC 28th macromolecular symposium, Amherst, 1982, p 247
38. Kaminsky W, Miri M, Sinn H, Woldt R (1983) Macromol Rapid Commun 4:417
39. Herwig J, Kaminsky W (1983) Halogen free soluble Ziegler catalysts with methylalumoxane as cocatalyst. Polym Bull 9:464
40. Kaminsky W, Lüker H (1984) Macromol Rapid Commun 5:225
41. Kaminsky W (1984) Naturwissenschaften 71:93
42. Kaminsky W (2004) J Polym Sci A Polym Chem 42:3911–3921
43. Schnutenhaus H, Brintzinger HH (1979) Angew Chem Int Ed Engl 18:777–778
44. Wild FRWP, Zsolnai L, Huttner G, Brintzinger HH (1982) J Organomet Chem 232:233–247
45. Wild FRWP, Wasiucionek M, Huttner G, Brintzinger HH (1985) ansa-Metallocene derivatives. IIV. J Organomet Chem 288:63–67
46. Ewen JA (1984) J Am Chem Soc 106:6355–6364
47. Kaminsky W, Külper K, Brintzinger HH, Wild FRWP (1985) Angew Chem 97:507–508
48. Kaminsky W, Külper K, Brintzinger HH, Wild FRWP (1985) Angew Chem Int Ed Engl 24:507–508
49. Kaminsky W, Miri M (1985) Ethylene propylene diene terpolymers produced with a homogeneous and highly active zirconium catalyst. J Polym Sci A Polym Chem 23:2151
50. Kaminsky W (1985) Polym Prepr 26(2):373
51. Kaminsky W, Külper K, Niedoba S (1986) Macromol Symp 3:377
52. Kaminsky W (1986) Angew Makromol Chem 145/146:149
53. Kaminsky W, Niedoba S (1987) CLB Chemie für Labor und Betrieb 38:398
54. Soga K, Shiono T, Takemura S, Kaminsky W (1987) Macromol Rapid Commun 8:305
55. Werner RW, Brintzinger HH, Rieger B, Zolk R (1990) Angew Chem Int Ed Engl 29(3):279–280
56. Arlman EJ, Cossee P (1964) J Catal 3:99–104
57. Cossee P (1960) Tetrahedron Lett 17:12–16
58. Cossee P (1960) Tetrahedron Lett 17:17–21
59. Cossee P (1964) J Catal 3:80–88
60. Breslow D, Newburg NR (1959) J Am Chem Soc 81:81–86
61. Green MLH (1972) Pure Appl Chem 30:373–388
62. Ivin KJ, Roony JJ, Stewart CD, Green MLH, Mahtab R (1978) J Chem Soc Commun 1978:604–606
63. Brookhart M, Green MLH (1983) J Organomet Chem 205:395–408
64. Corradini P, Barone V, Fusco R, Guerra G (1979) Eur Polym J 15:1133
65. Pino P, Muelhaupt R (1980) Angew Chem 92:869–887
66. Zambelli A, Sacchi MC, Locatelli P, Zannoni G (1982) Macomolecules 15:211–212
67. Zambelli A, Locatelli P, Sacchi MC, Tritto I (1982) Macromolecules 15:831–834

68. Farina M (1987) Top Stereochem 17:1–111
69. Corradini P, Guerra G, Vacatello M, Villani V (1988) Gazz Chem Ital 118:173–177
70. Cheng HN, Ewen JA (1989) Makromol Chem 190:1931–1934
71. Cavallo L, Guerra G, Oliva L, Vacatello M, Corradini P (1989) Polym Commun 30:16–19
72. Cavallo L, Guerra G, Vacatello M, Corradini P (1991) Macromolecules 2:1784–1790
73. Guerra G, Cavallo L, Moscardi G, Vacatello M, Corradini P (1994) J Am Chem Soc 116:2988–2995
74. Zambelli A, Proto A, Longo P (1995) In: Fink G, Mülhaupt R, Brintzinger HH (eds) Zeigler catalysts: recent scientific innovations and technological improvements. Springer, Berlin, pp 217–235
75. Corradini P, Guerra G, Cavallo L, Moscardi G, Vacatello M (1995) In: Fink G, Mülhaupt R, Brintzinger HH (eds) Zeigler catalysts: recent scientific innovations and technological improvements. Springer, Berlin, pp 237–249
76. Toto M, Cavallo L, Corradini P, Moscardi G, Resconi L, Guerra G (1998) Macromolecules 31:3431–3438
77. Dyachkovskii FS, Shilova AK, Shilov AE (1967) J Polym Sci C Polym Symp 16(4):2333–2339
78. Zefirova AK, Shilov AE (1961) Dokl. Akud Nuuk SSSR 136.599; Dokl. Chem (Engl. Translation) p 13677
79. Eisch JJ, Piotrowski AM, Brownstein SK, Gabe EJ, Lee FL (1985) J Am Chem Soc 107:7219
80. Jordan RF, Dasher WE, Echols SF (1986) J Am Chem Soc 108:1718–1719
81. Jordan RF, Echols SF (1987) Inorg Chem 26:383–386
82. Jordan RF, Bajgur CS, Willett R, Scott B (1986) J Am Chem Soc 108:7410–7411
83. Taube R, Krukowka L (1988) J Organomet Chem 347(1–2):C9–C11
84. Hlatky G, Turner H, Eckman R (1989) J Am Chem Soc 111:2728
85. Eshuis JJW, Tan YY, Teuben JH, Renkema J, Evens GG (1992) Organometallics 11:362–369
86. Eshuis JJW, Tan YY, Teuben JH, Renkema J (1990) J Mol Catal 62:277–287
87. Jordan RF (1991) Adv Organomet Chem 32:325–387
88. Borkowsky S, Baenziger NC, Jordan RF (1993) Organometallics 12:486–495
89. Jordan RF, Guram AS (1990) Organometallics 9:2116–2123
90. Hlatky G, Eckman R, Turner H (1992) Organometallics 11:1413
91. Hlatky G (2000) Chem Rev 100:1347
92. Bochmann M (2010) Organometallics 29:4711–4740
93. Bochmann M (1996) J Chem Soc Dalton Trans 1996:255–270
94. Chen EYX, Marks TJ (2000) Chem Rev 100:1391–1434
95. Li H, Marks TJ (2006) Proc Natl Acad Sci 103:15295–15302
96. Ustynyk LY, Fushman EA, Razavi A (2006) Kinet Catal 47(2):213–220
97. Riechert KH (1970) Angew Makromol Chem 12:175
98. Piers WE, Bercaw JE (1990) J Am Chem Soc 112:9406–9407
99. Krauledat H, Brintzinger HH (1990) Angew Chem Int Ed Engl 29:1412–1413
100. Prosenc MH, Janiak C, Brintzinger HH (1992) Organometallics 11(12):4036–4041
101. Leclerc MK, Brintzinger HH (1995) J Am Chem Soc 117:1651–1652
102. Burger BJ, Cotter WD, Coughlin EB, Chacon ST, Hajela S, Herzog TA, Kohn RO, Mitchell JP, Piers WE, Shapiro PJ, Bercaw JE (1995) In: Fink G, Muelhaupt R, Brintzinger HH (eds) Ziegler catalysts. Springer, Berlin
103. Grubbs RH, Coates GW (1996) Acc Chem Res 29:85–95
104. Herzog TA (2007) PhD Thesis, California Institute of Technology, Pasadena
105. Maurice Brookhart M, Malcolm LH, Green MLH, Parkin G (2007) PNAS 104(17):6908–6914
106. Dahlman M, Erker G, Nissinen M, Froehlich R (1999) J Am Chem Soc 121:2820–2828
107. Shapiro PJ (2002) Coord Chem Rev 231:67–81
108. Zachmanoglou CE, Melnick JG, Bridgewater BM, Churchill DG, Parkin G (2005) Organometallics 24:603–611
109. Peifer B, Welch MB, Alt HG (1997) J Organomet Chem 544:115–119
110. Alt HG, Milius W, Palackal SJJ (1994) Organomet Chem 472:113

111. Alt HG, Milius W, Palackal SJJ (1994) J Organomet Chem 472:113–118
112. Schertl P, Alt HG (1999) J Organomet Chem 582:328–337
113. Razavi A, Vereecke D, Peters L, Den Dauw K, Nafpliotis L, Atwood JL (1995) Homogeneous Ziegler–Natta catalysts. In: Fink G, Muelhaupt R, Brintzinger HH (eds) Zeigler catalysts. Springer, Berlin, pp 112–147
114. Kim I, Kim K, Lee MH, Do Y, Won M (1988) J Appl Polym Sci 70:973–983
115. Flory PJ (1953) Principles of polymer chemistry. Cornell University Press, Ithaca
116. Hamilton P, Song H, Luss D (2007) AIChE J 53(3):687–694
117. Liu J, Rytter E (2001) Macromol Rapid Commun 22(12):952–956
118. Razavi A (2008) Patent US 2008/0214759 Al, Total Petrochemicals Inc
119. Razavi A, Debras G (1998) Patent US 005,719,241A, Fina Research, S.A
120. Razavi A (2006) Patent US 2006/0,068,985 Al, Fina Technology Inc
121. Razavi A (2008) Patent US 2008/0,108,766 Al, Fina Technology Inc
122. Lauher JW, Hoffmann R (1967) J Am Chem Soc 98:1729
123. Alt HG, Zenk R, Milus W (1996) J Organomet Chem 514:257–270
124. Yano A, Endo K, Kaneko T, Sone M, Akitomo A (1999) Macromol Chem Phys 200:1542–1553
125. Alt HG, Jung M (1998) J Organomet Chem 568:87–112
126. Razavi A, Vereecke D (1999) Patent US 006,002,033A, Fina Research S. A
127. Resconi L, Cavallo L, Fait A, Piemontesi F (2000) Chem Rev 100:1253–1345
128. Boor J Jr (1979) Ziegler–Natta catalysts for polymerization. Academic, New York
129. Drago D, Pregosin PS, Razavi A (2000) Organometallics 19(9):1802–1805
130. Alt HG, Jung M, Kehr GJ (1998) J Organomet Chem 562:153–181
131. Ewen JA, Elder M, Jones LR, Haspeslagh L, Atwood JL, Bott SG, Robinso K (1991) Makromol Chem Makromol Symp 48/49:253–295
132. Alt HG, Koeppl A (2000) Chem Rev 100:1205–1221
133. Miller SA, Bercaw JE (2004) Organometallics 23:1777–1789
134. Alt HG, Zenk R (1996) J Organomet Chem 526:295–302
135. Alt HG, Zenk R (1996) J Organomet Chem 522:39–54
136. Razavi A, Marin V (2010) Patent US 2010/0,016,528 A1, Fina Technology Inc
137. Zuccaccia C, Stahl NG, Macchioni A, Chen MC, Roberts JA, Marks TJ (2004) J Am Chem Soc 126:1448–1464
138. Chen MC, Roberts JA, Marks TJ (2004) J Am Chem Soc 126:4605
139. Van der Leek V, Angermund K, Reffke M, Kleinschmidt R, Goretzki R, Fink G (1997) Chem Eur 3:585–591
140. Cavallo L, Guerra G, Vacatello M, Corradini P (1991) Macromolecules 24:1784–1790
141. Borreli M, Busico V, Cipullo R, Ronca S, Budzelaar PHM (2003) Macromolecules 36:8171–8177
142. Rappe AK, Polyakov OG, Bormann-Rochette LM (2007). In: Baugh LS, Canich JAM (eds) Stereoselective polymerization with single-site catalysts. CRC, Boca Raton, pp 169–200
143. Guerra G, Longo P, Corradini P, Resconi L (1997) J Am Chem Soc 119:4394–4403
144. Angermund K, Fink G, Jensen VR, Kleinschmidt R (2000) Chem Rev 100:1457–1470
145. Angermund K, Fink G, Jensen VR, Kleinschmidt R (2000) Macromol Rapid Commun 21:91–97
146. Tomasi S, Razavi A, Ziegler T (2007) Organometallics 26:2024–2036
147. Rowley CR, Woo TK (2011) Organometallics 30(8):2071–2074
148. Razavi A, Baekelmans D, Bellia V, De Bauwer Y, Hortmann K, Lambrecht M, Miserque O, Peters L, Van Belle, S (1999) Syndiotactic and isotactic specific metailocene catalysts with hapto-flexible cyclopentadienyl-fluorenyl ligand. In: Kaminsky W (ed) Metalorganic catalysts for synthesis and polymerization. Springer, Berlin, pp 236–247
149. Huttner G, Brintzinger HH, Bell LG, Friedrich P, Bejenke V, Neugebauer D (1978) J Organomet Chem 145:329–333
150. Kowala C, Wunderlich JA (1976) Acta Crystallogr B32:820–823

151. Rerek ME, Basolo F (1983) Organometallics 2:372–376
152. Schonberg PR, Paine RT, Compana DF, Duesler EN (1982) Organometallics 1:799–807
153. Rerek ME, Basolo F (1984) J Am Chem Soc 106:5908–5912
154. Nesmeyanov AN, Ustynyuk NA, Makraova LG, Andrinov VG, Struchkov YT, Andrae S (1978) J Organomet Chem 159:199
155. Basolo F (1986) Isr J Chem 27:233
156. Nesmeyanov NA, Ustynyuk LG, Makraova VG, Andrinov YT, Struchkov S, Andrae J (1978) Organomet Chem 159:199
157. Faller JW, Crabtree RH, Habib A (1985) Organometallics 4:929–935
158. Calhorda MJ, Veiros LF (2003) Inorg Chim Acta 350:547–556
159. Goncalves IS, Ribeiro-Claro P, Romao CC, Royo B, Tavares ZM (2002) J Organomet Chem 648:270–279
160. Calhorda MJ, Felix V, Lu´s F, Veiros LF (2002) Coord Chem Rev 230:49–64
161. Calhorda MJ, Veiros LF (2001) J Organomet Chem 635:197–203
162. Vicente J, Abad JA, Bergs R, Peter G, Jones PG, Carmen M, de Arellano R (1996) Organometallics 15:1422–1426
163. Vicente J, Abad JA, Bergs R, Jones PG, Carmen M, de Arellano R (1996) Organometallics 15:1422–1426
164. Kabi-Satpathy A, Bajgur CS, Reddy KP, Petersen JL (1989) J Organomet Chem 364:105–117
165. Jolly CA, Marynick DS (1989) Inorg Chem 28:2893–2895
166. Castonguay LA, Rappe AK (1992) J Am Chem Soc 114:5832–5842
167. Bierwagen EP, Bercaw JE, Goddard WA (1994) J Am Chem Soc 116:1481–1489
168. Chen MC, Marks TJ (2001) J Am Chem Soc 123:11803–11804
169. Chen EY-C, Marks TJ (2000) Chem Rev 100:1391–1434
170. Graf M, Angermund K, Fink G, Thiel W, Vidar R, Jensen R (2006) J Organomet Chem 691(21):4367–4378
171. Zurek E, Ziegler T (2001) Organometallics 21(1):83–92
172. Zurek E, Ziegler T (2004) Prog Polym Sci 29:107–148
173. Timothy A, Herzog TA, Deanna L, Zubris DL, Bercaw JE (1996) J Am Chem Soc 118:11988–11989
174. Miyake S, Bercaw JE (1998) J Mol Catal A Chem 128:29–39
175. Veghini D, Henling LM, Burkhardt TJ, Bercaw JE (1999) J Am Chem Soc 121:564–573
176. Price CJ, Zeits PD, Reibenspies JH, Miller SA (2008) Organometallics 27:3722–3727
177. Razavi A, Bellia V (2010) Patent US 2010/0,016,528 A1, Fina Technology Inc
178. Razavi A, Atwood JL (1995) J Organomet Chem 497:105–111
179. Razavi A, Vereecke D, Peters LD, Dauw K, Atwood JL (1995) Macromol Symp 89:345
180. Razavi A, Atwood JL (1996) J Organomet Chem 520:115–125
181. Razavi A, Bellia V, Baekelmans D, Slawinsky M, Sirol S, Peters L, Thewalt U (2006) Kinet Catal 47(2):257–267
182. Miller SA (2007) J Organomet Chem 692:4708–4716
183. Tomasi S, Razavi A, Ziegler T (2009) Organometallics 28(8):2609–2618
184. Tomasi S, Razavi A, Wang D, Ziegler T (2008) Organometallics 27(12):2861–2867
185. Min EY-J, Byers JA, Bercaw JE (2008) Organometallics 27(10):2179–2188
186. Gomez FJ, Waymouth RM (2002) Macromolecules 35:3358–3368
187. Razavi A, Hortmann K, Bellia V (2002) In: Hermann WA (ed) Synthetic methods of organometallic and inorganic chemistry, vol 10. Thieme, Stuttgart, pp 185–193
188. Razavi A (1992) Process for the preparation of metallocenes. Patent US 005,117,020A. Fina Research, S.A
189. Razavi A (2006) Catalyst comprising a metallocene with two tetrahydroindenyl ligand for producing a polyolefin. Patent US 007,041,756B2, Total Petrochemicals Research Feluy
190. Razavi A, Debras G (1998) Process for producing polyolefins and polyolefin catalysts. Patent US 005,719,241A, Fina Research, S.A

191. Przybyla C, Zechlin J, Steinmetz B, Tesche B, Fink G (1999) Influence of the particle size of silica support on the kinetics and the resulting polymer properties at the polypropylene polymerization with heterogeneous metallocene catalysts; part I: experimental studies and kinetic analysis. Metalorganic Catal Synth Polymerization 1999:321–332
192. Tisse VF, Prades F, Briquel R, Mckenna TFL (2010) Role of silica properties in the polymerisation of ethylene using supported metallocene catalysts. Macromol Chem Phys 211(1):91–102
193. Tisse VF, Briquel RM, Mckenna TFL (2009) Influence of silica support size on the polymerisation of ethylene using a supported metallocene catalyst. Macromol Symp Spec Issue React Eng Polyolefins 285(1):45–51
194. Bonini F, Fraaije V, Fink G (1995) Propylene polymerization through supported metallocene/MAO catalysts. J Polym Sci A Polym Chem 33(14):2393–2402
195. Marin V, Razavi A (2009) Fluorenyl catalysts composition and olefin polymerization process. Patent US 7,514,510 B2, Fina Technology, Inc
196. Marin V, Razavi A (2009) Syndiotactic polypropylene and methods for preparing the same. Patent US 7,538,167B2, Fina Technology, Inc
197. Marin V, Razavi A (2006) Process for preparation of substituted fluorene. Patent US 7,094,938, Fina Technology, Inc
198. Marin V, Razavi A (2008) Syndiotactic polypropylene and methods of preparing same. Patent US 2008/097,052 A1, Fina Technology Inc
199. Marin V, Razavi A (2008) Stereoregular fluorenyl catalyst compositions for olefin polymerization process gaining polymers with different properties. Patent WO 2008/014,217 A2 2008/0,131, Fina Technology Inc
200. Razavi A (2004) Synthesis of hydrogenated metallocene catalyst for olefin polymerization and polyolefins prepared thereby. Patent WO 2004/078,798 A2 2004/0,916, Fina Technology Inc
201. Razavi A (2002) Production of syndiotactic polyolefins by fluorenyl-containing metallocene catalysts. Patent EP 1,179,553 A1 2002/0,213, Fina Technology Inc
202. Razavi A (2000) Metallocene catalyst technology and environment. CR Acad Sci IIC Chem 3:615–625
203. De Rosa C, Gargiulo MC, Auriemma F, Ruiz de Ballesteros O, Razavi A (2002) Macromolecules 35:9083–9095
204. De Rosa C, de Ballesteros OR, Santoro M, Auriemma F (2003) Polymer 44:6267–6272
205. Stocker W, Schumacher M, Graff S, Lang J, Wittmann JC, Lovinger AJ, Lotz B (1994) Macromolecules 27(23):6948–6955
206. Lotz B, Lovinger AJ, Cais RE (1988) Macromolecules 21:2375
207. Lovinger AJ, Lotz B, Davis DD (1990) Polymer 31:2253
208. Lovinger AJ, Davis DD, Lotz B (1991) Macromolecules 24:552
209. Lovinger AJ, Lotz B, Davis DD, Schumacher M (1994) Morphology and thermal properties of fully syndiotactic polypropylene. Macromolecules 27(22):6603–6611
210. Tsukruk VV, Reneker DH (1995) Macromolecules 28(5):1370–1376
211. Harasawaa J, Ueharaa H, Yamanobea T, Komotoa T, Terano M (2003) Macromolecules 36:6472–6483
212. Thomann R, Wang C, Kressier RJ, Juengling S, Muelhaupt R (1995) Polymer papers. Polymer 36(20):3795–3801
213. Hahn T, Suen W, Kang S, Hsu SL, Stidham HD, Siedle AR (2001) Polymer 42:5813–5822
214. Loos J, Schauwienold A-M, Yan S, Petermann J, Kaminsky W (1997) Polym Bull 38:185–189
215. Lovinger AJ, Lotz B, Davis DD, Padden FJ Jr (1993) Macromolecules 26(14):3494–3503
216. Supaphol P, Spruiell JE, Lin J (2000) Polym Int 49:1473–1482
217. Supaphol P (2001) J Appl Polym Sci 82:1083–1097
218. Supaphol P (2001) J Appl Polym Sci 79:1603–1609

219. Eckstein A, Suhm J, Friedrich C, Maier RD, Sassmannshausen J, Bochmann M, Muelhaupt R (1998) Macromolecules 31:1335–1340
220. Wheat RW (1995) Rheological explanations for syndiotactic polypropylene behaviors. In: Proceedings of the polymers, laminations & coatings conference, TAPPI, Atlanta, pp 407–410
221. Eckstein C, Friedrich A, Lobrecht R, Spitz R, Muelhaup R (1997) Acta Polym 48:41–46
222. Thomann R, Kressler RJ, Setz S, Wang C, MueIhaupt R (1996) Polymer 37(13):2627–2634
223. Thomann R, Kressler RJ, Rudolf B, Muelhaupt R (1996) Polymer 37(13):2635–2640
224. Maier RD, Thomann R, Kressler RJ, Muelhaupt R, Rudolf B (1977) J Polym Sci B Polym Phys 35(7):1135–1144
225. Schardl JM, Sun L, Baumgartner AS, Boyle K (2004) Patent US 2004/0,034,167 A1, Fina Technology Inc

Adv Polym Sci (2013) 258: 117–142
DOI: 10.1007/12_2013_217

Published online: 16 May 2013

Polyolefins with Cyclic Comonomers

Laura Boggioni and Incoronata Tritto

Abstract Highly active metallocenes and other single-site catalysts have opened up the possibility to polymerize cycloolefins or to copolymerize them with ethene or propene. The polymers obtained show interesting structures and properties. The cycloolefins such as cyclopentene, norbornene, and their substituted derivatives are incorporated into the polymer chain either by addition or metathesis. An overview of copolymers obtained via addition copolymerization is here given. Materials with elastomeric properties or tactic polymers with high glass transitions and melting points can be obtained, depending on the wide range of different microstructures. Cycloolefin copolymers and homo- and copolymers of norbornene, in particula, are of great academic and industrial interest because of their properties and applications in optoelectronics, lenses, and coatings.

Keywords Catalysis · Cycloolefin copolymers · Metallocene

Contents

L. Boggioni and I. Tritto (✉)
Istituto per lo Studio delle Macromolecole (ISMAC), Consiglio Nazionale delle Ricerche (CNR), Via E. Bassini 15, 20133 Milano, Italy
e-mail: tritto@ismac.cnr.i

1 Introduction

The Ziegler and Natta discovery of catalysts for ethene polymerization (Ziegler 1953) and stereospecific propene polymerizations (Natta 1954), awarded with the 1963 Nobel Prize in Chemistry, generated searches for catalysts and cocatalysts for the polymerization of other olefins, of which the most interesting are the cyclic olefins. In the early 1960s, cycloolefins such as norbornene could be polymerized by using heterogeneous systems based on titanium, tungsten, or molybdenum halides and strong Lewis acidic cocatalysts [1–4]. The unsaturated 1,3-dimethylenecyclopentane repeating units in the polymer chain suggested that polymerization occurred via ring opening. Indeed, conventional heterogeneous Ziegler–Natta catalysts generally yield cycloolefin polymers containing both addition and ring-opening metathesis polymerized (ROMP) units [3]. Searches for catalysts for ROMP [5, 6] led to the development of commercial products based on polyalkenamers from cyclopentene, cyclooctene, norbornene, and dicyclopentadiene and more recently to "well-defined" catalysts based on a range of metals including titanium, tantalum, tungsten, and molybdenum thanks to advances in this area, especially by Grubbs and Schrock (awarded with the 2005 Nobel Prize in Chemistry jointly with Chauvin) [7–12].

After Kaminsky, Brintzinger, and Ewen discovered homogeneous metallocene/methylaluminoxane (MAO) catalysts for stereospecific α-olefin polymerization (for reviews on olefin polymerization, see [13–21]), the first report [22, 23] on addition cycloolefin polymerization without ROMP appeared. This stimulated a great interest in these polymers and in catalysts for cycloolefin polymerization (Fig. 1). Cycloolefins such as cyclopentene, cyclooctene, and norbornene can be polymerized via addition (Fig. 2). Polycycloolefins by metallocenes are difficult to process due to their high melting points and their low solubility in common organic solvents. However, metallocenes allow the synthesis of cyclic olefin copolymers (COC), especially of cyclopentene and norbornene with ethene or propene, which represent a new class of thermoplastic amorphous materials (Scheme 1) [24, 25].

There is tremendous interest in cycloolefin homo-[26] and copolymers [24, 25] because of the easy availability of the monomers and interesting polymer properties. Amorphous cycloolefin copolymers, namely norbornene with ethene, with excellent transparency, high refractive index, and variable glass transition temperatures are industrially produced (e.g., Topas). Polymers with cycloaliphatic repeating units display good thermomechanical properties, high optical clarity, and low dielectric constants and are suited for microelectronic and optical applications. Soluble saturated cycloaliphatic homopolymers can now be obtained using late transition metal catalysts (palladium, nickel, and cobalt) in high yield.

An overview of the state of the art on cycloolefin copolymerization is given here. The driving force influencing the reactivity in cycloolefin addition polymerization is both the ring strain of the cycloolefin and the non-planarity of the reacting double bond. The possibility or not of undergoing β-hydrogen elimination, which leads to isomerization and chain termination, has consequences on polymer structure and molar mass [24, 25].

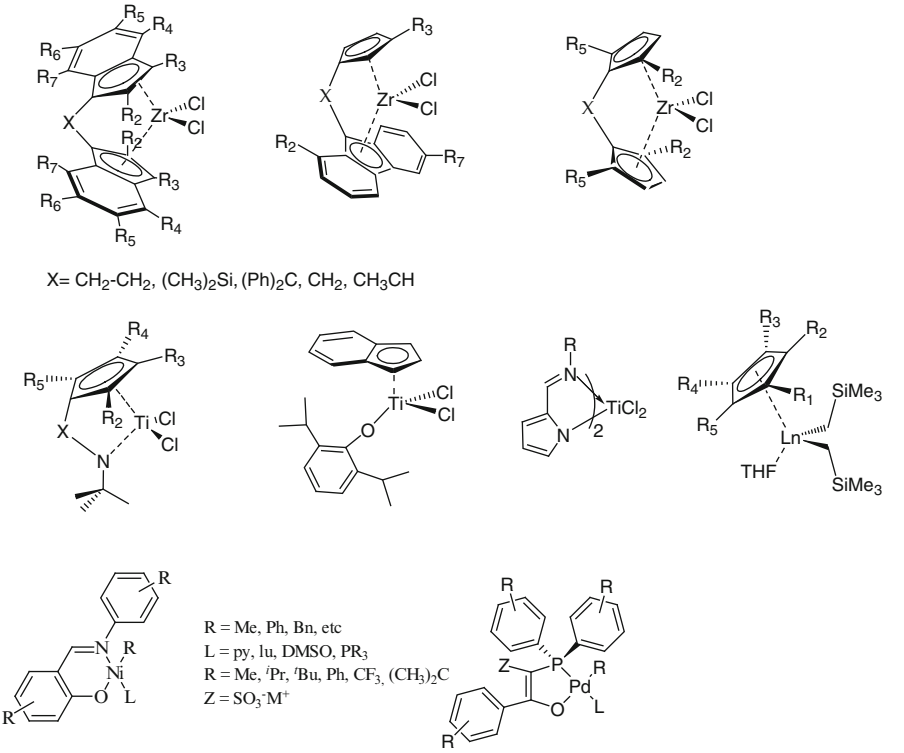

Fig. 1 Examples of metal catalysts that can homo- or copolymerize cyclic olefins and functionalized norbornenes

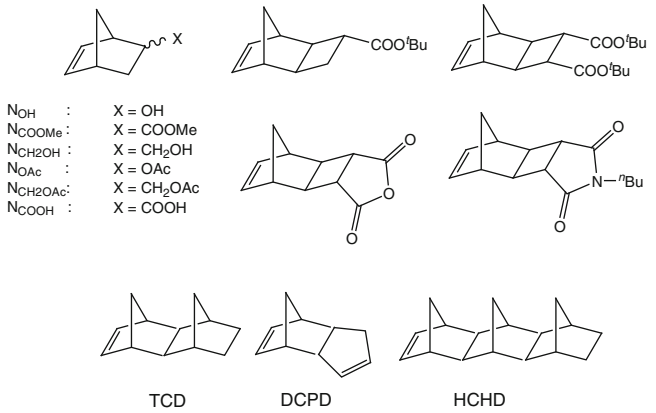

Fig. 2 Examples of cyclic olefins and functionalized norbornenes that can be homo- or copolymerized by transition metal catalysts

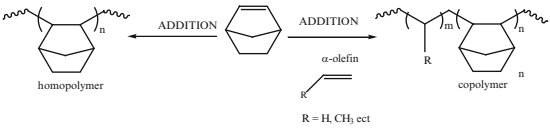

Scheme 1 Addition homo- and copolymerization of norbornene

2 Copolymers with Monocyclic Olefins

Copolymerization of cyclic olefins such as cyclopentene and norbornene with ethene or propene yield cycloolefin copolymers in which the presence of non-cyclic units introduce flexibility in the polymer chain. Thus, the copolymers are amorphous, processable, and soluble in common organic solvents. Early attempts at such copolymerizations were made by using heterogeneous $TiCl_4$/$AlEt_2Cl$ or vanadium catalysts, but real advancements were made utilizing metallocenes and other single-site catalysts, which are about ten times more active than vanadium systems and other Ziegler–Natta catalysts.

Cyclopentene can be copolymerized with ethene or propene using heterogeneous and homogeneous Ziegler–Natta catalysts [1, 27–35]. Crystalline or elastomeric copolymers are obtained, depending on the cyclopentene content and the ring opening or vinyl-type polymerization mechanism [27]. Metallocene/MAO catalysts are very active in the copolymerization of cyclopentene with ethene. In contrast to the homopolymerization of cyclopentene, the cyclic olefin is incorporated into the copolymer chain by 1,2-enchainment. The polymerization activity increases with increasing reaction temperature and reaches 19 kg of copolymer by 1 mol of catalyst in 1 s using a low zirconocene *rac*-[$Et(Ind)_2$]$ZrCl_2$ (**I-1** in Fig. 3) concentration of around 10^{-6} mol/L [28].

The activities and the molecular weights of the obtained copolymers are not much influenced by the molar ratio of cyclopentene/ethene in the starting mixture. Cyclopentene incorporation increases with decreasing polymerization temperature and increasing cyclopentene/ethene ratio. Statistic copolymers with cyclopentene units from 1.7 to 18 mol% are obtained.

^{13}C-NMR spectroscopy showed that cyclopentene is incorporated in the copolymer chain through a 1,2-insertion, without ring-opening metathesis. This is in contrast to the homopolymerization of cyclopentene, where 1,3-insertion was observed (Scheme 2). The 1,2-enchainment results from the easy coordination to the zirconium center when the last insertion is an ethene unit. The β-hydride elimination of a cyclopentene unit at the end of the growing chain, needed to form a 1,3-enchained cyclopentene unit, is relatively slow compared to a next ethene insertion. Therefore, it is difficult to synthesize copolymers with more than 50 mol% of cyclic olefin units. Higher incorporation rates up to 64 mol% of cyclopentene were obtained if highly substituted cyclopentadienyl/fluorenyl zirconium complexes such as *rac*-dimethylsilandiyl(ferroceno[2,3]inden-1-yl)(cyclopentadienyl)zirconiumdichloride were used [29]. The copolymers show small cyclopentene blocks with 1,3-enchained units and isolated 1,2-enchained units. The *cis*/*trans* ratio was quantified to be 10% *trans* of the 1,3-units and 2.9% *trans* of the 1,2-units, thus copolymers contain mainly *cis*-units.

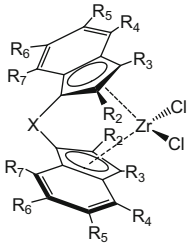

I

X=CH_2-CH_2,	all R=H	**(I-1)**
X=$(CH_3)_2$Si,	all R=H	**(I-2)**
	R_4-R_5=benz	**(I-3)**
	R_2=CH_3	**(I-4)**
	R_2=CH_3, R_4-R_5=benz	**(I-5)**

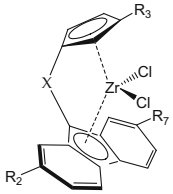

II

X=$(CH_3)_2$C,	all R=H	**(II-1)**
	R_3=CH_3, R_2=R_7=H	**(II-2)**
	R_3=*i*Pr, R_2=R_7 = H	**(II-3)**
	R_3=*t*Bu, R_2=R_7=H	**(II-4)**
X=$(CH_3)_2$Si,	all R=H	**(II-5)**
X=$(Ph)_2$C,	all R=H	**(II-6)**
	R_3=H, R_2=R_7=*t*Bu	**(II-7)**
X=$(Me)_3$Pen	all R=H	**(II-8)**
X=$(Me)_3$Pen	R_3=Ph, R_2=R_7=H	**(II-9)**

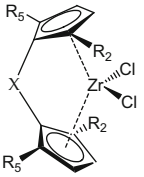

III

X=CH_2-CH_2, X=CH_2,	R=Me	**(III-1)** **(III-2)**
X=$(CH_3)_2$CH	R=H	**(III-3)**

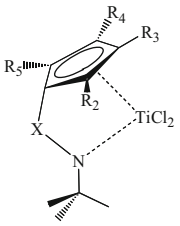

IV

X = Me_2Si,	R_2=R_3=R_4=R_5=CH_3	**(IV-1)**
	R_3=R_5=CH_3	**(IV-2)**
	R_4=*t*Bu	**(IV-3)**
	R_4-R_5=benz	**(IV-4)**
	R_1-R_5=benz, R_2-R_3=benz,	**(IV-5)**

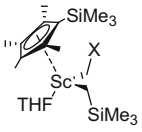

V

X=Me_3Si,	**(V-1)**
X=$PhMe_2$Si,	**(V-2)**
X=$C_6F_6Me_2$Si,	**(V-3)**

Fig. 3 Most frequently used metal catalyst precursors that can homo- or copolymerize cyclic olefins

Naga and Imanishi [30] studied the effects of the ligand structure of zirconocene catalysts on the copolymerization of cyclopentene (Cp) and ethene. They found that non-bridged zirconium complexes together with MAO as cocatalyst were not able to incorporate cycloolefin units into the polymer chain. The copolymers obtained with *rac*-[Et(Ind)$_2$]ZrCl$_2$ (**I-1** in Fig. 3) contained not only *cis*-1,2-units but also 20–30% *cis*-1,3-units of cyclopentene. DSC measurements showed multiple melting

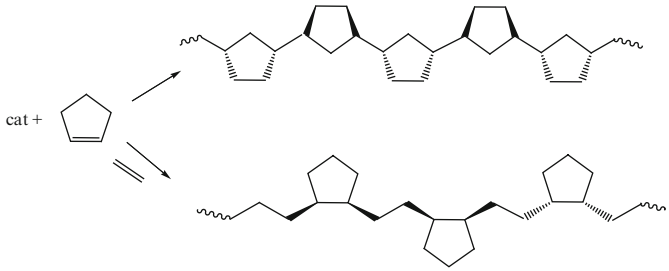

Scheme 2 Examples of microstructures of poly(cyclopentenes) (*above*) and of poly(E-*co*-cyclopentene) (*below*) obtained by 1,3- and 1,2-addition polymerization

endotherms and a broad composition distribution. One explanation for the broad composition or molecular weight distribution could be the fact that the chiral forms (*R*, *S*) and the small amounts of the *meso* form of the zirconocene complex produce different microstructures and molecular weights of the cyclopentene/ethene copolymers [31]. A narrow copolymer composition distribution was obtained with *rac*-[$Me_2Si(Ind)_2$]$ZrCl_2$ (**I-2** in Fig. 3).

Coates and Fujita [32] succeeded in the synthesis of highly alternating atactic cyclopentene/ethene copolymer using a bis(phenoximine)titanium dichloride complex activated by MAO. Copolymers show glass transition temperatures (T_g) between −27°C (27 mol% Cp) and 10.1°C (47 mol% Cp). Similar alternating copolymers were obtained by Waymouth and coworkers [33] using a constrained geometry titanium catalyst, dimethylsilylene[tetramethylcyclopentadienyl][*N-tert*-butyl]titanium dichloride, and modified MAO. The cyclopentene units are inserted by *cis*-1, 2-enchainment. Such a cyclopentene/ethene copolymer with nearly 50 mol% of Cp units shows a melting point of 182.5°C and T_g of 16.3°C.

If the C_2 zirconocenes *rac*-[$Et(Ind)_2$]$ZrCl_2$ (**I-1**) [36] or *rac*-[$Me_2Si(Ind)_2$]$ZrCl_2$ (**I-2**) activated by MAO are used, the resulting copolymers contain 2–5 mol% of Cp units incorporated by 1,2-enchainment mode. The molecular weights of the copolymers are low and lie between 35,000 (0°C) and 17,000 g/mol (30°C copolymerization temperature).

Cycloheptene and cyclooctene can be copolymerized with ethene, though copolymer yields are about 25% of that obtained with cyclopentene [28]. Copolymers with up to 4.5 mol% of cycloheptene and 1 mol% of cyclooctene could be produced using *rac*-[$Et(Ind)_2$]$ZrCl_2$/MAO (**I-1**) as catalyst. Alternating copolymers of cycloheptene and cyclooctene using a constrained geometry catalyst with a benzindenyl ligand were obtained by Lavoie and Waymouth [36].

Cyclohexene could not be copolymerized using *ansa*-metallocenes. Recently, copolymerization of ethene with cyclohexene with efficient cyclohexene incorporation by using non-bridged half-titanocenes containing an aryloxo ligand was reported by Nomura [37].

3 Ethene–Norbornene Copolymers

Norbornene can be copolymerized with olefins such as ethene and propene. Among these new cyclic olefin copolymers, made accessible from metallocenes [22, 28, 38–93], the ethene–norbornene (E–N) copolymers are the most versatile and interesting ones.

E–N copolymers are usually amorphous and display a wide range of T_g, from room temperature to about 220°C. They are characterized by high chemical resistance as well as good processability. They show excellent transparency and high refractive index, owing to their high carbon/hydrogen ratio, e.g., the refractive index is 1.53 for a 50:50 E–N copolymer. These properties make them suitable for optical applications such as coatings for high-capacity CDs and DVDs, for lenses, medical equipment, blisters, toner binder, and packaging. The industrially produced copolymers have norbornene contents between 30 and 60 mol% and T_g values of 120–180°C. After their first synthesis by Kaminsky [22, 28], E–N copolymers have been developed to commercial products such as TOPAS (see http//www.topas.com: [40]) from Ticona, while Mitsui produces APEL [41] by using vanadium-based catalysts.

The group 4 metallocene catalysts [22, 28] show much higher activity than traditional heterogeneous $TiCl_4/AlEt_2Cl$ or vanadium catalysts, and the fine-tuning of ligand substituents allows the control of copolymer properties and their structures, from random to alternating [23–25].

A variety of metallocene catalysts having C_1, C_2, C_{2v}, and C_S symmetry were studied for E–N copolymerization. Subsequently, homogeneous organometallic catalysts, including half-sandwich and cyclopentadienyl (Cp)-free group 4 metal catalysts, late transition metal catalysts, and more recently cationic rare earth metal half-sandwich alkyls have been reported to catalyze E–N copolymerization (Fig. 3) [24, 25, 42–57].

The resultant copolymer properties depend on different parameters, such as comonomer content and distribution throughout the polymer chain, as well as the configuration of the asymmetric carbons of the comonomer units. The microstructure of the copolymer can be controlled by the appropriate choice of reaction conditions and catalyst structure.

A description of the microstructure by ^{13}C NMR spectroscopy of these copolymers, as well as a detailed understanding of the processes and mechanisms involved in these copolymerizations, proved difficult to achieve. A number of groups took on this challenge using various methodologies, which included synthesis of model compounds, NMR pulse sequences, synthesis of series of copolymers with different norbornene content and using catalysts of different symmetries, synthesis of copolymers selectively ^{13}C-enriched, chemical shift prediction, and ab initio chemical shift computations. Such assignments enabled detailed information to be obtained on copolymerization mechanisms by Tritto et al. [24]. They employed a computer optimization routine, which allows a best fit to be obtained for the microstructural analysis by ^{13}C NMR spectra in order to derive the reactivity ratios for both first- and second-order Markov models (M1 and M2, respectively).

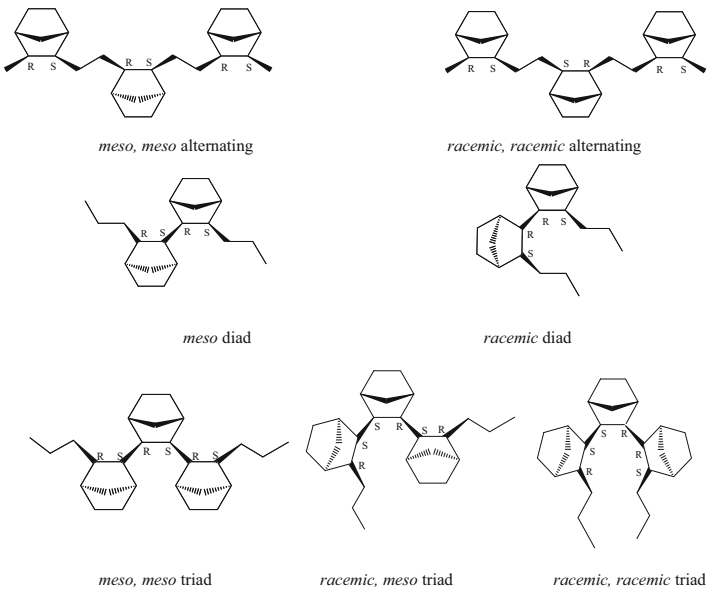

Fig. 4 Alternating (NENEN), diad (ENNE) and triad (ENNNE) sequences, showing the possible configurations

Arndt et al. [58, 59] gathered information about norbornene insertion and dimer and trimer microstructure by hydrooligomerization with metallocene catalysts known to produce atactic, isotactic, and syndiotactic poly(α-olefins); isolation; and characterization of model dimers and trimers. Norbornene was shown to undergo *cis-exo* insertion into the metal–carbon bonds, and the different stereochemistry of oligomers (and polymers) was demonstrated [58, 59].

Configuration of atoms C_2/C_3 in the ring of E–N copolymers can be either *S*/*R* or *R*/*S*, so two subsequent norbornene units can be either *erythro* di-isotactic (*meso*) or *erythro* di-syndiotactic (*racemic*). The possible stereochemical environments of norbornene in alternating sequences, diads, and triads are illustrated in Fig. 4. *Erythro* di-isotactic and *erythro* di-syndiotactic microstructures of ENENE and ENNE segments can be obtained, depending on the catalyst structure (for a recent review on catalysts for cyclic olefin copolymerization see [42]). The microstructure of the copolymer can be controlled by the appropriate choice of reaction conditions and catalyst structure.

Two trends common to almost all E–N copolymerizations by *ansa*-metallocenes are: (1) an increase in norbornene concentration in a polymerization feed results in a decrease in catalytic activity, probably due to the facility of coordination to the active sites, and in an increase of norbornene content in the copolymer up to a plateau, which depends on the catalyst structure; and (2) the molecular mass of the copolymer often increases with the increase in norbornene content.

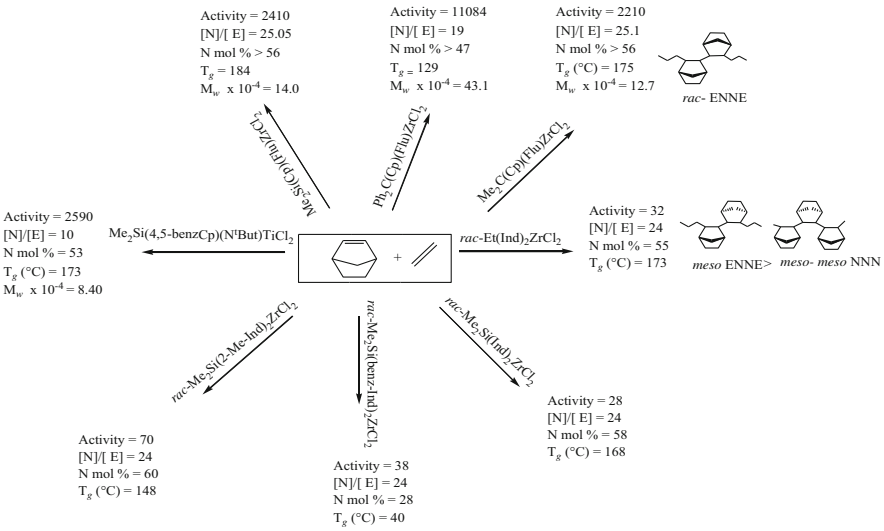

Fig. 5 Some E−N copolymerizations, showing activities and properties under the same conditions

Ansa-metallocenes with C_2 and C_s symmetries generate random copolymers containing norbornene microblocks [43, 44, 61, 62, 64–68, 92]. Copolymers with norbornene content well above 50 mol% and T_g values as high as 220°C can be synthesized. Metallocene symmetry and ligand substituents dictate polymerization activity, tacticity, and sequential distribution. The type of bridge has an influence on polymerization activity, norbornene content, and molar masses (Fig. 5).

Among the C_2-symmetric metallocenes, **I-1** is the most active. The C_s-symmetric **II-1**, as already known, turned out to be the most productive catalyst. Among the C_2-symmetric catalysts, **I-4** was shown to be noticeably more active than the others of the series. The microstructure was dominated by metallocene symmetry and ligand type. Precursor **I-3** produced copolymers with the highest norbornene content and the highest amount of *meso–meso* NNN sequences [68].

The C_s-symmetric **II-1**, **II-5**, and **II-6**, and the C_{2v}-symmetric **III-2** [68] showed higher activity than the C_2-symmetric metallocenes. Among these catalysts most active is complex **III-2**, while **II-5** shows the highest molecular mass [22]. The presence of a methyl substituent on α-carbons and the absence of substituents on the β-carbons in compound **III-2** are crucial to the high activity of this system.

Random copolymers having a norbornene content between 48 and 60 mol% showed T_g values that can reach about 200°C. A linear correlation between the amount of norbornene incorporated and the T_g measured was found for norbornene contents that were not too high [44]. Comparison of T_g values of copolymers with high norbornene content [68] led to the conclusion that there is no linear correlation between norbornene content and T_g values when copolymers with high norbornene content and different microstructures are considered.

Highly alternating stereoregular (isotactic) E−N copolymers were synthesized with the C_1-symmetric, bridged metallocenes **II 2-4**, **II-6** [61, 71] in the presence of an excess of norbornene. The copolymers obtained are crystalline if the norbornene content is higher than 37 mol%, and have melting points of 270–320°C.

Metallocene **I-5** gave a mainly alternating isotactic copolymer with trace amounts of ENNE sequences and a surprising significant amount of norbornene (up to ~10%) belonging to NNN triads [74]. Isotactic alternating copolymers with norbornene content above 37 mol% are semicrystalline. They feature T_g values of 100–130°C and T_m values of 270–320°C. They are still transparent owing to the small size of their crystalline regions (5 nm). Atactic alternating copolymers are amorphous with T_g values up to about 130°C.

Constrained geometry catalysts also copolymerize ethene and norbornene with lower activity than *ansa*-zirconocenes, but can give perfectly alternating copolymers [45]. C_1-symmetric, bridged monocyclopentadienyl titanium amido complexes $Me_2Si(Cp')(N^tBu)TiCl_2$ (where Cp′ = 2,4-Me_2Cp, 3-^{t}BuCp, indenyl) (**IV 2-4**) have also been shown to yield mainly alternating E−N copolymers by Waymouth and coworkers [46].

Random E–N copolymers with high molar masses and high norbornene content were produced by Shiono [53] by using the half-sandwich titanocene precatalyst $Me_2Si(Flu)(N^tBu)TiMe_2$ (**IV-5**) activated with MAO free from Me_3Al. The complex produces E–N copolymers with high molecular weights (up to 63,000 g/mol), narrow molecular weight distributions (M_w/M_n = 1.32) and an incorporation of norbornene up to 58 mol%.

Nomura [56] showed that non-bridged half-titanocenes containing anionic donor ligand of the type, Cp′TiX_2(Y) (where Cp′ = cyclopentadienyl group; X = halogen, alkyl; Y = anionic ancillary donor ligands such as aryloxo, ketimide etc.) displayed unique characteristics such as efficient incorporation of bulky olefins. Random E−N copolymers with high norbornene contents could be obtained with (Ind)$TiCl_2$(O-2,6-*i*$Pr_2C_6H_3$) (**V-1**) that exhibited higher norbornene incorporation than the Cp*-aryloxo analogue (**V-3**), the 1,2,4-$Me_3C_5H_2$-aryloxo analogue (**V-4**), and the constrained geometry catalyst (CGC, **IV-1**).

Although living α-olefin polymerizations with transition metal catalysts are still quite rare despite the modern efficient examples recently developed (for a recent review, see [69]), some E−N copolymerizations have been shown to be quasi-living or living. The molecular mass of E–N copolymers by catalyst **I-1**, at temperatures between 30 and 50°C and high norbornene feed fractions, increases with time for up to 1 h. The polydispersity can be as narrow as 1.1 at [N]/[E] = 28 [49], indicating that E−N copolymerizations are quasi-living under these conditions.

Fujita [55, 57, 76–78] and coworkers developed bis(pyrrolide-imine)Ti complexes (named PI catalysts), which give highly alternating E–N copolymers. These group 4 transition metal [57, 76–79] catalysts with electronically flexible nonsymmetric [N^N] chelate ligands displayed a marked tendency to produce E–N copolymers with a stereoirregular structure despite the C_2-symmetric nature of the catalysts. The E–N copolymerization with PI catalysts is living [55].

Hou reported the first example of efficient COC synthesis by rare earth metal catalysts. Cationic rare earth (group 3 and lanthanide) metal alkyls is an emerging new class of catalysts for the polymerization and copolymerization of various olefins, including cyclic olefins [80, 81]. The combination of half-sandwich scandium bis (alkyl) complexes such as $Sc(\eta^5\text{-}Cp)(CH_2SiMe_3)_2(THF)$ (for **VIII-1**, Cp = $C_5Me_4SiMe_3$; **VIII-2**, Cp = 1,3-$C_5H_3(SiMe_3)_2$; **VIII-3**, Cp = C_5Me_5) with 1 equivalent of a borate compound such as $[Ph_3C][B(C_6F_5)_4]$ showed excellent activity for E–N copolymerization [82]. Under appropriate conditions (25°C and 1 atm ethene), the $[Sc(\eta^5\text{-}C_5Me_4SiMe_3)(CH_2SiMe_3)_2(THF)]/[Ph_3C][B(C_6F_5)_4]$ system afforded an amorphous alternating E–N copolymer with M_n = 85,000 g/mol, M_w/M_n = 2.19, T_g = 118°C, and norbornene content of 44 mol%, with an activity as high as 25,200 kg/(mol Sc h).

The catalytic properties of the following half-sandwich bis(alkyl) rare earth complexes $[Ln(\eta^5\text{-}C_5Me_4SiMe_2R)(\eta^1\text{-}CH_2SiMe_3)_2(THF)]$ (Ln = Sc, R = Me; Ln = Sc, R = C_6F_5; Ln = Y, R = C_6F_5; Ln = Lu, R = C_6F_5) activated by $[Ph_3C][B(C_6F_5)_4]$ in copolymerization of ethylene with norbornene have been assessed by Ravasio et al. [83]. Both excellent activities and noticeable control in molar mass distributions were found. Copolymer microstructure has been elucidated at the tetrad level.

Detailed information on copolymerization mechanisms was obtained by Tritto et al. [88] by calculating the E–N reactivity ratios employing a computer optimization routine, which allows the best fit to be obtained for the microstructural analysis by ^{13}C NMR spectra. The theoretical equations relating copolymer composition and feed composition were fitted to the corresponding experimental data. The reactivity ratios for both first- and second-order Markov models (M1 and M2, respectively) were derived. The reactivity values agree with the reports that E–N copolymers obtained with **IV-1**/MAO are mainly alternating ($r_1 \times r_2 \ll 1$), the norbornene diad fraction is very low, and there are no norbornene triads or longer blocks ($r_2 \approx 0$).

The ranges of the reactivity ratios obtained at the lowest [N]/[E] feed ratio are r_1 = 2.34–4.99 and r_2 = 0.0–0.062. The r_2 values are in general smaller than those obtained for propene copolymerization. The highest $r_1 \times r_2$ values found for the copolymers prepared with catalyst **I-4** confirmed its tendency to give more random copolymers. The values of r_1, r_2, and $r_1 \times r_2$ for the E–N copolymers obtained with catalysts **IV-1** and **I-5** are comparable with those of alternating ethene–propene copolymers with metallocene catalysts. The results of the second-order Markov model also showed that all r_{11} values, as r_1, are similar to those found for ethene and propene copolymerization with metallocene catalysts with low reactivity ratios. Differences in r_{12} and in r_{22} are illuminating, since they clearly show the preference of the insertion of ethene or norbornene into E–N–Mt (Mt = Metal) and N–N–Mt, respectively. Parameter r_{12} increases in the order **IV-1** < **I-5** ≪ **I-1** < **I-2**, opposite to the tendency to alternate the two comonomers [88].

Poly(E-*co*-N)$_1$-*b*-poly(E-*co*-N)$_2$ and PE-*b*-poly(E-*co*-N), and thus new materials consisting of crystalline and amorphous segments that are chemically linked, were successfully synthesized with PI catalysts [90], rare earth catalysts [82], and fluorinated enolato-imine titanium catalysts [91].

4 Propene−Norbornene Copolymers

Propene−norbornene (P−N) copolymers were expected to feature higher T_g values than E−N copolymers with the same norbornene content and molar mass since polypropene has a higher T_g value than polyethene [66–68]. Moreover, differences in stereo- and regioregularity of propene units as well as in the comonomer distribution and the stereoregularity of the bicyclic units were expected to allow fine tuning of copolymer microstructure and properties. However, compared to E−N copolymers, reports regarding P−N copolymers are very limited [94–100].

The first report on synthesis of amorphous P−N copolymers by Arnold with **I-2**/MAO was shown to yield low polymerization activity but very high norbornene content (up to 98 mol%) [94]. Then, Tritto and colleagues [95, 96] tackled the synthesis and microstructural studies of P−N copolymers with C_2- and C_s-symmetric metallocenes and MAO as cocatalyst. Two *ansa*-metallocenes of C_2-symmetry, *rac*-[Et(Ind)$_2$]ZrCl$_2$ (**I-1**) and *rac*-[Me$_2$Si(Ind)$_2$]ZrCl$_2$ (**I-2**), effective for the synthesis of prevailingly isotactic and regioregular polypropene as well as E−N copolymers with a tendency to alternate, were selected [67]. **II-1**, which yields prevailingly syndiotactic polypropene and is very active in E−N copolymerization, was selected as a metallocene of C_s symmetry. The polymerization activities of **I-1** and **I-2** were found to be low compared to those obtained for E−N copolymerization. Under similar polymerization conditions, **II-1** allows for a lower norbornene incorporation than catalysts **I-1** and **I-2**. The M_w values as well as T_g values of P−N copolymers are lower than those of E−N copolymers.

The low activity was demonstrated to result from the difficulty of inserting a propene into the Mt−tertiary carbon bond formed after the norbornene insertion (Mt-N), which is even more sterically crowded than the sites formed after a propene (2,1) regioirregular insertion, less reactive than sites with a primary growing polypropene chain. However, at low norbornene/olefin ratio it is possible to obtain P−N copolymers that are relatively richer in norbornene than the E−N copolymers prepared in similar conditions. At higher norbornene/olefin feed ratios, the great amount of 1,3 propene misinsertions clearly revealed that the steric hindrance of the Mt−tertiary carbon bond, when norbornene is the last inserted unit, makes the next propene insertion difficult, causing low polymerization activities, molecular masses, and T_g.

Kaminsky and colleagues studied P−N copolymerization with the C_2-symmetric **I-2**, two C_s-symmetric [Me$_2$C(Cp)(Flu)]ZrCl$_2$/MAO (**II-5**) and [Ph$_2$C(Cp)(2,7-di^{t}BuFlu)]ZrCl$_2$ (**II-7**) systems and with the constrained-geometry catalyst **IV-1**. Copolymers and oligomers with a wide range of T_g were produced with satisfying activities, whereas the activities for **IV-1** were much lower. These studies confirmed that the high reactivity of the cyclic monomer makes accessible P−N copolymers with higher norbornene incorporation, but with lower molar masses than E−N copolymers [98, 101–103].

Shiono and colleagues succeeded in the synthesis of P–N copolymers with high norbornene content up to 71 mol% with catalyst (^{t}BuNSiMe$_2$Flu)TiMe$_2$ activated by Me$_3$Al-free methylaluminoxane (dried MAO) [100]. They had previously reported

that this metallocene when activated with dried MAO yields living propene and norbornene homopolymerization [99]. P−N copolymerizations were carried at 20°C under atmospheric pressure of propene. Dimethylmetallocene **IV-2** was activated by dried MAO, modified methylaluminoxane (MMAO), and $Ph_3CB(C_6F_5)_4/Oct_3Al$. The system activated by $Ph_3CB(C_6F_5)_4/Oct_3Al$ was the most active and yielded the copolymer with the lowest molecular weight and broadest molecular weight distribution. Dried MAO yielded the copolymer with the narrowest polydispersity. The norbornene content in the copolymer was almost proportional to the [N]/[P] feed ratio and the T_g of the P–N copolymers increased linearly against the norbornene content in the copolymers, from 53°C to 249°C.

The influence of propene pressure and temperature on activity, norbornene content, M_w, and T_g of P–N copolymers by **I-1** was assessed [101]. A decrease in norbornene content, M_w, and T_g was observed at high temperatures and pressures. The great number of 1,3 propene insertions found, especially at high temperature and pressure, occurring after an inserted norbornene unit confirmed that the difficulty in inserting a propene after norbornene is the limiting step in P–N copolymerization and that chain transfer reactions are likely to occur more often at a propene-last inserted-Mt bond. This originates the lower M_w values of P−N copolymers with respect to those of E−N copolymers. The highest molar masses obtained at room temperature were in the range of 40,000 g/mol.

With the aim of obtaining P−N copolymers with high norbornene content and high molar masses, Tritto and colleagues investigated the synthesis of P−N copolymers using *rac*-$Me_2Si(2\text{-Me-Ind})_2ZrCl_2$ (**I-4**) [102]. Indeed the 2-alkyl indenyl substitutions of C_2-symmetric zirconocenes are key in considerably increasing polypropene molar masses of the produced polymers. Methyl 2-substitution on the indenyl ligand in **I-4** was found to cause an unexpected and strong decrease in catalytic activity, molar fractions f_N, T_g, and M_n values. P–N copolymers with a maximum of 16 mol% of norbornene were obtained by **I-4** in contrast to those highly alternating copolymers obtained by **I-1**. Chain-end group analysis revealed a greater amount of 2-butenyl end groups, arising from termination at a Mt-P_{21}, than of vinylidene groups arising from termination at a Mt-P_{12}. The greater amount of 2-butenyl end groups in samples with lower molar fractions of triads containing the P_{21} unit and in samples obtained with **I-1** gives an evidence that the limiting step in P–N copolymerization is the difficulty in inserting a propene after norbornene, which causes 2,1 insertions with subsequent isomerization to 1,3 propene insertions as well as chain epimerization in starved propene conditions with **I-4**. The great decrease in the tacticity of the PP blocks in the copolymers prepared with **I-4** with increasing the norbornene content in the feed revealed that the difficulty of this catalyst in accommodating a norbornene into Mt-$P_{12}N$ makes unimolecular epimerization events probable.

^{13}C NMR experiments and ab initio theoretical chemical shift calculations, combined with rotational isomeric state (RIS) statistics of the P–N chain, gave the first assignment of the ^{13}C NMR spectra of P–N copolymers [95–97]. *Cis*-2,3-*exo* norbornene insertion is considered to occur into the metal–carbon bond as in

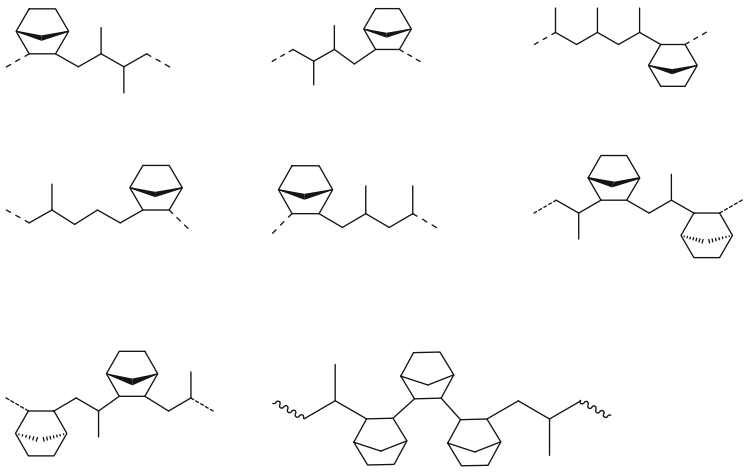

Fig. 6 Sequences observed in the ^{13}C NMR spectra of an isoctatic propene–norbornene copolymer with isolated norbornene units, alternating PNP sequences, and 1,2 or 2,1 and 1,3 propene insertions

E−N copolymerization. All propene consecutive monomer units have the methyls in *erythro* relationships, as in an isotactic polypropene chain.

Boggioni et al. [103] proposed a general scheme for describing the microstructure of P−N copolymers at triad level from ^{13}C NMR spectra. This scheme includes (1) definition of the possible triads composing the copolymer chain; (2) use of NMR techniques for assigning new signals; and (3) a best-fitting procedure to determine the copolymer microstructure [103]. This procedure, which allows for a quantitative analysis of copolymer sequences as accurate as possible, has been applied to analysis of the ^{13}C NMR spectra of a number of P−N copolymers prepared with catalyst precursors *rac*-[Et(Ind)$_2$]ZrCl$_2$ (**I-1**) and *rac*-[Me$_2$Si(2-Me-Ind)$_2$]ZrCl$_2$ (**I-4**).

The microstructural analysis by ^{13}C NMR of the copolymers gives evidence of the tendency of **I-1** to alternate propene and norbornene comonomers and of **I-4** not to alternate the comonomers, as well as information on the probability of insertion of norbornene and of the possible forms of propene insertion (P_{12}, P_{13}, and P_{21}) (Fig. 6). It is interesting that there are an unexpected number of triads containing propene misinsertions or regioerrors, which are greater in the series from **I-4** than from **I-1**. Regarding 1,3-enchained units, it is worth noting that the relevant amounts of $NP_{13}P_{12}$ in the series from **I-4** and of $NP_{13}N$ in the series from **I-1** reflect the different tendencies to alternate the comonomers of the two catalysts and the important penultimate effects with **I-4**.

Shiono used ^{13}C NMR spectroscopy to investigate the structure of the P−N copolymer with high norbornene content produced with catalyst dimethyl **IV-5** [100]. The author observed several signals for each carbon due to the different comonomer sequences and stereoisomers of the norbornene unit.

5 Copolymerization with Functionalized Norbornenes

The introduction of functional groups into cycloaliphatic polyolefin backbones could allow significant control of surface properties such as adhesion, wettability, dyeability, compatibility, and printability and could lead to COC with improved properties. Catalysts based on Ni and Pd are intrinsically less sensitive to functional groups than those based on the early transition metals currently employed in industry [104].

Open late transition metal catalysts based on palladium salts and complexes are highly active in norbornene homopolymerization in contrast to *ansa*-zirconocene catalysts, which have low activity because of steric hindrance. After Sen [105] reported on the dicationic system $[CH_3CN]_4Pd[BF_4]_2$ as a very active catalyst for norbornene addition polymerization, Risse investigated the homo- and copolymerization of norbornene and its derivates (e.g., ester substituents) with Pd(II) catalysts [106]. Goodall et al. recognized the potential of these polymers based on norbornene derivatives and used highly active catalysts based on cationic or neutral nickel and palladium complexes [107–109]. The homo- and copolymers of substituted norbornenes obtained have high decomposition temperatures, small optical birefringence, good transparency for short wavelength radiation, high plasma etch resistance, and are suitable for advanced photoresist composition in microelectronic industry. The palladium catalysts are less active than the nickel analogues. The ligand structure does not influence the polymer microstructure and properties, α-olefins act as chain transfer agents and allow control of the molecular weight. Promerus produces a range of homo-, co-, and terpolymers based on substituted norbornenes developed at BF Goodrich, such as Avatrel, Appear, and DUVCOR.

Brookhart breakthroughs [110] on late transition metals for olefin polymerization catalysts led to catalysts that allow incorporation of most polar functionalities. For example, N^N Pd-based systems tolerate acrylates, vinyl ketones, and silyl vinyl ethers, but they afford hyperbranched copolymers with functionalities located mainly at the end of ramifications, while, Ni-based systems give linear copolymers of ethene and methyl acrylate (MA) but with extremely low productivity. The norbornene derivatives have the functional group distant from the double bond and are more easily incorporated than functionalized α-olefins; however, a catalyst for the copolymerization of ethene with functionalized norbornenes must be both tolerant of functional groups and resistant to β-hydrogen elimination. Indeed, some late transition metals are often ineffective for the copolymerization of ethene with norbornene because 1-alkenes act as a chain transfer agent through β-hydrogen elimination.

Kaminsky et al. succeeded in E–N copolymerizations by using α-diimine palladium catalysts [111, 112]. The T_g values of E–N copolymers produced are very high and range from 98 to 217°C [111, 112]. Copolymers produced at norbornene molar fraction (x_N) ≥ 0.80, as well as homo-polynorbornenes, show no T_g values or T_m values under 350°C, and decompose above 350°C.

Grubbs introduced (salicylaldimino)nickel methyl complexes [113], which operate without requirement of a cocatalyst and allow the incorporation of bulky cycloolefins such as norbornene as well as functionalities into polyethene. Some promising results were reported on catalysts with nitrogen-based chelating ligands (see Fig. 7). The functionalized monomers so far copolymerized with ethene by Ni and Pd catalysts bearing nitrogen-based ligands are listed in Fig. 8. Copolymerization reactions of ethene with functionalized norbornene catalyzed by nickel (salicylaldiminato)-based catalysts are summarized in Fig. 7.

Complexes **VI-1** and **VI-2** were early reported as single-component catalysts for the copolymerization of ethene with functionalized norbornene derivatives N_{OH} and N_{COOMe}, affording P(E-*co*-N_{OH}) with N_{OH} incorporation of 22 wt%, $M_w = 17.2$ kg mol^{-1}, and $M_w/M_n = 1.6$ and P(E-*co*-N_{COOMe}) with N_{COOMe} incorporation of 12 wt% and $M_w = 73.8$ kg mol^{-1}, respectively. A more extensive study revealed that acetonitrile-containing catalyst **VI-2**, owing to the easier activation, gives a higher activity than the phosphine-containing analogues **VI-1** [114].

Copolymerization of ethene with functionalized norbornene derivatives was extended to monomers N_{CH2OH} and N_{OAc}. Monomers bearing ester groups (N_{COOMe} and N_{OAc}) resulted in less poisoning than the protic N_{CH2OH}, as showed by productivities and molar masses. Moreover, the higher the steric demand of substituent the lower the incorporation (in the order $N_{COOMe} < N_{OAc} < N_{CH2OH}$). This trend is ascribable to *endo* isomers of the monomer mixture, which after insertion are prone to give chelated intermediates that block the vacant coordination site of catalysts. Thus, tricyclononene-based functionalized monomers (TCN_{COOtBu}, $TCN_{(COOtBu)2}$, TCN_{AN}, TCN_{IM}) are more readily incorporated than bicyclic analogues because of the longer distance between the polar functionality and the olefin double bond. Interestingly, incorporation of monomer TCN_{COOtBu} could be tuned from 2 to 31 mol% through TCN_{COOtBu}/E feed ratio, though productivity dropped down with decreasing ethene concentration.

Bimetallic catalysts, which are generally and intrinsically more active than their monometallic analogues, can profit from cooperative effects arising from the close proximity of two metal centers [115–118]. A positive effect of dinuclearity was demonstrated by catalysts **VII-1**−**VII-3**/$B(C_6F_5)_3$ in copolymerization of ethene with functionalized norbornene derivatives N_{COOMe} and N_{CH2OAc}. A twofold higher activity as well as higher incorporation of functionalized monomer was observed in a series of E-*co*-N_{CH2OAc} copolymerizations by dinuclear **VII-1**−**VII-3**/$B(C_6F_5)_3$ with respect to the mononuclear analogues under the same conditions. Effect of dinuclearity on activity, incorporation, and best performance of catalyst **VII-3**, which possesses the terphenyl *o*-$C_6H_4(C_6H_4)_2$ group as bridging unit between the two salicylaldimine cores, was also confirmed for monomer N_{COOMe}. Experimental evidence and theoretical calculations suggested the effective action of a cooperative effect between the two metal centers [118].

Binuclear naphthyloxydiiminato nickel catalysts **VIII-1** and **VIII-2** activated by [Ni(cod)$_2$] efficiently copolymerize a variety of functionalized monomers from norbornene derivatives [119, 120]. The effective occurrence of eventual cooperative effects in copolymerization of ethene with monomers N_{OH}, N_{COOMe}, and

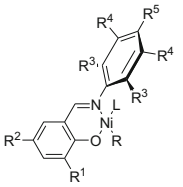

VI

R = Ph(PPh_3) ;	R^1 = 9-anth; R^2 = R^4=R^5=H; R^3 = ^{i}Pr	**(VI-1)**
R = Me(MeCN)]	R^1 = 9-anth; R^2 = R^4=R^5=H; R^3 = ^{i}Pr	**(VI-2)**

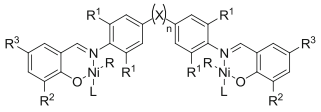

VII

n=1; X=CH_2;	R^1 = ^{i}Pr; R^2=9-Anth; R^3= H	**(VII-1)**
n=1; X=*o*-C_6H_4;	R^1=^{i}Pr; R^2=9-Anth; R^3=H	**(VII-2)**
n=1; X=*o*-$C_6H_4(C_6H_4)_2$	R^1 = ^{i}Pr; R^2=9-Anth; R^3=H	**(VII-3)**

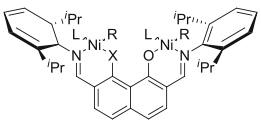

VIII

[NiClMe(PMe_3)$_2$]	X=OH	**(VIII-1)**
[NiCl(1-naph)(PPh_3)$_2$]	X=OH	**(VIII-2)**

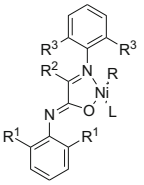

IX

[Ni(η^1-CH_2Ph)Cl(PMe_3)$_2$]	R^1=R^3=^{i}Pr; R^2=Me	**(IX-1)**
[Ni(η^1-CH_2Ph)Cl(2,6-lu))$_2$]	R^1=R^3=^{i}Pr; R^2=Me	**(IX-2)**
[Ni(η^1-C=OPh)Cl(py)$_2$]	R^1=R^3=^{i}Pr; R^2=Me	**(IX-3)**
[Ni(η^1-CH_2Ph)Cl(PMe_3)$_2$]	R^1=R^3=^{i}Pr; R^2=Et	**(IX-4)**
	R^1=R^3=^{i}Pr; R^2=$CH_2{}^i$Pr	**(IX-5)**
	R^1=R^2=R^3=^{i}Pr	**(IX-6)**
	R^1=R^3=^{i}Pr; R^2=Ph	**(IX-7)**
	R^1=R^3=^{i}Pr; R^2=4-$CF_3C_6H_4$	**(IX-8)**
	R^1=R^3=^{i}Pr; R^2=4-$MeOC_6H_4$	**(IX-9)**

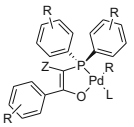

X

R = Me, L = DMSO, R = -OMe, Z = SO_3-M+	**(X-1)**
R = Me, L = py, R = -OMe, Z = SO_3-M+	**(X-2)**

Fig. 7 Most frequently used late transition metal catalyst precursors for the copolymerization of functionalized norbornenes

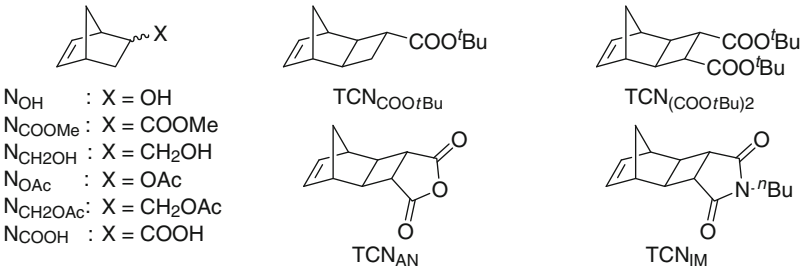

Fig. 8 Functionalized norbornenes that can be homo- or copolymerized by transition metal catalysts

N_{CH2OH} was demonstrated. Activities, as well as incorporation of functionalized monomers, of bimetallic catalysts were three- to fourfold higher than that of the monometallic analogue in identical conditions. Interestingly, the molar masses of copolymers were similar to those of copolymers of ethene with norbornene. Attempts to copolymerize N_{COOH} failed because the high acidity of the comonomer leads to catalyst deactivation.

Nickel complexes with α-iminocarboxamide ligands were intensively investigated in the copolymerization of ethene with functionalized norbornene derivatives N_{OH} and N_{OAc} [121]. Complex **IX-1** activated by $[Ni(cod)_2]$ as scavenger of PMe_3 yielded P(E-*co*-N_{AC}) copolymers containing 4–17 mol% incorporation of N_{AC} with excellent molar masses (M_n = 30–110 kg mol^{-1}). Catalyst **IX-1** preserved the ability to promote the controlled polymerization of ethene even in presence of N_{AC}, as confirmed by the linear time dependence of molar mass and the narrow molar mass distribution, even after 90 min of reaction [122]. Also, the hydroxyl-functionalized N_{OH} is readily incorporated into polyethene backbone, affording P(E-*co*-N_{OH}) copolymers with an incorporation of N_{OH} ranging from 5 to 18 mol% and possessing M_n = 11–56 kg mol^{-1}. Since hydroxyl functionality resulted in more poisoning than an acetyl group, the molar masses and activities were lower than those observed in E-*co*-N_{AC} copolymerization. In addition, the controlled nature of copolymerization was absent, as revealed by the nonlinear increase in molar masses with increasing reaction time as well as by the broader molar mass distributions. Very interestingly, catalyst **IX-1**/$[Ni(cod)_2]$ was exploited to prepare P(E-*co*-N_{AC}) copolymers with decreasing content of polar monomer. Thanks to the controlled nature of copolymerization and through complete conversion of N_{AC} it was possible to prepare "polar–apolar" block-copolymers that showed microphase separation [115]. Complexes **IX-1** and **IX-4–IX-9**/$[Ni(cod)_2]$ were exploited as catalysts for the copolymerization of ethene with N_{AC} to investigate eventual steric and perturbative effects of the group adjacent to imine (R2), by keeping the same bulky 2,6-*i*PrC_6H_4 as aryl frameworks. Both activity and incorporation of comonomer were sensitive to this modification. Productivity increased with increasing bulkiness of alkyl groups in the order *i*Pr (**IX-6**) > *i*Bu (**IX-5**) > Et (**IX-4**) > Me whereas incorporation behaved oppositely. In the series of aromatic substituents, i.e., complexes **IX-7–IX-9**, the higher the electron-withdrawing power the lower the activity. Incorporation was less influenced though lower than the alkyl-substituted analogues.

Copolymerization of ethene with norbornene and functionalized norbornenes in both non-aqueous and aqueous solutions could be carried out by (salicylaldimino) nickel methyl complexes [114, 123–125], square-planar nickel complexes containing anionic P,O-chelates [126], and by Pd phosphine aryl sulfonates [127–129].

Bazan reported on the synthesis of pseudo-tetrablock copolymers comprised of ethene and 5-norbornen-2-yl acetate, using the initiator system $(LiPr_2)Ni(\eta^1–CH_2Ph)(PMe_3)$ [$(LiPr_2)$ = *N*-(2,6-diisopropylphenyl)-2-(2,6-diisopropylphenylimino) propanamide] and 2.5 equivalents of $Ni(cod)_2$ [bis(1,5-cyclooctadiene)nickel [121, 130, 131]. Square-planar nickel complexes with anionic P,O-chelate ligands were used by Goodall and coworkers for the co- and terpolymerization of norbornene and 5-norbornene-2-carboxylic acid ethyl ester with ethene [126].

Also, complexes **IX-2**–**IX-3** with 2,6-lutidine and pyridine as neutral ligand, were demonstrated to act as single-component catalysts for the copolymerization of ethene with norbornene derivatives N_{OH} and N_{AC}, yielding comparable results to phosphine-based analogues apart from the molar mass distribution, which was evidently affected by a less-efficient activation [122].

The well-defined complex $[Pd(\kappa_2\text{-P,O-}\{2\text{-}(2\text{-}MeOC_6H_4)_2P\}C_6H_4SO_3)Me(dmso)]$ (**X-1**), having dimethylsulfoxide (dmso) as labile ligand, was investigated as a single-component catalyst for the copolymerization of ethylene with norbornene, affording P(E-*co*-N) in excellent yields and with molar masses significantly higher than those of polyethylene. Copolymer molar masses increased with norbornene concentration and reached values that are interesting for industrial applications. Such an increase, along with the presence of only terminal vinyl groups in the ^1H NMR spectra of copolymers, revealed that norbornene limits β-H elimination and thus both chain walking and chain termination. The more labile dmso, with respect to the pyridine in Claverie catalyst (**X-2**) due the more facile activation, leads to higher activities in E-*co*-N copolymerization. The use of the well-defined catalyst rather than the in-situ generated one leads to higher activity and a better control of copolymerization in terms of norbornene incorporation. Determination of microstructure and reactivity ratios revealed a strong inherent tendency to form alternating copolymers [129].

X-1 copolymerizes ethene with N_{OH} and N_{AC}. In the case of 5-norbornene-2-yl acetate, the activity and molar masses resemble those of E-*co*-N copolymerization.

6 Other Cycloolefin Copolymers

A drawback of E–N copolymers endowed with high T_g values is their brittleness at high norbornene content. The substitution of norbornene with a bulkier cycloolefin monomer could result in a more ductile COC by obtaining the same T_g values at a lower amount of cycloolefin content and thus copolymers with a higher amount of flexible ethene units in the chain. The properties of a COC based on bicyclic monomers can be varied by varying the norbornene content or the structure of the bicycloolefin; this includes norbornadiene, dicyclopentadiene (DCPD),

dimethanooctahydronaphthalene (DMON), or trimethanododecahydroanthracene (TMDA) [98, 132–144] or by terpolymerization (for an attempt at terpolymerization of ethene, norbornene and styrene see [143]).

Copolymerizations of ethene with bicyclic olefins, such as 2,5-norbornadiene and 5-vinyl-2-norbornene, have been investigated with metallocene catalysts. The secondary groups do not interfere with metallocene copolymerizations, and post-polymerization functionalization makes it possible to synthesize functionalized polyolefins [133–135].

DCPD is a very promising and attractive monomer because it contains two double bonds and both norbornene and cyclopentene units. If only one of the two double bonds is selectively copolymerized with ethene, it is possible to functionalize the remaining double bond (for a review on functionalization of C–C double bonds, see [136]). Nevertheless, the copolymerization of ethene with DCPD has not been extensively studied [137] because of the possibility of crosslinking reactions [137]. Hou [140] achieved alternating ethene–DCPD copolymerization in a controlled fashion over a wide range of temperatures (0–70°C) by using $[Sc(\eta^5\text{-}C_5Me_4SiMe_3)(CH_2SiMe_3)2(THF)]/Ph_3C][B(C_6F_5)_4]$. The highest catalytic activity was achieved at 50°C with a DCPD incorporation of ca. 44 mol% with T_g values between 101 and 125°C. Only the norbornene double bond was selectively copolymerized. Novel ethene–DCPD–styrene terpolymers, which are difficult to prepare with other catalyst systems, have also been achieved with excellent selectivity and activity.

Kaminsky copolymerized higher condensed cyclic olefin comonomers such as DMON or TMDA using metallocene catalysts [38, 98]. Low activities in DMON-ethene copolymerization and low incorporation were observed because of the increasing monomer bulk. Although the reactivity ratio for norbornene is similar to that of propene, reactivity ratios for DMON and TMDA are comparable to those of 1-butene and 1-hexene.

Recently, Lee and coworkers [141, 144] introduced the copolymerization of ethene with a regioselective partially hydrogenated tricyclopentadiene (HTCPD) by using $[8\text{-}(\eta^5\text{–}C_5Me_4)\text{-}2\text{-}Me(C_9H_8N)\text{-}\kappa N]TiMe_2$ ($C_9H_{10}NH$ = 1,2,3,4-tetrahydroquinoline) (**IV-6**) activated with $(Ph_3C)^+[B(C_6F_5)_4]^-$. A nearly alternating copolymer with a HTCPD content of 45 mol% was obtained with a satisfactory activity of 4.7×10^6 g/(mol Ti h) and a T_g value of 177°C, significantly higher than that of E–N copolymer at the same cycloolefin content. Tensile stress–strain curves showed more ductile properties than a high-T_g E–N copolymer with similar T_g.

Very recently, effective copolymerization of ethene and exo-1,4,4a,9,9a,10-hexahydro-9,10(1′,2′)-benzeno-l,4-methanoanthracene (HBMN) by CGC catalyst activated with $Al(iBu)_3/[Ph_3C][B(C_6F_5)_4]$ has been obtained [145]. E−HBMN copolymers show alternating E−HBMN sequences, high molecular weight, and T_g up to 207°C at comonomer incorporation of 30.4 mol%. The tensile test indicates that these copolymers are more flexible than E−N copolymers and other previously reported COC even at a higher T_g level.

7 Conclusions

Norbornene polymerization is the most versatile of the cycloolefin addition polymerizations. Single-site catalysts such as metallocene compounds, constrained geometry catalysts (CGCs), and nickel or palladium diimine complexes, used in combination with MAO or borate cocatalysts, are active for the copolymerization of norbornene with ethene. The structure of the norbornene homo- and copolymers can be widely influenced by the symmetry and structure of the ligands on the transition metal complexes.

Commercial ethene–norbornene copolymer products obtained using early transition metal catalysts are already available. E–N copolymers are usually amorphous and display a wide range of T_g, from room temperature to about 220°C. They are characterized by high chemical resistance and good processability [39]. They show excellent transparency and high refractive index owing to their high carbon/hydrogen ratio, e.g., the refractive index is 1.53 for a 50:50 E–N copolymer. These properties make them suitable for optical applications such as coatings for high-capacity CDs and DVDs, for lenses, medical equipment, blisters, toner binder, and packaging. During the last two decades, progress in metallocene catalysts for cycloolefin copolymerization has made possible the commercialization of E–N copolymers. A commercial plant for the production of COC material (E–N copolymer) was built in 2000 by Ticona in Oberhausen, Germany, with a capacity of 30,000 tons per annum. Mitsui produces E–N copolymers using vanadium-based catalysts. The industrially produced copolymers have norbornene contents of between 30 and 60 mol% and T_g values of 120–180°C. The copolymer densities are low and near 1. For many applications, these COC materials show better mechanical properties than comparable amorphous thermoplastics and are processable by all conventional methods.

By contrast, copolymerizations of norbornene with higher α-olefins or styrenes and conjugated dienes, or of polycycloolefins, still give low activity, low comonomer incorporation, and low molar masses. Thus, synthesis of new organometallic complexes with various metal centers and with ancillary ligands with appropriate structure will play an important role for their controlled copolymerization, which can lead to COC with desired physical, mechanical, and optical properties.

Late transition metal catalysts, which are more tolerant of polar functional groups than early transition metal catalysts, are most suitable and highly active for norbornene homopolymerizations or copolymerization with other cycloolefins. A range of tailor-made homo-, co-, and terpolymers based on substituted norbornenes for applications in electronic materials are produced and commercialized, but they need further development to be efficiently used in olefin–cycloolefin copolymerizations.

References

1. Natta G, Dall'Asta G, Mazzanti G, Pasquon I, Valvassori A, Zambelli A (1962) Makromol Chem 54:95
2. Dall'Asta G, Mazzanti G, Natta G, Porri L (1962) Makromol Chem 56:224
3. Sartori G, Ciampelli FC, Cameli N (1963) Chim Ind (Milan) 45:1478
4. Natta G, Dall'Asta G, Mazzanti G (1964) Angew Chem Int Ed Engl 3:723
5. Ivin KJ, Saegusa T (1984) Cycloalkenes and bicycloalkenes ring-opening polymerization, vol 1. Elsevier, London
6. Grubbs RH (2003) Handbook of metathesis. Wiley-VCH, Weinheim
7. Bielawski CW, Grubbs RH (2007) Prog Polym Sci 32:1
8. Buchmeiser MR (2000) Chem Rev 100:1565
9. Schrock RR (2006) Angew Chem Int Ed 45:3748
10. Grubbs RH (2006) Angew Chem Int Ed 45:3760
11. Schrock RR (2011) Dalton Trans 40:7484
12. Keitz BK, Fedorov A, Grubbs RH (2012) J Am Chem Soc 134:2040
13. Resconi L, Cavallo L, Fait A, Piemontesi F (2000) Chem Rev 100:253
14. Coates G (2000) Chem Rev 100:1223
15. Angermund K, Fink G (2000) Chem Rev 100:1457
16. Scheirs J, Kaminsky W (eds) (2000) Metallocene-based polyolefins. Wiley, Chichester
17. Kaminsky W (ed) (1999) Metalorganic catalysts for synthesis and polymerization: recent results by Ziegler-Natta and metallocene investigations. Springer, Berlin
18. Hlatky G (1999) Coord Chem Rev 181:243
19. Britovsek GJP, Gibson VC, Wass DF (1999) Angew Chem Int Ed Engl 38:428
20. McKnight AL, Waymouth RM (1998) Chem Rev 98:2587
21. Brintzinger HH, Fischer D, Mülhaupt R, Rieger B, Waymouth R (1995) Angew Chem Int Ed Engl 34:1143
22. Kaminsky W, Bark A, Arndt M (1991) Makromol Chem Macromol Symp 47:83
23. Kaminsky W, Arndt-Rosenau M (2000) In: Scheirs J, Kaminsky W (eds) Metallocene-based polyolefins. Wiley, Chichester, p 91
24. Tritto I, Boggioni L, Ferro DR (2006) Coord Chem Rev 250:212
25. Kaminsky W, Boggioni L, Tritto I (2012) Cycloolefin polymerization. In: Matyjaszewski K, Möller M (eds) Polymer science: a comprehensive reference, vol 3. Elsevier, Amsterdam, p 843
26. Blank F, Janiak C (2009) Coord Chem Rev 253:827
27. Dall'Asta G, Allegra G, Bassi IW, Corradini P, Ganis P (1962) Makromol Chem 58:242
28. Kaminsky W, Spiehl R (1989) Makromol Chem 190:515
29. Jerschow A, Ernst E, Herrmann W, Müller N (1995) Macromolecules 28:7095
30. Naga N, Imanishi Y (2002) Macromol Chem Phys 203:159
31. Kaminsky W, Schauwienold AM, Freidanck FJ (1996) Mol Catal A Chem 112:37
32. Fujita M, Coates GW (2002) Macromolecules 35:9640
33. Lavoie AR, Ho MH, Waymouth RM (2003) Chem Commun 2003: 864
34. Arnold M, Henschke O, Köller F (1996) Macromol Rep A 33(Suppl. 3–4):219
35. Naga N, Imanishi Y (2002) Polymer 43:2133
36. Lavoie AR, Waymouth RM (2004) Tetrahedron 60:7147
37. Wang W, Fujiki M, Nomura KJ (2005) Am Chem Soc 127:4582
38. Kaminsky W, Engehausen R, Kopf J (1995) Angew Chem Int Ed Engl 34:2273
39. Lamonte RR, Mc Nally D (2001) Adv Mater Process 3:1
40. Brekner MJ, Osan F, Rohrmann J, Antberg M (1994) Process for the preparation of chemically homogeneous cycloolefin copolymers, US Patent 5,324,801, p 199
41. Modern Plastics (1995) 72:137
42. Li X, Hou ZM (2008) Coord Chem Rev 252:1842
43. Ruchatz D, Fink G (1998) Macromolecules 31:4674

44. Ruchatz D, Fink G (1998) Macromolecules 31:4681
45. Harrington BA, Crowther DJ (1998) J Mol Catal A Chem 128:79
46. McKnight AL, Waymouth RM (1999) Macromolecules 32:2816
47. Lee BY, Kim YH, Won YC, Han JW, Suh WH, Lee IS, Chung YK, Song KH (2002) Organometallics 21:1500
48. Domski GJ, Rose JM, Coates GW, Bolig AD, Brookhart M (2007) Prog Polym Sci 32:30
49. Jansen JC, Mendichi R, Locatelli P, Tritto I (2001) Macromol Rapid Commun 22:1394
50. Bhriain NN, Brintzinger HH, Ruchatz D, Fink G (2005) Macromolecules 38:2056
51. Thorshaug K, Mendichi R, Boggioni L, Tritto I, Trinkle S, Friedrich C, Mülhaupt R (2002) Macromolecules 35:2903
52. Marconi R, Ravasio A, Boggioni L, Tritto I (1998) Macromol Rapid Commun 30:39
53. Hasan T, Shiono T, Ikeda T (2004) Macromolecules 23:8503
54. Shiono T (2011) Polymer J 43:331 and references therein
55. Yoshida Y, Matsui S, Fujita TJ (2005) Organomet Chem 690:4382
56. Nomura K (2009) Dalton Trans 8811and references therein
57. Matsui S, Yoshida Y, Takagi Y, Spaniol TP, Okuda JJ (2004) Organomet Chem 689:1155
58. Arndt M, Kaminsky W (1995) Macromol Symp 95:167
59. Arndt M, Engehausen R, Kaminsky W, Zoumis KJ (1995) Mol Catal A Chem 101:171
60. Provasoli A, Ferro DR, Tritto I, Boggioni L (1999) Macromolecules 32:6697
61. Arndt M, Beulich I (1998) Macromol Chem Phys 199:1221
62. Kaminsky W, Noll A (1993) Polym Bull 31:175
63. Kaminsky W, Arndt M (1997) Adv Polym Sci 127:143
64. Kaminsky W, Arndt-Rosenau M (2000) Homo- and copolymerization of cycloolefins by metallocene catalysts. In: Scheirs J, Kaminsky W (eds) Metallocene-based polyolefins, vol 2. Wiley, Chichester, p 89 and references there in
65. Kaminsky W, Beulich I, Arndt M (2001) Macromol Symp 173:211
66. Tritto I, Boggioni L, Sacchi MC, Locatelli P, Ferro DR, Provasoli A (1999) Copolymer microstructures of ethylene norbornene copolymers prepared with homogeneous metallocene based catalysts. In: Kaminsky W (ed) Metalorganic catalysts for synthesis and polymerization. Springer, Berlin, p 493
67. Tritto I, Boggioni L, Sacchi MC, Locatelli P, Ferro DR, Provasoli A (1999) Macromol Rapid Commun 20:279
68. Forsyth J, Pereña J, Benavente R, Perez E, Tritto I, Boggioni L, Brintzinger HH (1999) Macromol Chem Phys 202:614
69. Domski GJ, Rose JM, Coates GW, Bolig AD, Brookhart M (2007) Prog Polym Sci 32:30
70. Wendt RA, Fink G (2003) J Mol Catal A Chem 203:101
71. Herfert N, Montag P, Fink G (1993) Makromol Chem 194:3167
72. Wendt RA, Mynott R, Fink G (2002) Macromol Chem Phys 203:2531
73. Kaminsky W, Sperber O, Werner R (2006) Coord Chem Rev 250:110
74. Tritto I, Marestin C, Boggioni L, Sacchi MC, Brintzinger HH, Ferro DR (2001) Macromolecules 34:5770
75. Marconi R, Ravasio A, Boggioni L, Tritto I (2008) Macromol Rapid Commun 30:39
76. Yoshida Y, Matsui S, Takagi Y, Mitani M, Nitabaru M, Nakano T, Tanaka H, Fujita T (2000) Chem Lett 1270
77. Yoshida Y, Matsui S, Takagi Y, Mitani M, Nakano T, Tanaka H, Kashiwa N, Fujita T (2001) Organometallics 20:4793
78. Yoshida Y, Saito J, Mitani M, Takagi Y, Matsui S, Ishii S, Nakano T, Kashiwa N, Fujita T (2002) Chem Commun 1298
79. Matsui S, Spaniol TP, Takagi Y, Yoshida Y, Okuda JJ (2002) Chem Soc Dalton Trans 4529
80. Hou Z, Luo Y, Li XJ (2006) Organomet Chem 691:2734
81. Zeimentz PM, Arndt S, Elvidge BR, Okuda J (2006) Chem Rev 106:2404
82. Li X, Baldamus J, Hou Z (2005) Angew Chem Int Ed 44:962

83. Ravasio A, Zampa C, Boggioni L, Tritto I, Hitzbleck J, Okuda J (2008) Macomolecules 41:9565
84. Tritto I, Ravasio A, Boggioni L, Bertini F, Hitzbleck J, Okuda J (2010) Macromol Chem Phys 211:897
85. Bergström CH, Sperlich BR, Ruotoistenmäki J, Seppälä JV (1998) J Polym Sci A Polym Chem 36:1633
86. Wendt RA, Fink G (2001) Macromol Chem Phys 202:3490
87. Tritto I, Marestin C, Boggioni L, Zetta L, Provasoli A, Ferro DR (2000) Macromolecules 33:8931
88. Tritto I, Boggioni L, Jansen JC, Thorshaug K, Sacchi MC, Ferro DR (2002) Macromolecules 35:616
89. Tritto I, Boggioni L, Ferro DR (2004) Macromolecules 37:9681
90. Yoshida Y, Mohri J, Ishii S, Mitani M, Saito J, Matsui S, Makio H, Nakano T, Tanaka H, Onda M, Yamamoto Y, Mizuno A, Fujita T (2004) J Am Chem Soc 126:12023
91. Ravasio A, Boggioni L, Bertini F, Tritto I (2012) J Polym Sci A Polym Chem 50:867
92. Lee BY, Kim YH, Wona YC, Shim CB, Shin DM, Chung YK (2002) J Organomet Chem 660:161
93. Jansen JC, Mendichi R, Sacchi MC, Tritto I (2003) Macromol Chem Phys 204:522
94. Henschke O, Köller F, Arnold M (1997) Makromol Rapid Commun 18:617
95. Boggioni L, Bertini F, Zannoni G, Tritto I, Carbone P, Ragazzi M, Ferro DR (2003) Macromolecules 346:882
96. Boggioni L, Tritto I, Ragazzi M, Carbone P, Ferro DR (2004) Macromol Symp 218:39
97. Carbone P, Ragazzi M, Tritto I, Boggioni L, Ferro DR (2003) Macromolecules 36:891
98. Kaminsky W, Derlin S, Hoff M (2007) Polymer 48:7271
99. Hasan T, Nishii K, Shiono T, Ikeda T (2002) Macromolecules 35:8933
100. Hasan T, Ikeda T, Shiono T (2005) Macromolecules 38:1071
101. Boggioni L, Zampa C, Ravasio A, Tritto I, Ferro DR (2008) Macromolecules 41:5107
102. Boggioni L, Ravasio A, Zampa C, Ferro DR, Tritto I (2010) Macromolecules 43:4532
103. Boggioni L, Ravasio A, Boccia AC, Ferro DR, Tritto I (2010) Macromolecules 43:4543
104. Nakamura A, Ito S, Nozaki (2009) Chem Rev 109:5215
105. Sen A, Lai TW (1981) Am Chem Soc 103:4627
106. Mehler C, Risse W (1992) Macromolecules 25:4226
107. Goodall BL, Barnes DA, Benedikt GM, McIntosh LH III, Rhodes LF (1997) Polym Mater Sci Eng 76:56
108. Goodall BL (2003) Cycloaliphatic polymers via late transition metal catalysis. In: Rieger B, Baugh LS, Kacker S, Striegler S (eds) Late transition metal polymerization catalysis. Wiley-VCH, Weinheim, p 101
109. Hennis AD, Polley JD, Long GS, Sen A, Yandulov D, Lipian J, Benedikt GM, Rhodes LF, Huffman J (2001) Organometallics 20:2802
110. Johnson LK, Killian CM, Brookhart M (1995) J Am Chem Soc 117:6414
111. Kiesewetter J, Kaminsky W (2003) Chem Eur J 9:1750
112. Kiesewetter J, Arikan B, Kaminsky W (2006) Polymer 47:3302
113. Younkin TR, Connor EF, Henderson JI, Friedrich SK, Grubbs RH, Bansleben DA (2000) Science 287:460
114. Connor EF, Younkin TR, Henderson JI, Hwang S, Grubbs RH, Roberts WP, Litzau JJ (2002) J Polym Sci A Polym Chem 40:2842
115. Berkefeld A, Drexler M, Möller HM, Mecking S (2009) J Am Chem Soc 131:12613
116. Diamanti SJ, Khanna V, Hotta A, Coffin RC, Yamakawa D, Kramer EJ, Fredrick-son GH, Bazan GC (2006) Macromolecules 39:3270–3274
117. Rojas RS, Galland GB, Wu G, Bazan GC (2007) Organometallics 26:5339
118. Sujith S, Dae JJ, Na SJ, Park YW, Choi JH, Lee BY (2005) Macromolecules 38:10027
119. Li H, Marks TJ (2006) J Proc Natl Acad Sci USA 103:15295
120. Rodriguez BA, Delferro M, Marks TJ (2009) J Am Chem Soc 131:5902

121. Diamanti SJ, Ghosh P, Shimizu F, Bazan GC (2003) Macromolecules 36:9731
122. Rojas RS, Galland GB, Wu G, Bazan GC (2007) Organometallics 26:5339–5345
123. Bauers FM, Mecking S (2001) Macromolecules 34:1165
124. Sujith S, Joe DJ, Na SJ, Park YW, Choi CH, Lee BY (2005) Macromolecules 38:10027
125. Wehrmann P, Zuideveld M, Thomann R, Mecking S (2006) Macromolecules 39:5995
126. Benedikt GM, Elce E, Goodall BL, Kalamarides HA, McIntosh LH, Rhodes LF, Selvy KT, Andes C, Oyler K, Sen A (2002) Macromolecules 35:8978
127. Skupov KM, Marella PR, Hobbs JL, McIntosh LH, Goodall BL, Claverie JP (2006) Macromolecules 39:4279
128. Liu S, Borkar S, Newsham D, Yennawar H, Sen A (2007) Organometallics 26:210
129. Ravasio A, Boggioni L, Tritto I (2011) Macromolecules 44:4180
130. Diamanti SJ, Kanna V, Hotta A, Yamakava D, Shimizu F, Kramer EJ, Fredrikson GH, Bazan GC (2004) J Am Chem Soc 126:10528
131. Coffin RC, Diamanti SJ, Hotta A, Khanna V, Kramer EJ, Fredrickson GH, Bazan GC (2007) Chem Commun 3550
132. Kaminsky W, Bark A (1992) Polym Int 2:251
133. Dougnac VN, Quijada R, Palza H, Galland GB (2009) Eur Polym J 45:102
134. Lee DH, Yoon KB, Park JR, Lee BH (1997) Eur Polym J 33:447
135. Marathe S, Sivaram S (1994) Macromolecules 27:1083
136. Lane BS, Burgess K (2003) Chem Rev 103:2457
137. Naga NJ (2005) Polym Sci A Polym Chem 43:1285
138. Simanke AG, Mauler RS, Galland GB (2002) J Polym Sci A Polym Chem 40:471
139. Suzuki J, Kino Y, Uozumi T, Sano T, Teranishi T, Jin J, Soga K, Shiono TJ (1999) Appl Polym Sci 72:103
140. Li XF, Hou ZM (2005) Macromolecules 38:6767
141. Cho DJ, Wu CJ, Han WS, Kang SO, Lee BY (2006) Organometallics 25:2133
142. Na SJ, Wu CJ, Yoo J, Kim BE, Lee BY (2008) Macromolecules 41:4055
143. Sernetz FG, Mülhaupt R (1997) J Polym Sci A Polym Chem 35:2549
144. Yu ST, Na SJ, Lim TS, Lee BY (2010) Macromolecules 43:725
145. Hong M, Cui L, Liu S, Li Y (2012) Macromolecules 45:5397

Adv Polym Sci (2013) 258: 143–162
DOI: 10.1007/12_2013_211

Published online: 11 May 2013

Trialkylaluminum-Free Modified Methylaluminoxane as a Cocatalyst for Living Polymerization of Olefins

Takeshi Shiono

Abstract This article reviews living polymerization of olefins with several dimethyltitanium complexes by the use of trialkylaluminum-free modified methylaluminoxane (dMMAO) as a cocatalyst. The excellent solubility of dMMAO allows living coordination polymerization of olefins in aliphatic hydrocarbons. A chelating diamidodimethyltitanium complex (**1**) conducted living polymerization of propene in heptane at 0°C to produce atactic polymer. Metal oxide-supported dMMAO was also effective as a cocatalyst for the controlled polymerization of propene with **1**, where the propagation rate and the molecular weight distribution of the produced polymer were dependent on the metal oxide used. *ansa*-Dimethysilylene(fluorenyl)(*tert*-butylamido)dimethyltitanium (**2**) activated by dMMAO conducted living polymerization of propene at 0°C in chlorobenzene, toluene and heptane. The propagation rate and the *syndiotactic*(*syn*)-specificity of the catalyst were dependent on the solvent as follows: propagation rate, chlorobenzene > toluene > heptane; *syn*-specificity, chlorobenzene < toluene < heptane. The propagation rate and the *syn*-specificity were also dependent on the substituent on the fluorenyl ligand of **2**, and a highly active and *syn*-specific living polymerization was achieved by the use of a 3,6-di-*tert*-butyl substituted complex (**4**). Complex **2** and its derivatives such as **4** activated by dMMAO also conducted living homo- and copolymerization of norbornene and 1-alkene in toluene, which afforded a variety of tailor-made polyolefins composed of norbornene and 1-alkene.

Keywords 1-Alkene · Living polymerization · Modified methylaluminoxane · Norbornene · Propene · Single-site catalyst · Supported catalyst

T. Shiono (✉)
Graduate School of Engineering, Hiroshima University, Kagamiyama 1-4-1, Higashi-Hiroshima, 739-8527 Hiroshima, Japan
e-mail: tshiono@hiroshima-u.ac.jp

Contents

1 Introduction

Development of metallocene catalysts, which is strongly owing to the finding of methylaluminoxane (MAO) as a cocatalyst [1], has enabled us to produce a variety of uniform olefin copolymers as well as to control the stereoregularity of polyolefins [2, 3]. The success of metallocene catalysts stimulated the research on transition metal complexes for olefin polymerization [4, 5], so-called single-site catalysts, resulting in various transition metal complexes for living polymerization of olefins [6, 7]. Although several cocatalysts such as $B(C_6F_5)_3$, $Ph_3CB(C_6F_5)_4$, and $PhMe_2NHB(C_6F_5)_4$ have been developed [8], MAO is still one of the most important cocatalyst because of its universality for various transition metal complexes.

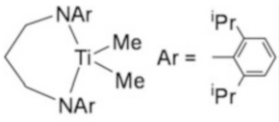

1

When MAO, which is the condensation product of water and Me_3Al and is usually supplied as a toluene solution, is used as a cocatalyst for living polymerization, Me_3Al remaining in the toluene solution should be removed to prevent the chain transfer via transmetalation. However, the removal of Me_3Al from MAO significantly decreases the solubility of MAO, even in toluene. Modified MAO (MMAO), which is the condensation product between water and the mixture of Me_3Al and $^iBu_3Al$, possesses good solubility in aliphatic hydrocarbons. We therefore prepared R_3Al-free MMAO and applied it as a cocatalyst [9]. Hereafter, dMAO and dMMAO denote Me_3Al-free MAO and R_3Al-free MMAO, respectively. This

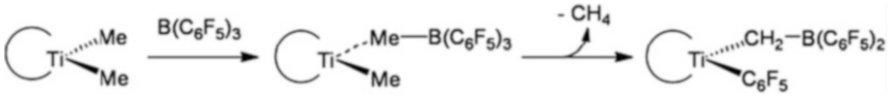

Scheme 1 Deactivation of **1**-$B(C_6F_5)_3$ [11]

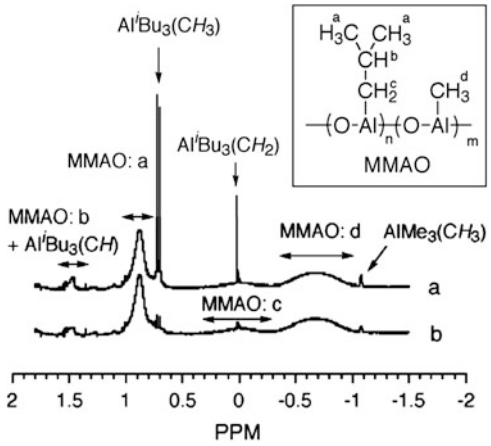

Fig. 1 ^{1}H NMR spectra of MMAO (*a*) and dMMAO (*b*) in THF-d_8 [13]

article reviews our work on the living polymerization of olefins using dMMAO combined with certain dimethyltitanium complexes.

2 Living Polymerization of Propene with a Chelating Diamidodimethyltitanium

2.1 Activation with dMMAO

McConville et al. demonstrated that living polymerization of 1-alkene proceeded with a chelating diamidodimethyltitanium (**1**) activated by $B(C_6F_5)_3$ at 23°C in bulk or CH_2Cl_2 solution [10]. The addition of toluene significantly retarded the activity because the active species formed a stable complex with toluene. They reported that the active species was deactivated in the absence of 1-alkene via the reaction shown in Scheme 1 [11]. These results prompted us to investigate propene polymerization with **1** activated by dMMAO, which was prepared from MMAO by repetitions of vacuum drying and successive re-dissolving in heptane [9].

Figure 1 displays the ^{1}H NMR spectra of MMAO and dMMAO in tetrahydrofuran-d_8. The contents of each Al species were calculated from the relative intensities of the ^{1}H NMR spectrum, which indicates that the treatment decreased the ^{i}Bu$_3$Al

Table 1 Effect of cocatalyst on propene polymerization with **1**[a]

Run	Cocatalyst	Ti (μmol)	Activity[b]	M_n[c] ($\times 10^4$)	M_w/M_n[c]	N/Ti[d] (mol/mol)
1	dMAO	20	7	20.9	3.52	0.02
2	dMMAO	20	321	29.2	1.16	0.46
3	dMMAO/SiO_2	20	235	66.1	1.34	0.15
4	dMMAO/SiO_2	10	89	124	1.43	0.03
5	dMMAO/Al_2O_3	10	102	49.2	2.17	0.09
6	dMMAO/MgO	10	4	27.2	2.48	0.01

[a]Polymerization conditions: heptane = 30 mL, propene = 1 atm, 0°C, polymerization time = 25 min, Al = 8.0 mmol (Run 1–2), Al = 4.0 mmol (Run 3–6)
[b]kg-PP mol-Ti^{-1} h^{-1}
[c]Determined by GPC using universal calibration
[d]Molar ratio of **1** and polymer chain calculated from yield and M_n

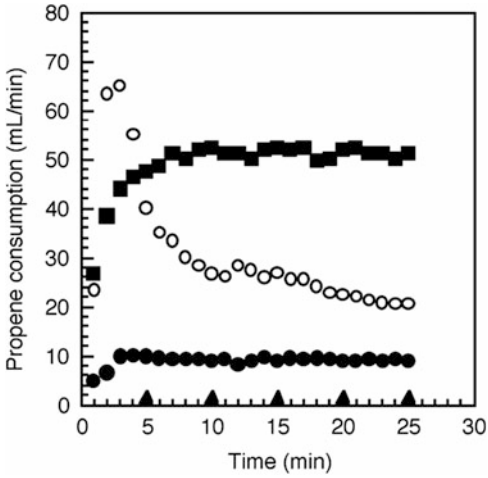

Fig. 2 Rate–time profiles of propene polymerization with **1** activated by dMMAO and dMMAO/SiO_2: *squares*, dMMAO (Ti = 20 μmol); *open circles*, dMMAO/SiO_2 (Ti = 20 μmol); *filled circles*, dMMAO/SiO_2 (Ti = 10 μmol); *triangles*, MMAO (Ti = 20 μmol) [12]

content from 1.3 to 0.1 mol%, keeping the Me_3Al content at approximately 0.1 mol%.

Propene polymerization was conducted in heptane with **1** using dMAO and dMMAO at 0°C under atmospheric pressure of propene. The results are shown in Table 1.

Both dMMAO and dMAO systems conducted polymerization, but the former showed about 50 times higher activity than the latter. The polymers obtained with dMMAO and dMAO had high M_n values of 290,000 and 209,000, respectively, and consequently the number of polymer chains (N) in the dMMAO system was 30 times larger than in the dMAO system. The polydispersity (M_w/M_n) of the polymer obtained with the dMMAO system was narrow ($M_w/M_n = 1.16$), whereas that with the dMAO system was broad ($M_w/M_n = 3.52$). The low N value and the broad M_w/M_n in the dMAO system are mainly due to the poor solubility of dMAO in heptane. MAO and MMAO did not show activity under the same conditions, probably due to the formation of the heterodinuclear complex with the remaining R_3Al.

The rate–time profile of propene polymerization with the dMMAO system is illustrated in Fig. 2, indicating a steady rate after a certain induction period. The

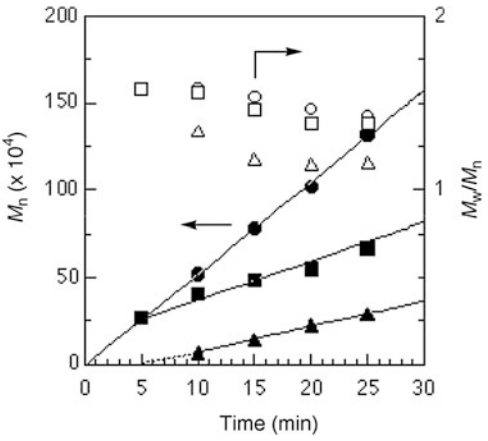

Fig. 3 Plots of M_n and M_w/M_n against polymerization time in propene polymerization with **1**: dMMAO/SiO_2 (Ti = 20 μmol), M_n (*filled squares*), M_w/M_n (*open squares*); dMMAO/SiO_2 (Ti = 10 μmol), M_n (*filled circles*), M_w/M_n (*open circles*); dMMAO (Ti = 20 μmol), M_n (*filled triangles*), M_w/M_n (*open triangles*) [12]. For polymerization conditions, see Table 1

dependence of molecular weight on polymerization time (t_p) was investigated by sampling during the polymerization, the results of which are shown in Fig. 3.

The M_n value increased almost linearly with increasing t_p with narrowing the M_w/M_n value from 1.4 to below 1.2, although the straight line of M_n against t_p did not go through the origin. The negative intercept and the narrowing of M_w/M_n are attributed to the slow initiation, as observed in Fig. 2. The results imply that the **1**-dMMAO system conducted living polymerization of propene in heptane at 0°C.

2.2 Activation with SiO_2-Supported dMMAO

Because dMMAO is readily soluble in heptane, unlike dMAO, we prepared SiO_2-supported dMMAO (dMMAO/SiO_2) to heterogenize this living polymerization system [12]. Propene polymerization was conducted at 0°C with **1** using dMMAO/SiO_2 as an activator and the rates of propene consumption against t_p are plotted in Fig. 2. When 20 μmol of **1** was used, the dMMAO/SiO_2 system showed a high consumption rate in the initial stage, but the rate gradually decreased because the produced polymer prohibited effective stirring. We then investigated the rate–time profile of the dMMAO/SiO_2 system with 10 μmol of **1** and found that the system showed a steady rate.

The time dependence of M_n and M_w/M_n in the dMMAO/SiO_2 system monitored by sampling is shown in Fig. 3. The dMMAO/SiO_2 system gave a high molecular weight polypropene (PP) even after 5 min of polymerization, regardless of the amount of Ti used, whereas the dMMAO system showed an induction period. The plot of M_n versus t_p with 10 μmol of Ti gives a straight line which goes through the origin. The M_w/M_n values, which were slightly broader than those of the homogeneous system, became narrow with increasing t_p. These results indicate the living nature of the dMMAO/SiO_2 system. In the case of 20 μmol of Ti with dMMAO/SiO_2, although the initial slope is the same as that of 10 μmol of Ti, it

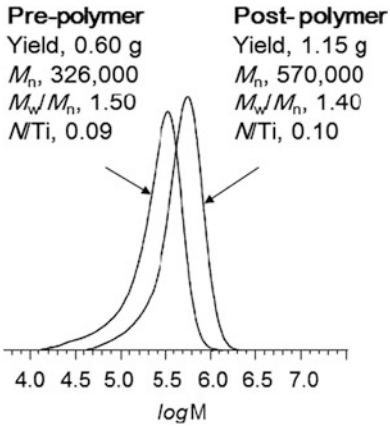

Fig. 4 Post-polymerization of propene with **1**-dMMAO/SiO_2 (Ti = 20 μmol) [12]

changes to a smaller value after 5 min of polymerization in response to the decrease in propene consumption rate. However, we confirmed the livingness by post-polymerization as shown in Fig. 4. The change of the slope in the dMMAO/SiO_2 system with 20 μmol of Ti is, therefore, ascribed to the decrease in propene concentration due to the ineffective stirring caused by the production of high molecular weight viscous polymer. These results imply that the **1**-dMMAO/SiO_2 system conducted living polymerization of propene in heptane.

The slope of the plot of M_n versus time with dMMAO/SiO_2 (Fig. 3) is larger than that with dMMAO, indicating that the propagation rate is enhanced by supporting dMMAO on SiO_2. Thus, dMMAO/Al_2O_3 and dMMAO/MgO were prepared and propene polymerization was conducted with these cocatalysts in place of dMMAO/SiO_2 [13]. Because the steady polymerization rates observed in these systems were accompanied by a linear increase in the M_n values with t_p, we can evaluate the propagation rate and the number of active centers from the M_n and the N values, respectively (Table 1).

The initiation efficiency of the homogeneous dMMAO system (46%) was higher than that of the heterogeneous dMMAO/SiO_2 system (15%) with 20 μmol of Ti. The lower initiation efficiency (3%) with 10 μmol of Ti in the dMMAO/SiO_2 system is probably due to the lower concentration of Ti and to impurities in the system. On the other hand, the M_n value for a 25-min polymerization decreased in the following order: dMMAO/SiO_2 > dMMAO/Al_2O_3 > dMMAO > dMMAO/MgO. That is, the propagation rate was enhanced by the modification of MMAO with SiO_2 or Al_2O_3, but suppressed by modification with MgO. The M_w/M_n value also depended on the metal oxide as follows: MgO > dMMAO/Al_2O_3 > dMMAO/SiO_2 > dMMAO.

To investigate the relationship between the supporting effects of dMMAO and the nature of the surface Al species of the cocatalysts, we conducted XPS analysis of dMMAO and the metal-oxide-supported dMMAOs, and investigated the binding energy (BE) of Al and the full width at half-maximum intensity (FWHM). The BE values of the supported MMAOs increased in the following order: dMMAO/MgO (74.7 eV) ≈ dMMAO (74.9 eV) < dMMAO/Al_2O_3 (75.3 eV) < dMMAO/SiO_2 (75.7 eV), which implies a decrease in electron density of Al in the cocatalyst,

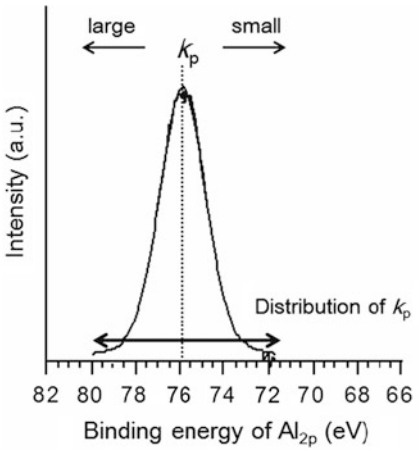

Fig. 5 Illustration of the relation between the XPS spectrum of MMAO and the propagation rate constant (k_p)

i.e., an increase in the Lewis acidity of dMMAO. This order is in good agreement with that of the M_n values. Thus, a cocatalyst with stronger Lewis acidity gives the active species with higher propagation rate, which can be interpreted by the separation of the active ion pair formed from the dimethyltitanium complex and the cocatalyst.

The FWHM of the XPS spectrum is an indicator of the heterogeneity of surface Al species. The FWHM value of dMMAO in the cocatalyst depended on the support used, and increased in the following order: MMAO (2.36 eV) < MMAO/SiO_2 (2.40 eV) < MMAO/Al_2O_3 (2.47 eV) < MMAO/MgO (2.65 eV). This order accords with that of the M_w/M_n values. Neither chain transfer nor deactivation occurred in the present systems. Thus, the distribution of propagation rate caused by the distribution of Lewis acidity should directly reflect the molecular weight distribution of the produced polymer, as illustrated in Fig. 5.

The ^{13}C NMR analysis of the produced polymers indicates that all the systems gave statistically atactic PPs.

3 Living Polymerization of Propene with *ansa*-Dimethysilylene(fluorenyl)(amido)-dimethyltitanium Activated with dMMAO

3.1 Effect of Solvents

We succeeded in regiospecific living polymerization of propene or 1-hexene with *ansa*-dimethysilylene(fluorenyl)(amido)dimethyltitanium (**2**) activated by $B(C_6F_5)_3$ in toluene at −50°C [14]. The use of dMAO as a cocatalyst raised the living polymerization temperature to 0°C, accompanied by an increase in activity and *syn*-specificity [*syn*-triad (*rr*) = 63%] [15]. We achieved living polymerization of propene with **1**-dMMAO in heptane. Thus, we investigated the effect of solvents

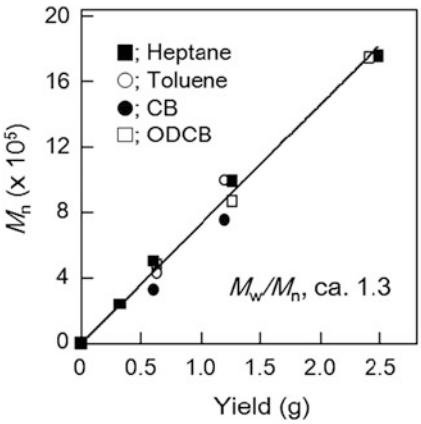

Fig. 6 Plots of M_n versus polymer yield in propene polymerization with **2**-dMMAO in various solvents [16]

in propene polymerization with **2** using dMMAO [16]. The solvents used were heptane, toluene, chlorobenzene (CB) and *o*-dichlorobenzene (ODCB).

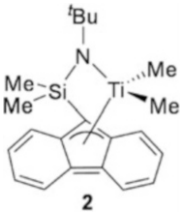

2

The livingness of the polymerization was investigated by a batch-type operation, changing the amount of charged propene. A good linear relationship was observed between the polymer yield and the M_n value, irrespective of the solvent used (Fig. 6), indicating that the living polymerization of propene should proceed in all the solvents used with almost the same initiation efficiency. The post-polymerization experiments in heptane and ODCB confirmed the livingness of the PPs produced in these solvents.

The effect of the solvents on propagation rate was investigated by semi-batch operation, indicating an extremely high propagation rate in ODCB compared with heptane. Rate enhancement by the addition of CH_2Cl_2 was observed in 1-alkene polymerization with **1**-B$(C_6F_5)_3$ [10] and propene polymerization with Cp_2TiPh_2–MAO [17]. The solvent effect on the propagation rate can be interpreted by the separation of the active ion pair: a polar solvent like ODCB gives a highly active separated ion-pair, while a non-polar solvent like heptane gives a less active contact ion-pair.

The *syn*-specificity of **2**-dMMAO was also dependent on the solvent, and the *rr* value of the produced PP decreased as follows: 74% (heptane) > 60% (toluene) > 46% (ODCB) > 42% (CB). The stereo-defect arising from "miss-selection of prochiral face" (*rmmr*) was independent of the solvent (4–5%), whereas the stereo-defect arising from "chain-migration without monomer insertion" (*rmrr*) increased according to the polarity of the solvent in the following order: heptane (10%) < toluene (19%) < ODCB (24%) < CB (26%). A similar solvent effect

Table 2 Propene polymerization with **2** and its analogues in heptane activated by dMMAO[a]

Catalyst	Al/Ti (mol/mol)	Time (min)	Activity[b]	M_n[c] ($\times 10^4$)	M_w/M_n[c]	N/Ti[d] (mol/mol)	rr[e] (%)	T_m[f] (°C)
2	400	11.0	660	16.1	1.31	0.75	73	89
3	200	3.0	2,280	20.8	1.65	0.55	81	92
4	200	3.0	2,320	19.6	1.46	0.60	93	142
5	100	0.5	11,400	19.3	2.92	0.50	61	–[g]

[a]Polymerization conditions: Ti = 20 μmol, cocatalyst = dMMAO, solvent = heptane, total volume = 30 mL, propene = 1 atm temperature = 0°C
[b]Activity in kg-polymer mol-Ti^{-1} h^{-1}
[c]Number average molecular weight and molecular weight distribution determined by GPC using monodisperse polystyrene standards
[d]Molar ratio of Ti and polymer chain calculated from yield and M_n
[e]Syndiotactic triad determined by ^{13}C NMR
[f]Melting temperature determined by DSC
[g]Not detected

was observed in propene polymerization with C_s-symmetric zirconcene catalysts, where *m*-dichlorobenzene, bromobenzene or CH_2Cl_2 was used [18–20].

3.2 Substituent Effects of Fluorenyl Ligand

The use of dMMAO enabled the living polymerization of propene in heptane, which afforded PP with the highest syndiotacticity among the solvents employed. We therefore synthesized a series of **2** analogues that possessed alkyl substituents on the fluorenyl ligand: 2,7-^{t}Bu$_2$, **3**; 3,6-^{t}Bu$_2$, **4**; 2,3,6,7-^{t}Bu$_4$ analogue, **5**.

The results of propene polymerizations with these complexes activated by dMMAO in heptane are shown in Table 2. The introduction of ^{t}Bu groups increased the activity regardless of the position on the fluorenyl ligand at the 2,7-position, **3**, or 3,6-position, **4** [21]. The post-polymerization experiments indicated the livingness of these systems at 0°C and 25°C, although the molecular weight distributions were slightly broad compared with that of ideal living polymerization due to slow initiation. The N values were almost the same regardless of the Ti complex used, indicating that the propagation rate was enhanced by the introduction of ^{t}Bu groups. The 2,3,6,7-^{t}Bu$_4$-substituted analogue, **5**, further increased the activity by one order of magnitude, although the molecular weight distribution became broad [22]. On the other hand, 3,6-substituted **4** showed the highest *syn*-specificity among the complexes used. Thus, complex **4** activated by dMMAO in heptane was found to be a highly active and highly *syn*-specific catalyst for living polymerization of propene.

Metallocene catalysts usually require a large excess of MAO or MMAO to achieve high polymerization activity. The effect of the amount of dMMAO was investigated by the living polymerization of propene with **4**-dMMAO, because the turnover-frequency (TOF) can be precisely evaluated from the number-average polymerization degree (P_n) of produced polymer and t_p as P_n/t_p. The relation between P_n/t_p and Al/Ti ratio is displayed in Fig. 7. The P_n/t_p value increased exponentially

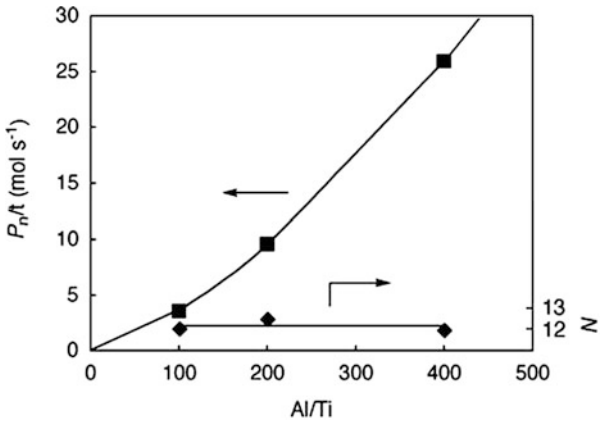

Fig. 7 Plots of P_n/t_p and N versus Al/Ti in propene polymerization with **4**-dMMAO [21]

against the Al/Ti ratio, keeping the N constant, indicating that a high Al/Ti ratio is necessary for high propagation rate, but not for high initiation efficiency.

The *syn*-specific living polymerization of propene was also achieved by Fujita et al. [23, 24] and Coates et al. [25] using bis(phenoxyimine)titanium derivatives (so-called FI catalysts) activated with dMAO. The active species of this catalyst is an octahedral Ti with a 2,1-inserted propagation chain, and the chain-end chiral carbon isomerizes the chirality of the Ti species one to the other in each monomer insertion to give the *syn*-PP. Fujita et al. succeeded in improving the *syn*-specificity ($rr = 94\%$) by tuning the bis(phenoxyimine) ligand [26]. The activity of propene polymerization with this catalytic system was significantly low, probably due to this stereospecific polymerization mechanism, because the system conducted living polymerization of ethene at very high activity [27].

One of the advantages of our *syn*-specific living polymerization is the high propagation rate for propene polymerization. We therefore investigated polymerization of 1-hexene, 1-octene, 1-decene, and 1-dodecene with **4**-dMMAO at 0°C in toluene [28]. Although the activity was decreased as the length of 1-alkene became longer, an activity of 9,500 kg-polymer mol-Ti^{-1} h^{-1} was observed in 1-dodecene polymerization to give a polymer with M_n value of 308,000 in a one-minute polymerization at an initial monomer concentration of 3.0 M. It was confirmed that living polymerization proceeded regardless of the alkyl chain length. TOF determined from P_n and t_p was found to decrease in the following order: 1-hexene (98 s^{-1}) > 1-octene (62 s^{-1}) > 1-decene (32 s^{-1}) > 1-dodecene (31 s^{-1}). On the other hand, the *syn*-triads of the produced polymers were approximately 0.85–0.88 with no relation to the alkyl length of 1-alkene.

3.3 Synthesis of Stereo-Block PP

The *syn*-specificity of the catalytic system was dependent on the Ti complex and the solvent as described above. The *syn*-specificity was also controlled by polymerization

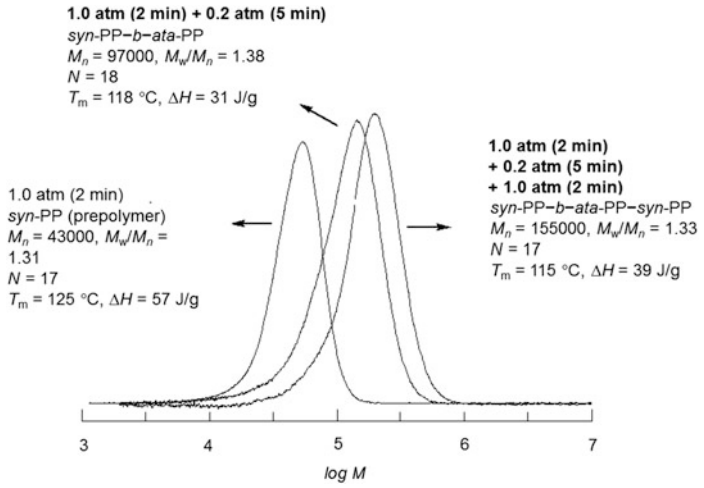

Fig. 8 Synthesis of stereo-block PP with **4**-dMMAO by pressure variation [32]

temperature and propene pressure (concentration). Stereo-block PPs composed of *syn*- and *ata*-sequences were synthesized by changing these conditions during the living polymerization of propene [29–31]. The synthesis of *syn*-PP-*block*-*ata*-PP-*block*-*syn*-PP by changing propene pressure is displayed in Fig. 8 [32].

4 Living Polymerization of Norbornene with *ansa*-Dimethysilylene(fluorenyl)(amido)-dimethyltitanium Activated with dMMAO

4.1 Homopolymerization of Norbornene

Complex **2**, which is effective for propene polymerization was found to conduct coordination-insertion-type polymerization of norbornene. In Table 3 are shown the effects of cocatalyst in norbornene polymerization with **2** in toluene at 20°C [33, 34].

dMAO and MMAO showed good activities (approximately 1,000 kg-polymer·mol-Ti^{-1}·h^{-1}), but MAO showed very poor activity due to Me_3Al in MAO. $Ph_3CB(C_6F_5)_4$ combined with R_3Al showed the highest activity. All the produced polymers possessed narrow molecular weight distributions. It should be noted that MMAO gave the narrowest M_w/M_n of 1.07 even in the presence of $^iBu_3Al$, probably due to the good solubility of MMAO, suggesting that dMMAO should not be necessary for living polymerization of norbornene with **2**. The chain transfer to R_3Al should be suppressed at the hindered propagation chain end of norbornene.

The effect of Al/Ti ratio on the yield and the M_n value are shown in Fig. 9. Both values increased proportionally with the Al/Ti ratio, keeping the narrow molecular weight distribution, which indicates that the propagation rate was enhanced by excess MMAO, as observed in propene polymerization with **4**-dMMAO.

Table 3 Polymerization of norbornene with **2** using different cocatalysts[a]

Cocatalyst	Time (min)	Activity[b]	Conversion[c] (%)	M_n[d] ($\times 10^4$)	M_w/M_n[d]	N/Ti[e]
dMAO	5	1,090	56	29.6	1.26	0.30
MAO	5	56	3	0.55	1.26	0.90
MMAO	3	953	29	7.9	1.07	0.60
$Ph_3CB(C_6F_5)_4$ + Oct_3Al[f]	2	4,820	95	33.5	1.40	0.50
$Ph_3CB(C_6F_5)_4$ + $^iBu_3Al$[f]	2	4,280	85	20.2	1.41	0.70
$Ph_3CB(C_6F_5)_4$[g]	10	–	–	–	–	–

[a]Polymerization conditions: Ti = 20 μmol, Al/Ti = 400, [norbornene] = 1.2 M, solvent = toluene, total vol. = 30 mL. Temperature = 20°C
[b]Activity = kg-polymer mol-Ti^{-1} h^{-1}
[c]Conversion was calculated from polymer yield
[d]Number average molecular weights and molecular weight distributions were measured by GPC using polystyrene standard
[e]Molar ratio of **2** and polymer chain calculated from yield and M_n
[f]B = 20 μmol, R_3Al = 400 μmol
[g]B = 20 μmol

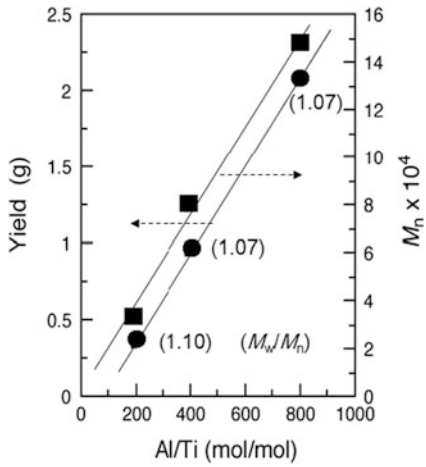

Fig. 9 Plots of yield and M_n values versus Al/Ti ratio in norbornene polymerization with **2**-MMAO [34]

4.2 Random Copolymerization of Norbornene and 1-Alkene

Complex **2** conducted random copolymerization of norbornene with ethene or propene in high activity combined with a suitable cocatalyst, and copolymers with narrow molecular weight distribution were obtained with dMAO [35–37]. There are many catalysts that can conduct copolymerization of ethene and norbornene [38] but very few for copolymerization of norbornene or its derivatives with 1-alkene [39–43]. We conducted copolymerization of norbornene with propene or 1-octene with **2**–**5** activated by dMMAO (Table 4) [44].

The activity of the copolymerization increased by the introduction of alkyl substituents on the fluorenyl ligand as observed in the propene polymerization.

Table 4 Copolymerization of norbornene with 1-alkene by **2**–**5** activated by dMMAO[a]

Catalyst	Comonomer	Time (min)	Activity[b]	M_n[c] ($\times 10^4$)	M_w/M_n[c]	NB[d] (mol%)	Conversion[e] NB (%)	T_g[f] (°C)
2[g]	Propene	3.0	1,880	15.1	1.10	79	40	292
3	Propene	2.0	3,000	16.7	1.14	81	43	291
4	Propene	1.0	4,920	15.9	1.33	76	34	285
5	Propene	0.5	17,100	23.2	1.30	71	57	250
2	1-Octene	5.0	340	5.3	1.19	80	22	213
3	1-Octene	1.5	800	4.9	1.15	82	17	233
4[h]	1-Octene	1.5	620	3.2	1.40	74	11	169
5	1-Octene	1.5	1,660	9.9	1.37	75	30	184

[a]Ti = 20 μmol, Al/Ti = 200, propene = 1.0 atm, 1-octene = 1.1 M, norbornene = 1.5 M (in propene copolymerization) or 0.7 M (in 1-octene copolymerization), solvent = toluene, total volume = 30 mL, temperature = 20°C
[b]Activity in kg-polymer mol-Ti^{-1} h^{-1}
[c]Molecular weight and molecular weight distribution were measured by GPC using polystyrene standards
[d]Norbornene content in copolymer determined by the ^{13}C NMR
[e]Norbornene conversion calculated from yield and comonomer content
[f]Determined by DSC
[g]Al/Ti = 400
[h]A different lot of dMMAO was used

The copolymers produced possessed high molecular weights and narrow molecular weight distribution with high T_g values irrespective of the Ti complex used. The activities of norbornene–propene copolymerization were too high to evaluate monomer reactivity ratios. Thus, the copolymerization abilities of each Ti complex were investigated with norbornene–1-octene copolymerization by changing the monomer feed ratio.

The T_g values of the copolymers thus obtained are plotted against the norbornene content in Fig. 10. The T_g value shows a linear relationship with the norbornene content in all the catalytic systems, indicating the formation of the uniform random copolymers regardless of the complex used. However, the slope of the straight line is dependent on the titanium complex. The results testified that the microstructures of the copolymers were dependent on the complex employed.

The monomer reactivity ratios ($r_N = k_{NN}/k_{NO}$ and $r_O = k_{OO}/k_{ON}$) determined by the Fineman–Ross method are shown in Fig. 10. These values indicate a preference for the insertion of norbornene, regardless of the last inserted monomer unit. The product of the reactivity ratios ($r_N \bullet r_O = 0.97$) obtained with **4** indicates a tendency for the formation of random copolymer, whereas the products of the reactivity ratios ($r_N \bullet r_O$: 2.5–3.5) obtained with **2**, **3**, and **5** imply a preference for the formation of the norbornene–norbornene sequence in the copolymer.

The living nature of the copolymerization with **5**-dMMAO, which showed the highest activity, was investigated by post-copolymerization. The results and the gel permeation chromatography (GPC) curves of the copolymers are shown in Fig. 11, implying that the copolymerization of norbornene and 1-octene with **5**-dMMAO proceeds in a living manner. The molecular weight distribution in the

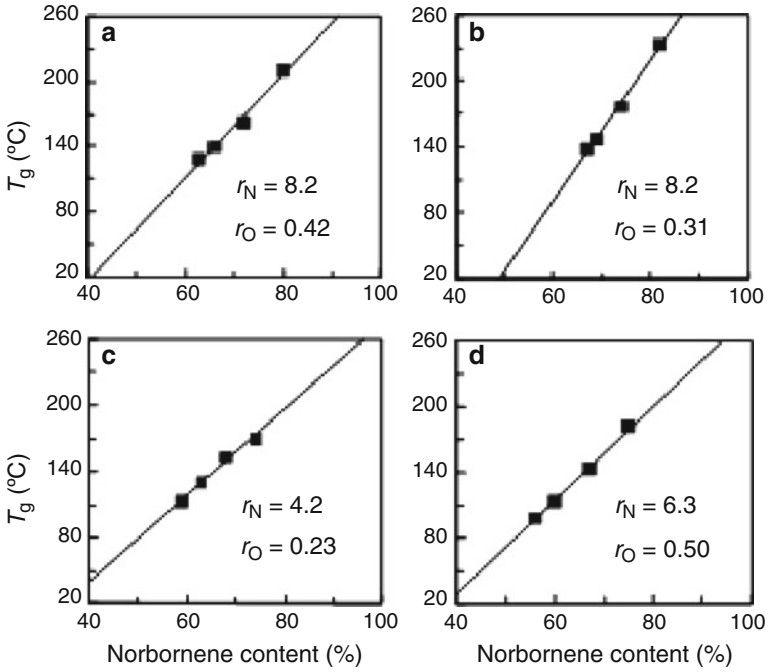

Fig. 10 Plots of T_g value versus norbornene content in poly(norbornene-*co*-1-octene) obtained with **2** (**a**), **3** (**b**), **4** (**c**), and **5** (**d**) activated by dMMAO [44]

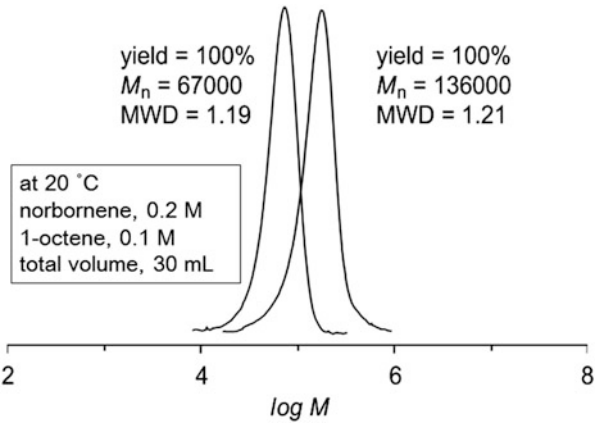

Fig. 11 Post-copolymerization of norbornene and 1-octene with **5**-dMMAO

post-copolymerization was narrower than in the copolymerizations shown in Table 4, suggesting that the broad molecular weight distribution of the latter comes from the physical inhomogeneity caused by the high activity of the catalyst, i.e., the temperature distribution in the reactor due to the heat of polymerization and/or the ineffective stirring due to the produced polymers. We have achieved

highly active living copolymerization of norbornene and 1-alkene with the tetraalkyl-substituted fluorenyl complex **5** activated by dMMAO.

4.3 Block Copolymerization of Norbornene and 1-Alkene

The most important role of living polymerization is to synthesize block copolymers. The Ti complexes **2**–**5** activated by dMAO or dMMAO were found to conduct living polymerization of propene, higher 1-alkene, and norbornene as well as their random living copolymerization. Thus, we can synthesize tailor-made copolymers composed of 1-alkene and norbornene with this catalytic system.

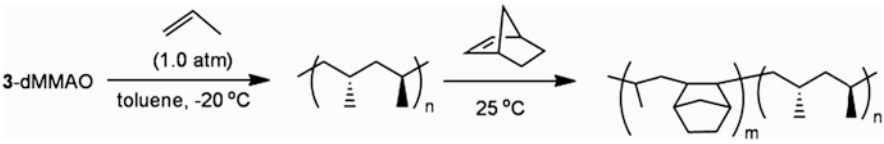

Scheme 2 Synthesis of *syn*-PP-*block*-poly(propene-*ran*-norbornene) with **4**-dMMAO [45]

As an example of the application of these living systems, we synthesized *syn*-PP-*block*-poly(propene-*ran*-norbornene) with **4**-dMMAO according to the procedure shown in Scheme 2 [45]. The PP obtained in the first step had an M_n value of 108,000, M_w/M_n value of 1.36 and melting point at 135°C. After the copolymerization, the yields were increased accompanied by an increase in M_n values (208,000–226,000), and a decrease in M_w/M_n values (1.21–1.32) regardless of the amount of norbornene added. The block copolymers showed both T_m (133–135°C) and T_g (93–311°C) that correspond to the crystalline *syn*-PP sequence and amorphous poly(propene-*ran*-norbornene) sequence, respectively, and the T_g values were controlled by the amount of norbornene added. These results indicate the formation of the expected block copolymers and the phase separation of the copolymers.

Although living polymerization is very useful for synthesis of monodisperse polymers and tailor-made block copolymers, one catalyst molecule (initiator) is necessary for one polymer chain. Catalytic synthesis of monodisperse polyolefins has been achieved by the combination of a living polymerization catalyst and a large excess of main group metal alkyls such as R_2Zn and R_3Al, where the propagating polymer chain on the transition metal exchanges with the metal alkyls reversibly much faster than the propagation rate. This kind of polymerization is referred to as coordinative chain transfer polymerization (CCTP) and the metal alkyls as chain shuttling reagents (Scheme 3) [46, 47]. A suitable combination of catalysts, which differ in copolymerization ability, produced multi-block copolymers in copolymerization of ethene with 1-octene in the presence of Et_2Zn

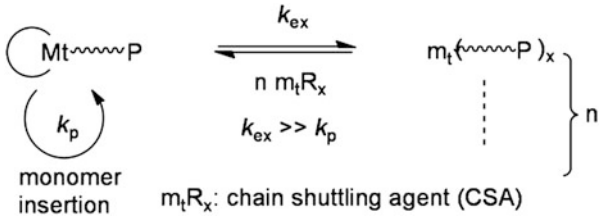

Scheme 3 Coordinative chain transfer polymerization (CCTP)

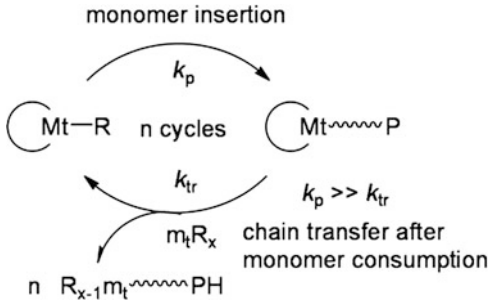

Scheme 4 Catalytic synthesis of monodisperse polymers with highly active living polymerization catalyst

as a chain shuttling reagent. The synthesis of multi-block copolymer with this mechanism is named chain-shuttling polymerization [48]. Ethene-based diblock copolymers were also synthesized by switching the monomer composition during CCTP [49].

On the other hand, the combination of a living polymerization catalyst and a suitable chain transfer reagent should give monodisperse polymers if the propagation rate is sufficiently faster than the chain transfer rate, and chain transfer occurs only after all the monomer is consumed (Scheme 4). Mitani et al. catalytically obtained monodisperse polyethene with a FI catalyst in the presence of a large excess of Et_2Zn by a sequential addition of the same amount of ethene [50]. We proved this concept in propene polymerization with **4**-dMMAO by controlling the amount of $^{i}Bu_3Al$ in dMMAO [51].

This concept was applied to the catalytic synthesis of block copolymer, as shown in Scheme 5 [52]. Block copolymerization of norbornene and propene was conducted with **4** activated by dMMAO containing a suitable amount of $^{i}Bu_3Al$, where propene was introduced before norbornene had been consumed. The propene-terminated chain end was transferred by $^{i}Bu_3Al$ after the propene had been consumption. The further sequential addition of norbornene and propene in the same way gave the same block copolymer without changing the M_n value or the narrow molecular weight distribution, indicating the catalytic synthesis of polynorbornene-*block*-poly(propene-*ran*-norbornene)-*block*-PP. We can conclude that the catalytic synthesis of block copolymers is possible by sequential addition of monomers in a highly active living polymerization system combined with a suitable kind and amount of chain transfer reagent.

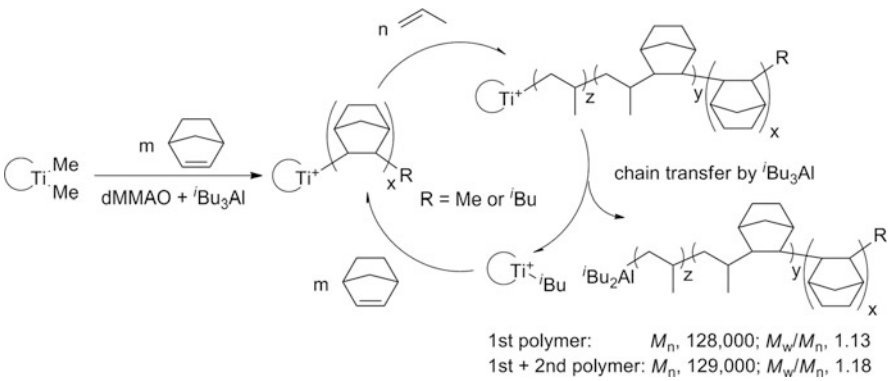

Scheme 5 Catalytic synthesis of monodisperse block polymers with **4**-dMMAO [52]

5 Conclusion

R_3Al-free MMAO (dMMAO) was found to be an effective cocatalyst for living polymerization of olefins with several dimethyltitanium complexes. The most important advantage of dMMAO is its solubility in aliphatic hydrocarbons. Living polymerization of propene was achieved with a chelating diamidodimethyltitanium (**1**) or *ansa*-dimethysilylene(fluorenyl)(amido)dimethyltitanium (**2**) activated by dMMAO in heptane. The *syn*-specificity of **2** depended on the polarity of the solvent, and heptane gave the highest *syn*-specificity although the activity was enhanced in halogenated solvents. The *syn*-specificity and activity of **2** were also dependent on the alkyl substituent of the fluorenyl ligand. The activity increased with the number of introduced alkyl groups, whereas the highest *syn*-specificity was obtained with the 3,6-^{i}Bu$_2$-substituted complex **4**. Thus, highly active and *syn*-specific living polymerization of propene was achieved with **4**-dMMAO in heptane. The catalytic system also conducted homo- and copolymerization of norbornene and higher 1-alkenes in a living manner, with high activity in toluene. The **4**-dMMAO system was also proved to be useful for catalytic synthesis of monodisperse block copolymers in the presence of a suitable amount of ^{i}Bu$_3$Al via selective chain transfer to ^{i}Bu$_3$Al after the monomer consumption. The characteristics of these catalytic systems can be applied to the development of novel olefin copolymers.

Acknowledgements The author acknowledges Tosoh Finechem Co. for donating cocatalysts.

References

1. Sinn H, Kaminsky W (1980) Adv Organomet Chem 18:99
2. Brintzinger HH, Fischer D, Muelhaupt R, Rieger B, Waymouth RM (1995) Angew Chem Int Ed Engl 34:1143

3. Kaminsky W (1996) Macromol Chem Phys 197:3907
4. Coates GW (2000) Chem Rev 100:1223
5. Gibson VC, Spitzmesser SK (2003) Chem Rev 103:283
6. Coates GW, Hustad PD, Reinartz S (2002) Angew Chem Int Ed 41:2236
7. Edson JB, Domski GJ, Rose JM, Bolig AD, Brookhart M, Coates GW (2009) Living transition metal-catalyzed alkene polymerization: polyolefin synthesis and new polymer architectures. In: Müller AHE, Matyjaszewski K (eds) Controlled and living polymerizations: from mechanisms to applications. Wiley, Weinheim, pp 167–239
8. Chen EY-X, Marks TJ (2000) Chem Rev 100:1391
9. Hagimoto H, Shiono T, Ikeda T (2002) Macromol Rapid Commun 23:73
10. Scollard JD, McConville DH (1996) J Am Chem Soc 118:10008
11. Scollard JD, McConville DH, Rettig SJ (1997) Organometallics 16:1810
12. Hagimoto H, Shiono T, Ikeda T (2002) Macromolecules 35:5744
13. Hagimoto H, Shiono T, Ikeda T (2004) Macromol Chem Phys 205:19
14. Hagihara H, Shiono T, Ikeda T (1998) Macromolecules 31:3184
15. Hasan T, Ioku A, Nishii K, Shiono T, Ikeda T (2001) Macromolecules 34:3142
16. Nishii K, Matsumae T, Dare EO, Shiono T, Ikeda T (2004) Macromol Chem Phys 205:363
17. Longo P, Oliva L, Grassi A, Pellecchia C (1989) Makromol Chem 190:2357
18. Herfert N, Fink G (1992) Makromol Chem 193:773
19. Chen M-C, Marks TJ (2001) J Am Chem Soc 123:11803
20. Busico V, Cipullo R, Cutillo F, Vacatello M, Van AV (2003) Macromolecules 36:4258
21. Cai Z, Ikeda T, Akita M, Shiono T (2005) Macromolecules 38:8135
22. Shiono T, Harada R, Cai Z, Nakayama Y (2009) Top Catal 52:675
23. Saito J, Mitani M, Mohri J-I, Ishii S-I, Yoshida Y, Matsugi T, Kojoh S-I, Kashiwa N, Fujita T (2001) Chem Lett 576
24. Sakuma A, Weiser M-S, Fujita T (2007) Polym J 39:193
25. Tian J, Hustad PD, Coates GW (2001) J Am Chem Soc 123:5134
26. Mitani M, Furuyama R, Mohri J-i, Saito J, Ishii S, Terao H, Kashiwa N, Fujita T (2002) J Am Chem Soc 124:7888
27. Saito J, Mitani M, Mohri J-I, Yoshida Y, Matsui S, Ishii S-I, Kojoh S-I, Kashiwa N, Fujita T (2001) Angew Chem Int Ed 40:2918
28. Cai Z, Ohmagari M, Nakayama Y, Shiono T (2009) Macromol Rapid Commun 30:1812
29. Nishii K, Shiono T, Ikeda T (2004) Macromol Rapid Commun 25:1029
30. Cai Z, Nakayama Y, Shiono T (2006) Kinet Catal 47:274
31. Cai Z, Nakayama Y, Shiono T (2010) Macromol Res 18:737
32. Cai Z, Nakayama Y, Shiono T (2008) Macromolecules 41:6596
33. Hasan T, Nishii K, Shiono T, Ikeda T (2002) Macromolecules 35:8933
34. Hasan T, Ikeda T, Shiono T (2004) Macromolecules 37:7432
35. Hasan T, Ikeda T, Shiono T (2004) Macromolecules 37:8503
36. Hasan T, Shiono T, Ikeda T (2004) Macromol Symp 213:123
37. Hasan T, Ikeda T, Shiono T (2005) Macromolecules 38:1071
38. Tritto I, Boggioni L, Ferro DR (2006) Coord Chem Rev 250:212
39. Henschke O, Koller F, Arnold M (1997) Macromol Rapid Commun 18:617
40. Kaminsky W, Derlin S, Hoff M (2007) Polymer 48:7271
41. Jung HY, Hong S-D, Jung MW, Lee H, Park Y-W (2005) Polyhedron 24:1269
42. Kaminsky W, Hoff M, Derlin S (2007) Macromol Chem Phys 208:1341
43. Li X, Nishiura M, Mori K, Mashiko T, Hou Z (2007) Chem Commun 4137
44. Cai Z, Harada R, Nakayama Y, Shiono T (2010) Macromolecules 43:4527
45. Cai Z, Nakayama Y, Shiono T (2006) Macromolecules 39:2031
46. Zhang W, Sita LR (2008) J Am Chem Soc 130:442
47. Zhang W, Wei J, Sita LR (2008) Macromolecules 41:7829
48. Arriola DJ, Carnahan EM, Hustad PD, Kuhlman RL, Wenzel TT (2006) Science 312:714

49. Hustad PD, Kuhlman RL, Arriola DJ, Carnahan EM, Wenzel TT (2007) Macromolecules 40:7061
50. Mitani M, Mohri J-i, Furuyama R, Ishii S, Fujita T (2003) Chem Lett 32:238
51. Cai Z, Shigemasa M, Nakayama Y, Shiono T (2006) Macromolecules 39:6321
52. Cai Z, Nakayama Y, Shiono T (2008) Macromol Rapid Commun 29:525

Adv Polym Sci (2013) 258: 163–178
DOI: 10.1007/12_2013_212

Published online: 19 April 2013

Novel Polyethylenes via Late Transition Metal Complex Pre-catalysts

Wen-Hua Sun

Abstract Late-transition metal complex pre-catalysts provide alternative promising catalytic systems for ethylene oligomerization and/or polymerization. Ethylene oligomerization using either iron or cobalt complex pre-catalysts is recognized as one of most active catalytic systems with high selectivity for α-olefins (up to 99%). New characteristic features are observed for the polyethylenes obtained from such late-transition metal catalytic systems. Highly linear polyethylene is usually obtained using the iron or cobalt complex pre-catalysts, whereas highly branched polyethylene is commonly formed by the nickel or palladium complex pre-catalysts. The causes for production of linear or branched polyethylenes are briefly explained according to the polymerization mechanism. Driven by demanding for new promising catalytic processes, the discussion is divided on the basis of models of complex pre-catalysts: a section on iron and cobalt complexes and another section on nickel and palladium complexes. The iron and nickel complex pre-catalysts receive more attention due to the relatively cheap and low toxicity metals from which they are derived.

Keywords Branched polyethylene · Ethylene oligomerization · Late-transition metal · Linear polyethylene · Polymerization

Contents

W.-H. Sun (✉)
Institute of Chemistry, Chinese Academy of Sciences, Beijing 100190, China
e-mail: whsun@iccas.ac.cn

Huge amounts of polyolefins provide cheap and light substances for the everyday world, for example they are used in the construction of furniture as well as for decorative and constructive parts. Other articles have highlighted the importance of Ziegler–Natta [1–4], Phillips [5], and the rapidly developing metallocene catalyst field [6–8]. Nothing is perfect in science, and therefore there is no end to the exploration of new catalysts in any catalytic system, including polyolefin formation. Although there are well-developed operating systems in olefin polymerization, industry is keen to develop new catalytic systems and to produce new polyolefin materials. With the knowledge accrued to date, it is reasonable to assume that late-transition metal complex pre-catalysts can provide alternative options in catalyst design and also potentially create new advanced and unique polyethylenes. With emphasis on the electronic configuration, 14-electron active species are common to both metallocenes [6–8] and late-transition metal pre-catalysts (Scheme 1), indicating a conceptual approach in designing metal complex pre-catalysts.

Scheme 1 Active species of metal complex pre-catalysts

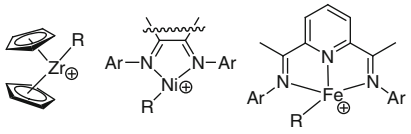

α-Diiminometal (nickel or palladium) complexes are highly active pre-catalysts in ethylene polymerization and their discovery marked a milestone in the area of ethylene reactivity [9–12]; in addition, bisiminopyridylmetal (iron and cobalt) chlorides were also found to polymerize ethylene and this discovery further enhanced the significant impact of late-transition metal complexes in polyolefin science [13–16]. Driven by these conceptual achievements and potential industrial applications, hundreds of research groups moved into the area to conduct extensive investigations of late-transition metal complex pre-catalysts in olefin polymerization. These research explorations included modification of existing models of complex pre-catalysts [17–31], monitoring of the active species and determining the catalytic mechanisms [32–40] as well as exploring suitable processes and applications. Furthermore, new complex pre-catalysts have been developed for iron and cobalt complexes [22–31, 41] as well as for nickel and palladium complexes [17–21, 42].

There are numerous review articles highlighting the progress of late-transition metal complex pre-catalysts in olefin polymerization [17–31, 41, 42], indicating their promising and potential applications. The petrochemical community should not expect too much of late-transition metal pre-catalysts, i.e. late-transition system do not compete with the operating catalytic systems. However, it would be very wrong to stop further exploration due to little pay-off in the short term. Late-transition metal complex pre-catalysts have shown high catalytic activities and relative low toxicity, exhibiting characteristic features for the obtained products. The selected topics for the discussion on late-transition metal pre-catalysts include: the characteristic differences in the polyethylenes obtained by various late-transition metal complex pre-catalysts (such polyethylenes are abbreviated as

LT-PE); the iron (with a smaller discussion of cobalt) pre-catalysts [22–31, 41], producing highly linear products either by oligomerization of α-olefins or polymerization to afford high-density polyethylenes (HDPEs) or polyethylene waxes; and the nickel complex pre-catalysts for yielding branched polyethylenes [17–21, 42] as extremely low-density polyethylenes (LDPEs) or polyethylene elastomers or gasoline depressants.

1 The Characteristic Features of LT-PE

To commercialize LT-PE will require an understanding of how the kind of polyethylene and its microstructure affects its properties and applications. Interestingly, LT-PE can be divided into two types depending on whether the microstructure is linear or branched. Highly linear polyethylenes (including oligomers) are commonly produced by iron and cobalt complex pre-catalysts [22–31, 41], whereas branched polyethylenes are formed by nickel and palladium complex pre-catalysts [17–21, 42]. The microstructural differences in LT-PE are caused by their characteristic mechanistic pathways of polymerization.

The linear products (oligomers and polyethylenes) could be simply explained as the constantly repeating of the processes of ethylene coordination and insertion (see Scheme 2: [**C**] and [**I**], respectively) but the termination stage will definitely control the chain length of the products, thereby obtaining oligomers, polyethylene waxes, or polyethylenes. In addition, in most cases the products were confirmed as having vinyl groups, therefore the oligomers would be useful α-olefins [43]. The polyethylene waxes and highly linear polyethylenes have been extensively used, and new challenges include production of value-adding polyethylenes with narrow polydispersity or finding efficient catalytic systems, of which the iron and cobalt complex pre-catalysts are highly potential and promising.

The polyethylenes obtained by nickel or palladium complex pre-catalysts are usually reported as branched products [17–21, 42], in which the main branches are methyl groups. Many proposed mechanisms (Scheme 2) are similarly reported in the literature, in which the polyethylenes with methyl branches are well illustrated [9–12, 17–21, 32–34, 44]. However, some longer alkyl branches are often observed within polyethylenes prepared using nickel catalytic systems [45, 46], therefore intermediates and potential mechanisms have been extensively proposed in order to complete the understanding of various alkyl-branched polyethylenes. The nickel and palladium catalytic systems commonly transfer ethylene into various branched products, including oligomers, polyethylene waxes, and polyethylenes. With the exception of the nickel-promoted SHOP process for α-olefins [47, 48], most nickel complex pre-catalysts transform ethylene into branched products and have low selectivity for vinyl-oligomers. Concerning branched polyethylenes, the current commercial processes require the co-polymerization of ethylene with an α-olefin. By employing nickel or palladium complex pre-catalysts, the branched polyethylenes are obtained by using solely ethylene, which reduces the additional cost of the co-monomer α-olefin. To enhance the properties and applications of

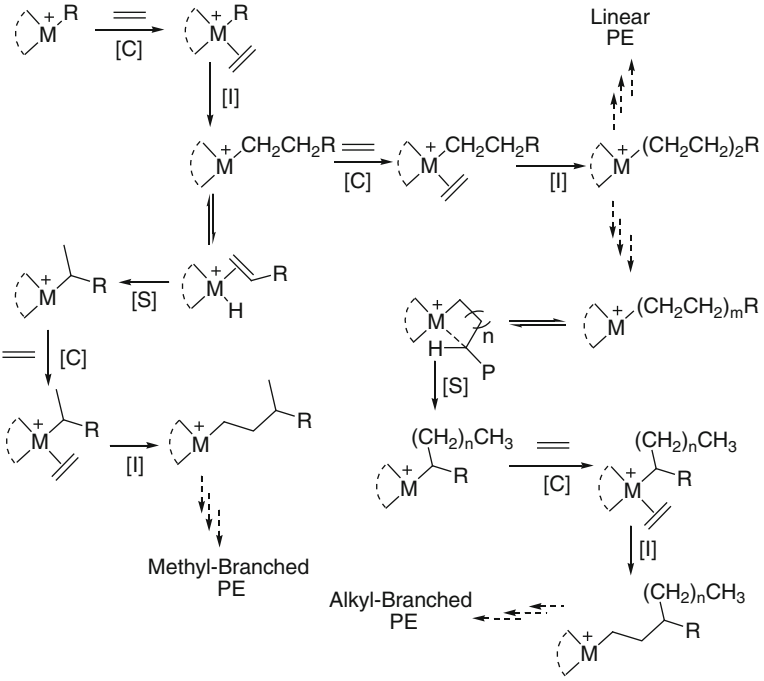

Scheme 2 Proposed mechanism of ethylene polymerization by late-transition metal pre-catalysts, indicating the formation of linear polyethylene, methyl-branched polyethylenes or various alkyl-branched polyethylenes. [*C*] coordination of ethylene, [*I*] chain propagation through ethylene insertion into M-polymeric alkyl group, [*S*] chain isomerization by β- or other (γ, δ, ε. . .)-hydrogen elimination

advanced polyethylenes, one needs to tailor the molecular weight and polydispersity as well as the number and types of branches present. It is likely that nickel pre-catalysts could be used to achieve new branched polyethylenes with new properties.

2 Variations in Iron and Cobalt Complex Pre-catalysts

In homogeneous catalysis, it is common for the first complex model to provide the best catalyst in terms of activity, as it tends to be the most studied. To have a useful catalytic model, various modifications are conducted in order to improve the productivity and selectivity, along with overcoming any problems in controlling the reaction parameters. That is exactly what happened with the bis(imino) pyridylmetal (iron or cobalt) chlorides in ethylene oligomerization and polymerization [13–16], which is well-reflected in the citations of the first publications in 1998. According to the Web of Science (December 3rd of 2012), there were

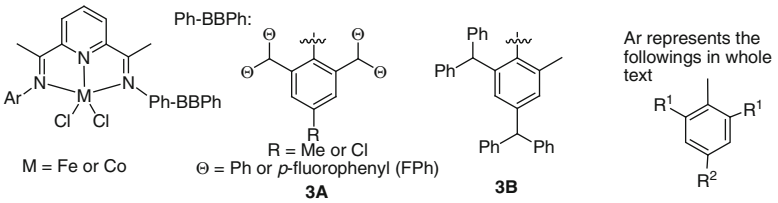

Scheme 3 Benzhydryl-substituted bis(imino)pyridylmetal complex pre-catalysts

707 citations for the Gibson group published on April 7 [13] and 983 for the Brookhart group published on April 29 [14]. Industrial trials were extensively conducted on the process of ethylene oligomerization in a joint adventure between DuPont and PetroChina, and on the process of ethylene polymerization targeting HDPE by BP with the assistance of Albemarle. The catalytic system of bis(imino) pyridyliron chlorides commonly proceed with ethylene oligomerization and polymerization together, but only the selective process producing either oligomerization or polymerization would be applicable in the petrochemical industry. Further modifications of the bis(imino)pyridyliron chloride complexes have been researched, and significant progress was made when revisiting the ambient-temperature-inactive benzhydryl-substituted bis(imino)pyridylmetal (iron or cobalt) chloride complexes (Scheme 3) [31, 49–52] [53, and unpublished data]. The exploration was inspired by the temperature-switching catalytic system of the 2-benzoxazolyl-6-iminopyridylcobalt chlorides, with ethylene oligomerization at room temperature, but ethylene polymerization at elevated reaction temperature [43]. These benzhydryl-substituted bis(imino)pyridylmetal (iron or cobalt) complex pre-catalysts [31, 49–52] [53, and unpublished data] do not show activity towards ethylene at room temperature; however, when the reaction temperature is elevated, they perform with high activities [up to 10^5 kg PE mol^{-1}(Fe) h^{-1}] in ethylene polymerization without any oligomers in the products.

The metal (iron or cobalt) complex pre-catalysts showed significant differences in their catalytic activities and resultant polyethylenes, depending on the substituents used in the ligands. Small fine tuning of the ancillary ligand set, even sometimes distant from the metal center, can result in dramatic changes to the resultant catalysis. For example, the iron analog pre-catalysts can give different options of polymerization conditions and properties of the obtained polyethylenes (Table 1). Although the molecular weights of these polyethylenes ranged from thousands to millions, high linearity is generally observed for these polyethylenes and, more importantly, narrow polydispersity for the obtained polyethylenes could be achieved through controlling the reaction parameters. Therefore, the bis(imino) pyridylmetal (iron or cobalt) complex pre-catalysts could potentially provide a catalytic process for producing HDPE or polyethylene waxes, though one more parameter should be considered as the operation temperature is between 70°C and 90°C for most olefin polymerization processes.

Table 1 Optimized polymerization results using iron complexes ligated by unsymmetrical bis(imino)pyridines bearing benzhydryl derivatives (under a pressure of 10 atm)

Pre-catalyst[a]													
Type	Θ	R	R^1	R^2	Co-catalyst	Al/Fe	T (°C)	Time (min)	Activity[b]	Mw[c]	Mw/Mn[d]	T_m[e] (°C)	References
3A	Ph	Me	Et	Me	MAO	1,500	60	30	22.3	99.8	8.3	132.7	[49]
3A	Ph	Me	Me	Me	MMAO	2,000	80	30	22.4	25.5	5.1	129.7	[49]
3A	Ph	Cl	Me	Me	MAO	2,500	80	30	14.3	23.0	2.8	130.2	[52]
3A	Ph	Cl	Me	Me	MMAO	2,500	60	30	24.6	42.0	5.1	128.6	[52]
3A	FPh	Me	Me	Me	MMAO	2,250	60	15	35.2	94.5	13.0	131.8	[53, and unpublished data]
3B	–	–	*i*Pr	H	MAO	3,000	60	30	26.2	18.7	4.4	128.4	[50]
3B	–	–	Et	Me	MMAO	3,000	70	30	23.3	12.1	3.5	127.6	[50]

MAO methylaluminoxane, *MMAO* modified methylaluminoxane

[a]See Scheme 1

[b]10^6 g mol^{-1} (Fe) h^{-1}

[c]Molecular weight, as determined by GPC

[d]Polydispersity (weight average molecular weight/number average molecular weight), as determined by GPC

[e]Melting temperature, as determined by DSC

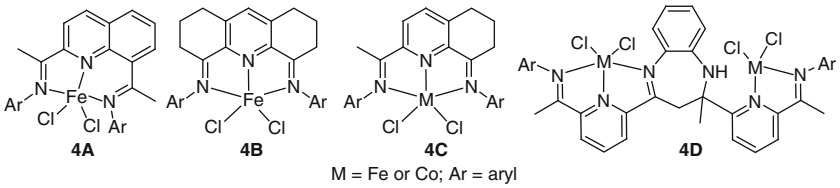

Scheme 4 New models of tridentate metal (Fe or Co) complex pre-catalysts

The required temperature parameter can be achieved by use of alternative *N*,*N*,*N*-tridentate iron and cobalt complex pre-catalysts. For example, 2,8-bis (1-aryliminoethyl)quinolylmetal (iron and cobalt) chlorides (**4A**, Scheme 4) are thermally stable up to 100°C under trial conditions [54]. 1,8-Diimino-2,3,4,5,6,7-hexahydroacridyliron complexes (**4B**, Scheme 4) [55] and 2,8-bis(arylimino)-5,6,7-trihydroquinolylmetal (iron and cobalt) complexes (**4C**, Scheme 4) [56, 57] were also found to polymerize ethylene very well. As a consequence, bi-metallic complex pre-catalysts (**4D**, Scheme 4) were successfully designed and showed high catalytic activity for ethylene reactivity [58, 59]. In general, iron and cobalt complex pre-catalysts can produce various ranges of highly linear polyethylenes according to the molecular weight and polydispersity (Table 2). From quantitative qualitative changes, the obtained polyethylenes can be rationally studied for their crystalline properties according to their molecular weights. The industrial application of such polyethylenes would still rely on the processes and properties of the obtained polyethylenes.

To the best of my knowledge, ethylene oligomerization by various bis(imino) pyridyliron chlorides commonly have by-products of polyethylene; even a trace amount of high molecular weight polyethylene will potentially block the pipeline of the process. Besides the above tridentate iron complexes for ethylene polymerization, other tridentate iron complex pre-catalysts have been developed (Scheme 5) [43, 60–65] through employing *N*-heteroatom cycles instead of one imino group. However, their catalytic systems mainly transfer ethylene into oligomers with additional formation of a little polyethylene wax (or low molecular weight products). In fact, these complex pre-catalysts are worthy of consideration for ethylene oligomerization.

Regarding the catalytic system for ethylene oligomerization, metal (iron and cobalt) complexes (Scheme 6) ligated by 2-imino-1,10-phenanthroline derivatives (**6A**, Scheme 6) [66–68], 2-(benzimidazol-2-yl)-1,10-phenanthroline derivatives (**6B**, Scheme 6) [69], or 2-(2-benzoxadozol-2-yl)-1,10-phenanthroline derivatives (**6C**, Scheme 6) [70] have shown unique and high activities, and especially high selectivity for α-olefins (Table 3). Moreover, a successful pilot process has now been achieved with 2-imino-1,10-phenanthrolyliron complex pre-catalysts at the 500-ton scale. Concerning the synthesis of 2-acetyl-1,10-phenanthroline, the same procedure was conducted for the first time by the groups of Solan [71] and ourselves [66–68].

Table 2 Representative results by the new tridentate iron complex pre-catalysts

Pre-catalyst[a]								Act[b]					
Type	R^1	R^2	Co-catalyst	Al/Fe	Pressure (atm)	T (°C)	Time (min)	Polymer	Oligomer	Mw[c]	Mw/Mn[d]	T_m[e] (°C)	References
4A	Me	H	MAO	3,000	30	100	30	7.61	0	99	2.8	–	[54]
4B	Me	Me	MAO	250	1.3	30	30	3.71	Trace	7.7	3.6	131.9	[55]
4C	Et	H	MAO	2,000	10	50	30	15.6	–	22.7	6.3	129.9	[56]
4D	Me	H	MMAO	1,000	30	30	30	4.14	6.18	–	–	–	[58]

MAO methylaluminoxane, *MMAO* modified methylaluminoxane

[a]See Scheme 4

[b]10^6 g mol^{-1} (Fe) h^{-1}

[c]Molecular weight, as determined by GPC

[d]Polydispersity, as determined by GPC

[e]Melting temperature, as determined by DSC

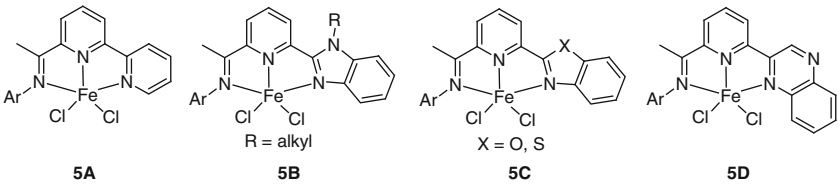

Scheme 5 2-Nitrocyclic-6-iminopyridyliron complex pre-catalysts

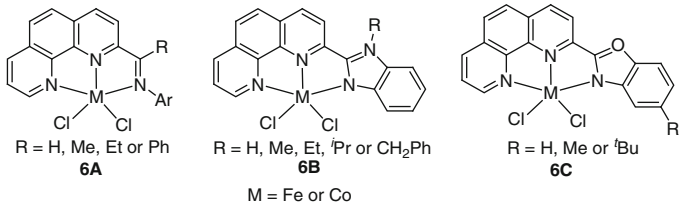

Scheme 6 Iron and cobalt complexes bearing 1,10-phenanthroline derivatives

Given that the pilot process required tens of kilograms of 2-acetyl-1,10-phenanthroline, new alternative synthetic methodologies were developed, which were scale-up synthetic procedures (Scheme 7). Driven by industrial considerations, namely cheap substances for the pre-catalyst, fine chemical companies are welcome to develop effective synthetic procedures and inform us; therefore the detailed conditions are provided and we await further improvements.

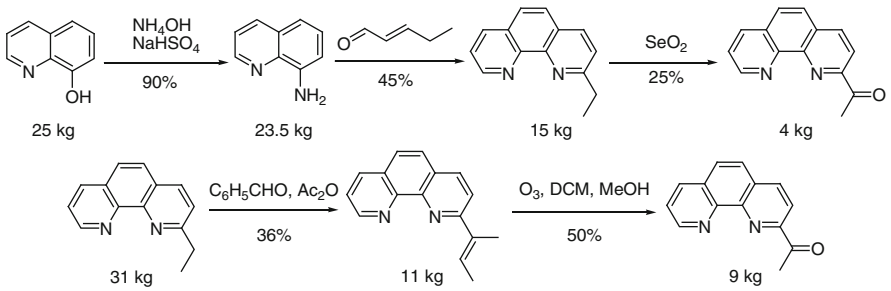

Scheme 7 Scaled-up synthetic procedures of 2-acetyl-1,10-phenanthroline

One additional issue should also be addressed concerning iron and cobalt complexes bearing bidentate ligands of 8-(benzimidazol-2-yl)quinolines (**8A**, Scheme 8) [72], 8-iminoquinolines (**8B**, Scheme 8) [73], or 2-iminoquinolines (**8C**, Scheme 8) [74]. These complexes also showed good catalytic activities towards ethylene oligomerization or polymerization. Their complex pre-catalysts show promising reactivity towards ethylene, though such bidentate ligands lack two

Table 3 Highly promising iron pre-catalysts in ethylene oligomerization

Pre-catalyst[a]									Oligomers			Waxes	
Type	R	R^1	R^2	Co-catalyst	Al/Fe	T (°C)	Time (min)	Pressure (atm)	A_o[b]	K[c]	α-O[d] (%)	A_w[e]	References
6A	H	*i*Pr	H	MAO	1,000	40	60	10	9.0	0.48	>97	Trace	[66]
6A	H	Me	Me	MMAO	500	20	30	1	0.95	0.65	>93	–	[67]
6A	H	Me	Me	MMAO	1,000	20	30	10	25.7	0.69	>95	40.7	[67]
6A	Me	Et	H	MAO	1,000	40	60	10	49.1	0.62	>94	14.6	[66]
6A	Me	Et	H	MMAO	500	0	30	1	1.34	0.52	>93	–	[67]
6A	Me	*i*Pr	H	MMAO	1,000	20	30	10	24.1	0.26	>93	–	[67]
6A	Et	Me	H	MAO	1,500	50	60	10	13.9	0.70	>95	12.1	[68]
6A	Ph	Et	H	MAO	1,000	40	30	10	23.0	0.52	>95	3.25	[66]
6A	Ph	Me	H	MMAO	500	20	30	10	0.80	0.62	>95	0.747	[67]
6B	H	–	–	MMAO	1,000	20	20	30	3.51	–	>92	–	[69]
6B	Me	–	–	MMAO	1,000	20	20	30	1.07	–	>82	–	[69]
6B	Et	–	–	MMAO	1,000	20	20	30	0.92	–	>81	–	[69]
6C	H	–	–	MMAO	800	20	20	10	1.89	–	80	–	[70]
6C	Me	–	–	MMAO	800	20	20	10	1.01	–	81.5	–	[70]
6C	*t*Bu	–	–	MMAO	800	20	20	10	0.91	–	83	–	[70]

MAO methylaluminoxane, *MMAO* modified methylaluminoxane

[a]See Scheme 6

[b]Activity for oligomers, in10^6 g mol^{-1} (Fe) h^{-1}

[c]Dissociation constant

[d]α-Olefin content (%), as determined by GC and GC–MS

[e]Activity for low-molecular-weight waxes, in 10^5 g mol^{-1} (Fe) h^{-1}

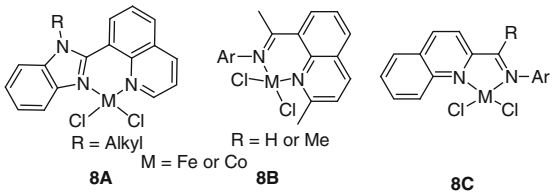

Scheme 8 *N*,*N*-Bidentate iron and cobalt complex pre-catalysts

of the electrons that tridentate ligands have. In fact, such chemistry was planned in the shadow of electrophilic active species of the well-known constrained-geometry complexes (CGC) [75–79].

In general, the cobalt complexes performed with slightly lower activity but with similar catalytic behavior as their iron analogs, though there were limited cases of cobalt analogs having better activities than their iron analogs. The abundance of iron, along with the lowest toxicity amongst metals, should be a favorable consideration in my view. The iron complex pre-catalysts are potentially promising for both ethylene oligomerization and polymerization.

3 The Nickel Complex Pre-catalysts

Similar catalytic behavior of nickel and palladium complex pre-catalysts has been observed in ethylene reactivity. The nickel complexes would be favored for industry because of their availability as a natural resource, whereas the palladium complexes would be widely used in academic studies with the advantage of effective NMR monitoring of the species. The nickel-promoted SHOP process for α-olefins [47, 48] illustrates its unique properties. Although the SHOP complex model has been extensively modified, there are a few catalytic systems of these modified complexes that are as efficient as the operating SHOP process. Therefore, nickel complex pre-catalysts in ethylene oligomerization will not be focused on here; instead the nickel complex pre-catalysts will be briefly discussed for ethylene polymerization, producing branched polyethylene.

There are numerous models of nickel complex pre-catalysts in ethylene polymerization, the study of which was initiated by a report on α-diiminonickel complexes. The obtained polyethylenes are commonly branched, including main methyl- and other alkyl-substituents. Concerning the ease of synthesis and handling of nickel complexes, the *N*,*N*-bidentate-type nickel complexes should be emphasized, especially with representative ligands such as α-diimino and 2-iminoethylpyridine derivatives, although other bidentate and tridentate ligands have been explored. The α-diimino ligands made from acenaphthylene-1,2-dione have been the most extensively studied (Scheme 9), and the resulting the nickel complexes (**9A**, Scheme 9) polymerize ethylene, affording polyethylene with various branches, but mainly methyl-substituents [9, 17–21]. Following these, the

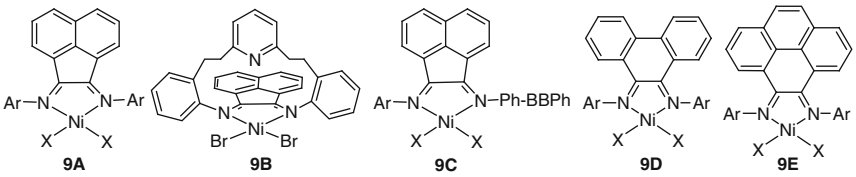

Scheme 9 Nickel complexes bearing α-diimino-type ligands

constrained an α-diimino compound was designed for the nickel complex pre-catalyst (**9B**, Scheme 9), which produced polyethylene of high molecular weight and narrow polydispersity [80]. Encouraged by the better thermal stability of iron complex pre-catalysts bearing benzhydryl-substituted ligands, the benzhydryl-substituted α-diimino ligands were developed for their nickel complexes (**9C**, Scheme 9) [81–83]. Indeed, the new nickel complexes showed better thermal stability and higher catalytic activities; moreover, the obtained polyethylenes had higher molecular weights and narrow polydispersity. The nickel complexes (**9C,** Scheme 9) are routinely and easily synthesized and, in addition to their high activities in ethylene polymerization, the properties and usefulness of the obtained polyethylene would be key in deciding whether the (pilot) processes should be conducted or not. In my personal view, the polyethylene obtained by nickel complex pre-catalysts (**9C**, Scheme 9) could be easily prepared in hundreds of grams and offers scientists the potential for detailed investigations in polymeric physics. With these results, the properties of the obtained polyethylene would necessarily be further investigated in order to evaluate their usefulness and applications. In addition, the pre-catalysts (**9D** and **9E**, Scheme 9) [84, 85] provide alternative models for controlling the synthesis of polyethylenes with different molecular weights and polydispersity (Table 4).

In addition to the α-diiminonickel complex pre-catalysts used in ethylene polymerization, another important model of complex pre-catalysts should be recognized, i.e., nickel complexes bearing 2-iminopyridine derivatives (**10A**, Scheme 10) [86–89] and bipyridine derivatives (**10B**, Scheme 10) [90]. Most of these produce both oligomers and polyethylenes, although interestingly the model (**10C**, Scheme 10) [91–93], either with or without substituents at the *ortho*-position to the nitrogen, could provide either oligomers or polyethylenes. The polyethylenes with narrow polydispersity could be varied with different molecular weights and, more importantly, the branches of the obtained polyethylenes could be also tuned to some degree to alter the number and the length of the carbon chains.

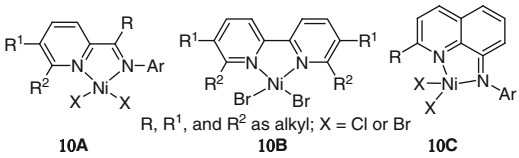

Scheme 10 Nickel complexes bearing pyridine-derivative bidentate ligands

Table 4 Ethylene polymerization by typical diiminonickel halides

Pre-catalyst[a]														
Type	X	R^1	R^2	Co-catalyst	Al/Ni	Pressure (atm)	T (°C)	Time (min)	Activity[b]	T_m[c] (°C)	Mw[d] (10^5 g mol^{-1})	Mw/Mn[e]	Brch[f]	References
9A	Br	*i*Pr	H	MAO	10	1	0	30	5.06	122	1,400	2.3	5	[9]
9A	Br	*i*Pr	H	MMAO	2,000	14	35	10	67.2	110	337	1.8	24	[17]
9B	–	–	–	MAO	3,000	14	35	10	Trace	–	–	–	–	[80]
9B	–	–	–	Me_2AlCl	3,000	14	35	10	0.016	131	56.4	2.2	3.6	[80]
9C	Br	*i*Pr	H	Et_2AlCl	600	10	20	30	10.9	49.1	942	2.7	–	[81]
9C	Br	*i*Pr	H	MAO	3,000	10	20	30	9.39	62.7	745	2.5	–	[81]
9D	Br	Me	H	MAO	2,000	1.2	0	60	1.58	124.9	195	5.9	7.0	[84]
9E	Cl	Me	Me	EASC	400	10	40	30	4.41	99.9	2.01	2.1	32	[85]
9E	Cl	Me	Me	MAO	1,500	10	40	30	3.43	116.2	3.49	2.3	35	[85]
9E	Br	Et	Me	EASC	300	10	40	30	3.63	107.5	3.87	2.1	33	[85]
9E	Br	Et	Me	MAO	1,000	10	40	30	3.53	115.8	7.33	2.2	29	[85]

EASC ethylaluminium sesquichloride, *MAO* methylaluminoxane, *MMAO* modified methylaluminoxane

[a]See Scheme 9

[b]10^6 g (PE) mol (Ni)$^{-1}$ h^{-1}

[c]Melting temperature, as determined by DSC

[d]Molecular weight, as determined by GPC

[e]Polydispersity, as determined by GPC

[f]Branches every 1,000 carbons, as determined by FT-IR

The polyethylene produced by the nickel catalytic systems could potentially become new functional materials because some of them have various types of alkyl branches (from methyl to hexyl branches). Surprisingly, the obtained polyethylenes are highly unique polyethylenes with narrow molecular polydispersity, but with various alkyl branches in different numbers and different lengths of carbon chain. Such polyethylenes with high molecular weights and narrow polydispersity can act as elastomer materials and have high transparency. That would be an advantage of using solely ethylene for highly branched polyethylene. These new polyethylenes could be available from laboratory suppliers in kilogram quantities for any polymer physicist to explore the properties and applications of such polyethylenes.

The chemistry of nickel-promoted ethylene polymerization is a new and interesting subject. More pre-catalyst models and catalytic behaviors are being explored, and the obtained polyethylenes investigated for their properties and potential applications. In assistance to polymeric chemists, more polymeric physicists are expected to join the research and this will definitely draw attention from both academic and industrial fields. These polyethylenes can provide a wide range of properties in various applications.

Much innovative and extensive research into transition-metal complex pre-catalysts in ethylene reactivity could not been included herein, but a few examples of complex models have been discussed in a limited manner in order to encourage more research and attract more consideration. The progress and achievements, indicated by the selected results, emphasize two characteristic species that can induce two different mechanistic polymerizations: highly linear products (either oligomers or polyethylenes) formed by the catalytic systems of iron or cobalt complexes, and branched polyethylenes formed by the catalytic systems of nickel and palladium.

References

1. Ziegler K, Gellert HG, Zosel K, Lehmkuhl W, Pfohl W (1955) Angew Chem 67:424
2. Ziegler K, Holzkamp E, Breil H, Martin H (1955) Angew Chem 67:541–547
3. Natta G (1955) J Polym Sci 16:143–154
4. Natta G, Pino P, Corradini P, Danusso F, Mantica E, Mazzanti G, Moraglio G (1955) J Am Chem Soc 77:1708–1710
5. McDaniel MP (2010) Adv Catal 53:123–606
6. Sinn H, Kaminsky W, Vollmer HJ (1980) Angew Chem Int Ed Engl 19:390
7. Kaminsky W (1996) Macromol Chem Phys 197:3907
8. Kaminsky W, Arndt M (1997) Adv Polym Sci 127:143
9. Johnson LK, Killian CM, Brookhart M (1995) J Am Chem Soc 117:6414
10. Killian CM, Tempel DJ, Johnson LK, Brookhart M (1996) J Am Chem Soc 118:11664
11. Svejda SA, Johnson LK, Brookhart M (1999) J Am Chem Soc 121:10634
12. Gates DP, Svejda SA, Oñate E, Killian CM, Johnson LK, White PS, Brookhart M (2000) Macromolecules 33:2320
13. Britovsek GJP, Gibson VC, Kimberley BS, Maddox PJ, McTavish SJ, Solan GA, White AJP, Williams DJ (1998) Chem Commun 1998:849

14. Small BL, Brookhart M, Bennett AMM (1998) J Am Chem Soc 120:4049
15. Small BL, Brookhart M (1998) J Am Chem Soc 120:7143
16. Britovsek GJP, Bruce M, Gibson VC, Kimberley BS, Maddox PJ, Mastroianni S, McTavish SJ, Redshaw C, Solan GA, Strömberg S, White AJP, Williams DJ (1999) J Am Chem Soc 121:8728
17. Gates DP, Svejda SA, Ate EO, Killian CM, Johnson LK, White PS, Brookhart M (2000) Macromolecules 33:2320
18. Helldörfer M, Backhaus J, Milius W, Alt HG (2003) J Mol Catal A Chem 193:59
19. Wegner MM, Ott AK, Rieger B (2010) Macromolecules 43:3624
20. Liu F-S, Hu H-B, Xu Y, Guo L-H, Zai S-B, Song K-M, Gao H-Y, Zhang L, Zhu FM, Wu Q (2009) Macromolecules 42:7789
21. Popeney CS, Guan Z (2010) Macromolecules 43:4091
22. Britovsek GJP, Gibson VC, Wass DF (1999) Angew Chem Int Ed 38:428–447
23. Gibson VC, Spitzmesser SK (2003) Chem Rev 103:283–315
24. Gibson VC, Redshaw C, Solan GA (2007) Chem Rev 107:1745–1776
25. Bianchini C, Giambastiani G, Rios IG, Mantovani G, Meli A, Segarra AM (2006) Coord Chem Rev 250:1391–1418
26. Bianchini C, Giambastiani G, Luconi L, Meli A (2010) Coord Chem Rev 254:431–455
27. Sun W-H, Zhang S, Zuo W (2008) C R Chim 11:307–316
28. Jie S, Sun W-H, Xiao T (2010) Chin J Polym Sci 28:299–304
29. Budagumpi S, Kim K-H, Kim I (2011) Coord Chem Rev 255:2785–2809
30. Xiao T, Zhang W, Lai J, Sun W-H (2011) C R Chim 14:851–855
31. Ma Z, Sun W-H, Li Z-L, Shao C-X, Hu Y-L, Li X-H (2002) Polym Int 51:994–997
32. Guan Z, Cotts PM, McCord EF, McLain SJ (1999) Science 283:2059
33. Deng L, Margl P, Ziegler T (1997) J Am Chem Soc 119:1094–1100
34. Deng L, Woo TK, Cavallo L, Margl PM, Ziegler T (1997) J Am Chem Soc 119:6177–6186
35. Tomov AK, Gibson VC, Britovsek GJP (2009) Organometallics 28:7033–7040
36. Bryliakov KP, Talsi EP, Semikolenova NV (2009) Organometallics 28:3225–3232
37. Fayet G, Raybaud P, Toulhoat H, de Bruin T (2009) J Mol Struct (Theochem) 903:100–107
38. Volbeda J, Meetsma A, Bouwkamp MW (2009) Organometallics 28:209–215
39. Barabanov AA, Bukatov GD, Zakharov VA (2008) J Polym Sci A Polym Chem 46:6621–6629
40. Trovitch RJ, Lobkovsky E, Chirik PJ (2008) J Am Chem Soc 130:11631–11642
41. Zhang W, Sun W-H, Redshaw C (2013) Dalton Trans 42. doi:10.1039/C2DT32337K
42. Gao R, Sun W-H, Redshaw C (2013) Catal Sci Technol. doi:10.1039/C3CY20691B
43. Gao R, Wang K, Li Y, Wang F, Sun W-H, Redshaw C, Bochmann M (2009) J Mol Catal A Chem 309:166–171
44. Musaev DG, Froese RDJ, Svensson M, Morokuma K (1997) J Am Chem Soc 119:367–374
45. Tang X, Sun W-H, Gao T, Hou J, Chen J, Chen W (2005) J Organomet Chem 690:1570–1580
46. Tang X, Cui Y, Sun W-H, Miao Z, Yan S (2004) Polym Int 53:2155–2161
47. Keim W, Kowaldt FH, Goddard R, Kruger C (1978) Angew Chem Int Ed Engl 17:466
48. Keim W, Behr A, Limbäcker B, Krüger C (1983) Angew Chem Int Ed Engl 22:503
49. Yu J, Liu H, Zhang W, Hao X, Sun W-H (2011) Chem Commun 47:3257–3259
50. Zhao W, Yu J, Song S, Yang W, Liu H, Hao X, Redshaw C, Sun W-H (2012) Polymer 53:130–137
51. Lai J, Zhao W, Yang W, Redshaw C, Liang T, Liu Y, Sun W-H (2012) Polym Chem 3:787–793
52. Cao X, He F, Zhao W, Cai Z, Hao X, Shiono T, Redshaw C, Sun W-H (2012) Polymer 53:1870–1880
53. W-H. Sun, W. Zhao, J. Yu, W. Zhang, X. Hao, C. Redshaw (2012) Macromol Chem Phys 213:1266-1273
54. Zhang S, Sun W-H, Xiao T, Hao X (2010) Organometallics 29:1168–1173
55. Appukuttan VK, Liu Y, Son BC, Ha C-S, Suh H, Kim I (2011) Organometallics 30:2285–2294
56. Zhang W, Chai W, Sun W-H, Hu X, Redshaw C, Hao X (2012) Organometallics 31:5039–5048

57. Sun W-H, Kong S, Chai W, Shiono T, Redshaw C, Hu X, Guo C, Hao X (2012) Appl Catal A Gen 447–448:67–73
58. Zhang S, Vystorop I, Tang Z, Sun W-H (2007) Organometallics 26:2456–2460
59. Zhang S, Sun W-H, Kuang X, Vystorop I, Yi J (2007) J Organomet Chem 692:5307–5316
60. Britovsek GJP, Baugh SPD, Hoarau O, Gibson VC, Wass DF, White AJP, Williams DJ (2003) Inorg Chim Acta 345:279–291
61. Xiao L, Gao R, Zhang M, Li Y, Cao X, Sun W-H (2009) Organometallics 28:2225–2233
62. Sun W-H, Hao P, Zhang S, Shi Q, Zuo W, Tang X, Lu X (2007) Organometallics 26:2720–2734
63. Chen Y, Hao P, Zuo W, Gao K, Sun WH (2008) J Organomet Chem 693:1829–1840
64. Sun W-H, Hao P, Li G, Zhang S, Wang W, Yi J, Asma M, Tang N (2007) J Organomet Chem 692:4506–4518
65. Gao R, Li Y, Wang F, Sun W-H, Bochmann M (2009) Eur J Inorg Chem 27:4149–4156
66. Sun W-H, Jie S, Zhang S, Zhang W, Song Y, Ma H, Chen J, Wedeking K, Fröhlich R (2006) Organometallics 25:666–677
67. Jie S, Zhang S, Sun W-H, Kuang X, Liu T, Guo J (2007) J Mol Catal A Chem 269:85–96
68. Zhang M, Zhang W, Xiao T, Xiang J-F, Hao X, Sun W-H (2010) J Mol Catal A Chem 320:92–96
69. Zhang M, Hao P, Zuo W, Jie S, Sun W-H (2008) J Organomet Chem 693:483–491
70. Zhang M, Gao R, Hao X, Sun W-H (2008) J Organomet Chem 693:3867–3877
71. Pelletier JDA, Champouret YDM, Cadarso J, Clowes L, Gañete M, Singh K, Thanarajasingham V, Solan GA (2006) J Organomet Chem 691:4114–4123
72. Xiao T, Zhang S, Kehr G, Hao X, Erker G, Sun W-H (2011) Organometallics 30:3658–3665
73. Song S, Zhao W, Wang L, Redshaw C, Wang F, Sun W-H (2011) J Organomet Chem 696:3029–3035
74. Song S, Xiao T, Redshaw C, Hao X, Wang F, Sun W-H (2011) J Organomet Chem 696:2594–2599
75. Stevens JC, Timmers FJ, Wilson DR, Schmidt GF, Nickias PN, Rosen RK, McKnight GW, Lai (Dow) S (1991) Eur Pat Appl 0416815A2
76. Canich (Exxon) JAM (1991) US Patent 5,026,798
77. McKnight AL, Waymouth RM (1998) Chem Rev 98:2587
78. Shapiro PJ, Cotter WD, Schaefer WP, Labinger JA, Bercaw JE (1994) J Am Chem Soc 116:4623
79. Shapiro PJ, Bunel E, Schaefer WP, Bercaw JE (1990) Organometallics 9:867
80. Leung DH, Ziller JW, Guan Z (2008) J Am Chem Soc 130:7538
81. Liu H, Zhao W, Hao X, Redshaw C, Huang W, Sun W-H (2011) Organometallics 30:2418–2424
82. Liu H, Zhao W, Yu J, Hao X, Redshaw C, Chen L, Sun W-H (2012) Catal Sci Technol 2:415–422
83. Kong S, Guo C-Y, Yang W, Wang L, Sun W-H, Glaser R (2013) J Organomet Chem 725:37
84. Li L, Jeon M, Kim SY (2009) J Mol Catal A Chem 303:110
85. Song K, Yang W, Li B, Liu Q, Redshaw C, Li Y, Sun W-H (2013) Dalton Trans. doi:10.1039/C2DT32343E
86. Laine TV, Klinga M, Leskelä M (1999) Eur J Inorg Chem 1999:959
87. Laine TV, Lappalainen K, Liimatta J, Aitola E, Lofgren B, Leskela M (1999) Macromol Rapid Commun 20:487
88. Hou X, Cai Z, Chen X, Wang L, Redshaw C, Sun W-H (2012) Dalton Trans 41:1617
89. Lai J, Hou X, Liu Y, Redshaw C, Sun W-H (2012) J Organomet Chem 702:52
90. Shao C, Sun W-H, Li Z, Hu Y, Han L (2002) Catal Commun 3:405
91. Yu J, Hu X, Zeng Y, Zhang L, Ni C, Hao X, Sun W-H (2011) New J Chem 35:178
92. Zhang L, Hao X, Sun W-H, Redshaw C (2011) ACS Catal 1:1213
93. Yu J, Zeng Y, Huang W, Hao X, Sun W-H (2011) Dalton Trans 40:8436

Adv Polym Sci (2013) 258: 179–232
DOI: 10.1007/12_2013_210

Published online: 12 June 2013

Functional Polyolefins Through Polymerizations by Using Bis(indenyl) Zirconium Catalysts

Jukka Seppälä, Esa Kokko, Petri Lehmus, Anneli Pakkanen née Malmberg, Kimmo Hakala, Sami Lipponen, and Barbro Löfgren

Abstract The discovery of metallocene catalysts has enabled synthesis of new polyolefin structures through the ability to incorporate comonomers that are not applicable using Ziegler–Natta or other conventional olefin polymerization catalysts. Extensive research has been carried out on the copolymerization behavior of different bis(indenyl) zirconium catalysts in order to understand their comonomer response, chain termination mechanisms, and chain-end isomerization. Metallocene-catalyzed copolymerization enables unforeseen material structures, leading to functional polyolefins with strongly or weakly interacting comonomers or long-chain branches. These copolymers show interesting technical properties like reactive functionality, compatibility, adhesion properties, and modified rheology.

Keywords Catalysts · Functional polyolefins · Long-chain branched polyethylenes · Olefin copolymers · Polyolefin compatibilization · Siloxy-substituted metallocenes

J. Seppälä (✉) and B. Löfgren
Department of Biotechnology and Chemical Technology, Aalto University, Espoo, Finland
e-mail: jukka.seppala@aalto.fi

E. Kokko and A. Pakkanen née Malmberg
Borealis Polymers Oy, Porvoo, Finland

P. Lehmus
Neste Oil Corporation, Technology Centre, Porvoo, Finland

K. Hakala
Borouge Pte Ltd, Innovation Centre, Ruwais, United Arab Emirates

S. Lipponen
Styrochem Finland Oy, Porvoo, Finland

Contents

Abbreviations

Ar	Aryl
a_T	Shift factor, $a_T = \eta_0(T)/\eta_0(T_0)$
Bn	Benzyl
Bu	Butyl
Bz	Benzoyl
cat	Catalyst
CD	Composition distribution
CGC	Constrained geometry catalyst
-*co*-SiF	-*co*-7-octenyldimethylfluorosilane
-*co*-SiPh	-*co*-7-octenyldimethylphenylsilane
Cp	Cyclopentadienyl
CSTR	Continuous stirred tank reactor
E_a	Flow activation energy, $a_T = \exp[(E_a/R) \times (1/T - 1/T_0)]$ (kJ mol^{-1})
Et	Ethyl
FTIR	Fourier transform infrared spectroscopy
G^*	Complex modulus, $G^* = [(G')_2 + (G'')_2]^{1/2}$ (Pa)
G'	Storage modulus, $G' = \cos\delta\,(\sigma/\gamma)$ (Pa)
G''	Loss modulus, $G'' = \sin\delta\,(\sigma/\gamma)$ (Pa)
HDPE	High-density polyethylene
HMW	High molecular weight

Ind	Indenyl
i-Pr	Isopropyl
LCB	Long-chain branching
LDPE	Low-density polyethylene
LLDPE	Linear low-density polyethylene
LVE	Linear viscoelasticity
MAO	Methylaluminoxane
M_0	Molecular weight of the repeat unit, for PE, $M_0 = 14.027$ g/mol
M_c	Critical molecular weight above which η_0 scales with $M_w^{3.6}$ for PE, $M_c = 3{,}500$ g/mol
M_e	Chain length for entanglements for PE, $M_e = 1{,}300$ g/mol
M_n	Number-average molecular weight
M_w	Weight-average molecular weight
Me	Methyl
MFR	Melt flow rate
mLLDPE	Metallocene-catalyzed linear low-density polyethylene
mol	Mole(s)
MTR	Mass transfer resistance
MWD	Molecular weight distribution, M_w/M_n, as determined by size exclusion chromatography
NMR	Nuclear magnetic resonance
p_E	Ethylene partial pressure in polymerization
Ph	Phenyl
Pr	Propyl
r_C	Reactivity ratio of comonomer
r_E	Reactivity ratio of ethylene
r_H	Reactivity ratio of comonomer (1-hexene)
rt	Room temperature
SEC	Size exclusion chromatography
SEC-MALLS	Size exclusion chromatography coupled with multi-angle laser light scattering
-Si $(CH_3)_2Ph$	Dimethylphenylsilane
$-Si(CH_3)_3$	Trimethylsilane
SSC	Single-site catalyst
T	Measurement temperature
T_0	Reference temperature
tan δ	Loss tangent, tan $\delta = G''(\omega)/G'(\omega)$ [−]
t-Bu	*tert*-Butyl
TMS	Trimethylsilyl
T_p	Polymerization temperature
ZN	Ziegler–Natta
γ	Shear strain [−]
γ	Shear rate (s^{-1})

δ	Phase angle, phase shift between stress and strain vectors
ε	Tensile strain [−]
η	Shear viscosity, $\eta = \sigma/\gamma$ (Pa s)
η^*	Complex viscosity, $\eta^* = G^*/\omega$ (Pa s)
η_0	Limiting viscosity at zero shear rate (Pa s)
η_E	Steady-state extensional (tensile) viscosity, $\eta_E = \sigma_E/\varepsilon$ (Pa s)
μSi	Microsilica
σ	Shear stress (Pa)
σ_E	Steady state tensile stress (Pa)
ω	Angular frequency (rad s^{-1})

1 Introduction

Through the discoveries of the last 30 years [1–4], metallocene catalysts have opened the window for new polyolefin structures through their ability to readily incorporate comonomers, which Ziegler–Natta or other conventional olefin polymerization catalysts have a limited ability of doing. Metallocenes have successfully been applied for the copolymerization of ethylene and various short and long chain 1-olefins, for example 1-octadecene [5], vinyl-terminated polypropylene oligomers [6], norbornene and styrene [7], and isobutene [8]. Vast interest in providing catalysts capable of producing isotactic or syndiotactic polypropylene has widened the selection of metallocenes available for ethylene polymerization.

The research group of Seppälä has studied extensively the copolymerization behavior of different bis(indenyl) zirconium catalysts and has determined their comonomer response, chain termination mechanisms, and the importance of chain-end isomerization to produce new polyolefin materials containing long-chain branching (LCB) or heteroatom-functionalized polyolefins giving unforeseen material properties.

The ability to incorporate bulky comonomer owes a lot to the tunability of the active site through ligand substitution. The very first metallocenes had limited copolymerization ability but the introduction of alkyl substituents, bridges to connect cyclopentadienyl rings, and ligand symmetry radically changed our view of the copolymerization properties of metallocenes. Then, further tuning of indenyl ligands through additional alkyl groups or heteroatom-bearing substituents like siloxy groups has further increased the possibilities for modification of the electronic and steric environment of metallocenes. Through these modifications, comonomer reactivity ratios of different metallocenes can vary by two orders of magnitude, from almost equal reactivity between ethylene and 1-olefin comonomer to those typically experienced with classical Ziegler–Natta catalysts. Additionally, activity in homogeneous polymerization can even exceed 100,000 kg polyethylene/mol catalyst using a suitable activator such as methylaluminoxane (MAO). There are also examples showing that tuning the electron density can significantly reduce the need for MAO by an order of magnitude compared to first-generation metallocenes.

Traditionally it was considered that ionic catalyst systems produce essentially linear polymeric architectures. This view changed, however, through analysis of the melt behavior of metallocene-based polyethylenes, which revealed the presence of long-chain branching (LCB) in these materials [9–14]. Interestingly enough, a long-chain branch structure is different to the structure exhibited by low-density polyethylene (LDPE) or Cr-based high-density polyethylene (HDPE) materials.

Some metallocenes produce essentially linear polyethylene whereas others are capable of producing almost crosslinked material at suitable polymerization conditions. Here, both comonomer response and ability to provide vinyl terminals have been seen as important in defining the degree of branching.

As is well known, polyethylene properties are dictated by molecular weight, molecular weight distribution (MWD) and branching. Short-chain branches of less than 40 carbon atoms influence the crystallinity and crystalline structure, whereas long-chain branches strongly affect the rheological properties of polyethylene, giving an additional tool for the modification of processing behavior to complement that provided by MWD. Thereby, metallocene polyethylenes with narrow MWD and LCB offer a possibility for multistage processes to produce materials with specifically tuned polymer property and processability combinations not available by conventional catalyst technology [15].

Another great challenge in polyolefin technology has been the production of polyolefins with polar functionalities. The most advanced method for producing functional polyolefins, in addition to free radical reactions and grafting reactions, is copolymerization with co-ordination catalysts.

Unfortunately, due to the Lewis acidity of the Ziegler–Natta catalysts, the copolymerization of polar functional olefins with these catalysts is not straightforward. The σ-donating polar groups have a higher tendency than the π-coordinating olefins to coordinate with the cationic complexes of these catalysts.

Single-site catalysts enable a broader range of alternative comonomers in ethylene and propylene copolymerizations through better comonomer response, which allows the use of much lower polar comonomer concentrations. Dramatically new technical properties could be achieved in polyolefin materials when the properties of polyolefins and polar comonomers were combined [16–18].

Functional polyolefins with significant contents of reactive alcohol, acid, ester, ether, silyl ether, amine, and amide groups have been successfully synthesized [19–22]. Even though these systems are not commercially feasible, the novel materials demonstrated gave a boost to the search for ways to fill this gap.

Some vinyl silanes were found to act feasibly as weakly interacting comonomers. Functional copolymers with ethylene and vinyl-$Si(CH_3)_3$, allyl-$Si(CH_{3)3}$, 3-butenyl-$Si(CH_3)_3$, 4-pentenyl-$Si(CH_3)_3$, 5-hexenyl-$Si(CH_3)_3$ or 7-octenyl-$Si(CH_3)_2Ph$ as comonomers were polymerized [23–25]. The short trialkylsilane monomers suffered from the electronic influence of silicon, which led to poor polymerization performance. In these cases, the chain end of the synthesized polyethylene-*co*-allyl-$Si(CH_3)_3$ consisted of reactive allylic silane groups and therefore the functionality and reactivity of these copolymers was higher than the weakly interacting trimethylsilane moiety can provide. Also it was found that the phenylene group in

the polyolefin pendant chain originating from 7-octenyl-Si(CH_3)$_2$Ph comonomer was effective and offered new possibilities for post-functionalization. In these approaches it has been possible to convert pendant groups in PE-*co*-SiPh and PP-*co*-SiPh to reactive fluorine, chlorine, methoxy, and ethoxysilane groups. In addition, hydrosilylation post-reactions were also investigated. Thus, synthesized reactive polyolefins have been shown to perform excellently as compatibilizers in polymer blends and composites [25–29].

2 Copolymerization Behavior of Bis(indenyl) Metallocenes

This section reviews copolymerization studies and aims to give an overview of research on ethylene-1-olefin copolymerization, the role of ligand substitution in copolymerization and the polymerization mechanisms involved. The copolymerization behavior of a group of siloxy-substituted complexes is discussed because they have the ability to be activated at low MAO ratios and some of them provide excellent comonomer response.

Scheme 1 displays metallocenes discussed in this paper. Table 1 summarizes selected literature data regarding ethylene reactivity ratios (r_E) in ethylene/1-olefin copolymerization.

Ligand substitution, transition metal (Ti, Zr, Hf), and the interannular bridge have distinctive effects on the copolymerization behavior. Electronic factors at the active site and the steric environment in the vicinity of the active site of a metallocene catalyst determine the reactivity of monomers and the structure of the copolymer. Many general conclusions about the influence of the ligand structure on the polymer structure [30] can be made, although the details of how the combination of electronic and steric effects determines the reactivities of reactants are not fully understood. General conclusions are the following:

- Substitution of Cp ligand decreases comonomer response [31]
- Bridged metallocene complexes have better comonomer response than non-bridged metallocenes
- Indenyl ligand substituted metallocenes have higher comonomer intake than tetrahydroindenyl ligand substituted ones
- Dimethyl silyl bridge improves comonomer response over ethyl bridge
- Hf complexes have higher comonomer reactivity than Zr analogues [32]
- Half metallocenes have typically high comonomer response but no stereo control
- *Meso* complexes have substantially higher comonomer response than their *racemic* counter parts
- Siloxy-substitution at 3-position significantly improves reactivity towards comonomer
- 4-Phenyl or benz[e]indenyl substitution further improves comonomer response

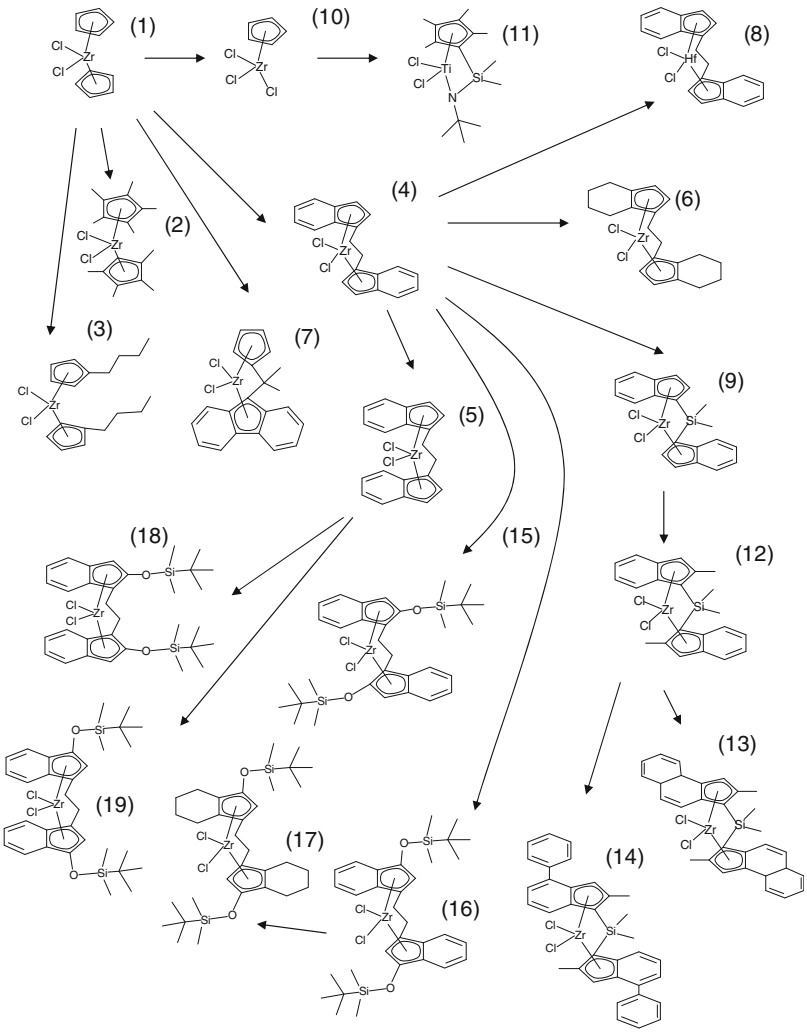

Scheme 1 Metallocene structures discussed in this chapter

Direct comparison of literature data regarding the copolymerization abilities of metallocene catalysts is difficult, as the copolymerization studies with longer 1-olefins have usually been carried out with a limited selection of catalysts under different polymerization conditions [6, 33–37]. Furthermore, some comparisons provide contradictory data, possibly due to differences in experimental setup control.

The basic zirconocene, Cp_2ZrCl_2 (**1**), is highly reactive towards ethylene and moderately reactive towards comonomer insertion [38]. The structure of the catalyst does not hinder free rotation of the ligands. This leads to a dramatic decrease in

Table 1 Ethylene and 1-olefin reactivity ratios (r_E) for selected metallocenes in ethylene/1-olefin copolymerization

	r_E (80°C)			r_E (40°C)	
Metallocene	C_2/C_6	C_2/C_6	C_2/C_{16}	C_2/C_6	C_2/C_8
1	114	112 ± 9	–	–	32.8 (0.05)
2	1,012	–	–	–	–
3	–	–	160 ± 13	–	–
4	–	48 ± 4 (<0.02)	51 ± 7	–	–
5	–	–	–	–	–
6	–	71 ± 4 (<0.03)	–	–	–
7	–	–	–	–	–
8	–	6 ± 1	–	–	–
9	–	26 ± 4	–	–	18.9 (0.014)
10	–	–	–	–	–
11	–	–	–	–	4.1 (0.29)
12	–	–	–	–	19.5 (0.013)
13	–	–	–	–	10.1 (0.118)
14	–	–	–	–	–
15	–	55 ± 3 (0.005)	63 ± 2 (0.002)	36 ± 3 (0.003)	–
16	–	30 ± 5 (0.004)	–	14 ± 4 (0.004)	–
17	–	19 ± 4 (0.006)	25 ± 1	16 ± 1 (0.005)	–
18	–	–	–	11 ± 1 (0.005)	–
19	–	–	–	10 ± 1 (0.001)	–
References	[31]	[51, 66, 88]	[66, 74]	[66, 74]	[36]

Values in parentheses (if shown) represent comonomer reactivity (r_C)

the comonomer response with increasing polymerization temperature. Furthermore, the substituent-free ligands do not promote any stereocontrol for the 1-olefin coordination, and the approaching 1-olefin can coordinate in regio- or stereo-irregular fashion. The resulting misinsertions inhibit chain growth and decrease the molecular weight drastically. Polypropylene produced with this catalyst is atactic and has a low molecular weight [30]. Pentamethyl substitution (**2**) of cyclopentadienyl significantly reduces comonomer response whereas an alkyl [e.g., methyl, ethyl, propyl or *n*-butyl (**3**)] substitution of the Cp ring reduces comonomer response only slightly compared to the unsubstituted **1**. These changes can be attributed to the increase in steric bulk around the active center [31].

The introduction of an interannular bridge between the ligands and the substitution of the cyclopentadienyl ligand with a C_2-symmetric ligand eliminates the free rotation and promotes stereocontrol for 1-olefin insertion. The very first synthesized metallocenes belonging to this category were *rac*-Et[Ind]$_2$ZrCl$_2$ (**4**) and its *meso*-isomer **5**. Hydrogenation of indenyl ligand yields *rac*-Et[H$_4$Ind]$_2$ZrCl$_2$ (**6**), which was the first metallocene catalyst shown to produce isotactic polypropylene [39, 40]. The comonomer response of this catalyst is also clearly higher than the response of **1** [33, 41].

The rigid structure of **6** prevents regio- and stereo-irregular insertions to a large extent. This is very true at low temperatures. At higher temperatures, ligand movement is allowed and the stereocontrol effect is removed [42]. The indenyl ligand forms a plane and improves the rigidity of the ligand compared to its hydrogenated tetrahydroindenyl analogue. *rac*-Et[Ind]$_2$ZrCl$_2$ (**4**) produces more isotactic polypropylene at low monomer concentration [43] and at a higher temperature than **6** [42]. Also, **4** exhibits better copolymerization ability than **6**. The gap-opening aperture of **4** and **6** has been reported by Busico et al. [44] to be 95° and 86°, respectively, which can be understood to reduce the probability of comonomer insertion for the latter [45, 46]. Electronic effects may also play a role in the better 1-olefin response. The electronic density around the central metal is lowered [47] when the alkyl ligand is substituted with an aromatic ligand.

Synthetic routes of C_2-symmetric metallocenes usually produce significant amounts of undesired *meso* isomer **5** in addition to the targeted *racemic* isomer **4**. The *meso* isomer does not provide stereocontrol in polypropylene polymerization due to the very open steric environment around the active site.

The changes in ligand symmetry alter the microstructure of the prepared polymer. Catalysts with C_S-symmetry enable the production of highly syndiotactic polypropylene [48]. An example of this is *i*Pr[Cp][Flu]ZrCl$_2$ (**7**). Based on the published reactivity ratios, this catalyst has better copolymerization ability than *rac*-Me$_2$Si[Ind]$_2$ZrCl$_2$ (**9**) [5, 35, 49].

Selection of the transition metal also has a significant effect on the copolymerization ability. Hf complexes have in general higher comonomer response than their Zr analogues; e.g., *rac*-Et[Ind]$_2$HfCl$_2$ (**8**) has almost an order of magnitude higher comonomer response than **5**. Not too many studies regarding the copolymerization behavior of Ti-metallocenes in comparison to their Zr analogues have been published. Based on the existing data, comonomer response appears to be at a similar level [41].

Other means of improving the comonomer reactivity is variation of the interannular bridge. In propylene polymerization, replacing the –CH$_2$CH$_2$– bridge with a shorter –Si(Me$_2$)– bridge increases the molecular weight and isotacticity [50]. *rac*-Me$_2$Si[Ind]$_2$ZrCl$_2$ (**9**) also has a higher comonomer response than **4** [51] or **6** [33].

Early development also included some half-metallocenes like CpZrCl$_3$ (**10**), which have been reported to give similar polymerization behavior to **1** [52]. Among this class of complexes belongs one of the highest comonomer response catalysts: SiMe$_2$[CpMe$_4$][*tert*-BuN]TiCl$_2$ (**11**), which has an extremely high comonomer response [53]. Even at 140°C, an r_E value as low as 8.8 has been determined [54]. The high comonomer response has been attributed to the low steric hindrance at the active site. However, electronic factors lower the activity of this half-metallocene catalyst [55].

Metallocene development has been driven largely by the search for high isotacticity for polypropylene. For example, the introduction of a 2-methyl substituent in the indenyl ligand provided (**12**). This metallocene has similar comonomer response to **9** but somewhat higher isotacticity [56]. Further development of this

catalyst family resulted in more sophisticated catalyst structures with improved copolymerization abilities. *rac*-Me_2Si[Me-Benz[e]Ind]$_2ZrCl_2$ (**13**) and *rac*-Me_2Si[2-Me-4-Ph-Ind]$_2ZrCl_2$ (**14**) are good examples of rational ligand design [56, 57]. Mülhaupt et al. applied these systems in ethylene-1-butene [36], ethylene-1-octene [58], and propylene-1-octene [59] copolymerization studies. In accordance with previous propylene homopolymerization studies they reported a beneficial influence of a 2-methyl substituent on the molar mass of the copolymers accompanied, however, by a simultaneous decrease in polymerization activity. Benzannelation of the indenyl ligand gave a beneficial influence on copolymerization activity and, furthermore, on the randomness and level of comonomer incorporation. The general character of the synergistic 2-methyl-4-aryl substitution was further demonstrated by Xu et al. [60], who synthesized a constrained geometry catalyst (CGC) having a 2-methylbenzindenyl ligand and applied it in ethylene-1-octene copolymerizations. Compared to the basic CGC catalyst with a Me_4Cp ligand, the activity and copolymerization ability of this rationally designed catalyst were slightly increased and the molar mass of the resulting copolymers was markedly increased.

2.1 Effect of Heteroatoms in the Ligand Framework

For tuning the electronic properties at the active site, the natural route for further development of metallocenes was the use of heteroatoms (N, O, S, P) in ligand substituents, which broadened the variety of metallocene complex families significantly. To study the electronic effects of ligand substituents, Piccolrovazzi et al. [61] and Collins et al. [62] in the early 1990s reported introduction of methoxy groups in the 4,7- and 5,6-positions of **4**, respectively. Their approach led to a drastic decrease in polymerization activity, which was explained as being due to interaction between the donor substituents and MAO, resulting in inductive electron withdrawal instead of electron donation. This also explains the low activity reported for 2-methoxy substituted bis(indenyl)zirconocenes [63]. Introduction of amino groups in the 2-position of indenyl ligands was found by Brintzinger et al. [64] and Luttikhedde et al. [65] to give modest activity after an induction time of several hours. The induction time was explained to result from inhibition of the reaction generating the active species, probably again as a consequence of an unfavorable interaction of the donor substituents with the MAO cocatalyst. Early successful developments in this area included various siloxy-substituted bis(indenyl) catalysts, e.g., **15**, **16**, and **17**. Sterically shielded 2-siloxy-substituted bis(indenyl) complexes were found by Leino et al. [66–68] not to suffer from induction periods and to give a considerable increase in ethylene polymerization activity compared to their unsubstituted analogues. An example of successful heteroatom substitution is highlighted by comparing the copolymerization behavior of two catalysts with different ligands, [1-*tert*-$BuSiMe_2$Oind] versus [1-*tert*-$BuSiMe_2$Ind]. The results have shown that the latter silyl-substituted catalyst has a poor comonomer response,

probably due to steric crowding, whereas the siloxy-substituted catalyst exhibits excellent copolymerization properties [69]. It is also noteworthy that such shielded siloxy-substituted complexes revealed highest polymerization activity at low Al(MAO)/Zr ratios. Reducing the amount of MAO in metallocene activation has been an important research objective due to the high cost of MAO [70]. Ewen et al. [71] also reported heteroatom-substituted aromatic ligands with a polymerization performance rivaling that of the corresponding unsubstituted complexes. Generally, the tuning of ligand properties with heteroatoms has been demonstrated to bear a high potential for extending the concept of rational ligand design.

2.2 *Copolymerization Behavior of Siloxy-Substituted Bis(indenyl) Zirconium Dichlorides*

Having found that siloxy-substituted complexes bear a high potential as highly active olefin polymerization catalysts, intensive research was directed towards optimizing the ligand design to improve the copolymerization behavior. It was soon found that the polymerization behavior of siloxy-substituted complexes depended markedly on the position of the siloxy substituent at the ligand [66].

Siloxy substitution at the 3-position of the indenyl ligand (**17**) was found to remarkably improve the 1-olefin copolymerization ability, whereas substitution at the 2-position (**15**) slightly reduced the copolymerization ability as compared to the unsubstituted **5**. The reason for this was suggested to be mainly the increased coordination gap aperture of the 3-siloxy-substituted complexes. Table 1 summarizes the ethylene reactivity ratio data obtained for the siloxy-substituted complexes **15**, **16**, and **17** The large difference in the ethylene and comonomer reactivity ratio values, the product of which is much below unity, emphasizes the prevailing tendency of the catalysts to produce copolymers with isolated comonomer units. The reason for the 15–40% lower incorporation of 1-hexadecene than 1-hexene was explained by the higher steric bulk and lower rate of diffusion of the longer α-olefin.

Furthermore, decreasing the temperature from 80°C to 40°C clearly improved the copolymerization ability of the hydrogenated **16**/MAO, while the influence of temperature on the comonomer response of the corresponding bis(indenyl) system **17**/MAO was less pronounced. This was also suggested to originate from contribution of steric effects. Fluctuation between the indenyl-backward and indenyl-forward conformations [72] in combination with the fluctuation of the hydrogenated six-rings of complex **16** is reduced at lower temperatures, resulting in less interference with the comonomer coordination. The copolymerization behavior of complex **17**, which has essentially planar indenyl moieties, could be understood to be considerably less influenced by the polymerization temperature.

Replacing the methyl groups at the silicon atom of **15** and **17** with bulkier *iso*-propyl groups was found to increase the ability of comonomer incorporation

[73]. This observation suggested that better shielding of the electron-rich oxygen in the siloxy substituent reduces the possibility of unfavorable interactions with the MAO cocatalyst. The enhancement of copolymerization ability due to improved shielding of the heteroatom is supported by the finding that the copolymerization ability of the less shielded **17** is negatively affected by increasing the Al(MAO)/Zr ratio.

In addition to enhancing copolymerization ability, 3-siloxy substitution was found to increase the sensitivity towards excess MAO, which was observed as a decreased comonomer incorporation and an increased induction time with an increasing Al(MAO) concentration. Increasing the temperature from 40°C to 80°C was found to shift the induction period to higher Al/Zr ratios. Using triisobutylaluminium (TIBA) had a similar effect to increasing the temperature. These observations indicate the presence of equilibrium reactions, which are shifted towards more rapid formation of the active sites by increasing temperature and decreasing MAO content. The open coordination sphere of the 3-siloxy-substituted complexes could be more subjected towards coordination of MAO to the donor substituents than it is for the 2-substituted complexes. Shortening of the induction period could be achieved by addition of TIBA, probably as a result of more efficient alkylation of the catalyst, since the alkylation by trimethylaluminum (TMA) has been reported to be extremely slow for 2-amino-substituted catalysts [47].

Siloxy substitution at the 2-position of the indenyl ligand resulted in immediate polymerization and extremely high polymerization activities at very low Al(MAO) concentrations [66]. At least two reasons were suggested for the enhanced polymerization activity of **15**/MAO at low MAO concentrations:

- Preservation of the electron-donating nature of the siloxy substituent in the presence of MAO is suggested to facilitate the formation of the active site and to stabilize the cationic metal center
- The weaker binding of the counterion to the cationic metallocene alkyl may increase the rate of monomer insertion into the metal–alkyl bond and thus increase the chain propagation rate

Finally, further manifestation of the good comonomer response of *meso* isomers was shown with siloxy-substituted **18** and **19**, which both provide excellent comonomer response although they decompose at higher temperatures [74].

In conclusion, siloxy substitution has been demonstrated to provide a family of highly active metallocene catalysts that reveal optimum polymerization properties at low Al(MAO) concentrations. Good comonomer response and the reduction of the required MAO amount are highly desirable features from an industrial point of view.

2.3 Chain Termination

In addition to the copolymerization ability, it is of special interest to understand the structure of end groups when defining a catalyst's potential to promote long-chain branch formation or to facilitate end-group functionalization. Moreover, analysis of

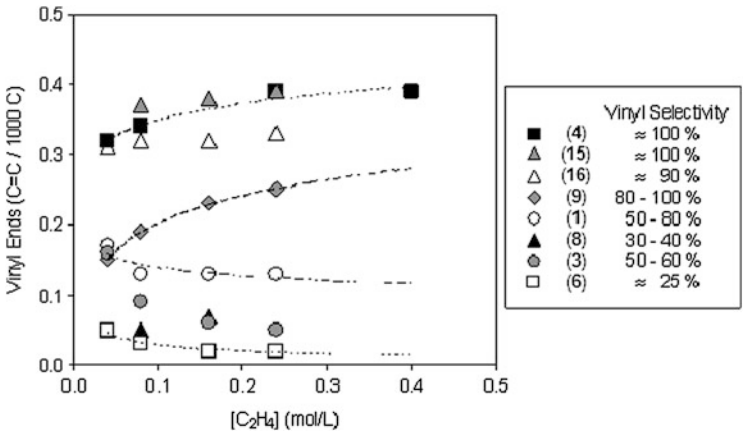

Fig. 1 Vinyl end-group content and selectivity in the homopolyethylenes produced with selected metallocenes. Vinyl selectivity has been calculated from the GPC (M_n) and FTIR data. Polymerization conditions: $T = 80°C$, MAO cocatalyst, solvent toluene. *Trendlines* are to guide the eye. Figure adapted from [168]

the polymer microstructure and end groups can reveal the mechanisms involved in the polymerization process.

The presence of different end-group types indicates that various chain transfer or isomerization reactions have participated in the polymerization. However, different mechanisms may produce the same end-group types. In these cases, the response to the changes in polymerization conditions may be utilized to reveal the reaction paths. The response to the polymerization temperature, monomer, comonomer, cocatalyst, and hydrogen concentration depend largely on the metallocene.

End groups of ethylene polymers are much less studied than those of propylene polymers. Only a handful of studies have been published on the subject [31, 37, 46, 51, 66, 75].

Figure 1 shows a comparison of the vinyl bond content of polyethylenes produced with several catalysts. In addition to the vinyl end groups, the polymers contained *trans*-vinylenes and a very small number of vinylidene double bonds [46, 51, 66].

The reaction path for *trans*-vinylene formation requires an isomerization reaction during chain transfer [76] or hydrogen liberation [37]. Vinylidene bonds may originate from a side reaction whereby a vinyl-terminated polyethylene is reincorporated into a growing chain, followed by a subsequent termination [46, 77].

The indenyl-substituted bridged Zr-catalysts (**4**, **9**, **15**, **16**) exhibit very high vinyl selectivity, which is typically almost 100%. A decrease in the monomer concentration slightly lowers the vinyl selectivity. Intermediate vinyl selectivities have been observed for non-bridged Cp metallocenes, e.g., **1** and **3**. The polyethylenes produced with the latter catalyst typically had lower vinyl contents

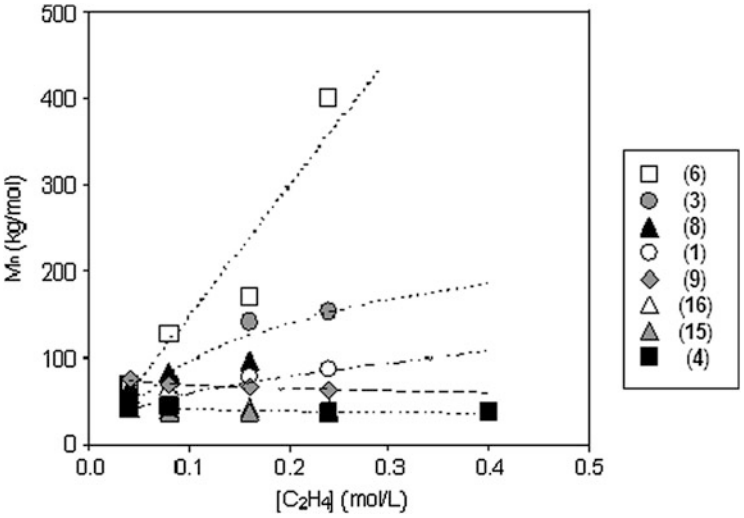

Fig. 2 Number average molecular weight of the homopolyethylenes as a function of ethylene concentration. Polymerization conditions: $T = 80°C$, MAO cocatalyst, solvent toluene. *Trendlines* are to guide the eye. Figure adapted from [168]

than those produced with **1**. The lowest vinyl selectivities and vinyl contents were in polyethylenes based on **6** and **8**. The introduction of a tetrahydroindenyl ligand or change of the central metal to Hf reduced the vinyl selectivity to the level of 25–40%.

Figure 2 shows the M_n as a function of ethylene concentration (C_E) for the same group of metallocenes. The indenyl-substituted bridged metallocenes (**4**, **9**, **15**, **16**) produced polyethylene with a constant M_n. The M_n of **6**-catalyzed polyethylenes, in turn, increased proportionally with the C_E. The M_n dependence of polyethylenes produced with the remaining set of metallocenes was neither independent nor linearly dependent on the ethylene concentration.

2.3.1 Effect of Hydrogen

Hydrogen acts as a chain transfer agent in olefin polymerization, reducing the molecular weight, but the response varies from one catalyst to another [43, 78]. In ethylene polymerization, hydrogen has been found to efficiently suppress the formation of *trans*-vinylenes, whereas the effect on the vinyl bonds is less pronounced [46, 51, 78].

The catalysts had marked differences in sensitivity towards hydrogen insertion and the resulting chain transfer. The hydrogen sensitivity of selected metallocenes is summarized in Table 2.

When **3** or **6** was used, the molecular weight decreased drastically and the vinyl bond content (C=C/1,000 C atoms) was very low correspondingly. The decrease in

Table 2 Effect of hydrogen on the polyethylene structure

Complex	H_2 feed (mmol/L)	M_w[b] (kg/mol)	M_n[b] (kg/mol)	*trans*-Vinylene content (C=C/1,000 C)	Vinyl content (C=C/1,000 C)
1	0.0	142	46	0.05	0.13
1	0.43	18	9	0.00	0.20
3	0.0	290	130	0.05	0.07
3	0.17	17	8	0.00	0.08
4	0.0	98	41	0.03	0.37
4	0.43	46	25	0.00	0.36
6	0.0	300	128	0.08	0.03
6	0.0[a]	1,000	400	<0.06	<0.02
6	0.13[a]	69	34	0.00	0.02
8	0.0	292	85	0.03	0.05
8	0.43	45	21	0.00	0.03
9	0.0	167	65	0.02	0.19
9	0.43	91	37	0.00	0.17

Polymerization conditions: $T = 80°C$; $C_E = 0.08$ mol/L; cocatalyst MAO. Data from [46, 51]
[a]$C_E = 0.24$ mol/L
[b]Molecular weights were determined by GPC; unsaturations by FT IR

the M_n was also very notable with **1** and **8**. The bis(indenyl)-substituted catalysts **4** and **9** had the lowest tendency towards hydrogen insertion under these polymerization conditions [46, 51].

The difference in the sensitivity towards chain transfer is attributed to the dominance of alternative chain transfer mechanisms. β-H elimination with **6** inherently produces Zr^+–H bonds. When **4** or **9** is used, chain transfer to the monomer was found to dominate. In this case, the active site is of the form Zr^+–CH_2CH_3 after the chain transfer reaction.

Based on the polymerization studies, several conclusions regarding the polymerization behavior and prevailing chain transfer mechanisms can be drawn:

- Chain transfer to the monomer is judged to be the major chain transfer mechanism with the indenyl bridged zirconium catalysts. This conclusion is based on the following two findings: (1) vinyl selectivity is approximately one unsaturation in each chain, which suggests that chain transfer to MAO is negligible, and (2) the M_n is independent of ethylene concentration, which rules out β-H elimination.
- β-H elimination is the dominant chain transfer mechanism with *rac*-Et[H_4Ind]$ZrCl_2$ (**6**). The M_n increases proportionally with the ethylene concentration, and the vinyl end-group selectivity is constant. Low vinyl end-group selectivity suggests that isomerization decreases the vinyl end-group selectivity, or that chain transfer to aluminum is present to some degree.
- Possibly, all three chain transfer routes play a significant role with unbridged metallocenes (e.g., **1** or **3**). Hf-based (**8**) also belongs to this class.

- The tendency towards chain transfer to hydrogen seems to be the highest with metallocenes prone to unimolecular β-H elimination. Metallocenes with high selectivity towards bimolecular β-H elimination are less reactive towards hydrogen.
- Isomerization tendency also appears to be the most significant with the catalysts for which β-H elimination dominates.

3 Long-Chain Branched Polyethylenes Formed In Situ

3.1 LCB Mechanism

Studies on the comonomer response and end group selectivity of bis(indenyl) zirconium catalysts led to further studies on the tendency of selected single-site catalyst systems under certain conditions to form long-chain branching.

Long chain branching (LCB) has several benefits relating to the polymer processability because it affects melt viscosity, temperature dependence of viscosity, melt elasticity, shear thinning, and extension thickening. The effect of LCB on the melt-state properties of polyethylene depends on the number, length, and distribution of the branches, on molecular weight, and on MWD.

The ability to produce polyethylene with low levels of LCB from ethylene monomer only is today considered to be reasonably common for single-site and metallocene catalysts. LCB is thought to occur via an in situ macromer copolymerization mechanism [12, 14, 46, 54, 79–87]. One manifestation of macromer insertion capability is the finding that crosslinked polymer is formed in copolymerization of ethylene and non-conjugated dienes with metallocene catalysts [88]. The in situ copolymerization mechanism (Scheme 2) was originally proposed to explain LCB in polymers with Constrained Geometry Catalyst (CGC) in a solution process [89–91]. According to this mechanism, the catalyst must first produce a vinyl-terminated polyethylene chain – a macromonomer – and then copolymerize it into another growing chain. Even when the fraction of chains with vinyl ends is relatively high, LCB incorporation would have to compete with insertion of short chained monomer and comonomer and only very low levels of LCB are expected to be incorporated. Following the mechanism, low ethylene concentration should favor LCB incorporation and lead to a more branched polymer. Increasing the amount of comonomer or hydrogen in the polymerization should result in less LCB due to a decreasing number of vinyl ends. Experimental data for these dependencies will be shown below.

The polymerization process also plays a role. In solution polymerization at high temperatures, polymer is dissolved and individual chains are assumed to have free mobility. The macromer can move from one site to another, and be copolymerized to a growing chain in a similar manner as other comonomers. However, in the particle forming process in a slurry or in gas phase, the polymer is not dissolved, but

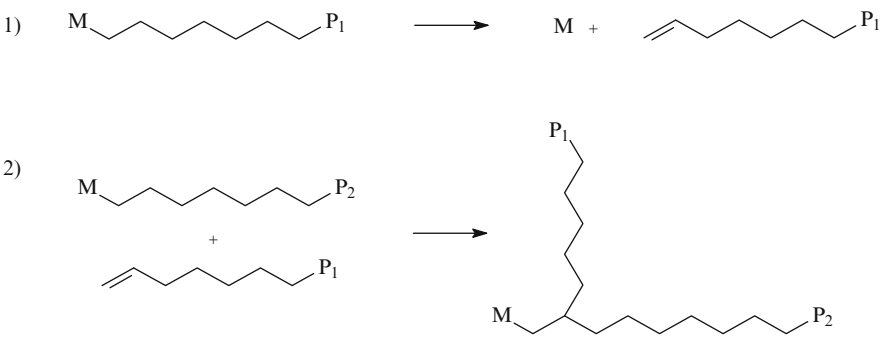

Scheme 2 Long-chain branch formation through incorporation of macromonomer in ethylene polymerization. The catalyst first produces another vinyl-terminated polyethylene chain (macromonomer) (*1*) and then copolymerizes it into another growing chain (*2*)

crystallizes and precipitates as particles as it is formed. Therefore, macromer might not move from one active site to another, but instead insertion of the macromer to another chain takes place at the same site where it was formed.

3.2 LCB Analytics

In contrast to the LCB in LDPE, a characteristic of the metallocene-LCB is the sparse amounts present. Three methods are well established for charactering this LCB: melt rheological measurements, ^{13}C-NMR, and SEC with multiple detectors (especially SEC-MALLS). Low shear rate melt rheology requires comparison to the results from conventional SEC for polymer average molecular weight and MWD. Analysis of LCB is best achieved with a combination of all these methods.

LCB density in single-site catalyzed polyethylenes is typically in the range of 0.01–0.2 branch points per 1,000 main chain carbons [14, 85, 91–93]. Sensitivity of modern ^{13}C-NMR instruments is by far sufficient to detect the low levels of 0.02 branches/1,000 carbon atoms that already have a significant impact on rheological behavior. Furthermore, ^{13}C-NMR is an attractive technique because it can give a number for the amount of LCB per chain. However, with regard to LCB determination, ^{13}C-NMR has a big drawback in that it cannot differentiate between side branches that are six carbons in length or longer. Therefore, it is of limited use in copolymers; moreover, it cannot differentiate between the rheologically significant difference between side chains of, e.g., 16 carbon atoms and 250 atoms in length.

SEC with multiple detectors, especially with multi-angle laser light scattering (SEC-MALLS), has high sensitivity towards high molecular weights and improved differentiation between LCB and linear high molecular weight species. SEC-MALLS has emerged as a complementary technique to detect low levels of LCB [86, 87, 94–97]. Multiple detector SEC most usefully yields information on the branching along with the MWD. Branched molecules have a smaller

radius of gyration than linear polymers and this result in a g-value of less than one in the SEC-MALLS. The g-value is the ratio of the radius of gyration of branched polymer to that of a linear polymer and, by definition, $g = 1$ for non-branched polymers. A decrease in the g-value towards higher molecular weight indicates an increased fraction of branched chains at the high M_W end. These components of long relaxation times have a large effect on low shear rheological responses.

Melt flow behavior in comparison with the molecular weight and MWD from SEC is a sensitive, yet relatively simple and reliable, way of detecting the LCB. This approach is however always indirect; one needs to compare the rheological responses to those of linear polymers of similar molecular weight and similar MWD. Even though the effects of the metallocene-generated LCB go beyond the effect of broadening the MWD [92, 93, 98–100], it may be a challenge to distinguish between these two. Characterization of the temperature dependence of rheological behavior [97, 100, 101] often offers a convenient way to distinguish between LCB and MWD effects.

The zero-shear viscosity η_0 of linear polymers scales exponentially with molecular weight [102] above the critical chain length M_c, but LCB polymers repeatedly deviate from this dependency. In comparison to linear polymers of similar M_w, polymers with low levels of LCB exhibit enhanced zero-shear viscosity values and, in a qualitative sense, ^{13}C-NMR-based LCB content often [85, 92, 93], but not always [100], correlates well with the viscosity increase. For long-chain branched LDPE, the η_0 in comparison to linear polyethylene of similar M_w is lower [103, 104]. A zero-shear viscosity η_0 value higher than that of the corresponding linear polymers of similar M_w is reported to occur at an LCB content of 0.2 LCB/10,000 C but the increase becomes more pronounced as the LCB content grows [85, 91, 92, 105, 106]. This feature of low amounts of LCB has also been utilized to explore the extent of metallocene LCB [13, 85, 106, 107].

Figure 3 illustrates utilization of the SEC-based M_w and the low shear rate viscosity to show LCB in narrow MWD metallocene-catalyzed polyethylene samples [94]. For this comparison, η_0 (from creep measurements) or complex viscosity $\eta^*(\omega = 0.01$ rad s^{-1} from oscillatory shear) values were plotted against the SEC-measured M_w. The solid line in Fig. 3 depicts literature-reported correlation of η_0 and M_w for linear polyethylenes [98]. Experimental η_0 results for a linear reference polyethylene sample (IUPAC5A) follow the literature relationship. In contrast, values of η_0 or $\eta^*(\omega = 0.01$ rad s^{-1}) for six experimental samples are up to 50-fold higher than the η_0 expected values for linear polymers of similar molecular weight. This deviation indicates a long-chain branched structure in the polymers. Figure 3 also shows the ^{13}C-NMR-determined values of branching (branches longer than six carbons) in these ethylene homopolymers. It is seen that even the samples with barely detectable amounts of LCB have clearly elevated low shear rate viscosity values.

Naturally, measures other than just a qualitative difference are of high interest and a variety of indices and procedures have been proposed as a measure for LCB from rheological behavior contra either the SEC-measured narrow MWD [93, 100, 106] or branching content from NMR [85, 106, 107]. Numerous approaches

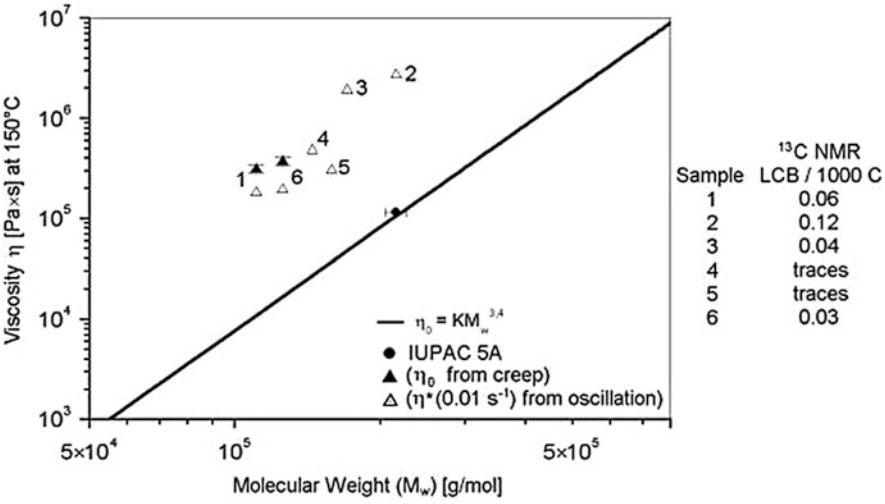

Fig. 3 Molecular weight dependence of the η_0 or $\eta^*(\omega = 0.01 \text{ rad s}^{-1})$ of linear (IUPAC5A) and long-chain branched polyethylenes. *Filled symbols* denote η_0 determined with creep experiments; *open symbols* give η^* from dynamic analysis at $\omega = 0.01$ rad s^{-1}. A deviation from the *solid line* indicates the presence of LCB. Reprinted from [94], with kind permission from Elsevier

have also been proposed for comparing the relative contributions of elastic and viscous responses from the dynamic rheological analysis [13, 96, 99, 108–111] with aim of describing the rheological polydispersity in the high molecular weight end of the MWD. Of the various ways to present low shear rheological data, plotting the phase angle δ against either frequency, ω, or complex modulus G^* (Van Gurp profile) have proven practical and are widely used to showing the effects and presence of a low amount of LCB [13, 84, 86, 96, 109–111]. Common to these procedures is that they start from the simple assumption that LCB varies only in the amount of branches.

Presence of LCB gives increased temperature dependence of the viscoelastic properties, giving increased value of the flow activation energy, E_a. Enhanced temperature sensitivity results from the additional relaxation processes that the long-chain branched chains require and that possess a different temperature dependence to the simple reptation [112, 113] and thus are not seen in linear polymers even when of broad MWD. Even though short-chain branching has almost no effect on the flow curves up to comonomer content of about 30 wt%, the E_a increases with comonomer level in linear polymers [97, 101, 107, 114, 115]. Thus, E_a of 25–28 kJ/mol is derived for HDPE samples and 30–34 kJ/mol for LLDPE samples [116, 117]. For higher E_a, the higher the comonomer content and the longer the comonomer is [97]. For long-chain branched LDPE, clearly higher values of above 50 kJ/mol are obtained [101, 117].

Flow E_a for polymers with a small amount of LCB cannot always be distinguished from the E_a of linear polymers [99, 115], but often E_a appears increase with

increasing LCB [13, 85, 91]. Thermorheological complexity is only seen with LCB samples and thus distinguishes the influence of LCB from the influence of short chain comonomers [97, 101, 116].

3.3 *Influence of the Catalyst and Polymerization Conditions on LCB*

Considering LCB formation via the copolymerization route, the vinyl end-group selectivity and comonomer response of the employed catalyst are important factors in determining the polymer structure. Besides the choice of catalyst, the choice of polymerization conditions may also suppress or enhance formation of LCB.

3.3.1 Catalyst Structure

Differences in vinyl end-group selectivity (data in Fig. 1) and the copolymerization ability (Table 1) suggest that metallocenes *rac*-Et[Ind]$_2$ZrCl$_2$ (**4**) and *rac*-Me$_2$Si[Ind]$_2$ZrCl$_2$ (**9**) would be more eager to produce LCB than metallocenes *rac*-Et[H$_4$Ind]$_2$ZrCl$_2$ (**6**) and bis(*n*-BuCp)$_2$ZrCl$_2$ (**3**) when activated. The rheological properties of homopolyethylenes made with these catalysts are in line with this thinking and with the in situ LCB mechanism.

Figure 4 shows the complex viscosity (η^*) as a function of oscillation frequency (ω) for homopolyethylenes produced with these MAO-activated catalysts under similar polymerization conditions [46, 51]. Sample characteristics are reported in Table 2. Polyethylenes prepared with catalysts **4**/MAO and **9**/MAO show low shear rate viscosity values [at η^* ($\omega = 0.02$ rad s^{-1})] that are 30- and 42- times higher than expected for linear polymers of the same M_w. In contrast, the melt viscosity is much smaller in polymers produced with the catalysts **6**/MAO and **1**/MAO. For polymers made with **3**/MAO**,** the low shear rate viscosity value is very close to the theoretical value, suggesting linear structure of the polymer.

Figure 5 shows dynamic modulus curves for the polyethylenes produced with MAO-activated metallocenes **1**, **3**, **4**, **6**, and **9**. All polymer samples had narrow M_w/M_n (2.2–2.5) and displayed no high molecular weight tailing in SEC [46, 51]. The modulus curves of polymers prepared with **3** and **6** are similar to the modulus curves of linear polymers of narrow MWD. In contrast, for the polymers based on **1**, **4**, and **9**, the elastic modulus (G') appears very large in comparison with the viscous modulus G''. Their rheological behavior suggests a much broader MWD than the SEC-based MWD. The contrast between SEC-measured MWD and rheological behavior is attributed to the presence of LCB in the polymers.

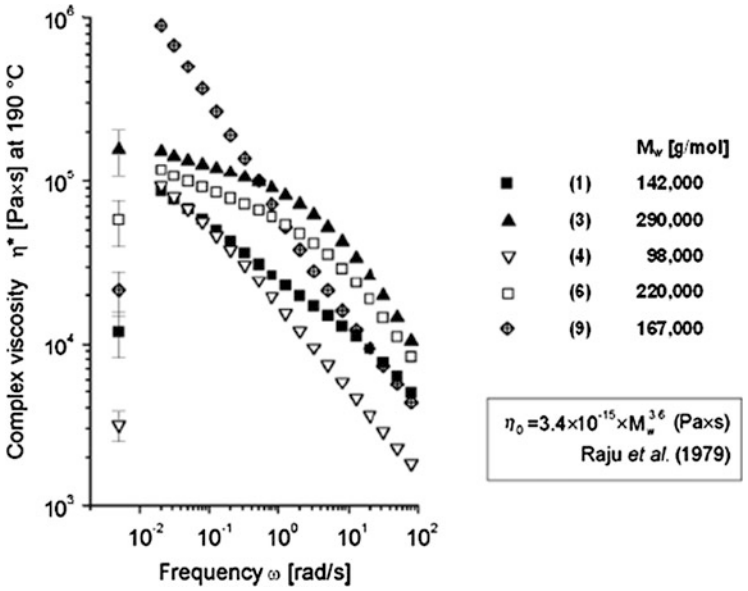

Fig. 4 Complex viscosity (η^*) curves of polyethylenes produced with selected MAO-activated catalysts under similar polymerization conditions. Single *points* shown at the *left* of the graph denote values for zero-shear viscosity (η_0) expected for a linear polymer of corresponding molecular weight. The expected zero-shear viscosity value was calculated from SEC-measured M_w with a formula originally reported by Raju et al. [102]. Adapted from [51, 168]

3.3.2 Effect of Ethylene Concentration

With in situ macromer incorporation as the LCB mechanism, the LCB content should change when the ratio [ethylene]/[vinyl terminated polyethylene chain] changes.

Figure 6 shows the η^* versus ω curves for polyethylenes produced at different ethylene concentrations (C_E) in a semi-batch slurry polymerization. Samples produced with lower C_E exhibit increasingly high values of low shear rate viscosity versus the SEC-measured M_W, and more pronounced shear thinning [46].

Interestingly, for the polymers produced with **1**/MAO, **3**/MAO, and **6**/MAO, a clear deviation from linearity is seen only at the lowest C_E. At high ethylene concentration, the difference between expected η_0 and measured $\eta^*(\omega = 0.02\,\mathrm{rad\,s^{-1}})$ values became smaller and the flow activation energy E_a values of these polymers were comparable to the values expected for linear polyethylenes [46, 51].

In addition to the semi-batch slurry experiments, **9**/MAO was used in solution in a continuous stirred tank reactor (CSTR) to further investigate the influence of [ethylene]/[macromonomer] ratio on LCB. Figure 7 shows a quantitative analysis of the ^{13}C-NMR-based LCB content in polyethylene as a function of the [ethylene]/[macromonomer] ratio [85]. The LCB content was the highest at low ratios and rapidly decreased with an increase in the [ethylene]/[macromonomer] ratio. This is in line with LCB formation via the copolymerization reaction.

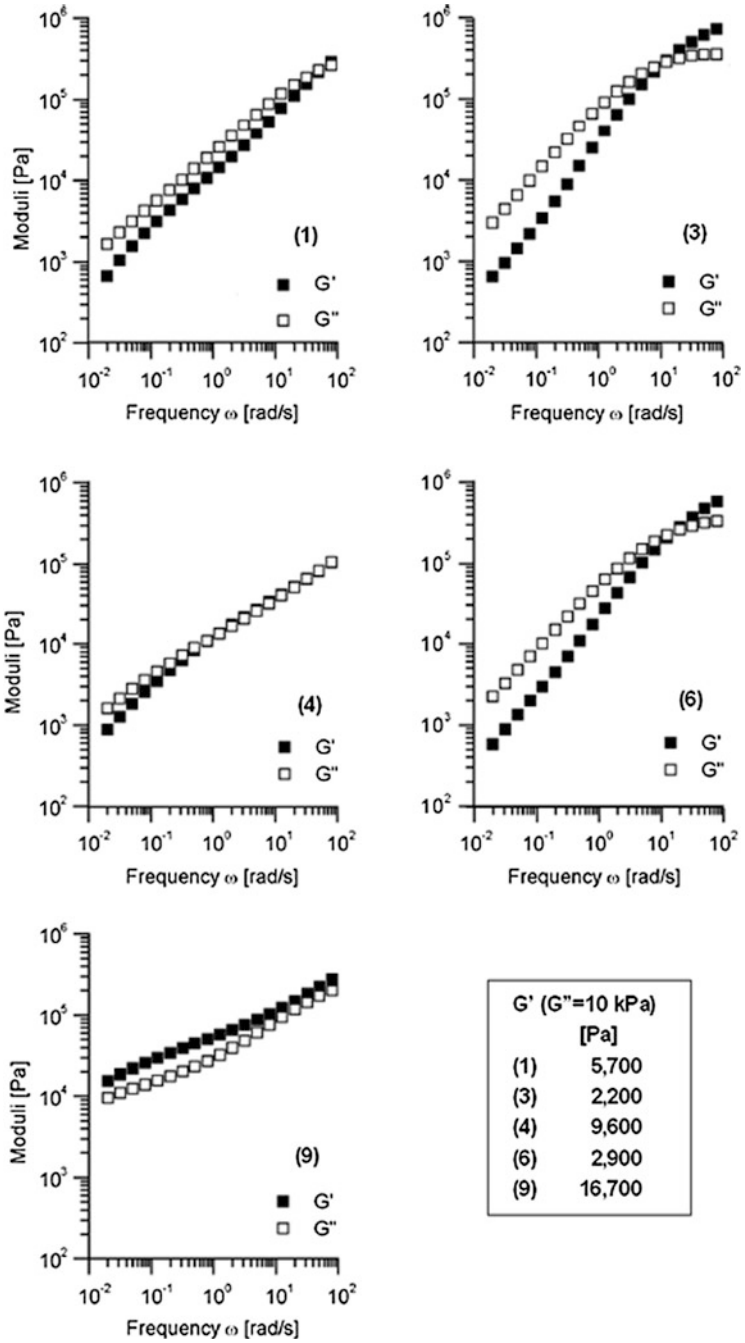

Fig. 5 Modulus (G' storage modulus, G'' loss modulus) curves of homopolyethylenes produced with metallocenes **1**, **3**, **4**, **6** and **9** activated with MAO. Polyethylenes **1**, **4** and **9** have greatly elevated G' values due to LCB, whereas **3** and **6** behave like linear polymers of narrow MWD. Adapted from [46, 168]

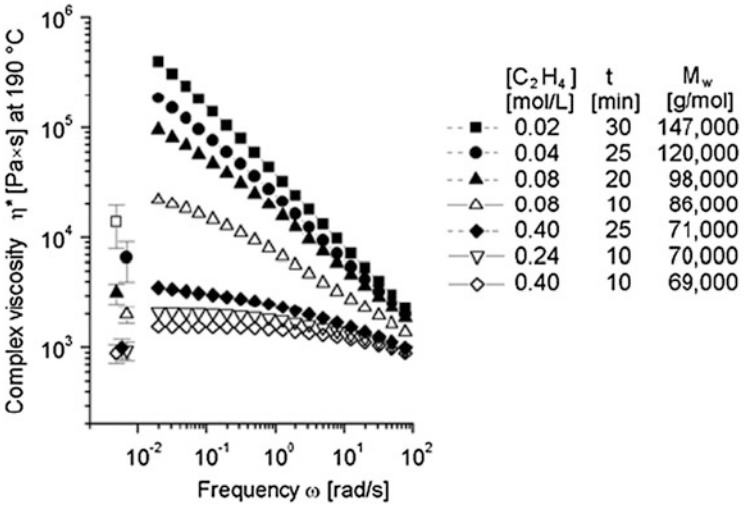

Fig. 6 Melt rheological behavior of polyethylenes polymerized with **4**/MAO varying the ethylene concentration and polymerization time. Single *points* shown at the *left* of the graph represent theoretical η_0 values [102] expected for a linear polymer of corresponding M_w. A decrease in the C_E results in the strongly elevated η^* at low shear rates and significant shear thinning. Note that for the samples with very high viscosity, the true zero-shear viscosity value η_0 would be much higher than the experimentally measured $\eta^*(\omega = 0.02 \text{ rad s}^{-1})$ value. Adapted from [51, 168]

3.3.3 Hydrogen Concentration

From the copolymerization mechanism it also follows that introduction of hydrogen would suppress LCB formation due to the decreasing number of vinyl ends, as preferred chain transfer to hydrogen leaves saturated chain ends. Table 3 shows the effect of hydrogen on the melt rheological properties [46]. For polymer polymerized with **4**/MAO at $C_E = 0.08$ M, introduction of hydrogen as chain transfer agent decreased the E_a value from 42 to 38 kJ/mol, and diminished the discrepancy between the theoretical and the experimentally measured low shear rate viscosity. The polymer produced by **6**/MAO without hydrogen at $C_E = 0.24$ M displayed melt rheological properties of a linear polymer with narrow MWD.

3.3.4 Effect of Comonomer

Ethylene copolymerization with 1-olefin comonomers decrease the polymer vinyl bond concentration because chain transfer to the comonomer ends the polymer chain with a vinylidene bond. Therefore, introducing a 1-olefin comonomer into the polymerization is expected to lead to lower LCB content, whereas use of

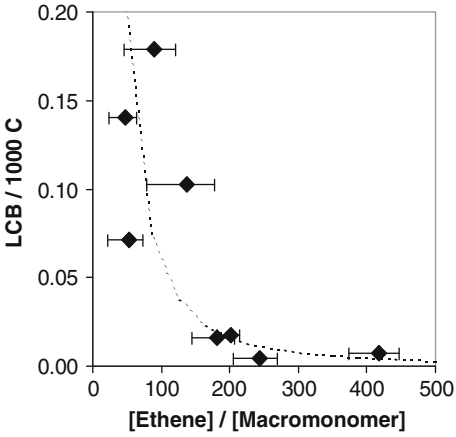

Fig. 7 Effect of estimated [ethylene]/[macromonomer] ratio on the NMR-measured LCB content in **9**/MAO-catalyzed polyethylenes produced in a continuous stirred tank reactor at 140°C. The reactivity of ethylene was estimated to be 75-fold that of macromonomer. Reprinted from [85], with kind permission from John Wiley and Sons

Table 3 Effect of hydrogen on the melt rheological properties of polyethylenes produced with catalysts **4**/MAO and **6**/MAO in a semibatch flow reactor at 80°C[a]

Catalyst	$[C_2H_4]$ (mol/L)	H_2 feed (mmol)	M_w (kg/mol)	M_w/M_n	Theoretical η_0[b] (Pa s)	η^*(0.02 rad s^{-1}) at 190°C (Pa s)	E_a (kJ/mol)
4	0.24	0.0	70	2.0	900	2,080	30
4	0.24	1.3	59	1.9	500	980	
4	0.08	0.0	98	2.4	3,200	94,000	42
4	0.08	0.5	65	2.1	700	5,930	38
6	0.24	0.4	69	1.9	900	1,200	27

Data from [46, 168]

[a]Polymerization medium was toluene

[b]Theoretical η_0 calculated using the equation $\eta_0 = 3.4 \times 10^{-15} \times M_w^{3.6}$ (Pa s) [102]

nonconjugated α,ω-dienes as comonomer would increase the vinyl bond concentration and thus the probability of LCB formation.

As shown in Table 4, introduction of 1-hexadecene as comonomer has a similar influence to hydrogen on the rheological properties of the polyethylene: the $\eta^*(\omega = 0.02$ rad $s^{-1})$ and G' values were lowered, indicating suppression of the LCB. The flow activation energy value, E_a remained almost unchanged due to two opposite effects at play simultaneously. For flow E_a, two different effects of the comonomer incorporation are present: an increase in the comonomer content in a linear polymer will increase E_a, but for the LCB, a decrease in the LCB content would decrease the E_a value.

The E_a values (26–28 kJ/mol) reported for **3**/MAO-catalyzed copolymers are considered to represent the properties of linear polymers in which only short-chain branching influences the melt behavior [46]. The calculated η_0 values are close to the measured values, and the flow activation energy E_a increases slightly with comonomer incorporation, as expected for a polymer with short-chain branching.

Table 4 Effect of comonomer 1-hexadecene on the properties of polyethylenes produced with catalysts **3**/MAO and **4**/MAO in a semibatch flow reactor at 80°C[a]

Catalyst	Comonomer content (mol%)	Vinyl content (C=C/1,000 C)	M_w (kg/mol)	M_w/M_n	Calculated η_0[b] (Pa s)	η^* (0.02 rad s^{-1}) at 190°C (Pa s)	E_a (kJ/mol)
4	0.0	0.4	98	2.4	3,200	94,000	42
4	0.8	0.5	74	2.2	1,200	8,100	42
4	3.4	0.4	64	2.0	700	1,680	41
3	0.0	0.1	290	2.3	160,000	152,000	29
3	0.3	0.1	183	2.0	30,000	28,900	27
3	1.2	0.1	80	2.0	1,500	2,700	34

Data from [46, 168]

[a]$[C_2H_4] = 0.08$ M; solvent, toluene

[b]Theoretical η_0 was calculated using equation $\eta_0 = 3.4 \times 10^{-15} \times M_w^{3.6}$ (Pa s) [102]

Table 5 Effect of catalyst and vinyl bond content on the properties of polyethylenes produced with Catalysts 3/MAO and 8/MAO in a semibatch flow reactor at 80°C[a]

Catalyst	1,7-octadiene content (mol%)	Vinyl content (C=C/1,000 C)	M_w (kg/mol)	M_w/M_n	Calculated η_0^b (Pa s)	η^* (0.02 rad s^{-1}) at 190°C (Pa s)	E_a (kJ/mol)
3	0.00	<0.1	77	2.2	1,300	1,410	27
3	0.15	0.7	63	1.8	640	740	
3	0.16	1.1	74	1.9	1,150	1,370	
3	0.27	1.5	65	1.9	720	2,270	33
8	0.00	<0.1	146	2.4	13,300	39,400	28
8	0.17	0.4	101	2.5	3,500	170,000	57
8	0.23	0.5	68	2.3	850	11,300	43

Data from [88]

[a]$[C_2H_4] = 0.40$ M, comonomer 1,7-octadiene, cocatalyst MAO, solvent toluene

[b]Calculated using equation $\eta_0 = 3.4 \times 10^{-15} \times M_w^{3.6}$ (Pa s) from [102]

To test the importance of vinyl bond content and copolymerization ability in LCB formation, we carried out a diene copolymerization series with two catalysts having very different comonomer responses, low inherent vinyl bond formation tendency, and very facile hydrogen reactivity. Concentration was kept high to avoid inherent LCB formation in the series. 1,7-Octadiene served as the diene comonomer. Polymerization results are summarized in Table 5.

Ethylene/1-octadiene copolymers produced with catalyst **3**/MAO, of low copolymerization ability, were linear or contained only a very small amount of LCB. The homopolymer that contained very few vinyl bonds was concluded to be essentially linear on the basis of its rheological properties. The copolymer with 1.5 vinyl bonds/1,000 carbon atoms had slightly elevated η^* versus η_0, G′, and E_a values. These rheological results suggest the presence of a small amount of LCB in this polymer. With an increase in diene feed, copolymer produced at low ethylene concentration with the **3**/MAO displayed relatively broad MWD ($M_w/M_n = 8.8$)

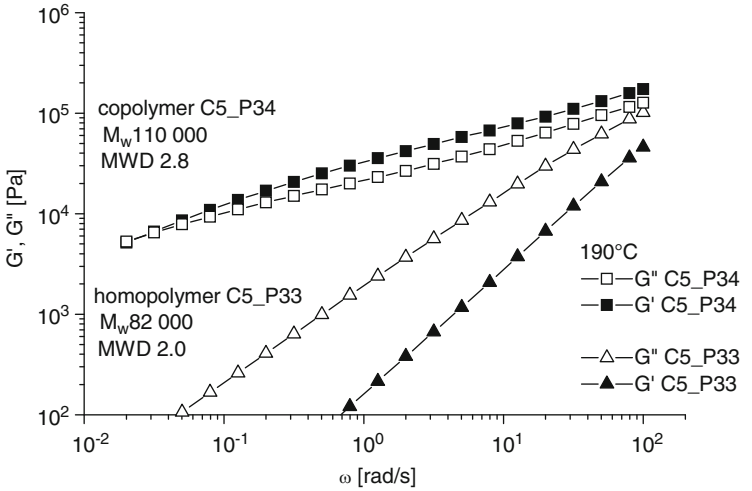

Fig. 8 Storage modulus G' (*filled symbols*) and loss modulus G'' (*open symbols*) as function of oscillation frequency for an ethylene homopolymer and an ethylene/1-hexene copolymer with **15**/MAO. Polymerization conditions: medium *n*-pentane, *p*(ethylene) = 2.5 bar, $T = 80°C$, $t = 30$ min. Copolymer contains 7.2 wt% 1-hexene. Reprinted from [81], with kind permission from American Chemical Society

when the polymer contained about 3.0 vinyl bonds/1,000 carbon atoms [88], suggesting significant branching at these conditions even using a catalyst with poor copolymerization ability and vinyl-selectivity.

Very different polymer properties were observed with catalyst **8**/MAO, of good comonomer response. The copolymers had drastically modified rheological properties even at very low diene content. Slightly higher diene comonomer feed resulted in the formation of a crosslinked polymer that was difficult to remove from the reactor due to gelation.

Experiments with a variety of single-site catalysts show that 1-olefin comonomer at low levels may actually increase the LCB behavior. This behavior has been reported by several groups using various bridged bis(indenyl) structures [81, 83, 85, 109, 115] in semi-batch slurry polymerizations as well as in the continuous gas phase [12] with supported and homogeneous catalysts, and with various short chain comonomers [12, 81, 83, 86, 97]. At large enough comonomer content, the chains produced appear non-LCB again [83, 86, 115].

Figure 8 shows low shear rate rheological results for an ethylene homopolymer and an ethylene/1-hexene copolymer with catalyst **15**/MAO [81]. Ethylene homopolymers by this catalyst exhibit the rheological behavior of linear chain polymers. In contrast, the copolymer displays a higher molecular weight and broader MWD than the corresponding ethylene homopolymers and, as shown in Fig. 8, in the copolymer melt the elastic behavior dominates even at the lowest frequencies. Behavior like this suggests the presence of widely different relaxation times, as in a crosslinked network structure (but the polymer was completely

Fig. 9 Illustration of possible structures of long-chain branched polyethylene. Multiple branched comb-like branching (*left*), one 3-arm branch (Y-structure; *center*) and two 3-arm branches (H-structure; *right*)

soluble in trichlorobenzene at 135°C, and crosslinking during measurements can be out ruled because the thermal stability of the polymers was perfect). We attribute this LCB enhancement effect by the 1-olefin comonomer to diffusion-controlled polymerization, in which the mass and heat transfer properties in the polymerization system have been changed by introduction of the comonomer. It is interesting to note that while these semi-batch polymerization experiments were run in pentane medium, similar ethylene/1-hexene copolymerization experiments with same catalyst but toluene as the medium yielded polymers with rheologically linear behavior [81].

3.4 Structure Considerations of the LCB

The branching mechanism for metallocene LCB shown in Scheme 1 suggests that the length of each segment is up to half the length of a chain. In copolymerization of vinyl-ended macromonomers with ethylene, assuming only one vinyl end per molecule, trifunctional branch points are formed rather than crosslinks. Whereas incorporating one macromonomer in the chain produces a Y-like structure, the architecture becomes more complex (tree- or comb-like) if several macromonomers are incorporated in a single growing chain. Figure 9 illustrates possible LCB structures.

A characteristic of metallocene LCB is the low amounts present: based on the ^{13}C-NMR experiments, one can conclude that there is less than one LCB in every four chains [85, 91, 93, 94, 105, 118]. Nevertheless, the impact on low shear rheology as well as on elongational rheology is strong. Modeling results [119] for the chain length distribution shows that the LCB distorts the MWD and forms a high M_w (HMW) tail. SEC-FTIR studies have shown that polymer chains in the HMW tail may be highly branched. Furthermore, SEC-MALLS measurements have been utilized [94, 103] to study the qualitative differences between LCB in metallocene polyethylenes and conventional LDPE. The following conclusions were made about metallocene polyethylenes: (1) LCB is present in far lower amounts, (2) long-chain branches are three times longer than for the LCB in LDPE, and (3) LCB is located specifically at the highest molar mass.

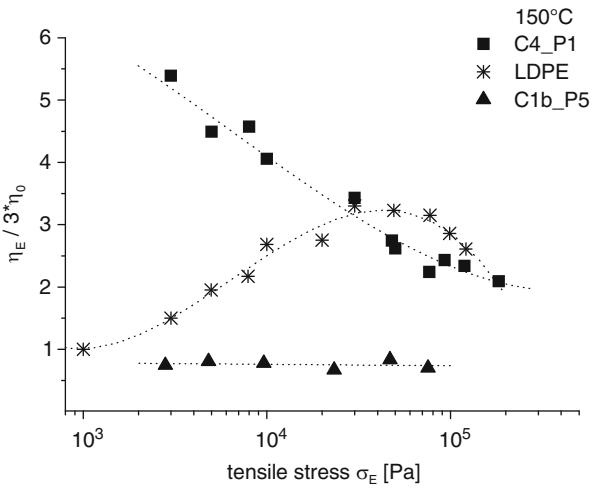

Fig. 10 Dependence of the steady-state tensile viscosity η_E on the tensile stress at 150°C for a LDPE and two metallocene samples. C4_P1 represents branched mPE and C1b_P5 represents linear mPE. *Curves* are fitted to the data points to guide the eye. Reprinted from [120], with kind permission from American Chemical Society

Metallocene-catalyzed LCB polyethylene thus consists of a mixture of linear and LCB chains, where the LCB structures make up only a small fraction of the total number of chains. Assuming the different ability of catalysts to incorporate vinyl-ended macromonomers in polymerization, it appears rational to expect differences in the amount, but also in the distribution, of the long-chain branches. Thereby, uneven LCB distribution (a few multiply branched chains versus several with only one branch) would lead to species with even longer relaxation times, which, even if present only in minor amounts, could be expected to alter the melt flow behavior even more than a star-like branch would do. In addition to increased LCB amount, multiple branched structures of high molar mass give a possible explanation for a gelation-resembling rheological response like the ones shown in Figs. 5 and 8.

Additional evidence on differences in distribution or structure of LCB was gained from elongation rheological experiments. Uniaxial elongation studies in the nonlinear range and low shear studies for polymers in the linear viscoelastic (LVE)-regime arranged the polymers in a different order in terms of apparently increasing LCB [120]. Figures 10 and 11 display steady-state elongational viscosity at various tensile stress values at 150°C for linear and long-chain branched metallocene-catalyzed polyethylenes [120]. Properties of the polymers are given in Table 6.

The linear metallocene polyethylene (mPE) reference, polymer C1b_P5, shows stress-independent steady-state viscosity throughout the stress range measured, whereas the LDPE shows strain hardening behavior typical for that range. At low stress, the response is equal to three times the LVE shear viscosity. Increasing the tensile stress leads to strain hardening up to a maximum stress, after which the response becomes extension thinning [121]. In contrast to the LDPE, the steady-state extensional viscosity (η_E) of branched mPE polymer C4_P1 appears

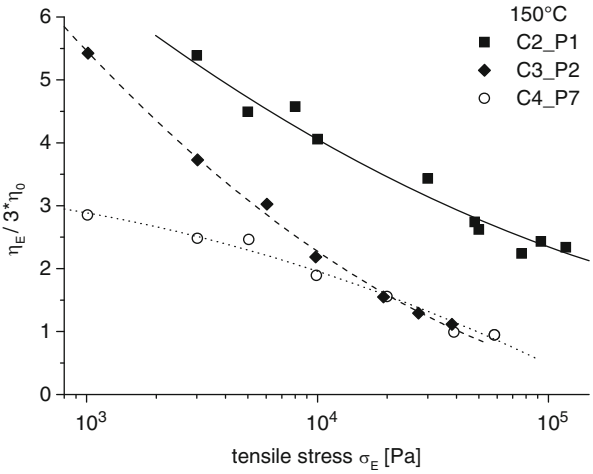

Fig. 11 Dependence of the steady-state tensile viscosity η_E on the tensile stress at 150°C for three metallocene-catalyzed polyethylenes differing in branching topology. *Curves* are fitted to the data points to guide the eye. Reprinted from [120], with kind permission from American Chemical Society.

continually to increase towards the low stress values, with strong strain hardening character.

Figure 11 shows elongation results for polymers prepared by metallocene catalyst systems prone to LCB branching formations. Interestingly, the polymers differ both in the maximum strain hardening value and in the extension rate at which this occurs. Moreover, the results for shear behavior (E_a and $\eta_0 - M_w$ discrepancy, Table 6) are in contradiction; the sample with highest flow activation energy in shear displays lower maximum values of extensional viscosity and, unlike the others, the values approach the η_E plateau maximum value within the rate/stress scale studied. Molecular weight differences offer no immediate explanation because the M_w values in the series were quite similar.

Melt elongational measurements provide a fingerprint of the structure of the highest molecular weight tail of the MWD as melt extensional viscosity bears extra sensitivity to long relaxation times in general [122–124]. In LDPE, increasing branch content enhances the nonlinear behavior and shifts the η_E maximum to higher values and lower extension rates [121]. Modeling [125] with an idealized H-architecture has shown that the dominant contribution to the increased relaxation times arises from the cross-bar segment of the H, because the arms relax on a much faster time scale. With monodisperse model polymers, the strain hardening character of H-topology has also been been experimentally shown [126] Star polymers are expected to follow the nonlinear behavior of linear melts (as they do in the nonlinear shear rheology), and experimental results with model polymer blends support this [126]. Reported results for single-site LCB in uniaxial extension range from little difference in strain hardening [92] with increasing (low) levels of LCB to very pronounced nonlinearity [105, 120].

In metallocene or generally single-site catalyzed LCB, we understand the components with the highest relaxation times to represent the structure or distribution of the long-chain branches. However, does the LCB spread out in a even

Table 6 Basic properties of metallocene copolymers and reference LDPE characterized with the melt elongational measurements

Sample	Type	Density (kg/m^3)	M_w^a (g/mol)	M_w/M_n	η_0 (190°C) (Pa s)	α ($\times 10^5$)^b	$E_{a\ (average)}$ (kJ/mol)
C1b_P6	Linear	924	82,000	3.1	3,130	0.01	33
C1b_P5	Linear	922	106,000	3.3	7,970	0.1	32
C4_P1	LCB	925	94,000	3.3	16,600	1.2	34
C5_P2	LCB	960	83,000	4.7	10,200	1.4	39
C6_P7	LCB	930	82,000	7.5	25,000	3.2	44
LDPE	LDPE	923	155,000^c	15^b	7,600		53

Data from [120]

[a]Values measured by SEC, uncorrected for branching effects

[b]Fraction of long-chain branch points.Values for the constants in Equations 1–3 by Janzen and Colby [106]: $K = 5.22 \times 10^{-6}$ (Pa s)/(g/mol), $B = 6.0$, $M_0 = 14.027$ g/mol, $M_c = 2{,}100$ g/mol, $M_{Kuhn} = 145.9$ g/mol

[c]From SEC-on line viscometer, $g' = 0.5$

manner, as in more chains bearing a single long branch, or is it concentrated in a few multiply branched chains? In the multiply branched case, differences in the molecular weight between the branch points would determine the degree of non-linearity and rate dependence of the extensional response. This being the case, the polymer C4_P7 represents a more even distribution of the LCB than the C4_P1. An alternative explanation, possibly acting simultaneously, could be differences in the number of the branch points.

3.4.1 LCB Dependence on the Polymerization Process

The polymerization process should significantly be able to alter the LCB topology. In a continuous system, such as the stirred tank reactor (CSTR) system, both monomer and macromonomer concentrations are constant after the steady state conditions are achieved. Monomer concentration is also constant in a semi-batch polymerization with continuous monomer feed but the macromonomer concentration increases as the polymerization proceeds.

In solution polymerization, the forming polymer remains dissolved in the solution because the polymerization temperature is above the polymer melting point. This allows for more free monomer and macromonomer mobility. Furthermore, in the CSTR, residence times are typically short to overcome reduced catalyst lifetime at higher temperatures [80, 82].

In slurry polymerization, the polymer precipitates from the solution partly or totally and this certainly limits the macromer mobility. Forming polymer encapsulates the active center and the polymerization occurs in the polymer phase [127], this is even more so the case with supported (immobilized) catalysts.

Further consideration of the origin of different topologies caused by the process conditions include heat and mass transfer effects. Heat and mass transfer limitations are more easily present in the semi-batch slurry polymerizations, where residence times are

longer and the particle formation itself could be a factor. Precipitation has a great influence on the mobility of the chains and on monomer diffusion rate coefficients.

All above-mentioned phenomena can play a role in the LCB formation. It appears reasonable to assume that most important are the monomer and the macromonomer concentrations in the vicinity of the active site. In the particle forming process, the situation could be described as diffusion-controlled long-chain branch formation enabled by vinyl-end formation and the good copolymerization ability of metallocenes. In solution, the decisive factors could be vinyl-end formation and good copolymerization ability with macromer mobility. The reported rheological behavior of LCB polyethylenes produced with mono-C_P amido catalysts in slurry [81, 83] differs from that for polymerizations carried out in solution [80, 91]. The rheologically complex behavior (like that shown in Fig. 8) and comonomer enhancement effect on LCB has much more often been reported in particle forming polymerizations [12, 81, 83]. Modeling efforts [119] for the chain length distribution produced with the in situ mechanism show that the LCB distorts the MWD and forms a high M_w tail.

Adapting the idea of elongational rheological response to reflect species with longest relaxation times [122–124], we interpret these differences as variations in long chain branching topology. The continuous processes can be better controlled for mass and heat transfer properties of the components and system. Therefore, it seems reasonable that the samples prepared in continuous processes would have more random branching structure, with branches distributed more evenly among the molecules. Branches in the polymers produced in a semi-batch system, on the other hand, may be less homogeneously distributed, forming a multiply branched high molar mass tail with very long relaxation time.

Despite the big effect on shear sensitivity at low shear rates, low levels of metallocene LCB do not necessarily yield any improvement at high shear rates [95, 128] In extensional flows, metallocene-LCB may improve melt strength and melt stability due to a strain hardening effect, giving improved film blowing stability and more even film thickness [119].

To summarize long-chain branch formation with metallocenes, as discussed above:

- The ability to incorporate long-chain branches appears reasonably common among metallocene catalysts. Experimental results for LCB formation with both CGC and conventional metallocene-catalyzed polymerizations are in line with an in situ copolymerization mechanism. For copolymerization of vinyl-terminated polyethylene molecules to occur, the first requirement is the presence of termination mechanisms producing vinyl-terminated macromonomers. Secondly, the catalyst must able to incorporate these macromonomers into a growing chain. Macromers probably do not move from one active site to another, but instead insertion of macromer to another chain takes place at same site where it was formed in a intramolecular incorporation manner.
- It is the catalyst structure that governs the feasibility of the LCB formation. The dominating termination reaction and its sensitivity to the presence of chain transfer agents are determined by the catalyst. Provided that vinyl ends are

formed, the copolymerization ability appears to be an even more important aspect. Structural features of the catalyst that influence the copolymerization ability are interannular bridge and size, and position of substituents in the ligands. In particular, the $Et(Ind)_2ZrCl_2$-based 3-siloxy-substituted complexes show high copolymerization ability towards short chain comonomers and a high tendency for LCB formation.

- Low shear rate rheological characterization in comparison with the molecular weight and MWD from SEC is a sensitive, yet relatively simple and reliable way of detecting the LCB. In accordance with the in situ mechanism, the rheological behavior of conventional metallocene-catalyzed ethylene homopolymers heavily depends on polymerization conditions such as ethylene pressure, hydrogen concentration, and polymerization time. Therefore, the LCB is not only a function of the catalyst but also of the polymerization. Moreover, any deviation from the polymerization rate-controlled polymerization conditions (e.g., due to the presence of mass and heat transfer limitations) offers a pathway to broadening of polymer structure in terms of MWD, comonomer distribution, and also the LCB.
- The level of long-chain branching by metallocene catalysts, however, is low and this complicates the characterization. Metallocene-catalyzed LCB polyethylene thus consists of a mixture of linear and LCB chains, where the LCB structures make up only a small fraction of the total number of chains.
- The first structure assumption for LCB is a three-arm star, but complex branches-on-branches structures may form through copolymerization of more than one vinyl-ended macromer in the chain. The branched molecules are located in the highest molecular weight end of the MWD. The LCB mechanism and the influencing factors, i.e., catalyst copolymerization ability and polymerization conditions, suggest that it is feasible that variations not only in the amount but also in the distribution of LCB can occur. However, it is postulated that the catalyst structure also plays a major role as regards distribution/topology of the long-chain branches along the chains.

4 Polymerization of Functional Comonomers with Olefins by Using Bridged Bis(indenyl) Catalysts

4.1 Polymerization of Strongly Interacting Comonomers

The coordination polymerization by transition-metal catalysts, such as Ziegler–Natta catalysts or metallocenes, is the most versatile method for preparing linear polyolefins under mild and controlled conditions. Unfortunately, attempts at direct incorporation of functional monomers during polymerization run into the problem of catalyst poisoning caused by the interaction of organic functionalities with the catalyst center [129].

The following methods have been suggested [130] to improve the polymerizability or copolymerizability of polar monomers by Ziegler-type catalysts:

- The polymerizable double bond is isolated from the heteroatom by a spacer, typically consisting of a long sequence of methylene units or a rigid cyclic unit
- The heteroatom is shielded by sterically demanding groups
- The electron-donating character of the heteroatom is decreased via attachment of electron-withdrawing substituents on or adjacent to it
- The polar monomers are precomplexed with a Lewis acid, typically an organoaluminum compound
- The catalyst components are chosen so that the deleterious effect of the heteroatom is minimized

Interest in homogeneous olefin polymerization catalysts, especially group 4 metallocenes has caused a dramatic increase in the number of publications describing the synthesis of functionalized polyolefins by direct copolymerization. Many soluble metallocenes, such as bridged zirconocenes, have much better ability to incorporate higher α-olefins than do Ti-based Ziegler–Natta catalysts. This also makes them better suited for copolymerizations involving, often very bulky, functional comonomers.

The copolymerization of a polar comonomer with nonpolar olefins by coordination polymerization is thought to be possible if the insertion of the polar comonomer takes place on the same active catalyst center as the nonpolar olefin according to the Cossee–Arlman mechanism [131, 132]. The prerequisite for this is that the polar comonomer coordinates to the metal center by its C=C double bond rather than by its polar group [133].

The most studied polar comonomers are those containing a functional group directly bound to the olefinic carbon. These include alkyl acrylates, vinyl ethers, and vinyl halides. Experimental and computational studies have elucidated the characteristic difficulties in copolymerizations of those comonomers with early- or late-transition-metal catalysts [134–138]. The coordination of the polar comonomers tends to be sterically and electrically unfavorable compared with the coordination of nonpolar olefins, and thus the incorporation rates are slow. An even more severe hindrance to successful copolymerization is the high barrier to subsequent monomer insertion after, for example, an inserted methyl acrylate unit, owing to the strong binding of the monomer polar end to the catalyst, i.e., formation of a stable chelate. On the other hand, in investigations of the reactions of vinyl chloride with group 4 metal catalysts [136] and a tantalum hydride model complex [133], 1,2-insertion of the vinyl chloride was found to be followed by selective β-Cl elimination. This means that in copolymerizations with nonpolar olefins, vinyl chloride acts as a chain transfer agent and no chlorine is incorporated into the polymer [139].

In our studies, functional long-chain alkene comonomers with different electronic and steric environments were selected for copolymerization experiments. Most of these comonomers can be considered derivatives of 10-undecenoic acid,

which means that they contain a long spacer of methylene carbons between the polymerizable double bond and the polar group. The spacer fades out the direct electronic effect of the polar group on the double bond and makes chelate formation after comonomer insertion improbable. Additionally, the effect of the polar groups on the electron density of the double bond is weak over the spacer of many atoms. Hence, the reactions of the polar group and the double bond can be considered as competing, but fairly independent of each other. On this basis it was anticipated that random-type copolymerization of these comonomers with ethylene and propylene would be possible.

4.1.1 Copolymerization Behavior of Oxygen-Functional Alkenes

Several alcohol-, ether-, acid-, ester- and ketone-functional alkenes (Fig. 12) were tested as comonomers in polymerization experiments [19, 21] A bridged zirconocene complex *rac*-Et(Ind)$_2$ZrCl$_2$ was selected as catalyst for the studies because it is a relatively good copolymerization catalyst and capable of both ethylene and propylene polymerizations. MAO was used as cocatalyst. MAO and the comonomers were pre-contacted for 15 min in the reactor just before the start of the polymerization.

The catalyst activity dropped significantly in the presence of every one of the oxygen-functional comonomers. As depicted in Fig. 13, of the different alcohols the more shielded ones (**6**, **8**) induced the least decrease in activity in propylene copolymerizations. The length of the spacer between the alcohol group and the double bond had no effect on the decline in activity. Comparison of the alcohol- and ether-functional comonomers (**4** versus **12** and **13**) in ethylene copolymerization showed that the catalyst activity was on the same level for all three comonomers. This means that methyl and trimethylsilyl groups are not good protecting groups for oxygen atoms. Among the carbonyl-containing comonomers, the carboxylic acid **15** and the more shielded ester **17** performed best in terms of catalyst activity, whereas the ketone comonomer **18** almost completely killed the catalyst.

In the studies of copolymerizations with propylene [19], it was found that a longer spacer favors the copolymerizability of the oxygen-functional comonomer. Double the amount of 10-undecen-1-ol **4** was incorporated into the polymer chain compared with the amount of 5-hexen-1-ol **5**. The comonomer **6** with methyl branches at α-position to the vinyl group did not copolymerize at all. The reactivities of carbonyl-functional comonomers **15** and **17** were about the same or slightly higher than the reactivity of 10-undecen-1-ol. A similar trend was found in the ethylene copolymerizations, where ether comonomers were incorporated to about the same degree as 10-undecen-1-ol (Fig. 14) [21].

From the different reactions of those comonomers with MAO known from the NMR studies [140, 141], it can be concluded that the formation of aluminum alkoxides is not crucial for comonomer incorporation. However, nonfunctional 1-undecene exhibited the highest relative reactivity. This could be inferred to derive from the smaller size of the comonomer, which does not react with aluminum-containing cocatalyst species.

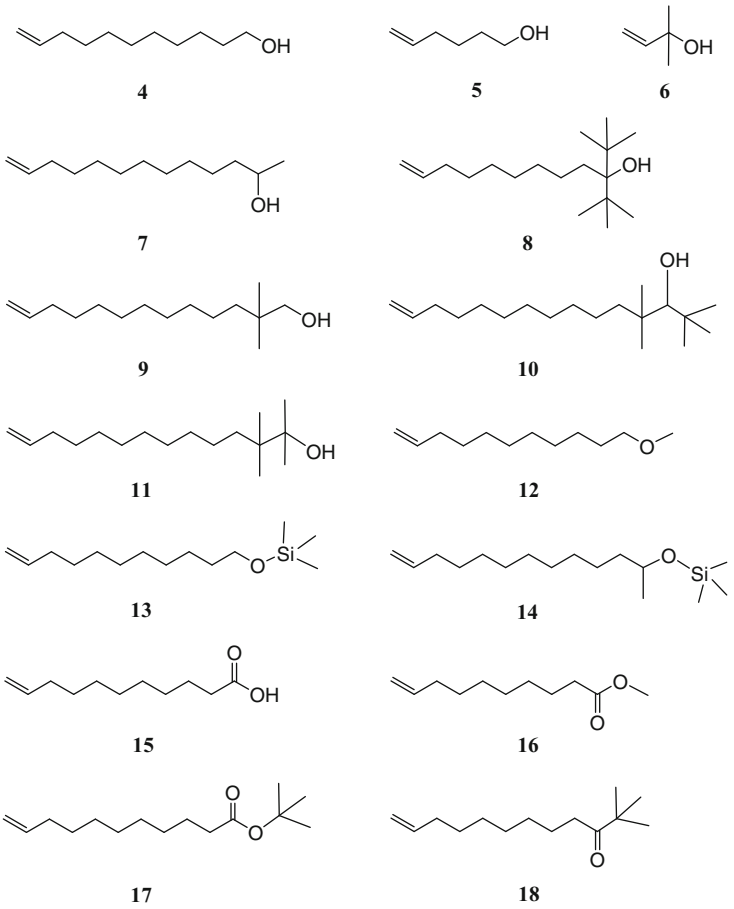

Fig. 12 Oxygen-functional comonomers: 10-undecen-1-ol (**4**); 5-hexen-1-ol (**5**); 2-methyl-3-buten-2-ol (**6**); 12-tridecen-2-ol (**7**); 2,2-dimethyl-3-(1,1-dimethylethyl)-11-dodecen-3-ol (**8**); 2,2-dimethyl-12-tridecen-1-ol (**9**); 2,2,4,4-tetramethyl-14-pentadecen-3-ol (**10**); 2,3,3-trimethyl-13-tetradecen-2-ol (**11**); 10-undecenyl methyl ether (**12**); 10-undecenyl trimethylsilyl ether (**13**); 12-tridecen-2-yl trimethylsilyl ether (**14**); 10-undecenoic acid (**15**); methyl 9-decenoate (**16**); *tert*-butyl 10-undecenoate (**17**); and 2,2-dimethyl-11-dodecen-3-one (**18**)

4.1.2 Copolymerization Behavior of Nitrogen-Functional Alkenes

Thirteen differently substituted long-chain amide- and amine-functional comonomers (Fig. 15) were studied in ethylene and propylene copolymerizations carried out with catalyst *rac*-Et(Ind)$_2$ZrCl$_2$ (for ethylene) or *rac*-Me$_2$Si(2-MeInd)$_2$ZrCl$_2$ (for propylene) [22]. As for the oxygen-functional comonomers, MAO was used as cocatalyst. Amide-functional comonomers were found to depress the catalyst activity even with high excess of MAO (Al/comonomer 40–80 mol/mol). Slightly less poisonous were monomers **19** and **20**, which contain active hydrogens

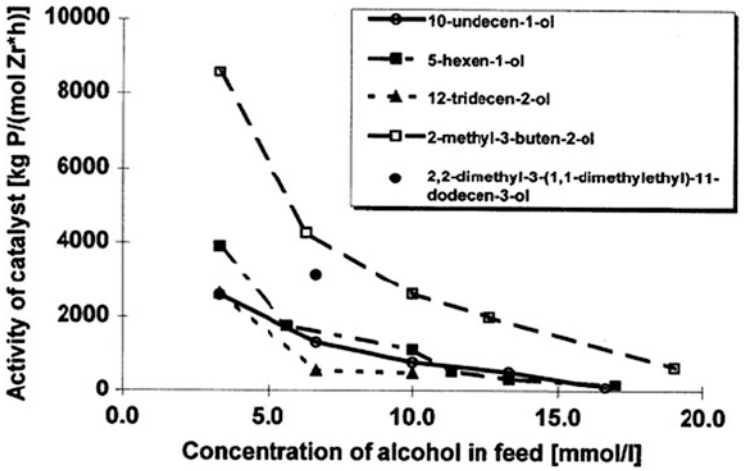

Fig. 13 Effect of different alcohol comonomers on the activity of the catalyst $Et(Ind)_2ZrCl_2$/MAO in propylene copolymerizations. Polymerization conditions: $T_p = 30°C$, $p_{propylene} = 3.0$ bar, Al/Zr = 4,000 mol/mol. Reprinted from [19], with kind permission from Elsevier

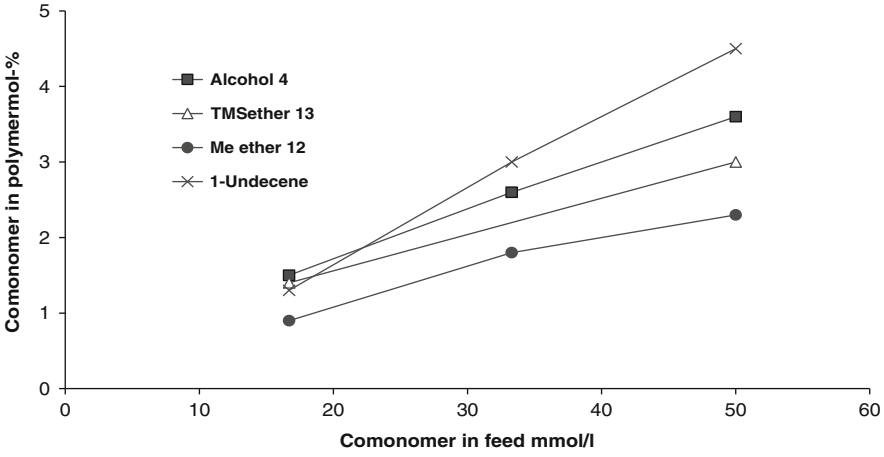

Fig. 14 Reactivity of different comonomers in copolymerizations with ethylene. Polymerization conditions: $T_p = 60°C$, $P_{ethylene} = 1.5$ bar, Al/comonomer = 4.0 mol/mol. Reprinted from [21], with kind permission from John Wiley and Sons

and are thus capable of reacting with TMA or MAO. No significant differences were observed in the dimethyl-, diethyl-, and diisopropyl-substituted amides.

Compared with the amides, the amine comonomers **24–31** were much better tolerated by the catalyst system. In ethylene copolymerizations, the catalyst activity remained at a moderate level, i.e., 1,000–3,000 kg polymer/(mol Zr h), when Al/comonomer ratios were 4–10 mol/mol. In the comparison of different amines,

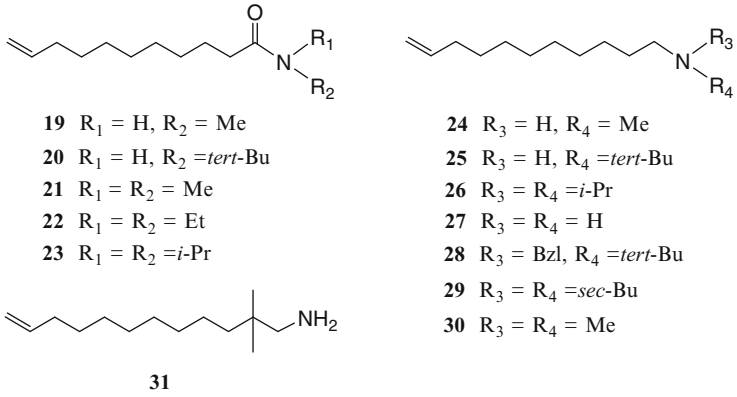

Fig. 15 Nitrogen-functional comonomers: *N*-methyl-10-undecenamide (**19**); *N*-*tert*-butyl-10-undecenamide (**20**); *N*,*N*-dimethyl-10-undecenamide (**21**); *N*,*N*-diethyl-10-undecenamide (**22**); *N*,*N*-diisopropyl-10-undecenamide (**23**); *N*-methyl-10-undecenylamine (**24**); *N*-*tert*-butyl-10-undecenylamine (**25**); *N*,*N*-diisopropyl-10-undecenylamine (**26**); 10-undecenylamine (**27**); *N*-benzyl-*N*-*tert*-butyl-10-undecenylamine (**28**); *N*,*N*-di-sec-butyl-10-undecenylamine (**29**); *N*,*N*-dimethyl-10-undecenylamine (**30**); and 2,2-dimethyl-11-dodecenylamine (**31**)

the increased bulkiness around nitrogen was found slightly to favor the catalyst activity.

Despite the low catalyst activity, all studied amides **19–23** formed copolymers with ethylene and propylene. The maximum amount of amide incorporated was 1.3 mol% with ethylene and 0.96 mol% with propylene. In the copolymerizations of amines with ethylene, the highest comonomer contents were on the same level (1.2 mol%), even though much higher comonomer concentrations could be used in the polymerizations. It seems that when the functional comonomers are better masked by the cocatalyst, the reactivities are at the same time decreased. Nonetheless, even the unhindered primary and secondary amines with acidic hydrogens were incorporated in the polymer chain. In this respect, the amines behave much like the alcohols and ethers, whereas amides resemble the less-shielded esters.

4.1.3 Properties of Functionalized Copolymers

The formation of true copolymers was confirmed in all copolymers studied by ^{13}C-NMR. The comonomers were present as isolated units arising from random-type incorporation of the comonomers. No consecutive comonomer units were detected by NMR, which means either that the concentration of comonomer dyads was below the sensitivity of the ^{13}C-NMR measurements or that formation of the dyads was suppressed. In copolymerizations of ethylene and higher α-olefins, the bridged bis(indenyl)-type metallocene catalysts, such as *rac*-Et(Ind)$_2$ZrCl$_2$,

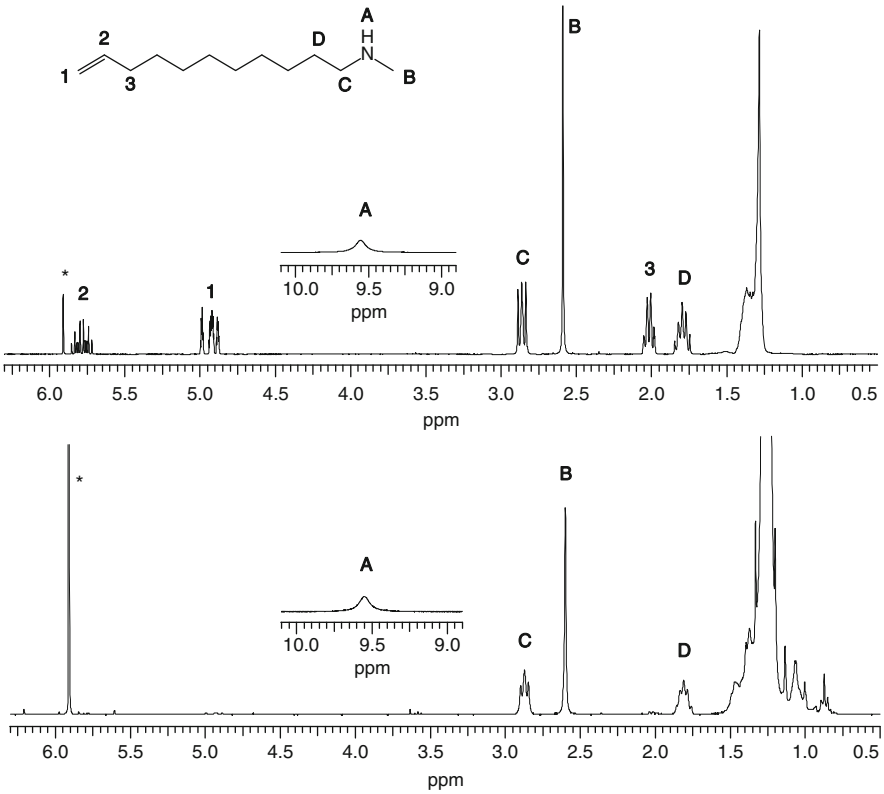

Fig. 16 ^{1}H-NMR spectra of amine 24 (*above*) and poly(ethylene-*co*-24) containing 1.3 mol% of amine units (*below*). The *asterisk* denotes a solvent resonance. Reprinted from [22], with kind permission from Springer Science and Business Media

have a tendency to form slightly alternating structures because of the lower relative reactivity of the bulkier comonomer at the comonomer propagating end [142]. The NMR and FTIR investigations revealed that in most cases the functional group in the copolymer was the same as that in the comonomer before polymerization. An example is the secondary amine **24** shown in Fig. 16. The absence of resonances from the free comonomer shows that it has been effectively removed by the washing procedure. As an exception, the trimethylsilyl ether functionality of comonomer **13** has been converted to the corresponding alcohol, as is clear from the FTIR (Fig. 17) and NMR spectra.

The NMR studies of copolymers containing an amide comonomer revealed some peculiarities. In all amide copolymers the amount of saturated end groups was higher than the amount of double bonds. Termination by chain transfer to aluminum results in the polymer chains having Al–C bonds, which normally undergo hydrolysis to saturated end groups during the polymer workup [140] . It has been reported that transfer to aluminum, which is normally a minor chain termination mechanism in metallocene-mediated polymerizations, may become

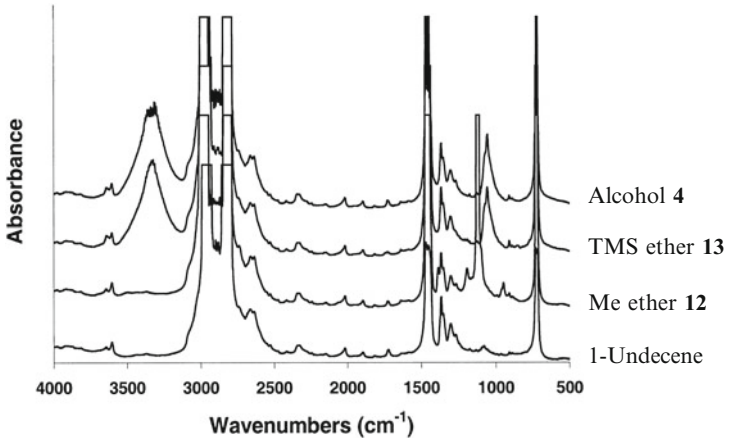

Fig. 17 IR spectra of ethylene copolymers with 1.3–1.8 mol% of functional units. Comonomers: alcohol **4**, trimethylsilyl ether **13**, methyl ether **12**, and 1-undecene. Reprinted from [21], with kind permission from John Wiley and Sons

dominant if the monomer insertion is delayed, as it is in cyclopolymerization of 1,5-hexadiene [143] and ethylene copolymerization with allylbenzene. In the ^{1}H-NMR spectra of ethylene–amide copolymers there was also a triplet signal at δ 3.5 ppm, which is typical of primary alcohols. The presence of hydroxymethylene groups in these copolymers was confirmed by ^{13}C-NMR spectroscopy (Fig. 18). A reasonable explanation for the emergence of the hydroxyl groups is as follows: since the polymer slurry was brought into contact with air a few minutes before the acidic ethanol was added, a fraction of the Al-functional chain ends may have been oxidized by oxygen and subsequently converted to hydroxyl groups by alcoholysis [18, 144]. However, this cannot explain the trace amounts of similar types of hydroxyl groups seen in the ^{1}H-NMR spectra of some of the propylene–amide copolymers. On this basis, it seems probable that a fraction of the amide functionalities was reduced to primary alcohol groups during either the polymerization or the acidic workup [145]. In ethylene–amide copolymers where the amount of hydroxyl groups was higher, it was not possible by NMR to differentiate between the hydroxyl groups at polymer chain ends and at the end of comonomer side chains.

Molar mass distributions of the prepared copolymers were measured by gel permeation chromatography (GPC). Relative to the molar masses of the corresponding homopolymers, the molar masses of the functionalized copolymers were always lower. This argues in favor of the ability of the functional comonomers to terminate the propagation of the polymer chain. The decreasing effect on the molar mass was most prominent with amides and amines. In general, the functional comonomers had a greater lowering effect on molar mass in the ethylene polymerizations. However, the molar masses of propylene copolymers were also

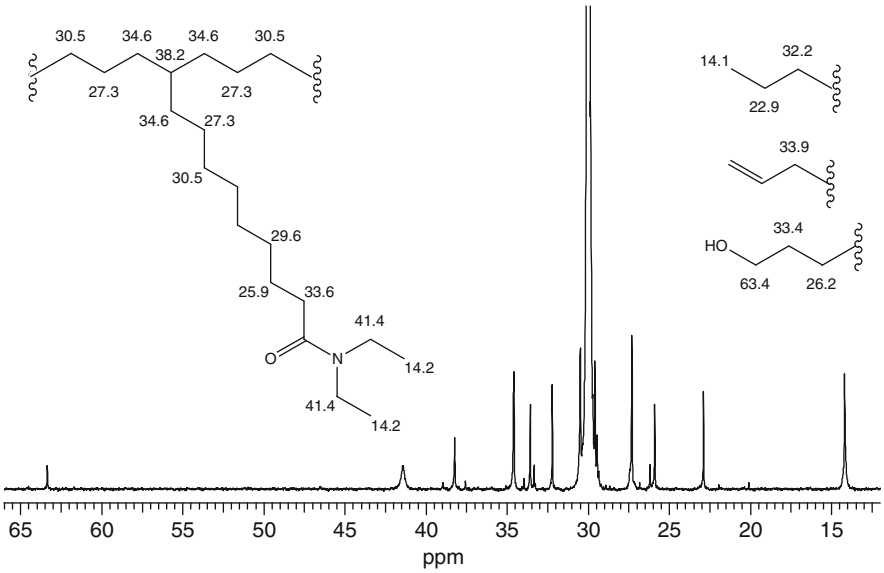

Fig. 18 ^{13}C-NMR spectrum of poly(ethylene-*co*-22) with 1.3 mol% of amide units. Reprinted from [22], with kind permission from Springer Science and Business Media

low because the complexes that were used are not capable of forming high molar-mass polypropylene.

As discussed above, NMR studies suggested that chain transfer to aluminum is an important chain-transfer mechanism especially in the copolymerizations involving amides or amines as comonomers. A comparison with the nonfunctional 1-undecene also demonstrates that the functional comonomers have a greater effect on the molar masses than do simple α-olefins [21]. In all cases, the molar mass distributions remained narrow, as is typical for single-site catalysts. This finding is contradictory to the results reported for ethylene-10-undecen-1-ol copolymerizations carried out with non-bridged zirconocene/MAO, where significant broadening of the molar mass distributions was observed [146]. The melting points of the homopolyethylenes prepared with the metallocene catalyst *rac*-Et(Ind)$_2$ZrCl$_2$ were measured by differential scanning calorimetry (DSC) to be 135–137°C. Incorporation of functional comonomer as side chains to the polyethylene chain resulted in a decrease in the melting temperatures of the copolymer, as illustrated in Fig. 19. The lower heat of fusion values with the increasing comonomer content provide additional support for lowering of the polymer crystallinity due to side chains. In a comparison with the nonfunctional comonomer 1-undecene [21], the change in the melting point with functional comonomers was found to follow approximately the same trend. This demonstrates that the incorporation of functional comonomers is random, and that the chain structure of the functionalized copolymers is similar to that of ethylene-α-olefin copolymers prepared with single-site catalysts.

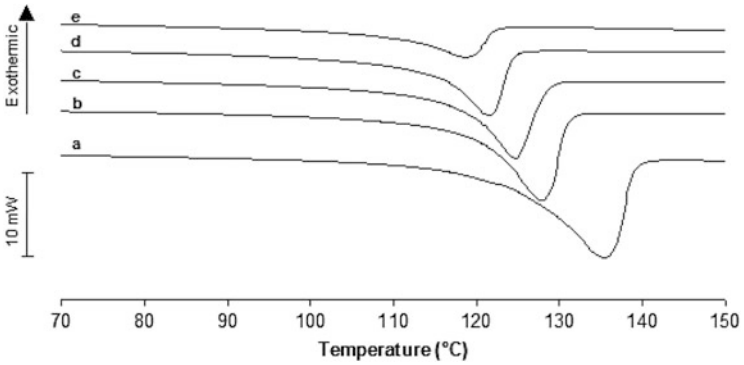

Fig. 19 DSC melting curves of ethylene homopolymer (*a*) and ethylene/10-undecen-1-ol copolymers containing 0.7 (*b*), 1.4 (*c*), 2.6 (*d*), and 3.6 mol% (*e*) of 10-undecen-1-ol. Data from the second heating are presented; heating rate 10°C/min

The melting points of the propylene homopolymers synthesized by zirconocene catalysts *rac*-Et(Ind)$_2$ZrCl$_2$ and *rac*-Me$_2$Si(2-MeInd)$_2$ZrCl$_2$ were 138°C and 148°C, respectively. In the case of amide **23**, a 12° lowering of the melting point (T_m) was obtained with incorporation of 1 mol% comonomer. All copolymers exhibited just one melting transition, which once again is an indication of homogeneous structure.

4.2 Polymerization of Weakly Interacting Comonomers

The metallocene-catalyzed polymerizations of Lewis acidic monomers normally proceed well if the electronic influence of the heteroatom (B, Si, Al) is diminished by a long spacer. However, when the heteroatom locates in the vicinity of the double bond, its behavior at the metallocene cation is altered. This was clearly seen in the studies of Guram et al. [147, 148], where the vinyl-Si(CH$_3$)$_3$ was found to coordinate with the cationic metallocene strongly via a secondary 2,1-insertion mechanism. This was explained as being due to the electropositive nature of silicon, which drives the electron density at the internal olefinic carbon and therefore favors the 2,1-insertion (Scheme 3a) [147, 148]. In contrast to vinyl-Si(CH$_3$)$_3$, allyl-Si(CH$_3$)$_3$ was found to coordinate with the metallocene catalyst via the primary 1,2-insertion mechanism [147]. The behavior of allylsilanes was rationalized on the basis of the formed polar transition state (Scheme 3b), which was stabilized by the β-effect of silicon [149]. This was also the reason for the promoted β-hydrogen abstraction after allylsilane insertions in the studies of Guram [148], Byun [150], Brandow [151], and Casey [152].

In our studies [23], ethylene was copolymerized with vinyl-Si(CH$_3$)$_3$ using Et(Ind)$_2$ZrCl$_2$/MAO catalyst, and the influence of the 2,1-insertion in the polymerization performance was seen in the weak comonomer uptake, low molar mass, and

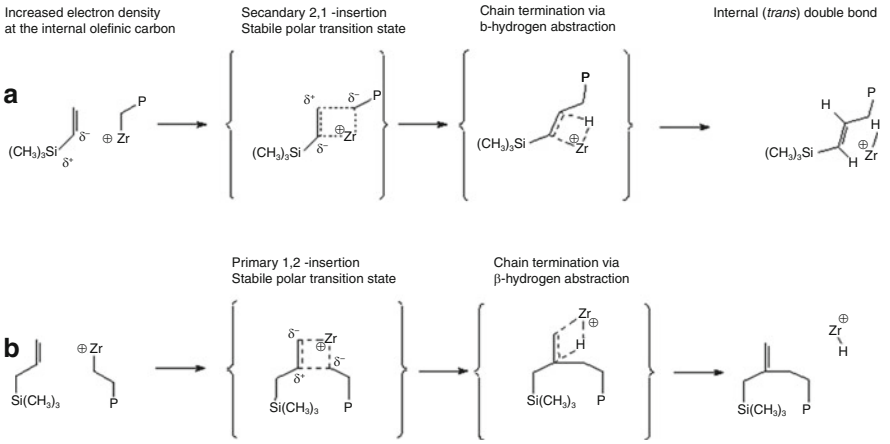

Scheme 3 Dominating insertion and termination mechanism of (**a**) vinyl-$Si(CH_3)_3$ and (**b**) allyl-$Si(CH_3)_3$ on the metallocene catalyst

decreased catalyst activity (Table 7, compare run 1 with runs 2–4). The strong presence of secondary insertion was confirmed by ^{1}H-NMR analysis, which revealed resonances that can be attributed to internal double bonds in the *trans*-position, formed after β-hydrogen abstraction of secondary inserted vinyl-$Si(CH_3)_3$.

In contrast to the vinyl-$Si(CH_3)_3$, the copolymerization of allyl-$Si(CH_3)_3$ and ethylene proceeded better because the comonomer uptake was clearly higher (Table 7, runs 5–9). However, these polymerizations also suffered from low molar mass copolymer and reduced catalyst activity. Both these disadvantages are in agreement with the above explanation of the formation of stable polar transition states that reduce the propagation rate and allow the chain termination reaction to take place. This hypothesis was further supported by the ^{1}H-NMR analysis, which showed an overwhelming concentration of chain-end allylic silane groups (Fig. 20a), which were obviously formed after primary 1,2-insertion of allyl-$Si(CH_3)_3$ (Scheme 3b) [23].

As an extension to the allylic silane groups formed in the chain end in polyethylene-*co*-allyl-$Si(CH_3)_3$, a clear indication of internal vinylene unsaturation was also found (Fig. 20a, triplet at 5.19 ppm [153], $J = 7.5$ Hz). Mechanistically, this unsaturation can be explained by the allylic activation taking place after the chain termination of primary inserted allyl-$Si(CH_3)_3$ [23]. Most interestingly, both of these unsaturations were in the allylic position of silicon and were therefore sensitive to electrophilic substitution [149]. This was seen when the normal acidic work-up procedure (after the polymerization step) was extended overnight, whereby all of the chain end and most of the internal allylic silane groups were cleaved off (Fig. 20b) [23].

In the next step, ethylene was copolymerized with 3-butenyl-$Si(CH_3)_3$ and the results were compared with those of the other copolymerizations [23]. With Et$(Ind)_2ZrCl_2$/MAO as catalyst, the 3-butenyl-$Si(CH_3)_3$ behaved like 1-alkenes if

Table 7 Metallocene/MAO-catalyzed copolymerization results

Run	Comonomer	Feed (mol/mol)	Polymer (mol%)	Activity (kg/mol P h)	M_w (kg/mol)	M_w/M_n
1	–	–	–	10,000	450	3.7
2	Vinyl-Si$(CH_3)_3$	0.25	0.3	4,400	92	2.1
3	Vinyl-Si$(CH_3)_3$	0.50	0.5	2,600	63	2.1
4	Vinyl-Si$(CH_3)_3$	1.0	0.7	1,300	39	2.0
5	Allyl-Si$(CH_3)_3$	0.25	1.4	6,100	48	2.0
6	Allyl-Si$(CH_3)_3$	0.35	1.8	5,800	45	2.0
7	Allyl-Si$(CH_3)_3$	0.50	2.3	5,300	38	2.0
8	Allyl-Si$(CH_3)_3$	1.0	3.7	1,900	25	2.0
9	3-Butenyl-Si$(CH_3)_3$	0.35	1.9	5,200	240	3.4
10	4-Pentenyl-Si$(CH_3)_3$	0.25	0.5	5,500	380	3.9
11	4-Pentenyl-Si$(CH_3)_3$	0.8	1.8	7,300	180	3.1
12	5-Hexenyl-Si$(CH_3)_3$	0.25	1.3	11,000	260	3.2
13	5-Hexenyl-Si$(CH_3)_3$	1.0	4.7	17,000	140	2.9
14	1-Hexene	0.35	2.0	13,000	240	2.9
15	1-Decene	0.25	1.4	12,000	260	3.1

Data from [23]
Conditions: $Et(Ind)_2ZrCl_2 = 1$ μmol; Al/Zr = 2,000; $P_{ethylene} = 0.7$ bar; $T = 40°C$; time = 20 min; toluene 300 mL
P Polymer

only the comonomer uptake and the molar mass of the copolymer are observed (Table 7, compare run 9 with runs 14–15). On the other hand, the polymerization performance of 3-butenyl-Si$(CH_3)_3$ also resembled that for allyl-Si$(CH_3)_3$ because the catalyst activity remained low and only chain-head groups formed after 1,2-insertion were present (Fig. 21b, doublet at 4.82 ppm, chain-head vinylidene after β-hydrogen abstraction). These strong indications for absence of 2,1-insertion were slightly odd because there were clear signs of secondary 2,1-monomer insertion when longer monomers were copolymerized with ethylene (Figs. 21a and 22a–c, resonances at 5.2–5.5 ppm). The electropositive nature of silicon would explain this behavior for allyl-Si$(CH_3)_3$, but not for 3-butenyl-Si$(CH_3)_3$ as then it should favor the 2,1-insertion (like vinylsilanes, but not as strongly). One explanation for these is that the 3-butenyl-Si$(CH_3)_3$ does also insert via a 2,1-mechanism but after that the chain termination is hindered, e.g., for steric reasons. This would also explain the observed low catalyst activities because the coordination of incoming monomer is normally slowed down when the former monomer is inserted via a 2,1-mechanism.

Like 3-butenyl-Si$(CH_3)_3$, the polymerization performance of 4-pentenyl-Si$(CH_3)_3$ (silane monomer of one methylene longer) was slightly different to that obtained for 1-alkenes (Table 7, compare runs 11–12 with runs 14–15) [23]. First of all, no sign of "positive comonomer effect" was observed, and the comonomer uptake was poorer. In addition, the ^{1}H-NMR spectra showed that the resonances at 5.2–5.5 ppm appeared more clearly in the spectrum of polyethylene-*co*-4-pentenyl-Si$(CH_3)_3$ than in the spectrum of polyethylene-*co*-1-alkene (Fig. 22c versus Figs. 21a and

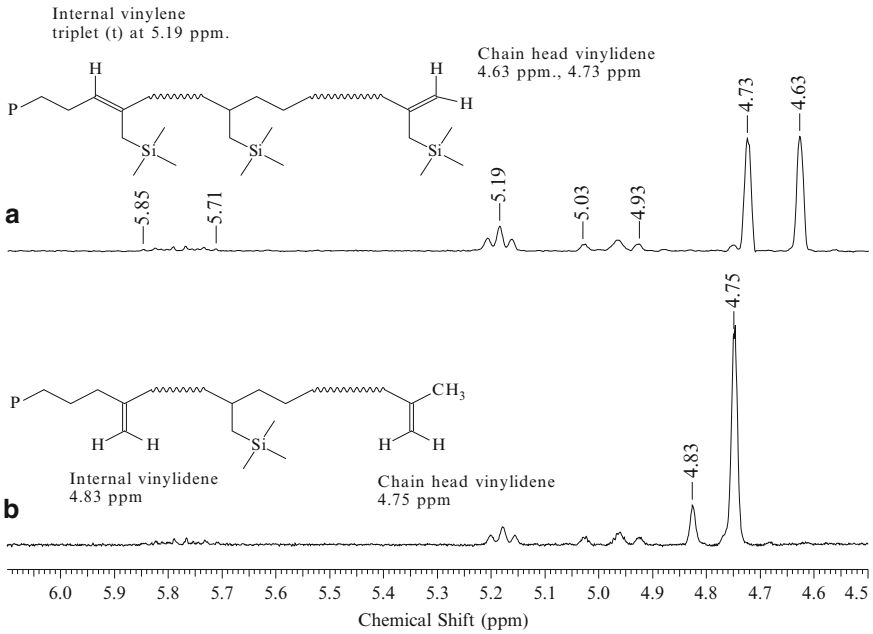

Fig. 20 Unsaturated area in ^{1}H-NMR spectra of polyethylene-*co*-allyl-Si(CH_3)$_3$ (see Table 7, run 7) after 2 h in acidic ethanol (normal work-up) (**a**), and after 24 h in acidic ethanol (**b**). Reprinted with permission from [23]. Copyright American Chemical Society

22a, b). The multiple/overlapping resonances at 5.4–5.5 ppm in ^{1}H-NMR spectrum are ordinarily explained by the internal vinylene unsaturation (*cis* + *trans*) formed after chain termination of secondary inserted 1-alkene (Scheme 4a), while the small resonances at 5.2–5.3 ppm are excluded [154]. However, now these resonances formed a clear coupling pattern (Fig. 22c, two doublets at 5.21–5.29 ppm., J(d) = 8 Hz, J(dd) = 15 Hz; and two triplets at 5.41 and 5.46 ppm., J(t) = 6 Hz, J(dt) = 15 Hz), which can be assigned to microstructure where the internal *trans*-vinylene unsaturation locates next to the branching point [153]. These kinds of internal unsaturations can be explained by the "allylic activation" mechanism [76, 142, 153, 155–157], which is also in agreement with our results (allylic activation and propagation after chain termination of 2,1-inserted comonomer; Scheme 4b) [23].

Finally, the polymerization performance of 5-hexenyl-Si(CH_3)$_3$ resembles well that obtained for 1-alkenes (Table 7, compare runs 12–13 with runs 14–15). Both of the comonomers resulted in similar results regarding the catalyst activities (positive comonomer effect) and the comonomer uptake. Also, the molar masses were decreased as much when compared with the molar mass of the homopolyethylene (Table 7, run 1) [23].

The study was extended by polymerizing olefins with monomer containing a dimethylphenylsilane group. The phenylsilane moiety was separated from the double bond by six methylene groups [7-octenyl-Si(CH_3)$_2$Ph] and that was

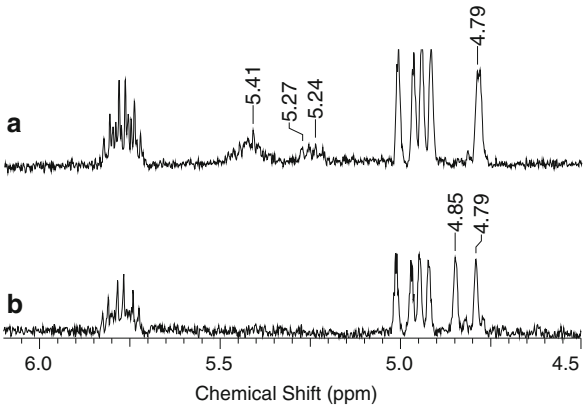

Fig. 21 The ^{1}H-NMR spectra of (**a**) polyethylene-*co*-1-hexene and (**b**) polyethylene-*co*-3-butenyl-Si(CH_3)$_3$. Reprinted with permission from [23]. Copyright American Chemical Society

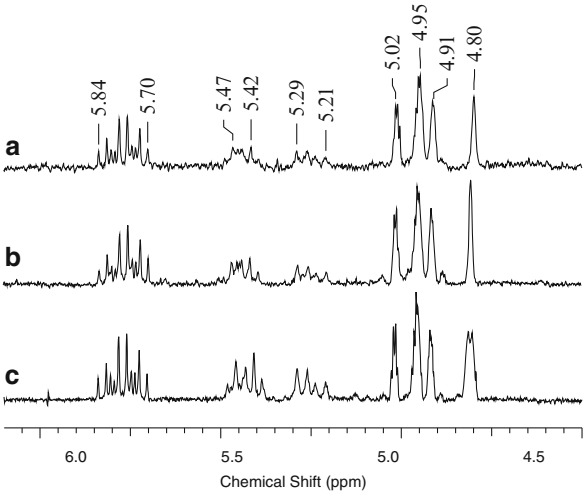

Fig. 22 The ^{1}H-NMR spectra of (**a**) polyethylene-*co*-1-decene, (**b**) polyethylene-*co*-5-hexenyl-Si(CH_3)$_3$, and (**c**) polyethylene-*co*-4-pentenyl-Si(CH_3)$_3$. Reprinted with permission from [23]. Copyright American Chemical Society

expected to be sufficient to hinder the electronic influence of silicon. Still, the polymerization performance of phenylsilane-containing monomer raises some questions from the perspective of the (active) benzyl ring because it has been found to interact with the electron-deficient metal centers through the π-aromatic system [158]. To study the polymerization performance of 7-octenyl-Si(CH_3)$_2$Ph, it was polymerized with ethylene [24] and propylene [25] and the microstructures of the formed copolymers (e.g., end groups, regio- and stereo-defects) were analyzed thoroughly. Finally, the results were compared with those obtained for polyethylene-*co*-1-decene and polypropylene-1-dodecene, but no clear deviations were observed. This indicated that there was no real interaction between the phenylsilane moiety and the cationic metal center of the metallocene catalyst [24, 25].

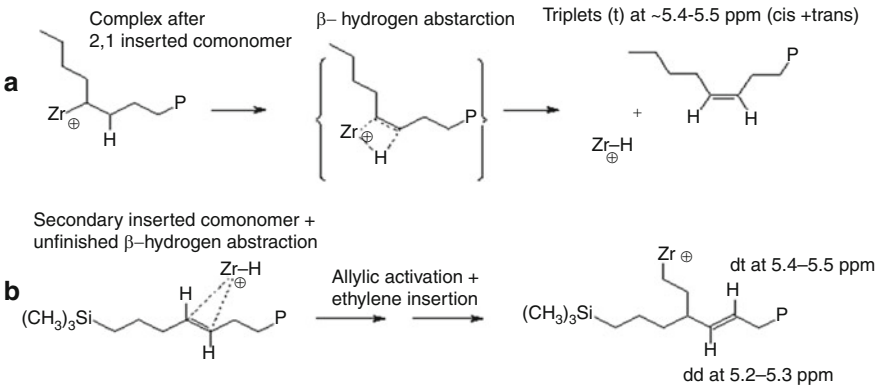

Scheme 4 The mechanisms for different unsaturations in the polyethylene chain; *P* polyethylene chain, *C* comonomer chain [23]

5 Functional Copolymers as Compatibilizers in Polyolefin Blends and Composites

Polymer–polymer blends are finding extensive application in the development of new materials. As an example, immiscible blends of polyolefins and engineering plastics offer novel types of polymers that synergistically combine the properties of their components [159]. Key to the physical properties of these blends is their morphology, i.e., the size and shape of the dispersed phase [160]. The phase morphology and its stability are largely controlled by interfacial adhesion.

In addition to polymer–polymer blends, new kinds of material can be obtained by adding fillers to the polyolefin matrix. The fillers are usually inorganic materials with polar hydrophilic surfaces and therefore they attract each other by van der Waals forces. This complicates their homogeneous compounding with hydrophobic nonpolar polyolefins, especially when high filler loadings or submicron sized fillers are used. If any form of aggregate remains in the polymer matrix, they can act as flaws (crack) resulting in a drastic decrease in the toughness of the composite. In addition, most of the fillers are less than optimally bonded with the nonpolar polyolefin matrix. Strong adhesion strength between these phases is usually required to ensure adequate mechanical properties of the composites [161–163].

One way to control the blend morphology, as well the filler dispersion and filler/matrix interaction in polyolefin composites, is to apply a compatibilizer, which acts as an interfacial agent promoting adhesion between the phases. Functionalized copolymers prepared by coordination copolymerization have many advantages over functionalized polyolefins prepared by radical polymerization or grafting. Coordination polymerization gives access to stereocontrol as well as to precise control of composition, crystallinity, molar mass, and their distributions.

5.1 *Functionalized Polyethylenes as Compatibilizers for Polyethylene/Polyamide Blends*

The functionalized ethylene copolymers described in Sect. 4.1 were investigated as compatibilizers in blends of commercial low-density polyethylene (40 wt%) and polyamide 6 (60 wt%) [164]. The compatibilizers differed in comonomer type (10-undecen-1-ol, 10-undecenoic acid, *N*-methyl-10-undecenylamine) and amount (0.2–1.2 mol%) as well as in molar mass (M_w 11–136 kg/mol) and crystallinity (ΔH_m 106–190 J/g). Blends containing 5 or 10 wt% of the compatibilizer were prepared by melt mixing of the polymers in a small-scale twin-screw extruder.

Blends containing 10 wt% of metallocene-based copolymer were found to be significantly tougher and stiffer than the uncompatibilized blend. This is a clear indication of the presence of the functionalized copolymer at the polyethylene/polyamide interface, which lowers the interfacial tension. Higher values of elongation at break for the compatibilized blends provide support for enhanced adhesion between the phases. The improved compatibility was also seen in the SEM micrographs as much finer morphology and a more ragged interface between the phases in the compatibilized blends. In the blends containing hydroxyl- or carboxyl-functional polyethylenes, a higher molar mass of the compatibilizer was found to be advantageous in terms of mechanical properties. This can be explained by enhanced entanglement formation with the polyethylene phase at higher molar mass [165, 166]. On the other hand, the *N*-methylamino-functional compatibilizer also gave a substantial increase in stiffness and toughness, even though it had the lowest molar mass of all compatibilizers.

Formation of chemical linkages between the functional groups of the functionalized polyethylenes and the terminal groups of the polyamide was verified by studying the IR spectra of the blends after dissolving the pure polyamide part with formic acid. Ester groups were found in blends containing hydroxyl-functional polyethylenes, indicating a grafting reaction between the hydroxyl groups and carboxyl end groups of polyamide. Similarly, in blends containing *N*-methylamino-functional polyethylene, the presence of amide groups arising from the reaction of the secondary amino groups with the carboxyl groups of the polyamide was evidence of graft copolymer formation. Carboxyl functionalities of acid-functional polyethylenes are assumed to form amide linkages with the amine end-groups of the polyamide, though it was not possible to obtain clear evidence by IR measurement because of the overlapping peaks from polyamide. It is also known that interfacial interactions can be substantially enhanced by the formation of hydrogen bonds between the blend components, so that covalent bonding is not a prerequisite for efficient compatibilization [167].

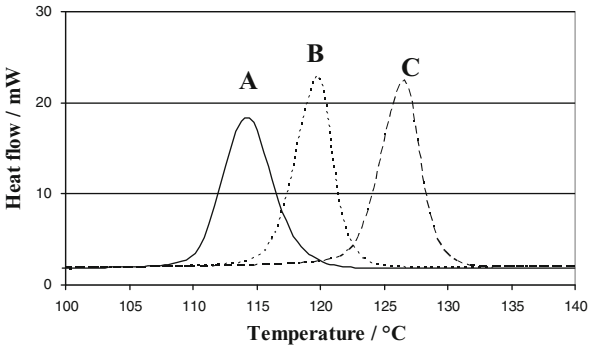

Fig. 23 DSC-cooling curves for (A) PP, (B) PP/μSi-composite (4 wt% of μSi), and (C) PP/μSi/PP-*co*-SiPh composite (4 wt% of μSi and 0.4 wt% of compatibilizer). Reprinted from [25], with kind permission from Elsevier

Table 8 Tensile properties of PP/μSi composites modified by functional PP

			Yield		Tensile	
Run	Composition	Modulus (MPa)	Strain (%)	Strength (MPa)	Strain (%)	Strength (MPa)
1	PP	860 ± 30	12.8 ± 0.3	29.1 ± 0.2	>1,500	~50
2	PP/μSi (30 wt%)	1,260 ± 30	5.2 ± 0.1	28.1 ± 0.1	500 ± 110	~26
3	+1.5 wt% PP-*co*-SiPh	1,250 ± 20	7.9 ± 0.2	31.9 ± 0.2	740 ± 30	~34
4	+1.5 wt% PP-*co*-SiF	1,240 ± 10	8.2 ± 0.1	32.3 ± 0.3	750 ± 30	~35

Data from [29]

5.2 *Weakly Interacting Compatibilizers in Polyolefin Composites*

The polyolefin composites are usually modified by a compatibilizer that contains some Lewis-basic reactive groups. Still, when a Lewis-acidic phenylsilane-functionalized compatibilizer, PE-*co*-SiPh, was used in a polyethylene/aluminum hydroxide composite, there were, indeed, some marks of influenced interaction at the filler/matrix boundary layer [28]. It was also found that phenylsilane-functionalized compatibilizer can actually react and form a covalent bond with the microsilica (μSi) filler. When polypropylene with pendant phenylsilane groups (PP-*co*-SiPh) was used as compatibilizer in a PP/μSi composite, the improved interaction between matrix and filler was seen as an increase in the crystallization temperature, i.e., stronger nucleation effect (Fig. 23) [25].

As an extension to this study, the μSi concentration in the composite was increased (from 4 wt% to 30 wt%), whereafter the influence of the PP-*co*-SiPh was also seen in the mechanical properties of the composites (Table 8, compare run 2 with run 3, increased yield and tensile values). A similar kind of increase in the mechanical properties was also achieved when a highly reactive Lewis-basic fluorosilane analogue was used in parallel (Table 8, compare run 3 .with run 4). This clearly supports the assumption that the PP-*co*-SiPh is able to form a strong bond with the μSi filler [29].

6 Outlook

Discovery of low pressure polyethylene and isotactic polypropylene 60 years ago started a material revolution that has improved the quality of life for nearly all people on earth. Today, these polyolefin materials account for more than 50% of all synthetic materials produced, ranging from commodities to various engineering level materials. The common denominator for all high-end polyolefin materials is the use of the most advanced catalyst and process technologies for manufacturing.

Further novel uses of polyolefins, as described in this paper, will most likely include their use in various composite and nanocomposite materials to further drive material property improvements. With the help of functional copolymers, polyolefins can be used in high purity applications through excellent polymer structure control, and in highly sophisticated polymer property/processing combinations where materials have been precisely developed to the specific application with the help of catalyst and process technologies.

Generally speaking, the polyolefin materials and catalysts reviewed here represent latest developments that have only partly been developed to the commercial scale. They still require optimization of the combination of feasible manufacturing and improvement in material properties. Further development is needed in adapting these novel polymerization techniques and catalyst systems to commercial scale operating conditions, while keeping in mind that existing polyolefin materials enjoy the benefits of scale that new developments need to overcome to find their way onto the market.

Even though these materials face challenges in replacing the existing high-end polyolefin materials, it is foreseen that many of these latest generation polyolefin-based materials will find their way to the people thanks to the feedstock availability, inertness, light weight, and facile large scale manufacturing technologies that gives them advantages over many other materials that have been around us for much longer than 60 years.

References

1. Severn JR, Chadwick JC (2008) Tailor-made polyolefins. Wiley-VCH, Weinheim
2. Kaminsky W (2004) J Polym Sci A 42:3911–3921
3. Mülhaupt R (2003) Macromol Chem Phys 204:289–327
4. Hoff R, Mathers RT (eds) (2010) Handbook of transition metal catalysts. Wiley, Hoboken
5. Koivumäki J, Fink G, Seppälä JV (1994) Macromolecules 27:6254–6258
6. Shiono T, Moriki Y, Soga K (1995) Macromol Symp 97:161–170
7. Imanishi Y, Naga N (2001) Prog Polym Sci 26:1147–1198
8. Shaffer TD, Canich JAM, Squire KR (1998) Macromolecules 31:5145–5147
9. Lai SY, Wilson JR, Knight GW, Stevens JC, Chum P-WS, Dow Chemical Company (1991) Elastic substantially linear olefin polymers. US Patent 5,272,236

10. Brant P, Canich JAM, Dias AJ, Bamberger RL, Licciardi GF, Henrichs PM, Exxon Chemicals (1993) Long chain branched polymers and a process to make long chain branched polymers. International Patent WO 94/07930
11. Howard P, Maddox PJ, Partington SR, BP Chemicals Ltd (1995) Polymerisation process and polyolefins obtained thereby. Patent EP 0 676 421 A1
12. Harrison D, Coulter IM, Wang S, Nistala S, Kuntz BA, Pigeon M, Tian J, Collins SJ (1998) Molecular Catalysis A 128:65–77
13. Vega JF, Santamaría A, Muñoz-Escalona A, Lafuente P (1998) Macromolecules 31:3639–3647
14. Malmberg A, Kokko E, Lehmus P, Löfgren B, Seppälä JV (1998) Macromolecules 31:8448–8454
15. Knuuttila H, Lehtinen A, Salminen H (2000) Metallocene catalyst technology in a bimodal polymerization process. In: Scheirs J, Kaminsky W (eds) Metallocene-based polyolefins. Wiley, Hoboken, pp 365–378
16. Boffa LS, Novak BM (2000) Chem Rev 100:1479–1493
17. Yanjarappa MJ, Sivaram S (2002) Prog Polym Sci 27:1479–1493
18. Seppälä J, Löfgren B, Hakala K, Helaja T, Anttila U (2001) Polym Mater Sci Eng 84:257–258
19. Hakala K, Löfgren B, Helaja T (1998) European Polym J 34:1093–1097
20. Aaltonen P, Fink G, Löfgren B, Seppälä J (1996) Macromolecules 29:5255–5260
21. Hakala K, Helaja T, Löfgren B (2000) J Polym Sci A 38:1966–1971
22. Hakala K, Helaja T, Löfgren B (2001) Polym Bull 46:123–130
23. Lipponen S, Seppälä J (2011) Organometallics 30:528–533
24. Lipponen S, Seppälä J (2002) J Polym Sci A Polym Chem 40:1303–1308
25. Lipponen S, Lahelin M, Seppälä J (2009) Eur Polym J 45:1179–1189
26. Lipponen S, Seppälä J (2004) J Polym Sci A Polym Chem 42:1461–1467
27. Lipponen S, Pietikäinen P, Vainio U, Seppälä J, Serimaa R (2007) Polym Polym Comp 15:343–355
28. Lipponen S, Seppälä J (2005) J Polym Sci A Polym Chem 43:5597–5608
29. Lipponen S, Nykänen A, Ruokolainen J, Seppälä J (2011) Polym Comp 32:1835–1841
30. Kaminsky W, Engehausen R, Zoumis K, Spaleck W, Rohrmann J (1992) Makromol Chem 193:1643–1651
31. Wigum H, Tangen L, Stövneng JA, Rytter E (2000) J Polym Sci A 38:3161–3172
32. Heiland K, Kaminsky W (1992) Makromol Chem 193:601–610
33. Denger C, Haase U, Fink G (1991) Makromol Chem Rapid Commun 12:697–701
34. Uozumi T, Soga K (1992) Makromol Chem 193:823–831
35. Yano A, Hasegawa S, Kaneko T, Sone M, Sato M, Akimoto A (1999) Macromol Chem Phys 200:1542–1553
36. Suhm J, Schneider MJ, Mülhaupt R (1998) J Mol Catal A Chem 128:215–227
37. Karol FJ, Kao S-C, Wasserman EP, Brady RC (1997) New J Chem 21:797–805
38. Kaminsky W, Schlobohm M (1986) Makromol Chem Macromol Symp 4:103–118
39. Kaminsky W, Külper K, Brintzinger H-H, Wild F (1985) Angew Chem 97:507–508
40. Ewen JA (1984) J Am Chem Soc 106:6355–6364
41. Chien JCW, He D (1991) J Polym Sci A 29:1585–1593
42. Busico V, Cipullo R, Caporaso L, Angelini G, Segre AL (1998) J Mol Catal A Chem 128:53–64
43. Carvill A, Tritto I, Locatelli P, Sacchi MC (1997) Macromolecules 30:7056–7062
44. Busico V, Cipullo R (1995) J Organomet Chem 497:113–118
45. Lehmus P, Härkki O, Leino R, Luttikhedde HJG, Näsman JH, Seppälä JV (1999) Macromol Chem Phys 199:1965–1972
46. Kokko E, Malmberg A, Lehmus P, Löfgren B, Seppälä J (2000) J Polym Sci A Polym Chem 38:376–388
47. Beck S, Brintzinger H-H (1998) Inorg Chim Acta 270:376–381
48. Ewen JA, Jones RL, Razavi A, Ferrara JD (1988) J Am Chem Soc 110:6255–6256

49. Herfert N, Montag P, Fink G (1993) Makromol Chem 194:3167–3182
50. Spaleck W, Antberg M, Rohrmann J, Winter A, Bachmann B, Kiprof P, Behm J, Herrmann WA (1992) Angew Chem Int Ed Engl 31:1347–1350
51. Kokko E, Lehmus P, Malmberg A, Löfgren B, Seppälä J (2001) In: Blom R, Follestad A, Rytter E, Tilset M, Ystenes M (eds) Organometallic catalyst and olefin polymerization, catalysts for a new millennium. Springer Verlag, Berlin, pp 335–345
52. Chien JCW, Wang B-P (1990) J Polym Sci A 28:15–38
53. Stevens JC (1993) In: Proceedings of the MetCon '93, Houston, 26–28 May 1993. Catalyst Consultants, Spring House, pp 157–170
54. Wang W-J, Yan D, Zhu S, Hamielec AE (1998) Macromolecules 31:8677–8683
55. Woo TK, Fan L, Ziegler T (1994) Organometallics 13:252–2261
56. Spaleck W, Küber F, Winter A, Rohrmann J, Bachmann B, Antberg M, Dolle V, Paulus EF (1994) Organometallics 13:954–963
57. Stehling U, Diebold J, Kirsten R, Röll W, Brintzinger H-H, Jüngling S, Mülhaupt R, Langhauser F (1994) Organometallics 13:964–970
58. Schneider MJ, Suhm J, Mülhaupt R, Prosenc M-H, Brintzinger H-H (1997) Macromolecules 30:3164–3168
59. Schneider MJ, Mülhaupt R (1997) Macromol Chem Phys 198:1121–1129
60. Xu G, Ruckenstein E (1998) Macromolecules 31:4724–4729
61. Piccolrovazzi N, Pino P, Consiglio G, Sironi A, Moret M (1990) Organometallics 9:3098–3105
62. Lee I-M, Gauthier WJ, Ball JM, Iyengar B, Collins S (1992) Organometallics 11:2115–2122
63. Winter A, Rohrmann J, Antberg M, Spaleck W, Herrmann WA, Riepl H (1994) Verfahren zur Herstellung eines Olefinpolymers unter Verwendung spezieller Metallocene. European Patent Application EP 582 195
64. Barsties E, Schaible S, Prosenc M-H, Rief U, Röll W, Weyand O, Dorer B, Brintzinger H-H (1996) J Organomet Chem 520:63–68
65. Luttikhedde HJG, Leino RP, Wilén C-E, Näsman JH, Ahlgrén MJ, Pakkanen TA (1996) Organometallics 15:3092–3094
66. Lehmus P, Kokko E, Härkki O, Leino R, Luttikhedde HJG, Näsman JH, Seppälä JV (1999) Macromolecules 32:3547–3552
67. Leino R, Luttikhedde HJG, Wilén C-E, Sillanpää R, Näsman JH (1996) Organometallics 15:2450–2453
68. Leino R, Luttikhedde HJG, Lehmus P, Wilén C-E, Sjöholm R, Lehtonen A, Seppälä JV, Näsman JH (1997) Macromolecules 30:3477–3483
69. Ekholm P, Lehmus P, Kokko E, Haukka M, Seppälä JV, Wilén C-E (2001) J. Polym. Sci. Part A: Polym. Chem 39:127–133
70. Kaminsky W (1995) Macromol Symp 97:79–89
71. Ewen JA, Jones RL, Elder MJ, Rheingold AL, Liable-Sands LM (1998) J Am Chem Soc 120:10786–10787
72. 'Piemontesi F, Camurati I, Resconi L, Balboni D, Sironi A, Moret M, Zeigler R, Piccolrovazzi N (1995) Organometallics 14:1256–1266
73. Härkki O, Lehmus P, Leino R, Luttikhedde HJG, Näsman JH, Seppälä JV (1999) Macromol Chem Phys 200:1561–1565
74. Kokko E, Lehmus P, Leino R, Luttikhedde HJG, Ekholm P, Näsman JH, Seppälä JV (2000) Macromolecules 33:9200–9204
75. Thorshaug K, Støvneng JA, Rytter E, Ystenes M (1998) Macromolecules 31:7149–7165
76. Lehmus P, Kokko E, Leino R, Luttikhedde HJG, Rieger B, Seppälä JV (2000) Macromolecules 33:8534–8540
77. Dang VA, Yu L-C, Balboni D, Dall'Occo T, Resconi L, Mercandelli P, Moret M, Sironi A (1999) Organometallics 18:3781–3791
78. Blom R, Dahl IM (1999) Macromol Chem Phys 200:442–449
79. Reinking MK, Orf G, McFaddin D (1998) J Polym Sci A Polym Chem 36:2889–2898

80. Wang W-J, Kolodka E, Zhu S, Hamielec A (1999) J Polym Sci A Polym Chem 37:2494–2957
81. Malmberg A, Liimatta J, Lehtinen A, Löfgren B (1999) Macromolecules 32:6687–6696
82. Kolodka E, Wang W-J, Charpentier PA, Zhu S, Hamielec AE (2000) Polymer 41:3985–3991
83. Walter P, Trinkle S, Suhm J, Mäder D, Friedrich C, Mühlhaupt R (2000) Macromol Chem Phys 201:604–612
84. Walter P, Trinkle S, Mühlhaupt R (2001) Polym Bull 46:205–213
85. Kokko E, Wang W-J, Seppälä JV, Zhu SJ (2002) Polym Sci Part A Polym Chem 40:3292–3301
86. Stadler F, Piel C, Klimke K, Kaschta J, Parkinson M, Wilhelm M, Kaminsky W, Münstedt H (2006) Macromolecules 39:1474–1482
87. Yang Q, Jensen M, McDaniel M (2010) Macromolecules 43:8836–8852
88. Kokko E, Pietikäinen P, Koivunen J, Seppälä JV (2001) J Polym Sci A Polym Chem 39:3805–3817
89. Hamielec AE, Soares JBP (1996) Prog Polym Sci 21:651–706
90. Soares JBP, Hamielec AE (1995) Polym React Eng 3:131–200
91. Yan D, Wang W-J, Zhu S (1999) Polymer 40:1737–1744
92. Wood-Adams PM, Dealy JM, DeGroot AW, Redwine OD (2000) Macromolecules 33:7489–7499
93. Wood-Adams PM, Dealy JM (2000) Macromolecules 33:7481–7488
94. Gabriel C, Kokko E, Löfgren B, Seppälä JV, Münstedt H (2002) Polymer 43:6383–6390
95. Wang W-J, Kharchenko S, Migler K, Zhu S (2004) Polymer 45:6495–6505
96. Piel C, Stadler F, Kaschta J, Rulhoff S, Münstedt H, Kaminsky W (2006) Macromol Chem Phys 207:26–38
97. Kessner U, Kaschta J, Stadler F, Le Duff C, Drooghag X, Münstedt H (2010) Macromolecules 43:7341–7350
98. Hatzikiriakos SG (2000) Polym Eng Sci 40:2279–2287
99. Shroff RN, Mavridis H (1999) Macromolecules 32:8454–8464
100. Shroff RN, Mavridis H (2001) Macromolecules 34:7362–7367
101. Mavridis H, Shroff RN (1992) Polym Eng Sci 32:1778–1791
102. Raju VR, Smith GG, Marin G, Knox JR, Graessley WW (1979) J Polym Sci Polym Phys Ed 17:1183–1195
103. Gabriel C, Münstedt H (2002) Rheologica Acta 41:232–244
104. Laun HM (1987) Prog Coll Polym Sci 75:111–139
105. Bin Wadud SE, Baird D (2001) J Rheol 44:1151–1167
106. Janzen J, Colby RHJ (1999) Mol Struct 485–486:569–584
107. Vega JF, Fernández M, Santamaría A, Muñoz-Escalona A, Lafuente P (1999) Macromol Chem Phys 200:2257–2268
108. Shroff R, Mavridis H (1995) Appl Polym Sci 57:1605–1626
109. Walter P, Heinemann J, Ebeling H, Mäder D, Trinkle S, Mühlhaupt R (2001) In: Blom R, Follestad A, Rytter E, Tilset M, Ystenes M (eds) Organometallic catalysts and olefin polymerization. Springer, Berlin, pp 317–341
110. Trinkle S, Friedrich C (2001) Rheol Acta 40:322–328
111. Trinkle S, Walter P, Friedrich C (2002) Rheol Acta 41:103–113
112. Graessley WW (1982) Macromolecules 15:1164–1167
113. Carella JM, Gotro JT, Graessley WW (1986) Macromolecules 19:659–667
114. Garcia-Franco CA, Harrington BA, Lohse DJ (2006) Macromolecules 39:2710–2717
115. Villar MA, Faill MD, Quijada R, Santos Mauler R, Vallés EM, Galland GB, Quinzani LM (2001) Polymer 42:9269–9279
116. Wasserman SH, Graessley WW (1996) Polym Eng Sci 36:852–861
117. Starck P, Malmberg A, Löfgren B (2002) J Appl Polym Sci 83:1140–1156
118. Stadler FJ, Karimkhani V (2011) Macromolecules 44:5401–5413
119. Beigzadeh D, Soares JBP, Duever TA, Hamielec AE (1999) Polym React Eng 7:195–205

120. Malmberg A, Gabriel C, Steffl T, Münstedt H, Löfgren B (2002) Macromolecules 35:1038–1048
121. Münstedt H, Laun H (1981) Rheol Acta 20:211–221
122. Kasehagen LJ, Macosko CW (1998) J Rheol 42:1303–1327
123. Münstedt H, Kurzbeck S, Egersdörfer L (1998) Rheol Acta 37:21–29
124. Münstedt H, Steffl T, Malmberg A (2005) Rheol Acta 45:14–22
125. McLeish TCB, Milner ST (1999) Adv Polym Sci 143:195–256
126. Lohse DJ, Xenidou M, Schulz DJ, Milner ST, Fetters LJ, Wright PJ, Hadjichristidis N, Pitsikalis M, Poulos Y, Avgeropoulos A, Sioula S, Paraskeva S, Velis G, Mendelson RA, García-Franco CA, Lyon MK, Sun T, Ruff CJ (2000) Polym Mater Sci Eng 82:123–124
127. Herrmann H-F, Böhm LL (1991) Polymer Comm 32:58–61
128. Hatzikiriakos SG, Kazatchkov IB, Vlassopoulos D (1997) J Rheol 41:1299–1315
129. Datta S (1991) Directly functionalized ethylene-propylene copolymers: synthesis and applications. Spec Publ R Soc Chem 87:33
130. Boor J Jr (1979) Ziegler–Natta catalysts and polymerizations. Academic, New York, pp 531–539
131. Cossee P (1964) J Catal 3:80
132. Arlman EJ, Cossee P (1964) J Catal 3:99
133. Ittel SD, Johnson LK, Brookhart M (2000) Chem Rev 100:1169
134. Strazisar SA, Wolczanski PT (2001) J Am Chem Soc 123:4728
135. Boone HW, Athey PS, Mullins MJ, Philipp D, Muller R, Goddard WA (2002) J Am Chem Soc 124:8790
136. Stockland RA Jr, Foley SR, Jordan RF (2003) J Am Chem Soc 125:796
137. Michalak A, Ziegler T (2001) J Am Chem Soc 123:12266
138. Philipp DM, Muller RP, Goddard WA III, Storer J, McAdon M, Mullins M (2002) J Am Chem Soc 124:10198
139. Gaynor SG (2003) Macromolecules 36:4692
140. Lehtinen C, Löfgren B (1997) Eur Polym J 33:115
141. Helaja T, Hakala K, Helaja J, Löfgren B (1999) J Organomet Chem 579:164–176
142. Resconi L, Camurati I, Sudmeijer O (1999) Top Catal 7:145
143. Mogstad A-L, Waymouth RM (1992) Macromolecules 25:2282
144. Kojoh S, Tsutsui T, Kioka M, Kashiwa N (1999) Polym J (Tokyo) 31:332
145. Wendt RA, Fink G (2002) Macromol Chem Phys 203:1071
146. Aaltonen P, Löfgren B (1995) Macromolecules 28:5353
147. Guram AS, Jordan RF (1990) Organometallics 9:2190–2192
148. Guram AS, Jordan RF (1993) J Org Chem 58:5595–5597
149. Brook MA (2000) Silicon in organic, organometallic and polymer chemistry. Wiley, New York, pp 552–607
150. Byun D-J, Shin S-M, Han CJ, Kim SY (1999) Polym Bull 43:333–340
151. Brandow GC, Mendiratta A, Bercaw JE (2001) Organometallics 20:4253–4261
152. Casey CP, Carpenetti DW, Sakurai H (2001) Organometallics 20:4262–4265
153. Busico V, Cipullo R, Friederichs N, Linssen H, Segre A, Castelli VVA, van der Velden G (2005) Macromolecules 38:6988–6996
154. Camurati I, Cavicci B, Dall'Occo T, Piemontesi F (2001) Macromol Chem Phys 202:701–709
155. Busico V, Caporaso L, Cipullo R, Landriani L, Angelini G, Margonelli A, Segre AL (1996) J Am Chem Soc 118:2105–2106
156. Richardson DE, Alameddin NG, Ryan MF, Hayes T, Eyler JR, Siedle AR (1996) J Am Chem Soc 118:11244–11253
157. Margl PM, Woo TK, Blöchl PE, Ziegler T (1998) J Am Chem Soc 120:2174–2175
158. Pellecchia C, Immirzi A, Pappalardo D, Peluso A (1994) Organometallics 13:3773–3775
159. Jois YHR, Harrison JB (1996) Macromol Sci Rev Macromol Chem Phys C36:433

160. Lambla M, Yu R X, Lorek S (1989) Coreactive polymer alloys. In: Utracki LA, Weiss RA (eds) Multiphase polymers: blends and ionomers. ACS Symposium Series, vol 395. American Chemical Society, Washington, pp 67–83
161. DeArmitt C, Hancock M (2003) Filled Thermoplastics. In: Rothon RN (ed) Particulate-filled polymer composites. Rapra Technology Limited, Shawbury
162. Rothon RN, Hancock M (2003) General principles guiding selection and use of particulate materials. In: Rothon RN (ed) Particulate-filled polymer composites. Rapra Technology Limited, Shawbury
163. Ashton DP, Briggs D, Liauw CM (2003) Analytical techniques for characterising filler surface. In: Rothon RN (ed) Particulate-filled polymer composites. Rapra Technology Limited, Shawbury
164. Anttila U, Hakala K, Helaja T, Löfgren B, Seppälä J (1999) J Polym Sci A Polym Chem 37:3099
165. Padwa AR (1992) Polym Eng Sci 32:1703
166. Filippi S, Chiono V, Polacco G, Paci M, Minkova LI, Magagnini P (2002) Macromol Chem Phys 203:1512
167. Sémeril D, Passaglia E, Bianchini C, Davies M, Miller H, Ciardelli F (2003) Macromol Mater Eng 288:475
168. Kokko E (2002) Metallocene-catalyzed ethylene polymerization: long-chain branched polyethylene. Acta Polytechnica Scandinavica, Chemical Technology Series, No. 290

Adv Polym Sci (2013) 258: 233–278
DOI: 10.1007/12_2013_209

Published online: 19 April 2013

Functional Polyolefins: Synthesis and Energy Storage Applications

T.C. Mike Chung

Abstract This chapter discusses our research into the functionalization of polyolefins (PE, PP etc.) that contain polar groups (such as OH and NH_2) in the side chains and chain end, as well as polyolefin graft and block copolymers containing both a polyolefin block and functional polymer blocks (acrylic and methacrylate polymers). In the late 1980s, our research on the functionalization of polyolefins was inspired by the development of homogeneous, single-site metallocene catalysts that showed excellent copolymerization capabilities and a well-controlled polymerization mechanism. We were curious to know how to apply this newly available technology to the direct polymerization (in-reactor) process to circumvent the inevitable deactivation of the transition metal cationic active site by functional (polar) groups containing basic O, N, and halides. Throughout the past two decades, we have developed an effective approach that is centered on specially designed "reactive" comonomers and chain transfer agents. These can deliver three essential properties during the polymerization process: (1) stability (no side reaction) of the active site; (2) solubility in the polymerization media for effective incorporation; and (3) versatility for interconversion to desirable functional groups under mild reaction conditions after polymerization (preferably a one-pot process). With the conjunction of suitable metallocene catalysts, a broad range of polyolefins with "reactive" sites in the side chains or chain end were prepared, and the incorporated reactive groups were interconverted into functional groups to form side-chain- or chain-end-functionalized polyolefins. Some active sites were also transformed into "living" radical or anionic initiator to initiate graft-from polymerization of polar monomers to obtain polyolefin graft and block copolymers (such as PP-*g*-PMMA and PP-*b*-PMMA). The resulting functional polyolefins show many desirable properties and applications. This chapter focuses on applications in the area of energy storage. Specifically, I will discuss the usage of new functional

T.C.M. Chung (✉)
Department of Materials Science and Engineering, The Pennsylvania State University, University Park, PA 16802, USA
e-mail: chung@ems.psu.edu

polypropylene polymers in the formation of dielectric thin films in capacitors that show significantly higher energy and power densities.

Keywords Block copolymer · Capacitor · Crosslinked polypropylene · Energy storage · Functional polyolefin · Graft copolymer · Hydroxylated polypropylene · Metallocene · Reactive chain transfer agent · Reactive comonomer

Contents

1 Introduction

Since the discovery of high-density polyethylene (HDPE) and polypropylene (PP) in the early 1950s, the functionalization of polyolefins [1, 2] has been a scientifically challenging and industrially important area of study. The continuing interest is driven by an impetus to improve on the poor interactive properties of polyolefins and apply them to higher value products, especially polymer blends and composites for which adhesion and compatibility with other materials are paramount. Despite significant research efforts [3, 4] in the past decades (since the beginning of the Ziegler–Natta era in the 1950s), both direct and post-polymerization approaches have yielded limited success.

Direct polymerization could be an ideal process [5–8] if the copolymerization of α-olefin (ethylene, propylene, etc.) with functional monomers was as effective and straightforward as the corresponding homopolymerization reaction. Unfortunately, some fundamental chemical difficulties, namely catalyst poisoning, are difficult to overcome and have prevented serious consideration of the direct process for commercial applications. The small number of catalytic (cationic) sites tend to form complexes with non-bonded electron pairs on N, O, and X (halides) of functional monomers, preferring to react with the π-electrons of the double bonds. The result is the deactivation of the active polymerization sites due to side reactions or the formation of stable complexes between catalysts and functional groups, thus inhibiting polymerization. Two general approaches are (1) protecting sensitive functional groups from the poisoning catalyst [9] and (2) employing late transition metal catalysts that are less oxophilic and more stable to heteroatoms [10–12]. So far, most experimental results show a significant decrease in catalyst

activity, forming branched polymer chain in late transition metal catalyst cases, which reduce polymer crystallinity and melting temperature.

Many current commercial functionalization processes are based on the post-polymerization process [13, 14]. Chemical modifications of the pre-formed polyolefins have been usually carried out in situ during the fabrication process to reduce the production cost, as well as to relieve concern (in many cases) surrounding the reduction of the processibility of polyolefins after the functionalization reaction. However, the combination of the inert nature of the polyolefin (requiring high energy) and a short reaction time (during processing) causes a great deal of difficulty in controlling the polymer composition and structure. There is no facile reaction site in the saturated PE, PP, and (ethylene propylene) EP polymers. The only successful tactic is to use a free radical initiator or radiation to activate the polymer by breaking some stable C–H bonds and forming free radicals along the polymer chain. The resulting polymeric radicals then undertake chemical reactions with some polar chemical reagents, such as maleic anhydride, acrylic acid, etc. However, such free radical chemistry is usually accompanied by many undesirable side reactions (crosslinking, degradation, oligomerization, etc.) and by-products. Overall, the current commercial process is far from ideal.

Despite its scientific challenges, energy storage has also long been an industrially important area and is an integral part of energy utilization efficiency [15]. Polyolefin (PE and PP) films are commonly used as separators in Li-ion batteries and dielectrics in capacitors for energy storage applications. Capacitors [16, 17] are passive electronic devices that store energy in the form of an electrostatic field. In their simplest form, capacitors consist of two conducting plates (positive and negative electrodes) separated by an insulating material called the dielectric, which can be air, ceramic, polymer, etc. In contrast to batteries, which have high energy density and low power density, capacitors usually exhibit high power density but very low energy density. The inherent scientific challenge is to increase the energy density of the capacitor, which is governed by the dielectric that separates the opposite static charges on two electrode surfaces. Recently, metallized polymer film capacitors [18, 19] have attracted a great deal of attention due to their desirable properties, such as light weight, low cost, and excellent processability for forming thin films with a large surface area. They also demonstrate flexibility and toughness under stress and the ability to be packaged into a desirable configuration. Currently, state-of-the-art polymer film capacitors are based on BOPP (biaxial-oriented PP) thin films [20, 21]. Despite the low energy density, in the range of 2–3 J/cm^3, BOPP shows almost no energy loss during charging–-discharging cycles and self-healing after a film puncture, which merely results in a gradual loss of capacitance so that they can be operated near the breakdown voltage with good long-term reliability. Many BOPP capacitors are currently used as pulse power capacitors in commercial and military devices.

Based on the energy density equation (Section 4), it is theoretically possible to increase the energy density of BOPP capacitors by increasing the PP dielectric constant (ε) and/or the applied electric field (E) controlled by breakdown strength. However, recent experimental results, studying several high dielectric

polymers and composites, show many complications. It is very difficult to find a new polymer that can fulfill all the required properties (i.e., high energy density, low energy loss, good processability, self-healing, long-term reliability, low cost, etc.). For example, the ferroelectric vinylidene fluoride (VDF)-based terpolymer with a high ε of over 60 can exhibit a high energy density of ~25 J/cm^3 at $E = 500$ MV/m [25–28], but this energy is accompanied by the hysteresis loops during polarization–depolarization cycles. This irreversible polarization behavior causes a minimum energy loss of ~30% that is transformed to heat, which must be instantaneously removed from the capacitor to prevent melting of the polymer thin film. In a large-scale energy storage device, the acceptable dielectric loss is less than 1%. In light of this, one of our approaches has been to adopt the newly developed PPs as the dielectrics, with the objective of improving the dielectric properties and maintaining the desirable properties of PP (i.e., low energy loss, good processability, self-healing, long-term reliability, low cost, etc.). In this chapter, I will summarize our experimental results on the application of hydroxylated polypropylene (PP–OH) to increase the dielectric constant (ε) and crosslinked polypropylene (x-PP) to increase breakdown strength (E) in capacitors.

2 New Functionalization Approach

In the early 1980s, the discovery of homogeneous single-site metallocene catalysts [22–25] provided an excellent opportunity to explore new functionalization approaches to circumvent the chemical difficulties in direct and post-polymerization processes. Comparing with heterogeneous (multiple active sites) Ziegler–Natta catalysts, one major advantage of single-site metallocene catalysts is the superior capability in the copolymerization reaction to form copolymers with narrow distributions of molecular weight and composition. In addition, the combination of tunable active site and well-controlled polymerization mechanism allows effective incorporation of large comonomers, including styrenic and cyclic comonomers, into PE and PP copolymers with a broad range of copolymer compositions. In the late 1980s, we were thinking about how to apply this new metallocene-mediated copolymerization capability into our functionalization chemistry [3, 29]. Scheme 1 illustrates the general reaction scheme, now called the "reactive" copolymer approach [30–33].

A comonomer that contains a "reactive" group should exhibit three essential properties: (1) good stability with metallocene catalyst, (2) good solubility with the reaction media, and (3) facile interconversion of reactive group into functional (polar) groups, such as OH and NH_2 groups, after polymerization [3, 34]. In previous years, we had identified three suitable "reactive" comonomers, i.e., borane monomer, *p*-methylstyrene (*p*-MS), and divinylbenzene (DVB), as illustrated in Scheme 1. In concert with the selected metallocene catalysts, the copolymerization reactions take place to form well-controlled "reactive" polyolefin copolymers with various reactive sites in the side chains. Subsequently, the incorporated reactive

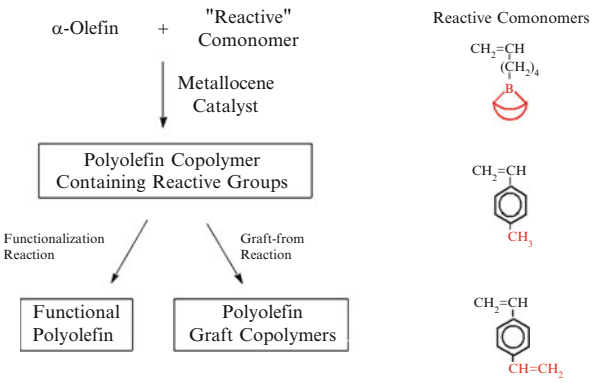

Scheme 1 The reaction route for preparation of functional polyolefin and graft copolymers using the reactive comonomer approach

groups can then be directly interconverted into functional groups or transformed into "living" radical or anionic initiator to initiate graft-from polymerization to obtain a broad range of polyolefin graft copolymers [35].

As illustrated in Scheme 2, this "reactive" copolymer approach has also been expanded to prepare polyolefins containing a terminal functional group and polyolefin diblock copolymers [29]. The well-controlled metallocene-mediated polymerization mechanism also leads to a precise control of the chain transfer reaction. With a suitable chain transfer agent containing a reactive group, the in-situ chain transfer reaction can happen to produce a polymer with a terminal reactive group. There are several facile "reactive" chain transfer agents, including simple borane species having H–B and CH_3–B moieties. With some selected metallocene catalysts (Section 2.2), the styrenic moiety also behaves as a chain transfer agent in the presence of H_2. In turn, this reactive end group opens up a convenient method to prepare chain-end-functionalized polyolefins and polyolefin diblock copolymers.

2.1 Polyolefins with Side Chain Functional Groups

As shown in Scheme 1, we have discovered three suitable "reactive" comonomers. The first is a borane-containing comonomer with a α-olefin moiety for copolymerization and a reactive borane group for the functionalization reaction. The initial idea was based on logic, mainly regarding the unique location of boron (B) in the Periodic Table, which is the only non-metallic and electron-deficient element. The Lewis acid nature of borane offers a very good chance of its coexistence with transition metals (Lewis acids). In addition, the size of the boron atom is relatively small, so steric protection can be effectively applied if needed. Therefore, an α-olefin containing a borane group should be able to be incorporated into the polymer using metallocene catalysis. Boron is situated next to carbon in the Periodic Table. Both elements are similar in atomic size and the B–C bond is covalent in nature, as is the regular C–C bond. The borane-containing polymers

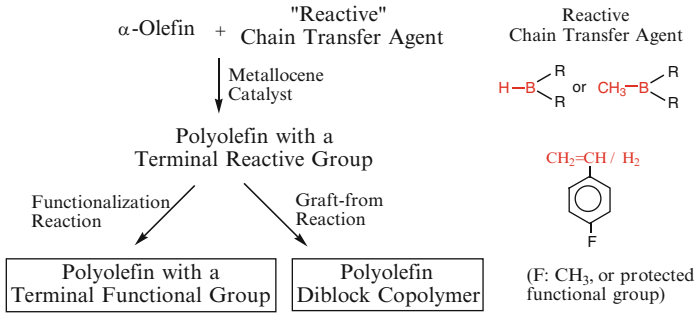

Scheme 2 The reaction route for preparation of chain-end-functionalized polyolefin and diblock copolymers using the reactive chain transfer approach

behave like regular hydrocarbon polymers with similar solution properties (solubility, viscosity). Therefore, the same reaction conditions and processes for α-olefin homopolymerization can be directly applied to its copolymerization reaction with a borane monomer. High molecular weight and high yield of borane-containing polymers are expected. On the other hand, the incorporated borane groups can be effectively transformed to a remarkably fruitful variety of functionalities under mild reaction conditions, as shown by Professor Herbert Brown [36]. Scheme 3 illustrates the general route to incorporation of borane monomers (the α-olefin-containing ω-borane group) into the polyolefin by the metallocene catalyst and the interconversion of the resulting borane-containing polyolefin to functional polyolefin copolymers [37, 38].

Table 1 summarizes the copolymerization results [39] between ethylene and borane monomer (5-hexenyl-9-BBN) using various homogeneous metallocene catalysts, including $[(\eta^5\text{-}C_5Me_4)SiMe_2\text{-}(\eta^1\text{-}NCMe_3)]TiCl_2$, $Et(Ind)_2ZrCl_2$, and Cp_2ZrCl_2, and heterogeneous Ziegler–Natta catalysts. The $[(\eta^5\text{-}C_5Me_4)SiMe_2\text{-}(\eta^1\text{-}NCMe_3)]TiCl_2$ CGC (constrained geometry complex) catalyst, with an open active site for accommodating a relatively large borane monomer, shows satisfactory copolymerization results at 150°C, similar to those in the preparation of linear low density polyethylene (LLDPE) polymers. Comparing runs I-I-1 to I-I-4, the concentration of borane groups in PE is basically proportional to the concentration of the borane monomer feed. In the $Et(Ind)_2ZrCl_2$/MAO catalyst system, about 50–60% of borane monomers were incorporated into the PE copolymers after a near half an hour of reaction time. It is unexpected that the catalyst activity systematically increases with the concentration of the borane monomer. Obviously, no retardation due to the borane groups is shown in these cases. The copolymerization of borane monomers in the Cp_2ZrCl_2/MAO system (shown in run I-III-2) is significantly more difficult. Only 1.22 mol% of the borane monomer is incorporated in the PE copolymer, even when a high concentration of the borane monomer used. On the other hand, the heterogeneous $TiCl_3 \cdot AA/Et_2AlCl$ catalyst shows no detectable amount of a borane group in the copolymer (as shown in run I-IV-1).

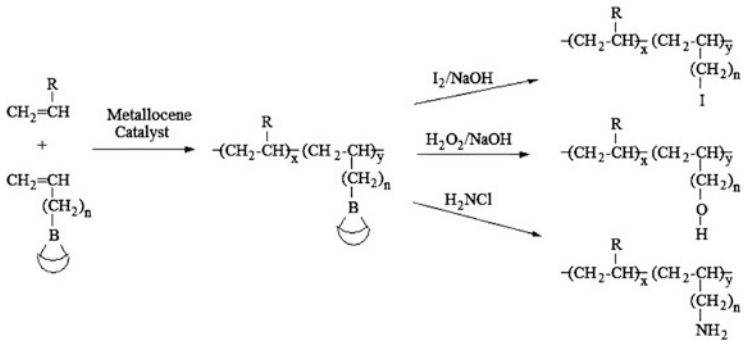

Scheme 3 Functionalization of polyolefin using "reactive" borane comonomer

Table 1 Copolymerization reactions between ethylene (M_1) and 5-hexenyl-9-BBN (M_2) using various catalysts, including [(η^5-C_5Me_4)$SiMe_2$-(η^1-$NCMe_3$)]$TiCl_2$/MAO (I), $Et(Ind)_2ZrCl_2$/MAO (II), Cp_2ZrCl_2/MAO (III), and $TiCl_3$ AA/Et_2AlCl (IV)

Run no.	Catalyst	Comonomers M_1/M_2 (psi/g)	Reaction temperature/ time (°C/min)	Catalyst activity (kg/mol·h)	Borane in PE (mol%)
I-I-1	I	450/0	150/5	2,100	0
I-I-2	I	450/2	150/5	2,000	1.46
I-I-3	I	450/4	150/5	2,200	2.75
I-I-4	I	450/8	150/5	2,800	4.65
I-II-1	II	40/0	30/70	350	0
I-II-2	II	45/0.22	30/30	480	1.25
I-II-3	II	45/0.61	30/30	660	2.15
I-II-4	II	45/0.82	30/30	850	2.30
I-III-1	III	45/0	30/70	110	0
I-III-2	III	45/5	30/70	210	1.22
I-IV-1	IV	80/10	60/110	1.3	0

The borane groups incorporated in PE were quantitatively converted to the corresponding hydroxy groups by reacting with $NaOH/H_2O_2$ reagents at 40°C for 1 h. Despite the heterogeneous reaction conditions in forming the PE–OH polymers, the interconversion reaction was very effective due to the high surface area of borane groups in the semicrystalline microstructure of the PE copolymers. The borane groups in the flexible side chains should be located in amorphous phases where the chemical reagents can be easily reached. It is very interesting to note that the resulting PE–OH, containing a hydroxy group located at the end of the flexible side chain, is structurally similar to that of LLDPE, with expected OH groups located at the end of each side chain. Figure 1 shows the gel permeation chromatography (GPC) curves for PE–OH polymers containing 0.5 and 1.2 mol% OH groups. The copolymers were prepared using the Et(Ind)2ZrCl2/MAO catalyst with ethylene/5-hexenyl-9-BBN comonomers. Overall, the copolymers have high molecular weight and narrow molecular weight distribution ($M_w/M_n < 3$). There is no indication of any negative influence of the borane group on the metallocene polymerization.

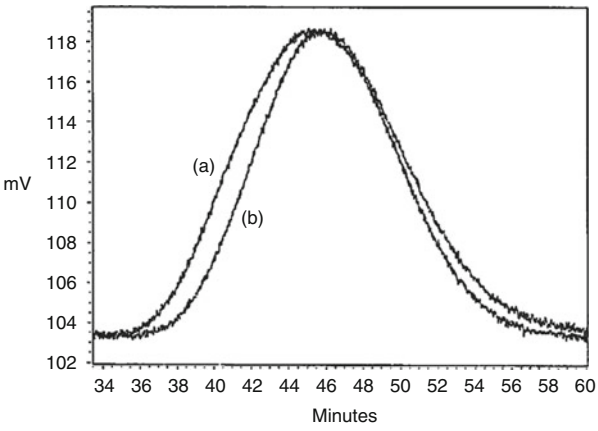

Fig. 1 GPC curves of poly (ethylene-*co*-5-hexenyl-9-BBN) copolymers containing (*a*) 0.5 and (*b*) 1.2 mol% of 5-hexenyl-9-BBN

A similar functionalization route was extended to higher α-olefin copolymers [31, 32]. Both isospecific metallocene and heterogeneous Ziegler–Natta catalysts were employed in propylene and 1-octene copolymerization reactions with 5-hexenyl-9-BBN. With the general phenomenon in Ziegler–Natta-mediated copolymerization, the bigger the size of the monomer the lower the reactivity and the more easily it can copolymerize the borane monomer with high α-olefins. Table 2 summarizes several copolymerization results for propylene and 5-hexenyl-9-BBN and for 1-octene and 5-hexenyl-9-BBN using the $TiCl_3$ AA/Et_2AlCl catalyst. It is obvious that propylene was preferentially polymerized and consumed in the propylene/5-hexenyl-9-BBN copolymerization. On the other hand, a significantly higher comparative comonomer reactivity was observed between 1-octene and 5-hexenyl-9-BBN.

Figure 2 compares infrared (IR) and differential scanning calorimetry (DSC) curves for three poly(1-octene) copolymers containing 15, 40, and 65 mol% of 1-hexen-6-ol units (runs II-II-1, II-II-2 and II-II-3, respectively), and two homopolymers, i.e., poly(1-octene) and poly(1-hexen-6-ol). The systematic increase in OH content, corresponding well with the borane comonomer mole ratio, indicates the comparative reactivity between 1-octene and 5-hexenyl-9-BBN. Only one glass transition temperature (T_g) is observed for each sample, which reveals the absence of a macroscopic phase separation, implying that the copolymer samples are fairly homogeneous. In fact, a linear relationship between the T_g and the weight fraction of either monomer has been taken as a qualitative indication of the homogeneity and random nature of the copolymer samples.

Based on the same three considerations (i.e., stability, solubility, and versatility) of the "reactive" comonomer, we also investigated *p*-methylstyrene (*p*-MS) [40–44]. The major advantages of *p*-MS are its commercial availability, easy incorporation into the polyolefin, and versatility in functionalization chemistry under various reaction mechanisms, including free radical, cationic, and anionic processes. The benzylic protons are known to be readily reactive in many chemical reactions (such as halogenation, metallation, and oxidation) to form a desirable functional group at the benzylic position under mild reaction conditions, as illustrated in Scheme 4.

Table 2 Summary of copolymerization reactions between propylene or 1-octene and 5-hexenyl-9-BBN using $TiCl_3$ AA/Et_2AlCl catalyst

Run no.	α-Olefin	Borane comonomer (mol%)	Reaction temperature / time (°C/min)	Borane in copolymer (mol%)	Molecular weight (g/mol)
II-I-1	Propylene	5	70/60	1.4	210,000
II-I-2	Propylene	10	70/60	2.6	183,000
II-I-3	Propylene	15	70/60	4.1	174,000
II-II-1	1-Octene	25	25/90	15	242,000
II-II-2	1-Octene	50	25/90	40	126,000
II-II-3	1-Octene	75	25/90	65	66,000

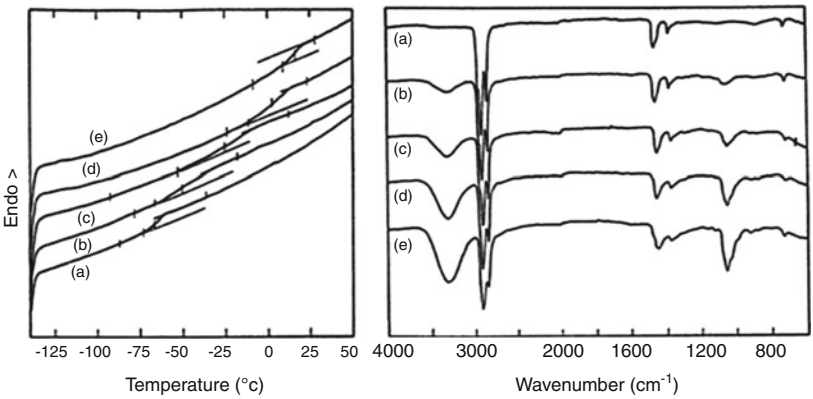

Fig. 2 Comparisons of DSC curves (*left*) and IR spectra (*right*) of (*a*) poly(1-octene) and its copolymers prepared by using (*b*) 25, (*c*) 50, and (*d*) 75 mol% of OH comonomers, and (*e*) poly (1-hexen-6-ol)

Table 3 summarizes some ethylene/*p*-MS copolymerization results using three metallocene catalysts: $[C_5Me_4(SiMe_2N^tBu)]TiCl_2$, $Et(Ind)_2ZrCl_2$, and Cp_2ZrCl_2 [40, 41]. As expected, the copolymerization efficiency follows the sequence of $[C_5Me_4(SiMe_2N^tBu)]TiCl_2 > Et(Ind)_2ZrCl_2 > Cp_2ZrCl_2$. The spatial opening at the active site of $[C_5Me_4(SiMe_2N^tBu)]TiCl_2$/MAO offers a high *p*-MS conversion and copolymers with a broad range of *p*-MS concentrations. In general, the catalyst activity systematically increases with the increase of *p*-MS content, due to the improvement of monomer diffusion in the lower crystalline copolymer structures. The catalyst activity attains a value of more than 2.4×10^3 kg polymer/mol Ti h (in run III-I-6), which is four times the value of homopolymerization of ethylene under similar reaction conditions. It is interesting to note that there exists a very small solvent (hexane and toluene) effect due to $[C_5Me_4(SiMe_2N^tBu)]TiCl_2$/MAO catalyst activity, yet a very significant difference in both $Et(Ind)_2ZrCl_2$ and Cp_2ZrCl_2 catalyst systems.

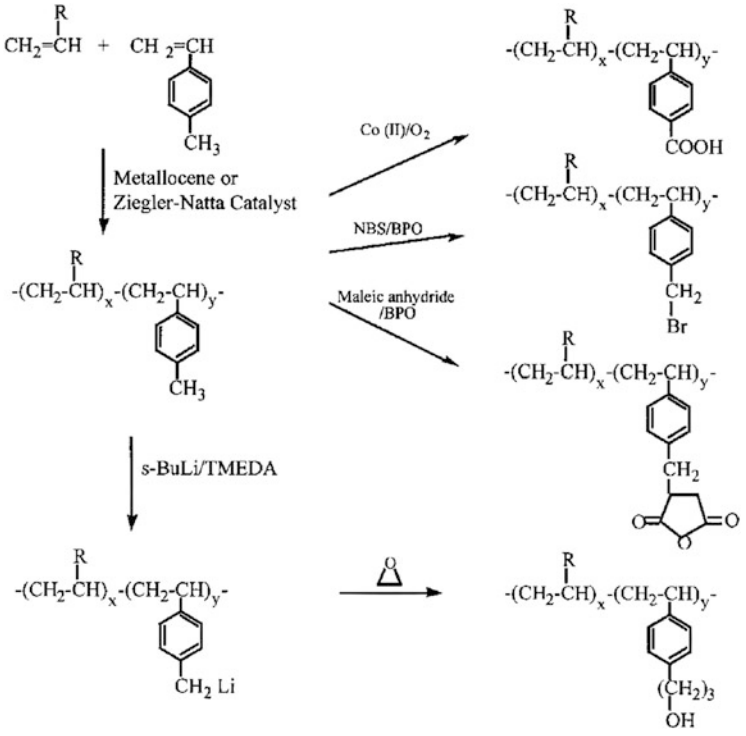

Scheme 4 Functionalization of polyolefin using "reactive" *p*-MS comonomer

The resulting poly(ethylene-*co*-*p*-methylstyrene) (PE-*p*-MS) copolymers show narrow molecular weight ($M_w/M_n = 2$–3) and composition distributions, implying the single-site polymerization mechanism. Figure 3 compares DSC curves between the PE homopolymer and several PE-*p*-MS copolymers prepared by the $[C_5Me_4(SiMe_2N^tBu)]TiCl_2$/MAO catalyst at 40°C in toluene. Even a small amount (~1 mol%) of *p*-MS comonomer incorporation has a significant effect to the crystallization of polyethylene. Overall, the melting point (T_m) and crystallinity (χ_c) of the copolymer are strongly related to the density of the comonomer; the higher the density, the lower the T_m and χ_c. Only a single peak is observed throughout the entire composition range and the melting peak completely disappears at ~10 mol% of *p*-MS concentration. A similar general trend was also observed in the DSC curves of PE-*p*-MS copolymers prepared by the $Et(Ind)_2ZrCl_2$/MAO catalyst. The systematic decrease in T_m and uniform reduction of the crystalline curve imply the homogeneous reduction of PE consecutive sequences. It is interesting to note that the T_m peak (ranging from 80°C to 45°C, as shown in Fig. 3, curve e) of the copolymer containing 9.82 mol% of *p*-MS covers a similar T_m range (45–55°C) as paraffin wax. This PE-*p*-MS copolymer consists of an average of 20–22 consecutive methylene units, which is in the molecular weight range of solid paraffin wax.

Table 3 Summary of copolymerization reactions between ethylene and *p*-methylene styrene using [(η^5-C_5Me_4)$SiMe_2$-(η^1-$NCMe_3$)]$TiCl_2$/MAO (I), Et(Ind)$_2ZrCl_2$/MAO (II), and Cp_2ZrCl_2/MAO (III) metallocene catalysts

Run no.	Catalyst	Comonomers E/*p*-MS (psi/M)	Solvent/ temperature (°C)	Catalyst activity (kg/mol·h)	*p*-MS in PE (mol%)
III-I-1	I	45/0.447	Hexane/30	1,200	13.5
III-I-2	I	45/0.912	Hexane/30	1,550	22.6
III-I-3	I	45/1.82	Hexane/30	1,590	40.0
III-I-4	I	45/0.447	Toluene/30	1,300	10.9
III-I-5	I	45/0.912	Toluene/30	1,740	21.6
III-I-6	I	45/1.82	Toluene/30	2,420	32.8
III-II-1	II	45/0.678	Hexane/50	1,290	5.16
III-II-2	II	45/0.678	Toluene/50	890	4.76
III-III-1	III	45/0.678	Hexane/50	1,420	2.20
III-III-2	III	45/0.678	Toluene/50	500	1.84

The copolymerization of propylene and *p*-MS [42] was investigated using iso-specific metallocene catalysts, including {$SiMe_2$[2-Me-5-Ph(Ind)]$_2$}$ZrCl_2$ and Et(Ind)$_2ZrCl_2$. Overall, these metallocene catalysts were not very effective in producing PP-*p*-MS copolymers, as measured by catalyst activity and *p*-MS incorporation. Compared to the results seen in the homopolymerization of propylene, the presence of even a small amount of *p*-MS in these cases shows severely reduced catalyst activity. These results are completely opposite to those observed in the corresponding ethylene/*p*-MS copolymerization reactions. The drastic difference is attributed to the steric jamming phenomenon in the cross-over reaction from *p*-MS to propylene, as illustrated in Scheme 5. It is well known that in metallocene catalytic polymerization, the insertion of the styrene monomer is predominately 2,1-insertion, whereas the 1,2-insertion of the propylene monomer is dominant. Once the propagating PP chain has a chance to react with the *p*-MS monomer via 2,1-insertion, the bulky *p*-phenyl group in the last unit of the growing chain (II in Scheme 5) is adjacent to the central metal atom and blocks the upcoming 1,2-insertion of a propylene unit. Because the homopolymerization of *p*-MS via the metallocene coordination mechanism is known to be near zero, the metallocene active site at the *p*-MS unit dramatically slows the propagation process.

The steric jamming problem can be overcome by adding a small amount of ethylene [43]. The sluggish propagating chain end of the *p*-MS unit allows the insertion of ethylene, which re-energizes the propagation process. In fact, the catalyst activity of ethylene/propylene/*p*-MS terpolymerization is higher than that of the corresponding ethylene or propylene homopolymerization reactions. These experimental results strongly support the steric jamming theory in the metallocene copolymerization of the propylene and styrenic monomer. Furthermore, it is peculiar to prepare ethylene/propylene/*p*-MS elastomers with a low T_g (below −45°C) and completely amorphous morphology. The incorporated *p*-MS units offer the "reactive" sites for a crosslinking reaction to form a stable EP network structure. With the unprecedented capability of the metallocene catalyst in copolymerization

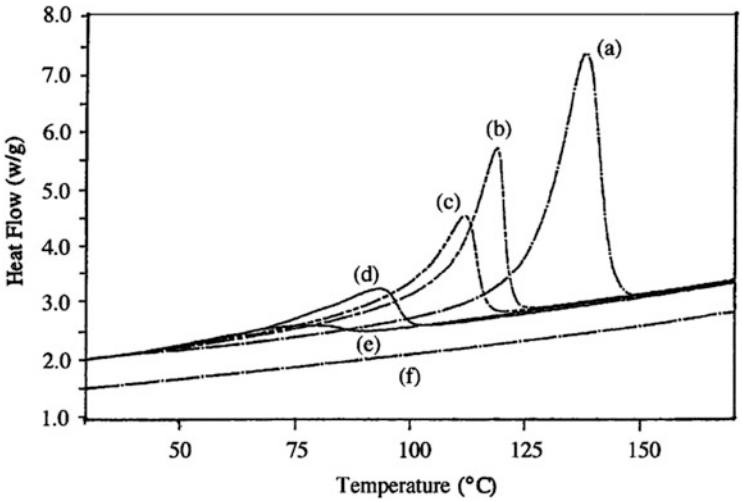

Fig. 3 The comparison of DSC curves between (*a*) PE and PE-*co*-*p*-MS copolymers with (*b*) 1.08, (*c*) 2.11, (*d*) 5.40, (*e*) 9.82 and (*f*) 18.98 mol% of *p*-MS comonomer units

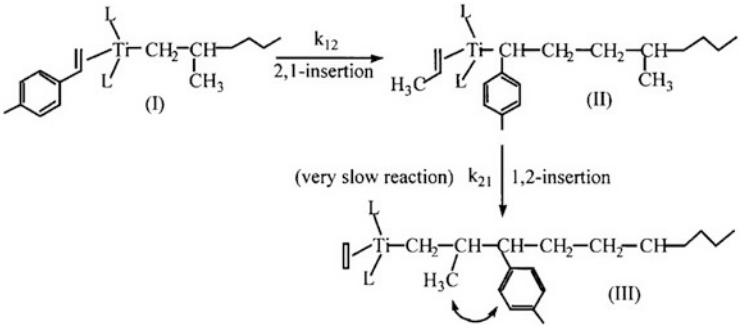

Scheme 5 Steric jamming phenomenon in the cross-over reaction from *p*-MS to propylene incorporation

reactions, it is also rather interesting to expand the polyolefin elastomer to new classes containing high α-olefins, such as 1-octene (instead of propylene), which can effectively prevent the crystallization of small consecutive ethylene units and provide low T_g properties. Table 4 summarizes the terpolymerization reactions of ethylene/propylene/*p*-MS (E/P/*p*-MS) and ethylene/1-octene/*p*-MS (E/O/*p*-MS) terpolymerization reactions using the $[C_5Me_4(SiMe_2N^tBu)]TiCl_2$/MAO catalyst [43]. Overall, this CGC metallocene catalyst shows excellent activity in all terpolymerization reactions, with comparative reactivities between ethylene/propylene and ethylene/1-octene and with good incorporation of *p*-MS in the resulting terpolymers. The incorporation of *p*-MS seems relatively insensitive to the ethylene/propylene or ethylene/1-octene feed ratio. Comparing runs IV-I-1 versus IV-I-2 and IV-I-3 (Table 4), with the same amount of ethylene and propylene feeds,

Table 4 Summary of ethylene/propylene/*p*-MS and ethylene/1-octene/*p*-MS terpolymerization reactions using [(η^5-C_5Me_4)$SiMe_2$-(η^1-$NCMe_3$)]$TiCl_2$/MAO catalyst

Run no.	Comonomers [E]/[P]/[*p*-MS] (mol/L)	Catalyst activity (kg/mol Ti h)	Terpolymers [E]/[P]/[*p*-MS] (mol%)	T_g (°C)
IV-I-1	0.13/0.28/0	4.9×10^3	53.9/46.10	−49.4
IV-I-2	0.13/0.28/0.03	3.8×10^3	50.7/48.6/0.7	−45.9
IV-I-3	0.13/0.28/0.05	4.1×10^3	54.4/43.8/1.8	−45.8
IV-I-4	0.12/0.35/0.05	4.0×10^3	46.1/52.3/1.6	−41.0
IV-I-5	0.14/0.25/0.03	4.4×10^3	56.3/43.1/0.6	−48.6
	[E]/[O]/[*p*-MS]		[E]/[O]/[*p*-MS]	
IV-II-1	0.25/0.89/0	5.6×10^3	41.4/58.6/0	−61.8
IV-II-2	0.25/0.89/0.13	4.2×10^3	40.0/54.5/5.5	−51.3
IV-II-3	0.20/0.80/0.10	5.8×10^3	54.2/43.0/2.7	−56.2
IV-II-4	0.40/0.80/0.10	8.0×10^3	61.1/36.0/2.9	−58.1
IV-II-5	0.40/0.80/0.20	7.8×10^3	60.3/36.3/4.4	−55.7

with or without *p*-MS, only a small reduction in molecular weight arises from the incorporation of *p*-MS. Furthermore, the polymer molecular weight is relatively high (M_w ~200,000 g/mol) and is not significantly dependent on the content of *p*-MS. The molecular weight distributions ($M_w/M_n < 2.5$), similar to most metallocene polymers, indicate a single-site reaction.

Figure 4 shows several DSC curves of EP-*p*-MS terpolymers [43]. Each curve has only a sharp T_g transition in a flat baseline, without any detectable melting point. The T_g is clearly a function of the propylene and *p*-MS contents. Comparing the ethylene/propylene copolymers (without *p*-MS units), the T_g transitions are linearly proportional to the propylene contents and level off at about −50°C with ~50% propylene content (similar results were reported for the ethylene propylene diene monomer case). The T_g transition significantly increases with the incorporation of *p*-MS into ethylene/propylene copolymers. It is interesting to compare runs IV-I-1 and IV-I-3, both with the ideal ~54 mol% ethylene content, in which the T_gs are −50 and −45°C, respectively. Overall, the composition of EP-*p*-MS material with low T_g of less than −45°C is very limited, only to polymers with <2 mol% of *p*-MS content. Despite the random terpolymer structure and the ideal (~55/45) ethylene to propylene ratio, a further increase of *p*-MS raises the T_g of the terpolymer to above −40°C. Evidently, the high T_g of both propylene (T_g of PP ~0°C) and *p*-MS [T_g of poly(*p*-MS) ~110°C] components preclude EP-*p*-MS from producing desirable elastomers containing both a high content of "reactive" *p*-MS and a very low T_g (below −50°C) transition. On the other hand, it is common to observe a T_g of less than −50°C in ethylene/1-octene/*p*-MS (EO-*p*-MS) terpolymers. The EO-*p*-MS sample, even with up to 5 mol% of *p*-MS, still shows a T_g less than −50°C. These results clearly demonstrate the advantages of the 1-octene comonomer (over propylene), which assures the formation of an amorphous polyolefin elastomer with low T_g and high *p*-MS content.

The primary objective of incorporating *p*-MS units in polyolefin surrounds its versatility in accessing a broad range of functional groups, as illustrated in

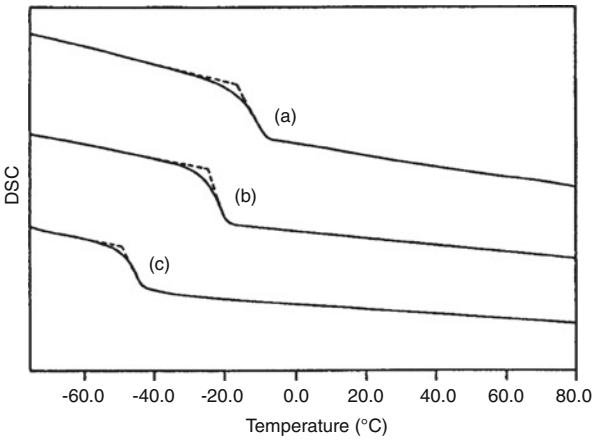

Fig. 4 Comparison of DSC curves of three EP-*p*-MS terpolymers having [E]/[P]/*p*-MS mole ratios of (*a*) 40.3/48.6/11.1, (*b*) 46.4/43.6/10.0, and (*c*) 54.4/43.8/1.8

Scheme 4. The benzylic protons are ready for many chemical reactions, such as halogenation, oxidation, and metallation. Many functionalization reactions take place exclusively at the *p*-CH_3 position. Therefore, the polymer backbone is untouched during functionalization and the extent of functionalization is governed by the concentration of *p*-MS groups. Figure 5 shows an ^{1}H NMR spectra of three functionalized PEs that were derived from the same PE-*p*-MS containing 1 mol% of *p*-MS units. In the carboxylated PE that was synthesized by bubbling CO_2 gas through a tetrahydrofuran (THF) slurry of the lithiated PE-*p*-MS copolymer, there are two new peaks at around 3.65 ppm and 7.1–7.4 ppm (see Fig. 5, curve a), corresponding to benzylic protons adjacent to the carboxylic acid (–COOH) group and *p*-C**H**$_2$COOH substituted aromatic protons, respectively. The degree of the carboxylation reaction (the ratio between [*p*-CH_2COOH] in the copolymer to [*p*-CH_3] in the starting copolymer) is 60.3%. By bubbling ethylene oxide gas through the lithiated PE-*p*-MS/THF suspension solution, a hydroxylated PE polymer containing *p*-(1-hydroxypropyl)styrene units was obtained. The ^{1}H NMR spectrum of the resulting polymer is shown in Fig. 5, curve b, with three new peaks at 3.71, 2.73, and 2.17 ppm corresponding to three types of CH_2 protons between the aromatic ring and the OH group. The efficiency of the functionalization reaction is 76.3%. The lithiated PE-*p*-MS suspended in THF solution was also reacted with methoxyl-9-BBN at room temperature, gave a borane-containing polymer, then converted to benzylic alcohol groups by hydrolyzing in the presence of NaOH/H_2O_2 in THF. Figure 5, curve c, shows the ^{1}H NMR spectrum of the resulting polymer. Two new peaks around 4.7 ppm and 7.1–7.4 ppm correspond to the benzylic protons next to the OH group and the aromatic protons of benzylic alcohol.

In addition, we also studied diene comonomers containing a styrenic moiety [45–48]. The objective was to incorporate pendant styrene groups into the polyolefin side chains, which are highly versatile for a broad range of reactions, including free radical, cationic, and anionic processes. With the advantages of metallocene catalysis, it is possible to select an active site with a specific stereo-opening that exhibits selectivity in olefin enchainment to provides high diene incorporation into

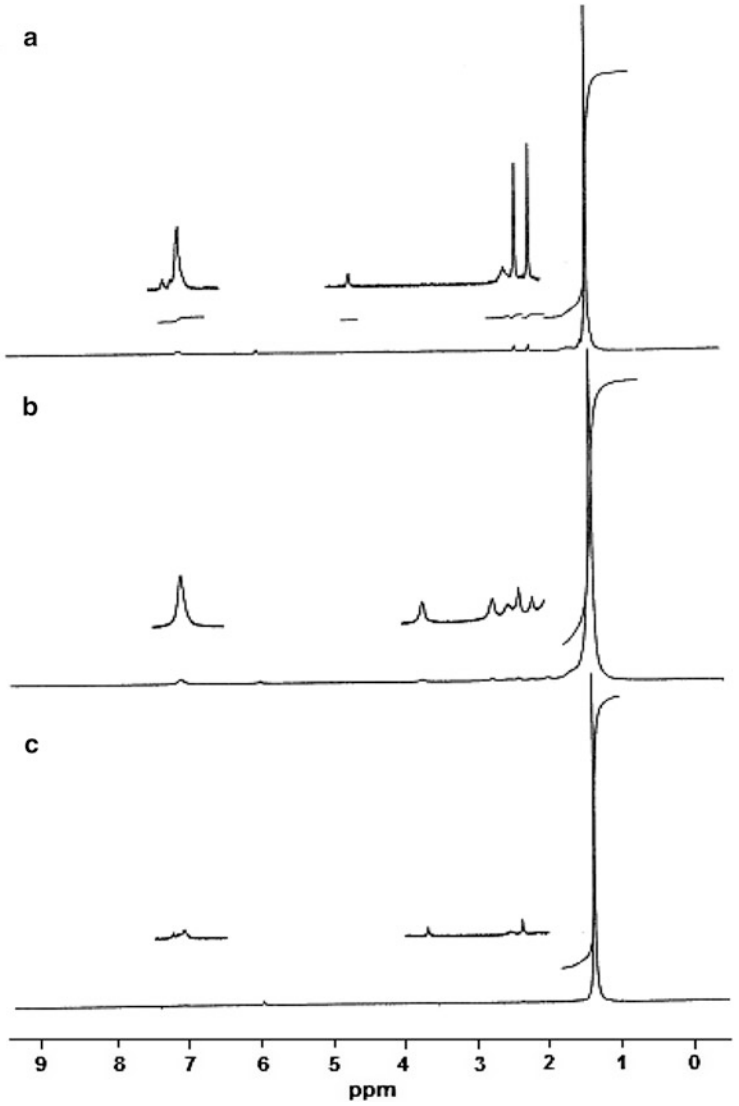

Fig. 5 ^{1}H NMR spectra of three functionalized PE polymers containing (**a**) ϕ-CH_2COOH, (**b**) ϕ-$(CH_2)_3$–OH, and (**c**) ϕ-CH_2–OH functional groups

the polyolefin without causing branching and/or crosslinking side reactions. Scheme 6 illustrates the general reaction scheme of a simple thermal process to form maleic anhydride-modified polyolefin and crosslinked polyolefin.

Table 5 summarizes the experimental results of the copolymerization reaction between ethylene and 1,4-divinylbenzene (DVB) using various metallocene catalysts, including Cp_2ZrCl_2, Ind_2ZrCl_2, *rac*-$Et(Ind)_2ZrCl_2$, $Me_2Si(Ind)_2ZrCl_2$, and $[C_5Me_4(SiMe_2N^tBu)]TiCl_2$ [45]. As expected, Cp_2ZrCl_2 and Ind_2ZrCl_2

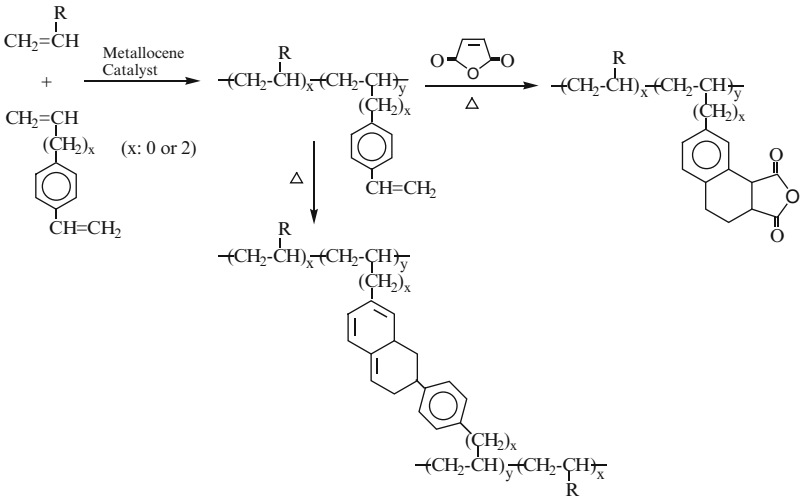

Scheme 6 Functionalization of polyolefin using "reactive" styrenic diene comonomer

exhibited very poor incorporation of styrenic monomers. Although $Me_2Si(Ind)_2ZrCl_2$ and$[C_5Me_4(SiMe_2N^tBu)]TiCl_2$, with open active sites, can incorporate styrene, the copolymers produced are largely insoluble. Evidently, both olefinic groups in DVB involve an enchainment reaction to form the crosslinked PE products. On the other hand, *rac*-$Et(Ind)_2ZrCl_2$/MAO is a suitable catalyst that shows good DVB incorporation. All poly(ethylene-*co*-1,4-divinylbenzene) copolymers obtained were completely soluble in common organic solvents, such as toluene and xylene, at elevated temperatures.

Figure 6 shows GPC curves of several ethylene/DVB copolymers. The polymer molecular weight systematically decreases with increasing DVB content, due to the lower polymerization reactivity of styrene and the increased rate of the chain transfer reaction after 2,1-insertion of the styrene unit. All copolymers exhibit narrow molecular weight distribution ($M_w/M_n \sim 2.3$), implying a single-site polymerization mechanism. Figure 7 shows an ^1H NMR spectrum of poly(ethylene-*co*-1,4-divinylbenzene) containing 7.2 mol% DVB units. In addition to the major peak at 1.3 ppm corresponding to ethylene units, several chemical shifts were observed at 5.2 and 5.7 ppm (doublet, CH=C$\mathbf{H}_2$) and 6.7 ppm (doublet of doublet, C$\mathbf{H}$=CH_2); aromatic proton peaks occurred at 7.1 and 7.4 ppm ($C_6\mathbf{H}_4$). The peak intensity ratios indicate that the mole ratio of the vinyl group to the phenyl group is near unity.

The poly[propylene-*co*-*p*-(3-butenylstyrene)] (PP-BSt) copolymers were prepared by a specific *rac*-$CH_2(3$-*t*-butyl-$Ind)_2ZrCl_2$ catalyst that exhibits highly favorable reactivity toward α-olefin over styrene moieties [48]. In other words, most of the BSt comonomers are incorporated through the α-olefin moiety. The incorporated BSt unit results in a pendant styrene moiety in the copolymer. Table 6 summarizes a set of PP-BSt copolymers. The appearance of the reacting polymer solution was dependent on the quantity of BSt used. In the high BSt case (run VI-7),

Table 5 Summary of copolymerization reactions between ethylene (M_1) and DVB (M_2) using Cp_2ZrCl_2 (I), Ind_2ZrCl_2 (II), *rac*-$Et(Ind)_2ZrCl_2$ (III), $Me_2Si(Ind)_2ZrCl_2$ (IV), and [(η^5-C_5Me_4)$SiMe_2$-(η^1-$NCMe_3$)]$TiCl_2$ (V) catalysts, in 100 toluene at 50°C for 30 min

Run no.	Catalyst	Comonomers M_1/M_2 (psi/mol)	Catalyst activity (kg/mol·h)	DVB in PE (mol%)	Solubility
V-I-1	I	20/0.05	1,880	0.5	Soluble
V-I-2	I	20/0.18	424	1.1	Soluble
V-II-1	II	20/0.05	1,976	0.6	Soluble
V-II-2	II	20/0.18	408	1.2	Soluble
V-III-1	III	20/0.03	3,616	1.5	Soluble
V-III-2	III	20/0.05	4,016	2.3	Soluble
V-III-3	III	20/0.08	4,464	3.3	Soluble
V-III-4	III	20/0.18	4,048	7.2	Soluble
V-IV-1	IV	20/0.03	3,296	–	Insoluble
V-IV-2	IV	20/0.05	4,280	–	Insoluble
V-V-1	V	20/0.03	2,584	–	Insoluble

a homogeneous solution was observed throughout the entire copolymerization reaction. In the case of low BSt (runs VI2-VI6), a slurry solution with white precipitates was observed at the beginning of the reaction. The precipitation is evidently due to the polymer crystallinity, which has long propylene sequences.

Figure 8 shows a typical ^{1}H NMR spectrum of PP-BSt copolymer (run VI-5). In addition to the major chemical shifts at 0.95, 1.35 and 1.65 ppm – corresponding to the methine, methylene, and methyl groups in polypropylene, respectively – there are several minor chemical shifts that are associated with the incorporated BSt comonomer units, including three distinctive olefinic proton chemical shifts at 6.7, 5.7, and 5.2 ppm and two equal intensity aromatic proton chemical shift bands at 7.1–7.2 and 7.3–7.4 ppm. With their relative chemical shift intensities, it is clear that most of the incorporated BSt units in the PP-BSt copolymer contain pendant styrene moieties. It is interesting to note that the same propylene/BSt copolymerization by the *rac*-$Me_2Si[2\text{-}Me\text{-}4\text{-}Ph(Ind)]_2ZrCl_2$ catalyst results in a long chain branched polypropylene (LCBPP) [49, 50] due to both olefinic and styrenic reactions.

The PP-BSt copolymers were completely soluble in xylene at an elevated temperature. However, the solution-encased PP-BSt copolymer films were crosslinked upon heating, due to a Diels–Alder [2+4] cycloaddition reaction between two pendant styrene units. The resulting crosslinked PP (x-PP) films were subjected to a vigorous solvent extraction to remove the soluble fraction that was not fully crosslinked into the network structure. Figure 9 compares the gel content after thermal treatment for 1 h under various temperatures for three PP-BSt copolymers with pendant styrene contents of 0.42 (run VI-3), 0.73 (run VI-5), and 8.6 mol% (run VI-7). The thermal regiospecific [2+4] cycloaddition reaction between two styrene units starts at a relatively low temperature (~80°C). However, the rate of the crosslinking reaction is highly dependent on the temperature and copolymer composition. In the low temperature range below 160°C (below melting temperature) with limited chain motion, the crosslinking efficiency of the

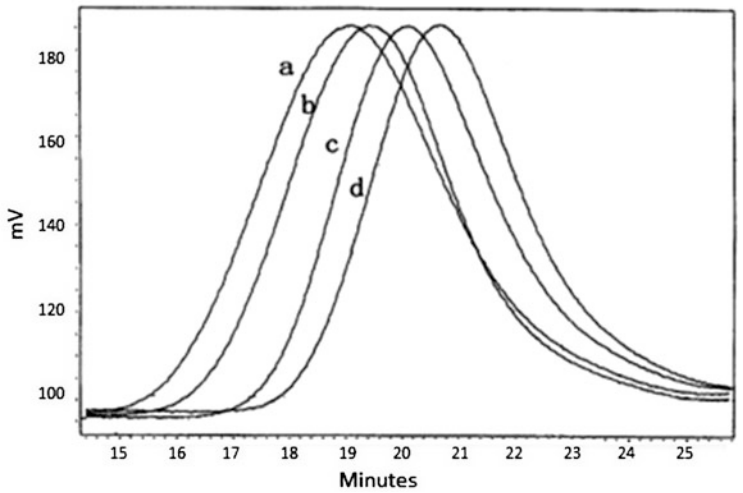

Fig. 6 GPC curves of (*a*) PE and three linear poly(ethylene-*co*-1,4-divinylbenzene) copolymers, containing (*b*) 1.5, (*c*) 2.3, and (*d*) 7.2 mol% DVB units, respectively (solvent, trichlorobenzene; temperature, 135°C)

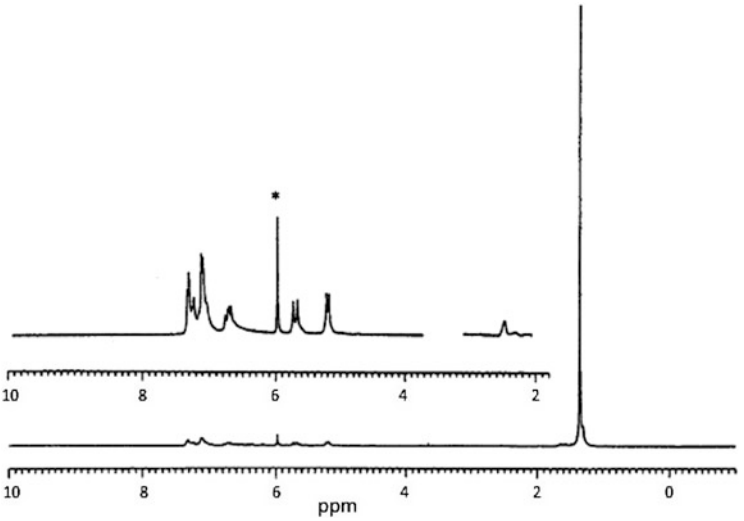

Fig. 7 ^{1}H NMR spectrum of poly(ethylene-*co*-1,4-divinylbenzene) with 7.2 mol% DVB units (solvent, $C_2D_2Cl_4$; temperature, 110°C)

PP-BSt copolymer is dependent on the concentration of pendant styrene (crosslinker) units. High crosslinker content is needed in order to observe an appreciable crosslinking reaction. It appears important to anneal the copolymer film at temperatures above 160°C (beyond its melting temperature) to achieve high

Table 6 Summary of propylene (M_1) and BSt (M_2) copolymerization reactions using *rac*-CH_2(3-*t*-butyl-Ind)$_2ZrCl_2$/MAO catalyst

Run no.	Comonomers M_1/M_2 (psi/mol)	Catalyst activity (kg/mol·h)	BSt in PP (mol%)	M_v (kg/mol)	T_m (°C)
VI-1	170/0	60	0	145	158
VI-2	170/0.5	46	0.16	246	154
VI-3	170/1	44	0.42	285	151
VI-4	170/2	38	0.53	231	150
VI-5	170/3	30	0.73	252	142
VI-6	170/4	30	0.88	201	140
VI-7	170/20	18	8.6	23	–

crosslinking efficiency, which is particularly important for the PP-BSt copolymer with <1 mol% of pendant styrene units. Beyond 200°C, the interchain reaction can effectively take place. Despite very different styrene contents, all three copolymers exhibit near completely crosslinked x-PP products.

2.2 *Polyolefins with a Chain-End Functional Group*

As shown in Scheme 2, we have extended the functionalization chemistry to prepare polyolefins with a terminal functional group. With the advantage of a well-defined metallocene-mediated α-olefin polymerization mechanism, our thought was to introduce a suitable "reactive" chain transfer agent that can be selectively incorporated at the polyolefin chain end. The in-situ formed "reactive" terminal group can be effectively interconverted to a terminal functional group under mild reaction conditions. A polymer containing a terminal functional group will not change the intrinsic properties, such as T_g and T_m, of the polymer. However, the terminal functional group presents a unique opportunity to serve as the connection site for constructing multi-segmented polymers, even polymers with complex supermolecular structures. In the polyolefin, the opportunity is even more intriguing due to the lack of functionality and difficulty in preparing polyolefin block/graft copolymers and long chain branched polymer structures. In our laboratory, we have investigated several organoboranes (containing the B–H and B–CH_3 moieties) as the chain transfer agents [51–55] for olefin polymerizations, as illustrated in Scheme 7. Given the facile ligand exchange between B–H (or B–CH_3) bonds and most metal-alkyl groups, it would be logical to expect a fast chain transfer reaction to take place in most metallocene catalyst systems. The resulting borane-terminated polyolefin is a highly versatile intermediate that can be converted into a broad range of polar group-terminated polyolefins and diblock copolymers containing both polyolefin and functional polymer segments (Section 3).

In the presence of a borane chain transfer agent containing a B–H (or B–CH_3) group, the metallocene-mediated propagating PP chain (I in Scheme 7) engages in a facile ligand exchange reaction (II) between C–M (where M indicates transition

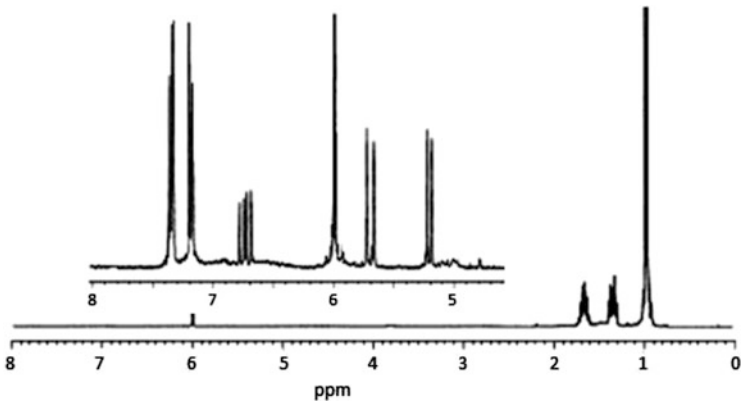

Fig. 8 ^{1}H NMR spectrum of a PP-BSt copolymer containing 0.73 mol% of *p*-(3-butenyl)styrene units (solvent, $C_2D_2Cl_4$; temperature, 110°C)

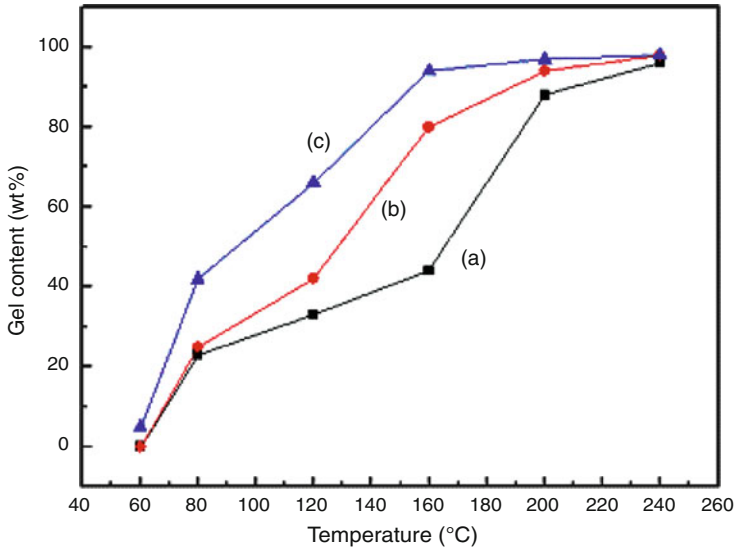

Fig. 9 Gel content after thermal treatment for 1 h under various temperatures for three PP-BSt copolymers with pendant styrene concentration of (*a*) 0.42 mol% (run VI-3), (*b*) 0.73 mol% (run VI-5), and (*c*) 8.6 mol% (run VI-7), respectively

metal) and B–H or (B–CH_3) bonds, due to the favorable acid–base interaction between the cationic metal center and anionic hydride. This ligand exchange reaction results in a borane-terminated polyolefin (III) and a new active site (IV) that can reinitiate polymerization. Ideally, this chain transfer reaction should not change the overall catalyst activity, and each polymer will contain a terminal borane group with an average polymer molecular weight that is inversely proportional to the molar ratio of [chain transfer agent]/[olefin]. The resulting

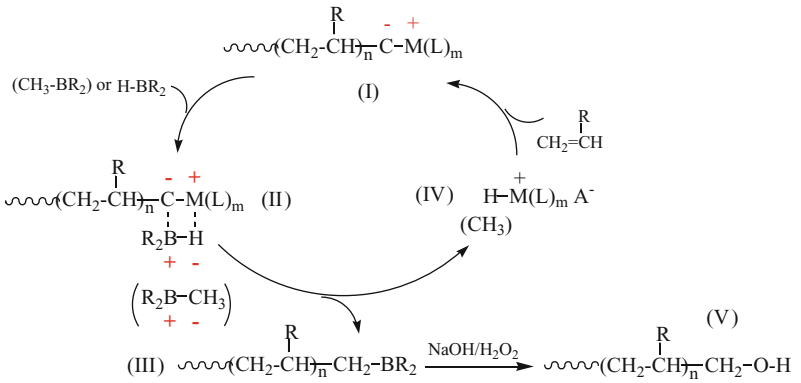

Scheme 7 Synthesis of chain functional polyolefin using borane chain transfer agent. *M* transition metal

borane-terminated polyolefin (III) can be converted into a hydroxy-terminated polyolefin (V) by treatment with $NaOH/H_2O_2$. There are some significant differences in applying the borane chain transfer agent containing B–H and B–CH_3 groups. Although the B–H group is more reactive toward the propagating PP chain (I) with a higher chain transfer constant, there are two potential side reactions that can derail the catalytic cycle shown in Scheme 7, namely hydroboration of the olefin monomer by borane and ligand exchange reactions between the borane and aluminum co-catalyst. Fortunately, borane compounds containing B–H groups usually form stable dimers that are unreactive towards olefins in typical olefin polymerization solvents (e.g., hexane, toluene). To eliminate the possibility of a ligand exchange reaction between B–H and Al-alkyl, we have found two solutions – either applying perfluoroborate co-catalyst or using purified methyl aluminoxane (MAO) (without trimethylaluminium, TMA) with a low reaction temperature (<35°C).

Table 7 summarizes the experimental results of ethylene polymerization in the presence of 9-BBN using two metallocene catalysts, $[Cp^*_2ZrMe]^+[MeB(C_6F_5)_3]^-$ and $[Cp^*_2ZrMe]^+[B(C_6F_5)_4]^-$ ($Cp^* = \eta^5$-C_5H_5, η^5-Me_5C_5), in toluene at 25°C [51]. To maintain the constant comonomer feed ratio, the reactions were carried out with rapid mixing and a short reaction time. After a 3–5 min reaction time, the polymer solution was quenched with anhydrous/anaerobic MeOH, and the resulting borane-terminated polyethylene (PE-*t*-B) was oxidized by $NaOH/H_2O_2$ to form a hydroxy-terminated polymer (PE-*t*-OH).

In essence, higher concentrations of a 9-BBN chain transfer agent resulted in lower molecular weights of the resulting polyethylene. The polymer molecular weight distribution is generally narrow, which is consistent with single site polymerization processes. The catalyst activity was also depressed in the presence of 9-BBN, which may reflect the competitive coordination at metallocene active sites between monomer and chain transfer agents. Figure 10 shows the plot of polymer number-average molecular weight (M_n) versus the mole ratio of ethylene/9-BBN

Table 7 Summary of metallocene-mediated ethylene (1 atm) polymerization in the presence of 9-BBN chain transfer agent, using $[Cp^*_2ZrMe]^+[MeB(C_6F_5)_3]^-$ (I), $[Cp^*_2ZrMe]^+[B(C_6F_5)_4]^-$ (II), $[(Ind)_2ZrMe]^+[MeB(C_6F_5)_3]^-$ (III), and $[Cp_2ZrMe]^+[MeB(C_6F_5)_3]^-$ (IV) catalysts

Run no.	Catalyst	9-BBN (mmol/L)	Catalyst activity (kg/mol·h)	M_n (kg/mol)	M_w/M_n
VII-I-1	I	0	2,333	85.2	2.0
VII-I-2	I	3.0	1,333	76.0	2.4
VII-I-3	I	4.5	1,366	55.5	2.9
VII-I-4	I	7.5	1,033	42.2	2.6
VII-I-5	I	12	800	19.4	2.7
VII-I-6	I	18	500	8.9	3.2
VII-I-7	I	23	167	3.7	4.0
VII-II-1	II	4.5	1,333	59.4	2.6
VII-II-2	II	7.5	1,000	46.2	2.5
VII-III-1	III	7.5	1,267	43.9	2.3
VII-IV-1	IV	7.5	1,667	46.9	2.1

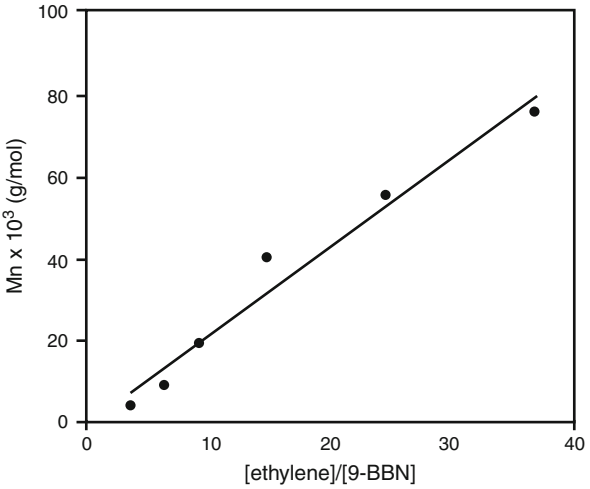

Fig. 10 Plot of the average molecular weights (M_n) of PE-*t*-B polymers versus the mole ratio of [ethylene]/[9-BBN] in the feed (runs VII-I-2 to VII-I-7)

for comparative runs VII-I-2 to VII-I-7 (see Table 7). The polymer's molecular weight is almost linearly proportional to the molar ratio of [ethylene]/[9-BBN]. It is clear that the chain transfer reaction with 9-BBN (with rate constant k_{tr}) is the dominant termination process, and competes with the propagating reaction (with rate constant k_p). The degree of polymerization (X_n) follows a simple comparative equation $X_n = k_p[\text{olefin}]/k_{tr}[\text{9-BBN}]$ with a chain transfer constant $k_{tr}/k_p \sim 1/75$.

A similar B–H chain transfer reaction was also applied to prepare borane terminated syndiotactic polystyrene (s-PS-*t*-B) using the $[Cp^*TiMe_2]^+[MeB(C_6F_5)_3]^-$ catalyst system [52]. The chain transfer reaction was clearly revealed by the systematic reduction of the polymer molecular weight with an increase in 9-BBN concentration. The catalyst activity was somewhat depressed if a high concentration of 9-BBN was present in the system, which reflects the competitive

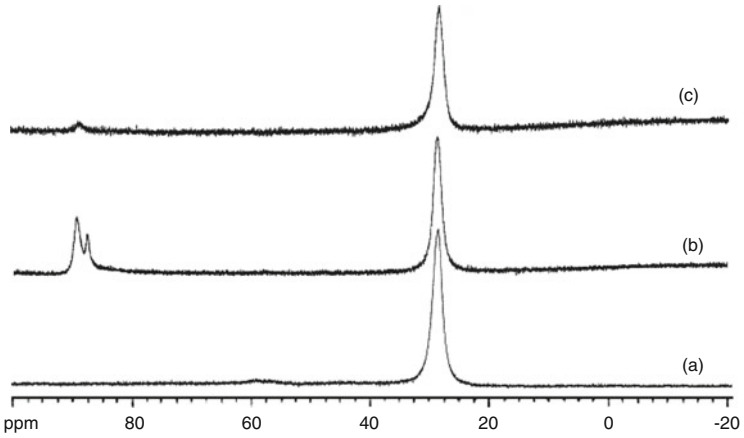

Fig. 11 ^{11}B NMR spectra comparison of (*a*) 9-BBN dimer and (*b*) the reaction adducts between 9-BBN dimer and commercial MAO (containing TMA) and (*c*) between 9-BBN dimer and the purified MAO (without TMA) in toluene at 20°C for 15 min

coordination at the titanocene active sites between monomers and chain transfer agents. The syndiotacticity and melting temperatures of all s-PS-*t*-B polymers are similar to those of the s-PS polymer. The 9-BBN chain transfer agent did not interfere with the regio- and stereoselective insertion process.

At the same time, the extension of this chemistry to prepare borane-terminated isotactic PP (i-PP-*t*-B) is much more difficult [54]. The iso-specific polymerization of propylene is limited to only a few steric-specific catalyst systems with a limited special opening for coordination. In addition, most of the iso-specific catalysts with only perfluoroborate activators show very poor catalyst activity. In other words, we have to use MAO activator and identify suitable reaction conditions. We can then carry out the metallocene-mediated propylene polymerization without encountering the ligand exchange reaction between B–H and Al–C moieties. Figure 11 shows the in-situ monitored ^{11}B NMR spectra of the reaction adducts between 9-BBN and two MAO activators, a commercial MAO andpurified MAO, at 20°C for 15 min [53]. The commercial MAO (containing trimethylaluminium, TMA) shows a facile methyl ligand exchange reaction with B–H in 9-BBN. On the other hand, the same reaction in the purified MAO (without TMA) is extremely slow. The results imply that the Al–CH_3 group in TMA is much more reactive toward the B–H group than that of MAO. However, temperature is also a big factor in the exchange reaction. Only about 1.5% of 9-BBN is consumed by the purified MAO in 15 min at 20°C, but it is almost completely consumed when the temperature is elevated to 50°C for 1 h.

The other approach to eliminating the concerns about the B–H chain transfer agent is to use trialkylborane (without B–H moiety), e.g., methyl-substituted 9-BBN (Me-B-9-BBN) and trimethylborane (TMB) that have a B–CH_3 moiety. Table 8 summarizes Cp_2ZrCl_2/MAO mediated ethylene polymerization in the presence of the Me-B-9-BBN chain transfer agent. For comparison, triethylborane (TEB) was also used as the chain transfer agent under similar polymerization

Table 8 Summary of Cp_2ZrCl_2/MAO-mediated ethylene polymerization in the presence of Me-B-9-BBN and TEB chain transfer agents at 50°C

Run no.	Transfer agent/borane concentration (mmol/L)	Catalyst activity ($\times 10^6$ g/mol·h)	M_v (kg/mol)
VIII-I-1	0	13	184
VIII-I-2	Me-B-9-BBN/0.1	12	137
VIII-I-3	Me-B-9-BBN/0.2	12	109
VIII-I-4	Me-B-9-BBN/0.4	9.8	94
VIII-I-5	Me-B-9-BBN/0.9	8.0	89
VIII-I-6	Me-B-9-BBN/1.2	8.3	81
VIII-I-7	Me-B-9-BBN/2.0	6.8	75
VIII-II-1	TEB/0.1	11	182
VIII-II-2	TEB/0.2	9.6	151
VIII-II-3	TEB/0.4	10	135
VIII-II-4	TEB/0.75	9.0	115
VIII-II-5	TEB/1.5	8.4	97
VIII-II-6	TEB/4.5	7.8	99

conditions. From a steric viewpoint, logically the reactivity of a borane chain transfer agent should follow the H–B > CH_3–B > C_2H_5–B sequence [54, 55].

The linear plot [54] of M_v (viscosity average molecular mass) versus the mole ratio of [ethylene]/[Me-B-9-BBN] indicates that chain transfer to Me-B-9-BBN constituted the most significant chain termination mechanism in the polymerization. Based on the slope and the resulting chain transfer constant, there is no significant difference between the two chain transfer moieties, the H–B group in 9-BBN and CH_3–B group in Me-B-9-BBN. This suggests that Me-B-9-BBN is a chain transfer agent almost as effective as 9-BBN in the Cp_2ZrCl_2/MAO-mediated ethylene polymerization. However, there is a significant reduction in chain transfer reactivity for TEB. The difference between TEB and Me-B-9-BBN must largely stem from a steric effect (C_2H_5–B versus CH_3–B) rather than an electronic effect (Lewis acidity), which makes the chain transfer reaction to Me-B-9-BBN more effective than that to TEB. Speculating along this logic, among trialkylborane chain transfer agents of various alkyl substituents, trimethylborane might have the highest reactivity.

It is most intriguing to expand chain transfer methodology to styrenic molecules [56–58] that usually serve as monomers during polymerization reactions. The research stems from an observation during the copolymerization of propylene and *p*-MS using the *rac*-$SiMe_2$[2-Me-4-Ph(Ind)]$_2ZrCl_2$/MAO complex. The reaction was completely stalled at the very beginning of the copolymerization process [42]. The catalyst's deactivation was speculated to be attributed to a steric jamming during the consecutive insertion of 2,1-inserted *p*-MS and 1,2-inserted propylene (k_{21} reaction), as illustrated in Scheme 5. This hypothesis was supported by the finding that a small amount of ethylene dramatically improving the catalyst activity. If the above hypothesis of catalyst deactivation proves correct, we may be able to take advantage of the dormant propagating site to react with hydrogen, which not only recovers the catalytic site but also produces PP polymer with a terminal *p*-MS group. Scheme 8 illustrates a general reaction scheme.

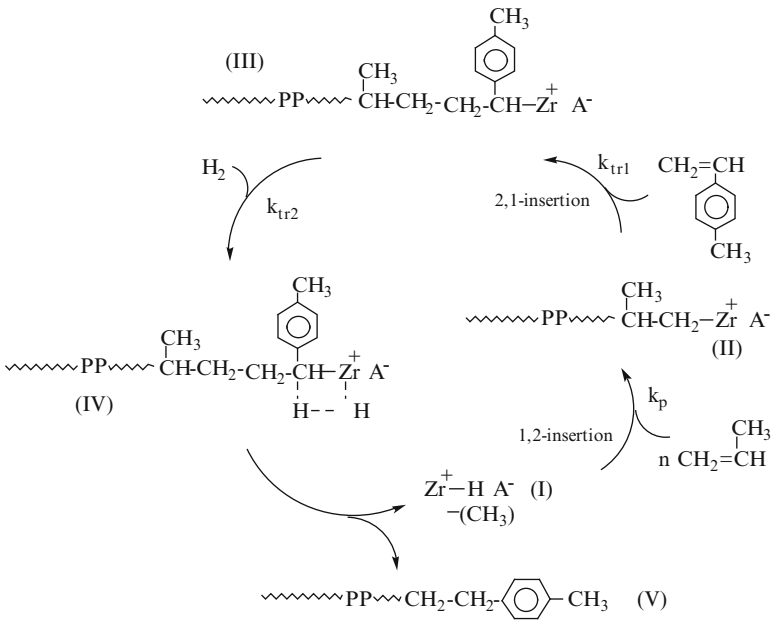

Scheme 8 Synthesis of chain functional polyolefin using styrenic chain transfer agent

During the polymerization of propylene (with 1,2-insertion manner), the propagation Zr–C site (II in Scheme 8) can also react with *p*-MS (with 2,1-insertion manner) to form a dormant propagating site (III) at the terminal *p*-MS unit. Although the catalytic Zr–C site in compound (III) becomes inactive to both propylene and *p*-MS, the dormant Zr–C site (III) can react with hydrogen to form *p*-MS terminated polypropylene (PP-*t*-*p*-MS) (V) and regenerate a Zr–H species (I) that is capable of reinitiating the polymerization of propylene and continuing the polymerization cycles. In other words, the ideal chain transfer reaction should not significantly affect the rate of polymerization, but reduce the molecular weight of the resulting polymer. The molecular weight of PP-*t*-*p*-MS should be linearly proportional to the molar ratio of [propylene]/[*p*-MS].

Figure 12 shows the GPC curves of a systematic set of PP-*t*-*p*-MS polymers prepared by *rac*-Me_2Si[2-Me-4-Ph(Ind)]$_2ZrCl_2$-mediated propylene polymerization with various amounts of the *p*-MS/hydrogen chain transfer agent [56]. The polymer's molecular weight clearly decreases with an increase in *p*-MS concentration. It is interesting to note that the polymer's molecular weight distribution stays relatively narrow (M_w/M_n = ~2), indicating a single site polymerization with a clean chain transfer reaction.

Table 9 summarizes two sets of propylene polymerizations using the *rac*-Me_2Si[2-Me-4-Ph(Ind)]$_2ZrCl_2$/MAO catalyst in the presence of *p*-MS/hydrogen and styrene/hydrogen chain transfer agents to form *p*-MS-terminated PP (PP-*t*-*p*-MS) and styrene-terminated PP (PP-*t*-St) polymers [56]. The in-situ chain transfer

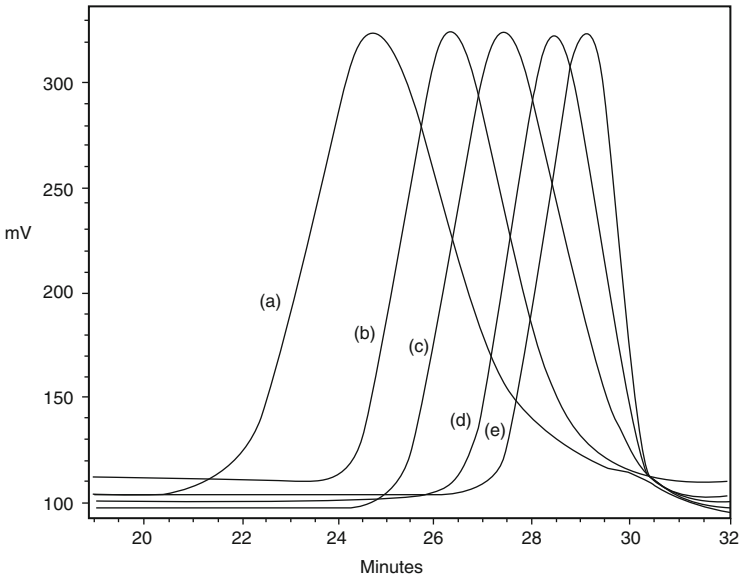

Fig. 12 GPC curves of (*a*) PP (control 1) and (*b–e*) several PP-*t*-*p*-MS polymers prepared by *rac*-$Me_2Si[2\text{-Me-4-Ph(Ind)}]_2ZrCl_2$-mediated propylene polymerization with various amounts (increasing from *b* to *e*) of *p*-MS/hydrogen chain transfer agent

reaction in the *rac*-$Me_2Si[2\text{-Me-4-Ph(Ind)}]_2ZrCl_2$/MAO-catalyzed polymerization of propylene is evidenced by its comparison with two control reactions that were carried out under similar reaction conditions – without the chain transfer agent (control 1) and with *p*-MS only (control 2). A small amount of *p*-MS effectively stops the polymerization of propylene. The introduction of hydrogen restores the catalyst activity, as shown in run IX-I-1, which exhibits about 85% of the catalytic activity of control 1 (without chain transfer agents). Hydrogen is clearly needed to complete the chain transfer cycle during polymerization, as shown in Scheme 8. In general, both *p*-MS/hydrogen and styrene/hydrogen chain transfer systems showed very similar results: the higher the concentration of the *p*-MS (or styrene), the lower the molecular weight of the resulting polymer. The polymer with very low molecular weight (just a few thousand) has been obtained and the molecular weight distribution is generally narrow, which is consistent with single site polymerization processes. The catalyst activity was also proportionally depressed with the concentration of *p*-MS (or styrene), which reflects the competitive coordination at metallocene active sites between monomer and chain transfer agents.

Figure 13 shows the plot of the polymer molecular weight (M_n) versus the mole ratios of [propylene]/[*p*-MS] and [propylene]/[St]. There is a linear proportionality between the polymer molecular weight and molar ratio of [propylene]/[*p*-MS] or [propylene]/[St]. It is clear that the chain transfer reaction to styrenic molecule (with rate constant k_{tr}) is the dominant termination process, with very high chain transfer constant $k_{tr}/k_p \sim 1/6.36$ and 1/7.5 for *p*-MS and styrene, respectively. The

Table 9 Two sets of the experimental results in *rac*-Me_2Si[2-Me-4-Ph(Ind)]$_2ZrCl_2$/MAO-catalyzed polymerization of propylene with *p*-MS/hydrogen and styrene/hydrogen chain transfer agents

Run no.	*p*-MS (mmol/L)	Catalyst activity (kg/mol·h)	*p*-MS in PP (mol%)	M_n (kg/mol)	M_w/M_n
Control 1	0	86,208	0	77.6	2.9
Control 2	30	0	–	–	–
IX-I-1	30	68,430	0.15	54.8	1.9
IX-I-2	76	33,664	0.41	25.8	2.3
IX-I-3	153	12,192	0.61	11.7	2.0
IX-I-4	305	4,704	1.47	4.4	1.8
IX-I-5	458	1,728	2.24	1.8	1.4
	Styrene (mmol/L)		Styrene in PP (mol%)		
IX-II-1	34	74,176	0.11	53.4	2.0
IX-II-2	86	28,512	0.33	26.1	1.7
IX-II-3	173	12,224	0.77	9.8	1.6
IX-II-4	346	6,720	1.45	4.6	1.5
IX-II-5	519	3,328	2.11	1.8	1.5

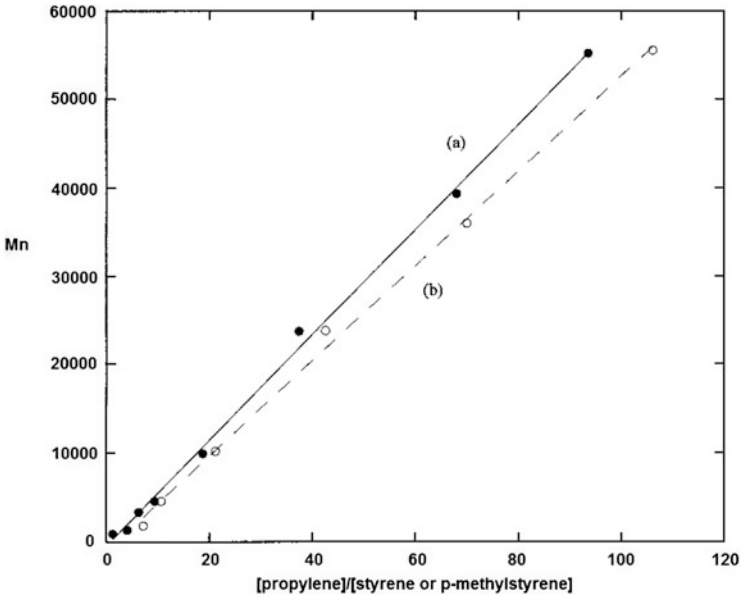

Fig. 13 Plots of number average molecular weights (M_n) of (*a*) PP-*t*-St and (*b*) PP-*t*-*p*-MS polymers versus [propylene]/[styrene] and [propylene]/[*p*-MS], respectively

cationic nature of the catalyst site is reflected in its higher reactivity to *p*-MS than to styrene during the chain transfer reactions.

End-group structures at both polymer chain ends provide direct evidence of the chain transfer reaction. This analysis was greatly benefited by the low molecular weight polymers. Figure 14 shows a ^{1}H NMR spectrum of PP-*t*-*p*-MS

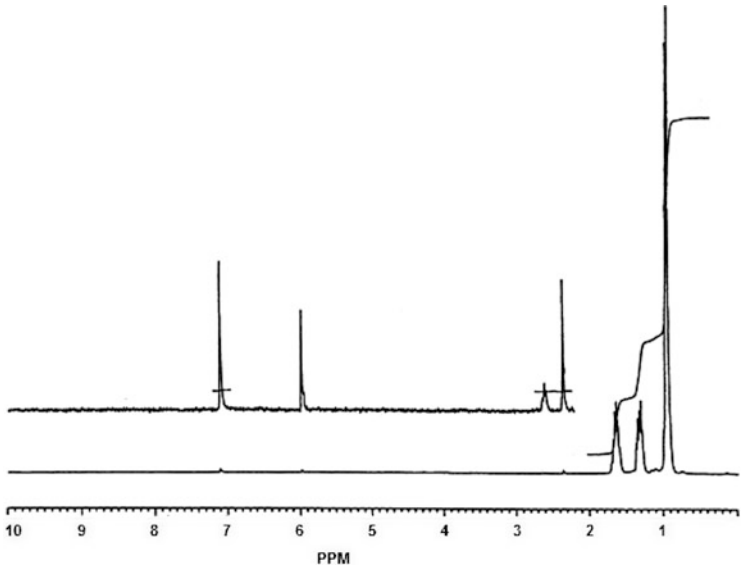

Fig. 14 ^{1}H NMR spectrum of a PP-*t*-*p*-MS polymer (M_n = 4,600)

(M_n = 4,600). In addition to the peaks between 0.9 and 1.7 ppm corresponding to protons in the PP chain, there are three peaks at 2.7, 7.1, and 2.35 ppm corresponding to –C**H**$_2$–C$_6$**H**$_5$–C**H**$_3$, respectively, located at the polymer chain end. The polymer molecular weight calculated from the chain-end group is quite consistent with that of the GPC result. We also measured the ^{13}C NMR spectrum of the PP-*t*-*p*-MS sample (M_n = 4,600 g/mol). In addition to three major peaks (δ = 21.6, 28.5, and 46.2 ppm) corresponding to the **C**H$_3$(mmmm), **C**H, and **C**H$_2$ groups in the PP backbone; the spectrum exhibits all of the carbon chemical shifts associated with both chain ends. The peak intensity ratio indicates both polymer chain ends (–CH$_2$–C$_6$H$_4$–CH$_3$ and –CH$_3$) with about a 1:1 mol ratio. It is important to note that there is no detectable vinyl group associated with the conventional chain transfer process (via β-H elimination), nor any chemical shifts for –**CH**–C$_6$H$_4$–CH$_3$ associated with the copolymerization reaction.

The same chain transfer reaction scheme can be applied to other styrene derivatives that contain a desirable functional group, such as Cl, OH, and NH$_2$. Three functionalized styrenic chain transfer agents (St-f) were investigated: *p*-chlorostyrene (St-Cl), dimethylisopropylsilane protected *p*-vinylphenol (St-OSi), and bis(trimethylsilane) protected *p*-ethylaminostyrene (St-NSi$_2$), as illustrated in Scheme 9, to prepare PP-*t*-St-Cl, PP-*t*-St-OH, and PP-*t*-St-NH$_2$ polymers with a terminal functional group [58].

No external protection agent is needed for St-Cl in *rac*-Me$_2$Si[2-Me-4-Ph (Ind)]$_2$ZrCl$_2$/MAO-catalyzed polymerization of propylene. However, both the OH and NH$_2$ groups are highly sensitive to the metallocene cationic site. The silane groups not only provide effective protection for both the OH and NH$_2$ functional

Scheme 9 Three functional styrenic derivatives used as the chain transfer agents in *rac*-Me_2Si[2-Me-4-Ph(Ind)]$_2ZrCl_2$/MAO-catalyzed polymerization of propylene

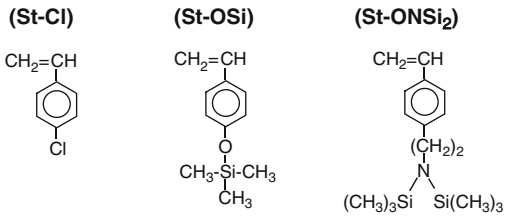

Table 10 Experimental results for *rac*-Me_2Si[2-Me-4-Ph(Ind)]$_2ZrCl_2$/MAO-catalyzed polymerization of propylene (100 psi) with St-Cl/H_2, St-OSi/H_2, and St-NSi_2/H chain transfer (CT) agents

Run no.	CT agent/concentration (mmol/L)	Catalyst activity (kg/mol·h)	CT agent in PP (mol%)	M_n (kg/mol)	M_w/M_n
X-I-1	St-Cl/144	70,435	0.12	46.1	2.1
X-I-2	St-Cl/289	45,673	0.22	18.7	2.1
X-I-3	St-Cl/433	36,106	0.39	8.4	1.9
X-II-1	St-OSi/198	26,995	0.10	52.5	2.2
X-II-2	St-OSi/396	8,318	0.20	22.0	2.0
X-III-1	St-NSi_2/125	31,655	0.08	58.9	2.3
X-III-2	St-NSi_2/250	10,066	0.19	24.2	2.3

groups during the metallocene catalysis but also can be completely deprotected by aqueous HCl solution during the sample workup procedure. The overall reaction especially benefits from the very small quantity of the chain transfer agent needed in the preparation of high polymers. Therefore, the additional protection–deprotection step causes almost no change in polymerization conditions.

Table 10 summarizes the experimental results involving three chain transfer agents, St-Cl/H_2, St-OSi/H_2, and St-NSi_2/H_2, in the *rac*-Me_2Si[2-Me-4-Ph(Ind)]$_2ZrCl_2$/MAO-catalyzed polymerization of propylene [58]. In all control reactions, a small amount of any styrene derivative (St-f) effectively stops the polymerization of propylene. The introduction of hydrogen restores the catalyst activity. Comparing with the homopolymerization of propylene (without the chain transfer agent), the catalyst activity was proportionally depressed with the concentration of St-f, which reflects the competitive coordination at metallocene active sites between monomer and chain transfer agents. Compared to the corresponding St-Cl cases, the consistently lower catalyst activity in St-OSi and St-NSi_2 cases may imply an effect (steric and/or electronic) from the bulky, protected functional group at the active site to slow the completion of the chain transfer reaction. Fortunately, this effect is small, especially in the preparation of a high molecular weight polymer that only requires a small concentration of the chain transfer agent. Overall, the PP molecular weight is governed by the chain transfer agent; the higher the concentration of the St-f, the lower the molecular weight of the resulting polymer. The plots of polymer molecular weight (M_n) versus the molar ratio of [propylene]/[St-f], including all three St-Cl/H_2, St-OSi/H_2, and St-NSi_2/H_2 chain transfer agents, are all linearly proportional. It is clear that the chain transfer reaction to St-f is the dominant termination process, with a chain transfer constant k_{tr}/k_p of 1/21 for

St-Cl/H_2, 1/48 for St-OSi/H_2, and 1/34 for St-NSi_2/H_2. It is intriguing that the k_{tr}/k_p values are significantly lower than those seen for styrene and *p*-MS under similar reaction conditions. The bulky, protected functional groups may reduce the frequency of the chain transfer reaction.

The terminal functional group at the polymer chain end provides direct evidence for the chain transfer reaction. Figure 15 shows the ^{1}H NMR spectra (with an inset of a magnified region and chemical shift assignments) of PP-*t*-St-OSi polymer ($M_n = 22.0 \times 10^3$, $M_w/M_n = 2.0$) and the corresponding PP-*t*-St-OH. In addition to three major peaks ($\delta = 0.95$, 1.35, and 1.65 ppm) for the C**H**$_3$, C**H**$_2$, and C**H** groups in the PP backbone, there are three minor chemical shifts at 0.25, 2.61, and 6.75–7.18 ppm (with an intensity ratio near 6/2/4) shown in Fig. 15a, corresponding to –OSi(C**H**$_3$)$_2$(*t*-Bu), –C**H**$_2$–Ph, and –CH_2–C_6**H**$_4$–OSi, respectively. The chemical shift for the silane protecting group completely disappears in Fig. 15b, indicating the occurrence of a very effective deprotection reaction during the sample workup step by using HCl solution. The equally split chemical shifts for the phenyl protons, combined with no detectable side product, further indicate the terminal *p*-alkylphenol moiety. The same clean ^{1}H NMR results were also observed in both PP-*t*-St-Cl and PP-*t*-St-NH_2 cases.

Overall, the experimental results strongly indicate a clean and effective reaction scheme. The combination of the facile in-situ chain transfer to St-f/H_2 during the catalytic polymerization of propylene and the subsequent complete deprotection reaction during the sample workup step affords a very interesting reaction scheme for the preparation of chain-end-functionalized i-PP with a Cl, OH, or NH_2 terminal group via a one-pot reaction process.

3 Polyolefin Block and Graft Copolymers

In addition to the preparation of functional polyolefins with side chain and chain-end functional groups (discussed above), the reactive groups (i.e., borane, *p*-MS, and pendant styrene units) in the polyolefin also provide convenient routes for preparation of polyolefin graft and block copolymers [52, 59–65], containing both a polyolefin block (PE, PP, s-PS, etc.) and functional polymer block (acrylic polymers), with good control of the molecular structure. In other words, instead of obtaining a functional group from a reactive group, the same reactive group can produce a functional polymer chain with hundreds and thousands of polar groups, which significantly increases the efficiency of the reactive group. In fact, the incorporated borane and *p*-MS groups have been transformed into "living" radical and anion macro-initiators, respectively, for initiating graft-from polymerization with well-controlled molecular structures. On the other hand, the incorporated DVB unit resembles a styrene monomer that can involve the subsequent polymerization reactions [49, 66]. A broad range of polyolefin graft and block copolymers have been prepared that have high functional (polar) group concentrations without compromising desirable polyolefin properties, such as crystallinity, melting

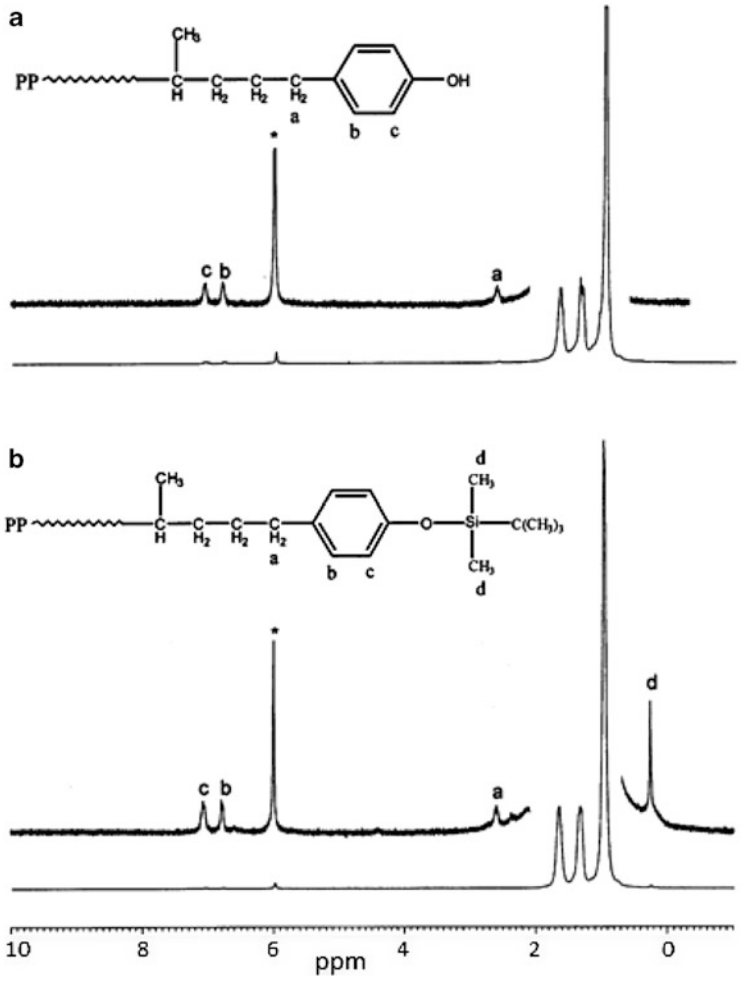

Fig. 15 ^{1}H NMR spectrum of (**a**) a PP-*t*-St-OSi polymer (run X-II-1) and (**b**) its corresponding PP-*t*-St-OH (solvent, $C_2D_2Cl_4$; temperature, 110°C). The groups corresponding to peaks *a–d* are indicated

temperature, elasticity, etc. They are highly effective interfacial agents for improving the compatibility of polyolefin blends and composites.

Scheme 10 illustrates a borane-terminated PE (PE-*t*-B), discussed in Sect. 2.2, which is transformed to the PE macro-initiator for forming a polyethylene-*block*-polymethylmethacrylate (PE-*b*-PMMA) diblock copolymer. The terminal borane group in PE (I) can be spontaneously oxidized to a peroxide (B–O–O–C) moiety (II) even at a very low temperature (−65°C). Due to the unfavorable ring strain increase by inserting oxygen into the C–B bonds in the bicyclic ring of 9-BBN, which destroys the stable double chair-form structure, the oxidation reaction selectively takes place at the C–B bond in the linear alkyl group to produce peroxyborane

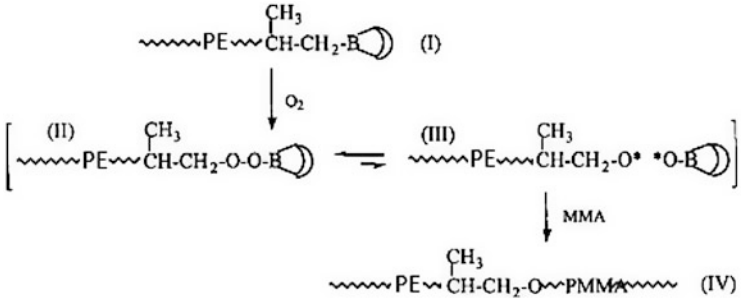

Scheme 10 PP-*b*-PMMA diblock copolymer prepared by PP-*t*-B polymer (macro-initiator) and a borane-mediated control radical graft-from polymerization

(C–O–O–B). The peroxyborane (II) behaves very differently from regular benzoyl peroxides, and consequently decomposes by itself even at ambient temperature. The decomposition reaction follows the homolytical cleavage of peroxide to generate an alkoxy radical (C–O*) and a borinate radical (B–O*). The alkoxyl radical (C–O*), located at the end of the polyolefin chain, is very reactive and can be used for the initiation of radical polymerization with the presence of free radical polymerizable monomers. On the other hand, the borinate radical (B–O*), stabilized by the empty p-orbital of boron through back-donating electron density, is too stable to initiate polymerization. However, the borinate radical may form a weak and reversible bond with the growing chain end during the polymerization reaction [67, 68]. Upon the dissociation of the electron pairs in the resting state, the growing chain end can then react with monomers to extend the polymer chain to form the diblock copolymer (IV). Overall, the reaction process resembles a transformation reaction from metallocene coordination polymerization to living free radical polymerization via a borane group at the polymer chain end. The reaction involves only one borane group per polymer chain. The entire reaction process provides the ultimate test for examining the efficiency of the borane reagent in the chain extension process.

Figure 16 compares the GPC curves of two PE-*b*-PMMA diblock copolymers and the starting PE-*t*-B polymer (M_n = 43,000 g/mol and M_w/M_n = 2.2) [51]. It is clear that the polymer continuously increases in molecular weight during the entire polymerization process. The polymer's molecular weight distribution is maintained at very constant and narrow levels (M_w/M_n = 2.0–2.4). The monochromatic increase of the copolymer molecular weight, with only a slight broadening in the molecular weight distribution and no detectable PE homopolymer, clearly point to the existence of a borane group at each PE chain end and a living radical polymerization of MMA in the chain extension process. The inset shows the linear plot of polymer molecular weight versus monomer conversion and compares the results with a theoretical line based on the polymer molecular weight estimated from [g of monomer consumed]/[mole of initiator]. A good match with the straight line through the origin strongly supports the presence of living polymerization in the reaction. Figure 17 shows the ^{1}H NMR spectra of three PE-*b*-PMMA copolymers

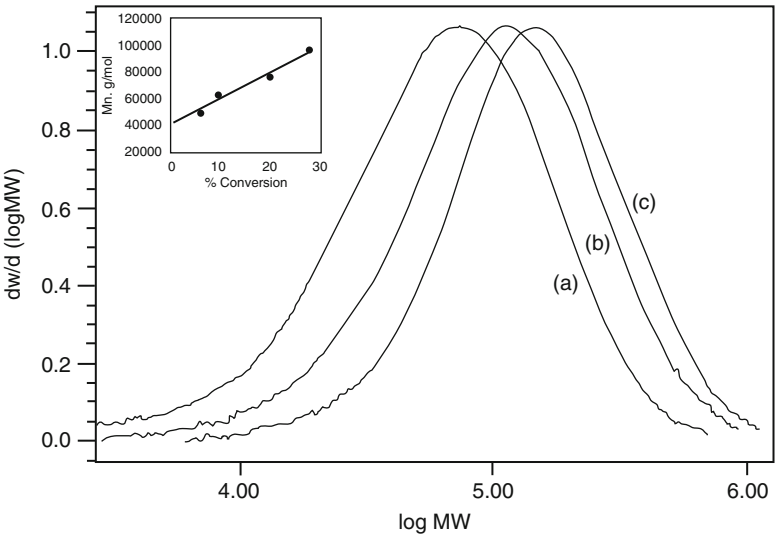

Fig. 16 GPC curves of two PE-*b*-PMMA diblock copolymers with (*a*) M_n = 98,000 g/mol and M_w/M_n = 2.3and (*b*) M_n = 62,000 g/mol and M_w/M_n = 2.4. (*c*) GPC curve for the starting PE-*t*-B polymer (M_n = 43,000 g/mol and M_w/M_n = 2.2). *Inset*: Plot of polymer molecular weight versus monomer conversion. The *line* indicates theoretical values estimated from [g of monomer consumed]/[mole of initiator].

that were sampled at different reaction times during the same chain extension process. The new peak at 3.58 ppm, corresponding to methoxyl groups (C**H**$_3$O) in PMMA, increased in intensity with the reaction time. Evidently, the PMMA segment in PE-*b*-PMMA grew with the reaction time, and a high molecular weight diblock copolymer with up to 85 mol% of PMMA copolymer (Fig. 17c) has been prepared. Considering that there is only one terminal borane group in each PE chain, these experimental results imply a very effective chain extension process.

On the other hand, the incorporated *p*-MS group in the polyolefin (the synthesis discussed in Sect. 2.2), provides the active site to transform metallocene polymerization to living anionic polymerization [56]. Scheme 11 illustrates the anionic reaction process from the PP-*t*-*p*-MS to the PP-*b*-PS diblock copolymer involving only one *p*-MS group per polymer chain. The entire reaction process provides an ultimate test for examining the efficiency of the chain transfer reaction to *p*-MS and the subsequent chain extension process.

The metallation reaction of *p*-MS-terminated polypropylene (PP-*t*-*p*-MS) (I in Scheme 11) was carried out under heterogeneous reaction conditions by suspending the powder form of PP in s-BuLi/TMEDA/cyclohexane solution. To examine the efficiency of the reaction, some of the metallated polymer (II) was terminated with Cl-Si(CH$_3$)$_3$ and examined by ^{1}H NMR measurement, showing about 85% conversion. Most of the lithiated PP-*t*-*p*-MS (II) was used to prepare diblock copolymers. By mixing polymer powder with styrene monomer in cyclohexane solvent, the living anionic polymerization took place to produce PP-*b*-PS diblock copolymer (III). After the reaction, the product was vigorously extracted by refluxing THF to

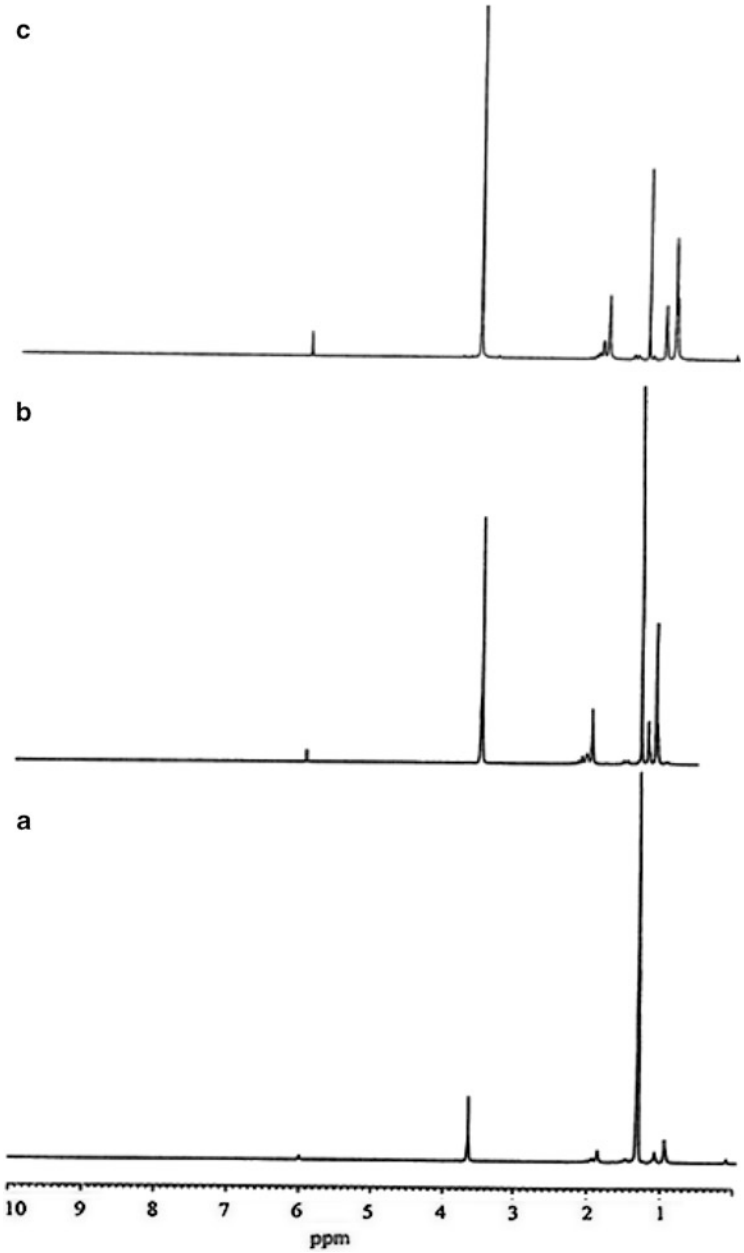

Fig. 17 ^{1}H NMR spectra of three PE-*b*-PMMA diblock copolymers containing (**a**) 22 mol%, (**b**) 40 mol%, and (**c**) 85 mol% of MMA units (solvent, $C_2D_2Cl_4$; temperature, 110°C)

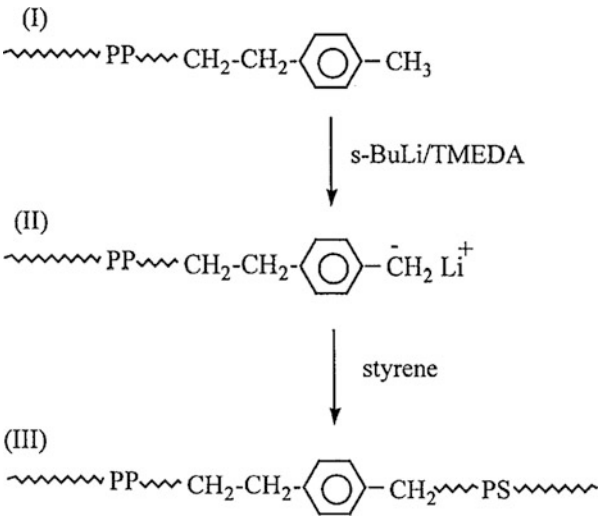

Scheme 11 PP-*b*-PS diblock copolymer prepared by PP-*t*-*p*-MS polymer (macro-initiator) and a living anionic graft-from polymerization

remove any PS homopolymer. In all cases (including high molecular weight PP-*t*-*p*-MS polymer cases), the soluble PS homopolymer fraction was negligible.

Figure 18 (top) shows the ^{1}H NMR spectra of PP-*b*-PS ($M_n = 44 \times 10^3$ g/mol; $M_w/M_n = 2.3$), and Fig. 18 (bottom) compares the GPC curve of PP-*b*-PS with the starting PP-*t*-*p*-MS ($M_n = 26 \times 10^3$ g/mol; $M_w/M_n = 2.3$). Despite the doubling of polymer molecular weight, the molecular weight distribution remains very constant. Diblock copolymer composition was calculated using the ratio of two integrated intensities between the aromatic protons ($\delta = 6.4$–7.3 ppm) in the PS segment and the methylene protons ($\delta = 1.35$–1.55 ppm) in the PP segment, along with the number of protons both chemical shifts represent.

Overall, the transformation from metallocene to living anionic polymerization was very effective (>80%), and the molecular structure of the copolymer could be easily controlled by the starting *p*-MS-terminated polyolefin and the quantity of monomer introduced during the living anionic chain extension reaction. This diblock reaction benefits from the known and well-defined living anionic polymerization process, and offers a complementary method to the previous one, i.e., transformation from metallocene to living free radical polymerization. The combination provides a powerful tool for preparation of a broad range of polyolefin diblock copolymers containing a metallocene-prepared polyolefin block and an anionic or free-radical-prepared polymer block.

4 Functional PP Capacitors for Energy Storage

As discussed, BOPP thin films are currently used as dielectrics in state-of-the-art capacitors [18–21], which can produce a energy density in the range of 2–3 J/cm^3 after applying a high external electric field ($E = 600$ MV/m). Despite the low

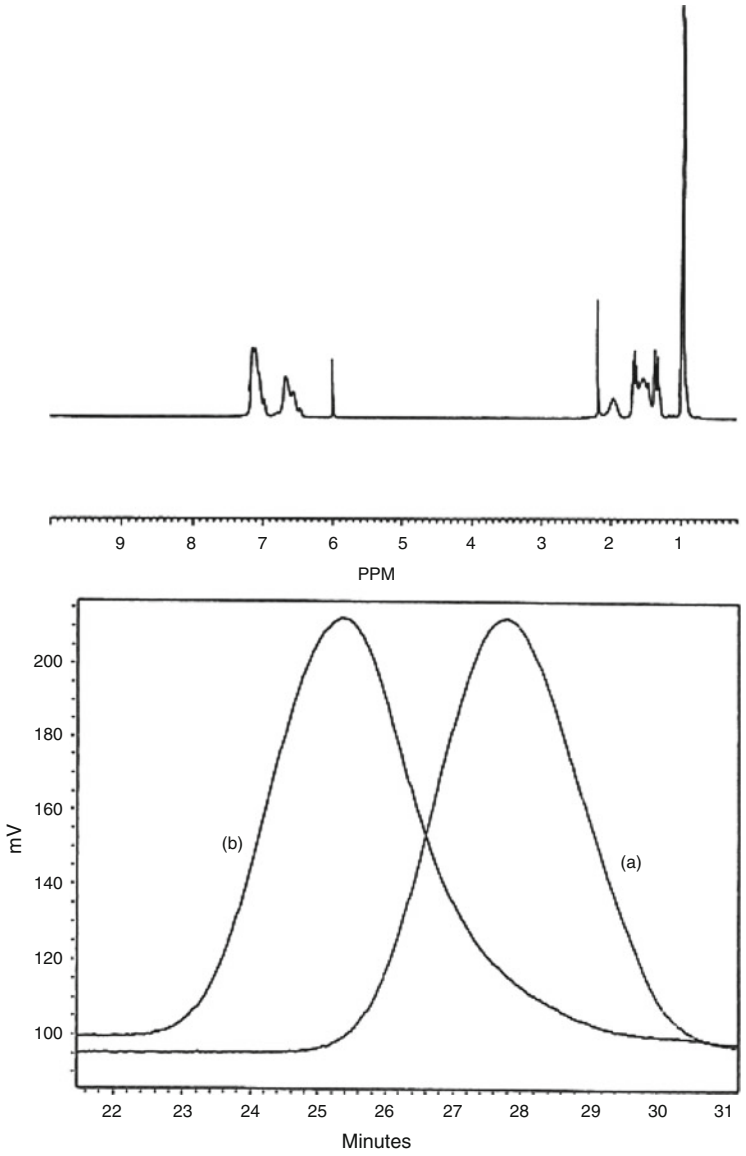

Fig. 18 (*Top*) ^{1}H NMR spectra of PP-*b*-PS diblock copolymer and (*bottom*) GPC curves of the starting PP-*t*-*p*-MS (*a*) and the resulting PP-*b*-PS (*b*) polymers

energy density, BOPP capacitors offer many advantages, including high power density, almost no energy loss, self-healing, and cost effectiveness. On the basis of the energy density equation (given below), a defect-free PP thin film with dielectric constant $\varepsilon = 2.2$, thickness $d = 10$ μm, and applied voltage $V = 5$ kV ($E = 500$ MV/m) can offer a maximum energy density of 2.4 J/cm^3, similar to that of experimental results.

$$\text{Energy density } (\text{J/cm}^3) = \frac{1}{2}\varepsilon\varepsilon_o E^2 = \frac{1}{2}\varepsilon\varepsilon_o (V/d)^2$$

($\varepsilon_o$is the permittivity of free space $= 8.85 \times 10^{-12}$ F/m)

Theoretically, a further increase in the polymer dielectric constant and/or the applied electric field controlled by breakdown strength results in a significantly higher energy density. In the past decade, many research groups have been investigating various polymer dielectrics using both the approaches of increasing dielectric constant (ε) and increasing breakdown strength (E). However, the results are mixed at best [22–24]. So far, there is no suitable material that can fulfill all the required properties (i.e., high energy density, low energy loss, good processability, self-healing, long-term reliability, low cost, etc.). The ε value in the polymer is contributed to by a combination of induced electronic polarization (σ and π electrons), ionization (ion pairs), and segmental motion (including dipole orientation); both electronic and ionic polarizations are fast and reversible, but the segmental chain motion in the viscoelastic polymer matrix is slow and usually not completely reversible in the capacitor application timescale (milliseconds). The slow randomization of the poled polar groups usually causes large hysteresis in the D–E loops (polarization–depolarization or charging–discharging cycles), resulting in large energy loss that significantly limits the capacitor applications. On the other hand, the breakdown strength is not completely understood. Some experimental results indicate strong dependence on the polymer (bond energy, molecular weight, etc.), film quality (morphology, uniformity of film thickness, impurities, and defects), and field distribution.

It is scientifically interesting to understand how it is possible to increase the dielectric activities (high ε value) in PP polymers without altering good polarization reversibility (thin D–E loops) and high breakdown strength (E) in order to achieve higher energy density in PP-based capacitors. I will summarize our experimental results by describing the application of hydroxylated polypropylene (PP–OH) to increase the dielectric constant [69] and crosslinked polypropylene (x-PP) to increase breakdown strength [70] in capacitors. As discussed in Sect. 2.1, PP–OH copolymers (with >4 mol% OH comonomer units) were prepared by both homogeneous and heterogeneous catalyst systems. Due to the large comonomer reactivity difference in the heterogeneous Ziegler–Natta polymerization, the resulting PP–OH copolymers have a tapered molecular structure [37], with the OH-containing side chain units concentrated at one end of the copolymer main chain. Therefore, the increase in comonomer content has less of an effect on the PP chain crystallization. Also discussed in Sect. 2.1, we have developed a new crosslinking chemistry to prepare the x-PP material. The x-PP thin films were obtained via solution casting the PP-BSt/xylene homogeneous solution then initiating a thermal crosslinking reaction between pendant styrene units at 220°C. This cycloaddition process results in uniform x-PP thin films (thickness ~10 μm) without forming any by-products. Impurities would have a detrimental effect on the film stability under high electric fields.

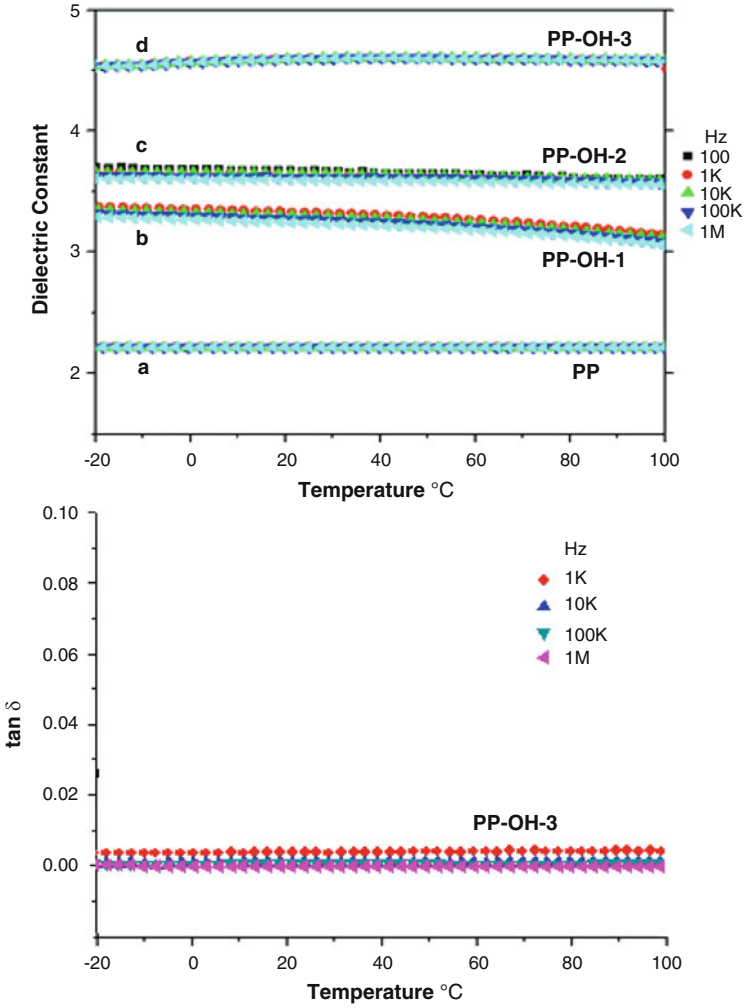

Fig. 19 (*Top*) Dielectric constants and (*bottom*) D–E loops for (*a*) PP and three PP–OH copolymers containing (*b*) 0.7, (*c*) 1.8, and (*d*) 4.2 mol% OH content

Figure 19 shows the dielectric constant (top) and dielectric loss (bottom) of several PP–OH copolymers (I) (Scheme 3) containing 0, 0.7, 1.8, and 4.2 mol% OH comonomer units, as well as the BOPP reference [69]. The dielectric constant increases proportionally with the OH content. The ε value of PP–OH-3 with 4.2 mol% of the OH comonomer content reaches about 4.6 (more than twice that of BOPP). It was a pleasant surprise to observe all PP–OH dielectric profiles resembling the PP profile, with a dielectric constant that is independent over a wide range of frequencies (between 100 and 1 MHz) and temperatures (between −20 and 100°C). These overlapping and flat dielectric constant lines imply a fast polarization response for the PP–OH (I)

copolymer, even under a relatively low electric field condition. At the same time, all PP–OH copolymers also exhibit a similar dielectric loss spectra (resembling that of BOPP); the loss maintains very low ($\tan \delta < 0.001$) frequency between the 1,000 and 1,000,000 Hz range and at temperatures between −20 and 100°C.

Figure 20 shows the D–E loops (top) and energy density (bottom) of several PP–OH copolymers containing 0, 0.7, 1.8, and 4.2 mol% OH comonomer units, as well as the BOPP reference [69]. All PP–OH copolymers exhibit similar linear and slim D–E loops (resembling BOPP); the slope of the D–E loop increases with the OH content, consistent with the dielectric results. In addition, the slope stays constant over a wide range of applied electric fields, up to $E = 600$ MV/m. The charge displacement of PP–OH-3 reaches 2.4 μC/cm^2 at 600 MV/m, which is double that of PP under the same applied electric field. Evidently, the dielectric loss remains very small, with even the PP–OH copolymers exhibiting significantly higher dielectric activities. Figure 20 (bottom) compares the energy density of the same four PP and PP–OH polymers. The energy density ($U_e = \int E dD_{\text{discharing}}$) is estimated from the discharging cycle in Fig. 20 (top), which clearly increases with the OH content and exponentially increases with the applied electric field. At the applied electric field $E = 600$ MV/m, the energy density for PP–OH-3 reaches 7.42 J/cm^3, which is more than double that shown in BOPP capacitors. Most importantly, the increase in energy density does not cause an increase in energy loss (the area enclosed by the charging–discharging cycle), which remains very low (similar to PP) for all PP–OH copolymers.

The OH groups in the flexible side chains clearly contribute to the polarizability of the PP–OH at an unexpectedly large scale, which may originate from the induced electronic polarization of OH groups along with the local dipole orientation. It is peculiar to observe polar group reversible polarization for the first time. As illustrated in Fig. 21, the flexible OH groups may form interchain H-bondings, with a network structure that provides reversible segment stability even when the temperature rises up to 100°C. A FTIR spectrum of PP–OH-3 also shows a broad OH absorption band peaked at 3,300 cm^{-1}, indicating H-bonding between OH groups in the PP–OH copolymer.

Figure 22a compares the breakdown strength of three x-PP copolymers, containing 0.7, 1.4, and 2.1 mol% crosslinkers units, and the corresponding linear PP polymer [70]. Figure 22b shows their Weibull distributions, with the estimated α and β values. All polymer films (thickness: 10–15 μm) were prepared by solution casting before thermal crosslinking. The chemical crosslinking has a significant effect on the breakdown strength and breakdown distribution – the higher the crosslinking density, the higher the breakdown strength (α value) and narrower the distribution (β value). The x-PP-3 thin film shows a breakdown strength between 620 and 670 MV/m, with a α value of 645 MV/m, which is almost the same as those of BOPP films that are carefully conditioned (through stretching and annealing) to increase chain orientation and crystallinity and to reduce defects. In addition, the x-PP-3 film exhibits a very narrow breakdown distribution with an exceptionally high β value of 42, indicating excellent dielectric reliability, which is

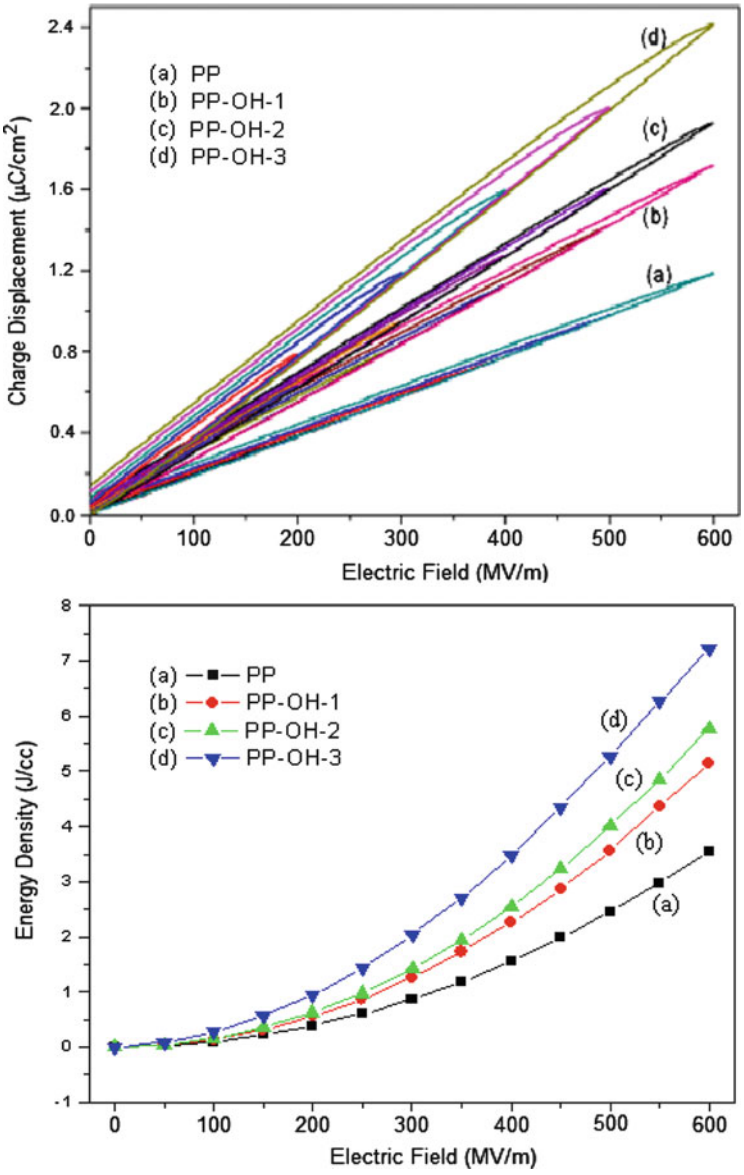

Fig. 20 (*Top*) D–E loops and (*bottom*) energy density for (*a*) PP and three PP–OH copolymers containing (*b*) 0.7, (*c*) 1.8, and (*d*) 4.2 mol% OH content under various applied electric fields

an important quality in capacitors. The combination of a high dielectric constant ($\varepsilon \sim 3$), relatively high breakdown strength (645 MV/m), and low energy loss in the x-PP-3 dielectric film offers a reliable energy density >5 J/cm^3, which is significantly higher than the 2–3 J/cm^3 typically shown in BOPP capacitors.

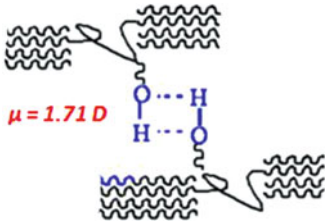

Fig. 21 Illustration showing the dipoles with a network structure via H-bonding between OH groups

In summary, we have systematically examined the structure–property relationship of PP copolymers containing various comonomer units. Both PP–OH and x-PP copolymers having a network structure show reversible polarization with low loss and narrow breakdown distribution. Their dielectric constant remains constant over a wide range of temperatures (between −20 and 100°C), frequencies (between 100 and 1 MHz), and applied electric fields (>600 MV/m). The PP–OH (having 4.2 mol% OH content)-based thin film capacitor displays a linear reversible charge storage capacity with high releasing energy density of >7 J/cm^3 (two to three times that of BOPP) after an applied electric field at $E = 600$ MV/m, without showing any significant increase in energy loss and remnant polarization at zero electric field.

5 Conclusions

It is both a scientific challenge and an industrial goal to develop a general method of preparing functional polyolefins and polyolefin block and graft copolymers containing a polyolefin block and a functional polymer block. The combination of a well-defined metallocene catalysis, the designed "reactive" comonomers (i.e., borane, *p*-MS/H_2, and styrenic dienes), and chain transfer agents (i.e., H–B and CH_3–B moieties, and St-f/H_2) offers a very attractive route with a convenient, direct polymerization process. The resulting functional polyolefins with side chains and chain-end functional (polar) groups show good control of molecular structures. Although only some examples are included in this chapter, this functionalization chemistry is very general, applicable to all polyolefins (including PE, PP, s-PS, and their co- and terpolymers), and can achieve most desirable functional (polar) groups. In addition, the "reactive" sites in the polyolefin permit the facile transformation of metallocene-mediated olefin polymerization to controlled radical or living anionic polymerization. This sequential polymerization process, with both changes of catalytic sites and monomers, allows for the employment of the best suitable polymerization mechanisms for preparing individual polymer blocks, including metallocene polymerization for polyolefins and controlled radical and anionic polymerization for functional (polar) polymers in the polyolefin block and graft copolymers.

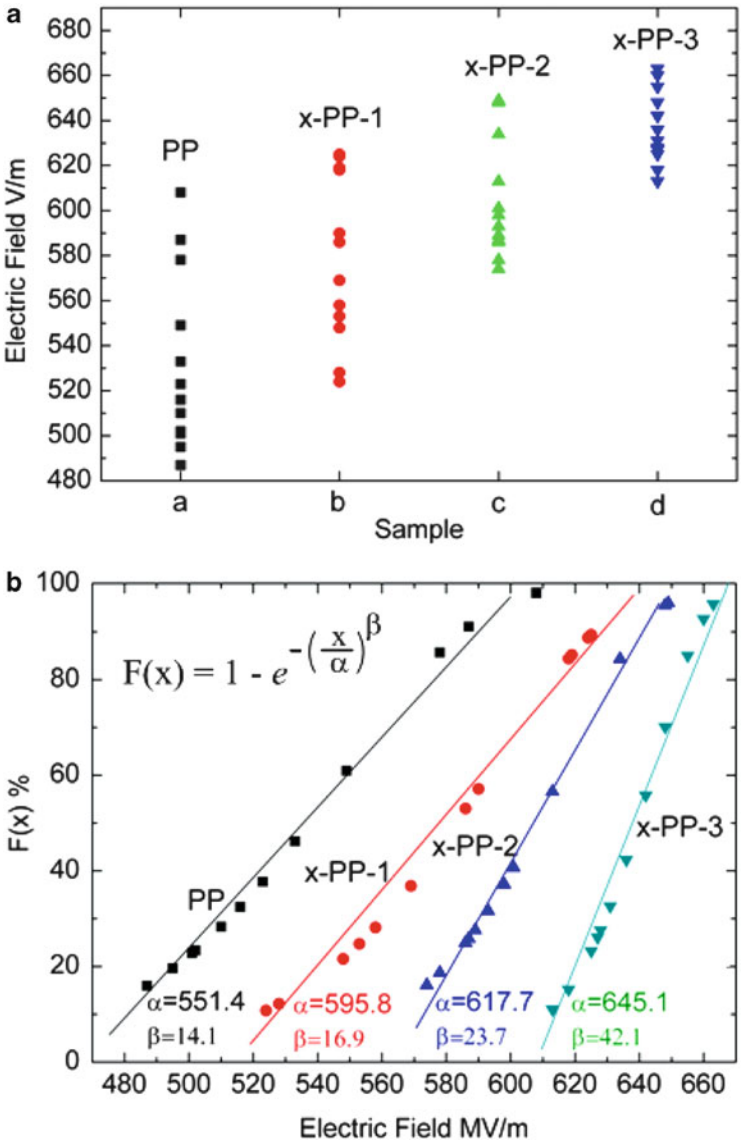

Fig. 22 (**a**) Breakdown strength and (**b**) Weibull distribution for PP, x-PP-1, x-PP-2, and x-PP-3 dielectrics with 0.7, 1.4, and 2.1 mol% crosslinkers, respectively

Both functional polyolefins and polyolefin block/graft copolymers have been shown to dramatically increase in polyolefin adhesion, compatibility, wettability, printability, and ion conductivity through functionalization [71–78]. Traditionally, they are the most difficult areas for polyolefin application and limit polyolefins in high-end applications. I have discussed new applications such as dielectrics for energy storage.

We have seen that a low concentration (a few mol%) of OH polar groups and crosslinking sites in PP can significantly increase energy density and breakdown strength without altering desirable dielectric properties.

References

1. Natta G, Mazzanti G, Longi P, Bernardini F (1958) Isotactic polymers of silicon-containing vinyl monomers. J Polym Sci 31:181
2. Lal J (1958) Polymerization of vinyl ethers by Ziegler catalysts. J Polym Sci 31:179
3. Chung TC (2002) Functionalization of polyolefins. Academic, London
4. Boor J Jr (1979) Ziegler–Natta catalysts and polymerizations. Academic, London
5. Heller J, Tszen DO, Parkinson DB (1963) Polymerization of *N*-vinylcarbazole with Ziegler-type catalyst systems. J Polym Sci 1:125
6. Hopkins E, Miller ML (1963) Polymerization of *t*-butyl acrylate in the presence of *n*-butyl lithium and titanium tetrachloride. Polymer 4:75
7. Bacskai R (1965) Copolymerization of α-olefins with ω-Halo-α-olefins by use of Ziegler Catalysts. J Polym Sci 3:2491
8. Clark KJ, Powell T (1965) Polymers of halogen-substituted 1-olefins. Polymer 6:531
9. Purgett MD, Vogl O (1988) Polymerization of w-alkenoate derivatives. J Polym Sci A Polym Chem 26:677
10. Johnson LK, Killian CM, Brookhart M (1995) New Pd(II)- and Ni(II)-based catalysts for polymerization of ethylene and α-olefins. J Am Chem Soc 117:6414
11. Johnson LK, Mecking S, Brookhart M (1996) Copolymerization of ethylene and propylene with functionalized vinyl monomers by palladium(ii) catalyst. J Am Chem Soc 118:267
12. Correia SG, Marques MM, Ascenso JR, Ribeiro AFG, Gomes PT, Dias AR, Blais M, Rausch MD, Chien JCW (1999) Polymerization with TMA-protected polar vinyl comonomers. II. Catalyzed by nickel complexes containing α-diimine-type ligands. J Polym Sci A Polym Chem 37:2471
13. Singh RP (1992) Surface grafting onto polypropylene – a survey of recent developments. Prog Polym Sci 17:251
14. Jagur-Grodzinski J (1992) Modification of polymers under heterogeneous conditions. Prog Polym Sci 17:361
15. Winter M, Brodd RJ (2004) What are batteries, fuel cells, and supercapacitors? Chem Rev 104:4245
16. Sarjeant WJ (1989) Advanced power sources for space missions, NAS-NRC (EEB) committee on advanced spaced based high power technologies. National Academy Press, Washington
17. Sarjeant W, Zirnheld JJ, MacDougall FW (1998) Capacitors. IEEE Trans Plasma Sci 26:1368
18. Reed CW, Cichanowski SW (1994) The fundamentals of aging in HV polymer-film capacitors. IEEE Trans Dielectr Electr Insul 1:904
19. Sarjeant WJ, MacDougall FW, Larson DW (1997) Energy storage in polymer laminate structures-ageing and diagnostic approaches for life validation. IEEE Electr Insul Mag 13:20
20. Rabuffi M, Picci G (2002) Status quo and future prospects for metallized polypropylene energy storage capacitors. IEEE Trans Plasma Sci 30:1939
21. Picci G, Rabuffi M (2000) Pulse handling capability of energy storage metallized film capacitors. IEEE Trans Plasma Sci 28:1603
22. Wang Z, Zhang ZC, Chung TC (2006) High dielectric VDF/TrFE/CTFE terpolymers prepared by hydrogenation of VDF/CTFE copolymers; synthesis and characterization. Macromolecules 39:4268
23. Zhang ZC, Chung TC (2007) Fluoro-terpolymer based capacitors having high energy density, low energy loss, and high pulsed charge-discharge cycles. Macromolecules 40:783

24. Zhang ZC, Chung TC (2007) The structure-property relationship of PVDF-based polymers with energy storage and loss under applied electric fields. Macromolecules 2007:9391
25. Sinn H, Kaminisky W (1980) Ziegler–Natta catalysts. Adv Organomet Chem 18:99
26. Wild FRWP, Zsolnai L, Huttner G, Brintzinger HH (1982) *ansa*-metallocene derivatives IV. Synthesis and molecular structures of chiral ansa-titanocene derivatives with bridged tetrahydroindenyl ligands. J Organomet Chem 232:233
27. Ewen JA (1984) Mechanisms of stereochemical control in propylene polymerizations with soluble group 4B metallocene/methylalumoxane catalysts. J Am Chem Soc 106:6355
28. Kaminsky W, Kulper K, Brintzinger HH, Wild FRWP (1985) Polymerization of propene and butene with a chiral zirconocene and methylalumoxane as cocatalyst. Angew Chem Int Ed Engl 24:507
29. Chung TC (2002) Synthesis of functional polyolefin copolymers with graft and block structures. Prog Polym Sci 27:39
30. Chung TC (1988) Synthesis of polyalcohols via Ziegler–Natta polymerization. Macromolecules 21:865
31. Ramakrishnan S, Berluche E, Chung TC (1990) Functional groups containing copolymers prepared by Ziegler–Natta process. Macromolecules 23:378
32. Chung TC, Rhubright D (1991) Synthesis of functionalized polypropylene. Macromolecules 24:970
33. Chung TC (1996) Functionalization of polyolefins using borane monomers and transition metal catalysts. Polym Mater Encyclopedia 4:2681
34. Chung TC (1999) Polyolefins containing reactive *p*-methylstyrene groups; from high Tm thermoplastics to low Tg elastomers. J Elastomers Plastics 31:298
35. Chung TC (1996) Polyolefin graft copolymers prepared by Borane approach. Polym Mater Encyclopedia 8:6412
36. Brown HC (1975) Organic syntheses via boranes. Wiley, New York
37. Chung TC, Rhubright D (1993) Kinetic aspects of the copolymerization between α-olefins and Borane monomers in Ziegler–Natta catalyst. Macromolecules 26:3019
38. Dong JY, Manias E, Chung TC (2002) Functionalized syndiotactic polystyrene polymers prepared by the combination of metallocene catalyst and Borane comonomer. Macromolecules 35:3439
39. Chung TC, Lu HL, Li CL (1995) Functionalization of polyethylene using Borane reagents and metallocene catalysts. Polym Int 37:197
40. Chung TC, Lu HL (1997) Synthesis of poly(ethylene-*co*-*p*-methylstyrene) copolymers by metallocene catalysts with constrained ligand geometry. J Polym Sci Polym Chem Ed 35:575
41. Chung TC, Lu HL (1998) Kinetic and microstructure studies of poly(ethylene-*co*-*p*-methylstyrene) copolymers prepared by metallocene catalysts with constrained ligand geometry. J Polym Sci Polym Chem Ed 36:1017
42. Chung TC, Lu HL (1999) Synthesis of poly(propylene-*co*-*p*-methylstyrene) copolymers and functionalization. J Polym Sci Polym Chem Ed 37:2795
43. Chung TC, Hong S, Lu HL (1998) Synthesis of new polyolefin elastomers, poly(ethylene-ter-propylene-ter-*p*-methylstyrene) and poly(ethylene-ter-1-octene-ter-*p*-methylstyrene). Macromolecules 31:2028
44. Lu B, Chung TC (2000) Synthesis of maleic anhydride grafted polyethylene and polypropylene with controlled molecular structures. J Polym Sci Polym Chem Ed 38:1337
45. Dong JY, Chung TC (2002) Synthesis of linear ethylene/divinylbenzene copolymers by metallocene catalysts. Macromolecules 35:2868
46. Dong JY, Hong H, Chung TC, Wang HC, Datta S (2003) Synthesis of linear polyolefin elastomers containing divinylbenzene units and applications in crosslinking, functionalization, and graft reactions. Macromolecules 36:6000
47. Gao C, Dong JY, Chung TC (2005) Hydrogen-assisted unique incorporation of 1,4-divinylbenzene in copolymerization with propylene using an iso-specific zirconocene catalyst. Macromol Rapid Commun 26:1936

48. Lin W, Shao Z, Dong JY, Chung TC (2009) Cross-linked polypropylene prepared by PP copolymers containing flexible styrene groups. Macromolecules 42:3750
49. Langston J, Dong JY, Chung TC (2005) One-pot process of preparing long chain branched polypropylene (LCBPP) using C_2-symmetric metallocene complex and A "T" reagent. Macromolecules 38:5849
50. Langston JA, Colby RH, Shimizu F, Suzuki T, Aoki M, Mike Chung TC (2007) Synthesis and characterization of long chain branched isotactic polypropylene (LCBPP) via metallocene catalyst and T-reagent. Macromolecules 40:2712
51. Xu G, Chung TC (1999) Borane chain transfer agent in metallocene-mediated olefin polymerization; synthesis of Borane-terminated polyethylene and diblock copolymers containing polyethylene and polar polymer. J Am Chem Soc 121:6763
52. Xu G, Chung TC (1999) Synthesis of syndiotactic polystyrene (s-PS) containing a terminal polar group and diblock copolymers containing s-PS and polar polymers. Macromolecules 32:8689
53. Chung TC, Xu G, Lu YY, Hu Y (2001) Metallocene-mediated olefin polymerization with B–H chain transfer agents; synthesis of chain-end functionalized polyolefins and diblock copolymers. Macromolecules 34:8040
54. Lin W, Dong JY, Chung TC (2008) Synthesis of chain end functional isotactic polypropylene by the combination of metallocene catalyst and Borane chain transfer agent. Macromolecules 41:8452
55. Lin W, Niu H, Chung TC, Dong JY (2010) Borane chain transfer reaction in olefin polymerization using trialkylboranes as chain transfer. J Polym Sci A Polym Chem 48:3534
56. Chung TC, Dong JY (2001) A novel consecutive chain transfer reaction to *p*-methylstyrene and hydrogen during metallocene-mediated olefin polymerization. J Am Chem Soc 123:4871
57. Dong JY, Chung TC (2002) Synthesis of polyethylene containing a terminal p-MS group; metallocene-mediated ethylene polymerization with a consecutive chain transfer reaction to P-MS and hydrogen. Macromolecules 35:1622
58. Dong JY, Wang ZM, Han H, Chung TC (2002) Synthesis of isotactic polypropylene containing a terminal Cl, OH, and NH_2 group via metallocene-mediated polymerization/chain transfer reaction. Macromolecules 35:9352
59. Chung TC, Jiang GJ (1992) Synthesis of poly(octene-*g*-MMA) copolymers. Macromolecules 25:4816
60. Chung TC, Jiang GJ, Rhubright D (1993) Synthesis of PP-*g*-PMMA copolymers by Borane approach. Macromolecules 26:3467
61. Chung TC, Janvikul W, Bernard R, Jiang GJ (1994) Synthesis of ethylene-propylene rubber graft copolymers by Borane approach. Macromolecules 27:26
62. Chung TC, Lu HL, Ding RD (1997) Synthesis of polyethylene-*g*-polystyrene and polyethylene-*g*-poly(p-methylstyrene) copolymers. Macromolecules 30:1272
63. Lu HL, Chung TC (1999) Synthesis of PP graft copolymers via anionic living graft-from reactions of polypropylene containing reactive p-methylstyrene units. J Polym Sci Polym Chem Ed 37:4176
64. Chung TC, Lu HL (1997) Functionalization and block reactions of polyolefins using metallocene catalysts and Borane reagents. J Mol Catal A Chem 115:115
65. Chung TC, Lu HL, Janvikul W (1997) A novel synthesis of PP-*b*-PMMA copolymers via metallocene catalysts and Borane chemistry. Polymer 38:1495
66. Gao C, Zou J, Dong JY, Hu YL, Chung TC (2005) Synthesis of PP graft copolymers by the combination of a PP copolymer containing pendant vinylbenzene groups and ATRP process. J Polym Sci Polym Chem Ed 43:429
67. Chung TC, Lu HL, Janvikul W (1996) A new "Living" radical initiator based on the oxidation adducts of alkyl-9-BBN. J Am Chem Soc 118:705
68. Zhang ZC, Chung TC (2006) Reaction mechanism of Borane/oxygen radical initiators during the polymerization of fluoromonomers. Macromolecules 39:5187

69. Yuan X, Matsuyama Y, Chung TC (2010) Synthesis of functionalized isotactic polypropylene dielectrics for electric storage application. Macromolecules 43:4011
70. Yuan X, Chung TC (2011) Cross-linking effect on dielectric properties of polypropylene thin films and applications in electric energy storage. Appl Phys Lett 98:62901
71. Chinsirikul W, Chung TC, Harrison I (1993) Adhesion improvement in polypropylene/aluminum laminates. J Thermoplastic Comp Mater 6:18
72. Lee SH, Li CL, Chung TC (1994) Evaluation of poly(propylene-*co*-hexen-6-ol) as an interfacial agent in PP/glass laminates. Polymer 35:2979
73. Chung TC, Lee SH (1997) New hydrophilic polypropylene membranes; fabrication and evaluation. J Appl Polym Sci 64:567
74. Chung TC, Rhubright D (1994) Polypropylene-*g*-polycaprolactone; synthesis and applications in polymer blends. Macromolecules 27:1313
75. Lu B, Chung TC (1999) New maleic anhydride modified polypropylene copolymers with block structure; synthesis and application in PP/nylon blends, Bing Lu and T. C. Chung. Macromolecules 32:2525
76. Wang ZM, Nakajima H, Manias E, Chung TC (2003) Exfoliated PP/clay nanocomposites using ammonium-terminated PP as the organic modification montmorillonite. Macromolecules 36:8919
77. Zhang M, Kim HK, Lvov SN, Chung TC (2011) New polyethylene based anion exchange membranes (PE-AEMs) with high Cl^- conductivity and good ion selectivity. Macromolecules 44:5937
78. Kim HY, Zhang M, Yuan X, Chung TC (2012) Synthesis of polyethylene-based proton exchange membranes containing PE backbone and sulfonated poly(arylene ethersulfone) side chains for fuel cell applications. Macromolecules 45:2460

Adv Polym Sci (2013) 258: 279–310
DOI: 10.1007/12_2013_219

Published online: 12 June 2013

Polyolefin Nanocomposites and Hybrid Catalysts

Markus Stürzel, Alexander Kurek, Melanie Anselm, Tobias Halbach, and Rolf Mülhaupt

Abstract The interplay of single- and multi-site catalysts with nanoparticles, nanostructure formation, and polymer crystallization represents the key to the development of advanced polyolefin materials for sustainable development. In polymerization filling technology, catalysts are supported on a great variety of nanofillers. In contrast to melt compounding, effective nanoparticle dispersion is readily achieved during catalytic olefin polymerization, independent of polyolefin molar mass. Novel families of in situ-formed polyolefin carbon hybrid materials are based upon single- and multi-layer graphene. Supported multi-site catalysts produce reactor blends as all "polyolefin" nanocomposites, reinforced by in situ-formed shish–kebab-like ultrahigh molecular weight polyolefin nanofibers.

Keywords Catalysis · Molecular reinforcement · Nanocomposites · Olefin polymerization · Polymerization filling · Polyolefin · Reactor blends · Single-site catalyst · Ziegler–Natta

Contents

M. Stürzel, A. Kurek, M. Anselm, T. Halbach and R. Mülhaupt (✉)
Freiburg Materials Research Center and Institute for Macromolecular Chemistry,
Stefan-Meier-Strasse 31, 79104 Freiburg, Germany
e-mail: rolfmuelhaupt@web.de

Abbreviations

CNT	Carbon nanotube
Cr-1	2,6-Bis-[1-(2,6-dimethylphenylimino) ethyl]pyridine chromium(III) chloride
Cr-3	η^5-[3,4,5-Trimethyl-1-(8-quinolyl)-2-trimethyl-silylcyclopentadienyl] chromium(III) chloride
EMI	Electromagnetic interference
Fe-2	2,6-Bis-[1-(2,6-dimethylphenyliminio)ethyl]pyridine iron(II) chloride
FG	Functionalized graphene
FI	Terunori Fujita-invented catalyst
GNP	Graphene nanoplatelets
GO	Graphite oxide
HDPE	High density polyethylene
LDPE	Low density polyethylene
LLDPE	Linear low density polyethylene
MAO	Methylaluminoxane
MLG	Multilayer graphene
MWCNT	Multi-walled carbon nanotubes
POSS	Polyhedral oligomeric silsesquioxane
iPP	Isotactic polypropylene
SWCNT	Single-walled carbon nanotubes
TEM	Transmission electron microscopy
TMA	Trimethylaluminum
UHMW	Ultrahigh molecular weight

1 Introduction

Since the pioneering advances of Ziegler and Natta during the 1950s, remarkable innovations in catalyst and process development stimulate the extraordinary commercial success of polyolefin materials, as reflected by the rapidly increasing growth of polyolefin production [1–3]. Today, polyolefin materials account for more than 40% of the 300 million tons of annual world plastics consumption. In an ideal way, polyolefins meet the demands of sustainable development and green chemistry. Produced in highly energy-, cost-, and resource-effective catalytic processes, free of solvents and problematic byproduct formation, polyolefins have a low carbon footprint and exhibit outstanding versatility in terms of the ability to tailor property profiles, processing, applications, and recycling. As hydrocarbon resins with high oil-like energy content, polyolefin wastes represent a valuable source of energy and of "renewable oil and gas," recovered from wastes by thermal cleavage of polyolefin chains [4]. In view of expanding their application in light-weight engineering and packaging, which is essential for reducing both fuel consumption and carbon dioxide emission in transportation, it is highly desirable

to further improve the balance of stiffness, strength, toughness, dimensional stability, scratch resistance, flame retardancy, electrical and thermal conductivity, as well as processing. Traditionally, this goal is achieved by compounding polyolefins with fillers and fibers [5]. In alternative strategies, both in situ nanostructure and hybrid formation are exploited, aiming at producing nanostructured polyolefin materials that can be processed in conventional injection molding, blow molding, extrusion, and spinning. Moreover, it is an important objective to combine effective matrix reinforcement with other functional properties such as electrical and thermal conductivity, scratch resistance, haptics, and barrier resistance against permeation of gases and liquids.

During the past decade, progress in nanotechnology has enabled the production of a great variety of nanoparticles. However, owing to their high surface area and strong interparticle interactions, many nanoparticles are rather difficult to disperse in highly viscous polymer melts. Therefore, it is beneficial to already disperse nanoparticles during catalytic olefin polymerization in gas phase or in low-viscosity polymerization media. This in situ composite formation eliminates special safety and handling procedures required for melt compounding of nanoparticles, owing to the potential health hazards associated with inhalation. Moreover, progress in heterogenous catalysis offers new opportunities for creating "all polyolefin" skeleton-like superstructures and multilayer composites without requiring the addition of alien materials. This 100% hydrocarbon nature of self-reinforced polyolefins is highly advantageous in view of combining effective recycling with the high resource and energy effectiveness typical for catalytic polymerization. The focus of this overview is on exploiting advanced polymerization catalysis in (nano)composite formation by means of in situ olefin polymerization on nanoparticle-supported catalysts and by reactor blend technology using multi-site catalysts.

2 Polyolefin Nanocomposites and Catalysis

One of the characteristic features of polymer composite materials is the formation of skeleton-like superstructures combining the rather flexible polyolefin matrix with highly rigid dispersed or co-continuous reinforcing phases. Typically, reinforcement is achieved by adding fibers and fillers such as talcum and calcium carbonate [6–11]. Compared with micron-sized fillers, nanometer-sized fillers with average diameter well below 100 nm can significantly change the polymer properties at much lower filler content. In fact, 10^9 nanoparticles are needed to substitute the same volume fraction equivalent to one micron-sized particle. As illustrated in Fig. 1, most of the polymer is allocated at the nanoparticle interface, whereas just a few percent of polymer covers the micron-sized filler surface. Converting bulk polyolefin into interfacial polyolefin can improve properties such as glass transition temperature, stiffness, strength, scratch resistance, and surface gloss [12].

Owing to their specific high surface area and interparticle interactions, nanofillers assemble and percolate at much lower filler content than microfillers.

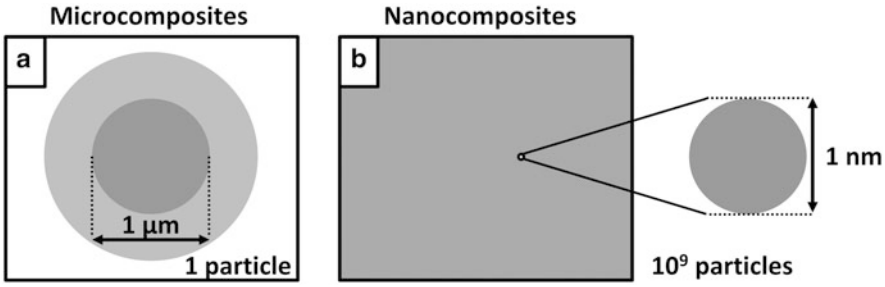

Fig. 1 Polymer composites containing micron- (**a**) and nanometer-sized (**b**) fillers

When using conducting nanofillers, the lower percolation threshold accounts for electrical conductivity at a fraction of conventional fillers. Percolation of highly anisotropic sheet-like nanofillers and their orientation in multilayer assemblies can simultaneously improve dimensional stability, stiffness, strength, toughness, electrical conductivity, and barrier resistance. Although controlled assembly of nanostructures is highly desirable, uncontrolled assembly and formation of large agglomerates is highly detrimental to mechanical as well as functional properties, causing premature mechanical failure at low stresses. Figure 2 displays important members of nanoparticle families used for in situ composite formation. Moreover, it should be mentioned that phase-separated polyolefin crystals of one- and two-dimensionally aligned polyolefins are also highly effective reinforcement agents.

In principle, two strategies are feasible for producing polyolefin nanocomposites by means of polymerization catalysis. In the first strategy, referred to as in situ polymerization, nanoparticles are added during catalytic polymerization. In a variation of this strategy, in situ composite formation, nanoparticles serve as catalyst support. The latter approach was named by Dubois as "polymerization filling technique" [13–18]. Since in both processes polyolefins are formed on the surface of the nanofillers, the nanoparticles are encapsulated in a polyolefin shell, thus promoting nanoparticle dispersion by preventing their agglomeration. It is important that nanoparticle-supported catalysts do not impair control of polyolefin morphology, as reflected by the formation of micron-sized polyolefin particles. In fact, the formation of sub-micron polyolefin particles can account for severe reactor fouling and even explosion hazards when dust-like, highly electrically insulating polyolefin nanoparticles are exposed to air and ignited by electrical discharge. Only the effective immobilization of catalysts on the filler surface prevents catalyst leaching, which can cause the severe reactor fouling typical for homogeneous catalysts.

In the second strategy, oriented crystallization of polyolefins, the production of in situ polyolefin (nano)fibers or (nano)sheets affords molecular polyolefin composites and effective polyolefin matrix reinforcement without requiring any alien fiber or fillers. Moreover, polyolefin reactor blends containing ultrahigh molecular weight (UHMW) polyolefin can produce in situ UHMW polyolefin

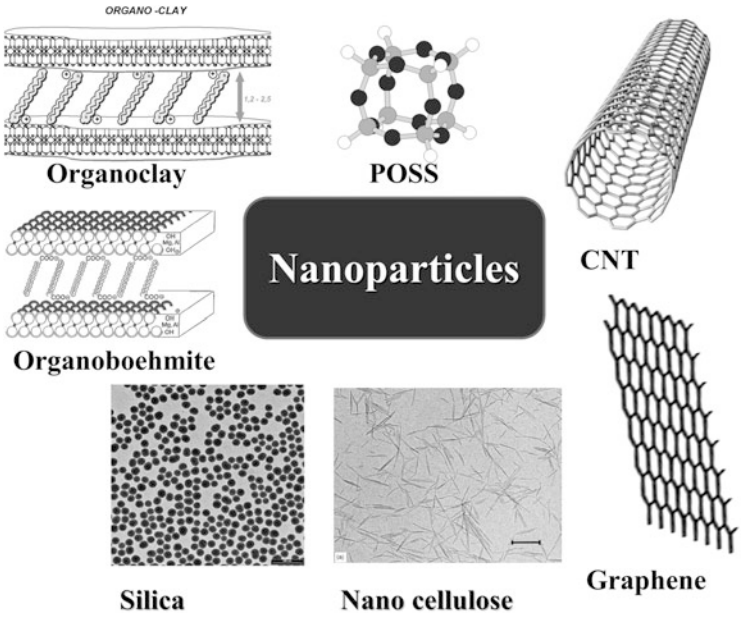

Fig. 2 Nanofiller families including molecules and inorganic nanoparticles

nanofibers as nucleating agents and highly effective reinforcement of the polyolefin matrix, especially when shish–kebab-like structures are formed. Since no alien fillers are needed, these materials are referred to as "all polyolefin" nanocomposites. This second strategy is of particular interest in view of sustainable development with effective recycling of polyolefin materials.

2.1 Polymerization Filling and In situ Nanocomposites

Similar to the immobilization of multi-site catalysts on various inorganic supports such as magnesium chloride, silica, and alumina, the (nano)fillers can be modified in order to enable in situ nanocomposite formation when used in modern catalysis [19]. Preferably, the filler is pretreated with methylaluminoxane (MAO) or other metal alkyls, which are adsorbed on the filler surface and in case of porous structures adsorbed within the pores, forming smaller pores with smaller radii. Since traces of water and hydroxyl groups can cause severe catalyst poisoning, aluminum alkyls are used as highly effective scavengers for rapid conversion of protic and polar impurities as well as surface groups. As illustrated in Fig. 3, in the case of single-site and post-metallocene catalysis, MAO-tethered filler surfaces function in the same way as support and catalyst activator. Examples include silicates, zeolites, boehmites, and functionalized polymer particles [20–27]. Alternatively, the catalyst is attached to the filler surface by covalent bond formation prior to its activation

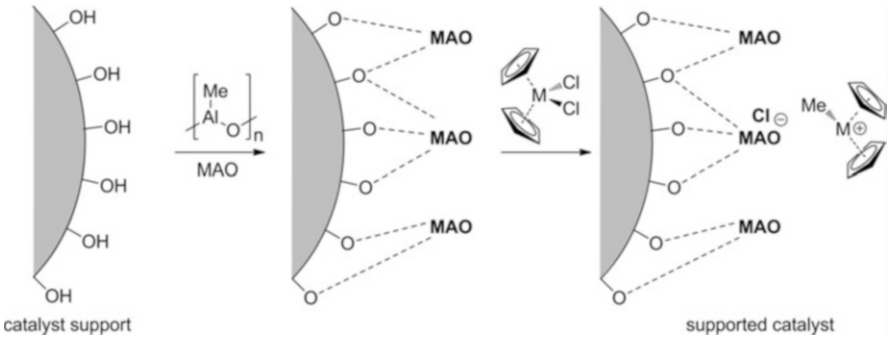

Fig. 3 Polymerization filling using MAO-tethered fillers as metallocene support

[20, 28]. When MAO activates the catalyst prior to contact with filler, the resulting catalyst is much more sensitive to catalyst poisoning by such surface groups. Therefore, non-polar fillers are preferred when injecting the pre-activated catalyst into the filler suspension [20]. In both approaches high catalyst activities are required. Increased demand of catalysts and activating alkyls, paralleled by lower catalyst activities and much higher catalyst residues, can adversely affect polyolefin oxidative stability. The metal alkyls located on the filler surface are fairly stable but are slowly oxidized upon exposure to air. Hence, the resulting peroxides consume the polymer antioxidants, such as sterically hindered phenols during melt processing, thus impairing long-term stability and processing of polyolefins.

A large variety of nanometer-scaled fillers have been employed, ranging from inorganic nanoparticles such as silica to organophilic modified nanoparticles including organoclay and boehmite. Ongoing research exploits the impact of "nanomolecules" polyhedral oligomeric silsesquioxane (POSS) and graphene (cf. Fig. 2). Whereas most in situ polymerization processes require non-polar reaction media, Mecking et al. succeeded in preparing nanocomposites by means of in situ ethylene polymerization in aqueous dispersions using aqueous dispersions of nanosilica from the Stöber process together with water-borne catalyst systems [29].

During the in situ polymerization, the filler is dispersed in the polymerization media prior to injection of the activated catalyst component. Upon initiating olefin polymerization, the polyolefin is formed at the filler surface, thus encapsulating the filler particles. In the polymerization filling technique the (nano)fillers are used as catalyst supports. Preferably, a washing step assures that all catalyst is immobilized on the filler surface and no homogeneous catalysts are formed as byproduct by leaching. The origins of polymerization filling date back to the early days of Ziegler–Natta catalysis. For example, in 1964 Ziegler catalysts were supported on cellulose to produce cellulose/polyolefin composites [30]. Since then a great variety of fillers have been used, including graphite, metals, metal oxide, and silicates [16]. For instance, Howard at Du Pont prepared highly filled UHMWPE composites

containing $CaCO_3$ and $Al_2O_3 \cdot 2\ H_2O$ by immobilizing $TiCl_4/AlR_3$ on the filler surfaces [31, 32]. Supporting tetraalkyl zirconium on predried alumina did not require the addition of aluminum alkyl cocatalysts [33–39]. In view of their applications as implant material, the much more uniform filler dispersion and improved mechanical properties of these UHMWPE composites show significant advantages compared to conventional compounding and powder blends. This is in accord with research reported by Dubois and coworkers, who demonstrated that the performance of kaolin- and barite-composites was far superior to that of melt-compounded composites [40, 41]. Supporting single-site catalysts on fillers enabled improved control of polyolefin molar mass and branching [42]. Kaminsky supported Cp_2ZrCl_2/MAO on starch, cellulose, and aluminum flakes [43]. Extensive studies on polymerization filling by means of filler-supported single-site catalysts were published by the group of Dubois [44], who employed a variety of microfillers such as kaolin, silica, glass beads [13], wollastonite, and magnesium hydroxide [45, 46]. Kaminsky and Zielonka [47] and Schoeppel and Reichert [48] reported the application of in-situ polymerization to form disperse micron-sized zinc and aluminum particles in HDPE, isotactic polypropylene (iPP) and poly(cyclopentene). At high metal content, the resulting Al/polyolefin composites exhibit metal-like high thermal conductivity without the electrical conductivity typical for metals, owing to the very effective encapsulation and insulation of the metal particles. However, at high Al content, the fire retardancy was drastically lowered, causing intolerable fire hazards in engineering applications. Similar polymerization filling strategies were developed for producing cellulose/polyolefin composites [49], HDPE/$CaCO_3$ nanocomposites [50], as well as iPP nanocomposites containing nanometer-sized alumina, magnesium oxide, and boron nitride [50]. The group of Marks exploited the in situ polymerization in the presence of TiO_2 and $BaTiO_3$ to produce dielectric polyolefin hybrid materials with high energy densities [51]. Recently, Rastogi et al. reported on the formation of UHMWPE nanocomposites prepared by polymerization filling using salicylaldimine catalysts supported on TiO_2, ZrO_2, hydroxyapatite, and carbon nanotubes (CNT). The resulting nanocomposites exhibited improved nanofiller dispersion and higher entanglement molar masses [52, 53].

With progress made in nanotechnology, polymerization filling has regained attractiveness in recent years for formation of in situ nanocomposites. Among nanoparticles, layered silicates such as clay minerals are of particular interest as catalyst supports. Polymerization between the individual clay layers can promote intercalation and exfoliation of individual layers, as reflected by dispersion of layer stacks or individual silicate layers within in the polyolefin matrix [54–57]. Prior to the in situ polymerization, the layered silicates such as montmorillonite are rendered organophilic by exchanging sodium cations in the layers for alkyl ammonium cations. A detailed overview on in situ polymerization based on organoclay and layered silicate is presented in Chap. 17 by Woo et al. For instance, HDPE and LLDPE nanocomposites containing exfoliated organophilic layered silicates were prepared by in situ polymerization in the presence of MAO-activated metallocene and diimine catalysts [58–60]. Half-sandwich-titanium complexes were supported on hectorite and montmorillonite to produce HDPE nanocomposites [46, 61]. Supporting

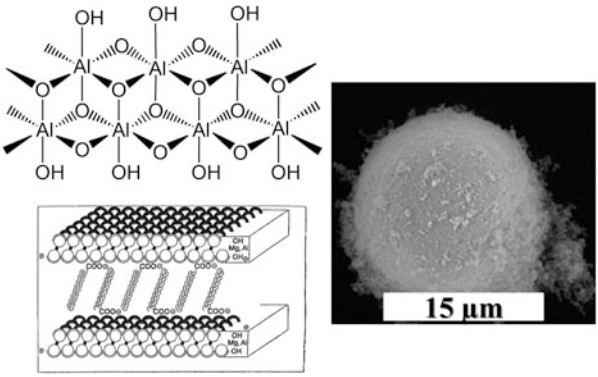

Fig. 4 Boehmite AlO(OH) (*above left*), boehmite rendered organophilic with carboxylate modification (*below left*) and SEM image of a boehmite powder (*right*)

bis(imino)pyridine-Fe on organophilic montmorillonite enabled partial exfoliation in ethylene polymerization and higher crystallinity compared to homogeneous in situ polymerizations [62]. Wei et al. [63] incorporated silica particles between clay layers by means of olefin polymerization on Cp_2ZrCl_2/MAO supported on clay/silica blends, affording enhancements in stiffness and particle morphology. Polymerization filling with traditional Ziegler catalysts [64, 65] as well as single-site metallocenes [66] afforded iPP nanocomposites containing exfoliated clay. Effective organoclay exfoliation and covalent attachment of exfoliated organoclay to the polyolefin matrix was achieved by Shin et al. who used vinyl-functional organoclay modification [67]. Coates et al. immobilized diimine-palladium catalysts in organophilic fluorohectorite modified with alkyl amonium cations [68]. Others immobilized diimine-nickel catalysts to obtain exfoliated clay with bimodal polyethylene [58, 69].

Nanometer-scaled boehmites are attractive support materials for single-site catalysts used for in situ nanocomposite formation [70–74]. Prepared from aluminum metal and alcohol in the Sasol process [75], nanometer-scaled boehmites are readily prepared and rendered organophilic by surface modification with various acids. Figure 4 displays the structure of double layer AlO(OH) and the corresponding alkane carboxylate-modified boehmite together with the morphology of boehmite particles, produced by self-assembly of nano-boehmite primary particles. In the Sasol process it is possible to vary the boehmite particle size between 20 and 80 nm by hydrothermal treatment of the 10-nm primary particles obtained during the sol–gel reaction [76–78]. Also, needle-like boehmites and boehmite nanorods with length of 200–400 nm were obtained [79]. Halbach and Mülhaupt have systematically examined the influence of boehmite size, shape, and aspect ratio (1–20) on composites based upon HDPE and poly(ethylene-*co*-1-octene) thermoplastic elastomers, synthesized by in situ polymerization and melt compounding [70]. As illustrated in Fig. 5, the boehmite nanofiller was dispersed in toluene and pretreated with MAO followed by addition of metallocene. With respect to the homogeneous Cp_2ZrCl_2/MAO, supporting the same metallocene on

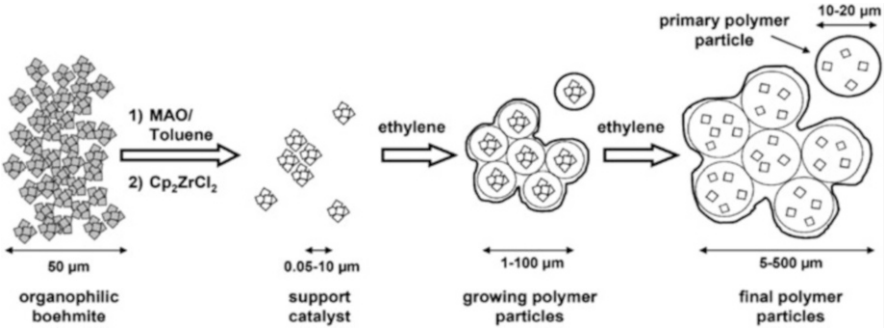

Fig. 5 In situ polymerization of boehmite/HDPE nanocomposites by in situ polymerization. (Reprinted with permission from [71]. Copyright 2008 American Chemical Society)

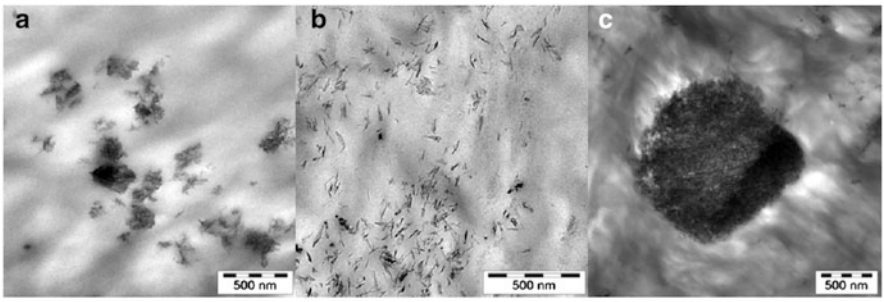

Fig. 6 Transmission electron microscopic images of boehmite/HDPE prepared by (**a**) masterbatch (10 wt% boehmite), (**b**) in situ polymerization (8 wt% boehmite content), and (**c**) melt compounding (10 wt% boehmite)

MAO-tethered boehmite accounted for 100% increase in catalyst activity. Although the homogenous catalyst caused severe reactor fouling, boehmite-supported metallocene catalysts afforded excellent morphology control without any indication of dust-like polyolefin particle formation.

During the in situ ethylene polymerization the boehmite nanoparticles deagglomerate and are encapsulated in HDPE. The hypothetical HDPE growth mechanism is displayed in Fig. 5 accounting for the formation of raspberry-like large HDPE granules containing effectively dispersed nano-boehmite primary particles inside. This in situ ethylene polymerization afforded composites with boehmite content up to 50 wt% without sacrificing melt processability. Such highly filled thermoplastic boehmite/HDPE composites are useful as masterbatches for melt compounding with neat polyolefins. The incorporation of the boehmite nanofillers improved the stiffness without sacrificing high elongation at break, especially when using boehmite with higher aspect ratio. From Fig. 6 it is apparent that the dispersion of nanometer-scaled boehmite by in situ polymerization is much more effective with respect to melt compounding. For effective matrix

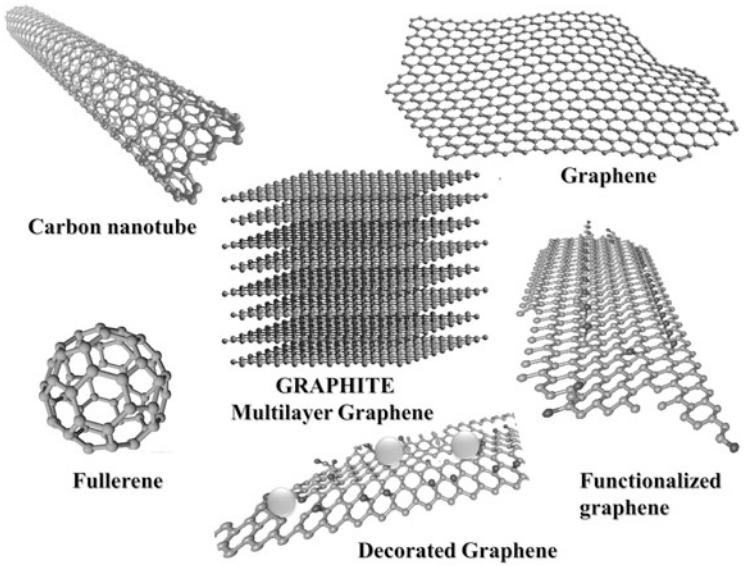

Fig. 7 The family of nanometer-scaled carbon allotropes

reinforcement a high aspect ratio is required. The investigation of iPP melt compounding revealed that non-modified boehmites are effective iPP nucleating agents, whereas the corresponding boehmites with organophilic modification function as anti-nucleating agents, slowing down iPP crystallization [80].

2.2 Polyolefin Carbon Hybrid Materials

Among conventional carbon materials, micron-sized graphite is an attractive filler for polyolefins, combining high electrical and thermal conductivity with excellent lubrication, abrasion resistance, thermo-oxidative and chemical stability, and barrier resistance. Typically, more than 20 wt% graphite is added to polyolefins, owing to the large percolation threshold of graphite microparticles. As illustrated in Fig. 7, graphite consists of graphene stacks. Graphenes are ultrathin but large two-dimensional polycyclic aromatic carbon polymers consisting of an hexagonal array of sp^2-hybridized carbon atoms in a honeycomb-like lattice [81]. With thickness of 0.3 nm for a single layer, the size of graphene sheets can be varied to the meter range. Important parameters governing the performance of polyolefin carbon hybrid materials include carbon particle size, shape, porosity, and surface functionality [82]. From the development of conducting carbon black it is well known that the percolation threshold required for electrical conductivity is drastically lowered when the carbon particle size is reduced well below 100 nm.

Table 1 Properties of MWCNT and graphene

Parameter	MWCNT	Graphene
Young's modulus (TPa)	0.2 [83], 0.8 [84]	1.0 [85]
Tensile strength (GPa)	11 [83], 63 [83], 150 [84]	130 [85]
Electrical conductivity (S cm^{-1})	Various[a]	6,000 [86]
Thermal conductivity (W $m^{-1}K^{-1}$)	3,000 [87, 88]	5,000 [89]
Specific surface area (m^2 g^{-1})	1,315 [90]	2,630 [91]

[a]Reported values vary as a function of structure and temperature; the electrical conductivity falls in the range of semiconductors and metals

Whereas isotropic carbon nanomaterials such as fullerenes offer limited prospects for polyolefin compounds, both carbon nanotubes and graphene are highly attractive with respect to their ultrahigh aspect ratio, extraordinary stiffness, as reflected by a Young's modulus of around 1 TPa, and their extremely fast electron transport (cf. Table 1).

Since the pioneering advances in CNT chemistry during the early 1990s, single- and multi-walled carbon nanotubes (SWCNTs and MWCNTs, respectively) have been rendered available in industrial processes such as catalytic chemical vapor deposition. Aligned CNTs are produced by catalytic chemical vapor deposition using cocatalysts [92], and also by decomposition of ferrocene–xylene complexes in a quartz-tube reactor [93]. According to Maruyama et al., SWCNTs are available by low temperature catalytic chemical vapor deposition at 550°C [94]. Many other approaches and the chemistry of CNTs have been reviewed by Smalley et al. [95, 96] and others [97–108]. However, in spite of the progress made in CNT production, their costs are high and still fail to meet the stringent cost-effectiveness requirements typical for polyolefin commodities. Since many processes produce large assemblies of CNTs, intense efforts are directed at improving CNT dispersion during melt processing of CNT/polyolefin compounds [109]. As an alternative strategy to melt compounding and high shear melt mixing in viscous polymer melts, the in situ polymerization of olefins in the presence of CNTs enables much easier CNT dispersion in low viscosity polymerization media, accompanied by CNT encapsulation in polyolefin. For instance, Kaminsky's group prepared MWCNT nanocomposites based upon iPP and syndiotactic polypropylene (sPP) [17, 110, 111]. Although CNT dispersion and wetting were improved, the fiber-pullout indicated poor interfacial adhesion. Remaining inhomogeneities, owing to incomplete MWCNT dispersion, and adhesion problems accounted for marginal improvements of strength and stiffness. In an attempt to incorporate more effective anchor points at the MWCNT surface, thus enabling covalent bond formation between CNT and MAO, the MWCNTs were functionalized [112]. However, such MWCNT modification requires an additional process step and cannot be integrated into the CNT preparation. MWCNTs are effective nucleating agents for the crystallization of both iPP and sPP, as reflected by increased crystallization temperatures. Bonduel et al. [113] employed metallocene-catalyzed in situ polymerization to produce MWCNT/HDPE nanocomposites. As a function of the cocatalyst type, it was possible to achieve improved morphology control in ethylene

polymerization [114]. Park et al. [115] investigated π–π interactions between MWCNT and the Cp ligand of Cp_2ZrCl_2, which was immobilized on MWCNT. They succeeded in preparing HDPE/MWCNT and UHMWPE/MWCNT nanocomposites. Tong et al. prepared HDPE/SWCNT nanocomposites by in situ Ziegler–Natta polymerization using $MgCl_2/TiCl_4$. Prior to the catalyst preparation, $MgCl_2$ in *n*-butanol was impregnated with SWCNT [116]. In spite of the progress made, the marginal improvement of the polyolefin/CNT property balance does not yet justify the high cost of CNT additives. In contrast to CNT, graphene offers unique opportunities both with respect to lower costs and high performance of polyolefin/carbon composites.

In 2004 Geim and Novoselov prepared defect-free graphene by peeling off individual graphene layers from highly orientated graphite. Their discovery triggered a boom in graphene research. As listed in Table 1, single layer graphene and CNT (SWCNT and MWCNT) exhibit similarly high performance with respect to their excellent mechanical and electrical properties [89, 117–127]. In contrast to CNT, however, graphene, as a two-dimensional polycyclic aromatic carbon polymer, forms electrically conductive, ultralight and optically transparent films that consist of only one carbon atom layer. Owing to thermal fluctuation, graphene does not form planar two-dimensional crystals but has a wavy structure [128, 129]. Graphene is highly impermeable, thus improving barrier resistance against permeation of gas and liquids. Hence, among carbon allotropes, only graphene is capable of simultaneously improving matrix reinforcement, electrical and thermal conductivity, as well as abrasion and barrier resistance. The envisioned applications of defect-free graphene include displays, carbon-based electronics, ultracapacitors. and organic solar cells [117, 119, 122, 130–133]. As illustrated in Fig. 7, the graphene family ranges from sub-micron graphite and multilayer graphene, also referred to as graphene nanoplatelets (GNP), to single-layer graphene. Whereas defect-free graphene additives, produced by chemical vapor deposition (CVD) and other "bottom-up" processes, are not cost-competitive with polyolefins, several "top-down" strategies are at hand, solving this cost/performance problem encountered for MWCNT/polyolefin composites. In principle, as illustrated in Fig. 8, there exist two routes toward producing graphene from graphite: (1) solution exfoliation and mechanical delamination of graphite, and (2) graphite intercalation and subsequent exfoliation.

Intercalation of graphite with sulfuric acid has been commercially used for many years to produce expandable graphite salts as flame retardants [134–136]. During combustion, the salt decomposes to expand graphite, accounting for intumescence [137–140]. The process for making expanded graphite can be modified to prepare functionalized graphene. Typically, graphite is swollen in sulfuric acid and oxidized to produce graphite oxide (GO), containing polar groups such as epoxy, hydroxyl, phenolic, and carboxylic acid groups [141]. As illustrated in Fig. 8, in the subsequent step, GO is chemically or thermally reduced. During thermal reduction, the functional groups decompose, evolving gases such as carbon monoxide and carbon dioxide, while de novo graphitization of the GO layers occurs. In this thermal reduction, rapid heating up to temperatures well above 400°C is required

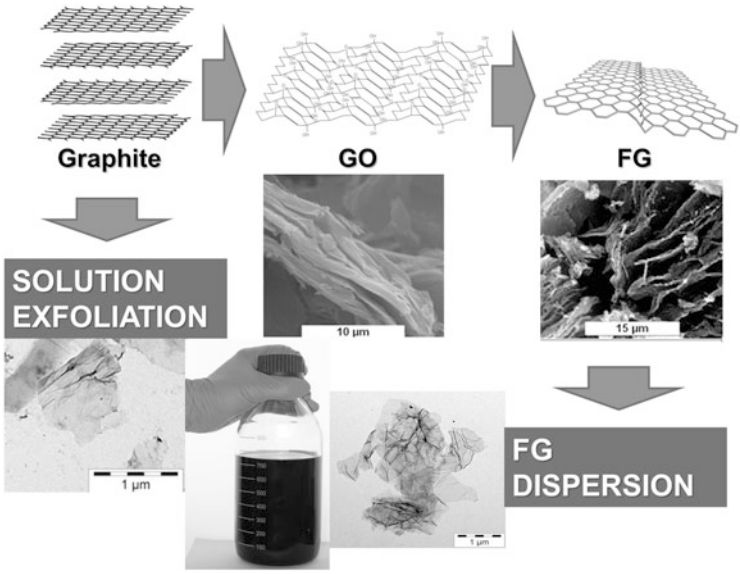

Fig. 8 Preparation of functionalized graphene (FG) dispersions from graphite via thermolysis of graphite oxide (*above*) and via solution exfoliation (*below*)

to build up pressure between the layers, causing expansion and exfoliation of graphene. The resulting functionalized graphene (FG) has an accordion-like architecture. Preferably, the functional groups are allocated at the edges of graphene and of graphene defects such as nanometer-sized holes (cf. Fig. 7), formed during thermolysis. This process is paralleled by a substantial increase in the specific surface area well above 600 m^2/g, approaching the specific surface area of ideal graphene (2,630 m^2/g). The oxygen content, reflecting the presence of functional groups, decreases from 40% to below 1% when increasing the temperature from 300°C to above 1000°C [142, 143], while simultaneously the electrical conductivity increases. Upon shearing, preferably in low viscosity media, individual FG are dispersed, as reflected by a massive increase in the specific surface area above 1,500 m^2/g [141, 144–147]. As is apparent from Fig. 8, FGs are not flat carbon molecules but have a wrinkled structure owing to the presence of the structural defects. The synthesis and properties of FG are the subject of several reviews [148–153]. Using high pressure homogenization, it is possible to produce stable graphene dispersion in polar solvents such as water, acetone and isopropanol without adding binders or dispersing agents [154]. In contrast to the preparation of functionalized CNTs, no additional process step is required for functionalization. The presence of functional groups is attractive for immobilization of catalysts and also for improving interfacial adhesion between FG and polyolefins. In recent years, several other routes have been introduced for exfoliation of graphene from graphite without requiring functionalization. For example, in solution, exfoliation graphite is swollen in polar solvents such as *N*-methyl-2-pyrrolidone (NMP) or butyrolactone

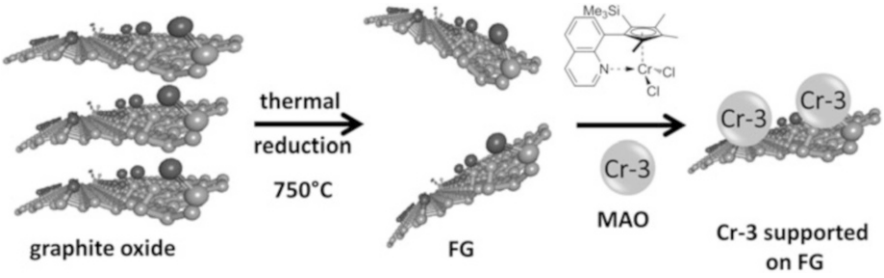

Fig. 9 Preparation of UHMWPE/FG composites by polymerization filling on FG/MAO/Cr-3 (Reprinted with permission from [72] Copyright 2008 American Chemical Society)

to produce single and multilayer graphenes upon shearing [155–163]. In supercritical carbon dioxide, graphite is intercalated, causing graphite expansion when the pressure is released [164, 165]. In mechanical delamination processes, graphene is exfoliated by grinding of graphite [166–168].

The graphite polymerization filling technique was pioneered by Dubois who successfully employed micron-sized graphite fillers to produce thermoplastic polyethylene/graphite composites with an effective filler dispersion [169]. However, in non-polar media, even in the presence of catalysts, graphite is not intercalated and does not produce dispersed graphene. Therefore, several groups have exploited FGs as intermediates for polymerization filling, thus producing FG/polyolefin composites such as FG/HDPE [170–172], FG/LDPE [173], FG/LLDPE [174], and FG/iPP [175], as well as UHMWPE containing nitrogen-doped graphene [176]. As illustrated in Fig. 9, Stürzel and Mülhaupt supported dichloro-η^5-[3,4,5-trimethyl-1-(8-quinolyl)-2-trimethylsilyl-cyclopentadienyl]chromium(III) (Cr-3) on MAO-tethered FG dispersions in *n*-heptane [72]. Owing to the presence of functional groups, very effective immobilization was achieved without leaching, even in the absence of washing steps.

Whereas the homogeneous Cr-3/MAO catalyst afforded broad particle size distributions with substantial amounts of dust-like polyethylene particles, thus accounting for severe reactor fouling, the FG/MAO/Cr-3 produced in situ FG/UHMWPE with much larger UHMWPE particle sizes and without producing fine particles and without any indication for reactor fouling (Fig. 10). In comparison to boehmite, nanometer-scaled carbon black, MWCNT, and graphite, FG gave the highest catalyst activities and produced FG/UHMWPE composites exhibiting simultaneously improved stiffness, strength, and elongation at break at FG content of only 1 wt%. Moreover, FG proved to be a very effective nucleating agent for UHMWPE crystallization.

Using a similar polymerization filling process, metallocenes such as $n\mathrm{Bu_2Cp_2ZrCl_2}$ were supported by Anselm and Mülhaupt on FG/MAO in order to copolymerize ethylene with 1-octene (cf. Fig. 11) [177]. As a function of the ethylene/1-olefin feed ratio, varied by increasing the 1-olefin content from 5 to 50 vol.-% at constant ethylene pressure of 5 bar, the catalytic copolymerization on FG/MAO/$n\mathrm{Bu_2Cp_2ZrCl_2}$

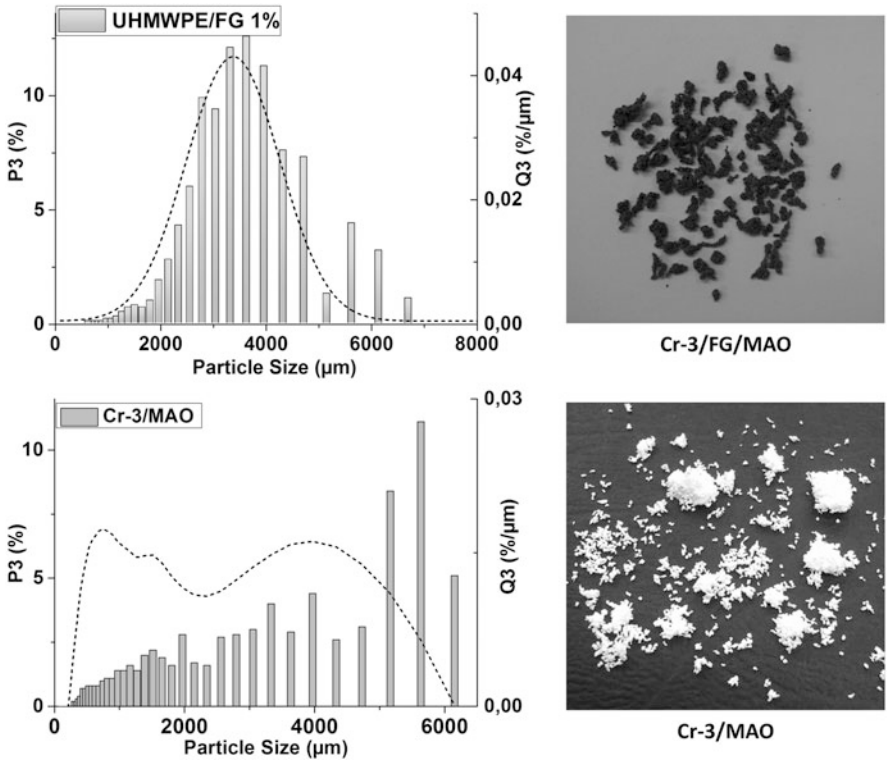

Fig. 10 Particle size distribution of UHMWPE/FG composites, containing 1 wt% Graphene prepared by ethylene polymerization on FG/MAO/Cr-3 (*above*) and the corresponding homogeneous Cr-3/MAO (*below*). (Reprinted with permission from [72] Copyright 2008 American Chemical Society)

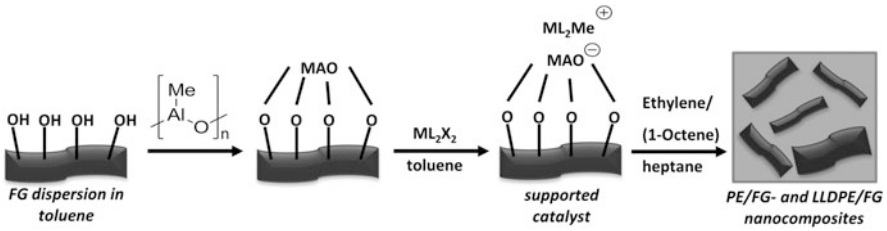

Fig. 11 Preparation of FG/poly(ethylene-*co*-1-octene) nanocomposites by polymerization filling using FG-supported $n\text{Bu}_2\text{Cp}_2\text{ZrCl}_2$/MAO

produced LLDPE and thermoplastic elastomers with 1-octene incorporation varying between 3 and 20 mol%. Both catalyst activity and 1-octene incorporation increased with increasing 1-octene content. From the TEM image in Fig. 12 it is apparent that uniform distribution of FG with the poly(ethylene-*co*-1-octene) matrix was achieved.

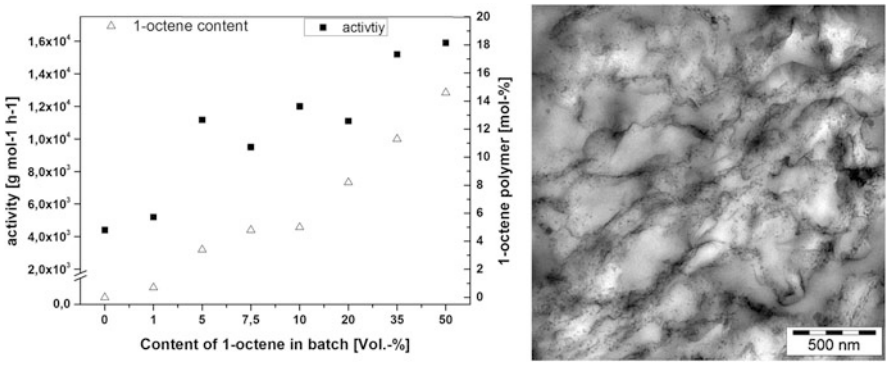

Fig. 12 Polymerization filling by means of ethylene/1-octene copolymerization on FG/MAO/nBu$_2$Cp$_2$ZrCl$_2$. Morphology by TEM reveals uniformly dispersed FG in the polyolefin matrix

The incorporation of uniformly dispersed graphene accounts for improved stiffness, strength, dimensional stability, and barrier resistance.

2.3 "All Polyolefin" Composites and Hybrid Catalysts

In self-reinforcing polyolefins, also referred to as "all polyolefin" composites and as molecular composites, the polyolefin forms both the matrix and reinforcing phases, thus eliminating the need to incorporate alien reinforcing agents [178, 179]. In comparison to conventional composites, containing inorganic and organic fibers with high densities, the much lower density of self-reinforced polyolefins is advantageous with respect to applications in lightweight engineering. Produced by highly active catalysts in solvent-free polymerization processes, combined with melt-processing, "all polyolefin" composites are highly cost-, energy-, and resource effective. They do not require prepreg formation and are readily recycled either by remelting or by thermal cleavage of polyolefin chains. This is essential for enabling quantitative recovery of oil and gas from wastes, which serve as a source of raw materials and energy. As pure hydrocarbon resins, self-reinforced polyolefins are considered to be environmentally benign, offering unique prospects for sustainable development. In principle, the self-reinforcement can be achieved either by 1D or 2D alignment of polyolefin chains by oriented crystallization, preferably of disentangled polyolefins. Hence, either in situ fiber-reinforced polyolefins or "all polyolefin" multilayer composites are formed. Since the interaction and load transmission between identical materials is superior, the in situ formed ultrastrong aligned polyolefins adhere very well to the polyolefin matrix, resulting in very effective stress transfer from the rather weak polyolefin matrix to the strong reinforcing phase. A comprehensive and general overview on strategies

for self-reinforced polymeric materials with a focus on processing technology has been presented by Kmetty and Karger-Kocsis [180] and others [181, 182].

Commercial self-reinforced "all PP" composites, marketed under the trade names Curv™, Pure™, and Armordon™, exploit lamination of extended chain polyolefins such as PP fabrics or stretched PP tapes with different PP grades in surface and core layers. In another approach, polyolefins are processed at temperatures around the melting temperature. Under these processing conditions, the polymer does not form highly entangled random coil polymer chains but crystallizes to produce a chain-extended, virtually non-entangled conformation. For instance, Ehrenstein and coworkers demonstrated that the elongational flow during extrusion of HDPE melt at temperatures very close to the melting temperature produces in situ polyethylene shish–kebab-like HDPE fibers as molecular reinforcement of the HDPE matrix [183]. The shish–kebab structure results from oriented crystallization in elongational flow combined with epitaxial growth of polyethylene crystals onto the extended chain polyethylene. Such self-reinforced HDPE exhibits substantially higher stiffness and strength, paralleled by highly reduced thermal shrinkage measured in the fiber direction. However, the narrow processing window and the limited scope of solid state extrusion hampered commercial application of this technology. For industrial applications it is highly desirable to enable self-reinforcement in conventional injection molding, extrusion, and blow molding processes. Although it is well known that the presence of UHMW polyethylene favors the formation of shish–kebab structures, most of the model HDPE blends containing UHMWPE were prepared by solution blending because in melt processing high amounts of UHMWPE caused a drastic increase in melt viscosity [184, 185]. Indeed, reactor blends of polyethylene with bimodal molar mass distribution, containing a few percent of UHMWPE, are produced on a commercial scale using cascade reactors, multi-zone reactors, and multi-site catalyst technology. As "tie molecules," slightly branched UHMWPE links together polyethylene crystals, thus accounting for the melt strengthening of blow-molded films and considerably improved fatigue resistance of HDPE pipes. Preferably, the bimodal polyethylenes are produced in reactor cascades polymerizing ethylene in the presence and absence of hydrogen. A massive improvement in mechanical properties was achieved when an α-olefin comonomer was incorporated exclusively into the UHMWPE fraction. The progress made in the development of bimodal polyethylenes and reactor cascade technology was reviewed by Böhm [186]. Since melt blending of UHMW polyethylene and low molecular weight polyethylene is rather difficult, owing to the poor melting of UHMWPE, the in situ formation of UHMWPE and HDPE reactor blends during polymerization is the synthetic method of choice.

During the last decade, remarkable progress in catalytic olefin polymerization, cascade and multistage- reactor technology has enabled precise control of molar mass distributions and particle growth [187–189]. Moreover, progress in supported single-site catalyst development has enabled unprecedented control of both molar mass distribution and selective incorporation of 1-olefin comonomers in high molecular weight fractions [190]. In addition to cascade and multi-staged reactor

system, it is possible to use a single reactor with multi-site catalysts, produced by blending together single-site catalyst on the same support. For instance, Kurek and Mülhaupt reported on the formation of polyethylene with tailored bi- and trimodal ultrabroad molar mass distributions [191]. Ethylene was polymerized on silica-supported post-metallocenes and half sandwich multi-site catalysts consisting of 2,6-bis-[1-(2,6-dimethylphenylimino) ethyl]pyridine chromium(III) chloride (Cr-1), 2,6-bis-[1-(2,6-dimethylphenylimino)ethyl]pyridine iron(II) chloride (Fe-2), and η^5-[3,4,5-trimethyl-1-(8-quinolyl)-2-trimethyl-silylcyclopentadienyl] chromium(III) chloride (Cr-3). Whereas UHMWPE is formed on Cr-3, Cr-1 produces wax-like HDPE with molar mass around 1,000 g/mol and Fe-2 produces medium range molar mass around 10^5 g/mol. In contrast to early catalyst generations, the Cr-3 catalyst is very robust and the UHMWPE molar mass produced by Cr-3 is independent of cocatalyst and molar ratio of Cr-1/Fe-2/Cr-3. As shown in Fig. 13, the mixing ratio of Cr-1/Fe-2/Cr-3 affords precise control of the reactor blend composition and molar mass distributions. At constant Cr-1/Fe-2 molar ratio, the UHMWPE content is exclusively controlled by increasing the Cr-3 content without affecting the average molar mass of UHMWPE. The resulting intimate, molecular blend of HDPE with in situ formed nanometer-scaled UHMWPE enables injection molding and blow molding of reactor blends containing more than 10 wt% UHMWPE [192]. According to the TEM image of the reactor blend, displayed in Fig. 14, shish–kebab UHMWPE nanofibers are formed during melt processing. Most likely, the UHMPE slowly crystallizes and forms UHMWPE extended chain crystals, which are highly effective nucleating sites for the lower molecular weight polyethylene with much higher crystallization speed. In the absence of micrometer-scaled UHMWPE, no large UHMWPE particles are found in the HDPE matrix. In comparison to the conventional talcum-filled polyethylene composites and the above mentioned HDPE nanocomposites containing boehmite and graphene, self-reinforced HDPE/UHMWPE reactor blends afford superior strength and stiffness but are composed exclusively of polyethylene.

In HDPE/UHMWPE reactor blend technology and processing of UHMWPE, the entanglement of polymer chains plays an important role. It is well known that the entanglement of (ultra)high molecular weight polyolefins accounts for high melt viscosity reflected by very low melt flow, slow chain mobility, and slow crystallization rates. As a result, UHMW polyolefins are difficult to process by conventional melt processing like extrusion and injection molding. Typically, UHMWPE is processed by compression molding, sintering, and solid state extrusion to produce sheets, plates, and rods, which require subsequent machining. Most of these UHMWPE materials still contain defects and grain boundaries resulting from incomplete melting and bonding of the micron-sized UHMWPE particles. To enable conventional processing and improve the properties of UHMWPE it is imperative to achieve disentanglement of polyethylene chains, enabling extended chain formation during crystallization. Special processing technology such as gel spinning was developed to produce ultrastrong disentangled extended-chain polyethylene fibers, exhibiting a tensile modulus equivalent to the theoretical value [193].

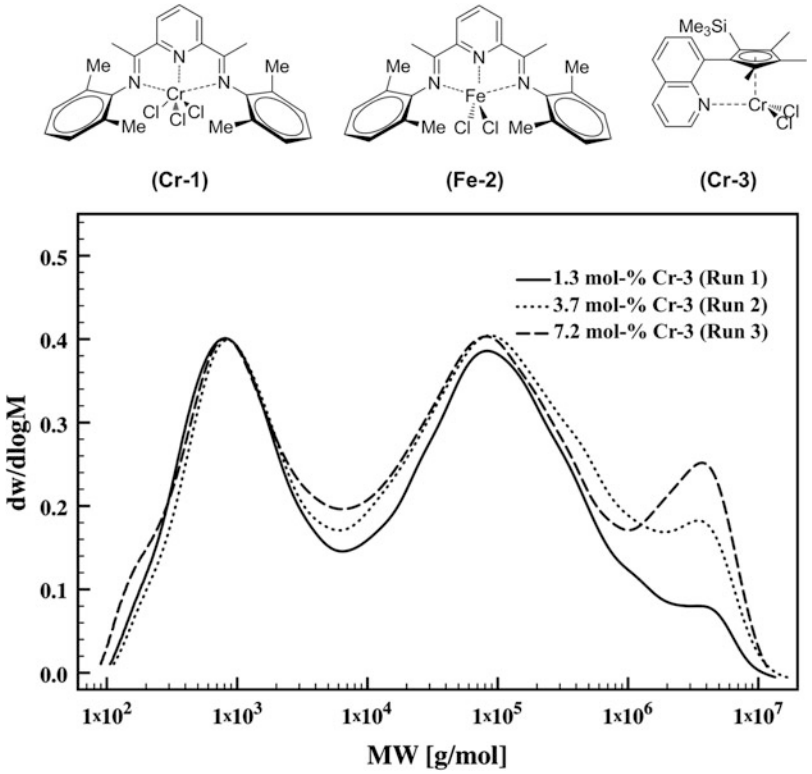

Fig. 13 Molar mass of HDPE/UHMWPE reactor blends prepared on silica-cosupported Cr-1/Fe-2/Cr-3 multi-site catalysts with variable amount of Cr-3 (Reprinted with the permission of [190] Copyright 2010 Wiley VCH)

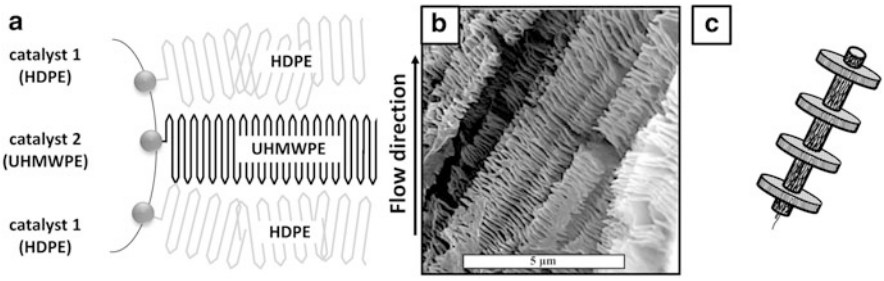

Fig. 14 Melt processing of HDPE/UHMWPE reactor blends (**a**), produced by multi-site catalysis, affords polyethylene reinforced with in situ formed shish–kebab UHMWPE nanofibers (**b**, **c**) [192]

In principle, it is possible to design catalysts producing disentangled polyolefin and extended chain polyolefin crystals. When polymerization takes place below the melting temperature, the polyolefin chains do not form highly entangled random coils. Lowering the polymerization rate relative to the crystallization rate, reducing the number of active sites, and designing novel catalyst systems enables the

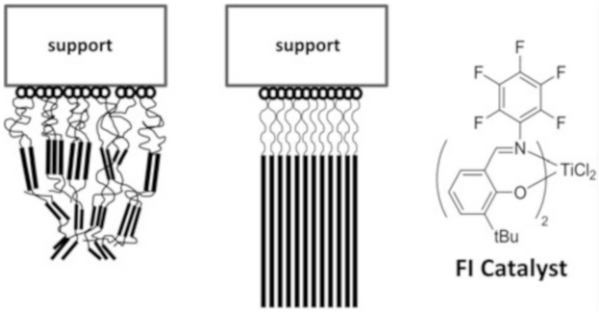

Fig. 15 Entangled (*left*) and disentangled (*center*) polyolefins prepared by catalytic olefin polymerization, e.g., by using the FI catalyst (*right*)

controlled oriented crystallization of extended chain polyolefins. In their pioneering advances, Smith, Chanzy and Rotzinger reported on a $VCl_4/AlEt_3$ catalyst producing disentangled polyethylene on the surface of a glass slide. They succeeded in producing ultrastrong fibers, films, and tapes drawn directly from disentangled virgin UHMWPE without using any solvents [194–196].

The advent of metallocene and post-metallocene catalysis has opened new possibilities for producing "disentangled" UHMWPE, e.g., using the supported FI catalyst displayed in Fig. 15. For instance, Rastogi and coworkers used phenoxy-imine-based catalysts supported on various nanoparticles (e.g., SWCNT, TiO_2, ZrO_2 and hydroxyapatite) to produce disentangled polyethylene at higher temperatures (25°C; 1 bar ethylene) with respect to the polyethylene produced on vanadium catalysts. After drawing in the solid state at temperatures between 125 and 145°C, disentangled polyethylene samples containing different nanoparticles exhibited high crystallinities (>90%) and high moduli at draw ratios >180. Attributed to the nature of the used supports, polymer–particle interactions influence the modulus and activity of the systems. Furthermore, the catalyst activity was significantly increased, most likely by scavenging of aluminum trimethyl by adding small amounts of sterically hindered phenols. It was concluded that modern metallocene catalysis based upon FI catalysts renders disentangled polyethylene readily available and prevents reactor fouling [52, 53, 197, 198]. Yet, in another approach towards disentangled UHMWPE Mecking et al. proposed the catalytic dispersion polymerization of ethylene in aqueous media [199]. LDPE can be used as dispersing agent at elevated temperatures (50°C), forming a stable dispersion of disentangled polyethylene in toluene [200].

3 Summary, Conclusions, and Outlook

The remarkable progress in catalytic olefin polymerization and single-site catalyst technology offers new opportunities for tailoring advanced highly energy-effective and sustainable polyolefin materials. As a function of the catalyst architectures, it is possible to tune polyolefin architectures and properties. Olefin copolymerization and multibranching homopolymerization afford precise control of short- and long-chain branching, thus enabling control of crystallization, density, elasticity, and

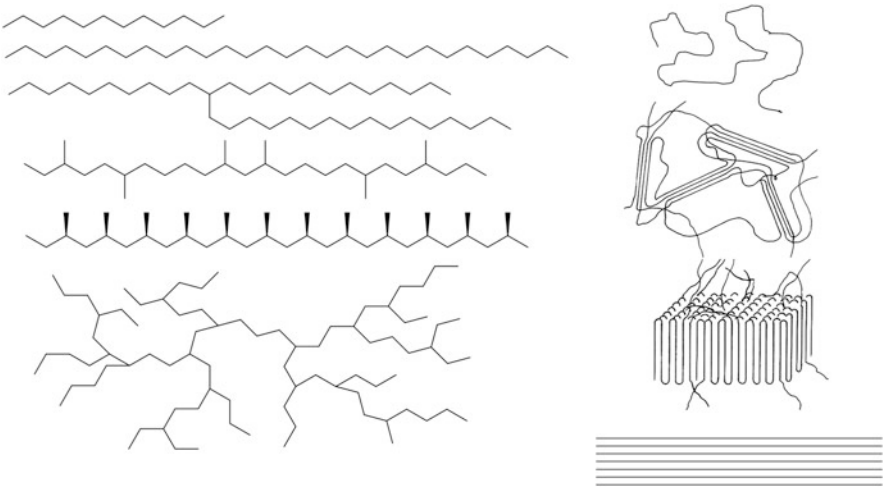

Fig. 16 Tailored polyolefins: from molecular engineering to controlled crystallization and formation of "all polyolefin" nanocomposites

shear thinning. Using reactor cascades, multizone reactors, and blends of single-site catalysts (hybrid catalysts), the molar mass distributions and molar mass-dependent branching are readily varied, thus improving processing, melt strengthening, and fatigue resistance. Morphology control by reactor granule technology eliminates the need for pelletizing extrusion and enables the in situ formation of reactor blends such as impact-modified polyolefins. As illustrated in Fig. 16, the tuning of molecular architectures controls the formation of specific polyolefin conformations such as random coil polyolefins that are typical for highly branched polyolefin elastomers, fringed micelles typical for thermoplastic elastomers and plastomers, chain-folded lamella typical for rigid polyolefin materials, and extended chain polyolefins crystals typical for high strength polyolefin fibers and "all polyolefin" composites.

Today, the interplay of catalysts with nanoparticles and nanostructure formation represents the key to novel generations of polyolefin materials exhibiting unique property combinations. In reactor blend and hybrid catalyst technology, nanophases are incorporated either by polymerization filling, using nanoparticle-supported catalysts, or by controlled polyolefin phase separation, including polyolefin crystallization and blend formation. Graphene-supported catalysts produce unique carbon/polyolefin hybrid materials combining reinforcement with barrier resistance and high electrical and thermal conductivity. Catalyst-mediated one- and two-dimensional alignment of polyolefin chains and disentanglement afford "all polyolefin" nanocomposites as advanced lightweight engineering plastics, exhibiting high cost-, energy-, eco-, and resource-effectiveness typical for catalytic olefin polymerization.

Acknowledgements The authors gratefully acknowledge the financial support of this work by the German Federal Ministry of Education and Research (BMBF) within the *multiKAT* project (project 03X3565C). Moreover, the authors are grateful to LyondellBasell for their longstanding support of our research on olefin polymerization.

References

1. Galli P, Vecellio G (2001) Technology: driving force behind innovation and growth of polyolefins. Prog Polym Sci 26:1287–1336
2. Qiao J, Guo M, Wang L, Liu D, Zhang X, Yu L, Song W, Liu Y (2011) Recent advances in polyolefin technology. Polym Chem 2:1611–1623
3. Pasquini N, Albizzati E, Addeo A (2005) Polypropylene handbook, 2nd edn. Hanser Publishers, Munich
4. Mülhaupt R (2013) Green polymer chemistry and bio-based plastics: dreams and reality. Macromol Chem Phys 214:159–174
5. Nwabunma D, Kyu T (2008) Polyolefin composites. Wiley, Hoboken
6. Manias E, Touny A, Wu L, Strawhecker K, Lu B, Chung TC (2001) Polypropylene/montmorillonite nanocomposites. Review of the synthetic routes and materials properties. Chem Mater 13:3516–3523
7. Usuki A, Hasegawa N, Kato M (2005) Polymer-clay nanocomposites. Adv Polym Sci 179:135–195
8. Zhou Y, Rangari V, Mahfuz H, Jeelani S, Mallick PK (2005) Experimental study on thermal and mechanical behavior of polypropylene, talc/polypropylene and polypropylene/clay nanocomposites. Mater Sci Eng A 402:109–117
9. Chan C-M, Wu J, Li J-X, Cheung Y-K (2002) Polypropylene/calcium carbonate nanocomposites. Polymer 43:2981–2992
10. Yang K, Yang Q, Li G, Sun Y, Feng D (2006) Morphology and mechanical properties of polypropylene/calcium carbonate nanocomposites. Mater Lett 60:805–809
11. Zuiderduin WCJ, Westzaan C, Huétink J, Gaymans RJ (2003) Toughening of polypropylene with calcium carbonate particles. Polymer 44:261–275
12. Mülhaupt R, Schall N, Engelhardt T (2001) Nanocomposites – auf dem Weg zur Anwendung. Kunststoffe 10:178–190
13. Alexandre M, Martin E, Dubois P, Marti MG, Jérôme R (2001) Polymerization-filling technique: an efficient way to improve the mechanical properties of polyethylene composites. Chem Mater 13:236–237
14. Bredeau S, Peeterbroeck S, Bonduel D, Alexandre M, Dubois P (2008) From carbon nanotube coatings to high-performance polymer nanocomposites. Polym Int 57:547–553
15. Dubois P, Alexandre M (2006) Performant clay/carbon nanotube polymer nanocomposites. Adv Eng Mater 8:147–154
16. Dubois P, Alexandre M, Hindryckx F, Jérôme R (1998) Polyolefin-based composites by polymerization-filling technique. J Macromol Sci Part C 38:511–565
17. Funck A, Kaminsky W (2007) Polypropylene carbon nanotube composites by in situ polymerization. Compos Sci Technol 67:906–915
18. Trujillo M, Arnal ML, Muller AJ, Bredeau S, Bonduel D, Dubois P, Hamley IW, Castelletto V (2008) Thermal fractionation and isothermal crystallization of polyethylene nanocomposites prepared by in situ polymerization. Macromolecules 41:2087–2095
19. Severn JR, Chadwick JC, Duchateau R, Friederichs N (2005) "Bound but Not Gagged"--immobilizing single-site α-olefin polymerization catalysts. Chem Rev 105:4073–4147
20. Hlatky GG (2000) Heterogeneous single-site catalysts for olefin polymerization. Chem Rev 100:1347–1376

21. Chadwick J, Severn J (2006) Single-site catalyst immobilization using magnesium chloride supports. Kinet Catal 47:186–191
22. Varkey SP, Lobo RF, Theopold KH (2003) Zeolite MCM-22 supported heterogeneous chromium catalyst for ethylene polymerization. Catal Lett 88:227–229
23. Xalter R, Halbach TS, Mülhaupt R (2006) New polyolefin nanocomposites and catalyst supports based on organophilic boehmites. Macromol Symp 236:145–150
24. Jang Y-J, Nenov N, Klapper M, Müllen K (2003) Organic nanoparticles with polypropyleneoxide chains as support for metallocene catalysts: ethylene homopolymerization and ethylene/α-olefin copolymerization. Polym Bull 50:343–350
25. Klapper M, Jang Y-J, Bieber K, Nemnich T, Nenov N, Müllen K (2004) New organic supports for metallocene catalysts applied in olefin polymerizations. Macromol Symp 213:131–146
26. Stork M, Koch M, Klapper M, Müllen K, Gregorius H, Rief U (1999) Ethylene polymerization using crosslinked polystyrene as support for zirconocene dichloride/methylaluminoxane. Macromol Rapid Commun 20:210–213
27. Nenov N, Koch M, Klapper M, Müllen K (2002) PEO-functionalized polystyrene as polymeric support in metallocene catalysed olefin polymerisation. Polym Bull 47:391–398
28. Mülhaupt R (2003) Catalytic polymerization and post polymerization catalysis fifty years after the discovery of Ziegler's catalysts. Macromol Chem Phys 204:289–327
29. Monteil V, Stumbaum J, Thomann R, Mecking S (2006) Silica/polyethylene nanocomposite particles from catalytic emulsion polymerization. Macromolecules 39:2056–2062
30. Orsino JA, Herman DF, Brancato JJ (1964) Patent US 3,121,698
31. Howard EG, Lipscomb RD, MacDonald RN, Glazar BL, Tullock CW, Collette JW (1981) Homogeneous composites of ultrahigh molecular weight polyethylene and minerals. 1. Synthesis. Ind Eng Chem Prod Res Dev 20:429–433
32. Howard EG, Glazar BL, Collette JW (1981) Homogeneous composites of ultrahigh molecular weight polyethylene and minerals. 2. Properties. Ind Eng Chem Product Res Dev 20:421–428
33. Howard EG Jr, (1975) Filled polyolefin compositions. Patent DE 245,911,8A1
34. Howard EG Jr (1978) Ethylene polymer/acrylonitrile polymer composites. Patent US 4,126,647A
35. Howard EG Jr (1983) Polymerization catalyst for 1-alkenes. Patent US 4,411,821A
36. Howard EG Jr (1992) Preparation of catalytically active fillers for polyolefin composites. Patent US 5,143,549A
37. Howard EG Jr (1993) Homogeneous, high-modulus, ultrahigh-molecular-weight polyethylene composites and their preparation. Patent WO 9303072A1
38. Howard EG Jr, Mahler W (1981) Large pore alumina-supported transition metal alkyl. Patent US 4,304,685A
39. Howard EG Jr, Sarafidis C (1980) Polymerization of propylene with a catalyst prepared in situ. Patent US 4,228,263A
40. Hindryckx F, Dubois P, Jerome R, Teyssie P, Marti MG (1997) Polymerization-filled composites prepared with highly active filler-supported Al/Ti/Mg catalysts. II. Properties of homogeneous polyethylene-based composites. J Appl Polym Sci 64:439–454
41. Hindryckx F, Dubois P, Jerome R, Teyssie P, Marti MG (1997) Polymerization-filled composites prepared with highly active filler-supported Al/Ti/Mg catalysts. I. Synthesis of homogeneous polyethylene-based composites. J Appl Polym Sci 64:423–438
42. Brintzinger HH, Fischer D, Mülhaupt R, Rieger B, Waymouth RM (1995) Stereospecific olefin polymerization with chiral metallocene catalysts. Angew Chem Int Ed 34:1143–1170
43. Kaminsky W (1996) New polymers by metallocene catalysis. Macromol Chem Phys 197:3907–3945
44. Pluta M, Alexandre M, Blacher S, Dubois P, Jerome R (2001) Metallocene-catalyzed polymerization of ethylene in the presence of graphite. II. Structure and electrical properties of the composites. Polymer 42:9293–9300

45. Alexandre M, Martin E, Dubois P, Garcia-Marti M, Jerome R (2000) Use of metallocenes in the polymerization-filling technique with production of polyolefin-based composites. Macromol Rapid Commun 21:931–936
46. Dubois P, Alexandre M, Jérôme R (2003) Polymerization-filled composites and nanocomposites by coordination catalysis. Macromol Symp 194:13–26
47. Kaminsky W, Zielonka H (1993) Polymerization of olefins in the presence of metal powders with homogeneous catalysts. Polym Adv Technol 4:415–422
48. Schoeppel W, Reichert KH (1982) Polymerization of ethene by Ziegler catalysts in the presence of fillers. Makromol. Chem Rapid Commun 3:483–488
49. Kaminsky W, Dutschke J, Maedler H, Miri M, Schlobohm M (1984) Process for the preparation of filled polyolefins. Patent DE3240382
50. Scharlach K, Kaminsky W (2007) PE/$CaCO_3$-nanocomposites synthesized by in-situ polymerization. J Zhejiang Univ Sci A 8:987–990
51. Guo N, DiBenedetto SA, Kwon D-K, Wang L, Russell MT, Lanagan MT, Facchetti A, Marks TJ (2007) Supported metallocene catalysis for in situ synthesis of high energy density metal oxide nanocomposites. J Am Chem Soc 129:766–767
52. Rastogi S, Lippits DR, Peters GWM, Graf R, Yao Y, Spiess HW (2005) Heterogeneity in polymer melts from melting of polymer crystals. Nat Mater 4:635–641
53. Ronca S, Forte G, Tjaden H, Yao Y, Rastogi S (2012) Tailoring molecular structure via nanoparticles for solvent-free processing of ultra-high molecular weight polyethylene composites. Polymer 53:2897–2907
54. Giannelis EP (1996) Polymer layered silicate nanocomposites. Adv Mater 8:29–35
55. Okada A, Usuki A (2006) Twenty years of polymer-clay nanocomposites. Macromol Mater Eng 291:1449–1476
56. Pavlidou S, Papaspyrides CD (2008) A review on polymer–layered silicate nanocomposites. Prog Polym Sci 33:1119–1198
57. Sinha Ray S, Okamoto M (2003) Polymer/layered silicate nanocomposites: a review from preparation to processing. Prog Polym Sci 28:1539–1641
58. Heinemann J, Reichert P, Thomann R, Mülhaupt R (1999) Polyolefin nanocomposites formed by melt compounding and transition metal catalyzed ethene homo- and copolymerization in the presence of layered silicates. Macromol Rapid Commun 20:423–430
59. Scheuermann GM, Rumi L, Steurer P, Bannwarth W, Mülhaupt R (2009) Palladium nanoparticles on graphite oxide and its functionalized graphene derivatives as highly active catalysts for the Suzuki−Miyaura coupling reaction. J Am Chem Soc 131:8262–8270
60. Heinemann J (2000) Herstellung von linearen, verzweigten und funktionalisierten Oligo/Poly (Ethen)en sowie von Polyolfin Nanokompositen durch katalytische Ethenpolymerisation. PhD Thesis, Albert-Ludwigs-University of Freiburg
61. Alexandre M, Dubois P, Sun T, Garces JM, Jerome R (2002) Polyethylene-layered silicate nanocomposites prepared by the polymerization-filling technique: synthesis and mechanical properties. Polymer 43:2123–2132
62. Ray S, Galgali G, Lele A, Sivaram S (2005) In situ polymerization of ethylene with bis (imino)pyridine iron(II) catalysts supported on clay: the synthesis and characterization of polyethylene–clay nanocomposites. J Polym Sci A Polym Chem 43:304–318
63. Wei L, Tang T, Huang B (2004) Synthesis and characterization of polyethylene/clay–silica nanocomposites: a montmorillonite/silica-hybrid-supported catalyst and in situ polymerization. J Polym Sci A Polym Chem 42:941–949
64. Ma J, Qi Z, Hu Y (2001) Synthesis and characterization of polypropylene/clay nanocomposites. J Appl Polym Sci 82:3611–3617
65. Mecking S, Held A, Bauers M (2002) Aqueous catalytic polymerization of olefins. Angew Chem Int Ed 41:544–561
66. Sun T, Garcés JM (2002) High-performance polypropylene–clay nanocomposites by in-situ polymerization with metallocene/clay catalysts. Adv Mater 14:128–130

67. Shin SYA, Simon LC, Soares JBP, Scholz G (2003) Polyethylene–clay hybrid nanocomposites: in situ polymerization using bifunctional organic modifiers. Polymer 44:5317–5321
68. Bergman JS, Chen H, Giannelis EP, Thomas MG, Coates GW (1999) Synthesis and characterization of polyolefin–silicate nanocomposites: a catalyst intercalation and in situ polymerization approach. Chem Comm 1999(21):2179–2180
69. Wang Q, Liu P (2005) Dual bimodal polyethylene prepared by intercalated silicate with nickel diimine complex. J Polym Sci A Polym Chem 43:5506–5511
70. Halbach TS, Thomann Y, Mülhaupt R (2008) Boehmite nanorod-reinforced-polyethylenes and ethylene/1-octene thermoplastic elastomer nanocomposites prepared by in situ olefin polymerization and melt compounding. J Polym Sci A Polym Chem 46:2755–2765
71. Xalter R, Pelascini F, Mülhaupt R (2008) Ethylene polymerization, on-line particle growth monitoring, and in situ nanocomposite formation using catalysts supported on arylsulfonic acid-modified boehmites. Macromolecules 41:3136–3143
72. Stürzel M, Kempe F, Thomann Y, Mark S, Enders M, Mülhaupt R (2012) Novel graphene UHMWPE nanocomposites prepared by polymerization filling using single-site catalysts supported on functionalized graphene nanosheet dispersions. Macromolecules 45:6878–6887
73. Sang L, Chen S-L, Yuan G, Zheng M, You J, Chen A, Li R, Chen L (2012) Metathesis of 1-butene and 2-butene to propene over Re_2O_7 supported on macro-mesoporous γ-alumina prepared via a dual template method. J Nat Gas Chem 21:105–108
74. Coiai S, Passaglia E, Augier S, Narducci P, Ciardelli F (2008) Organophilic boehmite nanoparticles by ATRP methacrylates polymerization: synthesis, characterization and dispersion in polypropylene. J Nanosci Nanotechnol 8:1803–1811
75. Bohnen FM, Siepen K (2001) Method for producing metal oxides dispersibles in organic solvents. Patent PCT/DE2000/002163
76. Bokhimi X, Toledo-Antonio JA, Guzmán-Castillo ML, Hernández-Beltrán F (2001) Relationship between crystallite size and bond lengths in boehmite. J Solid State Chem 159:32–40
77. Martens WN, Kloprogge JT, Frost RL, Bartlett JR (2002) A crystallite packing model for pseudoboehmite formed during the hydrolysis of trisecbutoxyaluminium to explain the peptizability. J Colloid Interface Sci 247:132–137
78. Nguefack M, Popa AF, Rossignol S, Kappenstein C (2003) Preparation of alumina through a sol–gel process. Synthesis, characterization, thermal evolution and model of intermediate boehmite. Phys Chem Chem Phys 5:4279–4289
79. Buining PA, Pathmamanoharan C, Jansen JBH, Lekkerkerker HNW (1991) Preparation of colloidal boehmite needles by hydrothermal treatment of aluminum alkoxide precursors. J Am Ceram Soc 74:1303–1307
80. Streller RC, Thomann R, Torno O, Mülhaupt R (2009) Morphology, crystallization behavior, and mechanical properties of isotactic poly(propylene) nanocomposites based on organophilic boehmites. Macromol Mater Eng 294:380–388
81. Pierson HO (1993) Handbook of carbon, graphite, diamond, and fullerenes properties, processing, and applications. Noyes Publications, Park Ridge
82. Wypych G (2009) Handbook of fillers, 3rd edn. ChemTec Publishing, Toronto
83. Yu M-F, Lourie O, Dyer MJ, Moloni K, Kelly TF, Ruoff RS (2000) Strength and breaking mechanism of multiwalled carbon nanotubes under tensile load. Science 287:637–640
84. Demczyk BG, Wang YM, Cumings J, Hetman M, Han W, Zettl A, Ritchie RO (2002) Direct mechanical measurement of the tensile strength and elastic modulus of multiwalled carbon nanotubes. Mater Sci Eng A 334:173–178
85. Lee C, Wei X, Kysar JW, Hone J (2008) Measurement of the elastic properties and intrinsic strength of monolayer graphene. Science 321:385–388
86. Du X, Skachko I, Barker A, Andrei EY (2008) Approaching ballistic transport in suspended graphene. Nat Nano 3:491–495
87. Hilding J, Grulke EA, George Zhang Z, Lockwood F (2003) Dispersion of carbon nanotubes in liquids. J Dispers Sci Technol 24:1–41

88. Kim P, Shi L, Majumdar A, McEuen PL (2001) Thermal transport measurements of individual multiwalled nanotubes. Phys Rev Lett 87:215502
89. Balandin AA, Ghosh S, Bao W, Calizo I, Teweldebrhan D, Miao F, Lau CN (2008) Superior thermal conductivity of single-layer graphene. Nano Lett 8:902–907
90. Peigney A, Laurent C, Flahaut E, Bacsa RR, Rousset A (2001) Specific surface area of carbon nanotubes and bundles of carbon nanotubes. Carbon 39:507–514
91. Stankovich S, Dikin DA, Dommett GHB, Kohlhaas KM, Zimney EJ, Stach EA, Piner RD, Nguyen ST, Ruoff RS (2006) Graphene-based composite materials. Nature 442:282–286
92. Terrones M, Grobert N, Olivares J, Zhang JP, Terrones H, Kordatos K, Hsu WK, Hare JP, Townsend PD, Prassides K, Cheetham AK, Kroto HW, Walton DRM (1997) Controlled production of aligned-nanotube bundles. Nature (Lond) 388:52–55
93. Andrews R, Jacques D, Rao AM, Derbyshire F, Qian D, Fan X, Dickey EC, Chen J (1999) Continuous production of aligned carbon nanotubes: a step closer to commercial realization. Chem Phys Lett 303:467–474
94. Maruyama S, Kojima R, Miyauchi Y, Chiashi S, Kohno M (2002) Low-temperature synthesis of high-purity single-walled carbon nanotubes from alcohol. Chem Phys Lett 360:229–234
95. Rinzler AG, Liu J, Dai H, Nikolaev P, Huffman CB, Rodriguez-Macias FJ, Boul PJ, Lu AH, Heymann D, Colbert DT, Lee RS, Fischer JE, Rao AM, Eklund PC, Smalley RE (1998) Large-scale purification of single-wall carbon nanotubes. Process, product, and characterization. Appl Phys A Mater Sci Process 67:29–37
96. Chiang IW, Brinson BE, Huang AY, Willis PA, Bronikowski MJ, Margrave JL, Smalley RE, Hauge RH (2001) Purification and characterization of single-wall carbon nanotubes (SWNTs) obtained from the gas-phase decomposition of CO (HiPco process). J Phys Chem B 105:8297–8301
97. Bachilo SM, Balzano L, Herrera JE, Pompeo F, Resasco DE, Weisman RB (2003) Narrow (n, m)-distribution of single-walled carbon nanotubes grown using a solid supported catalyst. J Am Chem Soc 125:11186–11187
98. Bandow S, Asaka S, Saito Y, Rao AM, Grigorian L, Richter E, Eklund PC (1998) Effect of the growth temperature on the diameter distribution and chirality of single-wall carbon nanotubes. Phys Rev Lett 80:3779–3782
99. Bronikowski MJ, Willis PA, Colbert DT, Smith KA, Smalley RE (2001) Gas-phase production of carbon single-walled nanotubes from carbon monoxide via the HiPco process: a parametric study. J Vac Sci Technol A 19:1800–1805
100. Colomer JF, Stephan C, Lefrant S, Van TG, Willems I, Konya Z, Fonseca A, Laurent C, Nagy JB (2000) Large-scale synthesis of single-wall carbon nanotubes by catalytic chemical vapor deposition (CCVD) method. Chem Phys Lett 317:83–89
101. Ivanov V, Nagy JB, Lambin P, Lucas A, Zhang XB, Zhang XF, Bernaerts D, Van TG, Amelinckx S et al (1994) The study of carbon nanotubules produced by catalytic method. Chem Phys Lett 223:329–335
102. Kitiyanan B, Alvarez WE, Harwell JH, Resasco DE (2000) Controlled production of single-wall carbon nanotubes by catalytic decomposition of CO on bimetallic Co–Mo catalysts. Chem Phys Lett 317:497–503
103. Li Y-L, Kinloch IA, Windle AH (2004) Direct spinning of carbon nanotube fibers from chemical vapor deposition synthesis. Science 304:276–278
104. Liu J, Casavant MJ, Cox M, Walters DA, Boul P, Lu W, Rimberg AJ, Smith KA, Colbert DT, Smalley RE (1999) Controlled deposition of individual single-walled carbon nanotubes on chemically functionalized templates. Chem Phys Lett 303:125–129
105. Meyyappan M, Delzeit L, Cassell A, Hash D (2003) Carbon nanotube growth by PECVD. A review. Plasma Sources Sci Technol 12:205–216
106. Su M, Zheng B, Liu J (2000) A scalable CVD method for the synthesis of single-walled carbon nanotubes with high catalyst productivity. Chem Phys Lett 322:321–326
107. Tasis D, Tagmatarchis N, Bianco A, Prato M (2006) Chemistry of carbon nanotubes. Chem Rev 106:1105–1136

108. Zhu HW, Xu CL, Wu DH, Wei BQ, Vajtai R, Ajayan PM (2002) Direct synthesis of long single-walled carbon nanotube strands. Science 296:884–886
109. Pegel S, Villmow T, Kasaliwal G, Pötschke P (2012) Polymer-carbon nanotube composites: melt processing, properties and applications. In: Bhattacharyya D, Fakirov S (eds) Synthetic polymer–polymer composites. Hanser, Munich
110. Kaminsky W, Funck A, Wiemann K (2006) Silica/polyethylene nanocomposite particles from catalytic emulsion polymerization. Macromol Symp 239:1–6
111. Wiemann K, Kaminsky W, Gojny FH, Schulte K (2005) Synthesis and properties of syndiotactic poly(propylene)/carbon nanofiber and nanotube composites prepared by in situ polymerization with metallocene/MAO catalysts. Macromol Chem Phys 206:1472–1478
112. Kaminsky W, Funck A (2008) In situ polymerization of olefins with nanoparticles by metallocene-catalysis. Macromol Symp 260:1–8
113. Bonduel D, Mainil M, Alexandre M, Monteverde F, Dubois P (2005) Supported coordination polymerization: a unique way to potent polyolefin carbon nanotube nanocomposites. Chem Comm 2005(6):781–783
114. Bonduel D, Bredeau S, Alexandre M, Monteverde F, Dubois P (2007) Supported metallocene catalysis as an efficient tool for the preparation of polyethylene/carbon nanotube nanocomposites: effect of the catalytic system on the coating morphology. J Mater Chem 17:2359–2366
115. Park S, Yoon SW, Lee K-B, Kim DJ, Jung YH, Do Y, Paik H-j, Choi IS (2006) Carbon nanotubes as a ligand in Cp_2ZrCl_2-based ethylene polymerization. Macromol Rapid Commun 27:47–50
116. Tong X, Liu C, Cheng H-M, Zhao H, Yang F, Zhang X (2004) Surface modification of single-walled carbon nanotubes with polyethylene via in situ Ziegler–Natta polymerization. J Appl Polym Sci 92:3697–3700
117. Bae S, Kim H, Lee Y, Xu X, Park J-S, Zheng Y, Balakrishnan J, Lei T, Ri Kim H, Song YI, Kim Y-J, Kim KS, Ozyilmaz B, Ahn J-H, Hong BH, Iijima S (2010) Roll-to-roll production of 30-inch graphene films for transparent electrodes. Nat Nano 5:574–578
118. Baughman RH, Zakhidov AA, de Heer WA (2002) Carbon nanotubes–the route toward applications. Science 297:787–792
119. Castro Neto AH, Guinea F, Peres NMR, Novoselov KS, Geim AK (2009) The electronic properties of graphene. Rev Mod Phys 81:109–162
120. Chen J, Hamon MA, Hu H, Chen Y, Rao AM, Eklund PC, Haddon RC (1998) Solution properties of single-walled carbon nanotubes. Science 282:95–98
121. Fan S, Chapline MG, Franklin NR, Tombler TW, Cassell AM, Dai H (1999) Self-oriented regular arrays of carbon nanotubes and their field emission properties. Science 283:512–514
122. Ferrari AC, Meyer JC, Scardaci V, Casiraghi C, Lazzeri M, Mauri F, Piscanec S, Jiang D, Novoselov KS, Roth S, Geim AK (2006) Raman spectrum of graphene and graphene layers. Phys Rev Lett 97:187401
123. Geim AK (2009) Graphene: status and prospects. Science 324:1530–1534
124. Geim AK, Novoselov KS (2007) The rise of graphene. Nat Mater 6:183–191
125. Novoselov KS, Geim AK, Morozov SV, Jiang D, Zhang Y, Dubonos SV, Grigorieva IV, Firsov AA (2004) Electric field effect in atomically thin carbon films. Science 306:666–669
126. Ren ZF, Huang ZP, Xu JW, Wang JH, Bush P, Siegal MP, Provencio PN (1998) Synthesis of large arrays of well-aligned carbon nanotubes on glass. Science 282:1105–1107
127. Saito S (1997) Carbon nanotubes for next-generation electronics devices. Science 278:77–78
128. Allen MJ, Tung VC, Kaner RB (2010) Honeycomb carbon: a review of graphene. Chem Rev 110:132–145
129. Ishigami M, Chen JH, Cullen WG, Fuhrer MS, Williams ED (2007) Atomic structure of graphene on SiO_2. Nano Lett 7:1643–1648
130. Eda G, Fanchini G, Chhowalla M (2008) Large-area ultrathin films of reduced graphene oxide as a transparent and flexible electronic material. Nat Nano 3:270–274

131. Stoller MD, Park S, Zhu Y, An J, Ruoff RS (2008) Graphene-based ultracapacitors. Nano Lett 8:3498–3502
132. Wang X, Zhi L, Müllen K (2008) Transparent, conductive graphene electrodes for dye-sensitized solar cells. Nano Lett 8:323–327
133. Wu J, Becerril HA, Bao Z, Liu Z, Chen Y, Peumans P (2008) Organic solar cells with solution-processed graphene transparent electrodes. Appl Phys Lett 92:263302–263303
134. Camino G, Duquesne S, Delobel R, Eling B, Lindsay C, Roels T (2001) Mechanism of expandable graphite fire retardant action in polyurethanes. In: Nelson GL, Wilkie CA (eds) Fire and polymers. ACS symposium series, vol 797. American Chemical Society, Washington, pp 90–109
135. Duquesne S, Bras ML, Bourbigot S, Delobel R, Vezin H, Camino G, Eling B, Lindsay C, Roels T (2003) Expandable graphite: a fire retardant additive for polyurethane coatings. Fire Mater 27:103–117
136. Horacek H, Pieh S (2000) The importance of intumescent systems for fire protection of plastic materials. Polym Int 49:1106–1114
137. Higginbotham AL, Lomeda JR, Morgan AB, Tour JM (2009) Graphite oxide flame-retardant polymer nanocomposites. ACS Appl Mater Interfaces 1:2256–2261
138. Song P, Cao Z, Cai Y, Zhao L, Fang Z, Fu S (2011) Fabrication of exfoliated graphene-based polypropylene nanocomposites with enhanced mechanical and thermal properties. Polymer 52:4001–4010
139. Xie R, Qu B, Hu K (2001) Dynamic FTIR studies of thermo-oxidation of expandable graphite-based halogen-free flame retardant LLDPE blends. Polym Degrad Stab 72:313–321
140. Schartel B, Braun U, Schwarz U, Reinemann S (2003) Fire retardancy of polypropylene/flax blends. Polymer 44:6241–6250
141. Hummers WS, Offeman RE (1958) Preparation of graphitic oxide. J Am Chem Soc 80:1339
142. Schniepp HC, Li J-L, McAllister MJ, Sai H, Herrera-Alonso M, Adamson DH, Prud'homme RK, Car R, Saville DA, Aksay IA (2006) Functionalized single graphene sheets derived from splitting graphite oxide. J Phys Chem B 110:8535–8539
143. Yang D, Velamakanni A, Bozoklu G, Park S, Stoller M, Piner RD, Stankovich S, Jung I, Field DA, Ventrice CA Jr, Ruoff RS (2009) Chemical analysis of graphene oxide films after heat and chemical treatments by X-ray photoelectron and Micro-Raman spectroscopy. Carbon 47:145–152
144. Dreyer DR, Park S, Bielawski CW, Ruoff RS (2010) The chemistry of graphene oxide. Chem Soc Rev 39:228–240
145. Kalaitzidou K, Fukushima H, Drzal LT (2007) A new compounding method for exfoliated graphite–polypropylene nanocomposites with enhanced flexural properties and lower percolation threshold. Compos Sci Technol 67:2045–2051
146. McAllister MJ, Li J-L, Adamson DH, Schniepp HC, Abdala AA, Liu J, Herrera-Alonso M, Milius DL, Car R, Prud'homme RK, Aksay IA (2007) Single sheet functionalized graphene by oxidation and thermal expansion of graphite. Chem Mater 19:4396–4404
147. Stankovich S, Piner RD, Chen X, Wu N, Nguyen ST, Ruoff RS (2006) Stable aqueous dispersions of graphitic nanoplatelets via the reduction of exfoliated graphite oxide in the presence of poly(sodium 4-styrenesulfonate). J Mater Chem 16:155–158
148. Balandin AA (2011) Thermal properties of graphene and nanostructured carbon materials. Nat Mater 10:569–581
149. Huang X, Yin Z, Wu S, Qi X, He Q, Zhang Q, Yan Q, Boey F, Zhang H (2011) Graphene-based materials: synthesis, characterization, properties, and applications. Small 7:1876–1902
150. Steurer P, Wissert R, Thomann R, Mülhaupt R (2009) Functionalized graphenes and thermoplastic nanocomposites based upon expanded graphite oxide. Macromol Rapid Commun 30:316–327
151. Terrones M, Botello-Méndez AR, Campos-Delgado J, López-Urías F, Vega-Cantú YI, Rodríguez-Macías FJ, Elías AL, Muñoz-Sandoval E, Cano-Márquez AG, Charlier J-C,

Terrones H (2010) Graphene and graphite nanoribbons: morphology, properties, synthesis, defects and applications. Nano Today 5:351–372
152. Wang G, Yang J, Park J, Gou X, Wang B, Liu H, Yao J (2008) Facile synthesis and characterization of graphene nanosheets. J Phys Chem C 112:8192–8195
153. Zhu Y, Murali S, Cai W, Li X, Suk JW, Potts JR, Ruoff RS (2010) Graphene and graphene oxide: synthesis, properties, and applications. Adv Mater 22:3906–3924
154. Tölle FJ, Fabritius M, Mülhaupt R (2012) Emulsifier-free graphene dispersions with high graphene content for printed electronics and freestanding graphene films. Adv Funct Mater 22:1136–1144
155. Bourlinos AB, Georgakilas V, Zboril R, Steriotis TA, Stubos AK (2009) Liquid-phase exfoliation of graphite towards solubilized graphenes. Small 5:1841–1845
156. Chung DDL (1987) Exfoliation of graphite. J Mater Sci 22:4190–4198
157. Hernandez Y, Nicolosi V, Lotya M, Blighe FM, Sun Z, De S, McGovern IT, Holland B, Byrne M, Gun'Ko YK, Boland JJ, Niraj P, Duesberg G, Krishnamurthy S, Goodhue R, Hutchison J, Scardaci V, Ferrari AC, Coleman JN (2008) High-yield production of graphene by liquid-phase exfoliation of graphite. Nat Nano 3:563–568
158. Lotya M, Hernandez Y, King PJ, Smith RJ, Nicolosi V, Karlsson LS, Blighe FM, De S, Wang Z, McGovern IT, Duesberg GS, Coleman JN (2009) Liquid phase production of graphene by exfoliation of graphite in surfactant/water solutions. J Am Chem Soc 131:3611–3620
159. Lu J, Yang J-x, Wang J, Lim A, Wang S, Loh KP (2009) One-pot synthesis of fluorescent carbon nanoribbons, nanoparticles, and graphene by the exfoliation of graphite in ionic liquids. ACS Nano 3:2367–2375
160. O'Neill A, Khan U, Nirmalraj PN, Boland J, Coleman JN (2011) Graphene dispersion and exfoliation in low boiling point solvents. J Phys Chem C 115:5422–5428
161. Pu N-W, Wang C-A, Sung Y, Liu Y-M, Ger M-D (2009) Production of few-layer graphene by supercritical CO_2 exfoliation of graphite. Mater Lett 63:1987–1989
162. Zhao W, Fang M, Wu F, Wu H, Wang L, Chen G (2010) Preparation of graphene by exfoliation of graphite using wet ball milling. J Mater Chem 20:5817–5819
163. Zhu Y, Stoller MD, Cai W, Velamakanni A, Piner RD, Chen D, Ruoff RS (2010) Exfoliation of graphite oxide in propylene carbonate and thermal reduction of the resulting graphene oxide platelets. ACS Nano 4:1227–1233
164. Jang BZ, Zhamu A (2012) Process for producing dispersible and conductive nano graphene platelets from non-oxidized graphitic materials. Patent US 2010/8216541
165. Zhamu A (2011) Mass production of pristine nano graphene materials. Patent WO/2011/014,347
166. Peukert W, Wasserscheid P, Hirsch A (2011) From molecules to materials: the cluster of excellence "Engineering of Advanced Materials" at Friedrich-Alexander University of Erlangen-Nuremberg. Adv Mater 23:2508–2513
167. Knieke C, Berger A, Voigt M, Taylor RNK, Röhrl J, Peukert W (2010) Scalable production of graphene sheets by mechanical delamination. Carbon 48:3196–3204
168. Knieke C, Berger A, Peukert W (2010) Graphene production with stirred media mills. MRS Proc 1259:1259-S12-01. doi:10.1557/PROC-1259-S12-01
169. Alexandre M, Pluta M, Dubois P, Jérôme R (2001) Metallocene catalyzed polymerization of ethylene in the presence of graphite, 1. synthesis and characterization of the composites. Macromol Chem Phys 202:2239–2246
170. Jiang X, Drzal LT (2010) Multifunctional high density polyethylene nanocomposites produced by incorporation of exfoliated graphite nanoplatelets 1: morphology and mechanical properties. Polym Compos 31:1091–1098
171. Wang L, Chen G (2010) Dramatic improvement in mechanical properties of GNs-reinforced HDPE nanocomposites. J Appl Polym Sci 116:2029–2034
172. Fim FdC, Basso NRS, Graebin AP, Azambuja DS, Galland GB (2012) Thermal, electrical, and mechanical properties of polyethylene–graphene nanocomposites obtained by in situ polymerization. J Appl Polym Sci 128(5):2630–2637. doi:10.1002/app.38317

173. Kuila T, Bose S, Hong CE, Uddin ME, Khanra P, Kim NH, Lee JH (2011) Preparation of functionalized graphene/linear low density polyethylene composites by a solution mixing method. Carbon 49:1033–1037
174. Kim H, Kobayashi S, AbdurRahim MA, Zhang MJ, Khusainova A, Hillmyer MA, Abdala AA, Macosko CW (2011) Graphene/polyethylene nanocomposites: effect of polyethylene functionalization and blending methods. Polymer 52:1837–1846
175. Xu J-Z, Chen C, Wang Y, Tang H, Li Z-M, Hsiao BS (2011) Graphene nanosheets and shear flow induced crystallization in isotactic polypropylene nanocomposites. Macromolecules 44:2808–2818
176. Choi B, Lee J, Lee S, Ko J-H, Lee K-S, Oh J, Han J, Kim Y-H, Choi IS, Park S (2013) Generation of ultra-high-molecular-weight polyethylene from metallocenes immobilized onto N-doped graphene nanoplatelets. Macromol Rapid Commun 34(6):533–538. doi:10.1002/marc.201200768
177. Anselm M (2012) Polyethylen- und Polyoctenamer-Nanokomposite durch Katalytische Polymerisation in Gegenwart von funktionalisierten Graphenen. PhD thesis, Albert-Ludwigs-University of Freiburg
178. Capiati NJ, Porter RS (1975) Tensile properties of ultradrawn polyethylene. J Polym Sci Polym Phys Ed 13:1177–1186
179. Capiati N, Porter R (1975) The concept of one polymer composites modelled with high density polyethylene. J Mater Sci 10:1671–1677
180. Kmetty Á, Bárány T, Karger-Kocsis J (2010) Self-reinforced polymeric materials: a review. Prog Polym Sci 35:1288–1310
181. Wang K, Chen F, Zhang Q, Fu Q (2008) Shish–kebab of polyolefin by "melt manipulation" strategy in injection-molding: a convenience pathway from fundament to application. Polymer 49:4745–4755
182. Gao C, Yu L, Liu H, Chen L (2012) Development of self-reinforced polymer composites. Prog Polym Sci 37:767–780
183. Pornnimit B, Ehrenstein GW (1991) Extrusion of self-reinforced polyethylene. Adv Polym Technol 11:91–98
184. Somani RH, Yang L, Zhu L, Hsiao BS (2005) Flow-induced shish–kebab precursor structures in entangled polymer melts. Polymer 46:8587–8623
185. Cao J, Gao X, Shen K (2012) Morphologies and mechanical properties of high-density polyethylene induced by the addition of small amounts of both low- and high-molecular-weight polyolefin under shear stress applied by dynamic packing injection molding. J Macromol Sci Part B 51:2519–2526
186. Böhm LL (2003) The ethylene polymerization with Ziegler catalysts: fifty years after the discovery. Angew Chem Int Ed 42:5010–5030
187. McKenna TFL, Di Martino A, Weickert G, Soares JBP (2010) Particle growth during the polymerisation of olefins on supported catalysts, 1 – nascent polymer structures. Macromol React Eng 4:40–64
188. Ruff M, Paulik C (2013) Controlling polyolefin properties by in-reactor blending: 2. particle design. Macromol React Eng 7:71–83
189. Ruff M, Paulik C (2012) Controlling polyolefin properties by in-reactor blending, 1–polymerization process, precise kinetics, and molecular properties of UHMW-PE polymers. Macromol React Eng 6:302–317
190. Chu K-J, Soares JBP, Penlidis A (2000) Variation of molecular weight distribution (MWD) and short chain branching distribution (SCBD) of ethylene/1-hexene copolymers produced with different in-situ supported metallocene catalysts. Macromol Chem Phys 201:340–348
191. Kurek A, Mark S, Enders M, Kristen MO, Mülhaupt R (2010) Mesoporous silica supported multiple single-site catalysts and polyethylene reactor blends with tailor-made trimodal and ultra-broad molecular weight distributions. Macromol Rapid Commun 31:1359–1363

192. Kurek A (2009) Maßgeschneiderte polyethylen-reaktorblends mit ultra-hochmolekularem polyethylen: steuerung von materialeigenschaften und nanostrukturbildung durch coträgerung von (post-) metallocenen. PhD thesis, Albert-Ludwigs University of Freiburg
193. Paul Smith PJL (1980) Ultra-high-strength polyethylene filaments by solution spinning/drawing. J Mater Sci 15:505–514
194. Rotzinger BP, Chanzy HD, Smith P (1989) High strength/high modulus polyethylene: synthesis and processing of ultra-high molecular weight virgin powders. Polymer 30:1814–1819
195. Smith P, Chanzy H, Rotzinger BP (1985) Drawing of virging ultrahigh molecular weight polyethylene: an alternative route to high strength fibres. Polym Commun 26:258–260
196. Smith P, Chanzy HD, Rotzinger B,P (1987) Drawing of virgin ultrahigh molecular weight polyethylene: an alternative route to high strength/high modulus materials. J Mater Sci 22:523–531
197. Ronca S, Romano D, Forte G, Andablo-Reyes E, Rastogi S (2012) Improving the performance of a catalytic system for the synthesis of ultra high molecular weight polyethylene with a reduced number of entanglements. Adv Polym Technol 31:193–204
198. Rastogi S, Yao Y, Ronca S, Bos J, van der Eem J (2011) Unprecedented high-modulus high-strength tapes and films of ultrahigh molecular weight polyethylene via solvent-free route. Macromolecules 44:5558–5568
199. Kolb L, Monteil V, Thomann R, Mecking S (2005) Aqueous dispersions of extraordinarily small polyethylene nanoparticles. Angew Chem Int Ed 44:429–432
200. Ronca S, Forte G, Ailianou A, Kornfield JA, Rastogi S (2012) Direct route to colloidal UHMWPE by including LLDPE in solution during homogeneous polymerization of ethylene. ACS Macro Lett 1:1116–1120

Adv Polym Sci (2013) 258: 311–340
DOI: 10.1007/12_2013_228

Published online: 12 June 2013

Polyolefin/Layered Silicate Nanocomposites Prepared by In Situ Polymerization

Naresh H. Tarte, Liqiang Cui, and SeongIhl Woo

Abstract This chapter briefely overviews the polymer-layered silicate nanocomposites, including the structure and properties of the layered silicates and their modifications. It also addresses the developments in synthesizing polyolefin/clay nanocomposites by olefin polymerization under catalysis of clay intercalated precatalysts. It mainly focuses on the synthetic routes, structural characterization, and properties of polyolefin/clay nanocomposites.

Keywords Coordination catalyst · In situ polymerization · Montmorillonite · Nanocomposite characterization · Polyolefin/clay nanocomposites · Preparation methods

Contents

N.H. Tarte
Department of Chemistry and Biology, Korea Science Academy of KAIST, 105-47 Baekyang gwanmoon-ro, Busanjin-gu, Busan 614-822, Republic of Korea

L. Cui
College of Chemical and Environmental Engineering, Shandong University of Science and Technology, Qingdao 266590, P. R. China

S. Woo (✉)
Departments of Chemical and Biomolecular Engineering, Chemistry, and Energy Science and Engineering, Graduate School of EEWS, Korea Advanced Institute of Science and Technology, 373-1 Guseong-dong, Yuseong-gu, Daejeon 305-701, Republic of Korea
e-mail: siwoo@kaist.ac.kr

Abbreviations

ATRP	Atom transfer radical polymerization
CEC	Cation-exchange capacity
CGC	Constrained geometry catalysts
DSC	Differential scanning calorimetry
FTIR	Fourier transform infrared spectroscopy
MAO	Methylaluminoxane
MMA	Methylmethacrylate
MMT	Montmorillonite
$Ni(acac)_2$	Nickel(II) acetylacetonate
NMP	Nitrous oxide-mediated living radical polymerization
NMR	Nuclear magnetic resonance
OMMT	Organically modified montmorillonite
PE	Polyethylene
PLS	Polymer-layered silicate
PMMA	Poly(methylmethacrylate)
PP	Polypropylene
RAFT	Reversible addition fragmentation chain transfer polymerization
ROMP	Ring-opening metathesis polymerization
ROP	Ring opening polymerization
SAXS	Small-angle X-ray scattering
TEA	Triethylaluminum
TEM	Transmission electron microscopy
T_g	Glass transition temperature
thf	Polytetrahydrofuran
TIBA	Tri(isobutyl)aluminum
TMA	Trimethylaluminum
WAXD	Wide angle X-ray diffraction
XRD	X-ray diffraction

1 Introduction

Interaction between inorganic layered materials and organic substances has attracted increasing interest from both scientific and industrial perspectives. The ability of clay minerals to induce or activate the polymerization of various unsaturated organic monomers has been known since the 1940s. During the early stage

of composite material development, it was observed by Friedlander [1] that montmorillonite (MMT) could catalyze the polymerization of butadiene and 4-vinyl pyridine. Subsequently, styrene could be polymerized [2–4] by mixing the monomer with dry, acid-washed MMT. Similarly, styrene could spontaneously polymerize when mixed with (dry) kaolinite and palygorskite [5]. However, the field of polymer-layered silicate (PLS) nanocomposites has gained momentum recently because two major findings have stimulated the revival of interest in these materials. First, the Toyota group [6] developed an attractive design for a Nylon-6 (N6)/clay nanocomposite in which individual silicate layers of about 1 nm thickness are homogeneously dispersed in a continuous matrix of Nylon-6. Very small amounts of layered silicate loadings resulted in pronounced improvement of thermal and mechanical properties. The second major finding was the observation by Vaia et al. [7] that it is possible to melt-mix polymers with layered silicates, without the use of organic solvents Today, efforts are being conducted globally, using almost all types of polymer matrices.

Polyethylene (PE) and polypropylene (PP) occupy about half the total production capacity in synthetic plastics. Having been an important field in both academy and industry for more than half a century, polyolefin nanocomposites are still attracting interest from numerous researchers due to their superior properties. Furthermore, preparation of coordination polymerization-induced PLS nanocomposites has many advantages, which include: (1) no unfavorable thermodynamic requirement for melt intercalation; (2) facile adjustment of clay loading and the accompanying nanocomposite properties; (3) no special demand on polyolefin molecular weights and no need for introduction of olefin oligomer modifiers; and (4) more homogeneous dispersion of clay layers in the polymeric matrix.

PLS nanocomposites are a relatively new class of materials that exhibit ultrafine phase dimensions, typically in the range of 1–100 nm [8]. Because of their nanometer size features, nanocomposites possess unique properties typically not shared by their more conventional microcomposite counterparts and, therefore, offer new technology and business opportunities [9–11]. For instance, many of the polymer properties can be significantly altered at very low clay loadings (2–8 wt%) in the nanocomposites whereas 30–40 wt% of the microfillers are required for the same effect in the case of conventional composites [11, 12]. PLS nanocomposites exhibit ultrafine phase dimensions, typically with 1–10 nm thickness [8]. The high aspect ratio (i.e., length: thickness ratio of about 100–1,000) of the clay platelets provides a large surface area and is considered to be responsible for the highly improved properties of these nanocomposites. These improvements can include better tensile strength and moduli [13–15], increased strength and heat resistance [12], decreased thermal expansion coefficient [14], decreased gas permeability [14, 16, 17], decreased flammability [18, 19], increased swelling resistance [13], biodegradability of biodegradable polymers [20], and enhanced ionic conductivity [21, 22]. The nanocomposites also show unusual chemical and physical phenomenon, such as highly anisotropic electrical conductivity [23] and photoactivity [24–26]. On the other hand, they are also considered to be unique model systems for the study of the structure and dynamics of polymers in confined environments.

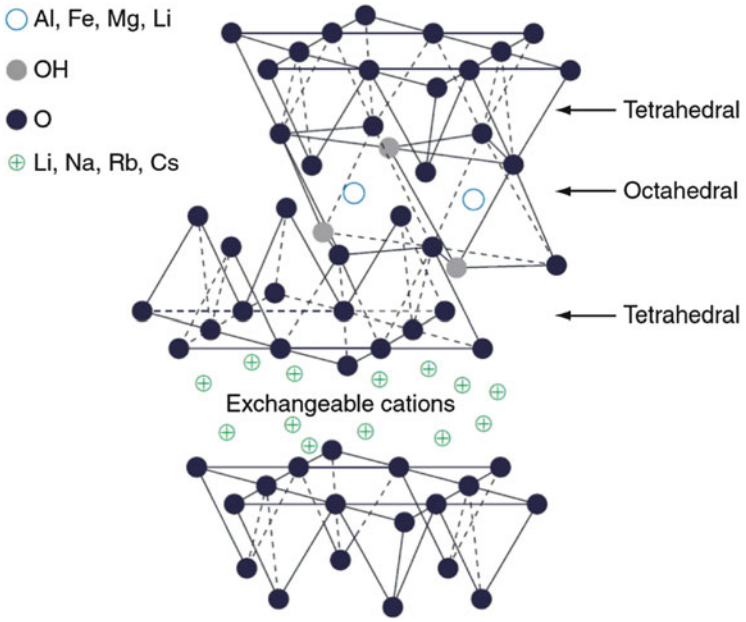

Fig. 1 Structure of 2:1 layered silicates. Reproduced from Giannelis et al. [115] Copyright (1999), with kind permission of Springer Science&Business Media

2 Structure and Properties of Layered Silicates

PLS nanocomposites are a hybrid between an organic phase (the polymer) and an inorganic phase (the silicate). The choice of the silicate determines the nanoscopic dispersion typical of nanocomposites. The silicates employed belong to the family of layered silicates also known as phyllosilicates, such as mica, talc, MMT, vermiculite, hectorite, saponite, etc [27]. Their crystal structure consists of layers made up of two silica tetrahedra fused to an edge-shared octahedral sheet of either aluminum or magnesium hydroxide (Fig. 1). Stacking of the layers leads to a regular van der Waals gap between the layers that is called the interlayer or gallery. Isomorphic substitution within the layers generates negative charges that are normally counterbalanced by cations residing in the interlayer space. In montmorillonite, the most familiar and common member of the smectite groups, the layer charge originates from the substitution of octahedral Al^{3+} by Mg^{2+}. Hectorite is also "octahedrally charged" with Li^{+} substituting for Mg^{2+} in the octahedral sheet. Saponite is tetrahedrally charged smectite with Al^{3+} replacing Si^{4+}.

MMT, hectorite, and saponite are the most commonly used layered silicates; their structures and properties are shown in Table 1. Layered silicates have two types of structure: tetrahedrally substituted and octahedrally substituted. In the case of tetrahedrally substituted layered silicates, the negative charge is located on the surface of silicate layers and, hence, the polymer matrices can interact more readily with these

Table 1 Chemical formula and characteristic parameters of commonly used 2:1 phyllosilicates

2:1 Phyllosilicates	Chemical formula	CEC (mequiv/100 g)	Particle length (nm)
Montmorillonite	$M_x(Al_{4-x}Mg_x)Si_8O_{20}(OH)_4$	110	100–150
Hectorite	$M_x(Mg_{6-x}Li_x)Si_8O_{20}(OH)_4$	120	200–300
Saponite	$M_xMg_6(Si_{8-x}Al_x)\ Si_8O_{20}(OH)_4$	86.6	50–60

CEC Cation exchange capacity, *M* monovalent cation, *x* degree of isomorphous substitution (between 0.5 and 1.3). Reproduced with permission from Sinha Ray and Okamoto [52] and with kind permission of Elsevier

than with octahedrally substituted material. Layer rigidity is an essential requirement for the pillaring of any lamellar solid. In the absence of such rigidity, attractive interactions between layers would result in distortion in the region between pillars, and such layer distortions would lead to collapse of the gallery pores.

3 Clay Surface Modifications

For all their advantages, including a large interlayer surface area (~700 m^2/g), high cation exchange capacity (~100 mol/kg), expansibility in water, and propensity for intercalating organic molecules, the MMTs and related phyllosilicates are naturally hydrophilic because of the presence of hydrated inorganic counterions such as Na^+ and Ca^{2+} in the interlayer space [27]. Obviously, in this pristine state, layered silicates are only miscible with hydrophilic polymers. Hence, the use of silicates as such greatly limits the class of miscible polymers. Treatment steps for use of coordination catalysts are required mainly to control the population of hydroxyl groups and surface acidity, and to scavenge impurities from the support surface before introduction of the catalyst precursor. Clay surface modifications are mainly achieved by organic modification of the clay, thermal treatment of the clay, and treatment of clay with alkylaluminum compounds.

3.1 Organic Modification of the Clay

One of the ways of overcoming the chemical incompatibility between mineral and polymer is to graft polar functional groups to either the mineral surface [28, 29] or the polymer chain [30–32]. The purpose of this treatment is to reduce the surface energy of MMT, increase the interlayer spacing of MMT, and create anchoring points for catalyst incorporation. This may be achieved by either intercalation of organic cations or grafting of organosilanes or suitable polymeric species to the silicate surface [29].

The excess negative charge of layered silicates and their ability to exchange ions can be quantified by a specific property known as the cation-exchange capacity (CEC) [9, 32], which is highly dependent on the nature of the isomorphous

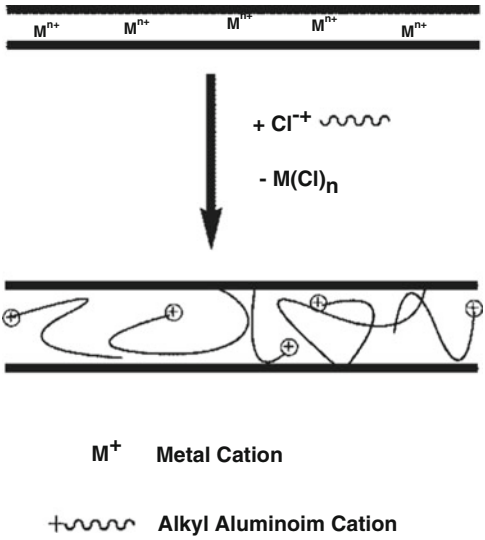

Fig. 2 Cation-exchange reaction between the silicate and an alkylammonium salt

substitutions in the tetrahedral and octahedral layers. The ability of MMT for cation exchange has been known for nearly a century [33] and it shows different CEC, ranging from approximately 0.9 to 1.2 mequiv/g [32, 34]. Hence, on the basis of the CEC of the clay, the content of the surfactant is usually about 35–45 wt%. Two types of organic cation-exchanged smectites may be distinguished. The first type of organically modified smectites is often referred to as "adsorptive clays" [35], which are formed by replacing the inorganic counterions in smectites with short-chain, compact cationic species, such as tetramethylammonium, tetraethylammonium, and trimethylphenylammonium [36]. The second type of organically modified smectites is obtained by intercalation of long chain alkyl ammonium ($[H_3N]R_þ$) or quaternary ammonium ($[CH_3]_3NR_þ$) ions, where R represents an alkyl chain (e.g., hexadecyl); these are called "organoclays" [37] or clay–organic complexes [38]. Natural clays, which may contain divalent cations such as calcium, are required to exchange these divalent cations with sodium prior to further treatment with organic cationic surfactant [39].

The cationic surfactants generally used to make the clay compatible with the polymer matrix (as shown in Fig. 2) include quaternary ammonium, quaternary phosphonium, imidazolium, and pyridinium salts [9, 39, 40]. The replacement of inorganic exchange cations by alkylammonium or alkylphosphonium cations on the gallery surfaces of clays not only serves to match the clay surface polarity with the polarity of the polymer, but it also expands the clay galleries. The organic cations lower the surface energy of the silicate surface and improve wetting with the polymer matrix. Organosilicates are thus much more compatible with most engineering plastics. Additionally, the organic cations may contain various functional groups that react with the polymer to improve adhesion between the inorganic phase and the matrix [41].

3.2 Thermal Treatment of the Clay

During support of the catalyst, the coordination catalyst must achieve a uniform distribution within the clay layers so that interlayer polymerization may take place, leading to clay exfoliation and dispersion into the formed polymer phase. Therefore, the compatibility between the clay surface, organic solvent, catalyst, cocatalyst, and polymer has a great impact on the effectiveness of in situ polymerization with clay. To achieve acceptable activities for in situ polymerization, the active sites immobilized on the clay surface should be shielded from side reactions that may lead to their deactivation. Pristine clays, such as Na^+-MMT, are hydrophilic and have a relatively high water content (up to 10 wt%), which acts as a poison for coordination catalysis [28, 29]. Depending on the clay structure, water may occur in three different forms [30] that can be determined using thermal gravimetric analysis: physically adsorbed water is generally released below 100°C; bound water is released below 300°C; and structural water is released around 600°C. Organic modification of clay can decrease the water content considerably [32]; however, water content is still large enough in the form of structural water to cause significant catalyst deactivation. During thermal treatment, physically adsorbed, bound, and structural water is removed at different temperature ranges as specified above, which results in changes in the clay porosity and acidity. In fact, the acidity, porosity, and cation exchange capacity of clays are closely related to their water content [42].

3.3 Treatment of Clay with Alkylaluminum Compounds

Treatment of clay with alkylaluminoxanes, such as MAO, TMA, TEA, TIBA etc., can remove the residual water on the clay surface and protect the upcoming coordination catalyst from deactivation [31]. The complete removal of water from clay requires thermal treatment at temperatures of about 400–600°C, which leads to the partial collapse of the clay structure and CEC reduction. Hence, treatment with alkylaluminum compounds and thermal treatment at moderate temperatures is required for further reduction of the adsorption of water. Additionally, treatment with alkylaluminum compounds will reduce the population of surface hydroxyl groups, which are also responsible for coordination catalyst deactivation [28].

4 Nanocomposite Structures

Generally in layered silicates, the layer thickness is of the order of 1 nm and has a very high aspect ratio (e.g. 10–1,000). A few weight percent of layered silicates that are properly dispersed throughout the polymer matrix thus create much higher

surface area for polymer–filler interaction as compared to conventional composites. From a structural point of view, polymer/clay composites can be generally classified into conventional composites and nanocomposites. In a conventional composite, the registry of the clay nanolayers is retained when mixed with the polymer, but there is no intercalation of the polymer into the clay structure. Consequently, the clay fraction in conventional composites plays little or no functional role and acts mainly as a filler agent for economic considerations. Depending on the strength of interfacial interactions between the polymer matrix and layered silicate, three classes of polymer/clay nanocomposites are described: phase-separated (immiscible nanocomposites), intercalated nanocomposites, and delaminated (or exfoliated) nanocomposites [43].

1. *Phase-separated microcomposites* are formed when the polymer is unable to intercalate with the silicate layers. This can also be called an immiscible system, which normally would not be regarded as a nanocomposite.
2. *Intercalated nanocomposites* are formed when one or a few molecular layers of polymer are inserted into the clay galleries in a crystallographically regular fashion, regardless of the clay-to-polymer ratio. Intercalation causes $<$20–30 Å separation between the silicate platelets. The result is a well-ordered multilayer structure of alternating polymeric and inorganic layers, with a repeat distance between them. Sometimes the silicate layers in intercalated nanocomposites are flocculated due to hydroxylated edge–edge interaction of the silicate layers.
3. *Exfoliated nanocomposites* are formed when the silicate nanolayers are individually dispersed in the polymer matrix, the average distance between the segregated layers being dependent on the clay loading. Its ordered structure is lost and the distance between the layers is of the order of the radius of gyration of the polymer. In this case, the polymer separates the clay platelets by 80–100 Å or more. Exfoliated or delaminated nanocomposites show greater phase homogeneity than intercalated nanocomposites. Notice that in the exfoliated case the surface area between organic and inorganic is increased compared with the intercalated materials. Hence, each nanolayer in an exfoliated nanocomposite contributes fully to interfacial interactions with the matrix. This structural distinction is the primary reason why the exfoliated clay state is especially effective in improving the reinforcement and other performance properties of clay composite materials. Exfoliation may be either “ordered” or “disordered” [44], which can be detected by X-ray diffraction (XRD) analyses.

It should be pointed out that many polymer/clay nanocomposite materials finally result in the formation of a mixture of exfoliated and intercalated structures [45]. The above types of nanocomposites are schematically compared with an immiscible system in Fig. 3.

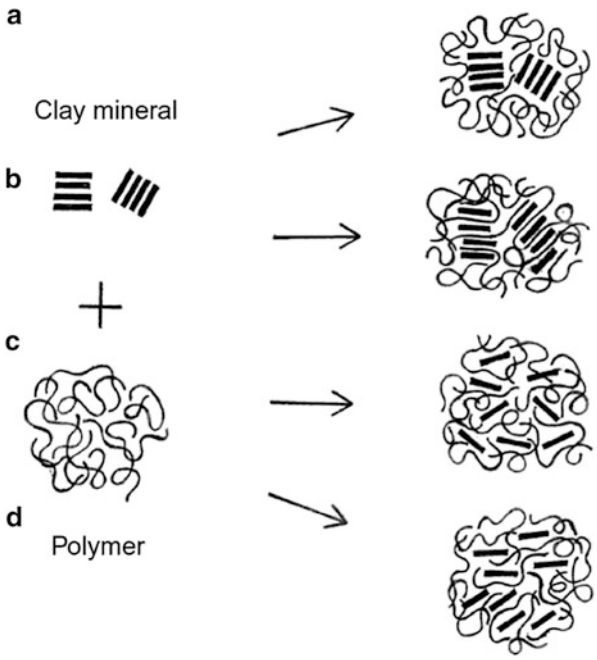

Fig. 3 Composite structures obtained using layered silicate: (**a**) conventional composite or microcomposite, (**b**) intercalated nanocomposite, (**c**) disordered exfoliated nanocomposite, and (**d**) ordered exfoliated nanocomposite. Reproduced with permission from Theng [116]

5 Techniques Used for the Characterization of Nanocomposites

Generally, the structure of nanocomposites has typically been established using XRD and transmission electron microscopy (TEM) observation. The XRD diffractograms and related TEM images produced by different types of hybrid are illustrated in Fig. 4 [21].

Using XRD, one can determine the spaces between silicate layers using Bragg's law: $\sin\theta = n\lambda/2d$, where λ corresponds to the wavelength of the X-ray radiation used, d the spacing between diffractional lattice planes and θ is the measured diffraction angle or glancing angle [9]. Hence, following Bragg's law, intercalation of the polymer chains increases the interlayer spacing, leading to a shift of the diffraction peak towards a lower angle. In the intercalated nanocomposites, the repetitive multilayer structure is well preserved, allowing the interlayer spacing to be determined; however, the exfoliated structures disrupt the coherent layer stacking, resulting in a featureless diffraction pattern. Thus, for exfoliated structures no more diffraction peaks are visible in the XRD diffractograms either because of a much too large spacing between the layers or due to a highly disordered nanocomposite structure [21, 46, 47].

XRD does not provide information concerning the spatial distribution of the silicate in the polymer matrix, nor the shape of the hybrid, since all its data are "averaged" over the whole of the sample. Furthermore, some layered silicates do

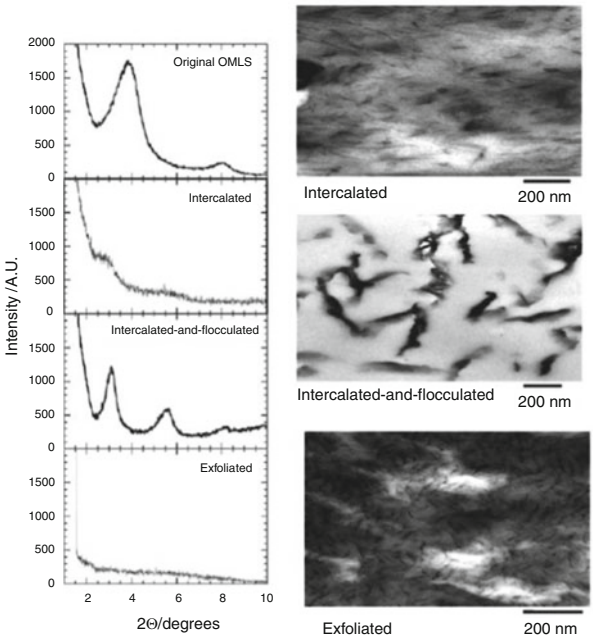

Fig. 4 Wide angle X-ray diffraction (*left*) and TEM analyses (*right*) of three different types of nanocomposite

not display well-defined basal reflections and it is difficult to determine the intensity pattern and the shape of the relative peaks. However, TEM can provide direct visual information about the morphology, atom arrangement, and spatial distribution of the phases and structural defects of a selected area of the translational mobility, as shown in Fig. 4 [48]. Because the silicate layers are composed of heavier elements (Al, Si, and O) than the polymer matrix (C, H, N, and O), the silicate sheets (which are the cross-sections of the silicate layers of ~1 nm thickness) are seen as dark lines in the TEM images [49, 50].

Van der Hart et al. [51] first used solid-state NMR (^{1}H and ^{13}C) as a tool for gaining greater insight into the morphology, surface chemistry and, to a very limited extent, the dynamics of exfoliated polymer/clay nanocomposites. The major objective in solid-state NMR measurement is to connect the measured longitudinal relaxations (T^{1}s) of ^{1}H or ^{13}C nuclei with the quality of clay dispersion [52].

Fourier transform infrared spectroscopy (FTIR) may find a difference between the bonding in different types of nanocomposites; however, the variations could be minute and hence this is an unreliable method for nanocomposite characterization [53, 54]. Nascimento et al. [55] presented for the first time the resonance Raman characterization of a polymer/clay nanocomposite formed by aniline polymerization in the presence of MMT.

Differential scanning calorimetry (DSC) provides further information concerning intercalation [7]. The many interactions that the intercalated chains of the polymer form with the host species greatly reduce its rotational and translational mobility. Such restricted mobility is responsible for the increased glass transition temperature (T_g) of the resultant nanocomposite.

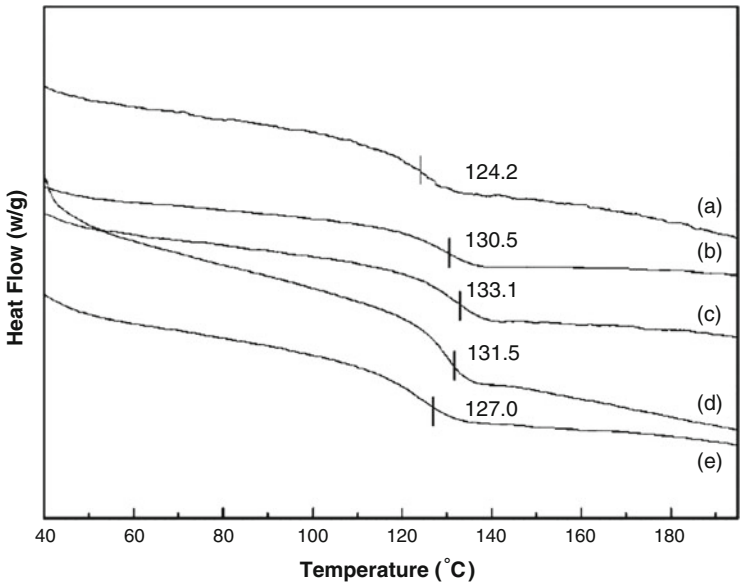

Fig. 5 DSC thermograms of (*a*) pure PMMA and (*b–e*) PMMA/clay nanocomposites with different clay contents: (*b*) 0.62 wt%, (*c*) 2.33 wt%, (*d*) 4.13 wt%, and (*e*) 10.4 wt%. Reproduced with permission from [56]

Recently, our group reported [56] DSC characterization of PMMA/clay nanocomposite prepared by in situ polymerization initiated with a $Ni(acac)_2$ catalyst in combination with MAO (Fig. 5). The pure PMMA exhibits T_g of ~124.28°C; in contrast, the PMMA/clay nanocomposites exhibit an increasing endothermic trend at ~127.0–133.18°C as an increasing amount of the clay is added.

Bafna et al. [57] developed a technique to determine the three-dimensional (3D) orientation of various hierarchical organic and inorganic structures in a PLS nanocomposite. The effect of compatibilizer concentration on the orientation of various structures in PLS nanocomposites using 2D SAXS and 2D WAXD for three different sample/camera orientations was studied.

A review of methods for the detailed characterization of polymer/clay nanocomposites is beyond the scope of this chapter. Valuable information on this area can be found in several literature reviews [11, 52, 58–60].

6 Methods of Nanocomposite Preparation

Intercalation of polymers in layered hosts, such as layered silicates, has proven to be a successful approach to the synthesis of PLS nanocomposites. These polymer/clay nanocomposites can be prepared in several ways, namely, solution exfoliation, melt intercalation, in situ polymerization, and template synthesis [9].

Intercalation of the polymer from solution is based on a solvent system in which the polymer or pre-polymer is soluble and the silicate layers are swellable. The layered silicate is first swollen in a solvent such as water, chloroform, or toluene. When the polymer and layered silicate solutions are mixed, the polymer chains intercalate and displace the solvent within the interlayer of the silicate. Upon solvent removal, the intercalated structure remains, resulting in PLS nanocomposite. The drawback of this method is the requirement for a suitable solvent. It has been shown that intercalation only occurs for certain polymer/solvent or monomer/solvent pairs [49].

In melt intercalation, the polymer and layered silicate mixture is annealed above the T_g in either static or flow conditions. Modified layered silicates are usually employed to promote intercalation. The polymer chains spread from the molten mass into the silicate galleries to form either intercalated or delaminated hybrids according to the degree of penetration. The critical factor that determines which type is obtained is probably linked to thermodynamic factors. This method is environmentally benign due to the absence of organic solvents. Furthermore, it is compatible with current industrial processes such as extrusion and injection molding. However, very careful attention has to be paid to finely tune the processing conditions to increase the compatibility of the clay layer surfaces with the polymer matrix.

The template synthetic method is based on the in situ hydrothermal crystallization of clay mineral layers (from a gel) using selected water-soluble polymers as templates [61]. Template synthesis is essentially limited to water-soluble polymers, and the synthetic clay mineral formed under the conditions described by the authors is a poorly ordered fluorohectorite. On the other hand, the method is potentially capable of promoting the dispersion of silicate layers in a one-step process.

In situ polymerization of monomers confined in molecule-sized spaces has been used to synthesize stereospecific polymers [62]. In this method, the layered silicate is swollen within the liquid monomer or a monomer solution so that polymer formation can occur between the intercalated sheets. Polymerization can be initiated either by heat or radiation, by the diffusion of a suitable initiator, or by an organic initiator or catalyst fixed through cation exchange inside the interlayer before the swelling step, as shown in Fig. 6.

Various in situ polymerization methods have been used in the production of well-dispersed silicate layers, including ROP [63–66] and ROMP [67–69]; controlled radical polymerization [63, 70–78] such as ATRP, NMP, and RAFT; cationic polymerization [79–81]; living anionic polymerization [82, 83]; and coordination polymerization [56, 60, 84–86]. In addition to the above in situ methods, nanocomposite preparations involving multimode [63] and click chemistry [69] have also been reported.

The scope of this contribution is limited to polyolefin nanocomposites prepared by in situ coordination polymerization techniques. Special emphasize is devoted to the synthetic routes and the resultant morphology of the nanocomposites prepared using the above-mentioned polymerization mechanism.

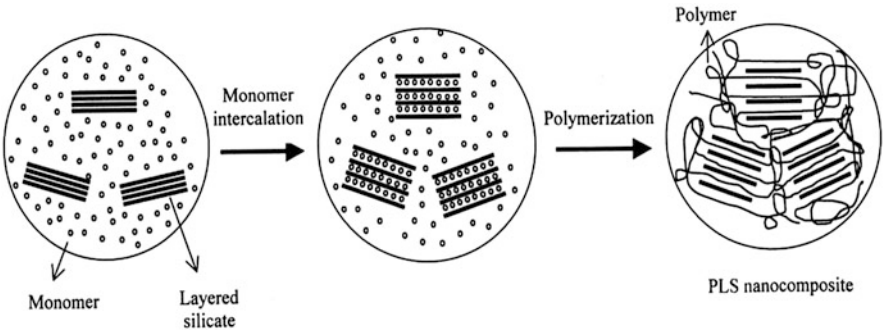

Fig. 6 Representation of in situ polymerization with clay

6.1 Polyolefin/Clay Nanocomposites by In Situ Polymerization of Olefins with a Coordination Catalyst

Polyolefins, which are normally defined as polymers based on alkene-1 monomers or α-olefins, are the most widely used group of thermoplastic polymers today. The use of many different coordination catalysts has been reported for the production of polyolefin/clay nanocomposites. The methods of in situ synthesis of polyolefin/clay nanocomposite by coordination catalysts mostly depends on the role of clay and can be divided into three categories: (1) clay as polymer filler, (2) clay as catalyst or cocatalyst support, and (3) Clay acts as a cocatalyst for coordination polymerization.

6.1.1 Clay as Polymer Filler

Heinemann et al. [87] first reported this method for synthesis of ethylene/clay blended nanocomposites in which the organically modified clay, the catalyst precursor, and the cocatalyst are added to the reactor and the polymerization is started by introduction of the olefin monomer. The authors found that in comparison to melt compounding, in situ ethylene homo- and copolymerization, catalyzed with MAO-activated zirconocene, nickel, and palladium catalysts with modified clay as filler, proved more effective in nanocomposite formation. This was evidenced by larger interlayer spacings and formation of exfoliated anisotropic nanosilicates with high aspect ratio. Only a few reports [88–91] have been published investigating this method, which seems to have the lowest polymerization activities compared with other methods. The activity values and the microstructure of the resultant nanocomposites can be improved by organic modification of MMT with polymerizable modifiers. Using this technique, Ren et al. [91] showed that the polymerizable MMTs were more exfoliatable than nonpolymerizable MMTs in the preparation of PE/MMT nanocomposites with very high activity values. A schematic representation of the clay modification and effect of amount of clay on nanocomposite microstructure is shown in Fig. 7.

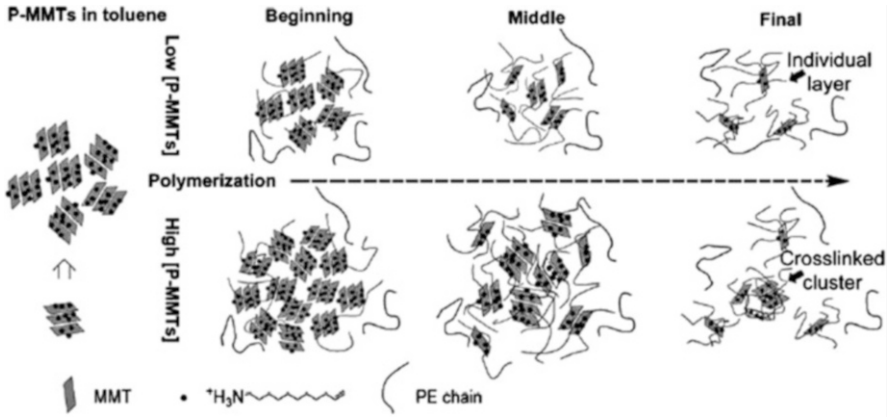

Fig. 7 Formation of PE/MMT nanocomposites via in situ ethylene polymerization in the presence of different concentrations of polymerizable MMTs (P-MMTs). Reproduced with kind permission from Ren et al. [91]

6.1.2 Clay as Catalyst or Cocatalyst Support

Kaminsky [92] was the first to report a method in which the filler surfaces were treated with metallocene-based catalyst for the production of filled polyolefins. In this method, at first under inert atmosphere, the clay surface is treated with an alkylaluminum compound to reduce the residual water content. In the second step, the catalyst or cocatalyst solution is impregnated onto the clay surface followed by washing with an anhydrous solvent to avoid excess catalyst leaching from the support during the polymerization. Additional alkylaluminum compounds may be used during the course of polymerization. This polymerization-filling technique is a widely used procedure for the synthesis of polymer/clay nanocomposites using coordination catalysts [60, 93, 94].

In order to show the advantages of catalyst or cocatalyst being supported on clay over simple addition of clay to the reactor, Kuo et al. [89] performed a comparative study of these two preparative methods. In method 1, they reacted $Et(Ind)_2ZrCl_2$, MAO, and an organoclay in the reactor and started the polymerization by introducing ethylene. In method 2, they reacted MAO-treated organoclay with the catalyst solution, and then used the product to polymerize ethylene. It was observed that in situ polymerization with method 2 led to higher catalyst activities and was less sensitive to clay loading. In addition, a finer and more homogeneous dispersion of polymer/clay particles was obtained for method 2. It was also reported that extending the MAO treatment time from 1.5 to 2.5 h, and the catalyst impregnation time from 0.5 to 2 h, had no appreciable effect on polymerization activity.

Tudor et al. [95] first used the in situ intercalative polymerization method for the preparation of PP/clay nanocomposites. They demonstrated the ability of soluble metallocene catalysts to intercalate inside silicate layers, and to promote the coordination polymerization of propylene. The silicate layers were modified by

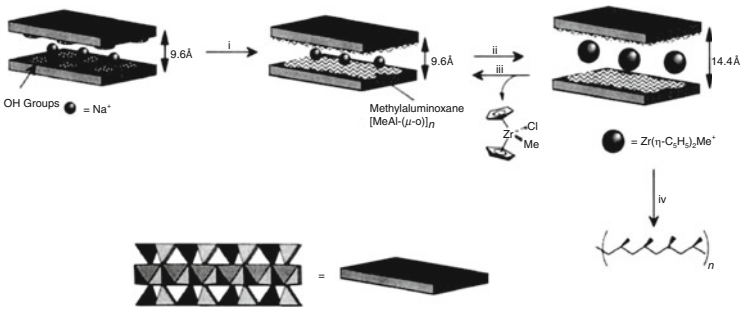

Fig. 8 Synthetic route of the modification and ion-exchange of Laponite with $[Zr(\eta\text{-}C_6H_5Me(thf))]^+$ BPh_4 and propene polymerization. Reproduced with kind permission from Tudor et al. [95]

MAO and then the cationic metallocene catalyst $\{Zr[\eta\text{-}C_6H_5Me(thf)]\}^+$ was intercalated in two clays (a synthetic fluorinated mica-type silicate and the modified synthetic hectorite) by ion-exchange reaction with the interlamellar cations of the layered silicates. Figure 8 shows a schematic route for preparation of PP/clay nanocomposites.

Subsequently, Sun and Garces [96] also reported the preparation of PP/clay nanocomposites by in situ polymerization with metallocene/clay catalysts. Recently, Wang and coworkers [97] used thermally treated naturally occurring palygorskite to support titanocene (Cp_2TiCl_2) catalyst. After activation by MAO, the supported catalyst initiated an in situ ethylene polymerization resulting in the exfoliated dispersion of the nanofibers into the polyethylene matrix. The activity of the supported catalyst was found to be even higher than its solution counterpart and the final PE/clay nanocomposite showed physical properties.

Huang et al. [88] reported a new approach for the effective stabilization of the PE/MMT nanocomposite structure against processing. The ethylene polymerization was conducted in the presence of *p*-methylstyrene using an OMMT-intercalated metallocene catalyst [$Et(Ind)_2ZrCl_2$ in combination with MAO]. The resultant *p*-methylstyrene-containing PE/OMMT nanocomposites were functionalized selectively on the benzyl group in the *p*-methylstyrene. The in situ-incorporated functional groups, including the pendant maleic anhydride groups and the polar PMMA side chains, significantly improved miscibility between the PE matrix and laminated silicate layers of MMT, leading to effective stabilization of the nanocomposite structure against processing.

Alexandre et al. [98] reported the preparation of PE/clay nanocomposite using Ti-based constrained geometry catalyst (CGC) catalyst. The MMT and hectorite were initially treated with TMA-depleted MAO and then intercalated with the CGC catalyst. Finally, addition of ethylene resulted in the formation of high molecular weight and exfoliated PE/clay nanocomposites. The vinyl groups were chemically linked to the silicate surface when copolymerized was carried out with ethylene inside the clay galleries using the nickel catalyst (Fig. 9). This method not only results in the effective exfoliation of the layered silicate but also in polyethylene chains that are chemically bonded to silicate surface.

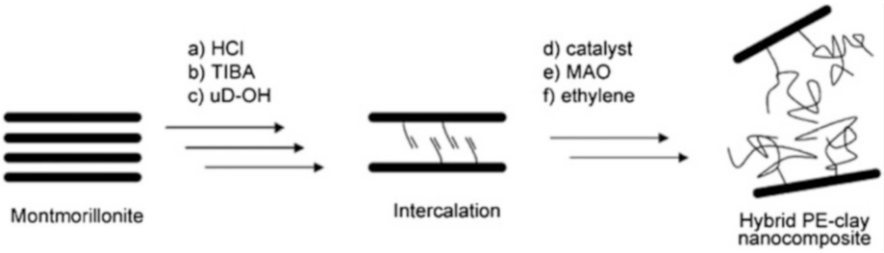

Fig. 9 Synthetic approach using bifunctional organic modifier to produce polyethylene chemically linked silicate layers prepared by in situ polymerization. Reproduced with kind permission from Alexandre et al. [98]

Shin and coworkers [99] prepared a hybrid PE/clay nanocomposite using [1,4-bis (2,6-diisopropylphenyl)-acenaphthenediimine]-dichloronickel catalyst. The chemical modification and intercalation of MMT were carried out with alkylaluminum and vinyl alcohol.

Ray et al. [93] treated organically modified MMT (OMMT) with a MAO solution after vacuum-drying at 100°C. The resulting MAO-treated clay was subsequently used for ethylene polymerization in the presence of 2,6-bis [1-(2,6-diisopropylphenylimino)ethyl]pyridine iron(II) dichloride with additional MAO in a glass reactor. In addition, they compared the methods of nanocomposite preparation and observed that the nanocomposite produced by catalyst supported on MAO-pretreated OMMT was more efficiently exfoliated than the nanocomposite produced when only a mixture of catalyst and clay was used. This result led them to conclude that at least some of the active centers resided within the clay galleries. Similarly, Guo et al. [100] in a separate studies successfully used pyridine diimine-based iron(II) catalysts for preparation of exfoliated PE/clay nanocomposites.

Bergman et al. [101] used Brookhart's single component palladium-based complex and the 1-tetradecylammonium cationically modified synthetic fluorohectorite for preparation of polyethylene nanocomposites. They first intercalated palladium catalyst into the galleries of modified fluorohectorite and exposed the dry powder to ethylene gas. Over a period of 2 h, they observed monomer consumption and a dramatic increase in the size of the silicate–catalyst composite. After 12 h, the orange colored palladium complex was unrecognizable; in its place was a large mass of colorless, rubbery polymer. The complete absence of diffraction peaks in the XRD patterns strongly suggested the formation of an exfoliated nanocomposite. It is noteworthy that this nanocomposite is formed without the use of MAO either for pretreatment of the silicate material or during polymerization. A schematic representation of nanocomposite formation by this method is given in Fig. 10.

Jin et al. [102] used organic salts with hydroxyl groups for the modification of MMT to produce MMT–OH. Because the hydroxyl groups in intercalation agents offer facile reactive sites for anchoring catalysts between silicate layers, they successfully anchored a Ti-based Ziegler–Natta catalyst at the inner surface of MMT for in situ production of exfoliated PENC. Figure 11 shows the $TiCl_4$ fixation

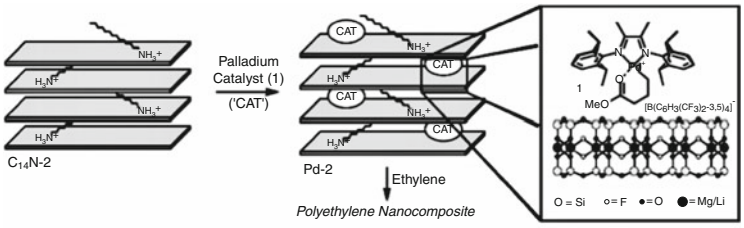

Fig. 10 Route for the preparation of PE/organically modified fluorohectorite nanocomposite using Brookhart's single-component palladium complex. Reproduced with kind permission from Bergman et al. [101]

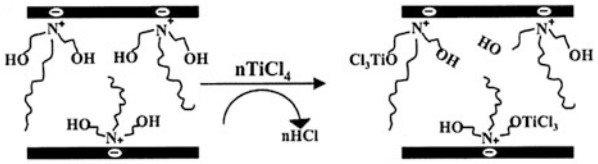

Fig. 11 Mechanistic representation of the fixing of $TiCl_4$ between the silicate layers of MMT–OH. Reproduced with kind permission from Jin et al. [102]

mechanism between silicate layers of MMT–OH. The polymerization of ethylene was conducted by injecting ethylene into the catalyst slurry (30–50°C, 4 bar). Comparison of the exfoliation characteristics of MMT–OH and nonintercalated montmorillonite showed that the feasibility of exfoliation during ethylene polymerization was highly dependent on the catalyst fixation method.

Recently, our group [103] used TEA-modified MMT to prepare exfoliated PMMA/clay nanocomposites by in situ polymerization using $Ni(acac)_2$ catalyst. A schematic representation is given in Fig. 12. The PMMA/clay nanocomposites are found to retain over 80% transparency, which is important for optical applications. In addition, the tensile strength of nanocomposites is up to 70 MPa for 7.26 wt% clay content, and the tensile modulus shows a value 20% higher than that of neat PMMA.

6.1.3 Clay Acts as a Cocatalyst for Coordination Polymerization

During the mid-1990s, a research group at Mitsubishi discovered that certain clays could be calcined and used to activate metallocenes [104]. McDaniel et al. [104] proposed that the metallocenes may be activated by the reaction between the clay cations and the metallocene, resulting in the formation "clay anions" and metallocene cations and sodium chloride. In this way a neutral metallocene can be activated, forming ion-pair active species such as metallocene cation and clay anion. A schematic representation of activation of metallocene by clay is shown in Fig. 13. The ion exchange of metallocenium cations with clay surfaces is also

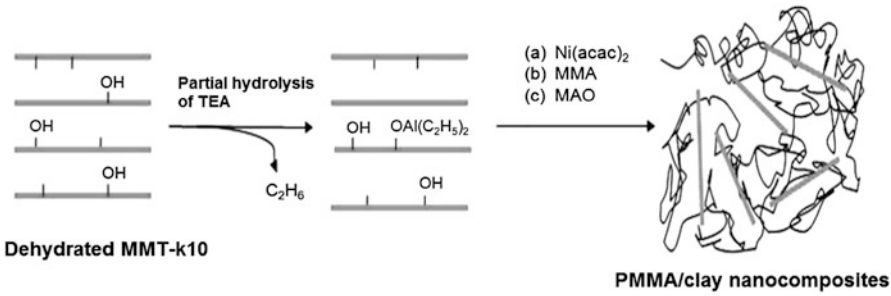

Fig. 12 Preparation of PMMA/MMT nanocomposite by in situ coordination polymerization using $Ni(acac)_2$ catalyst. Reproduced with kind permission from Cui et al. [103]

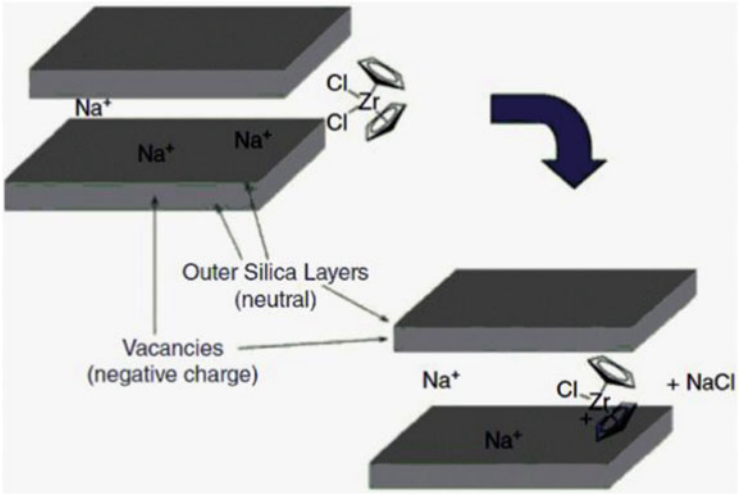

Fig. 13 Possible mechanism for metallocene activation on clay surface. Reproduced with kind permission from McDaniel et al. [104]

discussed by Chen and coworkers [105, 106]. During coordination polymerization, MAO has been proposed as being responsible for generation and stabilization of the cationic alkyl metallocene by acting as a counterion [92, 107], resulting in a species like $(L_2{\cdot}MtCH_3)^{+}{\cdot}(MAO{\cdot}X)^{-}$. Hence, in metallocene activation by clay, a similar role is thought to be played by the clay surface.

A number of reports [108] have shown that olefin polymerization catalysts can be activated by acidic clay surfaces when combined with alkylaluminum compounds such as trimethylaluminum or triisobuthylaluminum, generating catalysts that are very active for polymerization. Note that alkylaluminum compounds alone cannot properly activate metallocenes to high polymerization activities. In this approach, the clay surface is thought to be the sole location where polymerization takes place.

During in situ production of alkylaluminoxanes, water molecules present on the surface of pristine clay react with alkylaluminum compounds to produce MAO oligomers on the clay surface. The modified clay can then be used directly as a polymerization cocatalyst, or impregnated with a catalyst solution prior to polymerization. In this case, a high temperature thermal treatment to remove surface-bonded water molecules is not required.

Novokshonova et al. [109] reported a procedure in which the Al:H_2O ratio was lower than unity and alkylaluminum was added drop-wise to the clay solution until the evolution of volatiles (e.g., CH_4 in the case of TMA) stopped. Alternatively, in a second procedure, they used a Al:H_2O ratio equal to 1 and the alkylaluminum was added in a single step to the clay suspension. It was observed that the second procedure resulted in higher polymerization activities and no extra MAO was required during the polymerization. The authors suggested that higher degrees of alkylaluminum hydrolysis were obtained in the first procedure and that fewer alkyl groups remained available for alkylation reactions of the metallocene. On the other hand, higher Al:H_2O ratios resulted in partial hydrolysis of the alkylaluminum molecules and, consequently, more alkylaluminum molecules were available for metallocene alkylation. It was also found that the MAO formed on the clay surface had similar structure to that of commercial MAO.

Despite the fact that the presence of organic modifications on the clay surfaces enhances the dispersion of the clay nanolayers in nonpolar polymer matrices, the nanolayers tend to degrade rapidly under the high temperature required for polymer extrusion, leading to clay agglomeration and poor nanocomposite mechanical properties [110, 111]. Scott et al. [86] proposed a technique to overcome this problem by avoiding the use of clay organic modifiers. By comparing different clay treatments for catalyst support and in situ olefin polymerization, they showed that MMT treatment with mineral acid extensively disturbs its layered structure and increases its Lewis acidity. They proposed that the nickel complex can be activated for ethylene polymerization by binding a Lewis acid such as $B(C_6F_5)_3$ at the carbonyl group on the ligand backbone, generating a Zwitterionic adduct (Fig. 14). This catalyst was particularly effective at promoting polymerization solely on the clay surface, leading to effective clay dispersion in the polymer matrix, while not needing any cocatalyst or scavenger.

Unfortunately, this procedure was reported to be inadequate for metallocenes such as Cp_2ZrMe_2. The authors speculated that the low activity of the clay-supported metallocene was due to severe decomposition of the catalyst in contact with the strong Brønsted acidic surface of the clay. Scott et al. [86] also showed that the clay dispersion in the polyolefin matrix is stable during annealing at 170°C for 30 min and related this behavior to the high molecular weight and high viscosity at the test temperature (170°C).

In order to reduce the deactivating interaction between the coordination catalyst and the clay surface, Huang and coworkers [112] proposed an indirect supporting method in which a common support, such as $MgCl_2$ or SiO_2, is deposited onto the clay surface to increase the hydroxyl population on the clay surface where the loading of active catalyst occurs. It is well known that $MgCl_2$ dissolves in alcohols to form

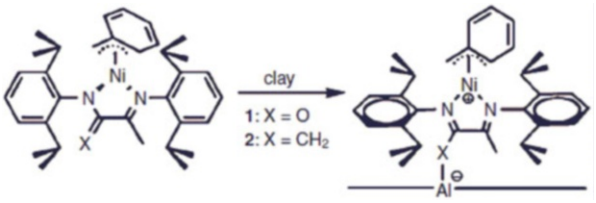

Fig. 14 Proposed mechanism of for nickel catalyst activation on the surface of clay. Reproduced with kind permission from Scott et al. [86]

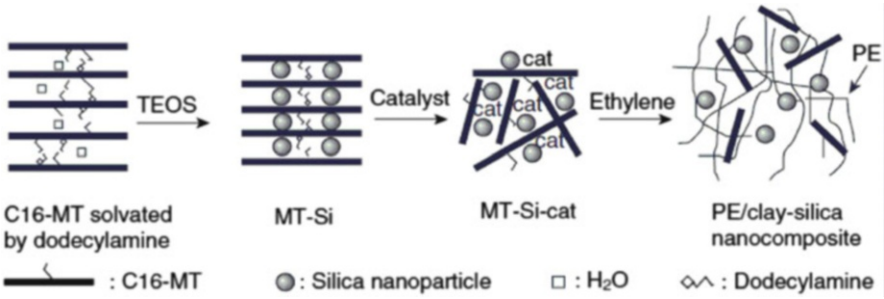

Fig. 15 Proposed mechanism for formation of montmorillonite–silica (*MT-Si*) and PE/clay–silica nanocomposites. Reproduced with kind permission from Huang et al. [112]

$MgCl_2{\cdot}n$ROH complexes and even MMT can swell in alcohols. When MMT is immersed in $MgCl_2$/alcohol solution, MMT can swell, thus allowing the diffusion of $MgCl_2{\cdot}n$ROH complexes into the space between the MMT layers. After removal of the alcohol, $MgCl_2$ as microcrystallites may deposit on and between the surfaces of layered MMT. The MMT-Si is prepared by a typical procedure in which 1 g OMMT was stirred with 5.1 g of dodecylamine at 50°C for 20 min, after which 43 g of tetraethylorthosilicate was added and stirred for the next 4 h. The resultant suspension was centrifuged, and the solid was subsequently dried to produce MMT-Si. The MMT-Si–Zr catalyst was prepared starting from purified MMT-Si (2.6 g) pretreated with 30 mL of MAO solution (1.0 mol/L in toluene) under argon. The prescribed amount of Cp_2ZrCl_2 solution (0.01938 mol/L in toluene) was then added to the MAO-treated MMT-Si support in toluene at 60°C. Figure 15 illustrates the preparation of MMT-Si–Zr and resultant PE nanocomposite.

We have recently developed [84] vanadium-based Ziegler–Natta polymerization of catalysts supported on clay/$MgCl_2$ hybrid supports. As $MgCl_2$ offers catalyst loading sites, the vanadium catalyst is avoided with a direct anchoring on the surface of the clay. Such intercalated catalyst clay/$MgCl_2$/$VOCl_3$ displays high activity for production of exfoliated PE-based clay nanocomposites. Compared with pure PE, all these nanocomposites showed enhancement of the melting temperature (T_m) and the thermal decomposition temperatures as well as significant improvement in the mechanical properties (shown in Table 2 and Fig. 16).

Table 2 Ethylene polymerization with intercalation catalyst V-MMT

Run no.	Initial clay loading (g)	Polymerization time (h)	Activity (kg_{PE}/mol_V h atm)	Clay mass fraction (wt%)	Extracted in decalin (%)	Temperature for 5 wt% loss[a] (°C)	Temperature for 10 wt% loss[a] (°C)
1[b]	0	2	2.60	0	82.7	367	419
2	0.15	12	50.7	1.61	73.4	388	422
3	0.10	24	28.0	2.43	40.4	403	444
4	0.10	12	36.2	3.76	23.4	426	498

Polymerization conditions: Al(*i*-Bu)$_3$ as cocatalyst, [Al]/[V] = 1,000, *n*-heptane 100 mL as solvent, room temperature, ethylene 1.2 atm

[a]Determined by TGA

[b]Homogeneous catalyst $VOCl_3$ as catalyst, [V] = 1.05 mmol, [Al]/[V] = 15, other conditions are same as for other samples

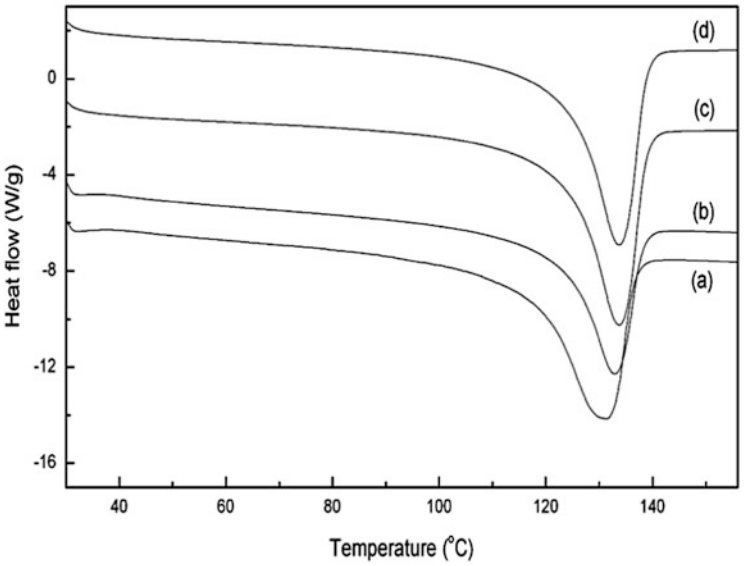

Fig. 16 DSC thermograms of pure PE (*a*), PE/clay 1.61 wt% (*b*), PE/clay 2.43 wt% (*c*), and PE/clay 3.76 wt% (*d*). Reproduced with kind permission from Cui et al. [84]

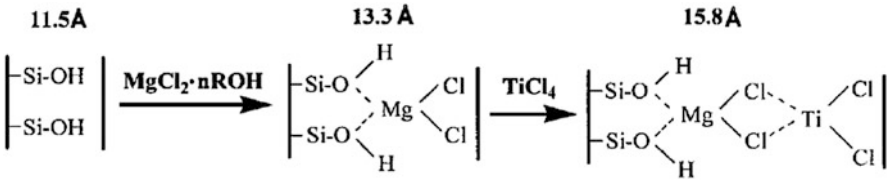

Fig. 17 Intercalation of $TiCl_4$ on MMT/$MgCl_2$ support. Reproduced with kind permission from Ma et al. [113]

Ma et al. [113] prepared PP/OMMT nanocomposites with improved dynamic mechanical properties and thermal properties using an OMMT/$MgCl_2$/$TiCl_4$ catalyst. At temperatures higher than T_g, with 8.1 wt% clay content, the PP nanocomposites exhibited a storage modulus three times higher than that of the pure PP. In a similar report, Yang et al. [114] prepared PE/MMT nanocomposites using a MMT/$MgCl_2$/$TiCl_4$ catalyst activated by $Al(Et)_3$. The catalyst was prepared by first diffusing $MgCl_2$ into the swollen MMT layers, followed by loading of $TiCl_4$ on the inner/outer layer surfaces of MMT/$MgCl_2$. The intercalation of MMT layers by $MgCl_2$ and $TiCl_4$ was demonstrated by the enlarged interlayer spacing, as determined by WAXD. They reported a significant improvement in the tensile strength of the resultant PE nanocomposite compared to that of virgin polyethylene of comparable molecular weight. Figure 17 shows a schematic representation of the reaction between the clay surface and the $MgCl_2$ and $TiCl_4$ loading.

7 Outlook

Organic/inorganic nanocomposites prepared by in situ polymerization methods have received extensive attention in recent years. Unlike microscale fillers, nanoscale fillers can offer excellent properties to a polymer matrix. Nanosized filler, with a few weight percent in the reinforced polymer nanocomposites, strongly influences the macroscopic properties of the polymer. The resultant polymer nanocomposites can significantly improve some of their properties, such as higher heat distortion temperatures, enhanced flame resistance, increased modulus, better barrier properties, reduced thermal expansion coefficient, and altered electronic and optical properties.

A wide variety of polymer/clay nanocomposites can be synthesized by in situ coordination polymerization methods, which gives the advantage of controlled molecular weight of the polymer nanocomposite. In the case of late transition metal-based coordination polymerization, the process is tolerant to the polar groups or to a little moisture in the clay or catalytic system. This moisture sensitivity can also be overcomed by treating the excess MAO or by in situ formation of MAO using TEA, TMA, or TIBA on the surface of clay, clay–$MgCl_2$, or clay–silica hybrid material.

Regarding synthesis of polyolefin nanocomposites with wider applications, copolymerization of ethylene with other olefinic monomers, including higher α-olefins and polar comonomers still needs to be investigated in more detail. To make the present coordination polymerization-induced formation of polyolefin/clay nanocomposites applicable to industrial bulk or slurry processes, more efforts are needed with regard to the preparation of catalytic species with regular morphology, prevention against re-aggregation or stacking recovery of the already intercalated or exfoliated MMT sheets, and the rheological properties of the nanocomposites with various structures and different MMT loadings.

References

1. Friedlander HZ (1963) Spontaneous polymerization in and on clays. ACS Polym Preprints 4:300–306
2. Bittles JA, Chaudhuri AK, Benson SW (1964) Clay-catalyzed reactions of olefins. I. Polymerization of styrene. J Polym Sci A2:1221–1231
3. Bittles JA, Chaudhuri AK, Benson SW (1964) Clay-catalyzed reactions of olefins. II. Catalyst acidity and mechanisms. J Polym Sci A2:1847–1862
4. Kusnitsyna TA, Ostrovskaya LK (1967) Catalytic activity of acid alumina-silicates in the styrene polymerization reaction. Vysokomolekulyarnye Soedineniya Seriya A9:2510–2514
5. Solomon DH, Rosser MJ (1965) Reactions catalysed by minerals. I. Polymerization of styrene. J Appl Polym Sci 9:1261–1271
6. Usuki AKY, Kawasumi M, Okada A, Fukushima Y, Kurauchi T et al (1993) Synthesis of nylon 6-clay hybrid. J Mater Res 8:1179–1184

7. Vaia RA, Ishii H, Giannelis EP (1993) Synthesis and properties of two-dimensional nanostructures by direct intercalation of polymer melts in layered silicates. Chem Mater 5 (12):1694–1696
8. Komarneni S (1992) Feature article. Nanocomposites. J Mater Chem 2(12):1219–1230
9. Alexandre M, Dubois P (2000) Polymer-layered silicate nanocomposites: preparation, properties and uses of a new class of materials. Mater Sci Eng R Reports 28:1–63
10. Fischer H (2003) Polymer nanocomposites: from fundamental research to specific applications. Mater Sci Eng C 23:763–772
11. Pavlidou S, Papaspyrides CD (2008) A review on polymer-layered silicate nanocomposites. Prog Polym Sci 33(12):1119–1198
12. Giannelis EP (1998) Polymer-layered silicate nanocomposites: synthesis, properties and applications. Appl Organometal Chem 12(10–11):675–680
13. Lan T, Pinnavaia TJ (1994) Clay-reinforced epoxy nanocomposites. Chem Mater 6 (12):2216–2219
14. Messersmith PB, Giannelis EP (1995) Synthesis and barrier properties of poly (ε-caprolactone)-layered silicate nanocomposites. J Polym Sci A Polym Chem 33 (7):1047–1057
15. Biswas M, Ray SS (2001) Recent progress in synthesis and evaluation of polymer–montmorillonite nanocomposites. Adv Polym Sci 155:167–221
16. Bharadwaj RK (2001) Modeling the barrier properties of polymer-layered silicate nanocomposites. Macromolecules 34(26):9189–9192
17. Xu R, Manias E, Snyder AJ, Runt J (2000) New biomedical poly(urethane urea)/layered silicate nanocomposites. Macromolecules 34(2):337–339
18. Gilman JW (1999) Flammability and thermal stability studies of polymer layered-silicate (clay) nanocomposites. Appl Clay Sci 15(1–2):31–49
19. Gilman JW, Jackson CL, Morgan AB, Harris R, Manias E, Giannelis EP, Wuthenow M, Hilton D, Phillips SH (2000) Flammability properties of polymer-layered-silicate nanocomposites. Polypropylene and polystyrene nanocomposites. Chem Mater 12 (7):1866–1873
20. Sinha Ray S, Yamada K, Okamoto M, Ueda K (2002) Polylactide-layered silicate nanocomposite: a novel biodegradable material. Nano Lett 2(10):1093–1096
21. Vaia RA, Vasudevan S, Krawiec W, Scanlon LG, Giannelis EP (1995) New polymer electrolyte nanocomposites: melt intercalation of poly(ethylene oxide) in mica-type silicates. Adv Mater 7(2):154–156
22. Wu J, Lerner MM (1993) Structural, thermal, and electrical characterization of layered nanocomposites derived from sodium-montmorillonite and polyethers. Chem Mater 5 (6):835–838
23. Mehrotra V, Giannelis EP (1991) Metal-insulator molecular multilayers of electroactive polymers: intercalation of polyaniline in mica-type layered silicates. Solid State Commun 77(2):155–158
24. Hutchison JC, Bissessur R, Shriver DF (1996) Conductivity anisotropy of polyphosphazene/montmorillonite composite electrolytes. Chem Mater 8(8):1597–1599
25. Ogawa M, Ishikawa A (1998) Controlled microstructures of amphiphilic cationic azobenzene-montmorillonite intercalation compounds. J Mater Chem 8(2):463–467
26. Ogawa M, Takahashi M, Kato C, Kuroda K (1994) Oriented microporous film of tetramethylammonium pillared saponite. J Mater Chem 4(4):519–523
27. Pinnavaia TJ (1983) Intercalated clay catalysts. Science 220(4595):365–371
28. Lagaly G, Ogawa M, Dékány I (2006) Clay mineral organic interactions. In: Bergaya F, Theng BKG, Lagaly G (eds) Handbook of clay science. Developments in clay science, vol 1. Elsevier, Amsterdam, pp 309–377
29. Ruiz-Hitzky E, Van Meerbeek A (2006) Clay mineral- and organoclay-polymer nanocomposite. In: Bergaya F, Theng BKG, Lagaly G (eds) Handbook of clay science. Developments in clay science, vol 1. Elsevier, Amsterdam, pp 583–621

30. Kato M, Usuki A (2000) Polymer–clay nanocomposites. In: Pinnavaia TJ, Beall GW (eds) Polymer–clay nanocomposites. Wiley, Chichester, pp 97–109
31. Koo CM, Kim MJ, Choi MH, Kim SO, Chung IJ (2003) Mechanical and rheological properties of the maleated polypropylene-layered silicate nanocomposites with different morphology. J Appl Polym Sci 88(6):1526–1535
32. Manias E, Touny A, Wu L, Strawhecker K, Lu B, Chung TC (2001) Polypropylene/montmorillonite nanocomposites. Review of the synthetic routes and materials properties. Chem Mater 13(10):3516–3523
33. Theng BKG (1974) The chemistry of clay-organic reactions. Wiley, Adam Hilger, London
34. Kornmann X, Lindberg H, Berglund LA (2001) Synthesis of epoxy–clay nanocomposites: influence of the nature of the clay on structure. Polymer 42(4):1303–1310
35. Brixie JM, Boyd SA (1994) Treatment of contaminated soils with organoclays to reduce leachable pentachlorophenol. J Environ Qual 23(6):1283–1290
36. Barrer RM (1978) Zeolites and clay minerals as sorbents and molecular sieves. Academic, London
37. Theng BKG, Churchman GJ, Gates WP, Yuan G (2008) Organically modified clays for pollutant uptake and environmental protection. In: Huang Q, Huang PM, Violante A (eds) Soil mineral–microbe–organic interactions. Springer, Berlin, pp 145–174
38. de Paiva LB, Morales AR, Valenzuela Diaz FR (2008) Organoclays: properties, preparation and applications. Appl Clay Sci 42(1–2):8–24
39. Zanetti M, Lomakin S, Camino G (2000) Polymer layered silicate nanocomposites. Macromol Mater Eng 279(1):1–9
40. Ishida H, Campbell S, Blackwell J (2000) General approach to nanocomposite preparation. Chem Mater 12(5):1260–1267
41. Krishnamoorti R, Vaia RA, Giannelis EP (1996) Structure and dynamics of polymer-layered silicate nanocomposites. Chem Mater 8(8):1728–1734
42. Heller-Kallai L (2006) Thermally modified clay minerals. In: Bergaya F, Theng BKG, Lagaly G (eds) Handbook of clay science. Developments in clay science, vol 1. Elsevier, Amsterdam, pp 289–308
43. Vaia RA, Giannelis EP (1997) Lattice model of polymer melt intercalation in organically-modified layered silicates. Macromolecules 30(25):7990–7999
44. LeBaron PC, Wang Z, Pinnavaia TJ (1999) Polymer-layered silicate nanocomposites: an overview. Appl Clay Sci 15(1–2):11–29
45. Huang X, Lewis S, Brittain WJ, Vaia RA (2000) Synthesis of polycarbonate-layered silicate nanocomposites via cyclic oligomers. Macromolecules 33(6):2000–2004
46. Vaia RA, Giannelis EP (1997) Polymer melt intercalation in organically-modified layered silicates: model predictions and experiment. Macromolecules 30(25):8000–8009
47. Beyer G (2002) Nanocomposites: a new class of flame retardants for polymers. Plast Addit Compd 4(10):22–28
48. Morgan AB, Gilman JW (2003) Characterization of polymer-layered silicate (clay) nanocomposites by transmission electron microscopy and X-ray diffraction: a comparative study. J Appl Polym Sci 87(8):1329–1338
49. Ma J, Xu J, Ren J-H, Yu Z-Z, Mai Y-W (2003) A new approach to polymer/montmorillonite nanocomposites. Polymer 44(16):4619–4624
50. Porter D, Metcalfe E, Thomas MJK (2000) Nanocomposite fire retardants-a review. Fire Mater 24(1):45–52
51. VanderHart DL, Asano A, Gilman JW (2001) NMR measurements related to clay-dispersion quality and organic-modifier stability in nylon-6/clay nanocomposites. Macromolecules 34 (12):3819–3822
52. Sinha Ray S, Okamoto M (2003) Polymer/layered silicate nanocomposites: a review from preparation to processing. Prog Polym Sci 28(11):1539–1641

53. Loo LS, Gleason KK (2003) Fourier transform infrared investigation of the deformation behavior of montmorillonite in nylon-6/nanoclay nanocomposite. Macromolecules 36 (8):2587–2590
54. Wu H-D, Tseng C-R, Chang F-C (2001) Chain conformation and crystallization behavior of the syndiotactic polystyrene nanocomposites studied using fourier transform infrared analysis. Macromolecules 34(9):2992–2999
55. Do Nascimento GM, Constantino VRL, Temperini MLA (2002) Spectroscopic characterization of a new type of conducting polymer–clay nanocomposite. Macromolecules 35 (20):7535–7537
56. Cui L, Tarte NH, Woo SI (2008) Synthesis and properties of poly(methyl methacrylate)/clay nanocomposites prepared via in situ polymerization with $Ni(acac)_2$ catalyst. J Appl Polym Sci 110(2):784–790
57. Bafna A, Beaucage G, Mirabella F, Mehta S (2003) 3D Hierarchical orientation in polymer–clay nanocomposite films. Polymer 44(4):1103–1115
58. Bhattacharya SN, Kamal MR, Gupta RK (2008) Polymeric nanocomposites: theory and practice. Carl Hanser, Munich
59. Ciardelli F, Coiai S, Passaglia E, Pucci A, Ruggeri G (2008) Nanocomposites based on polyolefins and functional thermoplastic materials. Polym Int 57(6):805–836
60. Dubois P, Alexandre M, Jérôme R (2003) Polymerization-filled composites and nanocomposites by coordination catalysis. Macromol Symp 194(1):13–26
61. Carrado KA (2000) Synthetic organo- and polymer–clays: preparation, characterization, and materials applications. Appl Clay Sci 17(1–2):1–23
62. Usuki A, Kojima Y, Kawasumi M, Okada A, Fukushima Y, Kurauchi T, Kamigaito O (1993) Synthesis of nylon 6-clay hybrid. J Mater Res 8(05):1179–1184
63. Di J, Sogah DY (2006) Exfoliated block copolymer/silicate nanocomposites by one-pot, one-step in-situ living polymerization from silicate-anchored multifunctional initiator. Macromolecules 39(15):5052–5057
64. Kubies D, Pantoustier N, Dubois P, Rulmont A, Jerome R (2002) Controlled ring-opening polymerization of ε-caprolactone in the presence of layered silicates and formation of nanocomposites. Macromolecules 35(9):3318–3320
65. Lepoittevin B, Pantoustier N, Devalckenaere M, Alexandre M, Kubies D, Calberg C, Jerome R, Dubois P (2002) Poly(ε-caprolactone)/clay nanocomposites by in-situ intercalative polymerization catalyzed by dibutyltin dimethoxide. Macromolecules 35(22):8385–8390
66. Viville P, Lazzaroni R, Pollet E, Alexandre M, Dubois P (2004) Controlled polymer grafting on single clay nanoplatelets. J Am Chem Soc 126(29):9007–9012
67. Yoonessi M, Toghiani H, Daulton TL, Lin J-S, Pittman CU (2005) Clay delamination in clay/poly(dicyclopentadiene) nanocomposites quantified by small angle neutron scattering and high-resolution transmission electron microscopy. Macromolecules 38(3):818–831
68. Yoonessi M, Toghiani H, Kingery WL, Pittman CU (2004) Preparation, characterization, and properties of exfoliated/delaminated organically modified clay/dicyclopentadiene resin nanocomposites. Macromolecules 37(7):2511–2518
69. Yoonessi M, Toghiani H, Pittman CU (2006) Orientation of montmorillonite clay in dicyclopentadiene/organically modified clay dispersions and nanocomposites. J Appl Polym Sci 102(3):2743–2751
70. Di J, Sogah DY (2006) Intergallery living polymerization using silicate-anchored photoiniferter. A versatile preparatory method for exfoliated silicate nanocomposites. Macromolecules 39(3):1020–1028
71. Konn C, Morel F, Beyou E, Chaumont P, Bourgeat-Lami E (2007) Nitroxide-mediated polymerization of styrene initiated from the surface of laponite clay platelets. Macromolecules 40(21):7464–7472
72. Li C-P, Huang C-M, Hsieh M-T, Wei K-H (2005) Properties of covalently bonded layered-silicate/polystyrene nanocomposites synthesized via atom transfer radical polymerization. J Polym Sci A Polym Chem 43(3):534–542

73. Salem N, Shipp DA (2005) Polymer-layered silicate nanocomposites prepared through in situ reversible addition-fragmentation chain transfer (RAFT) polymerization. Polymer 46 (19):8573–8581
74. Weimer MW, Chen H, Giannelis EP, Sogah DY (1999) Direct synthesis of dispersed nanocomposites by in situ living free radical polymerization using a silicate-anchored initiator. J Am Chem Soc 121(7):1615–1616
75. Wheeler PA, Wang J, Mathias LJ (2006) Poly(methyl methacrylate)/laponite nanocomposites: exploring covalent and ionic clay modifications. Chem Mater 18 (17):3937–3945
76. Zhao H, Argoti SD, Farrell BP, Shipp DA (2004) Polymer–silicate nanocomposites produced by in situ atom transfer radical polymerization. J Polym Sci A Polym Chem 42(4):916–924
77. Zhao H, Farrell BP, Shipp DA (2004) Nanopatterns of poly(styrene-block-butyl acrylate) block copolymer brushes on the surfaces of exfoliated and intercalated clay layers. Polymer 45(13):4473–4481
78. Zhao H, Shipp DA (2003) Preparation of poly(styrene-block-butyl acrylate) block copolymer-silicate nanocomposites. Chem Mater 15(14):2693–2695
79. Nese A, Sen S, Tasdelen MA, Nugay N, Yagci Y (2006) Clay-PMMA nanocomposites by photoinitiated radical polymerization using intercalated phenacyl pyridinium salt initiators. Macromol Chem Phys 207(9):820–826
80. Oral A, Tasdelen MA, Demirel AL, Yagci Y (2009) Poly(cyclohexene oxide)/clay nanocomposites by photoinitiated cationic polymerization via activated monomer mechanism. J Polym Sci A Polym Chem 47(20):5328–5335
81. Yu Y-H, Lin C-Y, Yeh J-M (2004) Poly(*N*-vinylcarbazole)-clay nanocomposite materials prepared by photoinitiated polymerization with triarylsulfonium salt initiator. J Appl Polym Sci 91(3):1904–1912
82. Fan X, Zhou Q, Xia C, Cristofoli W, Mays J, Advincula R (2002) Living anionic surface-initiated polymerization (LASIP) of styrene from clay nanoparticles using surface bound 1,1-diphenylethylene (DPE) initiators. Langmuir 18(11):4511–4518
83. Zhou Q, Fan X, Xia C, Mays J, Advincula R (2001) Living anionic surface initiated polymerization (SIP) of styrene from clay surfaces. Chem Mater 13(8):2465–2467
84. Cui L, Woo S (2008) Preparation and characterization of polyethylene (PE)/clay nanocomposites by in situ polymerization with vanadium-based intercalation catalyst. Polym Bull 61(4):453–460
85. Maneshi A, Soares J, Simon L (2011) Polyolefin–clay nanocomposites by in-situ polymerization. In: Mittal V (ed) In-situ synthesis of polymer nanocomposites. Wiley-VCH, Weinheim, pp 53–88
86. Scott SL, Peoples BC, Yung C, Rojas RS, Khanna V, Sano H, Suzuki T, Shimizu F (2008) Highly dispersed clay-polyolefin nanocomposites free of compatibilizers, via the in situ polymerization of α-olefins by clay-supported catalysts. Chem Commun 35:4186–4188
87. Heinemann J, Reichert P, Thomann R, Mülhaupt R (1999) Polyolefin nanocomposites formed by melt compounding and transition metal catalyzed ethene homo- and copolymerization in the presence of layered silicates. Macromol Rapid Commun 20(8):423–430
88. Huang Y, Yang K, Dong J-Y (2007) An in situ matrix functionalization approach to structure stability enhancement in polyethylene/montmorillonite nanocomposites prepared by intercalative polymerization. Polymer 48(14):4005–4014
89. Kuo S-W, Huang W-J, Huang S-B, Kao H-C, Chang F-C (2003) Syntheses and characterizations of in situ blended metallocence polyethylene/clay nanocomposites. Polymer 44 (25):7709–7719
90. Liu C, Tang T, Zhao Z, Huang B (2002) Preparation of functionalized montmorillonites and their application in supported zirconocene catalysts for ethylene polymerization. J Polym Sci A Polym Chem 40(11):1892–1898

91. Ren C, Du X, Ma L, Wang Y, Tang T (2010) The role of polymerizable organophilic clay during preparing polyethylene nanocomposite via filling polymerization. J Appl Polym Sci 117(3):1646–1657
92. Kaminsky W (1996) New polymers by metallocene catalysis. Macromol Chem Phys 197 (12):3907–3945
93. Ray S, Galgali G, Lele A, Sivaram S (2005) In situ polymerization of ethylene with bis (imino)pyridine iron(II) catalysts supported on clay: The synthesis and characterization of polyethylene–clay nanocomposites. J Polym Sci A Polym Chem 43(2):304–318
94. Shin S-YA, Simon LC, Soares JBP, Scholz G, McKenna TFL (2009) Gas-phase polymerization with transition metal catalysts supported on montmorillonite – a particle morphological study. Macromol Symp 285(1):64–73
95. Tudor J, Willington L, O'Hare D, Royan B (1996) Intercalation of catalytically active metal complexes in phyllosilicates and their application as propene polymerisation catalysts. Chem Commun 17:2031–2032
96. Sun T, Garcés JM (2002) High-performance polypropylene–clay nanocomposites by in-situ polymerization with metallocene/clay catalysts. Adv Mater 14(2):128–130
97. Li W, Adams A, Wang J, Blumich B, Yang Y (2010) Polyethylene/palygorskite nanocomposites: preparation by in situ polymerization and their characterization. Polymer 51(21):4686–4697
98. Alexandre M, Dubois P, Sun T, Garces JM, Jerome R (2002) Polyethylene-layered silicate nanocomposites prepared by the polymerization-filling technique: synthesis and mechanical properties. Polymer 43(8):2123–2132
99. Shin S-YA, Simon LC, Soares JBP, Scholz G (2003) Polyethylene–clay hybrid nanocomposites: in situ polymerization using bifunctional organic modifiers. Polymer 44 (18):5317–5321
100. Guo C-Y, Ke Y, Liu Y, Mi X, Zhang M, Hu Y (2009) Preparation and properties of polyethylene/montmorillonite nanocomposites formed via ethylene copolymerization. Polym Int 58(11):1319–1325
101. Bergman JS, Coates GW, Chen H, Giannelis EP, Thomas MG (1999) Synthesis and characterization of polyolefin–silicate nanocomposites: a catalyst intercalation and in situ polymerization approach. Chem Commun 21:2179–2180
102. Jin Y-H, Park H-J, Im S-S, Kwak S-Y, Kwak S (2002) Polyethylene/clay nanocomposite by in-situ exfoliation of montmorillonite during Ziegler–Natta polymerization of ethylene. Macromol Rapid Commun 23(2):135–140
103. Cui L, Tarte NH, Woo SI (2008) Effects of modified clay on the morphology and properties of PMMA/clay nanocomposites synthesized by in situ polymerization. Macromolecules 41 (12):4268–4274
104. McDaniel MP, Jensen MD, Jayaratne K, Collins KS, Benham EA, McDaniel ND, Das PK, Martin JL, Yang Q, Thorn MG, Masino AP (2008) Metallocene activation by solid acids. In: Severn JR, Chadwick JC (eds) Tailor-made polymers via immobilization of alpha-olefin polymerization catalysts. Wiley-VCH, Weinheim, pp 171–210
105. Mariott WR, Chen EYX (2003) Stereochemically controlled PMMA-exfoliated silicate nanocomposites using intergallery-anchored metallocenium cations. J Am Chem Soc 125 (51):15726–15727
106. Mariott WR, Escudé NC, Chen EYX (2007) Stereoregular P(MMA)-clay nanocomposites by metallocene catalysts: in situ synthesis and stereocomplex formation. J Polym Sci A Polym Chem 45(13):2581–2592
107. Kaminsky W, Strubel C (1998) Hydrogen transfer reactions of supported metallocene catalysts. J Mol Catal A Chem 128(1–3):191–200
108. Sun T, Garces JM (2003) Acidic lamellar aerogel nanoplate activated olefin polymerization with metallocene catalysts. Catal Commun 4(3):97–100
109. Novokshonova LA, Kovaleva NY, Ushakova TM, Meshkova IN, Krasheninnikov VG, Ladygina TA, Leipunskii IO, Zhigach AN, Kuskov ML (2005) Partially hydrolyzed alkylaluminums as the active heterogenized components of metallocene catalysts. Kinet Catal 46(6):853–860

110. Frankowski DJ, Capracotta MD, Martin JD, Khan SA, Spontak RJ (2007) Stability of organically modified montmorillonites and their polystyrene nanocomposites after prolonged thermal treatment. Chem Mater 19(11):2757–2767
111. Xie W, Gao Z, Pan W-P, Hunter D, Singh A, Vaia R (2001) Thermal degradation chemistry of alkyl quaternary ammonium montmorillonite. Chem Mater 13(9):2979–2990
112. Wei L, Tang T, Huang B (2004) Synthesis and characterization of polyethylene/clay–silica nanocomposites: a montmorillonite/silica-hybrid-supported catalyst and in situ polymerization. J Polym Sci A Polym Chem 42(4):941–949
113. Ma J, Qi Z, Hu Y (2001) Synthesis and characterization of polypropylene/clay nanocomposites. J Appl Polym Sci 82(14):3611–3617
114. Yang F, Zhang X, Zhao H, Chen B, Huang B, Feng Z (2003) Preparation and properties of polyethylene/montmorillonite nanocomposites by in situ polymerization. J Appl Polym Sci 89(13):3680–3684
115. Giannelis EP, Krishnamoorti R, Manias E (1999) Polymer–silicate nanocomposites: model systems for confined polymers and polymer brushes. Adv Polym Sci 138:107–147
116. Theng BKG (2012) Polymer-clay nanocomposites. In: Theng BKG (ed) Developments in clay science, vol 4. Elsevier, Amsterdam, pp 201–241

Adv Polym Sci (2013) 258: 341–362
DOI: 10.1007/12_2013_223

Published online: 12 June 2013

Iron Catalyst in the Preparation of Polyolefin Composites

Robert S.A. Meyer and Gerrit A. Luinstra

Abstract The polymerization of ethylene with bis(iminoaryl)pyridyl iron precursor is reviewed, with emphasis on the preparation of polyolefin composites by the in situ polymerization procedure. The catalytic properties are described. The rate of the polymerization is linearly dependent on the concentration of the active catalyst and the ethylene concentration. Bimodal distributions arise depending on the concentration of aluminum alkyls. Aluminum alkyls are chain transfer reagents and give access to polymeryl aluminum compounds that lead to polyethylene with a hydroxyl terminus after oxidation with air. The bis(iminoaryl)pyridyl iron dichloride can be supported on alumina, silica, and magnesium salts to give active catalysts after activation with aluminum alkyls, or vice versa, that are thermally robust. The iron complexes can also be used to prepare polyolefin (nano)composites from ethylene after immobilization on the filler in combination with aluminum alkyls.

Keywords Aluminum alkyl · Composite · Ethylene polymerization · Iron catalysis · Supported catalyst

Contents

R.S.A. Meyer and G.A. Luinstra (✉)
Institut für Technische und Makromolekulare Chemie, Fachbereich Chemie, Universität Hamburg, 20146 Hamburg, Germany
e-mail: luinstra@chemie.uni-hamburg.de

Abbreviations

a.u.	Arbitrary units
$BI^{R2}P$	Bis(iminoaryl)pyridyl with R as the *ortho* substituent of the iminoaryl moiety
C_p	Number of iron carrying alkyl chains
DIBAL	Di-isobutyl aluminum hydride
d-MAO	Dry MAO, MAO liberated from $AlMe_3$
DRIFT	Diffuse reflectance infrared Fourier transform spectroscopy
EBMAG	Ethyl butyl magnesium
EtOH	Ethanol
k_p	Rate constant for ethylene insertion in a iron alkyl bond
MAO	Methyl aluminoxane as the hydrolysis product of $AlMe_3$
Me	Methyl substituent
MMAO	Modified MAO, containing methyl and *t*-butyl groups
M_n	Number average molecular weight
M_w	Weight average molecular weight
PDI	Polydispersity index (M_w/M_n)
SEM	Scanning electron microscopy
TEAO	Tetraethyl aluminoxane
TEM	Transmission electron microscopy
TEOS	Tetraethoxy silane
TIBA	Triisobutyl aluminum
TMA	Trimethyl aluminum

1 Introduction

1.1 Polyolefins: Polymerization and Properties

The discovery of chromium (molybdenum) and titanium catalysts for the "low" pressure synthesis of polyethylene in the mid-1950s was a milestone in the preparation of plastics [1, 2]. Research efforts in the area have been greatly directed toward several "commercial" goals that comprise low production cost, which is related to an efficient process chain, and an appropriate property profile, which is related to a market requirement and/or an application [3]. The use of a supported catalyst that allows steering of the morphology of the product is an essential part of the production process [3, 4]. The property profile of polyolefins can be substantially extended by dispersion of fillers into the material (http://www.matweb.com/).

The performance of composites in mechanical, barrier, electrical, thermal, optical, and tribological applications etc. is dependent on reaching a good dispersion and adhesion of filler and matrix. Composites of polyolefins show the best mechanical and rheological properties when a good and lasting dispersion is reached of the filler or fillers in the matrix [5]. In many cases, the appreciable difference in polarity of polyolefin matrix and inorganic filler means that there is challenge in obtaining such a distribution. Several methods have been used for the preparation of composites. These methods include melt blending in an extruder or kneader, solution blending, and in situ polymerization or in situ particle formation [6]. The results of mixing and blending vary in quality depending on the filler, its surface treatment, and the procedures used (e.g., [7]). Although not established on a large scale, in situ polymerization has been shown to give finely dispersed fillers in polyolefins [8, 9]. In this process, the polymer is generated in the presence of the filler. Prerequisite is the compatibility of the polymerizing catalyst system and the filler. A lasting dispersion of filler in the matrix is reached in those cases where the polymer is wrapped around the filler. It may be anticipated that the latter can be reached if the polymer is formed on or in close vicinity to the surface.

An active polymerization system in the presence of a generic filler (clays/minerals, glass, carbon nanotubes, graphene) can be reached under the same requirements that lead to an active supported catalyst [8–16]. It has been reported that certain acid clays are capable of activating transition metal compounds for polyolefin formation and of forming an in situ filled polymer [10, 17]. The use of a combination of a transition metal complex and a polymerization activating agent in the form of aluminum alkyls or methyl aluminoxane (MAO) and derivatives [18, 19] is much more versatile and far less dependent on the type of filler and type of catalyst. Good results can be expected when the agent interacts and/or reacts with the surface of the filler and remains capable of initiating an olefin polymerization [20]. Many homogeneous catalysts can be activated for polyolefin formation in combination with aluminum alkyls or MAO and usually also with a support that has been coated with them [20]. This is thus a versatile route for generation of polyolefins of diverse microstructure, from high-density polyethylene (PE-HD) to linear low-density polyethylene (PE-LLD) and also to functionalized polyolefins [21].

The developments in homogeneous ethylene and propylene polymerization catalysis in the last 10–20 years have widened the scope of polyolefinic products attainable. Amongst these are: (1) complexes of early transition metals with non-metallocene ligands [22]; (2) nickel and palladium complexes, with chain walking leading to highly branched polyolefins (Pd) or chain straightening (Ni) in the case of 1-olefin polymerization [23]; (3) living olefin polymerization [24]; (4) catalytic preparation of end-functionalized polyolefins [21]; (5) (ternary) catalytic chain transfer polymerization [25] and chain shuttling [26]; and (6) facile synthesis of PE–LLDs and blends from ethylene by using a combination of a polymerization and/or an oligomerization catalyst (tandem catalysis) [27]. A spin-off of the discovery of further catalysts with easily accessible ligands is the fact that preparation has become less elaborate and time-consuming and is no longer the field of trained organometallic chemists working under Schlenk line conditions, thus allowing

faster industrial implementation. The discovery of tridentate bis(iminoaryl)pyridyl complexes of iron [28, 29] (and cobalt, and later also vanadium [30] and other metals [31]) with an extremely high activity for ethylene polymerization has been a milestone in that sense.

The primary products from iron catalysts are linear polyethylenes and aluminum polymeryls. The iron complexes can be prepared in a few simple steps and are not particularly sensitive to air, contrasting with many metallocenes of group III and IV or rare earth complexes. A body of literature on ethylene polymerization studies with these complexes allows a picture to be created of the catalytic action [31]. Here, a summary is given on the catalytic activity of these complexes, also in combination with solid supports, and an outlook towards the preparation of composites.

2 Ethylene Polymerization with Iron Catalysts

2.1 Combination of Aluminum Alkyls and Bis(iminoaryl)-pyridyl Iron Dichloride

The general consensus on the mechanistic details of transition metal-catalyzed polyethylene formation is that the active site comprises a metal with an alkyl group as active chain end and a free coordination site, with the metal incorporated in a ligand or in a salt crystal [32]. Ethylene is inserted in a *syn* fashion into the metal–carbon bond. Iron bis(iminoaryl)pyridyl dichloride ($BI^{R2}P\ FeCl_2$, where R denotes the *ortho* substituents on the aryl entity; Fig. 1) in combination with MAO or (tri)alkyl aluminum compounds (AlR_3) yields active ethylene polymerization systems [23]. Both the free coordination site and the alkyl group of the iron center thus originate from the interaction with the aluminum compounds.

Equation 1. Alkylation of iron complexes with AlR_3: proposed formation of an anionic ligand

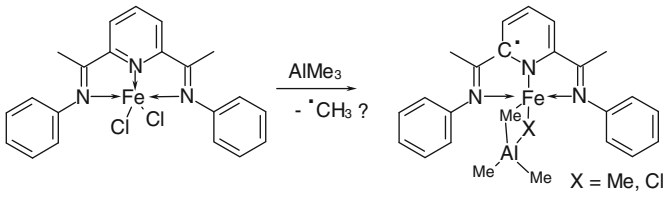

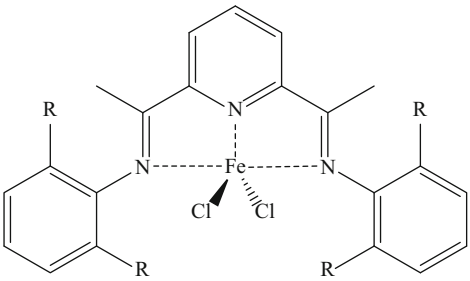

Fig. 1 Structure of bis (iminoaryl)pyridyl iron complexes $BI^{R2}P\ FeCl_2$, where R refers to the *ortho* substituents on the imino aryl part

Equation 2. Alkylation of iron complexes with MAO: proposed formation of a cationic complex

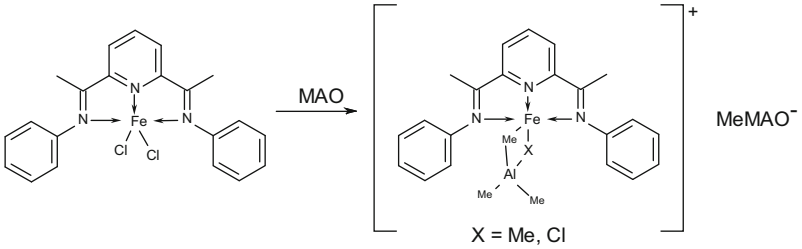

Molecular studies show that bimetallic complexes are generated with bridging alkyl and chlorides, reminiscent of proposals for Ziegler-type catalysts (1) and (2). The evidence is based mainly on NMR spectroscopy (^1H and ^2H). The paramagnetic BIP $FeCl_2$ complexes display large shifts and broad signals in the NMR spectra. The use of deuterated compounds simplifies the interpretation on account of the much smaller line width. In early studies on $BI^{Me2}P\ FeCl_2$, a terminal methyl bound to an iron(II) center was envisioned as completing the coordination sphere of dimethylated iron to arrive at a neutral complex (ligand)Fe(II)Me_2·$AlMe_3$, which would become active for polymerization after $AlMe_3$ dissociation [33]. The terminal methyl group, however, was not observable in either ^1H or ^2H NMR spectroscopy and is probably not present. In a later study on $BI^{iPr2}P\ FeCl_2$, it was shown that a formal reduction of the bis(imino)pyridyl moiety to a radical anion can take place, thus leading to a monoanionic ligand. Hence, only one negatively charged alkyl group is sufficient to balance the charges in a formal Fe(II) complex (1) [34]. It has concomitantly been argued that such neutral species are more likely to be the true catalysts. Ethylene polymerization with a catalyst system based on $BI^{iPr2}P\ FeCl_2$ and MAO with very small residual $AlMe_3$ (TMA) concentrations was almost two orders of magnitude less effective than with standard MAO containing up to 30% of free TMA [35]. This indeed seems to suggest that polymerization proceeds fast in a neutral complex. The generation of cationic alkyl species with a neutral bis(imino)pyridyl ligand in the case of MAO activation supports this idea. Model systems were prepared and found active for ethylene

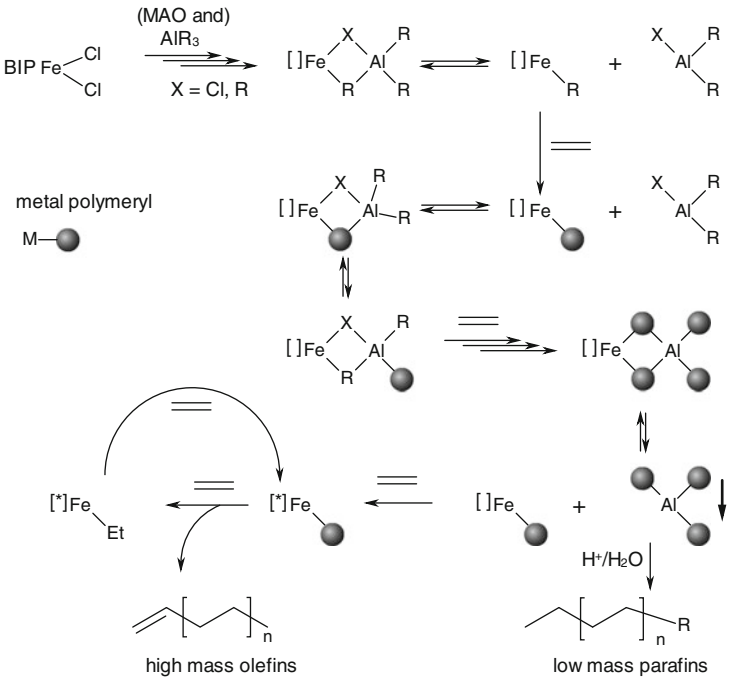

Scheme 1 Polymerization of ethylene with BIP $FeCl_2$ and aluminum alkyls; [] and [*] denote different or the same generic ligand surroundings for active iron catalysts, respectively

polymerization [36, 37]. The debate on the relevance for ethylene polymerization catalysis of either a neutral or cationic molecular system is not over and the products in (1) and (2) may eventually be precursors for the same catalytic species because they are closely related. The reactions shown in Scheme 1 may pertain to the catalytic properties of the BIP iron catalysts. The generic notation []Fe (and [*] Fe) is used to describe a cationic or neutral species with an intact or reduced BIP ligand.

The time-dependent UV spectra of mixtures of $BI^{iPr2}P$ $FeCl_2$ and MAO at several concentrations show that the interaction of the components leads to several species, which all are thermally labile. Some transformations are fast (minutes) and some proceed over hours at room temperature [38]. An interpretation is not offered. In the analogous vanadium(III) chloride complex, methylation of the *ortho* pyridyl carbon is found, leading to an mono-anionic ligand [30]. This reaction or comparable processes may also take place in the case of BIP FeCl complexes and may lead to further catalytic active species with different catalytic actions [39]. The identity of the active catalyst remains to be elucidated, as well as its oxidation state [34, 40–42]. In a recent review, the dissociation of the aluminum trialkyls from the complexes in (1) has been offered as a reaction leading to the actual catalyst (see Scheme 1) [43].

2.2 *Polyethylenes from Iron Catalysts*

The polyethylene products from (many) bis(imino)pyridyl iron dichloride/aluminum alkyl catalyst systems are bimodal and broadly distributed [35, 44]. This results from at least two different chain termination (transfer) reactions (Scheme 1). Next to the common β-hydrogen elimination of basically all polymerization catalysts, alkyl exchange between aluminum and iron terminates chain growth by a formal chain transfer reaction [27, 28]. The ease of such a reaction is easily envisioned in the bimetallic complexes of (1) and (2). The polyethylene obtained by bis(imino)pyridine iron catalysts after hydrolysis is thus a mixture of paraffins and vinylic compounds. The ratio is dependent on the ratio of aluminum alkyls to ethylene pressure. The higher the concentration of aluminum (or zinc [45]) alkyls, the shorter is the chain length of the polyethylene and the lower the percentage of olefinic chain ends. This is in a first approximation resulting from competition between the chain transfer process and propagation and β-hydrogen elimination. A reversible chain transfer is responsible for the Poisson distribution of the paraffins [45]. In the case of aluminum alkyls as activation agents, the distribution has an appreciably higher polydispersity index (PDI), probably because polymeryl trialkyl alumina is less effective in reaching the necessary coordination to iron for transmetallation and thus the transfer is not (completely) reversible. In addition, a molecular weight over the solubility limit brings a diffusion barrier to the reaction between the iron and the aluminum polymeryl. The solubility limit in toluene, a frequently used solvent, lies in the range of 500–1,000 Da. It has been argued on the basis of a resolution of GPC traces into Flory components [44] that several catalytic species need to be present to account for this behavior [46]. Such an analysis has typically been carried out for traditional $MgCl_2$-supported Ziegler catalysts, showing that several types of catalytic center are operative. The analysis in the case of the BIP $FeCl_2$ precatalysts arrives at the conclusion that two groups of catalytic reactions occur, one leading to low molecular weight products and one to high molecular weight products. Each of the groups is subdivided into several fractions, with a PDI of 2. The subfractions are thought to be generated from several types of closely related catalytic species. The two groups of products are accounted for by assuming that initially formed species decompose to further catalytically active species that generate the high molecular mass fraction. This indeed would account for the observed time dependence of the products formed during the course of the polymerization experiment. Higher molecular weights are predominantly formed at longer reaction times. This does not, however, contradict the explanation by Gibson that the formation of high molecular weight products results from the depleting concentration of chain transfer agents with reaction time [47]. Further work will be necessary to complete the mechanistic picture and to explain the kinetic behavior, and probably needs to encompass the precipitation of products with or without active catalyst and, for example, the matter of dormant species [48] (see chapter 2.3).

The concentration of the alkylating species certainly has a marked influence on the product constitution [47]. A typical distribution is shown in Fig. 2. The high

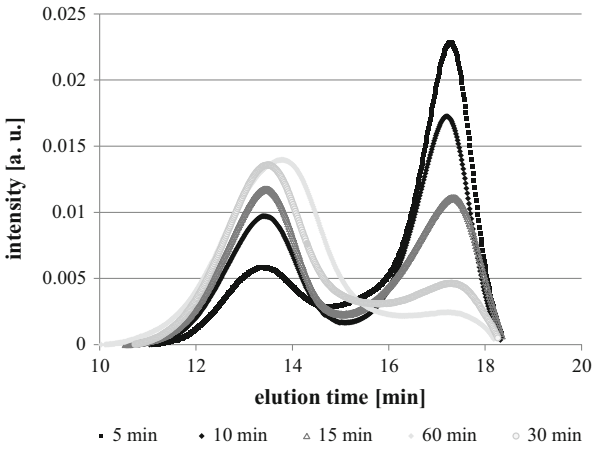

Fig. 2 Typical elugramm of iron-catalyzed ethylene polymerization as function of the reaction time

molecular weight products carry more olefinic endgroups than the low molecular weight fraction. We have found that very large excess of MAO or TEA (Al/Fe from 5,000 to 150,000) leads to basically paraffinic compounds with a PDI of 2 [49].

The production of bimodally distributed PE has been considered an advantage. Such products simultaneously have the excellent mechanical properties of high molecular weight PEs and the good flow properties of low molecular weight PEs. In industrial production of PE, such mixtures are produced using procedures such as physical blending, two stage polyreactions in cascade reactors, or ethylene polymerization with mixtures of catalysts. These methods are more elaborate and have higher costs than those using a single catalyst in a simple process. The options for PE formation using a single iron catalyst is nicely illustrated by recent finding using a catalyst with an asymmetric substituted bis(imino)pyridyl ligand, i.e., based on 2,4-dibenzhydryl-6-methylbenzamine and dialkyl anilines [50] or comparable complexes [51, 52]. BIP iron(III) complexes were also active and in addition produce branched 1-olefins; the reactivity was strongly dependent on the substitution pattern on the ligand [53]. The ligand substituents on the anilinic *ortho* positions are of importance for the ratio of the rates of β-hydrogen elimination and chain transfer to aluminum [54–59]. The rate of transfer to aluminum alkyls is also dependent on the type and concentration of aluminum compound as well as on the reaction time [35, 47, 60]. The concentration of chain transfer agent is probably also related to the conversion of the aluminum alkyl to aluminum polymeryl, the reversibility of the transmetallation reaction, and the solubility of aluminum polymeryls [47].

2.3 Kinetics of Polyolefin Formation

The polymerization reaction with homogeneous iron complexes usually has an induction phase with increasing activity, followed by a decay (Fig. 3) [47, 61, 62].

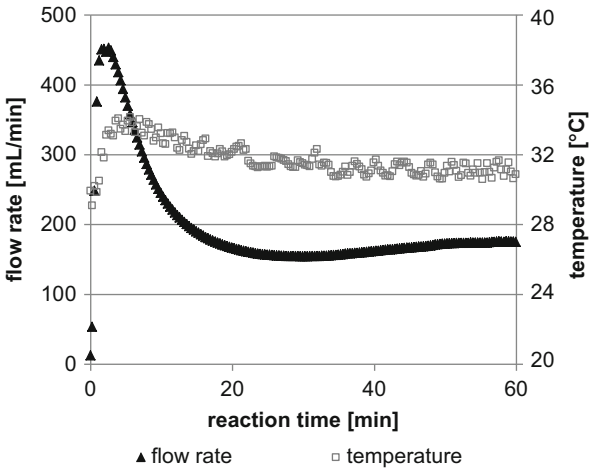

Fig. 3 Typical progress of a semibatch ethylene polymerization with BIP $FeCl_2$/TEA catalyst mixture

The rate of ethylene polymerization with the $BI^{iPr2}P$ $FeCl_2$/(M)MAO was originally reported to increase linearly with the ethylene concentration [29, 47]. This was found in other catalysts too and is consistent with the mechanism of a rate-determining ethylene insertion into the iron–carbon bond. For example, the average rate of polymerization over 30 min was found to be linearly dependent on the ethylene concentration in the case with the $BI^{Me2}P$ $FeCl_2$/MAO system as catalyst (Al/Fe = 400–1,400) [62]. The products had molecular weights in the range of waxes (Table 1), with PDI substantially below 2, showing that a typical single-site catalysis was operative. The rate in this system as well as with $BI^{iPr2}P$ $FeCl_2$ also increases linearly with the MAO concentration, probably on account of the linear increase in the number of active centers. The rate decreases with temperature.

We have used $BI^{Cl2}P$ $FeCl_2$/MAO [55] as catalyst system to address the reaction order in the catalyst and MAO at high concentration [49, 63]. Ethylene batch polymerizations with a ratio Al/Fe of 10,000 were evaluated on the basis of the time-dependent pressure drop to show that the reaction order in the catalyst is close to 1 (0.9 ± 0.2). The reaction order in MAO was close to zero (-0.2 ± 0.1) at a ratio of Al/Fe over 10,000. A decrease in overall activity with higher MAO concentrations has also been reported [50]. The overall rate of the BIP $FeCl_2$ (MAO)-catalyzed ethylene polymerization is thus likely to follow (3a) at "low" MAO concentrations. The dependence is explained by the increase in the number of active sites with increasing MAO concentration and a rate-determining ethylene insertion into an iron–carbon bond. At high concentration of cocatalyst, where the maximum concentration of active catalyst is reached, an inhibition may result because of coordination of aluminum alkyls to the active site (Scheme 1). The rate laws in (3) are thus indicative of a single catalyst species performing the ethylene polymerization [39].

Table 1 Selected data on BIP $FeCl_2$ catalytic action, dependence on iron, ethylene and aluminum concentration

Parameter/Ref.	Catalyst	Amount (μmol)	T (°C)	$p_{ethylene}$ (bar)	Ratio Al/Fe	Rate/activity/ productivity (min^{-1})
Fe						
[50]	**1**/MAO	0.07	25	2	10,000	0.02
[50]	**1**/MAO	0.34	25	2	10,000	0.1

Parameter/Ref.	Catalyst	Amount (μmol)	T (°C)	$p_{ethylene}$ (bar)	Ratio Al/Fe	Rate/activity/ productivity [kg/(mol_{Fe} bar h)]
Ethylene						
[48]	**2**/MAO/TIBA	0.57	50	2	100	5,260
[48]	**2**/MAO/TIBA	0.57	50	4	100	4,780
[48]	**2**/MAO/TIBA	0.57	50	6	100	4,980

Parameter/Ref.	Catalyst	Amount (μmol)	T (°C)	$p_{ethylene}$ (bar)	Ratio Al/Fe	Rate/activity/ productivity [kmol/(mol_{Fe}h)]
Ethylene						
[30]	**2**/MMAO	0.6	60	14		4,800
[30]	**2**/MMAO	0.5	60	28		7,000
[30]	**2**/MMAO	0.5	60	41		11,800

Parameter/Ref.	Catalyst	Amount (μmol)	T (°C)	$p_{ethylene}$ (bar)	Ratio Al/Fe	Rate/activity/ productivity [kg/(mol_{Fe}h)]
Al						
[51]	**3**/MMAO	1.5	20	10	1,000	2,450
[51]	**3**/MMAO	1.5	20	10	2,000	5,340
[51]	**3**/MMAO	1.5	20	10	3,000	8,400
[51]	**3**/MMAO	1.5	20	10	4,000	4,840

1: $BI^{Cl_2}P$ $FeCl_2$, **2**: $BI^{iPr_2}P$ $FeCl_2$, *MMAO* modified MAO, **3**: $BI^{Et_2(p\text{-}Me)}P$ $FeCl_2$+DBM: 2,4-dibenzhydryl-6-methyl phenyl is one of the aryl entities

Equation 3. Rate laws for polyolefin formation with BIP $FeCl_2$/MAO

At low [MAO]:

$$d[C_2H_4]/dt = k[C_2H_4]^1[MAO]^1[BIP\,FeCl_2]^1 \tag{3a}$$

At high(er) [MAO]:

$$d[C_2H_4]/dt = k[C_2H_4]^1[MAO]^{0-x}[BIP\,FeCl_2]^1 \quad (x > 0) \tag{3b}$$

The rate constants k_p of ethylene polymerization with MAO- and AlR_3-activated iron complexes have been evaluated by quenching with ^{14}CO [61]. Carbon monoxide has been shown to react with iron alkyls and form carbonyl-terminated polymer chains. The radioactivity in the polymer product was used to calculated the number

of actual growing chains during quenching. The quenching reaction is fast and is expected to compete effectively with deactivation processes during the polymerization of ethylene. Homogeneous $BI^{Me2}P$ $FeCl_2$ activated with triisobutyl aluminum (TIBA), a catalyst system with a fast activation and decay of the catalytic activity (minutes at 35°C), was evaluated in this way. The rate constant was evaluated by assuming a rate law $v = k_p[C_2H_4][Fe^*]$, where [Fe*] is the concentration of active sites. It was found that near the maximum rate (reached after about 2 min), 41% of the iron centers are catalytically active. This number decreases to 16% after 8 min. The rate constant for propagation near the maximum was 26,000 L mol^{-1} s^{-1}. $BI^{Me2}P$ $FeCl_2$ activated with MAO has k_p values in the same range [46]. The number of iron centers carrying an alkyl group is in this case less than 10% in the first 1.5 min and then decreases to 4% after 9 min. In contrast, it was found for $BI^{Me2}P$ $FeCl_2$ supported on Al_2O_3 and activated with TIBA that only about 1% of the iron centers carry an alkyl chain [61]. The rate constant k_p was determined to be 7,000 L mol^{-1} s^{-1}. This number increases to 18,000 L mol^{-1} s^{-1} when 5 vol% of dihydrogen is in the feed. The increase is interpreted as a reactivation of dormant species after 2,1-insertion of an in situ formed 1-olefin. A similar rate constant of 12,000–45,000 L mol^{-1} s^{-1} was measured in supported iron catalysts [64] (see chapter 2.4).

2.4 Ethylene Polymerization with Supported BIP $FeCl_2$

The catalytic properties of bis(imino)pyridyl iron catalysts (i.e., in the sense of activity, productivity, and thermal stability) can be enhanced by immobilizing the complex on inorganic materials. Thermal stability is of high relevance because many systems lose their initial activity within a few minutes at temperatures over 50°C [65, 66]. Support is also essential for preventing reactor fouling [16]. The BIP $FeCl_2$ catalysts are particularly easily heterogenized. Alumina, silica, and magnesium dichloride have been considered as standard supporting materials, and aluminum alkyls can be used to activate the catalyst and to influence the molecular weight and molecular weight distribution.

Supporting $BI^{Me2}P$ $FeCl_2$ on silica or alumina yields active polymerization catalysts after activation with TIBA or MAO. DRIFT analysis of the surfaces of the supported catalyst gives an indication that the iron complexes directly interact with hydroxide entities at the surface; interaction with the basic alumina is particularly prominent [67]. The productivity of the system after the addition of TIBA is in the range of 200–760 kg_{PE} g_{Fe}^{-1} in the supported catalyst at 5 bar of ethylene pressure. The activity of 41 kg_{PE} g_{Fe}^{-1} bar^{-1} h^{-1} is reached more slowly, as in the homogenous case, but remains constant over 60 min (Fig. 4). The addition of hydrogen at a pressure of 0.5 bar increases the activity and productivity by a factor of about 2. The stability of the catalytic system towards deactivation is favorably improved. Thus, higher polymerization temperatures of 80°C, with almost constant activity over at least 1 h are now feasible.

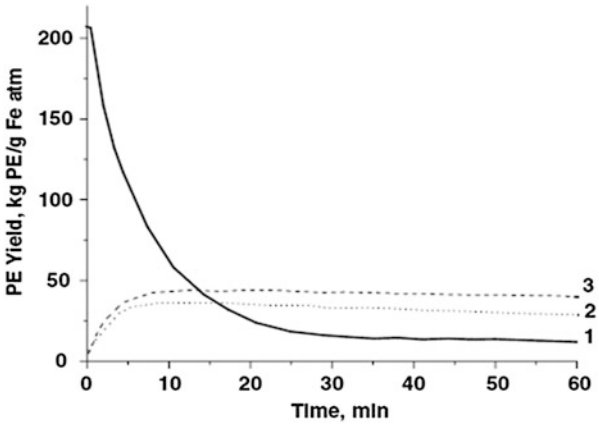

Fig. 4 Polymerization rate with time of $BI^{Me2}P$ $FeCl_2$/TIBA in heptane: *1* homogeneous at 35°C; *2* supported on SiO_2 at 80°C; and *3* supported on Al_2O_3 at 80°C [59]

A further study reports on silica as a support for $BI^{iPr2}P$ iron catalysts in more detail [68]. Consistently, no interactions could be found between the BIP $FeCl_2$ and the silica support, which was conditioned at several temperatures. The polymerization of ethylene at the support was effectuated by the addition of MAO (Al/Fe = 500–1,500/1). The rates of polymerization showed the usual dependence on reaction time, and the products were typically bimodal. In contrast to the Al_2O_3 support, no substantial increase in stabilization of the activity was observed. The catalysis is reminiscent of homogeneous catalysis and seems to proceed with little interaction with the surface of the support. The activities lie in the order of 4 ton mol_{Fe}^{-1} h^{-1} in the early stage (10 min) and 1 ton mol_{Fe}^{-1} h^{-1} average over 30 min at 1 bar ethylene pressure. The molecular weights are higher than in case of homogeneous polymerization, which is explained by a deactivation of part of the cocatalyst at the surface, leading to less chain transfer. Silica is a support that thus has little direct interaction with the BIP iron catalysts.

MAO and other aluminum alkyl derivatives react fast with the hydroxyl groups of the silica surface and cover it with an activating layer. Treating the silica with MAO prior to catalyst addition yields a much more suitable supporting material. Reaction of $BI^{iPr2}P$ $FeCl_2$ with silica-treated MAO gives evidence for the formation of an iron species with less electron density than the starting material [69]. This holds also for the chloride ions and is interpreted as removal of a chloride ion from the complex, consistent with (2). The solid support was used as catalyst in combination with several concentrations of added MAO. The activities obtained were 300–600 kg mol_{Fe}^{-1} h^{-1} at a ratio of Al/Fe between 250 and 500, lower than for the homogeneous system, but the molecular weights were higher (because of a lower MAO concentration). The morphology of the catalyst was advantageously mirrored in the product.

The pretreatment of SiO_2 with tetraethyl aluminoxane (TEAO) and exposure to $BI^{Me2}P$ or $BI^{iPr2}P$ $FeCl_2$ solution in dichloromethane gives an active supported catalyst with 0.6 wt% iron [70]. Polymerization of ethylene was effected at 1 bar and 30–50°C in toluene slurry containing various amounts of further TEAO

cocatalyst. The activity was on the order of one magnitude lower than for homogeneous polymerization under the same conditions (86–460 kg mol_{Fe}^{-1} h^{-1} bar^{-1}). The resulting products are bimodally distributed and show the usual dependence on the aluminum concentration. At lower ratios of Al/Fe (to about 500), low molecular weight products are thus progressively formed at higher ratios. Above a ratio of Al/Fe of 1,000, the molecular weight of the high molecular weight fraction increases as well as their relative weight. Chain transfer to aluminum thus becomes less important, probably also as result of diffusion limitations for the aluminum polymeryls formed in the process. The outcome of the reaction is thus very sensitive to the course of the polymerization. A much more elaborate approach in an earlier study, with tailoring of ligands that contain reactive entities towards silica surface Si–OH bonds, gave high activities (up to 40 ton mol_{Fe}^{-1} h^{-1} bar^{-1} in the first 5 min) and bimodal distributions [71].

Zeolite SBA-15 [72], a silicate with large channels (up to 30 nm), was also used as a support for $BI^{iPr2}P$ iron complexes [73]. The complexes were covalently anchored to the surface by the action of butyl lithium. It is inferred that an iron–oxygen bond is formed in the process as the molar ratio of Cl/Fe decreases from 2 to 0.29. The iron-loaded zeolite could be activated for ethylene polymerization by the addition of MAO in toluene solution. The activity of the system is at a high level of about 15% of the homogeneous complex (range of 200 kg mol_{Fe}^{-1} h^{-1} at 28°C). The molecular weight decreases with the amount of MAO (Al/Fe = 1,000–6,500), but the activity increases. The catalyst does not deactivate after the first minutes as was observed on other supports, and the system becomes thermally much more robust to allow excellent activities and productivities at 75°C (390 kg_{PE} mol_{Fe}^{-1} h^{-1} at a Al/Fe ratio of 2,500). The polyethylene is formed in bundles (Fig. 5), and is considered to be produced by extrusion polymerization [74].

Magnesium dichloride has become a preferred support for Ziegler-type catalysts for ethylene polymerization [75]. Several synthetic routes lead to useful magnesium chlorides in the sense of supporting a Ziegler catalyst. Titanium chlorides for example can be incorporated into the crystal surface of $MgCl_2$. Subsequent treatment with aluminum alkyls lead to highly productive ethylene polymerization catalysts. BIP $FeCl_2$ was also screened as catalyst precursor in magnesium-supported systems. $BI^{iPr2}P$ $FeCl_2$ was thus supported onto a $MgCl_2$ surface that was generated in situ from butyl ethyl magnesium (BEM) in combination with ethyl aluminum sesquichloride. Aluminum trialkyls (TEA, TIBA, DIBAL) were added to reach an ethylene polymerization system [76]. The activity of the system reaches the level of about 300 kg_{PE} g_{Fe}^{-1} h^{-1}. The catalyst system is more stable than the homogeneous MAO-activated iron complex. It shows only a minor decay in activity at that level after 60 min at temperatures as high as 60°C (at still higher temperature it does rapidly deactivate). Concomitantly, the molecular weight decreases from M_n = 230–30 kg mol^{-1} for polymerization temperatures of 40–80°C as a result of both increased rate of transfer to aluminum and increased β-hydrogen elimination.

Typical support precursors like the ethanol adduct of magnesium dichloride $MgCl_2 \cdot xEtOH$ also yield good substrates for iron catalysts, i.e., after pretreating by heating under vacuum and yielding alpha $MgCl_2$ types [77]. The activity of a

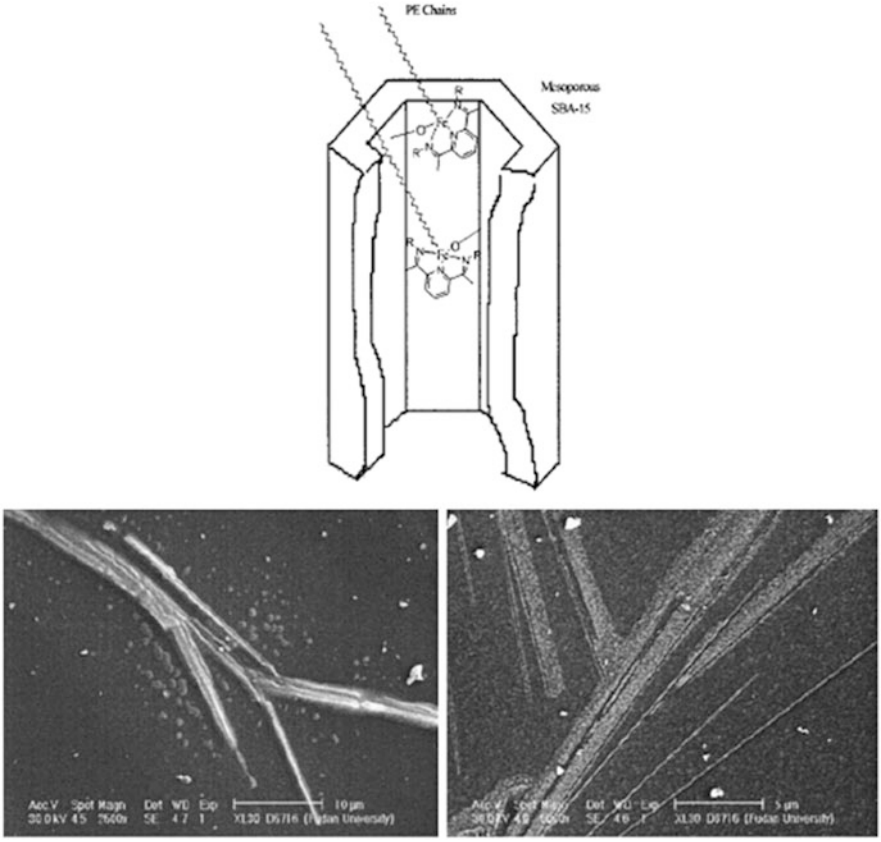

Fig. 5 Polymerization in zeolite SBA-15 channels. SEM images show formation of PE in bundles [73]

supported catalyst prepared by first contacting the thus-prepared $MgCl_2$ with a solution of $BI^{iPr2}P$ $FeCl_2$ and then with 500 equivalents of TEA is high (0.6–2 ton g_{Fe}^{-1} h^{-1}). The bulk density (to a high maximum of 390 g L^{-1}) of the polyethylene increases with the extent of dealcoholization of the $MgCl_2$ support. Moreover, the temperature stability of the catalyst increased substantially by supporting, and high activities (2.5 ton_{PE} g_{Fe}^{-1} bar^{-1} h^{-1}) were observed for more than 30 min (or even over hours at 70°C and 10 bar of ethylene pressure). The polymerization rate has an increasing and decreasing phase if dealcoholization is incomplete. The molecular weights (M_w) are up to the range of UHMWPE, i.e., 500 kg mol^{-1} (PDI 10.20). The melting temperature of 136–137°C is consistent with linear PE.

Dispersed activated $MgCl_2$ from Mg and butyl chloride is also useful as a substrate for iron catalysts [48]. The $BI^{Me2}P$ $FeCl_2$ may be directly immobilized onto this $MgCl_2$. Addition of TIBA at a relatively low ratio of Al/Fe = 500/1 in

heptane gives a catalyst that has high (70–200 kg g_{Fe}^{-1} h^{-1} bar^{-1}) and longstanding (>60 min) activity at temperatures higher than 60°C. The polyethylene is linear and is monomodal, although broadly distributed. Hydrogen is tolerated by the catalyst and increases the activity, as observed before, yet without a molecular weight regulation. 1-Olefins deactivate the catalyst system, possibly by allylic abstraction reactions and regeneration of the active center. In the latter case, the vinyl content per chain increases accordingly. The molecular weight of the product decreases with temperature from 415 to 16 kg mol^{-1} from 70°C to 90°C, respectively. The termination reactions at this low concentration of cocatalyst are basically only β-hydrogen eliminations. This may also explain the monomodal distribution.

The BIP iron catalyst on a support can be used to prepare in situ 1-olefins from ethylene. These can used to prepare PE–LLDs from ethylene through the action of a further catalyst. Fused silicas and MCM-41 were used as supports for the preparation of a catalyst capable of generating PE–LLD from ethylene. The catalyst was prepared by pretreating the silica particles with TMA and subsequently with gaseous H_2O to obtain a Lewis acidic and alkylating layer [78]. Titanocene and/or zirconenes in combination with a BIP catalyst were added either simultaneously or subsequently to the treated support. PE with several microstructures and distributions could be obtained in this way. Ethylene oligomerization with the supported iron catalyst is very effective (>50 ton mol_{Fe}^{-1} h^{-1}) and yields a products with M_n of 1,430 and PDI of about 10.

2.5 *Nanocomposites by BIP $FeCl_2$ Catalysis*

The generation of in situ composites – polymerizing ethylene in the presence of or on the surface of a filler – is a potentially efficient route for production of high performance polyolefin composites [79]. Of course, firstly, fragmentation of the filler particle needs to be kept within certain limits and, secondly, to avoid reactor fouling caused by melting of the polymer-filler ensemble, the activity of the resulting supported catalyst should be correspondingly lower (e.g., [7]). The BIP iron catalysts have been successfully used for the preparation of such composites. Phyllosilicates like glimmer (mica), montmorillonite, and/or saponite were used in some studies with the objective of achieving exfoliation and by that a molecular dispersion of silicate layers. In the case of mica, the catalyst was formed inside the silicate [80]. In a first step, iron(III) ions were loaded between the fluorotetrasilyllic layers and subsequently treated with $BI^{Me2(p\text{-}Me)}P$, $BI^{Me2}P$, or $BI^{iPr2}P$ ligands to locally prepare the BIP Fe complex. The resulting intercalated iron complex with $BI^{Me2(p\text{-}Me)}P$ was in this series particular active for the polymerization of ethylene after activation with MAO, TEA, or TIBA (500–890 g_{PE} g_{Fe}^{-1}). The molecular weights were in the range of 20–30 kg mol^{-1}. The morphology of the mica particles were replicated in the polymeric product. In another approach to the preparation of polyethylene composites from layered clays (mica, montmorillonite, saponite),

these were treated with dichloromethane solutions of BIP Fe Cl_2 [81]. Activation with TIBA was successful in achieving ethylene polymerization activities in the range of ton mol_{Fe}^{-1} h^{-1} bar^{-1} (Al/Fe = 500–1,500/1). It was found of importance to widen the layer distances in the supports by first exchanging the counterions with Mg^{2+}. The catalysts were active at 60°C and produced high molecular weight linear products (M_n = 20–46 kg mol^{-1}, M_w = 120–940 kg mol^{-1}) with large PDIs. A variation of the approach uses an acetyliminopyridine iron(III) complex successfully [82], but the material properties are not reported.

An earlier report describes the use of montmorillonite charged with organic ammonium ions as a starting material for the preparation of composites [83]. MAO was absorbed into the clay and the resulting solid treated with a suspension of $BI^{iPr2}P$ $FeCl_2$. The activity of the catalyst system was found in the usual range of a homogeneous iron catalyst (0.5–1 ton mol_{Fe}^{-1} h^{-1}) and was not dependent on the Al/Fe ratio between 250 and 1,760. The products showed the typical bimodal distribution, with the highest peak in the range of 50–150 kg mol^{-1}. The higher the concentration of clay, the lower the molecular weight. This was attributed to chain transfer reaction to aluminum, and is in agreement with the processes shown in Scheme 1. It was found that the crystal size of the linear PE was lower than that in pristine PE. Likewise, the crystallinity was lower. This is explained by a (partial) exfoliation of the silicate layers. A higher amount of clay resulted in a smaller amount of single layers and a higher Al/Fe ratio, with a higher percentage of exfoliation. These observations are probably related to the number of ethylene molecules that are polymerized between the layers. A higher aluminum concentration leads to more active centers. Rheologic studies show that a higher exfoliation leads to materials with higher storage moduli G′ and G″. The better the clay was dispersed, the higher the moduli. Exfoliation was not found when the catalyst was not previously absorbed onto the MAO-modified clay. These are typical results for in situ polymerization on a solid surface, with a large enhancement of the material properties.

We decided to use the catalytic properties of the $BI^{Cl2}P$ $FeCl_2$ complex to prepare aluminum polymeryls and turn these into polymeryl alkoxides for use as stabilizers for dispersing silica particles in polyethylene [49]. The objective was to reach a stable and fine dispersion of filler at high concentration in polyethylene and was addressed along different routes. Silica particles were chosen as generic filler material because they are easily generated by the "Stöber" process [84]. The routes are differentiated by the order of reactions. The first route comprises the steps of generating an alkoxy-functionalized polyethylene, with subsequent in situ generation of silica particles. The second synthesis uses the procedure of in situ polymerization.

The first route is based on generating sol–gel particles in an hydrophobic medium. Since the Stöber process is based on water or alcohol solvents and uses agents (ammonium hydroxide) that are not miscible with the polymerization medium of toluene, adaption was necessary. Higher alcohol (butanol, pentanol, octanol), toluene and toluene–ethanol mixtures were screened and, in addition to TEOS, TBOS (tetrabutoxy silane) was used as precursor [85]. It was found that the formation of defined and spherical particles is not easily achieved. For example, in a

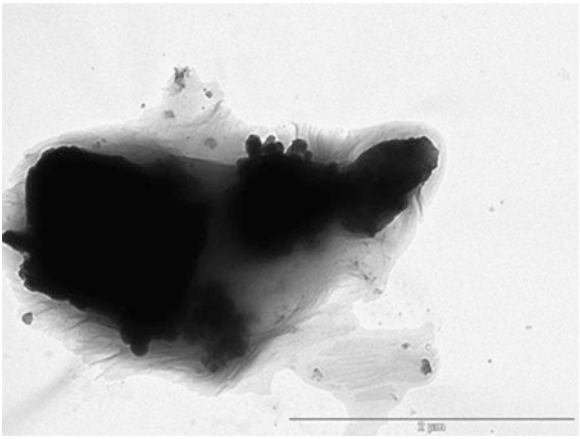

Fig. 6 TEM of polyethylene alkoxide composite with in situ formed silica particles

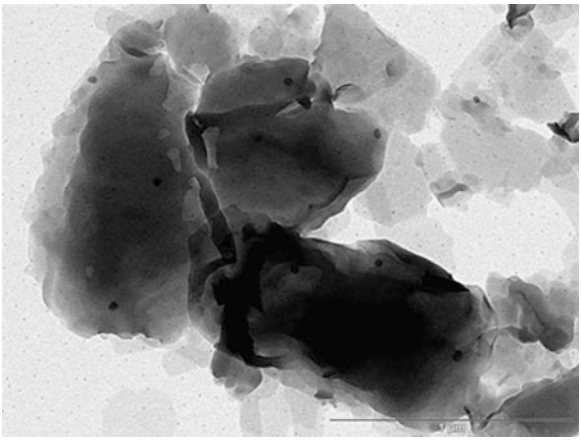

Fig. 7 Polyethylene silica composite from in situ polymerization on MAO-coated silica nanoparticles

toluene–ethanol mixture (11:1 by volume) the silica particles were in the range of micrometers and obviously the result of agglomeration of smaller initially formed solids (Fig. 6). A intimate contact between silica and polyethylene alkoxide is, however, easily recognized.

In the second approach, silica particles were generated in water by the sol–gel process and, subsequently, the surface was coated with MAO. The particles had a diameter of 86 nm, as measured by DLS (45 nm in TEM). Treatment of the particles with MAO in dry toluene yielded a corresponding MAO-coated filler. Addition of ethylene and $BI^{Cl2}P$ $FeCl_2$ yielded a composite of polyethylene (Fig. 7) with high activity. The dispersion of the particles in the matrix is good, no agglomerates are visible and distribution is homogeneous. It is inferred that the polyethylene is formed on the surface of the particles. As a consequence, the particles are intimately surrounded by polymer. The crystallization of the polyethylene was not influenced by the particles.

3 Summary, Conclusions, Outlook

The catalytic properties of BIP $FeCl_2$ and the options for preparation of various polyolefins, from low molecular weight aluminum polymeryls to low molecular weight 1-olefins for copolymerization to UHMWPE and mixtures, are presented. The catalysts are easily prepared and can be handled in air. The activities in combination with MAO, and more conveniently with aluminum alkyls, are of the highest level known for polyolefin formation. These catalyst are suitable for support on various inorganic carriers in a simple procedure to become thermally more robust catalysts, leading to the option of polymerizing ethylene at commercially relevant temperatures. The supported catalysts have about the same catalytic properties as the homogenous complexes and can lead to bimodally distributed products. Control over the molecular weight distribution can be reached by tuning the ligand and, more simply, the concentration of the cocatalysts. Hydrogen does not influence the molecular weight, but may improve the activity to some extent. The kinetics appear to be simple: the rate of ethylene consumption is linearly dependent on the concentration of active catalyst and on the ethylene pressure (concentration).

Polyolefin composites are likewise easily prepared by in situ polymerizations with the iron catalyst, i.e., after immobilization of BIP $FeCl_2$ complexes on the surface and activation with aluminum alkyls (including) MAO or by aluminum alkyl-coated filler and addition of the BIP $FeCl_2$ complex. The catalyst system of BIP $FeCl_2$/aluminum alkyl gives access to polymeryl aluminum compounds. The latter can be oxidized with air to yield polyethylene alkoxides or alcohols. Such compounds may prove interesting compounds for increasing the surface tension of polyethylene and are thus of importance, particularly for stabilizing the dispersion of inorganic nanoparticular fillers.

References

1. Hogan JP, Banks RL (1954) Polymers and production thereof. US Patent 2,825,721
2. Ziegler K, Breil H, Holzkamp E, Martin H (1953) Polymerization of ethylene. DE Patent 973,626 and (1954) US Patent 3,257,332
3. McDaniel MP (2009) Review of Phillips chromium catalyst for ethylene polymerisation. In: Hoff R, Mathers RT (eds) Handbook of transition metal catalysts. Wiley, Hoboken
4. Wu L, Wanke SE (2009) $MgCl_2$-Supported $TiCl_4$ catalysts for production of morphology-controlled polyethylene. In: Hoff R, Mathers RT (eds) Handbook of transition metal catalysts. Wiley, Hoboken
5. Yan XW, Wang J-D, Yang Y-R (2005) Polyethylene/clay nanocomposite: review of the synthetic routes and material properties. Cailiao Kexue Yu Gongcheng Xuebao 23(1):133–136
6. Ray SS, Okamoto M (2003) Polymer/layered silicate nanocomposites: a review from preparation to processing. Prog Polym Sci 28:1539–1641
7. Jones RF (1968) Filled and reinforced polyolefins. J Petrol Sci Eng 24(8):71–74
8. Nwabunma D, Tyu W (2008) Polyolefin composites. Wiley, Hoboken
9. Guo N, DiBenedetto SA, Tewari P, Lanagan MT, Ratner MA, Marks TJ (2010) Nanoparticle, size, shape and interfacial effects on leakage current density, permittivity, and breakdown strength of metal oxide-polyolefin nanocomposites: experiments and theory. Chem Mater 22:1567–1578
10. Alexandre M, Dubois P, Jerome R, Gareia-Marti M, Sun T, Garces JM, Millar DM, Kuperman A (1999) Polyolefin nanocomposites. Patent WO 99/47598

11. Weiss K, Wirth-Pfeifer C, Hofmann M, Botzenhardt S, Lang H, Bruning K, Meichel E (2002) Polymerisation of ethylene or propylene with heterogeneous metallocene catalyst on clay minerals. J Mol Catal A Chem 182(183):143–149
12. Tudor J, Willington L, O'Hare D, Royan B (1996) Intercalation of catalytically active metal complexes in phyllosilicates and their application as propene polymerisation catalysts. Chem Commun 1996:2031–2032
13. Sun T, Garces JM (2002) High-performance polypropylene-clay nanocomposites by in-situ polymerization with metallocene/clay catalysts. Adv Mater 14:128–130
14. Bergman JS, Chen H, Giannelis EP, Thomas MG, Coates GW (1999) Synthesis and characterization of polyolefin-silicate nanocomposites: a catalyst intercalation and in-situ polymerization approach. Chem Commun 1999:2179–2180
15. Dubois P, Alexandra M, Jerome R (2003) Polymerization-filled composites and nanocomposites by coordination catalysis. Macromol Symp 194:13–26
16. Hlatky GG (2000) Heterogeneous single-site catalysts for olefin polymerization. Chem Rev 1000:1347–1376
17. Scott S, Peoples B, Rojas R, Tanna A, Shimizu F (2007) Method for forming exfoliated clay-polyolefin nanocomposites. Patent WO 2007/146263
18. Malpass DB (2009) Commercially available metal alkyls and their use in polyolefin catalysts. In: Hoff R, Mathers RT (eds) Handbook of transition metal catalysts. Wiley, Hoboken
19. Ishihama Y, Isobe E, Maruyama Y, Sagae T, Suga Y, Uehara Y (1995) Catalyst for polymerizing an olefin and method for polymerizing the olefin. EP Patent 0683180
20. Guo N, DiBenedetto SA, Kwon D-K, Wang L, Russell MT, Lanagan MT, Facchetti A, Marks TJ (2007) Supported metallocene catalysis for in-situ synthesis of high energy density metal oxide nanocomposites. J Am Chem Soc 129(4):766–767
21. Amin SB, Marks TJ (2008) Versatile pathways for in-situ polyolefin functionalization with heteroatoms: catalytic chain transfer. Angew Chem Int Ed Engl 47(11):2006–2025. doi:10.1002/anie.200703310
22. Gibson VC, Spitzmesser SK (2003) Advances in non-metallocene olefin polymerization catalysis. Chem Rev 103(1):283–315
23. Ittel SD, Johnson LK, Brookhart M (2000) Late transition metal catalysts for ethylene homo and copolymerization. Chem Rev 100:1169–1203
24. Edson JB, Dornski GJ, Rose JM, Bolig AD, Brookhart M, Coates GW (2009) Living transition metal-catalyzed alkenen polymerization: polyolefin synthesis and new polymer architectures. In: Müller AHE, Matyjaszewski K (eds) Controlled and living polymerizations. Wiley, Weinheim
25. Kempe R (2007) How to polymerize ethylene in a highly controlled fashion. Chem Eur J 13:2764–2773
26. Arriola DJ, Carnahan EM, Hustad PD, Kuhlman R, Wenzel TT (2006) Catalytic production of olefin block copolymers via chain shuttling polymerization. Science 312:714–719. doi:10.1126/science.1125268
27. Quijada R, Rojas R, Bazan GC, Komon ZJA, Mauler RS, Galland GB (2001) Synthesis of branched polyethylene from ethylene by tandem action of iron and zirconium single site catalysts. Macromolecules 34:2411–2417
28. Britovsek GJP, Gibson VC, Kimberley BS, Maddox PJ, McTavish SJ, Solan GA, White AJP, Williams DJ (1998) Novel olefin polymerization catalysts based on iron and cobalt. Chem Commun 1998(7):849–850
29. Small BL, Brookhart M, Bennett AMA (1998) Highly active iron and cobalt catalysts for the polymerization of ethylene. J Am Chem Soc 120(16):4049–4050. doi:10.1021/J11802100s
30. Reardon D, Conan F, Gambarotta S, Yap G, Wang Q (1999) Life and death of an active ethylene polymerization catalyst. Ligand involvement in catalyst activation and deactivation. isolation and characterization of two unprecedented neutral and anionic vanadium(I) alkyls. J Am Chem Soc 121:9318–9325. doi:10.1021/j1190263x

31. Gibson VC, Redshaw C, Solan GA (2007) Bisiminopyridines: surprisingly reactive ligands and a gateway to new families of catalysts. Chem Rev 107:1745–1776. doi:10.1021/cr068437y
32. Cossée P (1964) Ziegler–Natta catalysis. I. Mechanism of polymerization of α-olefins with Ziegler–Natta catalysts. J Catal 3(1):80–88
33. Talzi EP, Babushkin DE, Semikolenova NV, Zudin VN, Zakharov VA (2001) Ethylene polymerization in the presence of iron(II) 2,6-bis(imine)pyridine complex: structures of key intermediates. Kinet Catal 42(2):147–153
34. Bryliakov KP, Talsi EP, Semikolenova NV, Zakharov VA (2009) Formation and nature of the active sites in bis(imino)pyridine iron-based polymerization catalysts. Organometallics 28:3225–3232. doi:10.1021/om8010905
35. Wang S, Liu D, Huang R, Zhang Y, Mao B (2006) Studies on the activation and polymerization mechanism of ethylene polymerization catalyzed by bis(imino)pyridyl iron(II) precatalyst with alkylaluminum. J Mol Catal A Chem 245(1–2):122–131. doi:10.1016/j.molcata.2005.09.023
36. Hoyt HM, Chirik PJ (2008) Single-component bis(imino)pyridine iron catalyzed olefin polymerization. In: Abstracts of papers, 236th ACS national meeting, INOR-707, Philadelphia
37. Bouwkamp MW, Lobkovsky E, Chirik PJ (2005) Bis(imino)pyridine iron(II) alkyl cations for olefin polymerization. J Am Chem Soc 127:9660–9966. doi:10.1021/j1524447
38. Schmidt R, Das PK, Welch MB, Knudsen RD (2004) *N*,*N*,*N*-Tridentate iron(II) and vanadium (III) complexes, part III, UV–visible spectroscopic studies of reactions of ethylene-oligomerization and polymerization catalysts with methyl aluminoxane cocatalysts. J Mol Catal A Chem 222(1–2):27–45. doi:10.1016/S1381-1169(04)00409-1
39. Bianchini C, Giambastiani G, Guerrero IR, Meli A, Passaglia E, Gragnoli T (2004) Simultaneous polymerization and Schulz–Flory oligomerization of ethylene made possible by activation with MAO of a 1-symmetric [2,6-bis(arylimino)pyridyl]iron dichloride precursor. Organometallics 23(26):6087–6089. doi:10.1021/om049313j
40. Cruz VL, Ramos J, Martinez-Salazar J, Gutierrez-Oliva S, Toro-Labbe A (2009) A theoretical study on a multicenter model based on different metal oxidation states for the bis(imino) pyridine iron catalysts in ethylene polymerization. Organometallics 28(20):5889–5895. doi:10.1021/om900534w
41. Britovsek GJP, Clentsmith GKB, Gibson VC, Goodgame DML, McTavish SJ, Pankhurst QA (2002) The nature of the active site in bis(imino)pyridine iron ethylene polymerization catalysts. Catal Commun 3(5):207–211
42. Tondreau AM, Milsmann C, Patrick AD, Hoyt HM, Lobkovsky E, Wieghardt K, Chirik PJ (2010) From synthesis and electronic structure of cationic, neutral and anionic bis(imino) pyridine iron alkyl complexes: evaluation of redox activity in single-component ethylene polymerization catalysts. J Am Chem Soc 132(42):15046–15059
43. Kissin YV, Qian CT, Xie GY, Chen YF (2006) Multi-center nature of ethylene polymerization catalysts based on 2,6-bis(imino)-pyridyl complexes of iron and cobalt. J Polym Sci A Polym Chem 44(21):6159–6170
44. Flory PJ (1953) Principles of polymer chemistry. Cornell University Press, Ithaca
45. Britovsek GJP, Cohen SA, Gibson VC, Maddox PJ, van Meurs M (2002) Iron-catalyzed polyethylene chain growth on zinc: linear *alpha*-olefins with a Poisson distribution. Angew Chem Int Ed 41(3):489–491
46. Barabanov AA, Bukatov GD, Zakharov VA, Semikolenova NV, Echevskaja LG, Matsko MA (2005) Kinetic peculiarities of ethylene polymerization over homogeneous bis(imino)pyridine Fe(II) catalysts with different activators. Macromol Chem Phys 206:2292–2298. doi:10.1002/macp.200500310
47. Britovsek GJP, Bruce M, Gibson VC, Kimberley BS, Maddox PJ, Mastroianni S, McTavish SJ, Redshaw C, Solan GA, Stroemberg S, White AJP, Williams DJ (1999) Iron and cobalt ethylene polymerization catalysts bearing 2,6-bis(imino)pyridyl ligands: synthesis, structures and polymerization studies. J Am Chem Soc 121(38):8728–8740
48. Mikenas TB, Zakharov VA, Echevskaya LG, Matsko MA (2007) Kinetic features of ethylene polymerization over supported catalysts [2,6-bis(imino)pyridyl iron dichloride/magnesium dichloride] with AlR_3 as an activator. J Polym Sci A Polym Chem 45(22):5057–5066. doi:10.1002/pola.22245

49. Scholtyssek JS (2012) Entwicklung einer dreistufigen in-situ Synthese von Polyethylen/Silica-Nanocomposites. PhD Thesis, Universität Hamburg
50. Zhao W, Yu J, Song S, Yang W, Liu H, Hao X, Redshaw C, Sun W-H (2012) Controlling the ethylene polymerization parameters in iron pre-catalysts of the type 2-[1-(2,4-dibenzhydryl-6-methylphenylimino)ethyl]-6-[1-(arylimino) ethyl]pyridyl iron dichloride. Polymer 53:130–137
51. Zhang W, Chai W, Sun W-H, Hu X, Redshaw C, Hao X (2012) 2-(1-(Arylimino)ethyl)-8-arylimino-5,6,7-trihydroquinoline iron(II) chloride complexes: synthesis, characterization and ethylene polymerization behavior. Organometallics 31:5039–5048
52. Smit TM, Tomov AK, Britovsek GJP, Gibson VC, White AJP, Williams DJ (2012) The effect of imine-crbon substituents in bis(imino)pyridine-based ethylene polymerisation catalysts across the transition series. Catal Sci Technol 2:643–655. doi:10.1039/2CY00448H
53. Görl C, Beck N, Kleiber K, Alt HG (2012) Iron(III) complexes with meta-substituted bis (arylimino)pyridine ligands: catalyst precursors for the selective oligomerization of ethylene. J Mol Catal A Chem 352:110–127. doi:10.1016/j.molcata.2011.10.011
54. Kaul FAR, Puchta GT, Frey GD, Herdtweck E, Herrmann WA (2007) Iminopyridine complexes of 3d metals for ethylene polymerization: comparative structural studies and ligand size controlled chain termination. Organometallics 26(4):988–999
55. Luinstra GA, Queisser J, Bildstein B, Görtz HH, Amort C, Malaun M, Krajete A, Werne G, Kristen MO, Huber N, Gernert C (2003) Highly active ethene polymerization catalysts with unusual imine ligands. In: Rieger B, Saunders Baugh L, Kacker S, Strigler S (eds) Late transition metal polymerization catalysis. Wiley-VCH, Weinheim
56. Britovsek GJP, Gibson VC, Kimberley BS, Mastroianni S, Redshaw C, Solan GA, White AJP, Williams DJ (2001) Bis(imino)pyridyl iron and cobalt complexes: the effect of nitrogen substituents on ethylene oligomerization and polymerization. J Chem Soc Dalton Trans 2001(10):1639–1644
57. Gibson VC, Solan GA (2009) Iron-based and cobalt-based olefin polymerisation catalysts. In: Guan Z (ed) Topics in organometallic chemistry. Springer, Berlin, doi:10.1007/3418_2008_10
58. Gibson VC, Solan GA (2010) Olefin oligomerizations and polymerizations catalyzed by iron and cobalt complexes bearing bis(imino)pyridine ligands. In: Bullock RM (ed) Catalysis without precious metals. Wiley-VCH, Weinheim. doi:10.1002/9783527631582.ch5
59. Kim I, Han BH, Ha Y-S, Ha C-S, Park D-W (2004) Effect of substituent position on the ethylene polymerization by Fe(II) and Co(II) pyridylbis-imine catalysts. Catal Today 93–95:281–285. doi:10.1016/j.cattod.2004.06.057
60. Wang Q, Li L (2004) Effect of aluminoxane on molecular weight and molecular weight distribution of polyethylene prepared by an iron-based catalyst. Polym Int 53:1473–1478. doi:10.1002/Pi.1565
61. Barabanov AA, Bukatov GD, Zakharov VA, Semikolenova NV, Mikenas TB, Echevskaja LG, Matsko MA (2006) Kinetic study of ethylene polymerization over supported bis(imino)pyridine iron (II) catalysts. Macromol Chem Phys 207:1368–1375. doi:10.1002/macp.200600122
62. Mahdavi H, Badiei A, Zohuri GH, Rezaee A, Jamjah R, Ahmadjo SJ (2007) Homogeneous polymerization of ethylene using an iron-based metal catalyst system. J Appl Polym Sci 103 (3):1517–1522. doi:10.1002/app.24949
63. Luinstra GA, Werne G (2001) Highly active single site catalysts with halogenated ligands. In: Abstracts of papers, 221st ACS national meeting, INOR-325, San Diego, 2001
64. Barabanov AA, Bukatov GD, Zakharov VA (2008) Effect of temperature on the number of active sites and propagation rate constant at ethylene polymerization over supported bis(imino) pyridine iron catalysts. J Polym Sci A Polym Chem 46(19):6621–6629. doi:10.1002/pola.22972
65. Small BL, Brookhart M (1999) Polymerization of propylene by a new generation of iron catalysts: mechanisms of chain initiation, propagation, and termination. Macromolecules 31:2120–2130
66. Kumar KR, Sivaram S (2000) Macromol Chem Phys 201(13):1513–1520

67. Semikolenova NV, Zakharov VA, Paukshtis EA, Danilova IG (2005) Supported catalysts based on 2,6-bis(imino)pyridyl complex of Fe(II): DRIFTS study of the catalyst formation and data on ethylene polymerization. Top Catal 32(1–2):77–82. doi:10.1007/s11244-005- 9262-3
68. Ray S, Sivaram S (2006) Silica-supported bis(imino)pyridyl iron(II) catalyst: nature of the support–catalyst interactions. Polym Int 55:854–861. doi:10.1002/pi.2020
69. Ma Z, Sun W-H, Zhu N, Li Z, Shao C, Hu Y (2002) Preparation of silica-supported late transition metal catalyst and ethylene polymerization. Polym Int 51:349–352. doi:10.1002/pi.853
70. Li L, Wang Q (2004) Synthesis of polyethylene with bimodal molecular weight distribution by supported iron based catalyst. J Polym Sci A Polym Chem 42:5662–5669
71. Kaul FAR, Puchta GT, Schneider H, Bielert F, Mihalios D, Herrmann WA (2002) Immobilization of bis(imino)pyridyliron(II) complexes on silica. Organometallics 21:74–82
72. Trewyn BG, Slowing II, Giri S, Chen H-T, Lin VS-Y (2007) Synthesis and functionalization of a mesoporous silica nanoparticle based on the sol–gel process and applications in controlled release. Acc Chem Res 40(9):846–853
73. Ma Z, Ke Y, Wang H, Guo C, Zhang M, Sun W-H, Hu Y (2003) Ethylene polymerization with a silica-supported iron-based diimine catalyst. J Appl Polym Sci 88(2):466–469. doi:10.1002/app.11749
74. Kageyama K, Tamazawa J, Aida T (1999) Extrusion polymerization: catalyzed synthesis of crystalline linear polyethylene nanofibers within a mesoporous silica. Science 285:2113–2115. doi:10.1126/science.285.5436.2113
75. Wu L, Wanke SE (2010) MgCl2-Supported TiCl4 catalysts for productions of morphology-controlled polyethylene. In: Hoff R, Mathers RT (eds) Handbook of transition metal polymerization catalysts. Wiley, Hoboken
76. Ohnishi R, Konakazawa T, Amano J, Fujimura T (2006) Temperature effect on ethylene polymerization with a catalyst prepared by mixing $Mg(C_2H_5)(n\text{-}C_4H_9)$, $Al(2H_5)_{1.5}Cl_{1.5}$ and iron(II)bis(imino)pyridyl complex. Polym Bull 56(1):1–8. doi:10.1007/s00289-005-0460-8
77. Xu R, Liu D, Wang S, Mao B (2006) Preparation of spherical $MgCl_2$-supported late-transition metal catalysts for ethylene polymerization. Macromol Chem Phys 207:779–786. doi:10.1002/macp.200500582
78. Schilling M, Bal R, Görl C, Alt HG (2007) Heterogeneous catalyst mixtures for the polymerization of ethylene. Polymer 48:7461–7475. doi:10.1016/j.polymer.2007. 10.042
79. Kaminsky W, Funck A, Scharlach K (2010) In situ generation of polyolefin nanocomposites. In Sabu T (ed) Recent advances in polymer nanocomposites: synthesis and characterisation. Brill, Leiden, pp 49–73. doi:10.1163/ej.9789004172975.i-438.19
80. Kurokawa H, Matsuda M, Fujii K, Ishihama Y, Sakuragi T, Ohshima M, Miura H (2007) Bis(imino)pyridine iron and cobalt complexes immobilized into interlayer space of fluorotetrasilicic mica: highly active heterogeneous catalysts for polymerization of ethylene. Chem Lett 36:8. doi:10.1246/cl.2007.1004
81. Hiyama Y, Kawada Y, Ishihama Y, Sakuragi T, Ohshima M, Kurokawa H, Miura H (2009) Catalytic behavior of bis(imino)pyrindine iron(II) complex supported on clay minerals during slurry polymerization of ethylene. Bull Chem Soc Jpn 82(5):624–626
82. Kondo T, Yamamoto K, Sakuragi T, Kurokawa H, Miura H (2012) Acetyliminopyridineiron (III) complexes immobilized in fluorotetrasilicic mica interlayer as efficient catalysts for oligomerization of ethylene. Chem Lett 41:461–463. doi:10.1246/cl.2012.461
83. Ray S, Galgali G, Lele A, Sivaram S (2005) In situ polymerization of ethylene with bis(imino) pyridine iron(II) catalysts supported on clay: the synthesis and characterization of polyethylene–clay nanocomposites. J Polym Sci A Polym Chem 43:304–318
84. Stoeber W, Fink A, Bohn E (1968) Controlled growth of monodisperse silica spheres in the micron size range. J Colloid Interface Sci 26(1):62–69
85. Yun DS, Kim HJ, Yoo JW (2005) Preparation of silica nanospheres: effect of silicon alkoxide and alcohol on silica nanospheres. Bull Korean Chem Soc 26(12):1927–1928

Index